

# SSD

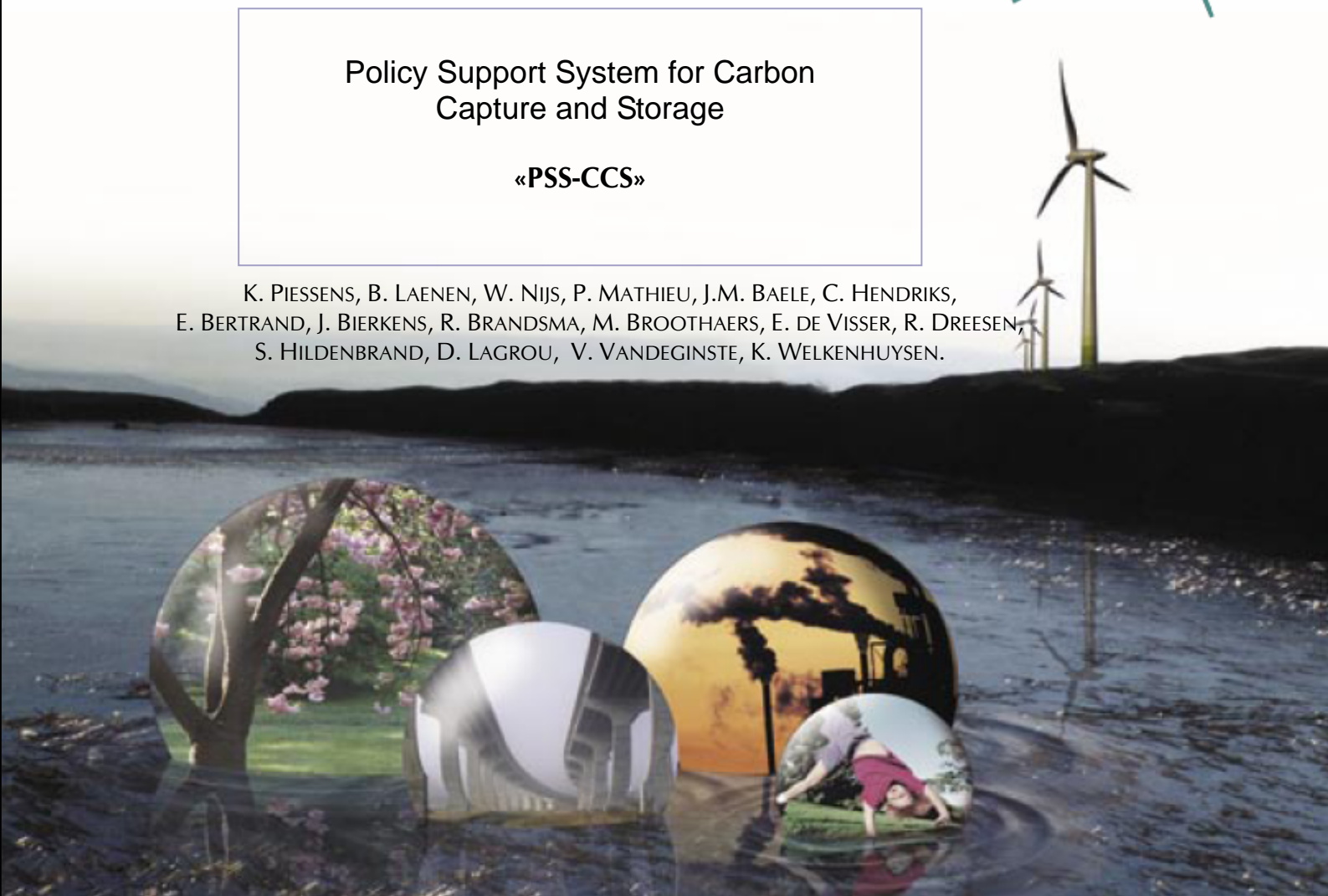
SCIENCE FOR A SUSTAINABLE DEVELOPMENT



## Policy Support System for Carbon Capture and Storage

«PSS-CCS»

K. PIESSENS, B. LAENEN, W. NIJS, P. MATHIEU, J.M. BAELE, C. HENDRIKS,  
E. BERTRAND, J. BIERKENS, R. BRANDSMA, M. BROOTHAERS, E. DE VISSER, R. DREESSEN,  
S. HILDENBRAND, D. LAGROU, V. VANDEGINSTE, K. WELKENHUYSEN.



ENERGY 

TRANSPORT AND MOBILITY 

AGRO-FOOD 

HEALTH AND ENVIRONMENT 

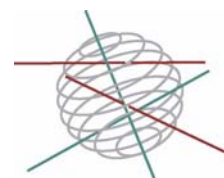
CLIMATE 

BIODIVERSITY 

ATMOSPHERE AND TERRESTRIAL AND MARINE ECOSYSTEMS 

TRANSVERSAL ACTIONS 

SCIENCE FOR A SUSTAINABLE DEVELOPMENT  
(SSD)



*Climate*

FINAL REPORT (Phase I)



Policy Support System for Carbon  
Capture and Storage

«PSS-CCS»

SD/CP/04A



Promotors

**Kris Piessens**

Royal Belgian Institute of Natural Sciences  
Geological Survey of Belgium

**Ben Laenen**

Vlaamse Instelling voor Technologisch Onderzoek (VITO)

**Philippe Mathieu**

Université de Liège

**Jean-Marc Baele**

Faculté Polytechnique de Mons

Authors

Kris Piessens, Veerle Vandeginste, Kris Welkenhuysen (RBINS)  
Ben Laenen, Roland Dreesen, Johan Bierkens, Matsen Broothaers  
Sandra Hildenbrand, David Lagrou, Wouter Nijs (VITO)  
Philippe Mathieu, Emmanuelle Bertrand (ULg)  
Jean-Marc Baele (FPM)  
Chris Hendriks, Erika de Visser, Ruut Brandsma (ECOFYS)

**September 2008**





D/2009/1191/1

Published in 2009 by the Belgian Science Policy

Rue de la Science 8

Wetenschapsstraat 8

B-1000 Brussels

Belgium

Tel: +32 (0)2 238 34 11 – Fax: +32 (0)2 230 59 12

<http://www.belspo.be>

Contact person:

*Mrs Sophie Verheyden* : +32 (0)2 238 36 12

Neither the Belgian Science Policy nor any person acting on behalf of the Belgian Science Policy is responsible for the use which might be made of the following information. The authors are responsible for the content.

No part of this publication may be reproduced, stored in a retrieval system, or transmitted in any form or by any means, electronic, mechanical, photocopying, recording, or otherwise, without indicating the reference:

Kris Piessens, Ben Laenen, Wouter Nijs, Philippe Mathieu, Jean-Marc Baele, Chris Hendriks, Emmanuelle Bertrand, Johan Bierkens, Ruut Brandsma, Matsen Broothaers, Erika de Visser, Roland Dreesen, Sandra Hildenbrand, David Lagrou, Veerle Vandeginste, Kris Welkenhuysen. ***Policy support system for carbon capture and storage «PSS-CCS»***. Final Report Phase 1. Brussels : Belgian Science Policy 2009 – 268 p. (Research Programme Science for a Sustainable Development)

## Technical Summary

The central goal of the project Policy Support System for Carbon Capture and Storage (PSS-CCS) is to build a tool capable of projecting the implementation of Carbon Capture and Storage in a Belgian context. Together with the simulator, a series of databases are needed on the three main elements in the CCS-chains: capture, transport and storage.

The report starts with a general introduction (chapter1) on climate change, mitigation techniques and CCS.

CO<sub>2</sub> concentrations in the atmosphere are on the rise due to human activities, and it seems advisable to control these levels in view of adverse climate effects. One of the possible techniques is Carbon Capture and Storage, which forms the main topic of this publication.

Capture refers to the separation of CO<sub>2</sub> into a concentrated stream. This can be done at large industrial sources, and in general three capture techniques are discriminated. In the post-combustion system, CO<sub>2</sub> is separated from the flue gases, produced by the combustion of the primary fuel in air. In the pre-combustion process, the primary fuel reacts with steam and air or oxygen in a first reactor to produce a mixture of mainly carbon monoxide and hydrogen. The carbon monoxide reacts then with steam in a second reactor to produce additional hydrogen, together with CO<sub>2</sub>. This mixture is then separated. In the oxy-fuel combustion system, primary fuel is combusted with oxygen instead of air to produce a flue gas that is mainly composed of water vapour and CO<sub>2</sub>.

After CO<sub>2</sub> capture, CO<sub>2</sub> is compressed for transport, commonly through pipelines. The CO<sub>2</sub> pressure should not drop below 7.5 MPa during the complete (pipeline) trajectory in order to avoid two-phase flow and to transport it at a sufficiently high density.

For geological storage, three types of formations are suitable: depleted oil and gas reservoirs, deep saline aquifers, and coal seams and (coal) mines. For the storage of CO<sub>2</sub> in a liquid or supercritical phase, CO<sub>2</sub> is commonly stored in formations below 800 m depth. Based on the lower CO<sub>2</sub> density compared to water, a sealed cap rock is required on top of the CO<sub>2</sub> storage reservoir. Additional trapping results from capillary forces, dissolution in formation water and mineral precipitation. In coal sequences, adsorption is an essential trapping mechanism.

Chapter 2 brings an overview of the current large CO<sub>2</sub> emitters in Belgium, which are potential targets for CCS projects and already give a first indication of the relevance of this technique for Belgium. The a technical overview is given on the main capture technologies that can be used in the power sector. At the end of this chapter, these techniques are compared regarding their performance and cost.

The current industry is an important starting point. The overview comprises Ammonia, Cement, Ethylene, Ethylene oxide, Glass, Hydrogen, Iron and Steel, Lime, Power, Refineries and other sectors. Current CO<sub>2</sub> production is dominated by sources that emit over 500 Mton/y, which is in general favourable for CCS projects. Pure CO<sub>2</sub> streams represent only a few percentages of the total emissions.

Capture technologies are relatively well described for the power sector. A comparison of the main technology types reveals clear differences regarding fuel price, capacity, charge factors, etc.. Nevertheless, the relevant economic parameter, which is the cost of electricity, is very comparable for all technologies. It is therefore not possible to identify which technology will dominate. In fact, it is likely that most of them will find their application.

The different geological storage options for Belgium are discussed in chapter 3. For the Flemish region the focus is on the aquifer storage options, while for the Walloon region coal gets most attention. For the international context, the storage options, capacities and costs in our neighbouring countries are assessed.

In Flanders, four aquifer complexes are considered. The Upper Cretaceous to Palaeocene carbonates occur at sufficient depth in the north of the Campine basin and in the Roer Valley Graben and have good injectivity and porosity. Seals are present in the overlying Cenozoic, but the target area is small.

The Lower Triassic sandstones of the Bundsandstein Formation have good porosity and are in the Roer Valley Graben overlain by sealing formations. Although the injectivity may be lower, it is regarded as a promising target for CO<sub>2</sub> storage.

The Upper Carboniferous sandstones, the Neeroeteren Formation, have good porosity and permeability, but sealing is incomplete or uncertain.

The Lower Carboniferous carbonates, known as the Dinantian carbonates, are used for the storage of natural gas. Sealing is guaranteed, but the capacity of individual structures is relatively small.

In the Walloon region, the coal deposits from Hainaut to Namur, and some sites near Huy and Liège, were selected as most promising for the storage of CO<sub>2</sub>. When assessing the storage potential, the whole coal sequence (coal, silt, sandstone) was taken into account. This new approach leads to a multiplication of the potential storage capacity.

The Dinantian aquifer is the best known aquifer target for CO<sub>2</sub> storage. It is especially its deepest and most horizontal part that is considered. This partly extends into France, and is considered as promising for CO<sub>2</sub> storage.

Belgium is a relatively small country. It also lacks gas or oil fields, which when depleted are often considered as first targets for CO<sub>2</sub> storage. Therefore also the storage potential in neighbouring countries is considered, more precisely for The Netherlands, Germany, France and the North Sea region. These show that exporting CO<sub>2</sub> would cost between 4 and 6 €/ton, except for the North Sea region where this would be 8 to 11€/ton.

Transport of CO<sub>2</sub> by pipeline is discussed in chapter 4, first by looking at the technical requirements of pipelines and CO<sub>2</sub> purity. This is followed by an estimation procedure for determining suited pipeline diameters, and discriminating the different cost aspects of pipeline construction and operation.

An enhanced formula for the calculation of pipeline diameters is proposed which allows to specifically include effects of height differences, local losses and frictional loss, and uses the Manning coefficients in order to avoid iterative calculation.

The Markal model is introduced in chapter 6. The reference energy scenario was extended by data on the capture technologies and a generalisation for transport and cost data in order to verify the potential impact of CCS on overall costs and emissions. The results of these forecasts are presented in chapter 7.

The Markal model is software that enables a user to represent a complex energy system as a linear system, as has been used to build a model for the electricity sector in Belgium. This is used as reference scenario, and is extended with data on capture technologies and in a more rudimentary way also transport and storage. These show that CCS can contribute significantly to decarbonisation of the electricity sector, up to 50%, when the CO<sub>2</sub> price is higher than 25 €/ton.

Chapter 8 describes the architecture and essential elements of the PSS simulator, as it was developed within the PSS-CCS project. It specifies how PSS is capable of making stochastic projections, and how it details routing costs and storage aspects. A demonstration of this potential is given in chapter 9.

PSS is a bottom-up simulator designed to provide ad-hoc projections for the implementation of CCS. In view of this particular scope, it is capable of making detailed cost estimates for

transport of CO<sub>2</sub> using least-cost pipeline routing and makes use of uncertainty predictions on the availability of CO<sub>2</sub> sinks. In general, it pays specific attention to uncertainty at scenario level.

Two scenarios, based on the main Markal scenario, are used to demonstrate its application and flexibility. These largely confirm the Markal results, but also highlight the hazards of technology lock-in and importance of open access to transport and storage infrastructure. The effects of these are significant, and may largely undo the anticipated environmental benefits of CCS.



**Table of contents**

<b>1 INTRODUCTION</b> .....	<b>11</b>
<b>1.1 Climate change</b> .....	11
1.1.1 Scientific background .....	11
1.1.2 Consequences of climate change .....	15
1.1.3 International policy .....	16
1.1.4 Belgian policy .....	18
<b>1.2 Carbon capture and storage</b> .....	20
1.2.1 Capture .....	20
1.2.2 Transport .....	21
1.2.3 Storage .....	22
<b>1.3 References</b> .....	23
<b>2 SOURCE TECHNOLOGY</b> .....	<b>25</b>
<b>2.1 Inventory of CO<sub>2</sub> emission from point sources in Belgium</b> .....	25
2.1.1 Introduction .....	25
2.1.2 Content and structure of the database .....	25
2.1.3 Sectors .....	30
2.1.4 Results and conclusions .....	44
<b>2.2 Post-combustion capture systems</b> .....	46
2.2.1 Basic process .....	46
2.2.2 Historical developments .....	46
2.2.3 Process chemistry .....	47
2.2.4 Limitations of the MEA process .....	50
2.2.5 CO <sub>2</sub> capture from gas versus coal-fired power plants .....	50
<b>2.3 Pre-combustion capture systems</b> .....	51
2.3.1 Basic process .....	51
2.3.2 Integrated Gasification Combined Cycle (IGCC) .....	51
2.3.3 Integral Reforming Combined Cycle (IRCC) .....	55
2.3.4 Limitations of the technology .....	55
<b>2.4 Oxy-fuel combustion capture systems</b> .....	57
2.4.1 Basic process .....	57
2.4.2 Oxy-fuel Pulverized Fuel boiler .....	57
2.4.3 Comparison with the air-firing case .....	60
2.4.4 Oxy-fuel gas turbine .....	60
<b>2.5 Performance and costs of power plants with CO<sub>2</sub> capture</b> .....	61
2.5.1 Introduction .....	62
2.5.2 Consistency of data and data processing .....	62
2.5.3 Plant performance .....	63
2.5.4 Costs .....	66
2.5.5 Prevision for 2030 .....	73
2.5.6 Conclusion .....	74
<b>2.6 References</b> .....	76
<b>3 Sink options</b> .....	<b>77</b>
<b>3.1 Storage site requirements</b> .....	77
<b>3.2 Flanders region</b> .....	77
3.2.1 Methodology .....	78
3.2.2 Upper Cretaceous to Palaeocene carbonates .....	82
3.2.3 The Lower Triassic sandstones .....	88
3.2.4 The Upper Carboniferous sandstones .....	96
3.2.5 The Lower Carboniferous carbonates .....	104
3.2.6 Conclusions .....	110

<b>3.3 Walloon Region</b> .....	112
3.3.1 Storage in (unmined) coal deposits.....	112
3.3.2 Storage in coal mines.....	125
3.3.3 Storage in aquifers.....	127
<b>3.4 International storage assessments</b> .....	129
3.4.1 Introduction.....	129
3.4.2 Assumptions to calculate CO <sub>2</sub> storage potential and costs outside Belgium.....	129
3.4.3 Methodology.....	130
3.4.4 Results.....	131
3.4.5 Conclusion.....	132
<b>3.5 References</b> .....	134
<b>4 Transport</b> .....	<b>137</b>
<b>4.1 Nature of CO<sub>2</sub> transport</b> .....	137
<b>4.2 CO<sub>2</sub> quality requirements for pipeline transport</b> .....	138
4.2.1 Introduction.....	138
4.2.2 Experience.....	138
4.2.3 Components in the captured CO <sub>2</sub> stream.....	139
4.2.4 Critical components in each step of the CCS system.....	141
4.2.5 Gas conditioning.....	143
<b>4.3 Cost estimation</b> .....	147
4.3.1 Pipeline investment cost factors.....	147
4.3.2 Determination of diameter and length of pipeline.....	149
4.3.3 Compressor cost.....	162
<b>4.4 References</b> .....	162
<b>5 Health, safety and environmental risks of underground CO<sub>2</sub>-sequestration</b> .....	<b>165</b>
<b>5.1 Introduction</b> .....	165
<b>5.2 Natural analogues</b> .....	166
<b>5.3 Experimental work and modelling</b> .....	167
<b>5.4 Human health and environmental hazards</b> .....	168
<b>5.5 Main mechanisms of CO<sub>2</sub> leakage</b> .....	170
5.5.1 Depleted oil and gas fields.....	172
5.5.2 Deep saline aquifers.....	174
<b>5.6 Risk assessment methodology</b> .....	176
5.6.1 Risk assessment.....	176
5.6.2 FEP–methodology and scenarios.....	177
<b>5.7 Environmental and human toxicology</b> .....	180
5.7.1 Effects on the environment.....	180
5.7.2 Ground- and drinking water.....	180
5.7.3 Surface water.....	182
5.7.4 Soil.....	182
5.7.5 Ecotoxicity studies.....	182
5.7.6 Effects on humans.....	183
5.7.7 Evaluation of environmental and health effects.....	192
<b>5.8 Case study and risk modelling</b> .....	193
5.8.1 Background - Leakage mechanisms.....	193
5.8.2 The Poederlee structure.....	195
5.8.3 The Verloren Kamp structure.....	202
<b>5.9 References</b> .....	205
<b>6 MARKAL Model</b> .....	<b>209</b>
<b>6.1 Markal methodology</b> .....	209
6.1.1 Presentation of Markal.....	209
6.1.2 Presentation of the electricity model.....	211
6.1.3 Limits of the model.....	212

<b>6.2 Reference scenario</b> .....	212
6.2.1 Policies and measures .....	212
6.2.2 Energy prices evolution .....	213
6.2.3 CO <sub>2</sub> emission factors.....	214
6.2.4 Electricity importation evolution .....	214
6.2.5 Electricity demand evolution .....	214
6.2.6 Heat demand evolution .....	215
6.2.7 Efficiency of generating facilities .....	215
<b>6.3 CCS scenarios</b> .....	215
6.3.1 Performance and costs of CO <sub>2</sub> capture technologies .....	215
6.3.2 Costs of CO <sub>2</sub> transport and storage.....	217
6.3.3 Scenarios .....	217
<b>7 Presentation and discussion of the MARKAL results</b> .....	<b>219</b>
<b>7.1 Model outputs</b> .....	219
<b>7.2 Comparison of different scenarios</b> .....	219
7.2.1 Major assumptions .....	220
7.2.2 Total cost and CO <sub>2</sub> emissions according to the different scenarios.....	220
7.2.3 Results and interpretation of technology choices .....	221
7.2.4 CO <sub>2</sub> storage: limitation of CO <sub>2</sub> injection rates.....	224
<b>7.3 Marginal Abatement Cost curves</b> .....	225
7.3.1 Proceeding.....	225
7.3.2 Results interpretation .....	226
<b>8 PSS simulator</b> .....	<b>233</b>
<b>8.1 Principles of bottom-up simulation</b> .....	233
<b>8.2 Environment and Architecture of PSS</b> .....	233
<b>8.3 The power of stochastic modelling</b> .....	235
<b>8.4 Router: determining pipeline trajectories</b> .....	236
8.4.1 Principles of raster routing.....	236
8.4.2 Geographic cost parameters.....	237
8.4.3 Advanced raster routing with Router .....	241
<b>8.5 Economer: NPV based project evaluation</b> .....	<b>242</b>
8.5.1 Methodology for ‘New Sources’ .....	242
8.5.2 Retrofit for ‘New Sources’ .....	247
8.5.3 Retrofit for ‘Old Sources’ .....	247
<b>8.6 PSS definition of CO<sub>2</sub> avoided</b> .....	249
<b>8.7 Sinkers: estimating storage capacity</b> .....	251
8.7.1 Introduction.....	251
8.7.2 Conceptual model .....	251
8.7.3 Expert input.....	253
8.7.4 Real Options calculation scheme .....	255
8.7.5 Presentation of results .....	256
<b>9 Preliminary results from PSS</b> .....	<b>257</b>
<b>9.1 Demo scenario</b> .....	257
<b>9.2 Scenario variants</b> .....	257
<b>9.3 Friendly scenario (export allowed)</b> .....	258
<b>9.4 Hostile scenario (no export possible)</b> .....	262
<b>9.5 Discussion of the Friendly and Hostile scenarios</b> .....	264
<b>10 Conclusions</b> .....	<b>267</b>



## 1 INTRODUCTION

### 1.1 Climate change

Climate change is currently a hot topic, receiving a lot of attention by the media, governments and the public. Worldwide, scientists evaluate the climate change and predict temperature changes in the future and its environmental impacts. Based on these predictions and assessments, they search for appropriate solutions and propose them to the governments, who need to make crucial decisions.

#### 1.1.1 Scientific background

##### 1.1.1.1 *Current climate change observations*

The observed increase of the global average atmospheric and ocean temperature, of the melting of snow and of the global average sea level proves without doubt the phenomenon of global warming (IPCC, 2007a; fig. 1-1):

- the average atmospheric temperature has increased by 0.74°C between 1906 and 2005;
- the average ocean temperature has increased to depths of at least 3000 m;
- the sea level has increased by 1.8 mm per year since 1961 (and 3.1 mm per year between 1993 and 2003);
- the extent of glaciers and snow has decreased.

Other climate changes include e.g. (IPCC, 2007a):

- the increase of precipitation in diverse regions;
- more intense and longer periods of drought in tropical and subtropical zones;
- higher frequency of intense precipitation.

##### 1.1.1.2 *Anthropogenic influence on climate change*

According to IPCC (2007a), there is a very high probability that human activities globally caused the warming since 1750. This warming is ascribed to the increase of atmospheric concentrations of CO<sub>2</sub>, CH<sub>4</sub>, N<sub>2</sub>O that cause an increase of the radiative forcing. The latter is used to quantitatively express the influence of changes in the atmospheric abundance of greenhouse gases and aerosols, in solar radiation and in land surface properties to alter the energy balance of the climate system. In this way, radiative forcing can be used to compare how a range of human and natural factors drive warming or cooling influences on global climate. Analysis of ice cores indicate that the CO<sub>2</sub>, CH<sub>4</sub> and N<sub>2</sub>O concentrations are significantly higher than the pre-industrial level (fig. 1-2) and that they are the highest in the last 650 000 years. The concentration of CO<sub>2</sub>, the main greenhouse gas of anthropogenic origin, increased from 280 ppm (pre-industrial) to 379 ppm in 2005 with an increase of the emission CO<sub>2</sub> from fossil fuels from 6.4 GtC/year in 1990 to 7.2 GtC/year in 2000-2005. The CH<sub>4</sub> concentrations changed from 715 ppb (pre-industrial) to 1774 ppb in 2005, while the emission (mainly due to agriculture and the use of fossil fuels) stayed relatively stable during the last decade. For N<sub>2</sub>O (its emissions mainly caused by agriculture), an increase was measured from 270 ppb (pre-industrial) to 319 ppb in 2005. The gases have induced a current radiative forcing that is the highest in the last 10 000 years. The positive radiative forcing related to CO<sub>2</sub> has increased by 20% in the last 10 years.

Other anthropogenic contributions to radiative forcing come from aerosols (primarily sulphate, organic carbon, black carbon, nitrate and dust) causing a total cooling effect, whereas emissions of ozone-forming chemicals (nitrogen oxides, carbon monoxide and hydrocarbons) and changes in halocarbons are characterized by a positive radiative forcing (IPCC, 2007a). Also changes in solar irradiance since 1750 produce a positive radiative forcing

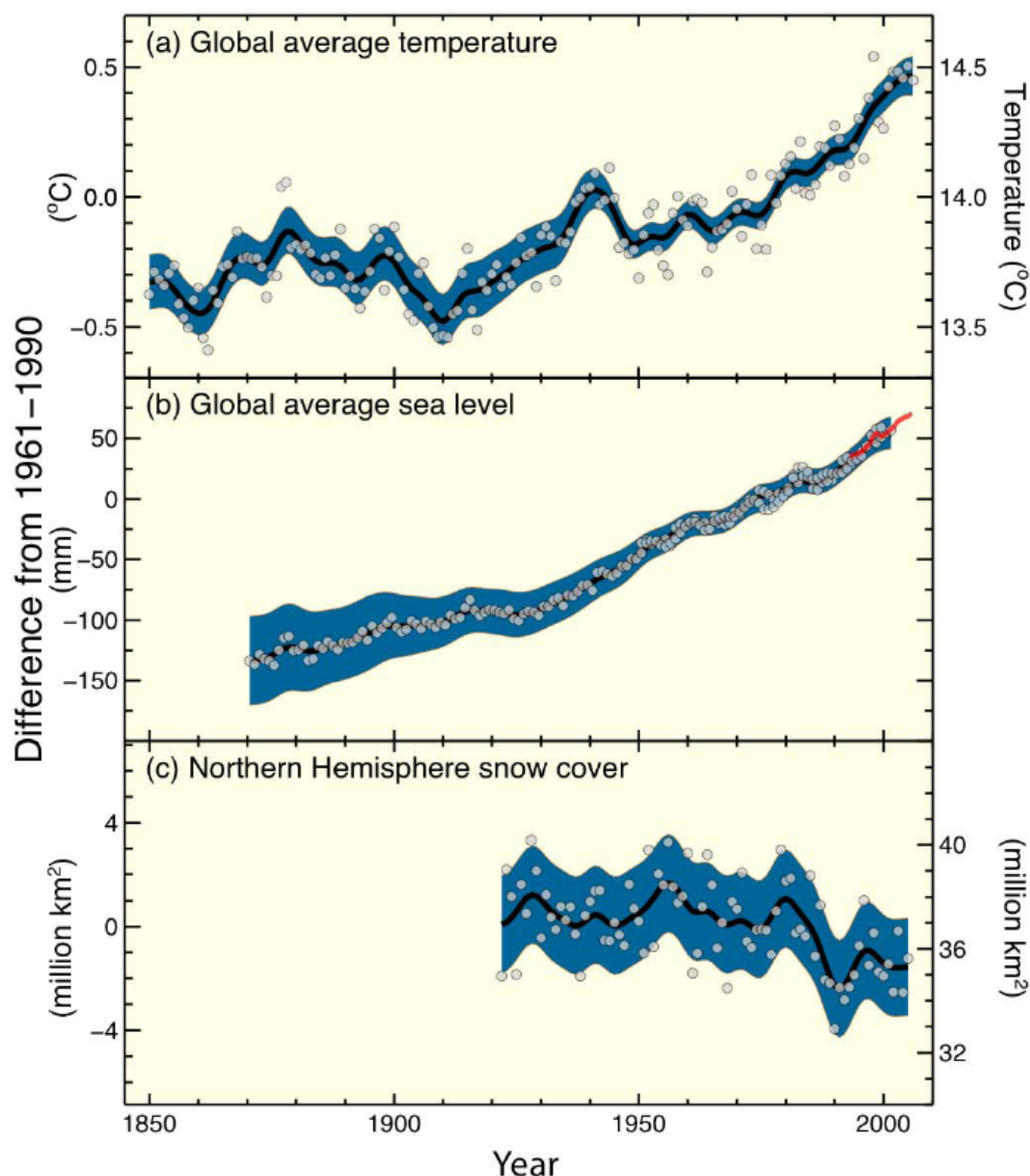


Figure 1-1: (From IPCC, 2007a) Observed changes in (a) global average surface temperature; (b) global average sea level rise from tide gauge (blue) and satellite (red) data and (c) Northern Hemisphere snow cover for March-April. All changes are relative to corresponding averages for the period 1961-1990. Smoothed curves represent decadal averaged values while circles show yearly values. The shaded areas are the uncertainty intervals estimated from a comprehensive analysis of known uncertainties (a and b) and from the time series (c).

The increase in global greenhouse gas emissions by 70% between 1970 and 2004 is mainly caused by the energy supply sector (increase of 145%). Direct emissions from transport, industry, land use (change) and forestry, agriculture and buildings increased by 120%, 65%, 40%, 27% and 26% respectively (IPCC, 2007c). The effect on global emissions of the decrease in global energy intensity (-33%) in the period 1970-2004 was smaller than the combined effect of global per capita income growth (77%) and population growth (69%).

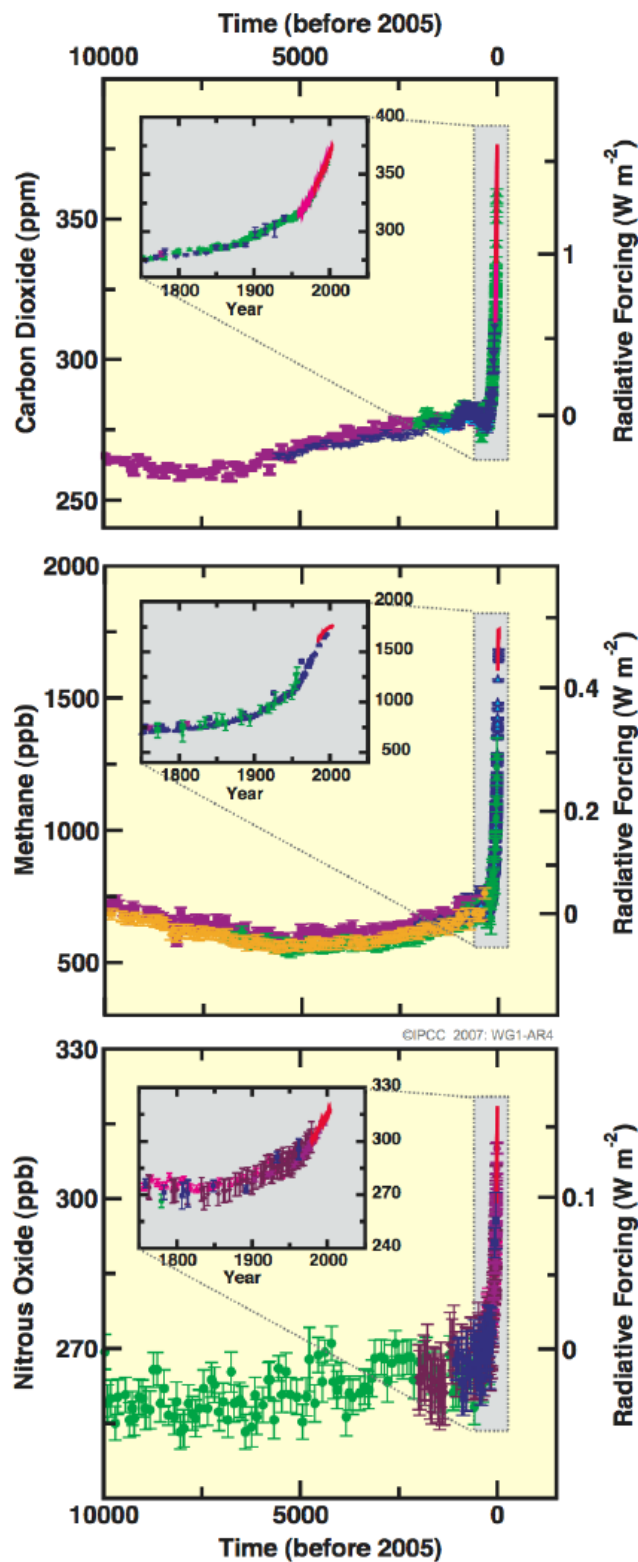


Figure 1-2: (From IPCC, 2007a) Atmospheric concentrations of  $\text{CO}_2$ ,  $\text{CH}_4$ ,  $\text{N}_2\text{O}$  over the last 10 000 years (large panels) and since 1750 (inset panels). Measurements are shown from ice cores (symbols with different colours for different studies) and atmospheric samples (red lines). The corresponding radiative forcings are shown on the right hand axes of the large panels.

### 1.1.1.3 Climate change predictions

According to climate prediction scenarios, a temperature increase of 0.2°C per decade occurs during the next 2 decades. The predictions for the average global warming till 2100 are highly dependent on the emission scenarios used and vary from 1.8 to 4°C increase compared to the 1980-1999 period (IPCC, 2007a; fig. 1-3). A mean global warming, expected to stabilize at a doubling of the CO<sub>2</sub> concentrations, will probably have a value between 2 and 4.5°C. The expected sea level increase by 2100 varies between 0.2 to 0.6 m compared to the 1980-1999 period. Furthermore, a pH-decrease by 0.14 to 0.35 of the oceans is expected by 2100.

Besides the global trends, some examples of regional trends, that are likely to occur, are the following (IPCC, 2007a):

- the expected warming is higher onshore and in the polar regions of the northern hemisphere;
- heat waves and heavy rainfalls will occur more often;
- a higher intensity of the tropical cyclones are predicted;
- higher rainfalls are expected in the polar regions, whereas a reduction is probable in most of the land areas.

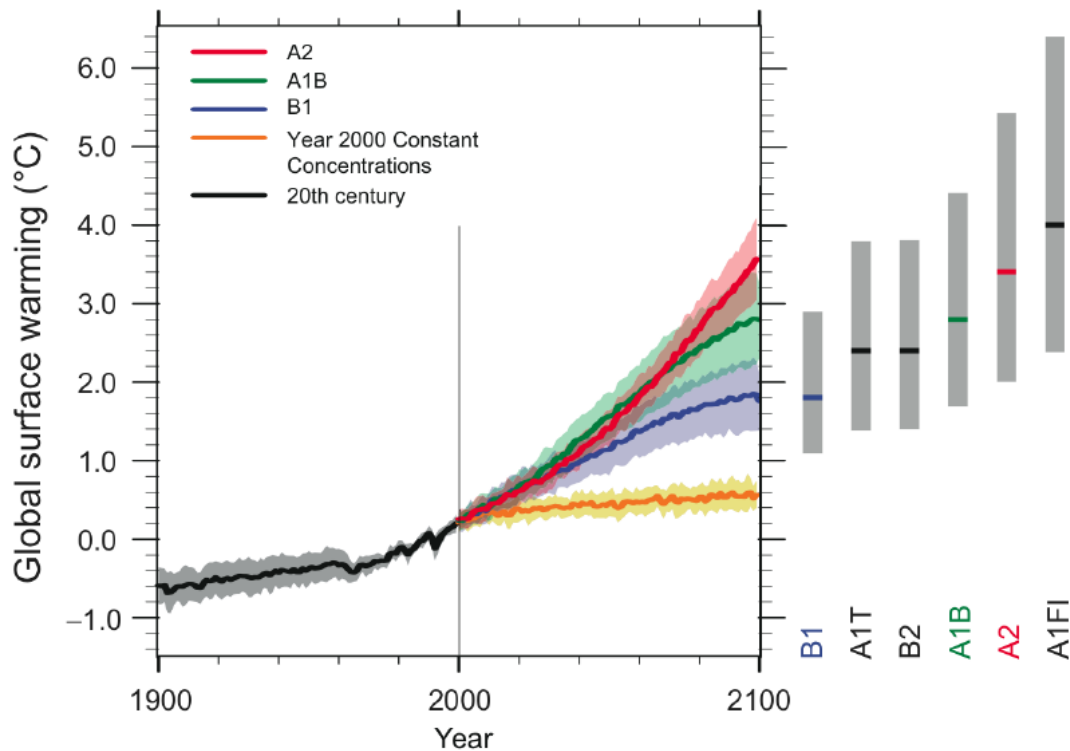


Figure 1-3: (From IPCC, 2007a) Solid lines are multi-model global averages of surface warming (relative to 1980-99) for the scenarios A2, A1B and B1, shown as continuations of the 20th century simulations. Shading denotes the plus/minus one standard deviation range of individual model annual averages. The orange line is for the experiment where concentrations were held constant at year 2000 values. The grey bars at right indicate the best estimate (solid line within each bar) and the likely range assessed for the six SRES marker scenarios. The assessment of the best estimate and likely ranges in the grey bars includes the AOGCMs in the left part of the figure, as well as results from a hierarchy of independent models and observational constraints.

## 1.1.2 Consequences of climate change

### 1.1.2.1 Current consequences

The observations demonstrate that there are consequences of the global climate change, especially the warming, for all continents and most oceans (IPCC, 2007b). These include e.g. changes in extent of snow and ice sheets and instability of soils in permafrost areas; warming of lakes and rivers with consequences for water quality; disturbance of biological systems such as earlier migration of birds and fish; changes in occurrences and amount of algae, plankton and fish in the oceans at higher latitudes. The global warming probably also influences agriculture at higher latitudes in the northern hemisphere, health (due to e.g. heat waves, migration of insects that transfer diseases) and changes in traditional activities in mountainous and arctic areas (IPCC, 2007b).

### 1.1.2.2 Future consequences

Future impacts due to climate change that may occur during this century, consist of (IPCC, 2007b):

- *with respect to water*: increased flow rate of rivers in arctic and some tropical areas in contrast to a decrease in most areas at moderate latitude; extension of areas subject to drought; more frequent and intense precipitations increasing the risk of flooding; decrease of glaciers and snow sheets resulting in a decrease of water availability in mountainous areas;
- *with respect to ecosystems*: the natural adaptation potential of diverse ecosystems will be surpassed by a combination of disturbances; decrease of terrestrial carbon; 20 to 30% of the plant and animal species are in danger of extinction for an average temperature increase of more than 1.5 to 2.5°C;
- *with respect to agriculture*: production increase in areas of moderate to high latitudes for a worldwide warming of less than 1 to 3°C, but production decrease in tropical areas; more extreme climate occurrences such as flooding and drought periods, affecting locally the agricultural production;
- *with respect to coastal areas*: high erosion and flooding risk in coastal areas; lagoons and mangroves are in danger by a higher sea level; coral reefs are endangered with a temperature increase of 2°C; increased acidification of ocean water due to higher CO<sub>2</sub> concentration influences shell formation;
- *with respect to human communities*: higher costs; industries, houses and communities in coastal areas, those that are highly dependent or sensitive on climate are at risk; poor communities are most at risk due to high dependency on local sources such as water and food production;
- *with respect to health*: higher health risk or mortality due to higher malnutrition, heat waves, flooding and drought, change in geographic distribution of transfers of diseases.
- The IPCC report (2007b) provides specific data on future impacts for specific regions:
  - *Africa*: higher water deficiency; lower food production; risk of flooding in populated areas;
  - *Asia*: higher risk of flooding, soil instability and disturbances in water provisions in Himalaya; higher flooding risk in coastal areas; interaction of climate change effects with fast economic and demographic growth and migration from the countryside to the city influences development in a negative way; higher risk of food deficiency due to lower agricultural production;
  - *Australia/New Zealand*: water deficiency due to less rainfall and higher evaporation; loss of biodiversity; risks related to higher sea level and intensity and frequency of storms affect coastal communities; positive changes such as longer vegetation period, shorter

period of frost, decrease of mortality due to cold and decrease of energy need during winter;

- *Europe*: mainly negative effects in Southern Europe such as regression of glaciers, longer growth seasons and health risks due to heat waves; diverse effects in Northern Europe such as decrease of energy need for heating, increase of agricultural production and growth of forests, but also winter flooding, endangered ecosystems, migration of species and increased health risks due to heat waves; in whole Europe, there is a higher risk of flooding, decrease of snow sheet, decrease of winter tourism and increased extinction of species;
- *Latin-America*: decrease of biodiversity, replacement of tropical rain forest by savanna, desertification of agricultural production areas; risk of flooding;
- *North America*: decrease of snow sheet in western mountains, more winter flooding and lower summer flow rate; higher risk of forest fires; higher agricultural production; more heat waves; risk and economic losses related to a higher sea level and more storms is negatively influenced by development of coastal areas and demographic growth;
- *Arctic areas*: decrease of thickness and extent of ice sheets and glaciers, changes in ecosystems, negative consequences for animals, higher vulnerability for invasive species; less energy need for heating, more possibilities for agriculture, but also negative effects on infrastructure and traditional life style of autochthon population;
- *Small islands*: infrastructure is endangered, less fresh water on islands, less tourists

### 1.1.3 International policy

#### **1.1.3.1 Adaptation to climate change and mitigation on short term**

Adapt to climate change is necessary. The development way, population growth, income and technological development can increase our vulnerability, while sustainable development can restrict it (IPCC, 2007b).

In order to mitigate greenhouse gas (GHG) emissions, measures were taken on an international level in 1992 by establishing the United Nations Framework Convention on Climate Change (UNFCCC). This Convention aims at the “stabilization of greenhouse gas concentrations in the atmosphere at a level that prevents dangerous anthropogenic interference with the climate system”. No mandatory limits on greenhouse gas emissions were set in this treaty in contrast to a later update, the Kyoto Protocol on Climate Change. For the UNFCCC, countries were grouped in Annex I (industrialized countries, agreeing to reduce their emissions to target levels below their 1990 emission levels), Annex II (developed countries which pay for costs of developing countries) and developing countries. The European Union stated in 1996 their view on the UNFCCC as the limitation of the temperature increase below 2°C compared to the pre-industrial level, which requires a stabilization of the greenhouse gases well below 550 ppmv CO<sub>2</sub> equivalent (D’haeseleer, 2007). One year later, the Kyoto Protocol to the UNFCCC was negotiated, whereby industrialized countries agreed to a legally binding reduction in greenhouse gas emissions of 5.2% below 1990 levels in the period 2008-2012. More than 160 countries and other governmental entities have ratified the Protocol. Important exceptions are the United States and Australia.

A series of instruments, each with advantages and disadvantages, are available for governments to stimulate mitigation actions: incorporating the climate policy in the development policy, regulatory measures and introduction of standards, taxes, licences, voluntary agreements, financial stimulations, information campaigns and research (IPCC, 2007c). Governments should also support technological development and innovation. The UNFCCC and the Kyoto Protocol realized a worldwide response to the climate change issue, improvement of a series national policy measures in several countries, development of a

world carbon market and the establishment of new institutional mechanisms that can form the foundation of mitigation efforts in the future (IPCC, 2007c). There are a lot of options to reduce the worldwide emissions of greenhouse gases through coordination on an international level. Potential agreements will receive more support when they are more environmental and cost efficient, taking account of distribution and equity and when they are feasible on institutional level (IPCC, 2007c).

### **1.1.3.2 Mitigation on long term**

Despite UNFCCC and Kyoto Protocol efforts, additional measures to reduce the emission of greenhouse gases are indispensable, certainly on a long term (IPCC, 2007b). The current policy to mitigate the greenhouse gas emissions will still lead to an emission increase during the following decades. In the scenario of an energy program dominated by fossil fuels (covering about 80% of the world primary energy need), a CO<sub>2</sub> emission increase of 45 to 110% compared to 2000 will be observed by 2030 and a total greenhouse gas emission increase of 25 to 90% (IPCC, 2007c). Future emission reductions need to be much stronger and an effort from all countries is required. It is necessary to manage energy demand, enhance energy efficiency, decarbonise our energy provision, and reduce deforestation (IPCC, 2007b). The mitigation efforts in the following 20 to 30 years will be determinative for the level of stabilization and related global warming on a long term (IPCC, 2007c). The intended long-term stabilization is an “overshooting” scenario, whereby the greenhouse gas emissions will peak within two decades, followed by substantial reductions of 30 to 60% (compared to the 2000 level) by 2050. Following the European Parliament, strong emission reductions of 15-30% by 2020 and 60-80% by 2050 compared to the 1990 levels should be undertaken by the developed countries (D’haeseleer, 2007).

Besides changes in behaviour and lifestyle, a series of technologies are currently available to decrease emissions significantly in sectors such as energy production, transport, buildings, industry, agriculture, forest and waste sector (IPCC, 2007c). The contribution of the different technologies can vary in time, region and intended stabilization level and also energy efficiency is important. Serious investments in carbon-poor technologies and technological improvements through research will be higher for lower intended stabilization levels (IPCC, 2007c). A decision on the appropriate stabilization level is accompanied by an iterative risk management process including mitigation and adaptation, taking into account actual and avoided climate change damages, co-benefits, sustainability, equity and attitudes to risk (IPCC, 2007c).

### **1.1.3.3 Sustainable development and climate change mitigation**

The transition to more sustainable development ways can contribute significantly to the mitigation of climate change. The choices of the options for mitigation are of major importance to optimize the synergies and to avoid interferences with other aspects of sustainable development (IPCC, 2007c). Several mitigation actions, such as those taken in the field of energy efficiency and renewable energies can provide advantages with respect to economy and energy safety and reduce the emission of pollution gases. Sustainable development can simultaneously enhance the adaptation and mitigation potential and reduce the vulnerability to climate change. In a lot of cases, synergies can be determined. The reduction options should be chosen and performed so that synergies become optimized and conflicts with other dimensions of sustainable development are avoided (IPCC, 2007c).

## 1.1.4 Belgian policy

### 1.1.4.1 Greenhouse gas emission trends of Belgium

Greenhouse gas (GHG) emissions decreased in Belgium by 1.3% in 2005 compared to the 1990 level (fig. 1-4). While emissions of methane, nitrous oxide and fluorinated gas decreased in the 1990-2005 period, CO<sub>2</sub> emissions increased by 3.6%. High GHG emissions are mainly caused by the transport sector and heating in residential, commercial and institutional sectors, whereas the emissions from the energy and processes of industries, agriculture and waste decreased mainly thanks to advances in energy efficiency and partial substitution of coal by gas (NIR, 2007). Public electricity and heat production is responsible for 20% of the GHG emissions. Electricity in Belgium is generated for 58% by nuclear plants, 38% by classic thermal power plants and 4% by pumping power stations, hydraulic energy and renewable energy (based on data from 2003).

### 1.1.4.2 Mitigation on short term

Under the Kyoto Protocol and the EU Burden Sharing Agreement, Belgium was assigned to reduce its greenhouse gas emissions for the 2008-2012 period by 7.5% compared to the 1990 level. The Belgian federal and regional governments have set specific reduction targets in the National Allocation Plan (NAP), by which Flanders is allowed to emit 83.37 Mt CO<sub>2</sub>, the Walloon region 50.23 Mt and the Brussels region 4.13 Mt from 2008 onwards. This means an emission reduction of 5.2% for Flanders, 7.5% for the Walloon region and an increase of 3.5% for Brussels compared to the 1990 level (NAP, 2004). Since more emission rights have been accorded than what is allowed for Belgium by the Kyoto Protocol, the deficit will be compensated by the federal government by using flexibility mechanisms. The NAP agreement provides that the regions can determine the extent to which and the way in which they use flexibility mechanisms themselves, in order to acquire additional allowances. Joint Implementation and the Clean Development Mechanism constitute possibilities by which countries can invest (after approval by UN services) in clean technologies abroad to reduce GHG emissions (D'haeseleer, 2007).

### 1.1.4.3 Climate policy after 2012

The Belgian climate policy should fit in the European Union policy to obtain a GHG emission reduction of 15 to 30% by 2020 and 60 to 80% by 2050 compared to the 1990 level. Different scenarios to mitigate GHG emissions by 2020 or 2050 were developed and analysed in the study of Federaal Planbureau (2006)

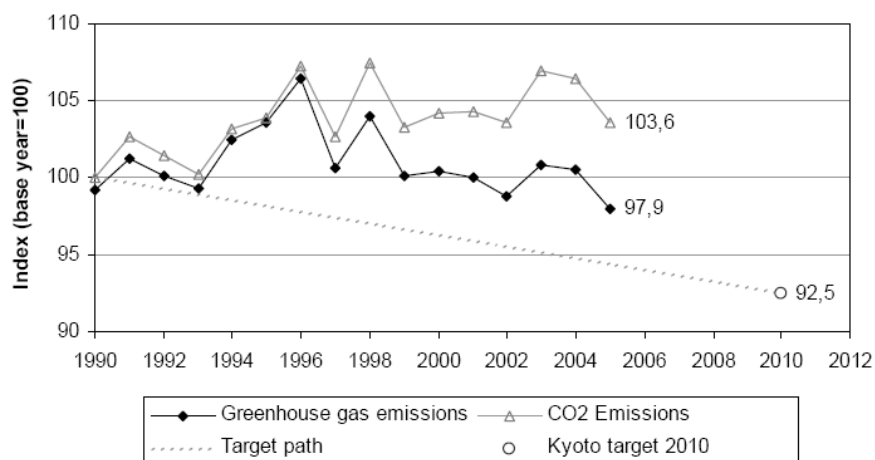


Figure 1-4: (From NIR, 2007) Greenhouse gas and CO<sub>2</sub> emission in Belgium from 1990 to 2005 (excl. LULUCF) compared with the Kyoto target.

For 2020, four scenarios to mitigate GHG emissions were developed and assessed compared to a reference scenario. Two scenarios correspond to reductions of 15 to 30% between 1990 and 2020 for the GHG emissions of the European Union. Two other scenarios study the impact for Belgium of additional measures involving wind energy, energy performance of buildings and transport (Federaal Planbureau, 2006).

To decrease the GHG emissions by 15 and 30% between 1990 and 2020 on the level of Europe-25, carbon values of 42 and 110 euro per ton CO<sub>2</sub>, respectively, would be needed. In Belgium, the reduction of GHG emissions lies between 4.8 and 13.7%, dependent on the scenario. This reduction has an impact on the evolution of the Belgian energy system, which results in a decrease in energy need and a decrease in the use of coal and oil in favour of gas and renewable energy sources for these scenarios. The change of CO<sub>2</sub> emissions of energy origin varies between +3.9% and -4.3% in 2020 compared to the 1990 level and, if additional policy measures are performed, between 13.1% and 19.1% dependent on the scenario.

Realizing the reduction objectives of the GHG emissions also influences the economy, arising from changes on the level of energy costs and through these, on the level of costs and prices of the different sectors. This impact also arises from the changes taken in the European context. In general, the impact of the scenarios on the economic activity, measured through gross domestic product (GDP), is rather neutral (between -0.06% and +0.03% of the GDP in 2020). The increase of the energy prices results in a significant increase of domestic costs and hence, to an inflation and loss of income and competition power. Moreover, the potential export market will show a slight decline, resulting in a decline of the economic activity. The decrease in social burden compensates the first negative consequences and the decrease of domestic demand and of the export is largely compensated by the decrease of import (a.o. import of energy). The impact on the employment will depend largely on the intended redistribution. In general, the original decrease of the activity leads to a loss of employment places, but this is largely compensated by a decrease of the social burden. New jobs are even created when taxes are used to reduce employer contributions. Finally, the different investigated scenarios demonstrate the possibility to increase the foreign balance and enhance the financing balance of the government.

For 2050, three levels (-50, -60 and -80%) to reduce GHG emissions are studied as objectives of the backcasting approach and placed in an evolution of sustainable development between 1990 and 2050 (Federaal Planbureau, 2006).

In the first scenario, an emission reduction of 50% by 2050 is obtained, based on the technological progress with a minimum of behaviour changes, by the maximal use of the existing potential of wind energy, solar energy, carbon capture and storage for the electricity plants, cogeneration, thermal insulation of buildings, transport. The technological progress requires an active policy, that also concerns demand control. In the second scenario, an emission reduction of 60% is obtained by changes in behaviour in addition to technological changes from the first scenario. This scenario includes a.o. the stabilization of the transport demand from now on till 2050, an increase of the average contribution of public transport (from 20 to 50%), the use of microcogeneration and heat pumps in buildings, the use of less energy demanding, long-lasting and more recyclable products. The emission reduction of 80% in 2050 is obtained in the third scenario by amplifying the changes in behaviour from the second scenario. This requires severe changes in the current consumption and production patterns and also a reduction of displacements by 50% between 2004 and 2050 and dominance of public transport.

An efficient world policy on climate changes should not moderate on the reduction of emissions by the international sea and air transport. The backcasting context for a sustainable development, with the objective of the change in consumption and production patterns shows the need of innovation and voluntary policy measures, for technological changes as well as

behavioural changes. The policy measures should be based on multi-actors (policy persons and community actors), multilevels (local decisions linked with decisions on world scale) and multidomains (to encourage the circulation of sectoral policy measures). Taking account of the high ambitions of the objectives, the Federaal Planbureau (2006) emphasizes the importance of the so-called transition policy due to which actions on short and medium term can be linked with actions on long term.

## **1.2 Carbon capture and storage**

Carbon capture and storage (CCS) has the potential to reduce CO<sub>2</sub> emissions on short term. It is an end-of-pipe solution that does not contribute to a decrease of the production of greenhouse gases, but it is very useful as a transition solution on the way towards other energy production mechanisms. CCS gains increasingly more attention internationally.

CCS comprises three steps, namely capture and concentration of CO<sub>2</sub> from emission gases, (often pipeline) transport to storage site and the storage of CO<sub>2</sub> in geological formations. These steps are introduced here only briefly, since the next chapters are dedicated to the elaborated description of the research performed on these technologies.

### **1.2.1 Capture**

In the CO<sub>2</sub> capture process, a concentrated (nearly pure) stream of CO<sub>2</sub> should be produced that is ready for transportation at high pressure to the storage site. There are three main systems to capture CO<sub>2</sub> from a primary fossil fuel (coal, natural gas or oil), biomass, or mixtures of these fuels: post-combustion, pre-combustion and oxy-fuel combustion systems (IPCC, 2005). These systems are schematically presented on figure 1-5. In the post-combustion system, CO<sub>2</sub> is separated from the flue gases, produced by the combustion of the primary fuel in air. Here, a liquid solvent (e.g. monoethanolamine) is used for CO<sub>2</sub> capture from this flue gas, which mainly consists of nitrogen. In the pre-combustion process, the primary fuel reacts with steam and air or oxygen in a first reactor to produce a mixture of mainly carbon monoxide and hydrogen. The carbon monoxide reacts then with steam in a second reactor to produce additional hydrogen, together with CO<sub>2</sub>. This mixture is then separated in a CO<sub>2</sub> stream and a hydrogen stream, which is a carbon-free energy carrier that can be combusted to generate power and/or heat. In the oxy-fuel combustion system, primary fuel is combusted with oxygen instead of air to produce a flue gas that is mainly composed of water vapour and CO<sub>2</sub>. The water vapour is then removed by cooling and compressing. This system requires the upstream separation of oxygen from air, with a purity of 95 to 99%.

Based on the IPCC report published in 2005, post-combustion and pre-combustion systems for power plants can capture 85-95% of the CO<sub>2</sub> processed in the capture plant. Capture and compression require roughly 10-40% more energy than an equivalent plant without capture, depending on the kind of system (IPCC, 2005). Consequently, the power plant with capture produces more CO<sub>2</sub> than the same plant without capture. The net amount of captured CO<sub>2</sub>, called CO<sub>2</sub> avoided, results in approximately 80-90% compared to a plant without capture. Oxy-fuel combustion systems are, in principle, able to capture nearly all produced CO<sub>2</sub>. However, the need for additional gas treatment systems to remove inert phases and pollutants (SO<sub>2</sub> and NO<sub>x</sub>) lowers the level of CO<sub>2</sub> captured to slightly more than 90% (IPCC, 2005).

CO<sub>2</sub> capture cost values range from 15 to 75 US\$, 5 to 55 US\$ and 25 to 115 US\$ per ton CO<sub>2</sub> net captured from a coal- or gas-fired power plant, from hydrogen and ammonia production or gas processing and from other industrial sources, respectively. These values depend on the plant type and size, location, efficiency, fuel type, fuel cost, capacity factor and cost of capital (IPCC, 2005).

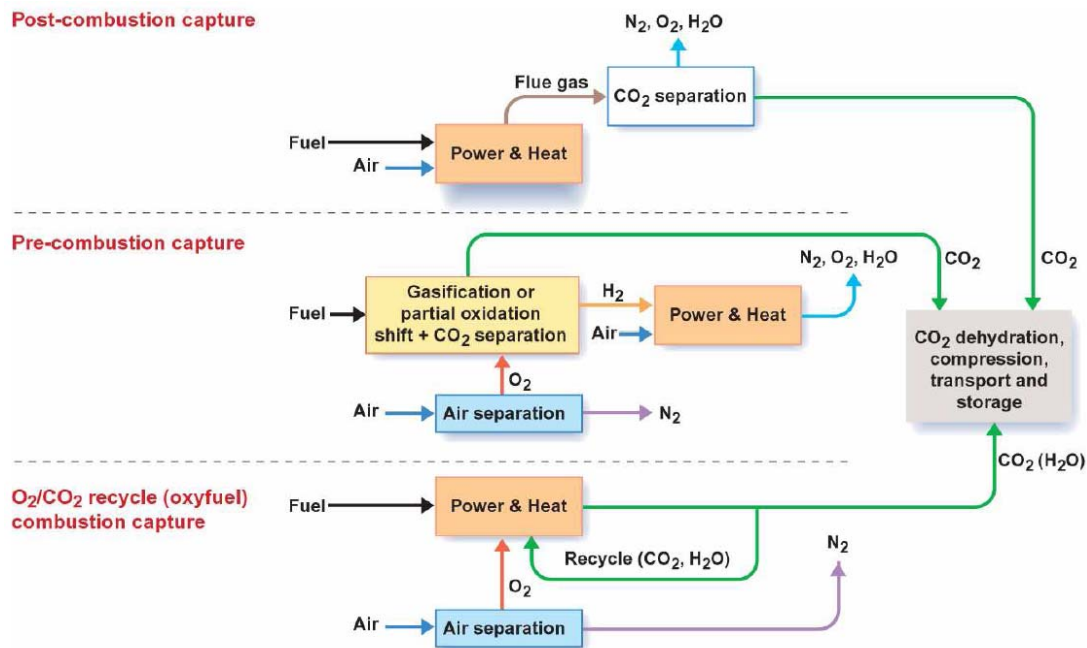


Figure 1-5: (From ZEP, 2006) Overview of CO<sub>2</sub> capture systems.

### 1.2.2 Transport

After CO<sub>2</sub> capture, CO<sub>2</sub> is compressed for transport, commonly through pipelines. The CO<sub>2</sub> pressure should not drop below 7.5 MPa during the complete (pipeline) trajectory in order to avoid two-phase flow and to transport it at a sufficiently high density. For CO<sub>2</sub> capture at power plants, the most energy efficient solution is to integrate the compressor into the power plant and the capture process (ZEP, 2006).

Although capture represents the highest cost and storage is critical with respect to security and long time monitoring, still, it is necessary to identify and structure transportation alternatives in order to analyse and evaluate future paths comprising CCS. Costs for CO<sub>2</sub> transport range from 1 to 8 US\$ per ton CO<sub>2</sub> transported (IPCC, 2005). This cost depends strongly on the distance and the quantity transported (CO<sub>2</sub> mass flow rate) and whether the pipeline is onshore or offshore, on hilly terrain and crosses many large rivers, highways and populated zones. Also, for long distances, additional booster stations may be needed. The pipeline cost also depends on (the fluctuation of) the steel price. CO<sub>2</sub> transportation by ship is commonly cheaper for distances of more than 1000 km (IPCC, 2005; fig. 1-6).

The risk and security issues related to this transportation have also to be investigated. High pressure pipelines for CO<sub>2</sub> transportation over long distances onshore are already used, mainly in the American EOR (Enhanced Oil Recovery) industry (IPCC, 2005). Minimum standards should be established for pipeline quality CO<sub>2</sub> for CCS purpose, which will be slightly different from those for EOR. Pipeline transport of CO<sub>2</sub> through populated areas requires detailed route selection, over-pressure protection, leak detection and other design factors (IPCC, 2005). The water content of the transported CO<sub>2</sub> flow should be very low, since moisture-laden CO<sub>2</sub> is highly corrosive to carbon-manganese steels, commonly used for pipelines. Otherwise, corrosion-resistant alloys or an internal polymer coating would be necessary, increasing the costs significantly. Accidents with current CO<sub>2</sub> pipelines are similar to natural gas pipelines with respect to frequency and its impact would not be more severe (IPCC, 2005).

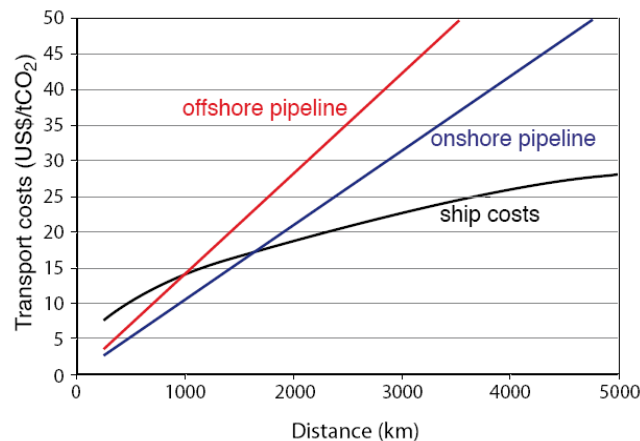


Figure 1-6: (From IPCC, 2005) Transport costs (expressed in US\$ per ton CO<sub>2</sub> transported) for onshore pipelines, offshore pipelines and ship transport, plotted in function of distance (in km). Pipeline costs are given for a mass flow rate of 6 million ton CO<sub>2</sub> per year. Ship costs include intermediate storage facilities, harbour fees, fuel costs, and loading and unloading activities. Costs include also additional costs for liquefaction compared to compression.

### 1.2.3 Storage

Besides geological storage, research is performed on ocean sequestration and onshore sequestration in diverse ecosystems. The storage potential is estimated at 50 to 100 billion ton CO<sub>2</sub> for reforestation and more than 1000 billion ton CO<sub>2</sub> for storage in oceans. These numbers are, however, highly uncertain and also the lack of specific possibilities, insufficient knowledge of biological and ecological consequences and uncertainty on feasibility on short term suggest that these options are not interesting for Belgium.

For geological storage, three types of formations are suitable, depleted oil and gas reservoirs, deep saline aquifers and coal seams and (coal) mines. Geological storage of CO<sub>2</sub> is ongoing in three industrial scale projects (projects in the order of 1 Mt CO<sub>2</sub> per year or more): the Sleipner project in an offshore saline formation in Norway, the Weyburn EOR project in Canada and the In Salah project in a gas field in Algeria. About 3 to 4 Mt CO<sub>2</sub> is annually captured and stored in this way (IPCC, 2005).

CO<sub>2</sub> injection is performed by using many similar technologies that were developed in the oil and gas exploration and production sector (IPCC, 2005). Several technologies, such as well-drilling, injection, computer simulation of storage reservoir dynamics and monitoring methods are optimized for CCS application. Experience from other kinds of geological storage or injection such as natural gas storage, deep injection of liquid wastes and acid gas disposal is an advantage here (IPCC, 2005). For the storage of CO<sub>2</sub> in a liquid or supercritical phase with a density of 50 to 80% of that of water, CO<sub>2</sub> is commonly stored in formations below 800 m depth (IPCC, 2005). Based on the lower CO<sub>2</sub> density compared to water, a sealed cap rock is required on top of the CO<sub>2</sub> storage reservoir. This physical trapping by e.g. a shale or clay layer prevents upward CO<sub>2</sub> migration, but still lateral migration is possible. Additional physical trapping results from capillary forces and also geochemical trapping (CO<sub>2</sub> reaction with the in situ fluids and host rock) is important for long-term entrapment of injected CO<sub>2</sub>. By the dissolution of CO<sub>2</sub> in water, the density of the CO<sub>2</sub>-laden water is higher than the surrounding water and consequently, it will sink in the formation. The dissolved CO<sub>2</sub> can also react with the rock minerals to form solid carbonate minerals. Another type of trapping is the preferential adsorption of CO<sub>2</sub> onto coal or organic-rich shales replacing gases such as methane.

Costs for geological storage in saline formations and depleted oil and gas fields vary from 0.5 to 8 US\$ per ton CO<sub>2</sub> net injected. Additional monitoring and verification costs of the geological storage (covering pre-injection, injection and post-injection monitoring) amount to 0.1 to 0.3 US\$ per ton CO<sub>2</sub> injected (IPCC, 2005).

### 1.3 References

- D'haeseleer W., 2007. Commission ENERGY 2030 Final report. Belgium's Energy Challenges Towards 2030. Commissioned by Minister Marc Verwilghen, Federal Minister of Energy.
- Federaal Planbureau, 2006. Het klimaatbeleid na 2012: Analyse van scenario's voor emissiereductie tegen 2020 en 2050. Federaal Planbureau, Economische analyses en vooruitzichten.
- IPCC, 1995. Second Assessment Report.
- IPCC, 2005. IPCC Special Report on Carbon Dioxide Capture and Storage.
- IPCC, 2007a. Fourth Assessment Report. Climate Change 2007: The physical science basis.
- IPCC, 2007b. Fourth Assessment Report. Climate Change 2007: Impacts, Adaptation and Vulnerability.
- IPCC, 2007c. Fourth Assessment Report. Climate Change 2007: Mitigation of Climate Change.
- NAP, 2004. Belgian National Allocation Plan. Federal government.
- NIR, 2007. Belgium's greenhouse gas inventory (1990-2005). National Inventory Report submitted under the United Nations Framework Convention on Climate Change.
- Van Tongeren P., Laenen B., Weyten H., 2004. Geotechnische en financiële aspecten van ondergrondse CO<sub>2</sub>-opslag in Vlaanderen. VITO report 2004/MAT/R/036
- ZEP, 2006. The final report from Working Group 1 Power Plant and Carbon Dioxide Capture. The European Technology Platform for Zero Emission Fossil Fuel Power Plants (ZEP).



## 2 SOURCE TECHNOLOGY

CO<sub>2</sub> capture will mainly be applied at large point sources such as fossil fuel power plants, fuel processing plants and other industrial plants, particularly for the manufacture of iron, steel, cement and bulk chemicals (IPCC, 2005). As introduced, the three main CO<sub>2</sub> capture technologies include post-combustion, pre-combustion and oxy-fuel combustion systems.

### 2.1 Inventory of CO<sub>2</sub> emission from point sources in Belgium

#### 2.1.1 Introduction

This inventory of large point sources of CO<sub>2</sub> in Belgium contributes to the process of developing a tool that provides for an economic evaluation of carbon capture and storage (CCS). This so-called Policy Support System (PSS) is primarily developed for the Belgian national context.

Ecofys has been asked to provide the project with an updated inventory of Belgian industrial CO<sub>2</sub> sources. The existing database on worldwide CO<sub>2</sub> emissions “IEA GHG CO<sub>2</sub> Emissions Database”, developed by Ecofys in the GESTCO-project (2003), has been used to update Belgian data on CO<sub>2</sub> sources.

The industries investigated are ammonia, cement, ethylene, hydrogen, iron & steel, power, refineries, other chemicals, lime and glass. Essential parameters that will be used as input for the economic calculations in the PSS project are collected for plants in these sectors. Among others these parameters included the size CO<sub>2</sub> streams, concentration CO<sub>2</sub> in the flue gas and location of the plant (geographical coordinates). Other parameters are needed to do calculations on CO<sub>2</sub> volumes, such as capacity, capacity factor, production, emission factors and so on.

#### 2.1.2 Content and structure of the database

##### 2.1.2.1 Information in the database

The data on industrial sources of CO<sub>2</sub> are summarized in a database that can easily be accessed and used in the Policy Support System to identify least cost options for carbon capture and storage. The threshold for CO<sub>2</sub> emissions included in the database has been set to 100 kilo tonne CO<sub>2</sub> per year, because carbon capture and storage is less interesting for small scale installations from an economic perspective. Besides, it requires a substantial effort to also include CO<sub>2</sub> emissions from small scale installations in the database.

The inventory of Belgian CO<sub>2</sub> sources contains information on the name and location of the plant, information on operation and production and on annual emissions of carbon dioxide. These parameters are essential for economic calculations in the PSS project. We continued the structure of the existing IEA GHG CO<sub>2</sub> emissions database, originally developed by Ecofys, for the Belgian emission inventory. Table 2-1 shows the entries (field names) of the records (point sources) in the database. A short description of each entry is given to clarify on the type of information included.

The compiled data on large stationary point sources in Belgium is obtained from several databases with industrial characteristics and from personal communications with representatives of the government and large industries.

Table 2-1: Structure of the CO<sub>2</sub> source database.

#	Field name	Description of field content	Remarks
1	Unit ID	Individual plant identification number	
2	Sector	Industrial sector	
3	Name of company	-	
4	Plant name	-	
5	Unit name	Unit names are assigned if more than one installation is operating on one production site	Units are only distinguished for the power sector (separate power production units) and for the iron & steel sector: to characterize part of the process. No distinction in units has been made for the other sectors.
6	City	-	
7	Country (NIMA)	-	Belgium for all entries
8	Latitude	Latitude coordinate of the production facility	The web based tool Maporama is used to find latitude and longitude coordinates on street level ( <a href="http://world.maporama.com/idl/maporama/">http://world.maporama.com/idl/maporama/</a> )
9	Longitude	Longitudinal coordinate of the production facility	
10	Status	Actual operational status of the plant	Five types of operational status have been included in the database: CON = under construction; OPR = operational; PLN = planned STN = shut down; RET = retired
11	Start-up Year	First year of operation	
12	Shut-down year	Last year of operation	
13	CO <sub>2</sub> reported (kt)	Emission reported by company or national environmental agency	The aim of including reported CO <sub>2</sub> emissions in the Belgian database is to compare them with calculated CO <sub>2</sub> emissions. Reported CO <sub>2</sub> emissions stem from: - EPER - EU-ETS - Walloon database - other publications (e.g. internet and annual reports)
14	CO <sub>2</sub> estimated (kt)	CO <sub>2</sub> emissions estimated with emission factor	CO <sub>2</sub> emissions are calculated on basis of the plants' technology, type of fuel, production (or operational time and capacity).
15	Concentration of CO <sub>2</sub> in flue gas (%)	Estimated concentration of CO <sub>2</sub> in the flue gas	Estimated on basis of type of industry, technology and fuel type used.
16	Product mix	Indication of the products of the plant	
17	Production	Annual production	
18	Unit of production	-	
19	Full load hours (h)	Full load hours or annual capacity	Capacity utilization
20	Capacity	Reported production capacity of the plant	
21	Unit of capacity	-	
22	Emission factor (kg CO <sub>2</sub> /tonne product)	CO <sub>2</sub> production per unit of production	
23	Technology	Indication of technologies used in the plant	For production processes where CO <sub>2</sub> emissions depend on both fuel and technology this entry is completed. For production process where CO <sub>2</sub> emissions are calculated on basis of the type of fuel only, this entry is left blank.
	Main fuel	More detailed description of fuel	
24	Fuel class	Categorization of fuels	All types of fuel in the entry "main fuel" are categorized under four main types of fuels being: coal, gas, oil, biomass/waste or unknown.
26	Reported emission - Information source	CO <sub>2</sub> emissions per facility as reported	
27	Reported emission - Year of report		
28	Last updated (year)	Last date that entry has been updated	
29	Information source other		
30	Reported start-up year		
31	Reported shut-down year		
32	Comments		

*a) IEA GHG CO<sub>2</sub> Emissions Database*

The IEA GHG CO<sub>2</sub> emissions database contains database entries on CO<sub>2</sub> point sources that are needed for the economic calculations in the PSS project. The information on Belgium point sources in the IEA GHG CO<sub>2</sub> Emissions Database is checked, completed, updated and revised by comparing the data to several other databases which are described below. Furthermore, information is collected by means of internet research and direct contacts with Belgian trade associations representing the various industries.

Ecofys has compiled the database as a pre-study for the IEA GHG R&D Programme's work on cost and potentials for reducing carbon dioxide emissions from fossil fuel use (IEA, 2002). The database structure and underlying formulas to calculate estimated CO<sub>2</sub> emissions are used in the Belgian emission inventory. The most recent update of the database by the IEA has been released in October 2006.<sup>1</sup> From this database, we extract the information on Belgium point sources of carbon dioxide<sup>2</sup>.

*b) European Pollution Emission Register (EPER)*

The EPER database is a European wide database containing industrial emissions to air and water. Currently, annual emissions from two reporting years (2001 and 2004) are available online. All EPER data are non confidential.

The first reporting year (2001) includes emissions from 9,000 industrial facilities in 15 EU member states as well as Norway and Hungary. About 42% of the EU's total carbon dioxide emissions in that year are covered. The second edition of the database has been launched end of 2006 and reports on annual emissions in the year 2004 for all 25 EU member states and Norway<sup>3</sup>. EPER covers all medium and large sized industrial point sources. The reporting threshold for CO<sub>2</sub> releases to air is 100 ktonne per year. Data is available on plant level and not on unit level. From this database we derive following data for updating the Belgium emission inventory: reported CO<sub>2</sub> emissions per facility and geographical coordinates of the facilities.

*c) World Electric Power Plant (WEPP) database*

The WEPP database is a global inventory of electricity generating units (Platts 2006). It contains design data and production figures for power plants of all sizes and technologies operated by regulated utilities, private power companies, and industrial or commercial auto producers. One important difference with the IEA GHG CO<sub>2</sub> emissions database is that database records are given on unit level instead of plant level. The WEPP database does not report on CO<sub>2</sub> emissions. From this database design parameters of power units are derived.

*d) Flemish CO<sub>2</sub> emissions*

The Flemish Institute for Technical Research (VITO) supplied a database to the project covering the CO<sub>2</sub> emissions of all Flemish CO<sub>2</sub> sources. The CO<sub>2</sub> emissions are calculated on basis of actual fuel consumption in the year 2000. The database is confidential since reported CO<sub>2</sub> emissions are linked to the companies emitting the CO<sub>2</sub>. Therefore, we used the reported CO<sub>2</sub> emissions only to check and compare information from other information sources. The combination of company name with CO<sub>2</sub> emissions will not be used as such in the new database. On installation level there are 67 installations that emit over 100 kton. Together these installations emitted 30.5 Mton CO<sub>2</sub> in 2000.

---

<sup>1</sup> See: [www.CO2captureandstorage.info/CO2emissiondatabase/database](http://www.CO2captureandstorage.info/CO2emissiondatabase/database)

<sup>2</sup> Report PH4/9 *Building the Cost Curves for CO<sub>2</sub> Storage: Part 1: Sources of CO<sub>2</sub>*

<sup>3</sup> See: [www.eper.cec.eu.int](http://www.eper.cec.eu.int)

In practice, it turned out that the names of the individual installations often do not correspond to the names of installations in other databases. Therefore, for only a limited number of installations it was possible to compare CO<sub>2</sub> emissions.

*e) Walloon CO<sub>2</sub> emissions database*

The Ministry of the Walloon Region supplied the project team with data on Walloon combustion installations. The database has been set up within the framework of the European Emissions Trading System (EU-ETS). Both verified emissions in 2005 and average emissions over the period 2000-2005 are covered. Included are installed capacities for combustion installations and production capacities for production plants in the steel sector. Carbon dioxide emissions are reported only for plants that fall under the ETS regime. This implies that among others process CO<sub>2</sub> emissions of industries in the chemical sector are not recorded. Data supplied by the Ministry are confidential. It is agreed that the data can be used without restriction in this project, but the resulting database is confidential and can not be distributed outside the project.

**2.1.2.2 Method to calculate CO<sub>2</sub> emissions**

The approach that is followed to obtain an up to date CO<sub>2</sub> emission inventory for Belgian CO<sub>2</sub> sources is based on the use of the structure and underlying formulas of the IEA GHG CO<sub>2</sub> emissions database. Belgian entries available in the IEA GHG CO<sub>2</sub> emissions database are copied to a separate Excel file to revise and update these figures.

*a) Method to calculate CO<sub>2</sub> emissions*

The key task of this study is to calculate CO<sub>2</sub> emissions for all entries in the Belgian database. Figure 2-1 shows a schematic presentation of the approach to calculate CO<sub>2</sub> emissions. The blue marked text boxes represent data that need to be collected; these data are used to estimate and calculate figures represented by white and orange text boxes.

The IEA GHG CO<sub>2</sub> emissions database calculates CO<sub>2</sub> emissions on basis of CO<sub>2</sub> emission factors and production information. The CO<sub>2</sub> emission factor depends on the type of fuel used in the process and the energy intensity of the process. Higher energy intensities actually result in a higher emission factor per unit product. If data are available, the CO<sub>2</sub> emission factor will be made dependent on technology type. For several sectors the calculation of CO<sub>2</sub> emissions follows a somewhat simpler method, because of insufficient data availability. In the glass sector for example, one generic CO<sub>2</sub> emission factor is used to calculate emissions without any further split up to technology type or fuel used.

*b) Step by step approach*

Following steps are undertaken in the process of supplying the project with an up to date CO<sub>2</sub> emission inventory for Belgium:

*1. Apply database structure of IEA GHG CO<sub>2</sub> emissions database to Belgian database*

The IEA GHG CO<sub>2</sub> emissions database covers following industrial sectors: power sector, chemical sector (ammonia, ethylene, and ethylene oxide), refineries, iron and steel plants, cement plants and natural gas processing facilities. Next to these sectors, the sectors lime and glass are added to the Belgian database.

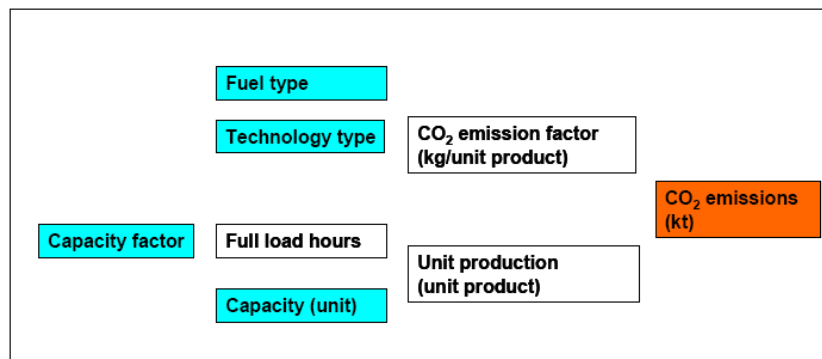


Figure 2-1: Schematic overview of the approach to calculate CO<sub>2</sub> emissions.

Another structural change compared to the IEA GHG CO<sub>2</sub> emissions database concerns the power sector. Whereas the original IEA GHG CO<sub>2</sub> emissions database presents data on plant level, we decided to include data on unit level for the Belgian inventory (available from the WEPP database). For the purpose of doing economic calculations on the possibilities of carbon capture unit level information is more useful than plant level information. Plant level CO<sub>2</sub> emissions are treated as one CO<sub>2</sub> volume whereas the CO<sub>2</sub> could come from different power units located at one site. As a consequence, presenting CO<sub>2</sub> emissions on plant level might lead to wrong conclusions on the type, size and costs of the capture technology to be applied and the possible need for a collection system for the CO<sub>2</sub> captured at different units at the site.

#### 2. Update the number of installations.

Following databases are used to update the information included in the IEA GHG CO<sub>2</sub> emissions database:

- European Pollution Emission Register (EPER)
- World Electric Power Plant (WEPP) database
- Database on Flemish CO<sub>2</sub> emissions (obtained from VITO)
- National Allocation Plan for Walloon CO<sub>2</sub> emitters

See section 2.1.2.1 for a more detailed description of the content of these databases.

#### 3. Collect published CO<sub>2</sub> emissions figures for each installation.

For verification reasons much effort has been given to collect published CO<sub>2</sub> emissions for each database entry. Estimated CO<sub>2</sub> emissions (spreadsheet column “CO<sub>2</sub> estimated (kt)”) are compared to published CO<sub>2</sub> emission figures for the same installation (see spreadsheet column “CO<sub>2</sub> reported (kt)”). One must be careful that estimated CO<sub>2</sub> emissions are calculated on basis of design parameters whilst published CO<sub>2</sub> emissions could be either based on annual production figures or also design parameters. Annual production figures could be very distinct from design parameters. In step 6 the estimated CO<sub>2</sub> emissions will be compared to published figures.

#### 4. Check whether other database entries than CO<sub>2</sub> emissions need updating and incorporate these changes.

The first version of the IEA GHG CO<sub>2</sub> emissions database has been created in the year 2002 and since then updates have been incorporated. For Belgium, estimated CO<sub>2</sub> emissions have last been updated in 2005, but no other changes have been made (e.g. added production capacity, company name).

*5. Attribute geographical coordinates to each plant.*

For the calculation of least cost carbon capture and storage options it is very important to assess the characteristics of the trajectory from source to storage site. Therefore the geographical coordinates (latitude and longitude) of CO<sub>2</sub> point source need to be available in the database. Most latitude and longitude coordinates are available from the EPER database, if not, they are calculated using the web based feature Maporama.<sup>4</sup>

*6. Compare reported CO<sub>2</sub> emissions to estimated CO<sub>2</sub> emissions.*

The published CO<sub>2</sub> emissions per database entry, as collected in step 3, are compared to estimated CO<sub>2</sub> emissions. We included this check of CO<sub>2</sub> emissions in the approach because for the purpose of the project it is very important to supply the project with correct CO<sub>2</sub> emission figures. Where there is a large difference between estimated and reported CO<sub>2</sub> emissions, applied formulas are checked.

### 2.1.3 Sectors

This section gives information per sector on the types of technology covered, data availability and the method to calculate CO<sub>2</sub> emissions. The aim of the section “data availability” is twofold. First, it points out which sources are used for published CO<sub>2</sub> emission figures and secondly reports on the data that are still missing.

#### **2.1.3.1 Ammonia sector**

##### *a) Technology*

In Europe, two main types of production processes for ammonia synthesis gas are currently in operation 1) steam reforming of natural gas or other light hydrocarbons and 2) partial oxidation of heavy fuel oil or vacuum residue. About 85% of world ammonia production is based on steam reforming concepts (European Fertilizers Manufacturers’ Association, 2000). Most plants use natural gas (methane) as feedstock for ammonia production. In Belgium, only steam methane reforming technology is applied.

In ammonia production processes two separate CO<sub>2</sub> streams can be identified:

- the flue gas stream from the burners (combustion process) and
- the pure CO<sub>2</sub> stream that is output from the reforming process.

The concentration of CO<sub>2</sub> in the flue gas is typically around 8% when natural gas is used as fuel. The CO<sub>2</sub> emissions from the primary reforming process (combustion) where natural gas is burned to supply heat to the process are about 500 kg per tonne ammonia produced. CO<sub>2</sub> emissions formed during the primary and secondary reforming processes are about 1200 kg per tonne ammonia (see fig. 2-2). The percentage of process CO<sub>2</sub> emissions in the total of CO<sub>2</sub> emissions of the ammonia production process amounts to 71%. The pure CO<sub>2</sub> stream is either vented to the atmosphere or used in other products, mainly for the production of urea.

Process CO<sub>2</sub> from the shift conversion is often used in the production of urea. The urea is formed by dehydrating the ammonium carbamate. Carbamate is produced by a reaction of CO<sub>2</sub> with ammonia. The amount of CO<sub>2</sub> that is used for this process is not vented to the atmosphere and is therefore not available for CO<sub>2</sub> storage.

##### *b) Data availability*

Reported CO<sub>2</sub> emissions are derived from the EPER database, which reports one CO<sub>2</sub> emission figure for both process and combustion processes. On basis of the CO<sub>2</sub> emission figures of the ammonia process as depicted in figure 2-2, we allocate 71% of the CO<sub>2</sub> emissions as reported by EPER to the process and 29% to the combustion part of ammonia production. Ammonia plants often produce other products in the same plant such as fertilizers

---

<sup>4</sup> Accessible via <http://world.maporama.com/idl/maporama/>

and nitric acid. The CO<sub>2</sub> emissions corresponding to these production processes are not included in the CO<sub>2</sub> emission calculations of the ammonia plants. The IEA GHG CO<sub>2</sub> emissions database nor other sources report urea manufacturing in Belgian ammonia plants.

c) Calculation of CO<sub>2</sub> emissions

Looking at the possibilities for carbon capture process CO<sub>2</sub> emissions and combustion CO<sub>2</sub> emissions are separately treated in this study. The cost-effectiveness of capturing pure streams of CO<sub>2</sub> must be reflected. For each ammonia production plant two entries are included for separately including process and combustion emissions of CO<sub>2</sub>.

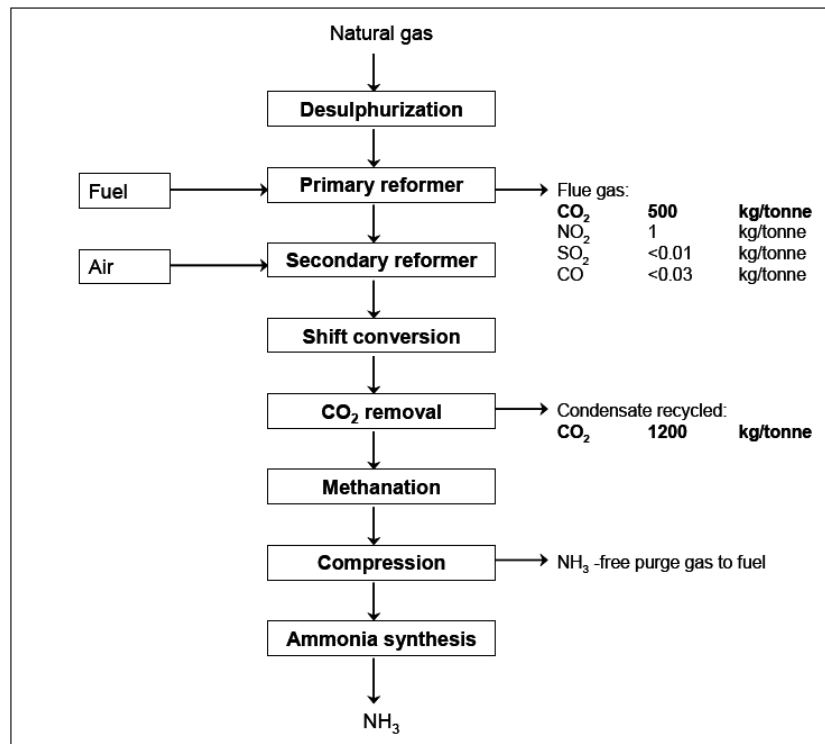


Figure 2-2: (From [www.efma.org](http://www.efma.org)) Typical emission levels in natural gas based steam reforming.

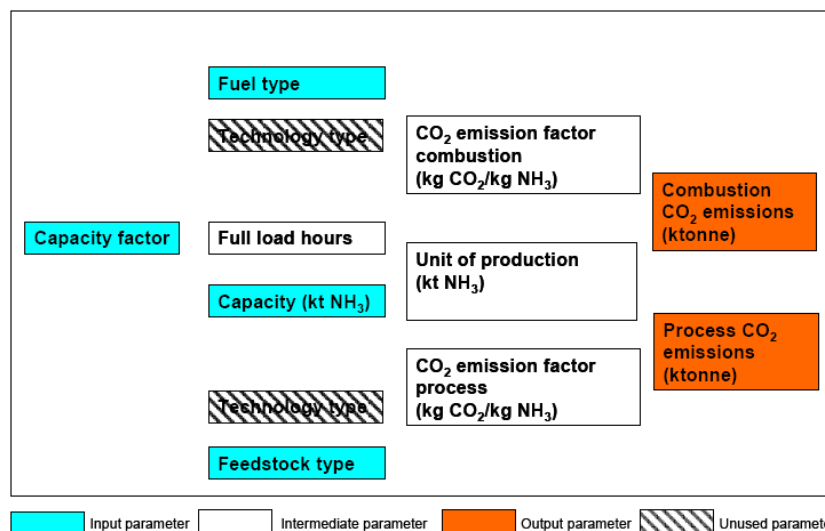


Figure 2-3: Schematic presentation of CO<sub>2</sub> emission calculation for ammonia plants.

The process and combustion CO<sub>2</sub> emissions for ammonia plants are calculated according to the schematic presentation in figure 2-3. The blue highlighted text boxes show what input parameters to the calculations of CO<sub>2</sub> emissions. White text boxes give the parameters calculated on basis of input parameters and the orange boxes are output parameters.

The capacity factor for ammonia plants is estimated at 92% (8000 hours at full load). Both CO<sub>2</sub> emission factors depend on the type of fuel used.

In case of urea production the CO<sub>2</sub> emissions are corrected for the use of CO<sub>2</sub> from this purpose. For the CO<sub>2</sub> used in urea plants we use a factor of 1400 kg/tonne urea.

### **2.1.3.2 Cement sector**

#### *a) Technology*

Cement manufacturing processes are classified according to the type of rotary kiln used for the clinker burning process. Four main process routes for manufacturing cement are distinguished; dry, semi-dry, semi-wet and wet processes. The first rotary kilns were of the wet type. New plants often use dry process kiln types because of a better fuel economy (see table 2-2 for comparison). Sometimes, wet processes are converted to dry process because of this improved fuel economy.

Two separate CO<sub>2</sub> streams result from cement production processes:

- Carbon dioxide produced during first step in cement manufacture: calcination of calcium carbonate (limestone) to lime
- Carbon dioxide in the flue gas from the combustion process.

Carbon dioxide emissions from the calcination of limestone and from the combustion of fuel are found in the exit gases from the kiln. The main source of carbon dioxide is the clinker production process. Clinker is the intermediate product from which cement is made. Process CO<sub>2</sub> emissions emitted during the clinker process are about 500 kg/tonne clinker.

Emissions from combustion during the cement making processes occur due to fuel use for the clinker burning process (pyroprocessing): fuel is burned in the rotary kiln and raw meal flows counter-current to a stream of hot gas. The amount of carbon dioxide emitted during this process is influenced by the technology applied and the type of fuel used; mostly coal and natural gas, but also fuel oil, petroleum, coke and alternative fuels. On average about 55 to 60% of the direct CO<sub>2</sub> emissions stem from process emissions and 40 to 45% from fuel combustion. The concentration of CO<sub>2</sub> in the flue gas is relative high and generally between 20 and 30%, depending on fuel type and technology applied (IEA R&D, 1999).

#### *b) Data availability*

In the IEA GHG CO<sub>2</sub> emissions database following clinker manufacturing technologies have been classified: dry preheating, semi-dry, wet, semi-wet and dry pre-calcinating.

Information on Belgium cement companies is derived from the World Directory on Cement published by the European Cembureau (in short WCD). The latest edition available (1996) gives information on more than 2100 cement plants worldwide. The database includes (amongst other) information on company name and location, clinker capacity, technologies applied, initial year of operation and type of fuel. The data on Belgium plants is not complete. For most plants information on the type of technology used, fuels used, number of kilns is missing.

#### *c) Calculation of CO<sub>2</sub> emissions*

For cement plants one CO<sub>2</sub> emission figure is calculated including both process and combustion CO<sub>2</sub> emissions from cement manufacturing. The CO<sub>2</sub> emissions that are formed directly from the combustion process are fuel and technology related as can be seen in figure 2-4. The CO<sub>2</sub> emission factor for the clinker process is set to a fixed figure of 450 kg/tonne clinker.

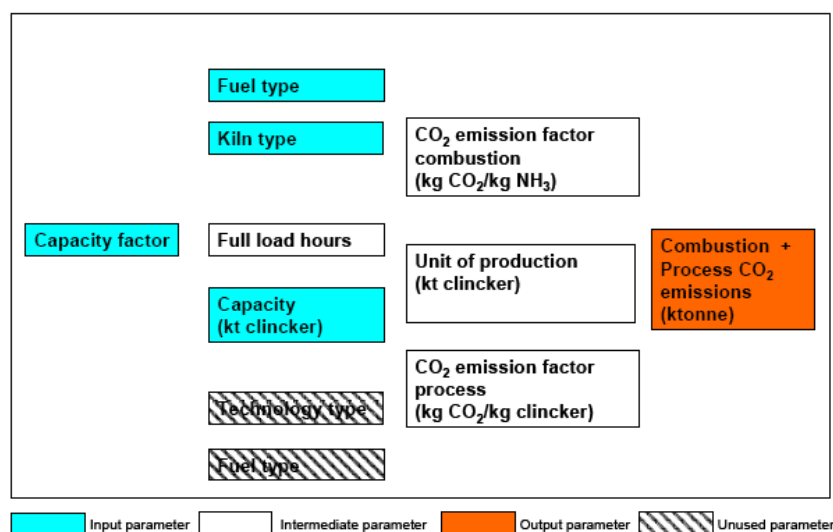


Figure 2-4: Schematic presentation of CO<sub>2</sub> emission calculation for cement plants.

Table 2-2: Specific energy consumption for clinker production per technology and emission factor per fuel type.

<b>Technology</b>	<b>GJ/t</b>
<i>Dry process</i>	3.6
<i>Dry process with precalcination</i>	3.3
<i>Semi-dry process</i>	4.0
<i>Semi-wet process</i>	4.8
<i>Wet process</i>	5.9
<i>Other and not-defined processes</i>	4.0

<b>Emission factor</b>	<b>kg/GJ</b>
<i>Emission factor coal</i>	104
<i>Emission factor fuel oil</i>	76
<i>Emission factor gas</i>	56
<i>Emission factor pet coke</i>	76
<i>Emission factor hv fuel oil</i>	86
<i>Emission factor other fuel</i>	86

Table 2-2 gives an overview of the specific energy consumption for clinker production per technology and the emission factors per fuel used in the calculations.

Although it is known that some cement kilns also burn biomass, the available information sources do not report the use of biomass in Belgian cement plants. Therefore the use of biomass is not taken into account.

### 2.1.3.3 Ethylene

#### a) Technology

The bulk of industrial ethylene is produced in crackers requiring high levels of energy. Carbon dioxide is formed during the combustion of gas oil and/or naphtha. The concentration of CO<sub>2</sub> in the flue gas is about 10-15%. A small fraction of the emission is a pure stream of

CO<sub>2</sub> (>99%). In Western-Europe the fuels used for ethylene production are mainly naphtha (80%) and gas oils (16%). The remainder (4%) are LNG including refinery gas.

#### b) Data availability

Data on ethylene production are already incorporated in the IEA CO<sub>2</sub> emissions database. Reported CO<sub>2</sub> emissions, if they are available, are derived from the EPER database (2001 and 2004 figures). Past years the Belgium ethylene plants have undergone expansion of the production capacity. The production capacity of Fina Antwerp Olefins increased from 1.2 Mt ethylene per year to 1.4 Mt ethylene per year in 2002 (ICIS, 2002).

#### c) Calculation of CO<sub>2</sub> emissions

For ethylene production no specific technology has been identified. The CO<sub>2</sub> emission factor is based on the type of fuel used and energy intensity of the product (fig. 2-5). It is assumed that only naphtha and gas oils are used in Belgium. On a national scale the specific energy consumption is known: for Belgium it is 34.9 GJ/tonne ethylene. The CO<sub>2</sub> emission factor is found by multiplying the specific energy consumption for ethylene production with the CO<sub>2</sub> emission factor of naphtha and gas oil (72.6 tonne CO<sub>2</sub> per GJ) (AEA Technology, 1999). The capacity factor is set to 90%.

### 2.1.3.4 Ethylene oxide

#### a) Technology

Ethylene oxide is formed by reacting gaseous ethylene and oxygen over a solid catalyst. The main by-products are carbon dioxide and water. The CO<sub>2</sub> in the product gas is very pure, almost 100%. The ratio between the two reactions (i.e. formation of ethylene oxide on the one hand and formation of CO<sub>2</sub> and H<sub>2</sub>O on the other hand) is mainly determined by the catalyst used. CO<sub>2</sub> is removed and either vented or used.

#### b) Data availability

Data on ethylene oxide production are already incorporated in the IEA CO<sub>2</sub> emissions database. Reported CO<sub>2</sub> emissions, if they are available, are derived from the EPER database (2001 and 2004 figures).

#### c) Calculation of CO<sub>2</sub> emissions

Carbon dioxide emissions are calculated on basis of a fixed CO<sub>2</sub> emission factor for ethylene processes (460 kg CO<sub>2</sub>/tonne ethylene oxide). On basis of annual ethylene oxide production the CO<sub>2</sub> emissions are calculated (fig. 2-6). A capacity factor of 80% was assumed.

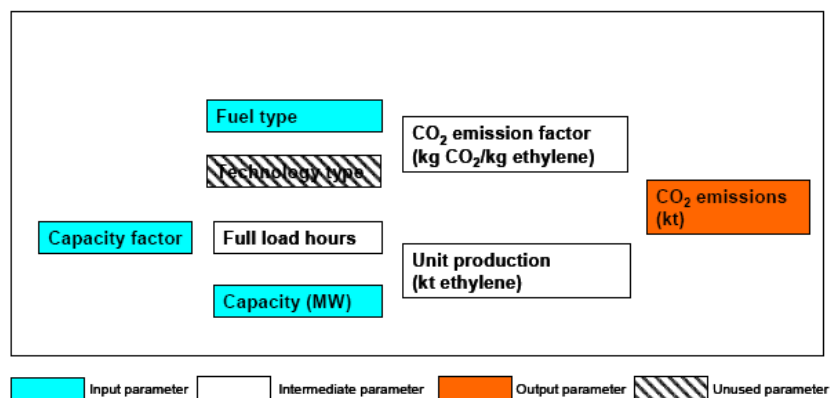


Figure 2-5: Schematic presentation of CO<sub>2</sub> emission calculation for ethylene plants.

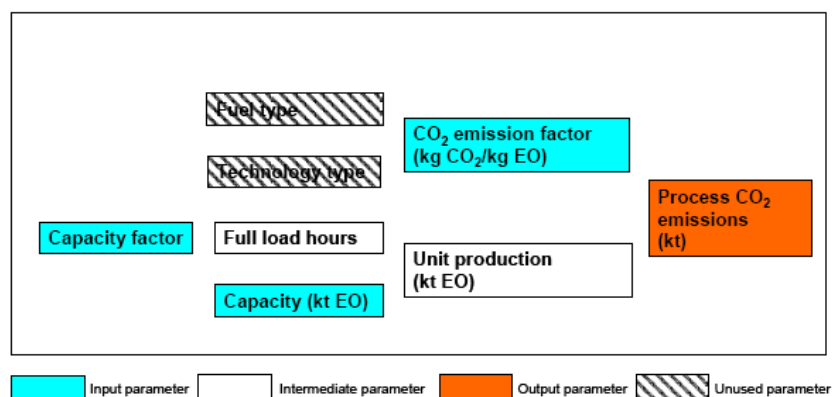


Figure 2-6: Schematic presentation of CO<sub>2</sub> emission calculation for ethylene oxide (EO) plants.

### 2.1.3.5 Glass

#### a) Technology

Glass manufacturing is a high-temperature, energy-intensive activity. Carbon dioxide emissions result from the combustion of fuels (fuel emissions) and from the decarbonisation of raw materials (process emissions). The glass sector knows various sub sectors such as container glass, flat glass, continuous filament glass fibre, domestic glass and special glass. These processes all have very typical CO<sub>2</sub> emissions, which can vary significantly between the processes.

The production of 1 tonne of glass in a gas-fired furnace generates approximately 600 kg CO<sub>2</sub>, of which 450 kg arises from fossil fuels combustion and 150 kg from the dissociation of carbonate raw material (CaCO<sub>2</sub> and dolomite) in the batch (World Bank Group, 2007).

#### b) Data availability

There is not much information on the percentage of CO<sub>2</sub> in the flue gases from glass manufacturing processes. Carbon dioxide in the flue gas stems from the combustion of the fuel and from the limestone used in the process. In Matveev et al. (1991) the concentration of CO<sub>2</sub> in the flue gas is reported at 10%. We use this figure in our calculations.

#### c) Calculation of CO<sub>2</sub> emissions

Carbon dioxide emissions from glass production processes are directly linked with the type of glass produced, the type of fuels used, process energy efficiency and the use of cullet. The production processes for specific glass types give rise to very different levels of carbon dioxide emissions. In this study we estimate CO<sub>2</sub> emissions on basis of average CO<sub>2</sub> emissions for glass production without further specification per type of glass product. Figure 2-7 shows the approach to calculated CO<sub>2</sub> emissions for glass manufacturing processes. Process and combustion CO<sub>2</sub> emissions are summed up.

The average specific energy consumption for the European glass industry is set at 7.50 GJ per tonne of glass (for the year 2000)<sup>5</sup>. The specific CO<sub>2</sub> emissions (process and combustion) for the European glass industry are estimated at 600 kg CO<sub>2</sub> per tonne of glass (for the year 2000). The annual capacity factor for glass manufacturing plants is estimated at 90% (8000 full load hours).

<sup>5</sup> CPIV <http://www.cпивglass.be>

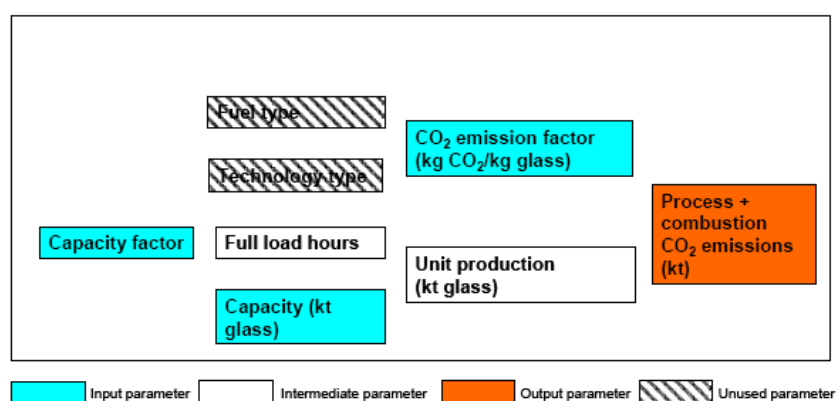


Figure 2-7: Schematic presentation of CO<sub>2</sub> emission calculation for glass manufacturing plants.

### 2.1.3.6 Hydrogen

#### a) Technology

Currently, the most dominant hydrogen production technology is steam methane reforming (SMR) of natural gas. Worldwide, about 95% of the total hydrogen production is produced by means of the reforming of natural gas. For lighter hydrocarbons, e.g. natural gas and naphtha, steam reforming is the most widely used technology. For heavier hydrocarbons, for example heavy oil, partial oxidation technology is more suited.

In the IEA GHG CO<sub>2</sub> emissions database hydrogen production technology is categorized following technology groups:

- cryogenic
- membrane
- PSA
- partial oxidation
- steam reforming
- steam naphtha reforming
- residue gasification

#### b) Data technology

Capacity figures of the only hydrogen production plant in Belgium were already incorporated in the IEA GHG CO<sub>2</sub> database. The reported CO<sub>2</sub> emissions (for comparison) are derived from the VITO database covering CO<sub>2</sub> emissions in the Flanders region in 2000.

Table 2-3: Emission factors and CO<sub>2</sub> concentration for different hydrogen production technologies.

<i>Technology</i>	<i>Emission factor (kg CO<sub>2</sub>/kg H<sub>2</sub>)</i>	<i>Concentration</i>	<i>Technology class</i>
<i>Cryogenic</i>	4.0	100%	Pure source
<i>Membrane</i>	4.0	100%	Pure source
<i>Partial oxidation</i>	8.3	100%	Pure source
<i>Steam methane reforming</i>	4.0	100%	Pure source
<i>Steam naphtha reforming</i>	5.2	100%	Pure source
<i>Residues</i>	20.0	100%	Pure source
<i>PSA</i>	4.0	11%	Flue gas
<i>Other</i>	4.0	11%	Unknown

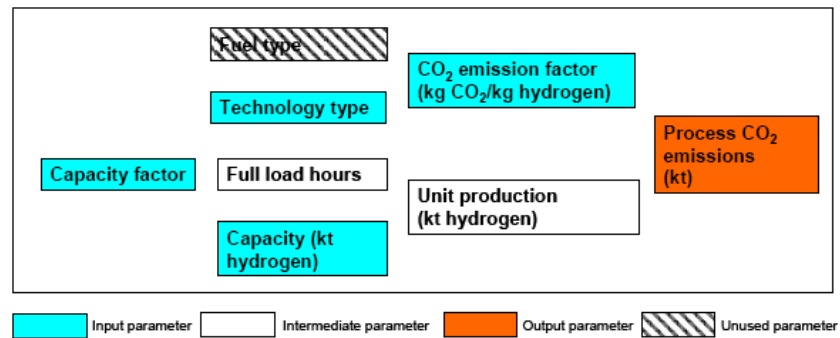


Figure 2-8: Schematic presentation of CO<sub>2</sub> emission calculation for hydrogen plants.

### c) Calculation of CO<sub>2</sub> emissions

For each of the above defined processes for the production of hydrogen emission factors are given in the IEA GHG CO<sub>2</sub> Emissions Database. The CO<sub>2</sub> emission factors depend on the technology used for hydrogen production (see table 2-3). Figure 2-8 presents the approach followed in calculating CO<sub>2</sub> emissions for hydrogen production facilities.

## 2.1.3.7 Iron and Steel sector

### a) Technology

Two principal types of steelmaking technology in use today are the primary integrated steel mills and the scrap based minimills (De Beer et al., 2003). All Belgian iron and steel plants are characterized either as ‘integrated plant’ or ‘mini-mill’. The production process of integrated steel mills is split up in different process steps, which are derived from De Beer et al. (2003):

- coke oven (treatment of ore and raw materials)
- sintering plant (sintering, ore handling, screening scrap)
- furnaces (iron making)
- oxygen furnace (steel making)
- rolling mills (rolling and finishing)

### b) Data availability

In the IEA GHG CO<sub>2</sub> emissions database iron and steel plants are characterized as integrated plant, minimill, mini-integrated plant. In Belgium, the different processes that make up an integrated steel plant are not per definition located on one site. From the perspective of carbon capture and storage opportunities it is therefore useful to keep the processes apart. Therefore, the integrated plants are split up in separate processes:

- coke oven
- sintering
- blast furnace
- basic oxygen furnace
- continuous casting
- rolling mills

The database with Walloon combustion installations and CO<sub>2</sub> emissions reports on process level for the iron and steel sector and give production capacities of stage products.

The IEA GHG CO<sub>2</sub> emissions database assumes 15% CO<sub>2</sub> (by volume) in the flue gas for integrated steel plants producing flat & long products. For other steel production processes and other steel products no CO<sub>2</sub> concentrations have been defined.

Since we use a division in process steps we cannot use the overall CO<sub>2</sub> concentration of 15% in the Belgian database. It proved that data on CO<sub>2</sub> concentrations for each process step are scarce. Only for the process step of steel production in an oxygen steel work data could be found. The off-gas from an oxygen-steel furnace typically contains 16% CO<sub>2</sub> and 70% carbon monoxide (IPCC, 2005). The drawback of calculating CO<sub>2</sub> emissions on process level (instead of plant level) is that for some process steps concentrations of CO<sub>2</sub> in the flue gas are missing.

*c) Calculation of CO<sub>2</sub> emissions*

For integrated steelworks the process steps of iron making and steel making were considered (figure 2-9). Treatment of ore and raw materials were not considered. CO<sub>2</sub> emissions stem from the blast furnace, having an emission factor of 1140-1400 kg CO<sub>2</sub>/tonne steel (mean value: 1270 kg CO<sub>2</sub>/tonne steel). If all processes that make up the integrated steel plant are located at one site the emission factor as used in the IEA GHG CO<sub>2</sub> emissions database is used: 1.27 kg CO<sub>2</sub>/kg steel. However, if this is not the case, CO<sub>2</sub> emissions are calculated on basis of the CO<sub>2</sub>-emissions per tonne *stage product*. In table 2-4 the process steps with intermediate products and corresponding CO<sub>2</sub>-emissions are given. In rolling and finishing operations different steel products are formed.

For EAF a specific energy consumption of 4551 MJ per tonne of liquid steel was assumed, of which 89% is electricity and 11% is fossil fuel (coal, coke, carbon in iron) (IISI, 1998). Further it was assumed that electricity was provided by the electricity grid thus resulting in zero emission at the steel site. Using an emission factor of 0.28 kg CO<sub>2</sub>/MJ for fossil fuel combustion, results in a steel making emission factor of 140 kg CO<sub>2</sub>/tonne steel.

Table 2-4: CO<sub>2</sub> emissions of integrated steel plants per process step (De Beer et al. 2003).

<b>Technology</b>	<b>Processes involved</b>	<b>Stage product</b>	<b>Low value</b>	<b>High value</b>
			Tonne CO <sub>2</sub> / tonne stage product	Tonne CO <sub>2</sub> / tonne stage product
<i>Coke oven</i>	Coke making, pelletising	Coke	0.25	0.32
<i>Sintering</i>	Sintering Ore handling Screening scrap	Agglomerate (sinter product)	0.18	0.19
<i>Blast furnace</i>	Iron making	Pig iron	1.30	1.60
<i>Basic oxygen furnace</i>	Steel making	Liquid steel	-0.04	0.04
<i>Continuous casting</i>	Casting	Steel (semi-finished)	0.01	0.01
<i>Rolling mills</i>	Rolling Finishing	Steel products: - hot rolled coil - cold rolled sheet/tinplate - semi-finished steel product - steel plate - section - tinplate/ galvanised steel	0.13 0.16 0.15 0.17 0.19 0.11	0.21 0.25 0.19 0.3 0.22 0.16

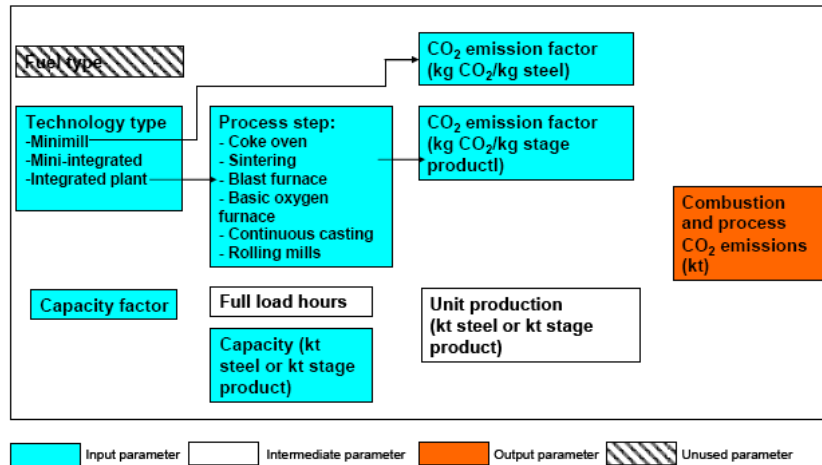


Figure 2-9: Schematic presentation of CO<sub>2</sub> emission calculation for iron and steel plants.

### 2.1.3.8 Lime

#### a) Technology

Lime is used in various sectors, but the steel making sector (40%) and the building and construction sector (20%) are largest consumers of lime. Belgium counts six lime producing plants with varying types of kilns used. Most frequently used in Belgium plants are rotary shaft kilns (8) and regeneration shaft kilns (14) on a total of 29 kilns (European Commission, 2001).

The production process of lime involves the burning of the limestone/chalk to obtain carbon dioxide and lime. Different types of kilns (process vessel) exist for the production of lime. In the European Union “other shaft kilns” and “parallel-flow regenerative shaft kilns” are used most. In 1995, 14 kilns were of the regenerative shaft type, 8 kilns were rotary kilns, 5 kilns were of the annular shaft type and 2 kilns were of other type in Belgium (IPPC, 2001).

Following reaction occurs at kiln temperatures of approximately 1000 °C:



This lime burning process is the main source of emissions and is also the principal user of energy in lime production.

The consumption of fossil fuels in the furnace to fuel the burning process typically produces flue gases with low CO<sub>2</sub> levels comparable to those in the power industry. The concentration of CO<sub>2</sub> in the flue gases depend on the type of fuels used and the excess air level used for optimal combustion conditions. The product gas using coke contains 40-42% CO<sub>2</sub>, while the product gas of using oil or gas contains 28-32% CO<sub>2</sub> (IPPC, 2001). In this study we will use an average CO<sub>2</sub> concentration of 30% for all types of lime kilns.

#### b) Data availability

The lime sector is not included as separate sector in the IEA GHG CO<sub>2</sub> emissions database. All Belgium lime kilns can be found in the Walloon region. From the database with Walloon installations, six lime producing companies are selected that have CO<sub>2</sub> emissions above 100 kt per year. Lime plant production capacities (tonnes/day) are derived from this database. Reported CO<sub>2</sub> emissions are derived from the latest version of the EPER database from November 2006.

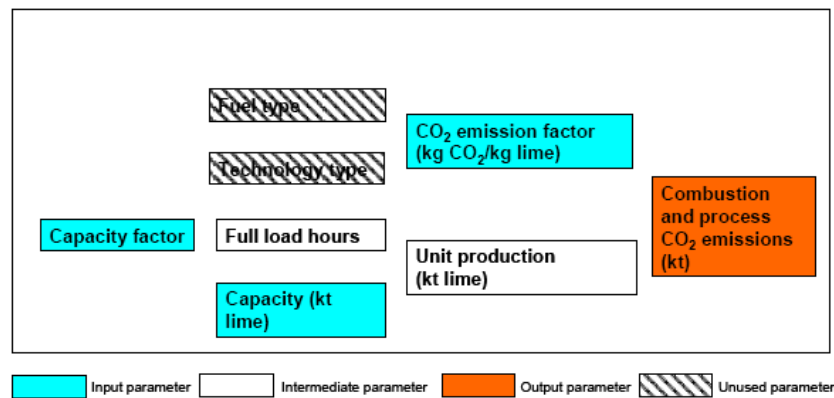


Figure 2-10: Schematic presentation of CO<sub>2</sub> emission calculation for lime plants.

### c) Calculation of CO<sub>2</sub> emissions

The CO<sub>2</sub> emission factor for the lime production process is derived from the Reference Document on Best Available Techniques in the Cement and Lime Manufacturing Industries (European Commission, 2001). The dissociation of limestone produces up to 750 kg of carbon dioxide (CO<sub>2</sub>) per tonne of lime, depending on the composition of the limestone and the degree of calcination. Although various types of kilns are identified for the production of lime, we use one general figure for specific CO<sub>2</sub> emissions because the lack of data on CO<sub>2</sub> emissions per type of process. Figure 2-10 gives an overview of the CO<sub>2</sub> emission calculation for lime plants.

The capacity of these lime production installations is given in tonnes per day (t/d) and yearly production is calculated based on assumed 8000 full load hours per year.

### 2.1.3.9 Power sector

#### a) Technology

The power sector comprises all electricity-only and combined heat and power (CHP) installations. Electricity and heat generated for industrial purposes is included in this sector. For example, on site electricity generation for iron and steel making processes is categorized as part of the power sector.

#### b) Data availability

For the power sector, data collection has been done on installation level (this deviates from data collection in the IEA GHG CO<sub>2</sub> emissions database). All database entries stem from the WEPP database (Platts, 2006). The WEPP database does not report CO<sub>2</sub>-emissions, but these are calculated on basis of installation capacity (MW), type of fuel and type of technology.

For the power sector data are collected on installation level, which is different from the IEA GHG CO<sub>2</sub> emissions database where data are collected on plant level. Difficulties with data collection on plant level are that no insight is given in the number of installations and the possible need for a central collection system for CO<sub>2</sub>. The infrastructure needed to collect CO<sub>2</sub> from several small power units increases the costs of CCS systems.

The VITO database reports CO<sub>2</sub> emissions on installation level, but the names of the installations are not comparable those in the WEPP database. Therefore, reported emissions for Belgium power installations are not included.

Table 2-5: Overview of capacity factors and emission factors for the Belgium power sector Source emission factors (IEA 2004).

Country	Fuel class COAL		Fuel class GAS		Fuel class OIL	
	capacity factor	emission factor kg CO <sub>2</sub> /MWh	capacity factor	emission factor kg CO <sub>2</sub> /MWh	capacity factor	emission factor kg CO <sub>2</sub> /MWh
Belgium	0.61	1014	0.42	384	0.33	473

c) Calculation of CO<sub>2</sub> emissions

In the database the number of full load hours is set dependent on the type of fuel used. The main fuel classes are coal, gas, oil and other fuels. Generally, coal fired plants are used as base load power plants and have a high load factor and number of full load hours (and capacity factor). Oil-fired plants have lowest number of full load hours. The number of full load hours used to calculate the electricity production is derived from the IEA publication “CO<sub>2</sub> emissions from fuel combustion, 1971-2004”, which gives capacity factors per fuel class on a country basis. For Belgium the capacity factors are given in table 2-5.

As can be seen from figure 2-11 the CO<sub>2</sub> emission factor for power units is calculated from the fuel type, technology type and the configuration of the unit. The database gives only capacities for the power part of the plants/units. The CO<sub>2</sub> emission factor is corrected for the CO<sub>2</sub> emissions for heat production in case of combined heat and power configuration.

If the type of fuel used is not known an average emission factor of 76 kg CO<sub>2</sub>/GJ is applied.

The CO<sub>2</sub> emission factor of biomass is originally set to zero in the IEA GHG CO<sub>2</sub> emissions database. However, when identifying opportunities for CO<sub>2</sub> capture the actual emissions from biomass fuelled plants need to be calculated. An emission factor of 110 kg CO<sub>2</sub> per GJ biomass has been assumed derived from (SenterNovem, 2006).

The technology types as used in the database are presented in table 2-6. Each technology is characterized as either steam turbine technology or combined cycle technology or gas turbine technology. On basis of this characterization in technology class and the fuel used, the concentration of CO<sub>2</sub> in the flue gas is defined.

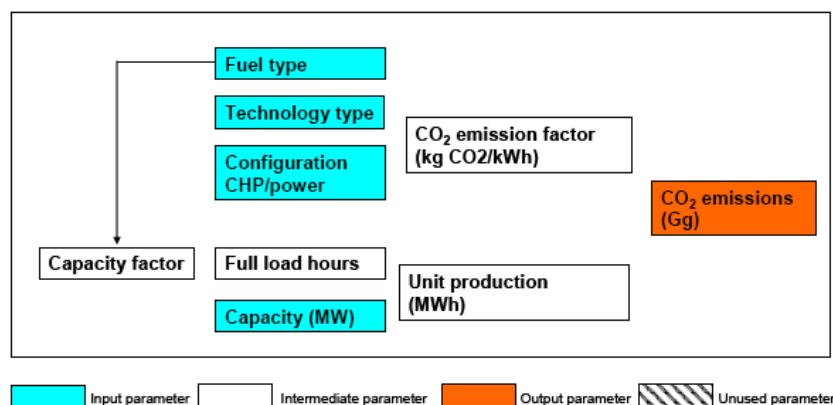


Figure 2-11: Schematic presentation of CO<sub>2</sub> emission calculation for power units.

Table 2-6: Overview of technology types and technology classes for power unit

<i>Abbr.</i>	<i>Technology</i>	<i>Class</i>
<i>CC</i>	Combined-cycle	GT CC
<i>CC/D</i>	Combined-cycle with heat recovery for desalination	GT CC
<i>CC/S</i>	Combined-cycle with steam sendout	GT CC
<i>CCSS</i>	Combined-cycle single shaft configuration	GT CC
<i>CHP</i>	Combined heat and power	GT CC
<i>CRY</i>	Cryogenic	other
<i>FC</i>	Fuel cell	FC
<i>GT</i>	Gas/combustion turbine	GT CC
<i>GT/C</i>	Gas turbine in combined-cycle	GT CC
<i>GT/D</i>	Gas turbine with heat recovery for desalination	GT CC
<i>GT/H</i>	Gas turbine with heat recovery	GT CC
<i>GT/S</i>	Gas turbine with steam sendout	GT CC
<i>GT/ST</i>	Gas turbine and steam turbine	GT CC
<i>GT/T</i>	Gas turbine in topping configuration	GT CC
<i>IC</i>	Internal combustion (reciprocating engine or diesel engine)	GT CC
<i>IC/C</i>	Internal combustion engine in combined-cycle	GT CC
<i>IC/H</i>	Internal combustion engine with heat recovery	GT CC
<i>IC/S</i>	Internal combustion engine with steam sendout	GT CC
<i>ST</i>	Steam turbine	ST
<i>ST/C</i>	Steam turbine in combined-cycle	ST
<i>ST/D</i>	Steam turbine with heat recovery for desalination	ST
<i>ST/H</i>	Steam turbine with heat recovery	ST
<i>ST/S</i>	Steam turbine with steam sendout	ST
<i>unk</i>	Unknown	ST

### 2.1.3.10 Refineries

#### a) Technology

The main sources of CO<sub>2</sub> from refineries are power plants, furnaces and boilers, flares and process vent emissions. Around 2% of emissions stem from hydrogen production. The concentration of CO<sub>2</sub> in the flue gases is typically 3% for gas turbines, 13% for other combustion equipment and >99% for hydrogen production. The total CO<sub>2</sub> emission varies with the level of complexity of the plant.

#### b) Data availability

Capacity figures of Belgium refining plants have already been incorporated in the IEA GHG CO<sub>2</sub> emissions database. There are no grounds to change these capacity figures. Reported CO<sub>2</sub> emissions for refineries are derived from the latest EPER database published in November 2006.

The differences between reported and estimated values of CO<sub>2</sub> emissions are significant and could be explained by the CO<sub>2</sub> emission value that we assume for all refinery processes in Belgium. It could very well be that some processes are more complex and have higher CO<sub>2</sub> emissions per unit output than what is assumed here.

Start-up and shut-down years are not known for the Belgian refineries. It is therefore assumed that the installations started operation in 2000 and will retire in 2040, i.e. the lifetime is set to a maximum of 40 years.

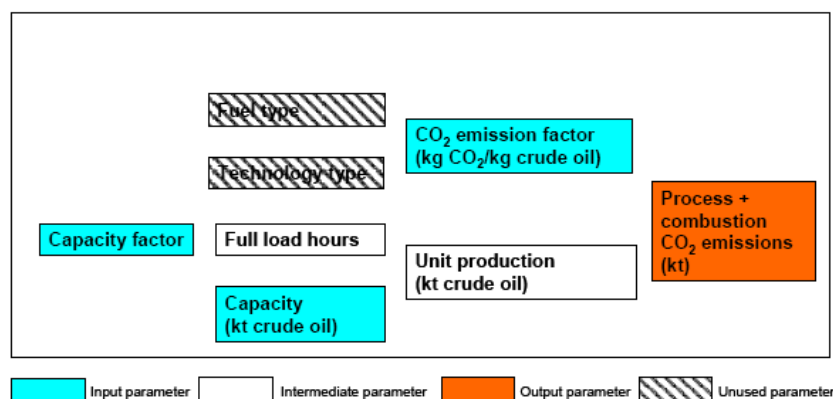


Figure 2-12: Schematic presentation of CO<sub>2</sub> emission calculation for refineries.

### c) Calculation of CO<sub>2</sub> emissions

The specific CO<sub>2</sub> emissions for refineries range from 20 to 820 kg of CO<sub>2</sub> per tonne of crude processed (European Commission, 2001). The specific CO<sub>2</sub> emissions depend on the complexity of the refinery. More complex refineries that produce more types of products tend to have higher specific CO<sub>2</sub> emissions. For the purpose of calculating CO<sub>2</sub> emissions we assume a fixed CO<sub>2</sub> emission factor of 219 kg CO<sub>2</sub>/tonne crude oil for all Belgium refineries. Figure 2-12 shows the approach of calculating CO<sub>2</sub> emissions.

### 2.1.3.11 Other

#### a) Technology

The sector “other” includes all plants that could not be included in one of the other sectors and comprises most chemical plants and pulp and paper mills. Due to the broad range of products produced by chemical plants no uniform approach to calculate CO<sub>2</sub> emissions could be set up. It has also been decided to make pulp and paper no separate sector, since calculations of CO<sub>2</sub> emissions are rather complex and for a detailed investigation on energy use and emissions of pulp and paper mills in Belgium.

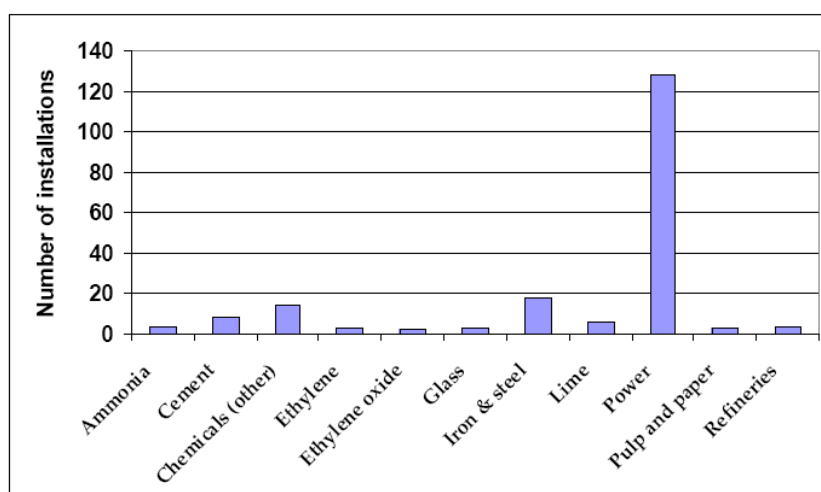


Figure 2-13: Number of installations in the database, categorized per sector.

For the sector “other” it is agreed to use reported CO<sub>2</sub> emissions in further calculations. In the column “CO<sub>2</sub> estimated (kt)” reported CO<sub>2</sub> emissions will be presented.

*b) Data availability*

See next section.

*c) Calculation of CO<sub>2</sub> emissions*

CO<sub>2</sub> emissions are not calculated for plants in this “other” sector since plants are too different to use one methodology to calculate emissions. Estimated CO<sub>2</sub> emissions are set equal to reported CO<sub>2</sub> emissions. For most plants CO<sub>2</sub> emissions are derived from the EPER database.

## 2.1.4 Results and conclusions

The aim of this part of the project was to include all large Belgian industrial point sources of CO<sub>2</sub> in the database. Larger installations are more interesting for application of carbon capture, because of the higher volumes of CO<sub>2</sub> that could be captured. Much effort has been given to including present figures for installations that emit over 100 kt CO<sub>2</sub> annually. Small scale installations are included in the power sector, where information is given on unit level. Figure 2-13 shows the number of installations included in the database per sector. The actual number of plants in the iron and steel sector is lower than what is presented here, because the volume of CO<sub>2</sub> emissions is allocated to the different process steps.

The properties of the CO<sub>2</sub> stream that could be input to a capture process are important, the size and costs of the capture technology to be applied are highly dependent on it. In general, a high concentration of CO<sub>2</sub> in the flue gas or off-gas tends to reduce the specific costs of CO<sub>2</sub> capture. Less conditioning and purification steps are needed for pure sources of CO<sub>2</sub>. Figure 2-14 provides an overview of the total CO<sub>2</sub> emissions split up according to the amount of CO<sub>2</sub> in their product gas. For some plants the concentration of CO<sub>2</sub> in the flue gas is not known (a.o. iron and steel sector) and therefore 25% of the CO<sub>2</sub> emissions could not be classified in one of the concentration categories. It shows that the capture potential from pure CO<sub>2</sub> sources is only marginal compared to the amount of CO<sub>2</sub> that might be captured from fossil fuel combustion sources.

Flue gases with lowest concentrations of CO<sub>2</sub> (3%) can be found in the power sector and result from the combustion of natural gas in combined cycles. The CO<sub>2</sub> concentration corresponding to the combustion of coal is set to 15% in this study.

The volume of CO<sub>2</sub> that per stationary source is available for capture should also be considered when options for CCS are identified (figure 2-15). In general, the capture costs per tonne CO<sub>2</sub> for small scale sources of CO<sub>2</sub> are higher compared to large scale sources of CO<sub>2</sub>. Figure 2-16 shows that a large part of total CO<sub>2</sub> emissions from industrial sources becomes available in volumes of CO<sub>2</sub> of over 500 kt. Almost two-third of the CO<sub>2</sub> emissions in the power sector stem from sources that emit over 500 kt CO<sub>2</sub> per year.

The main aim of the database is to collect and present accurate data on carbon dioxide emissions from Belgian industrial sources. Carbon dioxide emissions are calculated on basis of type of technology and/or fuel use. Besides, reported carbon dioxide emissions are given where available. Both figures have their limitations. Estimated carbon emissions could deviate from actual CO<sub>2</sub> emissions because information on technology type or fuels is missing and as a consequence not included in the calculations. For example, for ammonia production no technology classification is included and CO<sub>2</sub> emissions are calculated on fuel only. On the other hand, published data reflect CO<sub>2</sub> emissions in a specific year with that year’s specific running hours, fuel use etc.

For use in the economic simulator of this project it is advised to use estimated CO<sub>2</sub> emissions in economic calculations. These CO<sub>2</sub> emissions are based on installed capacities and also cross-checked with actual CO<sub>2</sub> emissions.

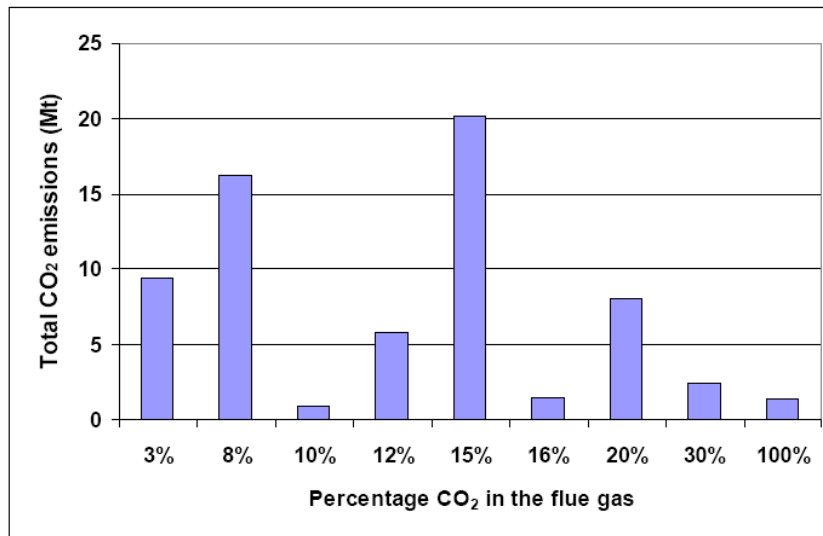


Figure 2-14: Total CO<sub>2</sub> emissions according to the concentration of CO<sub>2</sub> in the flue gas.

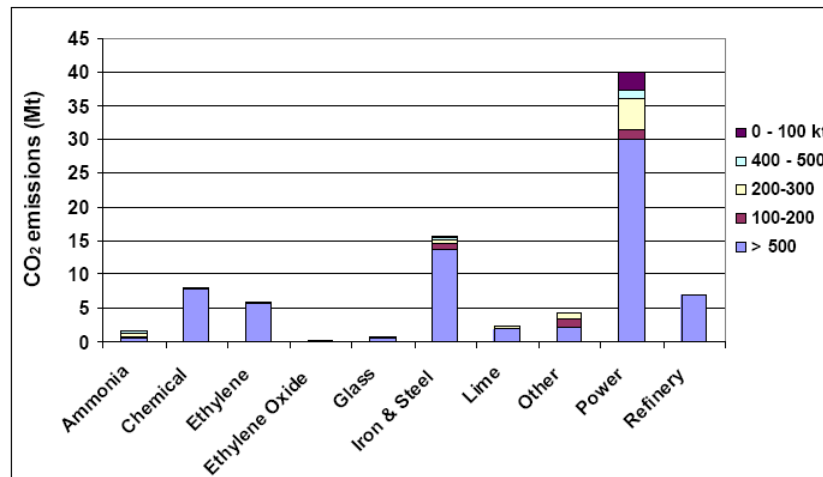


Figure 2-15: Volume of CO<sub>2</sub> streams that could be input to the capture process.

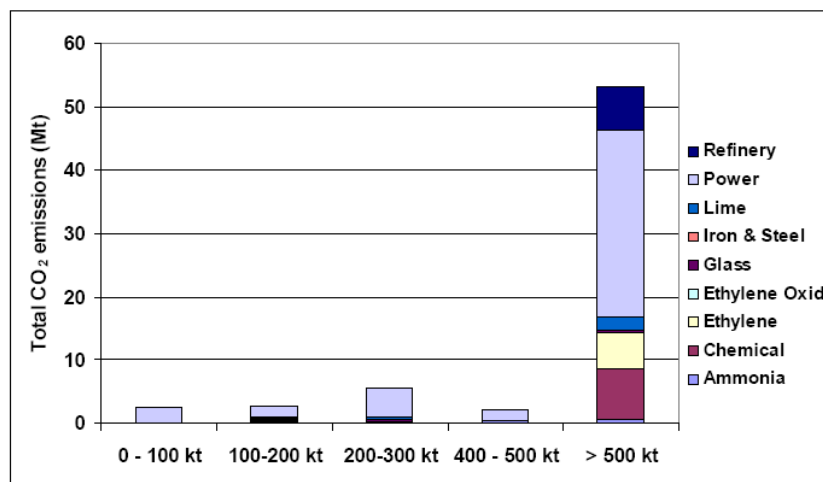


Figure 2-16: Volume of CO<sub>2</sub> streams per size class.

## 2.2 Post-combustion capture systems

### 2.2.1 Basic process

Under low CO<sub>2</sub> partial pressure conditions, as in the case of combustion flue gases (as low as 30-150 mbar), chemical absorption systems tend to be the most efficient, as the process is accompanied by a chemical reaction that enhances the overall mass transfer from gas to liquid phase. A continuous scrubbing system is used to separate CO<sub>2</sub> from the flue gas stream. It consists of two main elements: an absorber where CO<sub>2</sub> is absorbed into a solvent, and a regenerator (or stripper), where CO<sub>2</sub> is released (in concentrated form) and the original solvent is recovered. Typically, about 75% to 95% of the CO<sub>2</sub> is captured using this technology, producing a nearly pure CO<sub>2</sub> stream (> 99%).

High CO<sub>2</sub> loading and low heat of desorption are essential for atmospheric flue gas CO<sub>2</sub> recovery. The solvents must also have low byproduct formation and low decomposition rates, to maintain solvent performance and to limit the amount of waste materials produced (IPCC, 2005). The important effect of contaminants on the solvent is discussed later.

### 2.2.2 Historical developments

The idea of separating CO<sub>2</sub> from flue gas streams started in the 1970s, not with concern about the greenhouse effect, but as a potentially economic source of CO<sub>2</sub>, mainly for enhanced oil recovery (EOR) operations. Several commercial CO<sub>2</sub> capture plants were constructed in the US in the late 1970s and early 1980s. CO<sub>2</sub> was also produced for other industrial applications such as carbonation of brine and production of products like dry ice, urea and beverages. Some of these CO<sub>2</sub> capture plants are still in operation today, but all these plants are much smaller than a typical power plant. The first commercial CO<sub>2</sub> sequestration facility (exploited by Statoil) was launched in Norway in September 1996 in reaction to a Norwegian carbon tax. Since then, Statoil has been storing about 1 million tons of CO<sub>2</sub> per year from the Sleipner West gas field in a sandstone aquifer 1000 m beneath the North Sea. The international research community is closely monitoring this facility.

All these plants capture CO<sub>2</sub> with processes based on chemical absorption using a monoethanolamine (MEA)-based solvent. MEA is an organic chemical belonging to the family of compounds known as amines. It was developed over 60 years ago as a general, non-selective solvent to remove acidic gas impurities (e.g. H<sub>2</sub>S, CO<sub>2</sub>) from natural gas streams. The process was then adapted to treat flue gas streams for CO<sub>2</sub> capture. The following three absorption processes are commercially available for CO<sub>2</sub> capture in post-combustion systems (IPCC, 2005):

The Fluor Daniel ® ECONAMINE™ Process - This process was acquired by Fluor Daniel Inc. from Dow Chemical Company in 1989. It is a MEA-based process (30% by weight aqueous solution) with an oxygen inhibitor. The inhibitor helps in two ways – it reduces solvent degradation and equipment corrosion. It may be noted that this process is not applicable to reducing gas streams that contain large amounts of CO and H<sub>2</sub>, or contain more than 1 ppmv of H<sub>2</sub>S, or contain less than 1%vol O<sub>2</sub>. It has been used in many plants worldwide recovering up to 320 tons of CO<sub>2</sub> per day in a single train for use in beverage and urea production.

The Kerr-McGee/ABB Lummus Crest Process – This process uses a 15-20% by weight aqueous MEA solution. This technology can capture more than 96% of the CO<sub>2</sub> from flue gases, but the lower solvent concentration leads to economic disadvantages in terms of greater capital requirements (due to larger equipment size) and higher energy requirements (due to higher amount of dilution water per unit of solvent). The largest capacity experienced for this process is 800 tons of CO<sub>2</sub> per day utilizing two parallel trains.

The Kansai Electric Power Co., Mitsubishi Heavy Industries, Ltd., KEPCO/MHI Process - The process is based upon sterically-hindered amines and already three solvents (KS-1, KS-2 and KS-3) have been developed. In this process, low amine losses and low solvent degradation have been noted without the use of inhibitors or additives. The first commercial plant at 200 tons of CO<sub>2</sub> per day recovery from a flue gas stream has been operating in Malaysia since 1999 for urea production (equivalent to the emissions from a 10 MWt coal-fired power plant).

Post-combustion capture is thus a well-established technology but needs scaled-up engineering and optimization to be able to be applied to a 500 – 1000 MWe power plant (ZEP, 2006). Amine-based systems are similar to other end-of-pipe environmental control systems used at power plants. These units are operated at ordinary temperature and pressure. An existing plant can thus easily be retrofitted with an amine system. However, optimal heat integration may not be achievable, and is likely to lead to much higher energy penalty due to steam extraction necessary for the solvent regeneration. A major effort is being made worldwide to improve this process in the light of its potential role in CO<sub>2</sub> abatement. Thus, one can anticipate future technological advances.

### 2.2.3 Process chemistry

Absorption processes in post-combustion capture make use of the reversible nature of the chemical reaction of an aqueous alkaline solvent, usually an amine, with an acid gas (IPCC, 2005). The process chemistry is complex, but the main reactions taking place are:

- **CO<sub>2</sub> Absorption:**  $2 \text{R-NH}_2 + \text{CO}_2 \rightarrow \text{R-NH}_3^+ + \text{R-NH-COO}^-$
- **MEA Regeneration:**  $\text{R-NH-COO}^- + \text{R-NH}_3^+ + (\text{Heat}) \rightarrow \text{CO}_2 + 2 \text{R-NH}_2$

Pure MEA (with R = HO-CH<sub>2</sub>CH<sub>2</sub>) is an “unhindered” amine that forms a weakly bonded intermediate called “carbamate” that is fairly stable. Only half a mole of CO<sub>2</sub> is absorbed per mole of amine, as shown in the CO<sub>2</sub> absorption equation above. On application of heat, this carbamate dissociates to return CO<sub>2</sub> and amine solvent, as shown in the second equation above. Since the carbamate formed during absorption is quite stable, it takes lot of heat energy to break the bonds and to regenerate the solvent.

For other “hindered” amines (e.g., where R is a bulky group), the carbamate formed is not stable, and an alternate reaction leads to the formation of bicarbonate ions and hence a higher theoretical capacity of one mole of CO<sub>2</sub> per mole of amine, as shown in the following CO<sub>2</sub> absorption equation:

- **CO<sub>2</sub> Absorption:**  $\text{R-NH}_2 + \text{CO}_2 + \text{H}_2\text{O} \rightarrow \text{R-NH}_3^+ + \text{HCO}_3^-$
- **MEA Regeneration:**  $\text{HCO}_3^- + \text{R-NH}_3^+ + (\text{less Heat}) \rightarrow \text{CO}_2 + \text{H}_2\text{O} + \text{R-NH}_2$

The regeneration of these amines requires lesser amount of heat energy as compared to the unhindered amines. But the CO<sub>2</sub> uptake rate of hindered amines is very low. Efforts are underway to formulate better solvents by combining favourable properties of these two groups of amines.

#### a) Process equipment

Before entering the CO<sub>2</sub> capture plant, the flue gas has to be pre-cleaned to minimize degradation of the solvent. This is usually a combination of particulate removal, SO<sub>2</sub>-stripping in the Flue Gas Desulfurization unit (FGD), and reduction of NO<sub>x</sub> by means of a Selective Catalytic Reactor (SCR). Then, the CO<sub>2</sub> capture process is typically comprised of the following equipment as shown in figure 2-17:

#### b) Direct contact cooler

The flue gases coming out of a power plant are quite hot. The temperature of flue gas may be ranging from as low as 60°C (in case of coal-fired power plants with wet SO<sub>2</sub> scrubbers) to more than 550°C (in case of natural gas-fired simple cycle power plants). It is desirable to

cool down the flue gases to about 45-50°C, in order to improve absorption of CO<sub>2</sub> into the amine solvent (the absorption being an exothermic process is favoured by low temperatures), to minimize solvent losses (higher temperature may lead to solvent losses due to evaporation and degradation), and to avoid excessive loss of moisture with the exhaust gases. In case of coal-fired power plant applications that have a wet FGD unit upstream of the amine system, the wet scrubber helps in substantial cooling of the flue gases, and additional cooler may not be required.

*c) Flue gas blower*

The flue gas has to overcome a substantial pressure drop as it passes through a very tall absorber column, countercurrent to the solvent flow. Hence the cooled flue gas has to be pressurized using a blower before it enters the absorber.

*d) Absorber*

This is the vessel where the flue gas comes in contact with the amine-based solvent (amine in a water solution, with some additives). At absorber temperatures typically between 40 and 60°C, the amine reacts chemically with the CO<sub>2</sub> in the flue gas to form a weakly bonded compound (carbamate). The scrubbed gas is then washed and vented to the atmosphere. The column may be plate-type or a packed one. Most of the CO<sub>2</sub> absorbers are packed columns using some kind of polymer-based packing to provide large interfacial area.

*e) Lean/rich cross heat exchanger*

The CO<sub>2</sub>-loaded solvent needs to be heated in order to strip off CO<sub>2</sub> and regenerate the solvent. On the other hand, the regenerated (lean) solvent coming out of the regenerator has to be cooled down before it could be circulated back to the absorber column. Hence these two solvent streams are passed through a cross heat exchanger, where the rich (CO<sub>2</sub>-loaded) solvent gets heated and the lean (regenerated) solvent gets cooled.

*f) Regenerator (stripper)*

This is the column where the weak intermediate compound (carbamate) formed between the amine-based solvent and dissolved CO<sub>2</sub> is broken down at elevated temperatures (100°C – 140°C) and pressures not very much higher than atmospheric pressure. CO<sub>2</sub> gets separated from the solvent to leave reusable solvent behind. In case of unhindered amines like MEA, the carbamate formed is stable and it takes large amount of energy to dissociate. The regenerator also consists of a separator where CO<sub>2</sub> is separated from most of the moisture and evaporated solvent, to give a fairly rich CO<sub>2</sub> stream.

*g) Reboiler*

The regenerator is connected with a reboiler which is basically a heat exchanger where low-pressure steam generally extracted from the power plant is used to heat the loaded solvent.

*h) Steam extractor*

In case of coal-fired power plants that generate electricity by means of a steam turbine, a part of the LP/IP steam has to be diverted to the reboiler for solvent regeneration. Steam extractors are installed to take out steam from the steam turbines.

*i) Reclaimer*

Presence of acid gas impurities (SO<sub>2</sub>, SO<sub>3</sub>, NO<sub>2</sub> and HCl) in the flue gas leads to the formation of heat stable salts in the solvent stream, which cannot be dissociated even on application of heat. In order to avoid accumulation of these salts in the solvent stream and to recover some of this lost amine, a part of the solvent stream is periodically distilled in this vessel. Addition of caustic helps in freeing of some of the amine. The latter is taken back to the solvent stream while the bottom sludge (reclaimer waste) is sent for proper disposal.

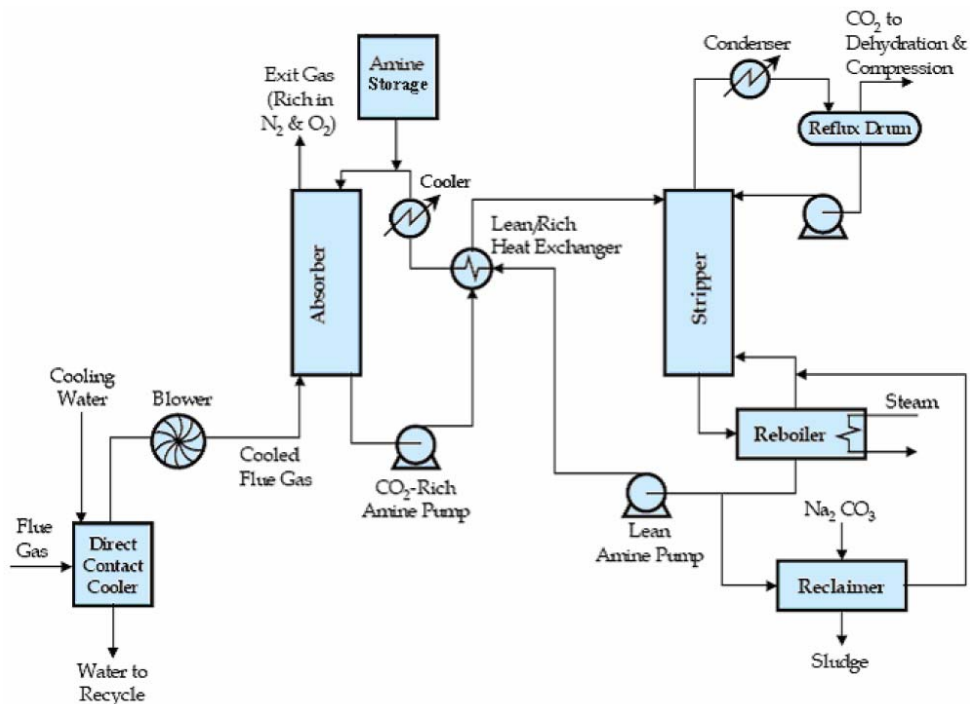


Figure 2-17: Typical amine absorption process for CO<sub>2</sub> recovery from flue gas.

#### j) Solvent processing area

The regenerated solvent has to be further cooled down even after passing through the rich/lean cross heat exchanger using a cooler, so that the solvent temperature is brought back to an acceptable level (about 40°C). Also, in order to make up for the solvent losses, a small quantity of fresh amine solvent has to be added to the solvent stream. So, the solvent processing area primarily consists of solvent cooler, amine storage tank, and a mixer. It also consists of an activated carbon bed filter that adsorbs impurities (degradation products of the amine) from the solvent stream.

#### k) CO<sub>2</sub> drying and compression unit

The multistage compression unit with inter-stage cooling and drying yields a final CO<sub>2</sub> product at the specified pressure that contains moisture and other impurities (e.g. N<sub>2</sub>) at acceptable levels.

The purity and pressure of CO<sub>2</sub> typically recovered from an amine-based chemical absorption process are as follows:

- CO<sub>2</sub> purity: 99.9% by volume or more (water saturated conditions)
- CO<sub>2</sub> pressure: 0.5 bar (gauge)

Values for the heat requirement for the leading absorption technologies are between 2.7 and 3.3 GJ/ton CO<sub>2</sub>, depending on the solvent process. Typical values for the electricity requirement are between 0.06 and 0.11 GJ/ton CO<sub>2</sub> for post-combustion capture in coal-fired power plants and 0.21 and 0.33 GJ/ton CO<sub>2</sub> for post-combustion capture in natural gas-fired combined cycles. Compression of the CO<sub>2</sub> to 110 bar will require around 0.4 GJ/ton CO<sub>2</sub> (IEA GHG, 2004). The performance of the chemical solvent in the operation is maintained by replacement, filtering and reclaiming, which leads to a consumables requirement. Typical values for the solvent consumption are between 0.2 and 1.6 kg/ton CO<sub>2</sub> (IPCC, 2005). In addition, chemicals are needed to reclaim the amine from the heat stable salt (typically 0.03–0.13 kg NaOH/ton CO<sub>2</sub>) and to remove decomposition products (typically 0.03–0.06 kg

activated carbon/ton CO<sub>2</sub>). The ranges are primarily dependent on the absorption process, with KS-1 being at the low end of the range and ECONAMINE™ at the high end (IPCC, 2005).

#### 2.2.4 Limitations of the MEA process

Although the MEA-based absorption process is the most widespread technology available for capture of CO<sub>2</sub> from power plant flue gases, it has its own disadvantages. The main problems are listed as follows:

A key feature of amine systems is the large amount of heat required to regenerate the solvent. The stable carbamate ion requires substantial energy to break the bonds. Substantial electrical energy is also needed for solvent circulation pumps, flue gas fans and CO<sub>2</sub>-compressor. This heat and electricity requirement reduces the net efficiency of the power plant if it is extracted internally (by de-rating the power plant). Alternatively, a much bigger power plant needs to be built in order to achieve the same “net” power generation capacity, as it would have been without CO<sub>2</sub> capture.

Some of the solvent is lost during the process because of a variety of reasons including mechanical, entrainment, vaporization and degradation. All the solvent entering the stripper is not regenerated. Flue gas impurities, especially sulphur oxides and nitrogen dioxide react with MEA to form heat-stable salts, thus reducing the CO<sub>2</sub>-absorption capacity of the solvent. Proprietary inhibitors are available that make the solvent tolerant to oxygen. Flue gas NO<sub>x</sub> is not a major problem because most of the NO<sub>x</sub> is nitric oxide (NO), whereas only NO<sub>2</sub> (typically about 5% of total NO<sub>x</sub>) is reactive. But SO<sub>2</sub> does degenerate MEA solvent, so very low inlet concentrations (on the order of 10 ppm) are desirable to avoid excessive loss of (costly) solvent. However, untreated flue gases of coal-fired power plants contain about 700 to 2500 ppm SO<sub>2</sub> (plus roughly 10-40 ppm NO<sub>2</sub>). The interaction of SO<sub>2</sub> with CO<sub>2</sub> control system is thus particularly important. The heat-stable salts that are formed may be treated in a side stream MEA-reclaimer, which can regenerate some of the MEA. Technologies such as electrodialysis are also being proposed for this purpose.

Corrosion control is very important in amine systems processing oxygen-containing gases. In order to reduce corrosion rates, corrosion inhibitors, lower concentrations of MEA, appropriate materials of construction and mild operating conditions are required.

Besides novel solvents (requiring less energy for regeneration), novel process designs are also currently becoming available. Research is also being carried out to improve upon the existing practices and packing types. Another area of research is to increase the concentration levels of aqueous MEA solution used in absorption systems as this tends to reduce the size of equipment used in capture plants. Methods to prevent oxidative degradation of MEA by de-oxygenation of the solvent solutions are also being investigated. In addition to this, the catalytic removal of oxygen in flue gases from coal firing has been suggested to enable operation with promising solvents sensitive to oxygen.

#### 2.2.5 CO<sub>2</sub> capture from gas versus coal-fired power plants

There are economic advantages in capturing CO<sub>2</sub> from coal-fired power plants compared to Natural Gas Combined Cycle (NGCC) power plants. These are as follows:

The CO<sub>2</sub> content in the flue gas from coal-fired power plants is 3 – 4 times more concentrated than that from a NGCC plant. Given plants with equal power export, if we assume an efficiency of 45% for coal-fired and 55% for NGCC (together with 90% and 80% CO<sub>2</sub> capture respectively), then it will be possible to aggregate more than twice the volume of CO<sub>2</sub> at a coal-fired power plant compared to a NGCC plant. The investment in infrastructure will therefore be higher on a CO<sub>2</sub> captured per unit basis.

The higher content of O<sub>2</sub> in the flue gas from a NGCC plant increases the thermal energy necessary for regeneration and increases degradation of the solvent, causing higher operation costs per ton of captured CO<sub>2</sub>.

## 2.3 Pre-combustion capture systems

### 2.3.1 Basic process

A pre-combustion capture process typically comprises a first stage of reaction producing a mixture of hydrogen and carbon monoxide (called synthesis gas or syngas) from a primary fuel (IPCC, 2005). The two main routes are to add steam (reaction 1), in which case the process is called ‘steam reforming’, or oxygen (reaction 2) to the primary fuel (IPCC, 2005). In the latter case, the process is often called ‘partial oxidation’ when applied to gaseous and liquid fuels and ‘gasification’ when applied to a solid fuel, but the principles are the same.

Steam reforming



Partial oxidation



This is followed by the ‘shift’ reaction to convert CO to CO<sub>2</sub> by the addition of steam (reaction 3):

Water Gas Shift Reaction



Finally, the CO<sub>2</sub> is removed from the CO<sub>2</sub>/H<sub>2</sub> mixture. The concentration of CO<sub>2</sub> in the input to the CO<sub>2</sub>/H<sub>2</sub> separation stage can be in the range 15-60% (dry basis) and the total pressure is typically 20-70 bar (IPCC, 2005). The CO<sub>2</sub> partial pressure is thus higher than in post-combustion capture. The separated CO<sub>2</sub> is then available for storage.

### 2.3.2 Integrated Gasification Combined Cycle (IGCC)

Coal and other hydrocarbons have been gasified for the production of chemicals, fertilizers, and synthetic fuels for more than half a century. However, it is only in the last 20 years that gasification has been used for the production of electricity using the Integrated Gasification Combined Cycle (IGCC) process. As illustrated in figure 2-18 and explained in the next sections, this nomenclature means that the design is based upon: (1) an integrated; (2) gasification “island”; and (3) a combined cycle “island”. The IGCC power plant is thus a combined cycle power plant which burns synthesis gas instead of natural gas.

#### 2.3.2.1 Existing IGCC power plants

There are currently five commercial-size, coal-based IGCC plants: the Wabash power station and the Polk power station in the United States, the Buggenum power station and the Puertollano power station in Europe and the Negishi power station in Japan.

#### 2.3.2.2 Gasification and Gas cooling and cleaning

Modern gasification technologies generally fall into three categories depending upon the flow conditions in the gasifier: moving bed, fluidized bed and entrained flow. For current and near-

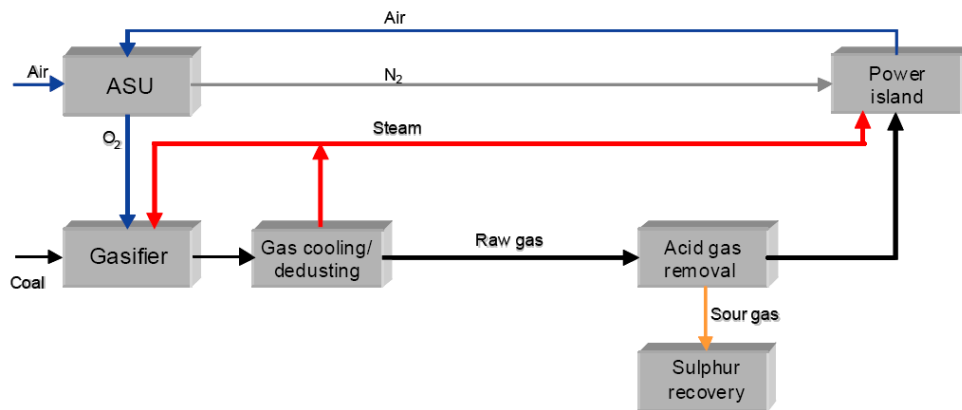


Figure 2-18: (From ZEP, 2006) IGCC process without CO<sub>2</sub> capture.

Future IGCC processes, the gasification technologies applied in the five commercial-scale plants (Shell, GE and Conoco Phillips) constitute the most matured entrained flow gasification technologies for high-rank coals which need temperatures of about 1500°C (ZEP, 2006). GE and Conoco Phillips are slurry fed processes whereas the other technologies use dry feeding systems (cf. table 2-7).

The Future Energy process is another entrained flow gasification option. For highly reactive low-rank coals (e.g. lignite) the High Temperature Winkler (HTW) gasification process is also available as a fluidized bed process at moderate process temperature (900°C) (ZEP, 2006).

The raw synthesis gas contains some pollutants which have to be eliminated before introducing the gas in the gas turbine. Due to the reducing conditions under which gasification occurs, the sulphur from the coal does not convert into SO<sub>2</sub>, but into H<sub>2</sub>S and COS instead. Similarly, the nitrogen from the coal is transformed into NH<sub>3</sub> and HCN. These components are more readily removed than NO<sub>x</sub> and SO<sub>2</sub> in combustion systems.

The synthesis gas is generally produced at high temperature (depending on the gasifier type) and must be cooled before it can be cleaned with existing technology (~400°C). Cooling can be accomplished by water quench or in a heat recovery boiler.

In the first case, the products from gasification are quenched with water, the saturated gas is cooled and condensed water and minor impurities (alkaline components, halogens, ammonia...) are removed. The gas is then passed through a hydrolysis reactor (that converts

Table 2-7: Salient characteristics of major gasification technologies.

<b>Technology Name/ Design Feature</b>	<b>GE Energy (formerly Texaco)</b>	<b>E-Gas (ConocoPhillips)</b>	<b>Shell</b>
<i>Feed System</i>	Coal in Water Slurry	Coal in Water Slurry	Dry Coal. Lock Hopper & Pneumatic Conveying
<i>Gasifier Configuration</i>	Single Stage Downflow	Two Stage Upflow	Single Stage Upflow
<i>Gasifier Wall</i>	Refractory	Refractory	Membrane Wall
<i>Pressure (psig)</i>	500-1000	Up to 600	Up to 600
<i>Notes</i>	Offered as Quench or with Heat Recovery	Currently only offered with Heat Recovery	Currently only offered with Heat Recovery

COS into H<sub>2</sub>S and hydrolyses HCN) and fed to an acid gas removal plant for removal of sulphur compounds. The sulphur compounds are converted to elemental sulphur in a Claus plant with tail gas treating. The clean fuel gas is passed through a turbo-expander and fed to the gas turbine combined cycle plant.

In the second case, the gasifier product gas is quenched with recycle fuel gas and cooled in a heat recovery boiler before being fed to a dry particulate removal unit (cyclone and filter). Some of the gas is recycled as quench gas and the remainder is scrubbed with water, reheated, passed through a hydrolysis reactor and fed to an acid gas removal plant. The clean fuel gas is fed to the gas turbine combined cycle plant. The steam produced in the heat recovery boiler is typically routed to the heat recovery steam generator (HRSG) of the combined cycle to increase steam turbine power generation.

The main disadvantage of cold gas cleaning is the energy loss during syngas cooling and reheating and the reduction of its sensible heat. By performing hot gas cleaning, exergy losses are decreased. The high sensible heat of hot gas is directly provided to the gas turbine. So, efficiency can be increased by 1 to 1.5% points. Furthermore, resorting to costly heat recuperators (exposed to harsh operating conditions) can be avoided. Hot gas cleaning is still in development but some units are currently at the demonstration stage.

### **2.3.2.3 CO<sub>2</sub> capture**

To adapt the IGCC process to achieve the CO<sub>2</sub> capture, some modifications are required as shown in figure 2-19.

As already mentioned, it is necessary to convert CO (the major raw gas constituent) to CO<sub>2</sub> by reaction with water (Water Gas Shift Reaction). This stage ensures that all carbon-containing constituents occur largely as CO<sub>2</sub> and can be captured in the downstream CO<sub>2</sub> scrubbing unit. This reaction is exothermic and thus decreases efficiency of the global process. The shift stage can basically be integrated into the process path as a sour shift or as a sweet shift if it is respectively put upstream or downstream of sulphur removal. Both variants are completely proven on a commercial scale in applications of the chemical industry. In the sour shift case, downstream sulphur is removed (as shown in fig. 2-19) or is separated together with CO<sub>2</sub>. A COS catalyst to hydrolyze COS to H<sub>2</sub>S is not required since shift catalyst copes with such. The selection between them depends on the desired degree of CO conversion and the overall carbon capture rate of the plant and is influenced by different techno-economic issues (ZEP, 2006).

A quench gasifier utilizes the heat of the gasification reaction to provide a very high level of saturation and is an ideal preparation for a shift reactor. In the other case, medium pressure steam has to be provided for the shift reaction.

There are several commercial possible methods to separate CO<sub>2</sub>: Absorption (chemical, physical), adsorption, cryogenic separation, and membranes. The most common is the physical (Rectisol<sup>TM</sup>, Purisol<sup>TM</sup> and Selexol<sup>TM</sup>), or chemical-physical, absorption when the pressure available in the syngas is over 20-30 bar, and the chemical absorption with minor pressures. In a zero emission process design with large amounts of CO<sub>2</sub> to be captured the physical variant is the preferred option (ZEP, 2006). When H<sub>2</sub>S is separated together with CO<sub>2</sub>, the solvent is selectively regenerated to produce separate CO<sub>2</sub> and sulphur compound streams. An option that is being considered in some countries is to separate H<sub>2</sub>S and CO<sub>2</sub> together, resulting in a concentration of H<sub>2</sub>S in the CO<sub>2</sub> stream between 1-5%.

Depending on the CO<sub>2</sub> separation process and the final specifications of CO<sub>2</sub> impurities admitted for geological storage, CO<sub>2</sub> purification may be necessary prior to the compression step. The CO<sub>2</sub> pressure is determined by the subsequent transportation and storage requirements (ZEP, 2006).

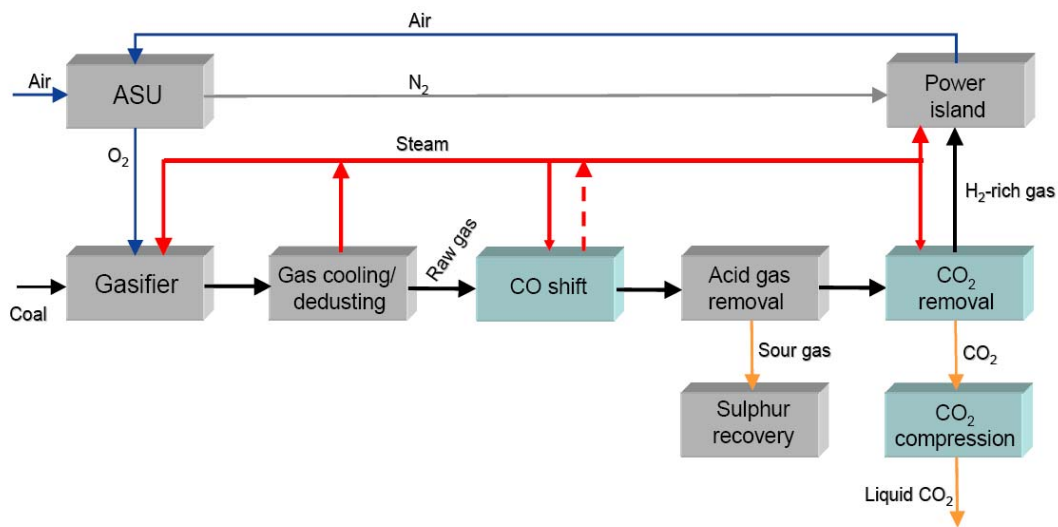


Figure 2-19: (From ZEP, 2006) IGCC process with CO<sub>2</sub> capture.

For the use of the H<sub>2</sub> stream in a combined cycle, no purification step is needed but some conditioning is required for the combustion in the gas turbine in order to keep NO<sub>x</sub> values low. It is achieved through the lowering of flame temperature by injection of steam or waste nitrogen from the Air Separation Unit (ASU) enabling both NO<sub>x</sub> control and increase of power output of the gas turbine (ZEP, 2006). Modified burners are required for the combustion of H<sub>2</sub>-rich gases and consequently adaptations of the gas turbine itself are necessary.

#### 2.3.2.4 Air Separation Unit

The oxygen required by gasification is generated in a cryogenic ASU. Gasification requires between only 1/3 and 1/5 of the theoretical amount of oxygen required for total combustion. Air supply of the ASU is ensured completely or partly by the gas turbine compressor (full or partial integration) or completely by a separate compressor (no integration). The level of ASU integration must be determined by weighing up the influence of efficiency, costs and operational flexibility (ZEP, 2006). It is the general consensus among IGCC plant designers that the preferred design today is one in which the ASU derives 25 to 50% of its oxygen supply from the gas turbine compressor and the rest from a separate air compressor.

Table 2-8: Features of commercially available reforming technologies.

	<i>Steam reforming</i>	<i>Partial oxidation</i>	<i>Autothermal reforming</i>
<i>Abbreviation</i>	SMR	POX	ATR, CPO
<i>Catalyst</i>	Ni	-	Partial oxidation: - Steam reforming: Ni
<i>Pressure</i>	15-40 bar	> 150 bar	20-40 bar
<i>Temperature</i>	750-900°C	1200-1600°C	850-1100°C
<i>Reaction</i>	$\text{CH}_4 + \text{H}_2\text{O} \leftrightarrow \text{CO} + 3\text{H}_2$	$\text{CH}_4 + \frac{1}{2} \text{O}_2 \leftrightarrow \text{CO} + 2\text{H}_2$	$\text{CH}_4 + \frac{1}{2} \text{O}_2 \leftrightarrow \text{CO} + 2\text{H}_2$ $\text{CH}_4 + \text{H}_2\text{O} \leftrightarrow \text{CO} + 3\text{H}_2$
<i>Enthalpy</i>	+206.2 MJ/kmol CH <sub>4</sub>	-35.7 MJ/kmol CH <sub>4</sub>	Exothermic
<i>H<sub>2</sub>/CO ratio</i>	3.6	1.8	1.8-3.7

A significant feature of the ASU and an incentive for further R&D is the high power demand (~10% of the gross power output and ~15% of the plant capital cost) with its strong impact on overall plant efficiency (ZEP, 2006).

### 2.3.3 Integral Reforming Combined Cycle (IRCC)

In the natural gas case a similar process configuration as described in figure 2-19 will be applied replacing the gasification by a reforming step of the natural gas and doing without dedusting.

The main reforming technologies available today are described below:

- Conventional steam methane reforming (SMR), in which the main reaction is steam reforming, which takes place in long catalyst filled reformer tubes. Heat for the highly endothermic reaction is provided by burning fuel gas.
- (Non-catalytic) partial oxidation (POX), in which the main reaction is partial oxidation. Natural gas is mixed with oxygen or air in a burner and partially oxidized at high temperature and high pressure to obtain reasonable reaction rates. The heat is mainly generated by the exothermic partial oxidation reaction.
- Catalytic partial oxidation (CPO), in which the main reaction is partial oxidation. A mixture of natural gas and an oxidant can be ignited on the surface of a noble metal catalyst (e.g. rhodium or palladium). The extremely high reaction rates allow very short residence times. This technology is not commercially available for large scale applications today.
- Autothermal reforming (ATR), in which there are two main reactions: partial oxidation and steam reforming. Natural gas is mixed with oxygen, or air, and steam in a mixer/burner. In the combustion chamber partial combustion reactions are taking place, followed by methane steam reforming reaction and shift conversion to equilibrium over the catalyst bed. The overall reaction is exothermic, resulting in a high outlet temperature, typically 850-1000°C.

(There is sometimes an interchange of terms for what is above described as CPO and ATR). Table 2-8 summarizes the features of these technologies.

In addition to the reformer technology choices described above, the installation of a catalytic prereformer, operating at approximately 500°C, can be considered to increase the overall fuel conversion efficiency. A prereformer converts most of the heavier hydrocarbons while the main reformer unit preferably converts methane to CO and H<sub>2</sub>.

For current and near-future IRCC processes the Autothermal Reforming ATR and Partial Oxidation POX constitute the most common technologies for the conversion of natural gas. The catalyst based ATR enables larger capacities per unit with higher cold gas efficiencies whereas POX allows lower investment costs. (The ‘cold gas efficiency’ is the ratio of the heating value of the produced synthesis gas to the heating value of the primary fuel.)

The concept of both steam- and air-side integration is common in IGCC systems. However, there are new possibilities for integrating the reforming plant with the combined cycle. An example is given for integrating the reforming plant air-side with natural gas plants using autothermal reformers (ATR) (fig. 2-20). Oxygen blown ATRs may also be used by inclusion of an ASU.

### 2.3.4 Limitations of the technology

The technology presents some disadvantages, here expressed for IGCC plants for which we possess more experience. These disadvantages are all linked to the technology’s degree of maturity:

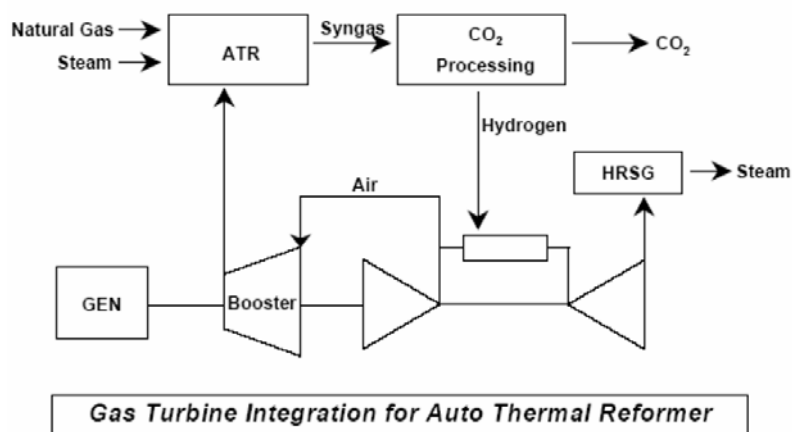


Figure 2-20: Autothermal reformer air integration.

The capital costs of IGCC plants are very high, significantly more (~10-30%) than those of conventional coal-fired units. This is partly because of the complex technologies involved, and partly because the technology is not yet ‘off-the-shelf’. This means that design and manufacturing costs are greater than will be the case once IGCC is fully commercialized. (IGCC technology is not perceived to be mature, so its risks and costs are not clearly understood.)

IRCC plants based on natural gas have not been applied because the NGCC process with much higher efficiencies and lower costs is today’s technology of choice for power generation from natural gas. An application is only justifiable in the case of IRCC with CO<sub>2</sub> capture.

The reliability of current IGCC plants has been lower than anticipated and certainly lower than is desirable for a commercial power station. One reason for this is that some of the individual component parts have yet to be fully optimized for use in an IGCC; another is that the overall design of the IGCC is rather complex and problems with one part of the plant can rapidly cascade into other areas. (The operating performance of IGCC has only been demonstrated at a handful of facilities, which have reached 80% availabilities, but not the 90% and higher availability preferred for commercial base-load coal generation)

The operational flexibility of IGCC plants is poor compared with other power generating technologies. Start-up times from cold are very long, typically 40-50 h (in contrast with a conventional boiler, which takes perhaps 8-10 h). The ability to follow load has yet to be fully demonstrated.

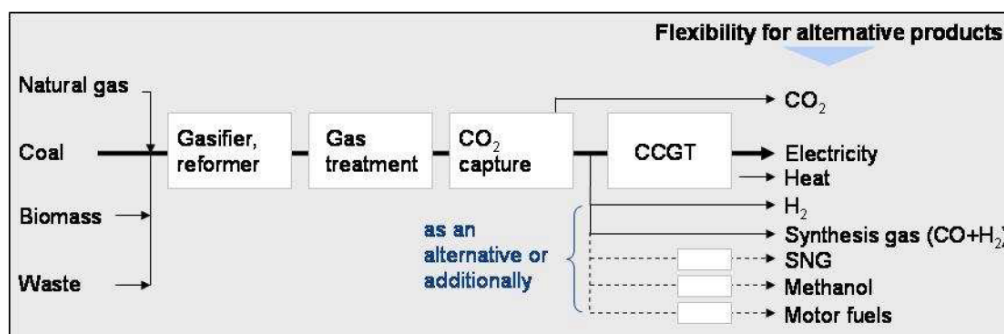


Figure 2-21: (From ZEP, 2006) Feedstock flexibility / Product flexibility.

## 2.4 Oxy-fuel combustion capture systems

### 2.4.1 Basic process

The oxy-fuel combustion process involves burning a carbonaceous fuel in either pure oxygen or a mixture of pure oxygen and a CO<sub>2</sub>-rich recycled flue gas. The combustion products then consist essentially of CO<sub>2</sub> and water vapour together with excess oxygen required to ensure complete combustion of the fuel (IPCC, 2005). It will also contain small quantities of Ar, N<sub>2</sub>, NO<sub>x</sub>, SO<sub>x</sub> and other constituents (HCl, Hg...) from feed oxygen, air leakage into the system from the atmosphere and fuel. The advantage of the process is that the flue gas is not diluted with nitrogen as when air is used for firing, and therefore can be disposed of with minimal further downstream processing.

Combustion of a fuel with pure oxygen has a combustion temperature of about 3500°C which is far too high for existing power plant materials. The combustion temperature is therefore controlled by the proportion of flue gas (and gaseous or liquid-water) recycled back to the combustion chamber (IPCC, 2005).

### 2.4.2 Oxy-fuel Pulverized Fuel boiler

In case of power generation based on coal (hard coal, lignite) or other solid fossil fuels, the power generation process is based on conventional boiler and steam cycle technology (fig. 2-22).

The CO<sub>2</sub>-rich gas resulting from the combustion process is cleaned from particles and after separation of the recycle stream, the main part of the water content is removed through condensing by cooling in a flue gas condenser, undesirable components are removed and CO<sub>2</sub>

### Oxyfuel (O<sub>2</sub>/CO<sub>2</sub> recycle) combustion capture

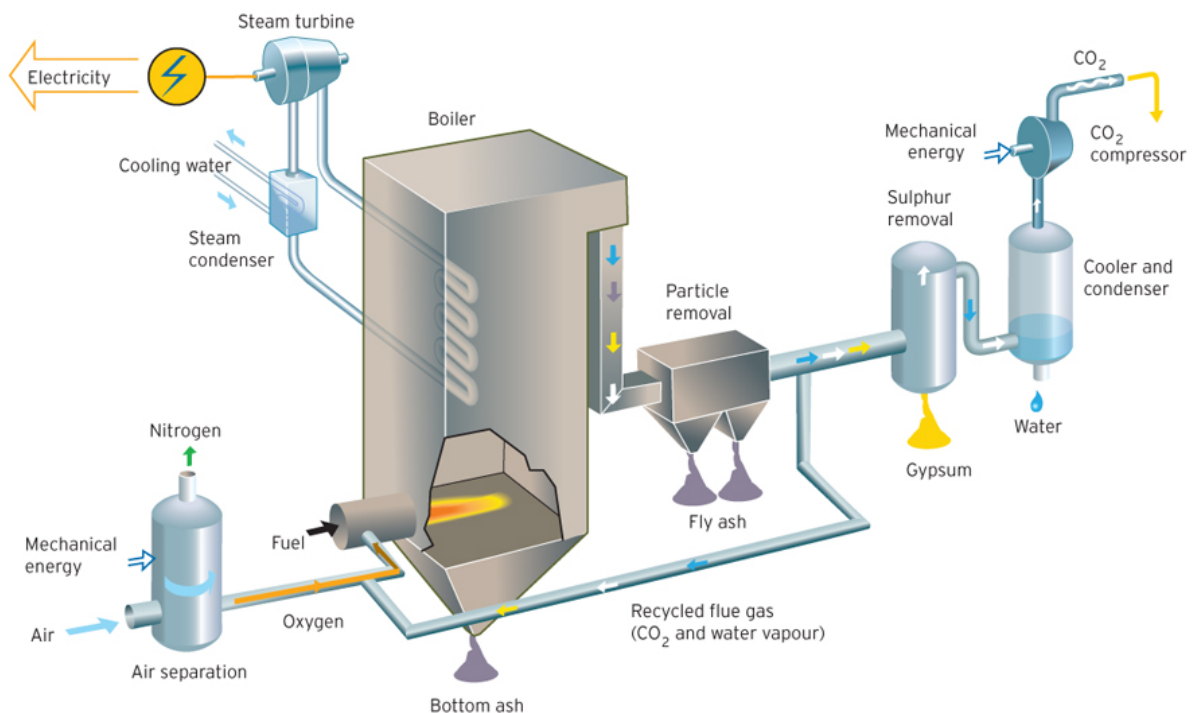


Figure 2-22: (From Vattenfall website) Oxy-fuel PF boiler.

is compressed and dried before being transported to a storage site. In case the content of non-condensable gases is too high, these gases are removed from the CO<sub>2</sub> during the compression/liquefaction process.

#### **2.4.2.1 Combustion process and boiler**

The combustion process can be based on pulverized fuel (PF) combustion or fluidized bed combustion or any other type of solid fuel combustion arrangement.

Many studies have so far been focusing on retrofit of existing PF boilers, where the boiler geometry is determined by the air-firing case, and where it has been a target for the O<sub>2</sub>/CO<sub>2</sub> recycle case to obtain combustion conditions (flame temperature, heat transfer) as similar as possible to those of the air-firing case. The flame temperature and heat capacity of gases to match fuel burning in air occurs when the feed gas used in oxy-fuel combustion has a composition of approximately 35% by volume O<sub>2</sub> and 65% by volume of dry recycled CO<sub>2</sub> (cf. 21% by volume O<sub>2</sub> and the rest nitrogen in air).

Most likely, a first generation of new oxy-fuel boilers will also adopt this boiler design philosophy. With increasing knowledge and refined tools for modelling of combustion in an O<sub>2</sub>/CO<sub>2</sub> atmosphere, it will be possible to refine the boiler design for the second and third generations of boilers. A major target will be to reduce the rate of, or even entirely avoid externally recycled flue gas. To maintain the flame temperature within acceptable limits, internal recycling of flue gas inside the boiler can be used. This will reduce the size of the boiler significantly, which means that the efficiency loss due to thermal radiation to the environment will be reduced, and will also reduce the electric power requirement for the flue gas recirculation fans. A significant reduction of the boiler size will also lead to a reduction in boiler investment cost, since the cost of the boiler is more or less proportional to the weight of the boiler parts.

When oxy-fuel combustion is applied to a Circulating Fluidized Bed (CFB) boiler, opportunities to significantly reduce the amount of flue gas recycle exist. A CFB boiler can provide very good temperature control even in highly exothermic conditions through the recirculation of bed material, thereby minimizing the need for flue gas recycling, and the boiler size and cost can thus be reduced in an easier manner than for the PF case. Alstom have reported that pilot scale testing of oxy-fuel CFB with O<sub>2</sub> concentrations of up till 70% is being performed.

The main equipment for the oxy-fuel combustion process is commercially available; however some adjustments in design are necessary. Validation and scale-up verification in pilot and demonstration projects is necessary for reaching a fully commercial level (ZEP, 2006).

Process integration is a very important part of the development in order to be able to increase the efficiency and make use of some of the waste heat generated in the air and CO<sub>2</sub> compression trains (ZEP, 2006).

#### **2.4.2.2 Flue gas treatment**

Conventional technology will be used for the flue gas clean-up, i.e. electrostatic precipitator (ESP) or bag house filters for particle removal. Wet FGD process with an external oxidation reactor is used for sulphur removal in the case of PF plants. Direct injection of limestone for sulphur removal could be an option for CFB boilers.

Inert gases must be reduced to a low concentration to avoid increasing the critical pressure of CO<sub>2</sub> in the pipeline transportation and possible two-phase flow developing, leading to CO<sub>2</sub> purities of around 95-98% minimum. The report on oxy-fuel combustion carried out by IEA GHG gives an example of the low temperature purification process to remove the inerts. The impure CO<sub>2</sub> from the boiler is first cooled by direct contact water scrubbing in a packed tower, to condense water vapour, remove traces of ash and dissolve soluble gases such as SO<sub>3</sub>

and HCl. Very little SO<sub>2</sub> or NO<sub>x</sub> is removed in this water scrubbing process. The ambient temperature CO<sub>2</sub> at atmospheric pressure is then compressed to a processing pressure of about 30 bar followed by drying in a dual-bed thermally regenerated desiccant drier. Oxygen, nitrogen and argon are removed from the CO<sub>2</sub> by low temperature processing. The impure CO<sub>2</sub> is thus cooled against evaporating lower pressure liquid CO<sub>2</sub> streams to a temperature of -55°C, close to its triple point, which reduces the partial pressure of CO<sub>2</sub> in the uncondensed gas stream to about 5 bar, corresponding to a typical concentration of approximately 20-25 mole% CO<sub>2</sub>. The purified CO<sub>2</sub> streams leaving the cold equipment are finally compressed in a second stage of CO<sub>2</sub> compression.

The requirements of enhanced oil recovery of oxygen content below around 10 ppmv are not reached by the low temperature inerts removal. Indeed, this results typically in an oxygen content of 1 mole% and a total inerts level of 2-5 mole%. This oxygen could be removed by using a fuel rich combustor, or using a catalytic combustor, to consume the oxygen present in the CO<sub>2</sub> before inerts removal. Another solution is to incorporate distillation of the liquid CO<sub>2</sub> to remove oxygen. This allows us to reach purities of 10 ppmv O<sub>2</sub> in the CO<sub>2</sub> without adding other impurities that might be created by fuel rich combustion.

Table 2-9 shows three different options for CO<sub>2</sub> purification from an oxy-fuel-fired coal combustion system. Actual powers will depend upon the type of coal burned and the amount of air inleakage there is into the boiler, since this will dictate the level of inerts that must be removed from the raw CO<sub>2</sub>, together with issues such as cooling water temperature. However, the figures of table 2-9 are consistent. One can see that low purity CO<sub>2</sub>, as produced by the process described above, gives the highest capture of the contained CO<sub>2</sub>. Increasing the purity of the CO<sub>2</sub> decreases recovery by 2% with a 1% reduction in power, which represents overall a reduction in capture efficiency. To reach the higher purities required by EOR leads to around 5% increase in power. Therefore, one can say that the extra penalty of achieving EOR-grade CO<sub>2</sub> from oxy-fuel-fired coal combustion is both feasible and tolerable as an extra energy penalty.

#### 2.4.2.3 Air Separation Unit

Although energy required for CO<sub>2</sub> separation is quite low, important energy consumption originates from the energy needed for oxygen production constituting the main part of efficiency penalty.

The Air Separation Unit is a key component in the oxy-fuel concept (ZEP, 2006). A variety of technologies have been developed to separate air, but cryogenic distillation is the most effective solution for large-scale oxygen production and high oxygen purity.

Full-scale power plants with CO<sub>2</sub> capture will require quantities of oxygen which is about four times the largest ASU delivered so far (ZEP, 2006). It was found to be more economic to design the air separation units for only 95% O<sub>2</sub> purity instead of 99.5% to comply with practical levels of air leakage into boilers and to separate the associated argon and nitrogen in

Table 2-9: Power, recovery and purity in oxyfuel CO<sub>2</sub> purification.

CO <sub>2</sub> purity	Oxygen content	CO <sub>2</sub> recovery	Power <sup>1</sup> from 1 to 110 bar, kWh/tonne CO <sub>2</sub> captured
95.9 mol%	0.9 mol%	89.0%	168.5
98 mol%	0.4 mol%	87.0%	166.5
99.97 mol%	10 ppmv	87.4%	177.1

<sup>1</sup> Power includes adiabatic compression without credit for steam system feed water heating, so numbers may appear high compared to intercooled compression

the CO<sub>2</sub> inert gas removal system. The extra power required for higher purity oxygen is indeed not compensated by a reduction in power in the CO<sub>2</sub> purification system.

The energy required to separate oxygen from air and produce 95% O<sub>2</sub> at a typical oxy-fuel application pressure of 1.7 bar is 220 to 265 kWh/ton O<sub>2</sub>.

Another future option could be Ion Transport Membranes (ITM) yielding a 100% selectivity to oxygen. Several international programmes are ongoing. As for now this technology seems better suited for natural gas cycles than coal steam cycles; IGCC is however a feasible application (ZEP, 2006).

### 2.4.3 Comparison with the air-firing case

Compared to the air-firing case, oxy-fuel combustion presents several advantages:

NO<sub>x</sub> emissions are lower than in the air-firing case due to largely reduced thermal NO<sub>x</sub> formation from the absence of nitrogen in the feed gas - with the partial recycling of NO<sub>x</sub> also reducing the formation and net emissions originating from the fuel bound nitrogen (This NO<sub>x</sub> reduction arises from dilution effects and the reaction of NO<sub>x</sub> in the recycle gas with hydrocarbon radicals from the fuel (the "reburning" mechanism)). Studies have demonstrated that the conversion ratio of fuel-N in coal to exhausted NO<sub>x</sub> is automatically and significantly reduced to one quarter or one sixth of that by conventional air combustion.

The overall heat transfer is improved because of the higher emissivity of the CO<sub>2</sub>/H<sub>2</sub>O gas mixture in the boiler compared to nitrogen and the improved heat transfer in the convection section. These improvements, together with the recycle of hot flue gas, increase the boiler efficiency and steam generation by about 5%. In the air-fired boiler, a large quantity of inert nitrogen is heated as a consequence of the combustion process, and although this nitrogen is cooled down again, it has a temperature above the ambient as the exhaust gas is released. The heat loss with the flue gas in a conventional air-fired boiler amounts to up to 10%. A significant part of this loss is the heat energy that leaves with the nitrogen in the flue gas. In the O<sub>2</sub>/CO<sub>2</sub> recycle combustion boiler, there is no bulk nitrogen in the gas path, which in turn means that the heat losses with the flue gas can be significantly reduced.

Hot recycling of the flue gas prior to CO<sub>2</sub> purification and compression reduces the size of all unit operations in the stream leaving the boiler to a fifth that of similar equipment deployed in conventional air blown combustion systems. The low temperature (-55°C) CO<sub>2</sub> purification plant integrated with the CO<sub>2</sub> compressor will not only remove excess O<sub>2</sub>, N<sub>2</sub>, argon but can also remove all NO<sub>x</sub> and SO<sub>2</sub> from the CO<sub>2</sub> stream, if high purity CO<sub>2</sub> is required for storage. This eliminates the need to deploy conventional selective catalytic reduction for NO<sub>x</sub> removal and flue gas desulphurization to purify the gas. The overall reduction in flow volumes, equipment scale and simplification of gas purification steps will thus have the benefit of reducing both capital and operating costs of equipment deployed for combustion, heat transfer and final gas purification.

Almost pure oxygen will be available for the combustion process in the boiler. This means that it will be possible to control and optimize the combustion process through the injection of oxygen in dedicated areas inside the boiler and that the boiler design will have an additional degree of freedom compared to conventional air-fired boilers, which can be taken advantage of to control combustion conditions, emission formation and temperature distribution.

### 2.4.4 Oxy-fuel gas turbine

The oxy-fuel process can also be adapted to natural gas firing, a schematic is provided in figure 2-23. Both steam- and combined cycles are feasible but the combined cycle will likely be preferred due to efficiency and cost.

The natural gas is burnt using oxygen from an air separation unit in a gas turbine cycle using

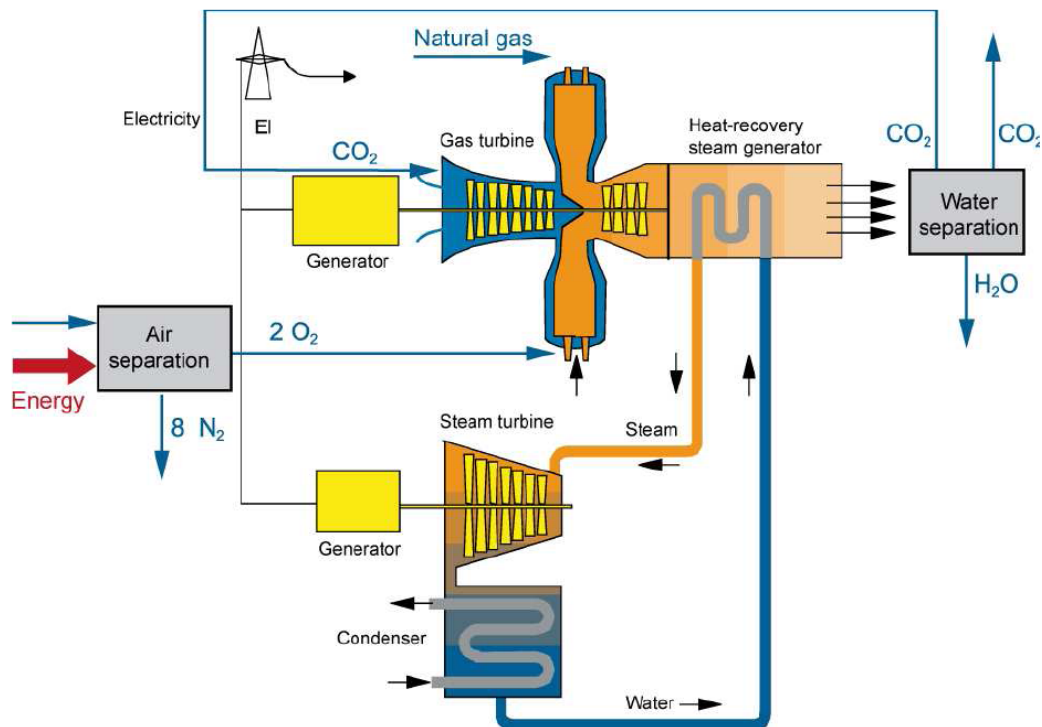


Figure 2-23: (From Sintef) Simplified thermal cycle for oxy-fuel-firing gas turbine based power generation.

recycled CO<sub>2</sub> as working fluid. The resulting flue gases are cleaned up if required, and the water is removed in a flue gas condenser. A part of the resulting CO<sub>2</sub>-rich product gases are recycled to the compressor and the other part is brought to the CO<sub>2</sub> compression and flue gas-conditioning unit.

A number of different designs of the thermodynamic cycle exist, to optimize efficiency and make use of existing technology (see for example the MATIANT cycle at <http://www.ulg.ac.be/genienuc/>). In any case changes are needed for the gas turbine compressor and turbine blading, the combustor and the air system (cooling and balancing); basically a new engine will have to be made. One could argue that this technology should strictly not be denoted a current and near-term technology. However, the cycle is feasible and recent studies have concluded that the Semi Closed Oxy-Fuel Combustion Combined Cycle (SCOF-CC) has good potential and limited techno-economic hinders for realisation.

## 2.5 Performance and costs of power plants with CO<sub>2</sub> capture

This section deals with the three leading technologies for capture of CO<sub>2</sub> in power plants, i.e., post-combustion capture, pre-combustion capture and oxy-fuel combustion. Performance, costs and emissions data for coal and natural gas-fired power plants<sup>6</sup> are gathered in a database, which has been developed in order to supplement the initial database of the Markal model provided by VITO. Sensitivities to various potentially significant parameters are assessed.

<sup>6</sup> Lignite will have a role to play in countries where it is abundant. Since it is not the case in Belgium, we will not take it into account in our database.

### 2.5.1 Introduction

Several relevant studies from literature have been reviewed. The main source of information is probably the ‘IPCC Special Report on Carbon Dioxide Capture and Storage (2005)’ which collects the results of many recent studies. Some studies carried out by the IEA GHG are also taken into consideration. Next to these two major sources, data coming from reports realised by Ecofys, DOE, SFA Pacific... are added to the database.

An important remark is that all the figures are only estimates for inexistent power plants or plants in demonstration projects and not statistics collected on existing plants. Features like availability, operation and maintenance costs... cannot be measured.

We focus here on new power plants. Some studies about retrofit are available but the results are too dependent on the studied case (number of years of power plant to be retrofitted, necessity for upgrade of components...). Furthermore, old power plants to be retrofitted have already a low efficiency and adding capture cuts the latter by ~10% points so increasing fuel consumption in an unacceptable way. This makes retrofit not an interesting option. It could however be interesting from an economic point of view according to CO<sub>2</sub> price.

### 2.5.2 Consistency of data and data processing

After gathering studies, some characteristics have been calculated and compared with values given in the reviewed studies. This allowed us to find some mistakes which are probably careless mistakes in data reporting.

Performance varies according to the different assumptions used in the studies, i.e. type of fuel, characteristics of the cycle... The reference power plants without CO<sub>2</sub> capture assume highly efficient commercially demonstrated technologies. Coal refers to bituminous coals although the composition or lower heating value is unknown and can vary greatly<sup>7</sup>.

Literature reports a fairly wide range of costs. The range is mainly due to the variability of site-specific factors, especially the design, operating and financing characteristics of the power plants, and the type and cost of fuel used. In addition, uncertainty still remains about the performance and cost of current and future capture technologies.

The costs reported in the various studies are expressed in different currencies (€ or US\$) and for different base years. We decided to convert all the costs in constant<sup>8</sup> euros of 2005 (currency and base year used in the Markal database). The Gross Domestic Product deflator (of the United States or Euro Area) has been chosen as an inflation index like advised by VITO and the exchange rate is an annual average value. To convert dollars of 2001 into euros of 2005, we thus first apply the inflation to obtain dollars of 2005 and then the exchange rate in 2005 to convert dollars into euros.

Capital costs reported by different organizations or authors may not always include the same items. The terms used to report capital costs may further disguise such differences and lead to misunderstandings about what is and is not included. For example, power plant cost studies often report a value of capital cost that does not include the cost of interest during construction or other so-called ‘owners costs’<sup>9</sup> that typically add at least 10-20% to the ‘total capital requirement’ (TCR) of a system. However, the capital cost breakdown is not reported in the reviewed studies and thus such omissions cannot be discovered. We made the choice not to modify the data because of the lack of information. The costs do not include development costs or costs which are specific to first-of-a-kind plants.

---

<sup>7</sup> We call bituminous coal a coal with a lower heating value contained between 24.4 and 36.1 GJ/kg (average value of 30.2 GJ/kg) and with a carbon content between 45 and 86% (average value of 65.5%).

<sup>8</sup> Current price (nominal price) includes the effect of general price inflation. Constant price (real price) refers to a value from which the overall effect of general price inflation has been removed.

<sup>9</sup> Refer to cost components that are typically Owner responsibility.

For each technology and each characteristic, an average value has been derived from the relevant studies as a representative value. However, not all technologies have a similar level of development. Some technologies are well-known and therefore we have a lot of information on them while others have not been studied in detail. Wider and narrower ranges between high and low values of a characteristic thus tend to reflect the relative number of studies for each technology, rather than inherent uncertainties in this characteristic.

To conclude, the figures presented in this section have to be used cautiously. We will have to wait until power plants with capture are developed at a commercial stage in a grid to get more exploitable data.

## 2.5.3 Plant performance

### 2.5.3.1 Efficiency

The net plant efficiencies of power plants with and without CO<sub>2</sub> capture are shown in table 2-10, on a lower heating value (LHV) basis. The absolute and relative efficiency losses when adding capture are calculated by comparison with the reference plant. Here the reference plant is assumed to be a plant of the same type and design as the plant with CO<sub>2</sub> capture. For coal, a Pulverized Coal-fired power plant (PC) is the reference plant for post-combustion and oxy-fuel combustion capture and an Integrated Gasification Combined Cycle (IGCC) is the reference plant for pre-combustion capture. For gas, a Natural Gas Combined Cycle (NGCC) is the reference for all the capture technologies.

No distinction is made here between the kinds of solvent used in post-combustion capture. Most studies are based on monoethanolamine (MEA) utilization, some are based on KS-1 utilization. In the same way, results do not make a distinction between the different gasifier technologies in pre-combustion capture.

The reference plants chosen for each capture technology do not have the same characteristics, which makes comparison difficult (see the Pulverized Coal-fired and NGCC power plants). We can however draw some trends.

With regard to **coal technologies**, the **post-combustion capture** is responsible for the highest penalty. CO<sub>2</sub> is removed from flue gas, hence a big mass flow rate and a low concentration. For low CO<sub>2</sub> partial pressure, we have to use chemical absorption to carry out the capture.

Table 2-10: Net plant efficiencies of CO<sub>2</sub> capture technologies.

<i>Fuel</i>	<i>CO<sub>2</sub> capture technology</i>	<i>Net efficiency (% LHV)</i>	<i>Absolute efficiency loss (% points)</i>	<i>Relative efficiency loss (%)</i>
<i>Coal</i>	PC	42.7		
	Post-combustion	32.9	9.9	23
	IGCC	43.8		
	Pre-combustion	37.0	6.7	15
	PC	44.7		
<i>Gas</i>	Oxy-combustion	36.0	8.7	19
	NGCC	56.6		
	Post-combustion	48.8	7.8	14
	NGCC	57.1		
	Pre-combustion	49.9	7.2	13
	NGCC	57.0		
	Oxy-combustion	46.4	10.7	19

The efficiency penalty thus results from two main reasons:

1. The solvent regeneration (by using low-pressure steam) requires a lot of energy (The heat consumption for regeneration of the KS-1 solvent is lower than for MEA and the flue gas fan power consumption is lower, partly due to the use of structured instead of random packing in the absorber).
2. Furthermore CO<sub>2</sub> is recovered at near atmospheric pressure and has still to be compressed to 110 bar.

In **pre-combustion capture**, CO<sub>2</sub> is removed from the fuel before combustion. The fuel gas mass flow rate is hence small and CO<sub>2</sub> partial pressure is high, allowing the use of physical solvents for capture. This leads to advantages compared to post-combustion capture.

The physical solvents need lower energy for regeneration (which is carried out by solvent depressurization) than that required by chemical solvents.

The energy consumption for CO<sub>2</sub> compression is also lower in the IGCC plants because CO<sub>2</sub> is recovered at elevated pressures.

However, the IGCC plants have additional energy losses which do not occur in the post-combustion capture plants.

The fuel gas has to be passed through the shift reactor prior to CO<sub>2</sub> removal and the shift reaction is highly exothermic (about 15% of the heat of combustion of CO is not converted into heat of combustion of H<sub>2</sub> but dissipated like heat). Even though most of the exothermic heat is recovered in steam generators, this means that energy bypasses the gas turbine and is fed directly into the lower efficiency steam cycle.

If the synthesis gas is quenched with water before being fed to the shift converter, sufficient steam is already present in the fuel gas to undergo the shift reaction. In the other case, medium pressure steam has to be added to the fuel gas fed to the shift converter, resulting in further energy losses.

Another energy loss in IGCC plants with capture is due to the impacts of shift conversion and CO<sub>2</sub> separation on the performance of the combined cycle. In plants without capture, CO<sub>2</sub> produced by combustion of the fuel gas is expanded in the gas turbine. In plants with capture, CO<sub>2</sub> is separated and is not available for expansion.

The use of a hydrogen-rich fuel gas in the plants with CO<sub>2</sub> capture also has other impacts on the combined cycle performance; in particular the expansion gas has a higher steam concentration, which increases the rate of heat transfer to the turbine blades. In order to maintain the same blade temperature, the turbine inlet temperature has to be reduced, which reduces the turbine efficiency.

Generally, all this gives a lower penalty compared to post-combustion capture.

In **oxy-fuel combustion** systems, oxygen is used to burn the fuel so that the flue gas consists mainly of CO<sub>2</sub> and water vapour. The process thus presents the following advantage.

Condensation is used to separate CO<sub>2</sub> from flue gas which does not require much energy.

The efficiency penalty is however high because of the two following reasons.

The air separation units which produce oxygen for combustion consume a lot of energy and hence increase the efficiency loss. This is slightly offset by a small overall reduction in losses in the main power generation units, for example due to the deletion of the FGD plant.

The energy consumption for CO<sub>2</sub> compression is higher than in the post-combustion capture plant because the volume of gas fed to the CO<sub>2</sub> compressors is higher, due to the presence of impurities (inerts). Secondly, some additional compression is required to drive the cryogenic separation unit which removes impurities part way through the CO<sub>2</sub> compression.

With regard to natural gas-fired plants,

The efficiency reduction for **post-combustion capture** is lower than for coal-fired plants. Although the fan power consumptions are higher in the gas-fired plants because a greater volume of flue gas has to be processed per unit of fuel, the solvent-regeneration heat

consumption is lower because less CO<sub>2</sub> has to be captured, natural gas having a lower carbon content per unit of energy than coal.

In **pre-combustion capture**, the power plant with capture is compared to a NGCC plant. Penalty includes energy losses related to the natural gas conversion into syngas and to the shift reaction, to the Air Separation Unit if oxygen is supplied to the reformer and to CO<sub>2</sub> separation.

Compared to the oxy-fuel combustion coal plant, the energy consumption for CO<sub>2</sub> compression of the **oxy-fuel combustion** NGCC plant is lower because less CO<sub>2</sub> is produced. Nevertheless, the efficiency reduction due to the power generation and due to the oxygen plant is substantially greater, resulting in a greater overall efficiency loss for capture. The quantity of oxygen required per MW of fuel is about 15% lower in the NGCC plant (Davison, 2007) but the oxygen is produced at high pressure to be fed to the gas turbine, resulting in a higher overall energy consumption. The working fluid in the Brayton cycle is now mainly CO<sub>2</sub> which has less good compression and expansion characteristics than air and flue gas.

Recent significant improvements in the post-combustion capture processes and more detailed heat integration between the CO<sub>2</sub> capture unit and the power plant lead to lower efficiency penalties than those presented here. An update should be considered. In the same way, it seems that studies on oxy-fuel combustion are based on more advanced reference power plants.

It has not been possible to obtain the breakdown of efficiency penalty for the figures presented here but this has been done in a recent study<sup>10</sup> carried out by IEA GHG.

### 2.5.3.2 Emissions

#### a) CO<sub>2</sub> emissions

The quantities of CO<sub>2</sub> emitted by the three capture technologies are shown in table 2-11. The CO<sub>2</sub> capture system efficiency and the percentage of CO<sub>2</sub> avoided are also shown. The CO<sub>2</sub> avoided is obtained by subtracting the emissions of a plant with CO<sub>2</sub> capture from the emissions of the reference plant without capture as defined above. This could also be evaluated for another baseline plant (like a Pulverized Coal plant or a NGCC plant).

The quantities of emissions avoided are lower than the quantities captured because of the reduction in efficiency, which results in a greater production of CO<sub>2</sub>. The percentages of CO<sub>2</sub>

Table 2-11: CO<sub>2</sub> emissions of CO<sub>2</sub> capture technologies

<i>Fuel</i>	<i>CO<sub>2</sub> capture technology</i>	<i>CO<sub>2</sub> specific emission (t/MWh)</i>	<i>CO<sub>2</sub> captured (%)</i>	<i>CO<sub>2</sub> avoided (%)</i>
<i>Coal</i>	PC	0.771		
	Post-combustion	0.112	89	85
	IGCC	0.745		
	Pre-combustion	0.100	89	87
	PC	0.761		
<i>Gas</i>	Oxy-combustion	0.079	92	90
	NGCC	0.363		
	Post-combustion	0.051	88	86
	NGCC	0.361		
	Pre-combustion	0.058	86	84
	NGCC	0.367		
	Oxy-combustion	0.014	97	96

<sup>10</sup> Davison J., Performance and costs of power plants with capture and storage of CO<sub>2</sub>

captured shown in table 2-11 are not necessarily the technical limits or economic optima for each of the technologies. The plants do not all produce the same purity of CO<sub>2</sub>. If high purity is required, purification units need to be installed. However, some CO<sub>2</sub> is lost during the purification decreasing the capture efficiency. It is the case for oxy-fuel combustion capture for which the inerts removal severely penalizes the system. The relative merits of the technologies therefore depend on the CO<sub>2</sub> quality requirements.

#### *b) Resource consumptions and other emissions*

Resource consumptions and emissions (different from CO<sub>2</sub>) are not mentioned in the reviewed studies. These are given in the above-mentioned study. Emissions to the atmosphere from plants without capture depend on environmental legislation and do not represent the practical limits for each technology.

For each type of fuel and power generation technology, CO<sub>2</sub> capture results in an increasing fuel consumption and outputs of wastes and by-products per unit of net electricity output. This does not hold for SO<sub>x</sub> emissions to the atmosphere which are reduced.

The best technology, from an environmental point of view, will depend on the relative importance given to the consumption of different resources and the environmental impact of different types of wastes and emissions.

In the model described further, it will be necessary to specify the NO<sub>x</sub> and SO<sub>2</sub> emissions of power plants. For power plants without capture, these emissions will be considered as being similar to values in the above-mentioned study since the latter are based on environmental legislation and have to be respected. For power plants with capture, SO<sub>2</sub> emissions are proportional to the efficiency but, for NO<sub>x</sub> emissions, it is more delicate. In post-combustion and pre-combustion capture, the flue gas input to a CO<sub>2</sub> solvent scrubbing unit must have low concentrations of SO<sub>2</sub> and NO<sub>x</sub>, as these substances result in the loss of solvent and the flue gas thus need to be pre-treated. For example, the SO<sub>2</sub> specification is set at 10 ppmv (6% O<sub>2</sub>) by Fluor's and 1 ppmv by MHI's amine scrubbing unit suppliers. Some of the remaining NO<sub>x</sub> and SO<sub>2</sub> will be captured in the capture process. So the emissions are not directly proportional to the efficiency. In this case, it is better to use the existing values. For the IRCC with capture, we will consider the NO<sub>x</sub> emissions as equal to those of the NGCC plant without capture because NO<sub>x</sub> emissions come mainly from the combustion in the gas turbine.

#### **2.5.3.3 Others**

Further information about capture technologies is given in table 2-12. The availability factor represents the fraction of the year that the capacity is available to operate. It constitutes a limit to the capacity factor defined in section 2.5.4.1. It is important to pay attention to the fact that the availability factor mentioned here is not the value that these technologies present today. 85% is rather a **minimum value** to reach in order to be able to use these technologies for commercial base-load generation. It is still a problem for pre-combustion capture plants which currently reach a maximum of 80% availability given their high complexity and integration rate. Post-combustion capture NGCC plants will probably be able to reach a higher value. We generally consider that a 90% and higher availability is required for commercial base-load generation. Concerning the technical lifetime of these technologies, pre-combustion capture plants are penalized by the gas turbine and the gasification unit.

#### **2.5.4 Costs**

In this section, the costs include only the power plant and capture technologies and not the additional costs of CO<sub>2</sub> transport and storage.

Table 2-12: Availability factor and technical lifetime of CO<sub>2</sub> capture technologies.

<i>Fuel</i>	<i>CO<sub>2</sub> capture technology</i>	<i>Availability factor (%)</i>	<i>Lifetime (year)</i>
<i>Coal</i>	PC		
	Post-combustion	85	40
	IGCC		
	Pre-combustion	85	25
	PC		
<i>Gas</i>	Oxy-combustion	85	40
	NGCC		
	Post-combustion	90	40
	NGCC		
	Pre-combustion	85	25
	NGCC		
	Oxy-combustion	85	40

#### 2.5.4.1 Costs of power generation

The effect of CO<sub>2</sub> capture on the cost of electricity is one of the most important measures of economic impact. The cost of electricity (COE) for a power plant can be calculated as:<sup>11</sup>

$$\text{COE} = [(\text{TCR})(\text{FCF}) + (\text{FOM})] / [(\text{CF})(8760)(\text{kW})] + \text{VOM} + (\text{HR})(\text{FC}) \quad (4)$$

where

COE = levelized cost of electricity (€/kWh)

TCR = total capital requirement (€)

FCF = fixed charge factor (fraction/year)

FOM = fixed operation and maintenance costs (€/year)

VOM = variable operation and maintenance costs (€/kWh)

HR = net plant heat rate or the opposite of the efficiency (kJ/kWh)

FC = unit fuel cost (€/kJ)

CF = capacity factor (fraction)

8760 = total hours in a typical year (hour/year)

kW = net plant power (kW)

The fixed charge factor (also known as the capital recovery factor) is the proportion of the yearly repayment of the TCR compared to the initial TCR payment<sup>12</sup>. For example, if you have a loan of 100 € over a period of 15 years and the FCF is 9%, then 9 € have to be paid for the next 15 years. The capacity factor is the period of time during which the power plant is in use and is limited by the availability factor.

The incremental COE is the difference in electricity cost with and without CO<sub>2</sub> capture. The equation shows that many factors affect this incremental cost. For example, the total capital cost as well as the fixed and variable costs associated with plant operation and maintenance (O&M) include many different items. Similarly, the fixed charge factor reflects assumptions about the plant lifetime and the effective interest rate (or discount rate) used to depreciate

<sup>11</sup> For simplicity, the value of FCF is applied to the Total Capital Requirement. More detailed calculations of COE based on a year-by-year analysis apply the FCF to the total capital cost excluding owner's costs, which are separately accounted for in the years prior to plant start-up.

<sup>12</sup> In its simplest form, FCF can be calculated from the project lifetime,  $n$  (years), and annual interest rate,  $i$  (fraction), by the equation:  $\text{FCF} = i / [1 - (1+i)^{-n}]$ .

Table 2-13: Total Capital Requirement and O&M costs of CO<sub>2</sub> capture technologies

<i>Fuel</i>	<i>CO<sub>2</sub> capture technology</i>	<i>TCR (€<sub>2005</sub>/kW)</i>	<i>Increase in TCR (%)</i>	<i>Net output (MW)</i>	<i>FOM (€/kW.y)</i>	<i>VOM (€/GJ)</i>
<i>Coal</i>	PC	1134		540	28.7	1.07
	Post-combustion	1902	67	444	33.5	1.32
	IGCC	1234		528	35.8	1.22
	Pre-combustion	1754	42	468	41.9	1.34
	PC	1084		605	27.0	1.07
	Oxy-combustion	1571	54	495	40.8	1.10
<i>Gas</i>	NGCC	487		536	10.8	0.57
	Post-combustion	880	81	459	13.8	0.70
	NGCC	405		645	10.8	0.57
	Pre-combustion	885	119	632	15.8	0.71
	NGCC	454		404	10.8	0.57
	Oxy-combustion	1047	130	383	16.3	0.58

capital costs. Assumptions about any of the factors can have a pronounced effect on overall cost results.

Finally, because several of the parameter values in the equation may change over the operating life of a facility (such as the capacity factor, unit fuel cost, or variable operating costs), the cost of electricity may also vary from year to year. To include such effects, an economic evaluation would calculate the net present value (NPV) of discounted costs based on a schedule of year-to-year cost variations. However, most engineering-economic studies use the above equation to calculate a single value of ‘levelized’ COE over the assumed life of the plant. The levelized COE is the cost of electricity, which, if sustained over the operating life of the plant, would produce the same NPV as an assumed stream of variable year-to-year costs. In most economic studies of CO<sub>2</sub> capture, however, all parameter values are held constant, reflecting (either implicitly or explicitly) a levelized COE over the life of the plant.

In the table below, representative values of the Total Capital Requirement derived from the relevant studies are shown. Operation and maintenance costs are rarely mentioned in the studies. These have hence been taken from the VITO Markal database (coming from European model PRIMES) when available or estimated in the other case.

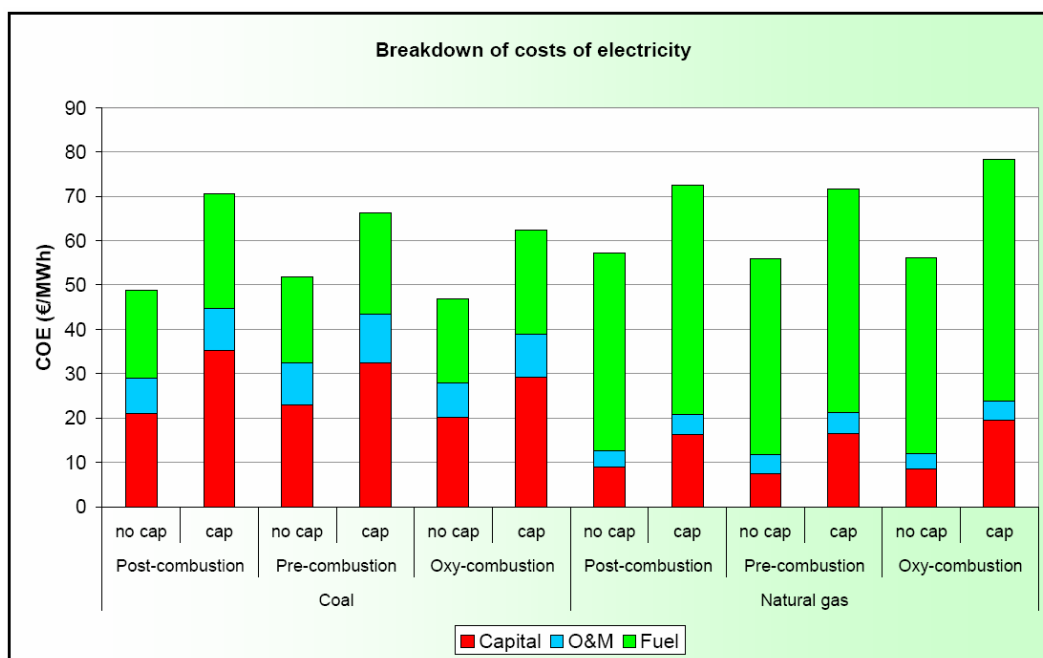
For coal-fired power plants, the IGCC reference plant is the most expensive. However, it also requires the lowest increase in capital cost for capture (table 2-13). Indeed, only a CO shift reactor and a CO<sub>2</sub> solvent scrubbing reactor have to be added. CO<sub>2</sub> is regenerated in successive flashes and we save the first stages of compression. Oxy-combustion capture has the lowest TCR. For natural gas-fired power plants, pre-combustion and post-combustion capture result in a similar TCR (however, the reference plants have not the same TCR). The increase in TCR for the natural gas fired oxy-fuel combustion plant is the highest (table 2-13). It is said that the cost of the combined cycle unit (excluding the oxygen plant and CO<sub>2</sub> compression) increases by 40% per MW of gross output compared to a reference plant. The average plant sizes are also reported in the table. The range of variation is very high. These differences in plant sizes affect the economic comparisons, because plants normally have economies of scale, i.e. the cost per unit output usually decreases with increasing plant size.

The costs of electricity obtained in the various studies are difficult to compare given capacity factors, fixed charge factors and fuel costs used to calculate them could differ greatly. For that reason, they have been recalculated with the following values:

- Capacity factor = 80%
- Fixed charge factor = 13%
- Fuel price: Coal = 2.35 €/GJ – Natural gas = 7 €/GJ

Table 2-14: Cost of electricity of CO<sub>2</sub> capture technologies.

<i>Fuel</i>	<i>CO<sub>2</sub> capture technology</i>	<i>COE (€ (2005)/MWh)</i>	<i>Increase in COE (%)</i>
<i>Coal</i>	PC	49	
	Post-combustion	71	45
	IGCC	52	
	Pre-combustion	66	28
	Oxy-combustion	62	33
<i>Gas</i>	NGCC	57	
	Post-combustion	72	27
	NGCC	55	
	Pre-combustion	72	30
	Oxy-combustion	78	39


 Figure 2-24: Breakdown of costs of electricity of CO<sub>2</sub> capture technologies.

The capacity factor and fixed charge factor are average values observed in the studies. We notice that fixed charge factors range from 9.4 up to 17.3%. These values are quite high and reflect great risk-investment. Natural gas price is very fluctuating, the value of 7 €/GJ has been chosen for calculation. Calculated values are shown in table 2-14.

According to these figures, coal-fired oxy-fuel combustion and pre-combustion capture plants have the lowest COE. However, these results are highly influenced by values taken as assumptions. Most important sources of variability are assumptions on the CO<sub>2</sub> capture system energy requirement, power plant efficiency, fuel type, plant capacity factor and fixed charge factor.

In figure 2-24, the COE are broken down into capital charges, operation and maintenance and fuel costs. For gas-fired plants, the contribution of capital costs is relatively low compared to coal plants.

### 2.5.4.2 Costs of CO<sub>2</sub> captured and avoided

The cost of CO<sub>2</sub> captured can be defined as:

$$\begin{aligned} \text{Cost of CO}_2 \text{ Captured (€ / ton CO}_2\text{)} \\ = [(\text{COE})_{\text{capture}} - (\text{COE})_{\text{ref}}] / (\text{CO}_2, \text{ captured} / \text{kWh}) \end{aligned} \quad (5)$$

where

COE = levelized cost of electricity (€/kWh)

CO<sub>2</sub>, captured / kWh = total mass of CO<sub>2</sub> captured (in tons) per net kWh for the plant with capture

The subscripts ‘capture’ and ‘ref’ refer to the plant with and without CO<sub>2</sub> capture, respectively. If the CO<sub>2</sub> captured at a power plant can be sold at this price (e.g., to the food industry, for enhanced oil recovery...), the COE for the plant with capture would be the same as for the reference plant having higher CO<sub>2</sub> emissions.

We can observe that this parameter is often used to compare the technologies, which is not correct. The cost of CO<sub>2</sub> captured is interesting, but does not take into account the emissions that are still emitted. Therefore, it can not be used to compare technologies and it can only be used **indicatively** to compare with international CO<sub>2</sub> price. The relevant variable to compare the technologies is the cost of electricity including penalization of CO<sub>2</sub>. Even if the €/ton captured is cheaper for a certain technology, it could become more interesting to use another technique if CO<sub>2</sub> prices increase.

The cost of CO<sub>2</sub> avoided reflects the average cost of reducing atmospheric CO<sub>2</sub> mass emissions by one unit while providing the same amount of useful product as a ‘reference plant’ without CCS. The avoidance cost can be defined as:

$$\begin{aligned} \text{Cost of CO}_2 \text{ avoided (€ / ton CO}_2\text{)} = \\ [(\text{COE})_{\text{capture}} - (\text{COE})_{\text{ref}}] / [(\text{CO}_2 / \text{kWh})_{\text{ref}} - (\text{CO}_2 / \text{kWh})_{\text{capture}}] \end{aligned} \quad (6)$$

where

CO<sub>2</sub> / kWh = CO<sub>2</sub> mass emission rate (in tons) per kWh generated, based on the net plant capacity for each case

Note that while this equation is commonly used to report a cost of CO<sub>2</sub> avoided for the capture portion of a full CCS system, strictly speaking it should be applied only to a complete CCS system including transport and storage costs (since all elements are required to avoid emissions to the atmosphere).

Table 2-15: Cost of CO<sub>2</sub> captured and avoided.

<i>Fuel</i>	<i>CO<sub>2</sub> capture technology</i>	<i>CO<sub>2</sub> captured (€ (2005)/tCO<sub>2</sub>)</i>	<i>CO<sub>2</sub> avoided (€ (2005)/tCO<sub>2</sub>)</i>
<i>Coal</i>	PC		
	Post-combustion	24	33
	IGCC		
	Pre-combustion	19	23
	Oxy-combustion	18	23
<i>Gas</i>	NGCC		
	Post-combustion	41	49
	NGCC		
	Pre-combustion	46	54
	Oxy-combustion	50	62

As already specified, the ‘reference plant’ is assumed here to be a plant of the same type and design as the plant with CO<sub>2</sub> capture. According to the kind of questions to treat, this reference plant could be any technology which produces electricity.

The costs of CO<sub>2</sub> captured and avoided have been calculated and reported in table 2-15.

The cost of CO<sub>2</sub> avoided is higher than the cost of CO<sub>2</sub> captured because the quantity of emissions avoided are lower than the quantity of emissions captured as explained above. The lowest cost of CO<sub>2</sub> avoided is realised by pre-combustion and oxy-combustion capture technologies for coal-fired plants. Costs per ton of CO<sub>2</sub> are higher for the gas-fired plants because less CO<sub>2</sub> emission is avoided per kWh of electricity generated.

### 2.5.4.3 Sensitivity

#### a) Sensitivity to fuel price

The fuel price is different at different locations and varies over time. Coal price is predicted to be relatively stable in the projection period; this is not the case for natural gas price. The following two graphs show the sensitivity of the cost of electricity of plants with capture to the natural gas and coal price. There is a linear relationship between fuel price and cost of electricity (fig. 2-25 and 2-26). For natural gas power plants, the cost of electricity would increase by 7.45 €/MWh for each 1 €/GJ increase in natural gas price. For coal-fired plants, this increase would be of 10.25 €/MWh for each 1 €/GJ increase in coal price. Contrary to what we could think, the sensitivity to coal price is higher because the efficiency of coal-fired power plants is much lower than that of natural gas-fired power plants. Pay attention to the fact that these costs of electricity have been calculated by keeping the other values like capacity factor and fixed charge factor constant.

#### b) Sensitivity to fixed charge factor and to capacity factor

Sensitivity to FCF and CF can be seen in the two graphs below (fig. 2-27 and 2-28). We note that coal technologies (in solid lines) are more sensitive given their higher capital cost.

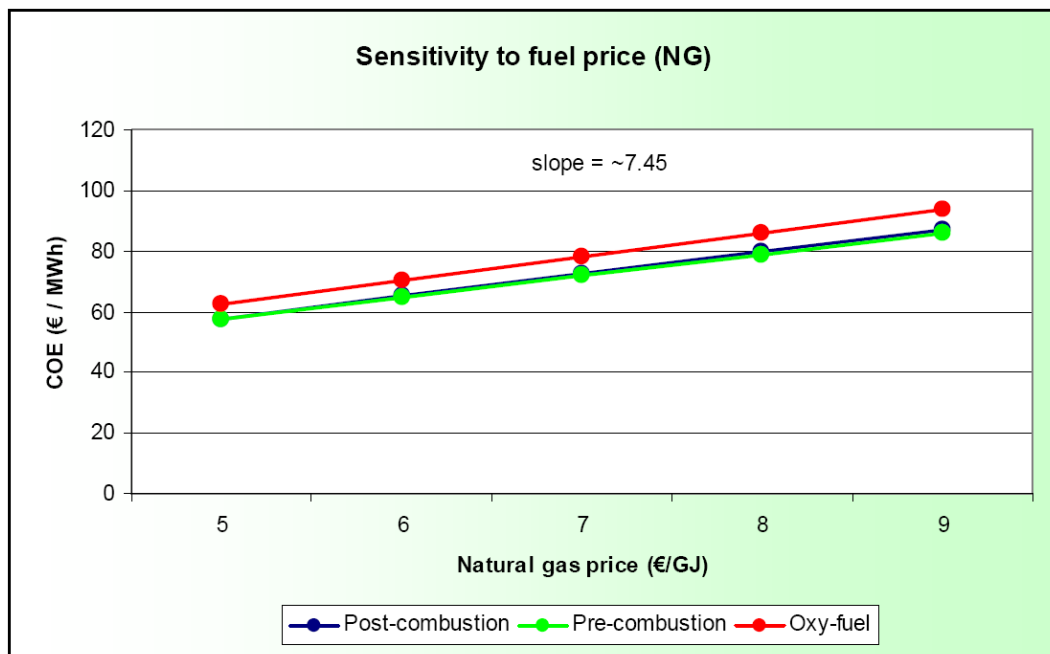


Figure 2-25: Sensitivity of the cost of electricity to natural gas price.

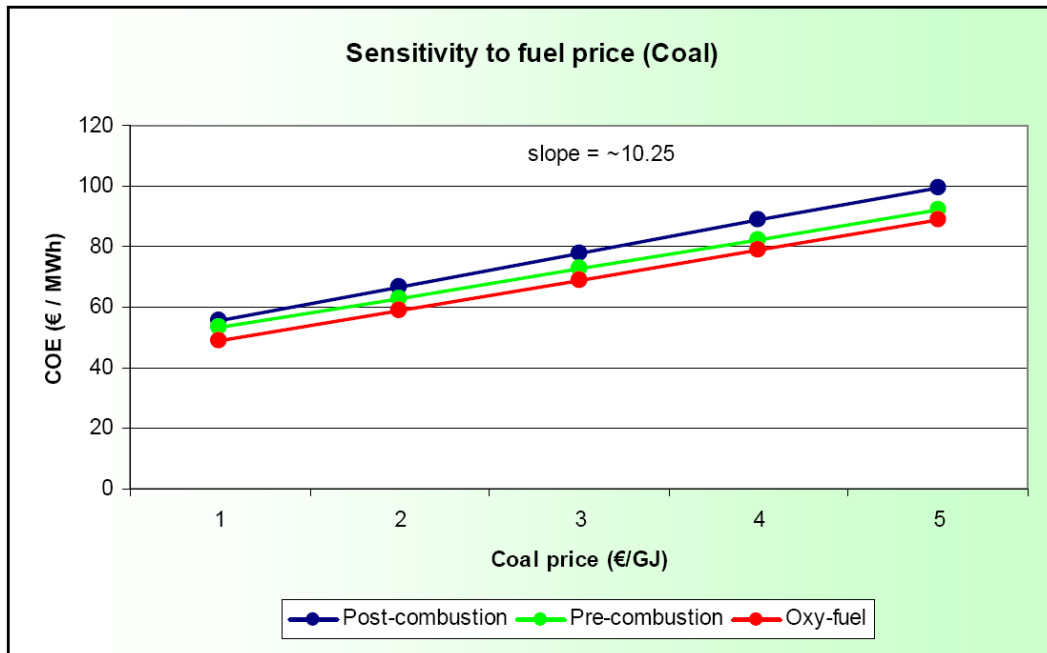


Figure 2-26: Sensitivity of the cost of electricity to coal price.

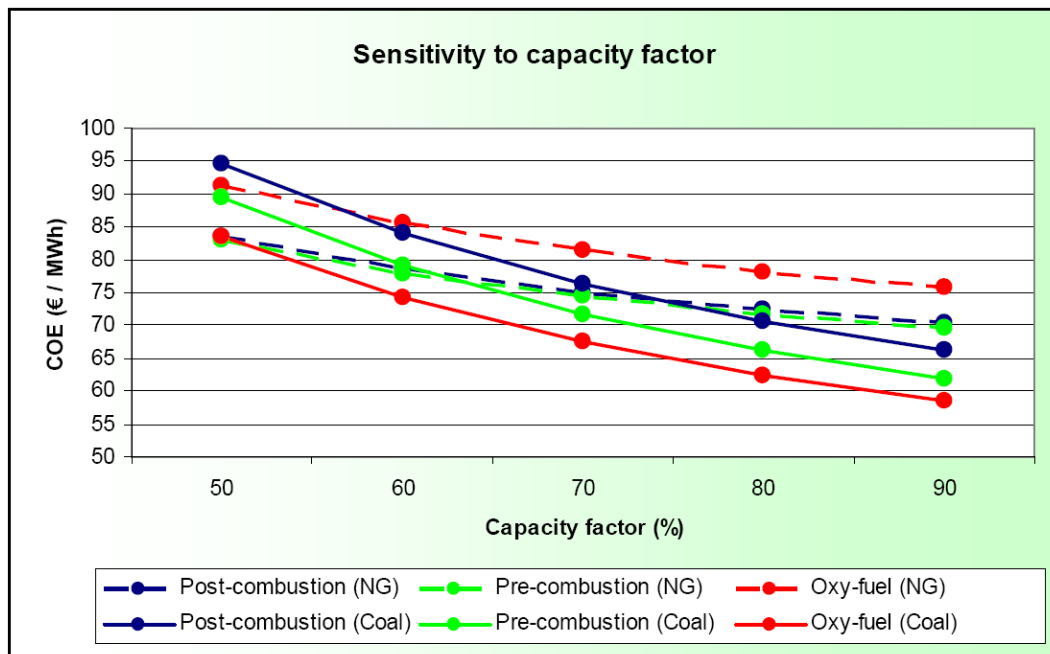


Figure 2-27: Sensitivity of the cost of electricity to capacity factor.

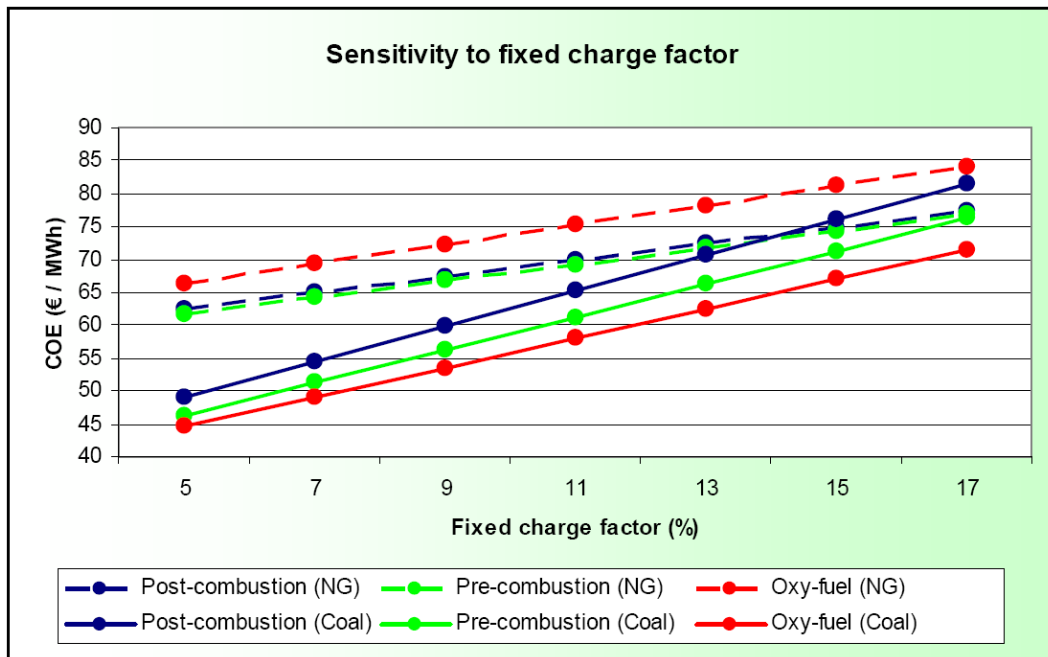


Figure 2-28: Sensitivity of the cost of electricity to fixed charge factor.

### 2.5.5 Prevision for 2030

The efficiency of all of the power generation technologies will improve in the future mainly due to development of more advanced gas and steam turbines (fig. 2-30). The performance and costs of CO<sub>2</sub> capture technologies are also expected to improve in the future due to technology developments and ‘learning by doing’ (fig. 2-29). In order to estimate the performance and costs of technologies until 2030, we used coefficients (shown in table 2-16) derived from data in the Markal database (coming from European model PRIMES) when they were available or estimated them in the other case.

These coefficients are used in an equation of the type:

$$y = a \cdot x^{TL} \quad (7)$$

Table 2-16: Technological learning coefficients for prevision until 2030.

<i>Fuel</i>	<i>CO<sub>2</sub> capture technology</i>	<i>TL (TCR)</i>	<i>TL (efficiency)</i>	<i>Start year (calendar year)</i>
<i>Coal</i>	PC	-0.074	0.029	
	Post-combustion	-0.124	0.044	2025
	IGCC	-0.096	0.039	
	Pre-combustion	-0.138	0.052	2030
	PC	-0.074	0.029	
<i>Gas</i>	Oxy-combustion	-0.124	0.044	2025
	NGCC	-0.025	0.032	
	Post-combustion	-0.076	0.049	2025
	NGCC	-0.096	0.039	
	Pre-combustion	-0.138	0.052	2030
	NGCC	-0.025	0.032	
	Oxy-combustion	-0.076	0.049	2050

where

y = value of the characteristic in the year in question  
 a = value of the characteristic in 2001  
 x = difference between the year in question and the reference year (2000)  
 TL (for technological learning) is the coefficient

These coefficients do not take into account the effect of the mass-production on cost reduction but only the technological learning. No major improvement is assumed. CO<sub>2</sub> emissions follow the same path as the efficiency (fig. 2-31); the coefficients (opposite of the efficiency coefficients) do thus not take into account an increase in CO<sub>2</sub> capture system efficiency. Technological learning is considered similar for post-combustion and oxy-fuel combustion capture while the pre-combustion capture undergoes the most important changes. The possibilities of improvement and integration are higher.

In the last column, the year in which the technologies will be available is estimated according to the technological knowledge and the development previsions of 2005.

The evolution of the Total Capital Requirement, the efficiency, the CO<sub>2</sub> emission and the COE of power plants with CO<sub>2</sub> capture are plotted out in the following graphs (fig. 2-29, 2-30, 2-31 and 2-32 respectively).

### 2.5.6 Conclusion

The relevant variable to compare the technologies is the COE (including penalization of CO<sub>2</sub>). We can see that the costs of electricity of the different technologies are very similar. Although not studied in this section, the CO<sub>2</sub> price for the non-captured CO<sub>2</sub> will impact on the COE. The COE of coal technologies will increase more than the COE of gas technologies, resulting in an even more reduced difference between technologies. A change in fuel price or capacity factor or fixed charge factor... can also change the order of ranking of the costs. It is likely that the fixed charge factor will be higher for the pre-combustion capture technology. The lifetime of this technology is after all shorter and at this moment the technology is still not very reliable. There is also significant scope for improvement in all of the technologies. According to interest given to one or other technology, the cost relativities could change in the future. In conclusion, it is very difficult to predict which of the technologies will be the least costly or will be deployed first.

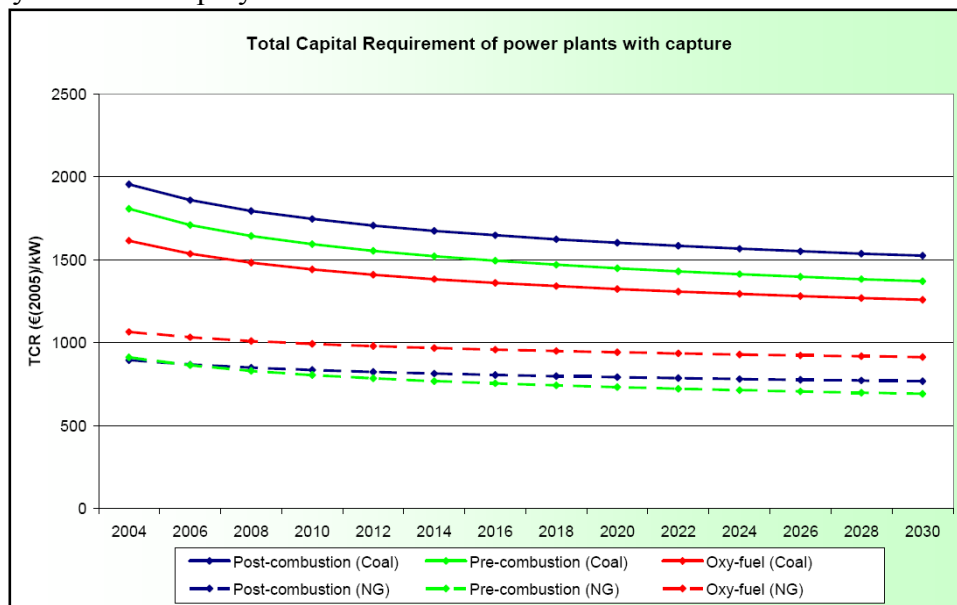


Figure 2-29: Evolution of the Total Capital Requirement of CO<sub>2</sub> capture technologies until 2030.

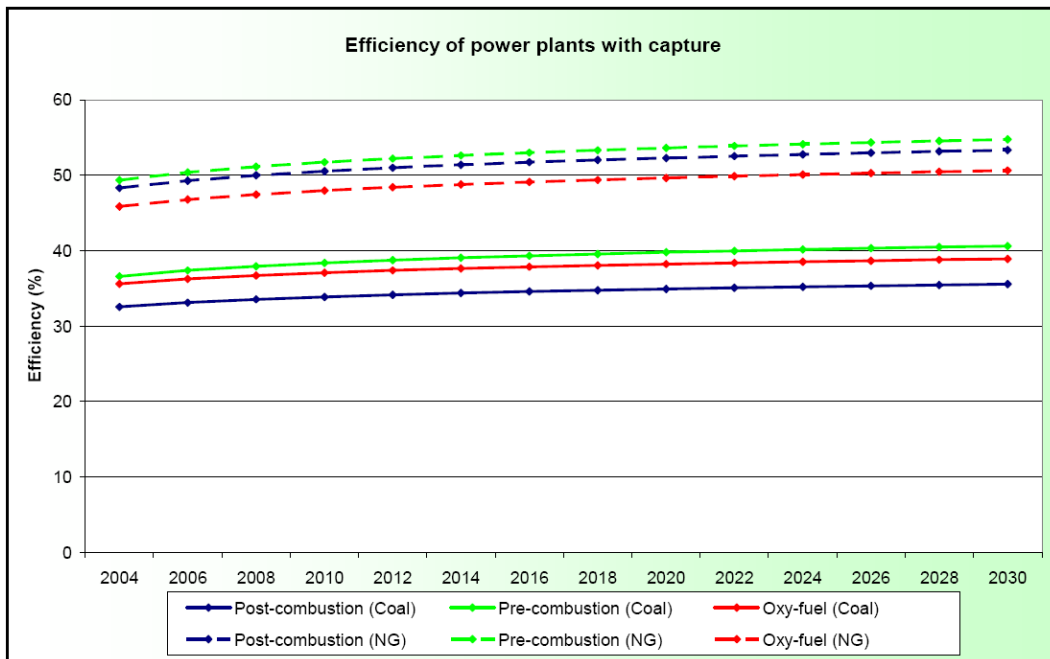


Figure 2-30: Evolution of the efficiency of CO<sub>2</sub> capture technologies until 2030.

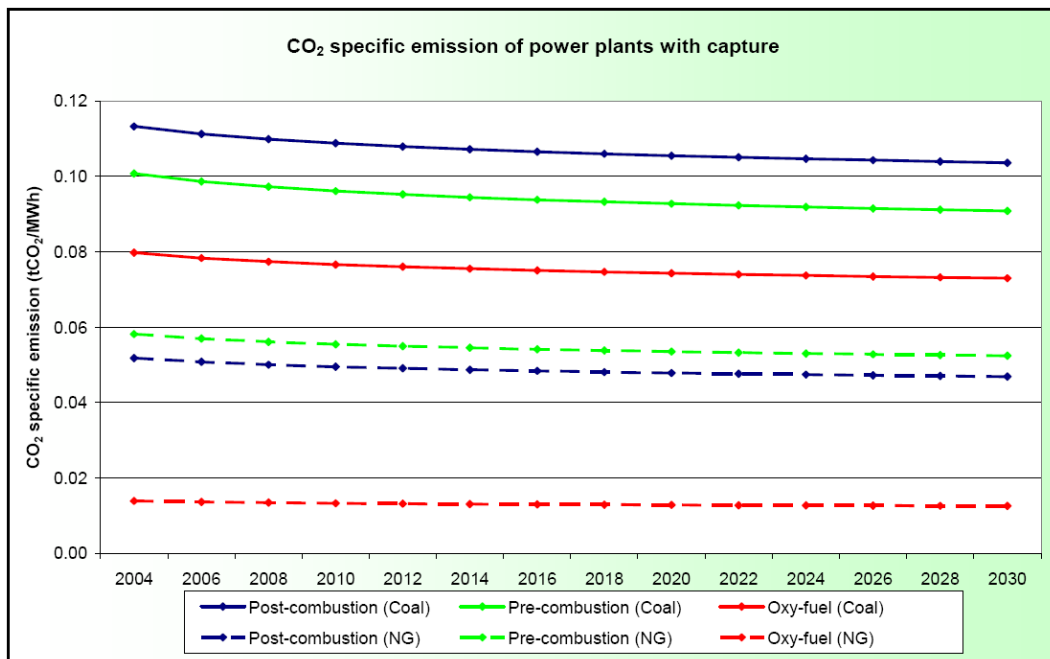


Figure 2-31: Evolution of the CO<sub>2</sub> specific emission of CO<sub>2</sub> capture technologies until 2030.

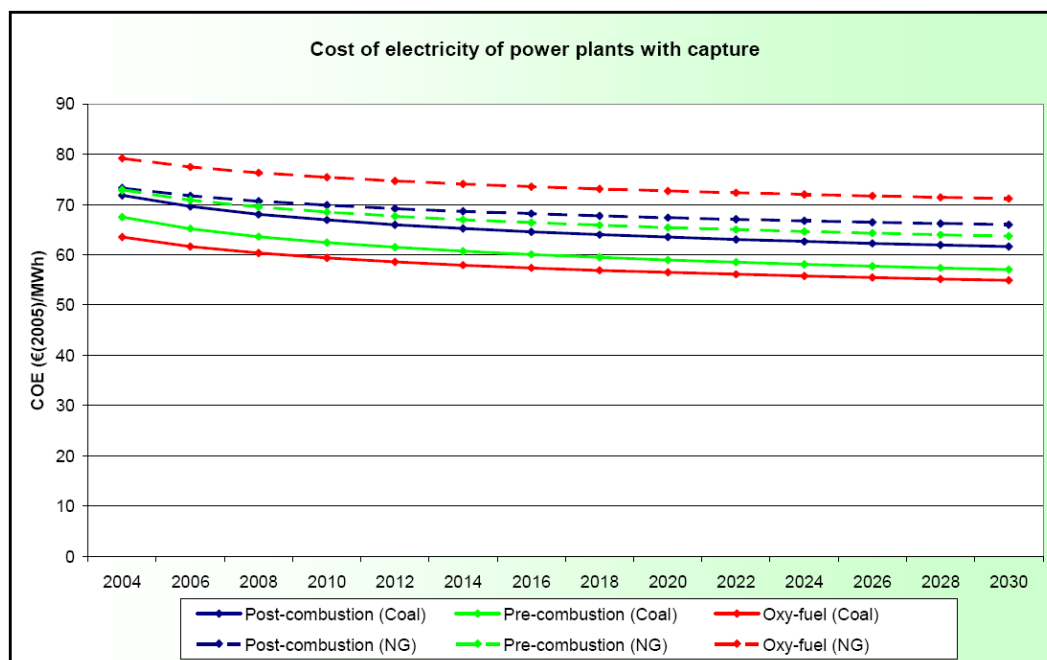


Figure 2-32: Evolution of the cost of electricity of CO<sub>2</sub> capture technologies until 2030.

## 2.6 References

- De Beer, J., J. Harnisch and M. Kerssemeeckers (2003) *Greenhouse Gas Emissions from Iron and Steel Production*, by order of the IEA Greenhouse Gas R&D Programme, report nr. PH3.30, September 2003.
- European Commission (2001) Reference Document on Best Available Techniques in the Cement and Lime Manufacturing Industries, December 2001.
- European Fertilizers Manufacturers' Association (2000) Best Available Techniques for Pollution Prevention and Control in the European Fertilizer Industry, Booklet No 1 of 8: Production Of Ammonia, June 2000.
- ICIS (2002) Fina Antwerp Olefins considers further expansion work, in: ICIS News 20/06/2002
- IEA GHG (1999) The Reduction of Greenhouse Gas Emissions from the Cement Industry, PH3/7, May, 112 pp.
- IEA Technology (1999) The reduction of greenhouse gas emissions from the oil refining and petrochemical industry, IEA Greenhouse Gas R&D Programme, June 1999.
- IEA (2002) Building the Cost Curves for CO<sub>2</sub> Storage: Part 1: Sources of CO<sub>2</sub>, Report PH4/9, by order of the IEA Greenhouse Gas R&D Programme, July 2002.
- IEA, 2004. Prospects for CO<sub>2</sub> Capture and Storage. Energy Technology Analysis. International Energy Agency, OECD/IEA France.
- IEA (2006) *IEA GHG CO<sub>2</sub> Emissions Database*, last update: October 2006.
- IPCC (2005) *IPCC Special Report on Carbon Dioxide Capture and Storage*, prepared by Working Group III of the IPCC, New York, United States.
- IPPC – Integrated Pollution Prevention and Control (2001) Reference Document on Best Available Techniques in the Cement and Lime Manufacturing Industries, December 2001.
- Matveev, V. A., I. S. Il'yashenko, A. B. Zhimalov, V. V. Maksimov and I. B. Smulyanskii (1991) *Rational fuel use in glass furnaces*, in: Glass and Ceramics, Volume 48, May 1991, pp. 185-188.
- Platts (2006) *World Electric Power Plant Database*, prepared by Platts, a division of the McGraw-Hill Companies, Inc., last update: March 2006.
- SenterNovem (2006) Dutch list of energy carriers and standard CO<sub>2</sub> emission factors.
- World Bank Group (2007) *Environmental Health and Safety (EHS) Guidelines*, April 2007, [www.ifc.org/ifcext/enviro.nsf/content/EnvironmentalGuidelines](http://www.ifc.org/ifcext/enviro.nsf/content/EnvironmentalGuidelines).
- ZEP, 2006. The final report from Working Group 1 Power Plant and Carbon Dioxide Capture. The European Technology Platform for Zero Emission Fossil Fuel Power Plants (ZEP).

## 3 Sink options

### 3.1 Storage site requirements

There are several aspects to consider when selecting a CO<sub>2</sub> storage site. Whether an aquifer formation has suitable reservoir properties depends on characteristics such as porosity and permeability, as well as on heterogeneities within the reservoir (e.g., faults, clay beds or cemented layers). Furthermore, formations with good sealing capacity should be present on top of the reservoir rock. Injection may occur in flat extended aquifers, however, onshore preference at least initially is given to closed structures. In these cases, the geometry of reservoir and seal rocks allow to trap or to confine the gas. As long as practical experience with underground CO<sub>2</sub> storage is missing, this additional safety measure may help to build confidence in the technique. Moreover, the reservoir should also be present below a certain depth (800 m), to ensure injection of CO<sub>2</sub> in a supercritical state. This is done both for efficiency and safety reasons (Bachu, 2003). The maximal depth is mainly determined by site-specific technical and economical factors. These conditions should be fulfilled in a favourable location, but that is outside the scope of the sink inventory.

### 3.2 Flanders region

This section presents a sink inventory with an overview of potential reservoir formations (aquifers) for the storage of CO<sub>2</sub> in the subsurface of Flanders. By lack of detailed reservoir data, the inventory is only a first step that specifies on which aquifers any future research in the field of geological CO<sub>2</sub> sequestration should focus.

In the central part of Flanders, the subsurface is constituted by the Lower Palaeozoic Brabant Massif. It is built up of deformed and metamorphosed rocks with low porosity and permeability. Therefore, this part of Flanders cannot be considered for storage. Suitable geological formations occur only southwest and northeast of the Brabant Massif.

To the southwest of the Brabant Massif, aquifer formations are present, but not at sufficient depth. Therefore, this region is not further elaborated in the sink inventory. Northeast of the Brabant Massif, several aquifer formations are present. This region is located in the provinces of Antwerp and Limburg. Geologically, it makes up the Campine Basin.

Based on currently available data (geological maps and layer models of the Belgian subsurface), four stratigraphic intervals were selected as potential reservoir formations within the Campine Basin (see also Laenen et al., 2004):

- the Upper Cretaceous to Palaeocene carbonates;
- the Lower Triassic sandstones;
- the Upper Carboniferous sandstones;
- the Lower Carboniferous carbonates.

Cenozoic aquifer formations are not considered, because they are located at a depth less than 800 m.

This section briefly discusses the geological setting for each of the four selected aquifers. An overview is given of the stratigraphy and of the lithology of the formations. Some petrographical characteristics may be presented as well. A summary is given of porosity and permeability data of the potential reservoir formation. The presence of sealing formations is discussed, as well as the possibility of trapping structures. A target area is outlined, where the potential reservoir formation is present at sufficient depth and where sealing formations occur. An assessment of the storage potential is given for each reservoir formation. If possible, a case study is presented to indicate the type and scale of structure that can be expected.

### 3.2.1 Methodology

#### **3.2.1.1 Outlining target areas**

The present sink inventory started from available geological maps and layer models of the Belgian subsurface. Based on this information, areas in which potential storage formations and proper sealing can be expected, were delineated, and potential storage aquifers were selected. For each of the selected formations, reservoir properties were considered, as well as characteristics of sealing formations and the potential presence of traps. These data were used to outline target areas for each of the selected formations. Within the target areas, the formations are present at sufficient depth, and appropriate sealing formations and traps are expected to occur. Zones with low and high potential can be distinguished, due to differences in depth or sealing.

A minimal depth of 800 m is postulated, to ensure injection of CO<sub>2</sub> in a supercritical state. It is anticipated that CO<sub>2</sub> will be in a supercritical state below this depth, based on pressure and temperature conditions observed in the Belgian subsurface (Laenen et al., 2004). CO<sub>2</sub> should be stored as a dense, liquid or supercritical phase, both for efficiency and safety reasons (Bachu, 2003). The efficiency of CO<sub>2</sub> storage in an aquifer depends on the amount of CO<sub>2</sub> that can be stored per unit volume of accessible pore space. The latter is directly related with the density of the CO<sub>2</sub> in the reservoir. Moreover, a higher density will add to the safety of the storage, as the upward migration of CO<sub>2</sub> is driven by buoyancy, and therefore depends on the density difference between the injected CO<sub>2</sub> and the original formation water.

No stringent maximal depth was defined for the inventory. The maximal depth for aquifer storage is mainly determined by technical and economical factors. These can only be determined under specific, site-dependent conditions. In general, development costs will increase with depth, whereas storage efficiency and safety can be expected to increase.

#### **3.2.1.2 Porosity & permeability measurements: different techniques**

It is important to know the techniques used to measure the porosity or permeability. For example, the permeability to air is much higher than the permeability to brine. Helium porosity values are higher than other measuring techniques, whereas point-counting data are lower. Combining the results of different techniques can lead to a wrong interpretation of the reservoir properties.

For the Triassic sandstones, point-counting data can be compared to data obtained by other techniques. Point-counting data are consistently lower. For the Bree Member, point-counting gives an average porosity value of 4.3%, whereas other techniques lead to an average of 14.7%. For the Bullen Member, point-counting data indicate an average porosity value of 12.2%, versus 14.9% for other techniques. For the Gruitrode Member, the average values are 2.6% and 11.2% respectively. These low values have a significant effect on the overall averages where all techniques are combined.

For the sandstones of the Neeroeteren Formation, point-counting indicates porosity values in the same range as data obtained by other techniques.

#### **3.2.1.3 Contribution of different lithologies**

For the Lower Triassic and Upper Carboniferous sandstones a further differentiation was made between different lithologies. Based on available core descriptions from a selection of wells, the percentage of each lithology within the designated formation was calculated. The following lithologies were distinguished: conglomerate, coarse sandstone, medium-grained sandstone, fine sandstone, siltstone, and mudstone. In the Upper Carboniferous sequence, coal layers were included as well.

Three boreholes were selected for the Upper Carboniferous sandstones (Neeroeteren Formation): KB146 (Neerglabbeek), KB161 (Opplabbeek-Louwelsbroek), and KB172 (Gruitrode-Ophovenderheide). Percentages were calculated separately in each borehole. The largest section of the Neeroeteren Formation was drilled in these boreholes. Two boreholes were selected for the Lower Triassic sandstones: KB172 (Gruitrode-Ophovenderheide) for the Gruitrode Member, and KB121 (Meeuwen-Bullen) for the Bullen Member. These wells contain the reference sections for both members. No detailed core descriptions were available for the Bree Member.

If porosity values are available for all lithologies, the percentages can be used to calculate a weighted average for the porosity. The contribution of each lithology can also be taken into account for calculations or estimations of reservoir properties.

#### **3.2.1.4 Calculation of accessible pore volume**

The storage capacity of the selected aquifers was calculated in 2 ways. The first method calculates the amount of CO<sub>2</sub> that can be stored in the aquifer formation per square kilometre. The second method focuses on selected potential storage sites. In this case, the geometry of the anticipated structures was included in the assessment.

For the assessment of the storage potential, the amount of CO<sub>2</sub> that can be stored as a free phase and by mineral trapping were taken into account. Dissolution trapping was not included, as this would involve the incorporation of a transport term to describe the interaction between the free CO<sub>2</sub> body and the surrounding formation water and movements of the formation water. This would involve a hydrological evaluation of the selected aquifers, which is out of the scope of the present inventory.

Mineral trapping is a relatively slow process. It is generally assumed that it will not contribute significantly to the potential during the injection. However, as mineral trapping chemically binds the injected CO<sub>2</sub>, it can add to the safety of the storage on the medium to long term (Bertier et al., 2006; Hitchon, 1996).

The parameters that are of primary importance to assess the storage potential per square kilometre are the thickness of the reservoir units, the reservoir pressure and temperature, the accessibility of the pore space and the irreducible water content. The latter parameter depends on the wetting properties of the injected fluid and the original formation water, as well as on the pore space characteristics of the host rock.

Pressure and temperature are a function of depth and therefore vary from location to location. Differences in depth were not taken into account directly. When the impact on diagenesis and compaction is neglected, it is however reasonable to assume that the rock-related reservoir properties of sedimentologically and diagenetically homogenous reservoir units that extend over a limited depth range, as is the case for the potential storage aquifers in Belgium, do not vary significantly. These parameters can be translated into accessible pore space. This factor is constant for a specific aquifer within a specific area. The storage potential at any site within the area is derived by multiplying the accessible pore space by the anticipated density of the CO<sub>2</sub>.

To evaluate the impact of lateral variations in reservoir properties, a detailed reservoir screening over the entire area of interest has to be carried out. To this end, sufficient observation points (e.g., wells, seismic data, outcrops) are needed. In Belgium, the necessary data for such an assessment of the potential storage aquifers is not available. The available data however do allow to get grip on the overall storage potential of the selected aquifers. Lateral variability in the reservoir properties was taken into account using Monte- Carlo runs on an Excel-based storage model (see below). The distributions for the reservoir properties were obtained from lithological and petrophysical observations on key wells within the target areas. The wells were selected based on the type and quality of the available data (e.g.,

detailed core description, petrographical data, petrophysical analyses). Moreover, they were chosen in function of the expected lateral variations in the reservoir properties (e.g., sedimentological or diagenetic trends).

For essential reservoir parameters such as porosity and permeability, the probability distributions used in the Monte-Carlo runs are in most cases based on a limited number of samples. The intra-well variability usually is higher than the expected lateral variability within a sedimentologically and diagenetically homogeneous region. In order to estimate the lateral variability in such a case, all samples from a homogeneous region were grouped. Subsets of 5 samples were taken at random from this group. Subsequently, the average values for each of the sub-groups were used to estimate the probability distribution used in the Monte-Carlo runs.

The results of petrophysical investigations were compiled and compared with lithological descriptions of key wells. In cases where sufficient petrophysical data are available, the samples were grouped per lithology and average properties were calculated for each of the lithologies. This led to a better understanding of the porosity and permeability distribution throughout the formation, allowed to delineate potential reservoir units (e.g., estimate contribution of pay zones). This also allows an assessment of the lateral variability of reservoir characteristics based on the core descriptions of the key wells.

The free storage capacity of the aquifer was calculated using the following formula:

$$SC = \rho_g \times S_g \times V \times \text{poro} \times (1 - \beta_r \times (2 \times P_h - P_r)) \quad (8)$$

with

SC = storage potential (kg)

$\rho_g$  = density of CO<sub>2</sub> under reservoir conditions (kg/m<sup>3</sup>)

$S_g$  = CO<sub>2</sub> saturation for the corresponding capillary pressure (no units)

V = rock volume of the reservoir (m<sup>3</sup>)

Porosity = effective porosity of the reservoir (m<sup>3</sup>/m<sup>3</sup>)

$\beta_r$  = matrix compressibility of the reservoir (m<sup>2</sup>/N)

$P_h$  = normal hydrostatic pressure (Pa)

$P_r$  = reservoir pressure (Pa)

Gas saturation, density of the CO<sub>2</sub> and pore volume all depend on the pressure within the reservoir. Under static conditions, the pressure at the CO<sub>2</sub>-water contact in an infinite or unconfined aquifer can be taken to equal the corresponding hydrostatic pressure for the completely water-filled reservoir. The pressure within the CO<sub>2</sub> column is defined by the pressure at the CO<sub>2</sub>-water contact, the distance towards the CO<sub>2</sub>-water contact and the density of the CO<sub>2</sub>.

The density of the CO<sub>2</sub> is also function of the reservoir temperature, and hence of the heat flux through the reservoir. The latter can be subdivided in a conductive and a convective heat flux. The sum of the two through the reservoir was kept constant and equals the regional heat flux estimated from available temperature measurements. The convective heat flux was derived from the density difference over the CO<sub>2</sub> column, using an iterative optimization procedure. The diffusive heat flux was derived by subtracting the convective from the total heat flux.

The density of the CO<sub>2</sub> was calculated using the equation of state published by Span & Wagner (1996). For all cases, the density at the top of the reservoir and at the CO<sub>2</sub>-water contact was calculated. The lowest of the two values was taken as CO<sub>2</sub> density under reservoir conditions. Temperatures and pressures were calculated using linear temperature-depth and pressure-depth relationships.

For the Buntsandstein Formation and the Carboniferous Limestone Group, the storage volume within a specific antiformal structure was calculated. The studied reservoirs are the Verloren

Kamp structure (Buntsandstein) and the Poederlee dome (Carboniferous Limestone Group). Both structures were recognized on seismic profiles. The Poederlee reservoir has been explored by well 030W0371. For both sites, a general geometrical model was built based on the available seismic data. Reservoir properties were derived from existing deep wells drilled in the structure or in the vicinity. To assess the storage potential, the same approach was used as for the entire aquifers.

### 3.2.1.5 Calculation of injectivity

The injectivity of the reservoirs is an important factor with respect to their CO<sub>2</sub> storage capacity. A throughout assessment of the injectivity should include the development of a numeric reservoir model of each of the potential CO<sub>2</sub> storage sites. At the moment, this is not possible due to lack of proper geometric and petrophysical data. Without this data, numeric models can only be approximate at the best. The necessary information can only be obtained by new geophysical exploration (mainly seismic acquisition), the drilling of deep wells and the performance of stem and reservoir tests.

Alternatively, analytic models have been developed that can be used for a first assessment of the behaviour a reservoir. These models make a number of assumptions to simplify the flow equations. For the model used here, the most important assumptions are:

- the reservoir is homogeneous and isotropic
- the reservoir has an infinite horizontal extend
- the reservoir is fully confined and there is no recharge or leakage
- flow in the aquifer complies with Darcy's law
- the well is operated in a permanent flow regime.

Under these assumptions, the relation between pressure at the bottom of a well and the injection or extraction rate for radial flow is given by (Gaussens, 1986):

$$P_f^2 - P_g^2 = \frac{\mu \times Q}{\pi \times h \times k} \times \left[ \ln\left(\frac{r}{a}\right) + S + S_p \right] \quad (9)$$

where

$P_f$  = pressure at the bottom of the well (Pa)

$P_g$  = pressure in the gas reservoir (assumed to be uniform) (Pa)

$Q$  = rate (m<sup>3</sup>(n)/s)

$a$  = well radius (m)

$h$  = height of the reservoir (m)

$\mu$  = viscosity of the gas (Pa.s)

$r$  = flow radius (m)

$k$  = gas permeability (m<sup>2</sup>)

$r$  = pressure influence radius (m)

$S$  is the dimensionless skin factor of the well.  $S_p$  is a term to correct for the pressure drop due to incomplete penetration of the gas reservoir.  $S_p$  was calculated using the analytical solution derived by Muskat (Gaussens, 1986):

$$S_p = (1 - R_g) * \ln(R/a) / R_g \quad (10)$$

where

$$R_g = \frac{h_p}{h} \times \left( 1 + 7 \times \sqrt{\frac{a}{2 \times h_p}} \times \cos\left(\frac{h_p}{h}\right) \right) \quad (11)$$

$h_p$  = penetration height of the well

The assumption that the well is operated in a permanent flow regime is met if at a finite distance from the well the pressure stays constant. In case on an underground gas storage,

there is no guaranty that this situation will occur. On the contrary, the calculations show that the influence zone will gradually extend with time. However, as a first approximation, the disturbed zone of an injection/production at a constant rate can be calculated using an adapted form of the Gray formula:

$$R_t = 1.5 \times \sqrt{K \times t} \quad (12)$$

where

$R_t$  = radius of the disturbed zone

$t$  = time elapsed since the start of injection / production

$K$  = diffusivity of the gas-saturated interval and is defined as:

$$K = k_g / (\varphi_g \times \mu_g \times \beta_g) \quad (13)$$

where

$k_g$  = permeability of gas

$\varphi_g$  = gas saturated porosity

$\mu_g$  = viscosity of the gas

$\beta_g$  = compressibility of the gas

In the light of these above mentioned assumptions and the simplification with respect to the influence zone of the injection/extraction, it is clear that the results obtained by equation 9 should be used with care.

The radial equation can be used to estimate the injectivity or productivity of a well under a constant injection or extraction regime. The productivity index is defined as:

$$I_p = \frac{P_f^2 - P_g^2}{Q} \quad (14)$$

where

$P_f$  = pressure at the base of the well (Pa)

$P_g$  = pressure in the gas reservoir (Pa)

$Q$  = production or injection rate (m<sup>3</sup>/s)

The advantage of this definition is that the productivity index is independent of the pressure and allows an easy evaluation of the flow regime. For darcian flow,  $I_p$  is a linear function of the rate.

For a first-estimate calculation of the injectivity for under other conditions than those used in base scenarios, an alternative production index was calculated:

$$PI = Q / (P_f - P_g) \quad (15)$$

The reported values are normalized to 1 m filter length.

For each potential reservoir level, the injectivity was calculated for a favourable, an intermediate and a poor storage scenario. For all cases it is assumed that the filter height is 50, that the injection well has a diameter of 200 mm and zero skin, and that the compressibility of water is  $5 \times 10^{-10} \text{ m}^2/\text{N}$ . The petrophysical data used for the assessments are summarized in the discussion of the various reservoir levels.

### 3.2.2 Upper Cretaceous to Palaeocene carbonates

The Upper Cretaceous to Lower Palaeocene (Danian) carbonate sequence, known from the classical outcrops around Maastricht, extends also in the subsurface of northern Belgium under a thick Cenozoic cover. The Upper Cretaceous strata gradually dip to the north and unconformably overlie Permian to Jurassic, Devonian-Carboniferous or Cambrian to Silurian rocks. Generally the stratigraphic hiatus increases towards the south.

Because of the minimal cut-off depth of 800 m in this sink inventory, only a very limited area of the present carbonate sequence in North Belgium can be selected as target area (fig. 3-1).

### 3.2.2.1 Brief description of geological setting

Within Flanders, the CO<sub>2</sub> storage potential of the Cretaceous to Palaeocene sequence is restricted to two geological regions (fig. 3-1):

The **Roer Valley Graben**: this zone in the north-eastern extremity of Belgium is separated from the *Campine Basin* by the *Feldbiss fault zone* which brings the top of the Cretaceous below the minimal depth of 800 m. In the Molenbeersel borehole (KB198, the only borehole reaching the base of the Cretaceous in the Roer Valley Graben) the top of the Cretaceous is situated at a depth of 1220 m, and the Cretaceous limestone sequence has a thickness of about 60 m. The reduced total thickness of the Cretaceous in the Roer Valley Graben in comparison with the Campine Basin is due to the fact that the Roer Valley Graben was inverted (uplifted block) during the Late Cretaceous. It was flooded by the sea only by Late Maastrichtian times. The uplifted Roer Valley Graben generated a detrital input to the Campine Basin which resulted in a sandy Aken (Santonian) and silty Vaals Formation (Campanian) in the eastern Campine Basin.

The **Campine Basin**: geographically this area contains roughly the Antwerp and Limburg Campine area and is limited to the south and west by the Brabant Massif. To the northeast it is bordered by the Roer Valley Graben. As the Cretaceous sequence gradually dips to the north, the sequence deepens in that direction. In the Antwerp Campine area, Cretaceous strata are present at a depth of 600 to 800 m, with a thickness of up to 300 m. In the Meer borehole (KB149; Vandenberghe et al., 1988), the northernmost deep borehole in Belgium, the top of the Cretaceous was reached at a depth of 808 m, with a thickness of 378 m.

### 3.2.2.2 Stratigraphy and lithology

For the Maastricht type area a very detailed lithostratigraphic subdivision of the Cretaceous sequence is available (Felder & Bosch, 2001). A brief overview of lithostratigraphic units in use in Belgium is given by Robaszynski et al. (2001). As for the Campine Basin and Roer Valley Graben only subsurface data (destructive boreholes and geophysical well logs) are available, a less detailed stratigraphic subdivision can be drawn up for this area. A recent study by Dusar and Lagrou (2007) presents a state-of-the-art overview and revision of the subsurface lithostratigraphy of the Cretaceous in northern Belgium (table 3-1).

In the eastern part of the Campine Basin, along the boundary faults of the Roer Valley Graben, the Cretaceous sequence starts with sand of the Aken Formation. The overlying Vaals Formation consists of glauconite-bearing marly sand, gradually shifting into silty marl towards the west. In the Antwerp Campine area, it is difficult to distinguish the Vaals Formation from the overlying Gulpen Formation (Zeven Wegen Member), which is made up of white chalk. In the east also the Zeven Wegen chalk Member is slightly sandy, but it is still easily distinguishable as a characteristic white chalk facies ('Schreibkreide'). Coarse-grained calcarenites are present in the Maastricht and Houthem formations.

Within the Roer Valley Graben, only 60 m of Cretaceous sediments are present. They are calcarenites of the Maastricht and Houthem formations.

### 3.2.2.3 Petrophysics and petrography of potential reservoirs

The Upper Cretaceous to Lower Palaeocene in North Belgium can be subdivided in 3 lithological units:

Coarse to fine calcarenites of the Houthem and Maastricht formation. These sediments are of Maastrichtian to Palaeocene (Danian) age. They make up the Upper Cretaceous aquifer.

Fine calcarenites, chinks and marls of the Gulpen Formation, Campanian to Maastrichtian age. These are considered to form an aquitard.

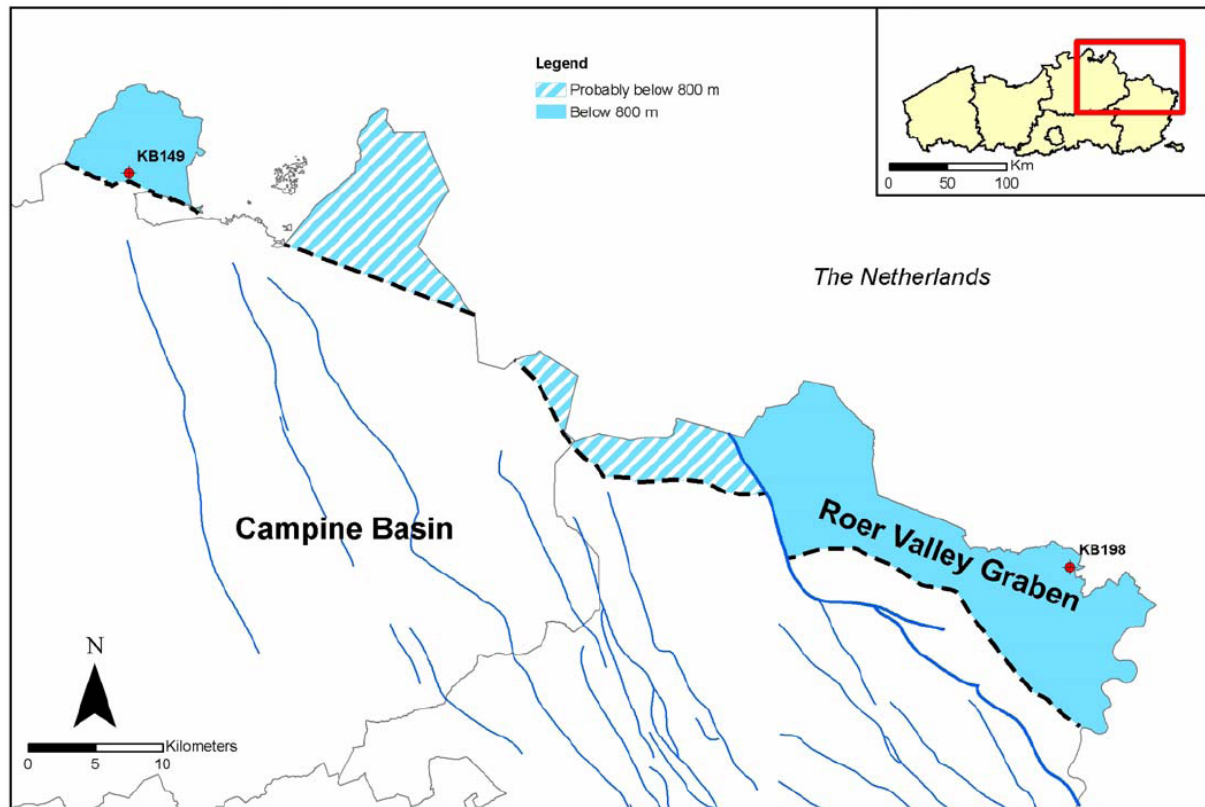


Figure 3-1: The target area of the Upper Cretaceous in the Campine Basin and Roer Valley Graben. Only two boreholes reached the top of the potential reservoir formation below 800 m depth: Molenbeersel (KB198) and Meer (KB149). Blue area: present at a depth of 800 m or more with high confidence or proven by boreholes; hatched blue area: expected to be present at a depth of 800 m or more.

Table 3-1: Cretaceous stratigraphic subdivision of the Limburg and Antwerp Campine area (after Felder, 2001 ; Robaszynski et al., 2001).

<b>Chronostratigraphy</b>	<b>Formation</b>	<b>Member</b>	<b>Brief lithological description</b>
<i>Danian</i> (from 61.7 ± 0.3 Ma)	Houthem		Pale beige soft fine to coarse-grained calcarenite
<i>Maastrichtian</i> (from 70.6 ± 0.6 to 65.5 ± 0.3 Ma)	Maastricht		Pale soft coarse-grained calcarenite
			Pale soft fine calcarenite with silex at the base
			Pale beige fine silex-bearing hard calcarenite
	Gulpen	Lanaye-Lixhe	Pale grey very fine calcarenite with thick silex bands White fine-grained chalk with many black silex bands
<i>Campanian</i> (from 83.5 ± 0.7 to 70.6 ± 0.6 Ma)	Vaals	Vijlen	Mainly pale grey silty chalk with fine silex (partly channel fill)
		Beutenaken	Grey marl Grey marly chalk
		Zeven Wegen	White fine-grained chalk
		Upper	Glauconite-bearing fine sand and silt (east) – marl (west)
<i>Santonian</i> (up to 83.5 ± 0.7 Ma)	Aken	Lower	Green clayey glauconite-bearing sandy marl
			Quartz sand with lignite

Table 3-2: Compilation of porosity and permeability measurements from laboratory-results on cores. For the Campine Basin the measurements are coming from the Loenhout area, for the Roer Valley Graben from the Molenbeersel borehole (“classical” porosity and permeability measurements, not further specified).

<b>Lithological unit</b>	<b>Campine Basin<sup>1</sup></b>	<b>Roer Valley Graben<sup>2</sup></b>
<i>Houthem and Maastricht Aquifer</i>	Effective porosity: 19-37% Horiz. perm: 3-140 mD Max. thickness: 67.5 m	Porosity: 10-20% Permeability: 0.01 to 12 mD Thickness: 60 m
<i>Gulpen Aquitard</i>	Effective porosity: 28-33% Horiz. perm: 0.3-8 mD Thickness: 270.5 m	Not present
<i>Vaals and Aken Aquifer</i>	Vaals: Effective poro: 19-29% Horiz. perm: 0.5-45 mD Thickness: Vaals 40 m; Aken: not present below 800 m	Not present

<sup>1</sup> Reference borehole for Campine Basin: KB149 Meer.

<sup>2</sup> Reference borehole for Roer Valley Graben: KB198 Molenbeersel.

Marls, chalks and sands of the Vaals and Aken formations. These are sediments of Santonian to Campanian age. Locally, the sands may constitute an aquifer.

Given the minimum cut-off depth of 800 m and the petrophysical properties of the different lithostratigraphic units (table 3-2), only the Houthem and Maastricht calcarenites can be taken into account for CO<sub>2</sub> storage. The calcarenites occur below the cut-off depth in the Roer Valley Graben and in the north of Belgium (area of Meer borehole). The thickness of the Houthem and Maastricht calcarenites in the Roer Valley Graben is 60 m (Molenbeersel borehole), whereas in the north of Belgium it is 67 m (Meer borehole).

The sands and silts of the Aken and Vaals formations also have favourable reservoir properties in the eastern part of the Campine Basin, along the boundary faults. However, they are situated in the depth interval of 450 till 600 m. Therefore, they cannot be taken into account for geological CO<sub>2</sub> storage under supercritical conditions.

The Gulpen Formation consists of chalks with high porosity (30-40%), but the permeability is low. It can be considered as a tight formation that will act as an aquitard and that can even act as a chemical trap for underlying potential reservoirs.

#### a) Petrography

##### 1. Calcarenites

Petrographically the yellowish calcarenite is a weakly cemented coarse to fine-grained bioclastic grainstone, consisting of irregular, poorly sorted skeletal fragments of echinoids, molluscs, brachiopods, bryozoa, annelides and foraminifera. The average grain size of the bioclasts is about 150 µm.

The calcarenites have a high pore volume (40%). Porosity mainly is intergranular type with intragranular porosity due to pores in the bioclasts and fossil fragments (Dubelaar et al., 2006). The cement mainly is syntaxial sparite preferentially formed around echinoid bioclasts. Two discontinuities of sedimentary origin often occur in the limestone and will influence the reservoir properties of the rock sequence. *Silicifications* in certain horizons cement the bioclasts and fill the pore volume, with even zero porosity for the flint layers. *Hardgrounds* are bored, often encrusted, discoloured horizons developed on the sea floor and point to an interruption in sedimentation (hiatus). The higher degree of cementation in these horizons leads to lower porosity and permeability values. Both hardgrounds and silicified horizons can

result in reservoir compartmentalization, and have to be taken into consideration in the reservoir evaluation.

## 2. Chalk

Chalk is a soft, fine-grained, white-to-greyish variety of limestone. Chalk is composed of shells of such minute marine organisms as foraminifera, coccoliths, and rhabdoliths. The purest varieties contain up to 99% calcium carbonate in the form of the mineral calcite. In the Campine Basin, the chalks are sandy or silty to the east (direction Roer Valley Graben), whereas to the west, they become more marly. Marl is a mixture of clay and calcium carbonate (35-65%). They are characterized by a low to very low permeability and can be considered to be tight.

### b) Karstification of the Cretaceous

The Cretaceous in Belgium is an important aquifer used for production of drinking water. The top layers of the calcarenites of the (Houthem and) Maastricht Formation are known for their high permeability, which decreases fast with depth. Traditionally, this phenomenon is attributed to a fissured top of the Cretaceous, with closed fissures at greater depth. However, many observations in the outcrop zone and underground quarries point to karstification in the top of the Cretaceous as reason for the augmentation of the permeability. Not only at shallow depth but also in a seismic study in the Mol-Dessel area at a depth of about 570 m, sinkholes with a width of 500 m and a depth of 30 m are recognized (NIRAS/ONDRAF, in prep.). This karstification might also be present below the 800 m cut-off depth, and can contribute significantly to the overall reservoir properties.

#### 3.2.2.4 Structure and sealing

In the Campine Basin, the relatively undisturbed Cretaceous to Lower Palaeocene carbonate sequence is slightly dipping to the north. If any structures are present, these will be flat extended domes. Considering the uncertainty in time-depth conversion in the seismic profiles, flat structures need to be handled with caution.

On the other hand, the Roer Valley Graben is an intensively disturbed area with NW-SE oriented faults. Roll-over structures bounded by faults are recognized on seismic lines perpendicular to the faults (campaign PLM84; Demyttenaere, 1989). However, the closure of the structures remains to be proven by seismic lines parallel to the faults. The faults should displace the reservoir in such a way that it is juxtaposed against an impermeable rock. Moreover, the fault plane has to be sealed by smearing of the clay-rich formations.

Formations sealing the Cretaceous aquifers are situated in the Cenozoic sequence. Three impermeable clay intervals can be distinguished, belonging to the Landen, Ieper and Rupel groups.

Table 3-3: Average useful reservoir volume of the chalks.

Area	Surface (km <sup>2</sup> )	Reservoir thickness (m)	Porosity (%)	Permeability measured (mDarcy)	Permeability used in model (mDarcy)	Accessible porosity* (10 <sup>6</sup> m <sup>3</sup> /km <sup>2</sup> )
Campine Basin	200	65	29.3 ± 8.5	65 ± 59	0.15 x e <sup>0.20xporo</sup>	10.6: 8.0 – 13.2
Roer Valley Graben	200	60	14.5 ± 4.7	2.5 ± 4.4	1.14 x 10 <sup>-3</sup> x e <sup>0.524xporo</sup>	0.11: 0 – 0.42

\* mean value and 10% and 90% percentiles

Table 3-4: Injectivity of the chalks in the Campine basin for three porosity and permeability conditions based on the analytical model described in section 3.2.1.5.

<i>Scenario</i>	$\Phi$ (%)	<i>K (mDarcy)</i>	<i>PI</i> ( $m^3(n)/s.bar.m$ )	<i>Ip (bar<sup>2</sup>.h/m<sup>3</sup>)</i>
<i>high</i>	37	140	0.049	0.026
<i>medium</i>	29	65	0.023	0.055
<i>low</i>	20	5	0.00196	0.665

### 3.2.2.5 Outline of target area

In the north of Belgium, the top of the potential carbonate reservoir is encountered at 808 m depth in the Meer borehole (KB149; fig. 3-1). According to data from the geological atlas of the deep subsurface of The Netherlands (TNO-NITG, 2001), the Cretaceous also occurs at a depth of more than 800 m in a band close to the Dutch border (hatched areas on the map). In a large part of the Roer Valley Graben, the depth is sufficient as well. The Cretaceous is only encountered in one borehole (KB198, Molenbeersel). In all areas, sealing formations are present within the Cenozoic sequence (clay layers).

### 3.2.2.6 Reservoir volume

Table 3-3 shows the estimated storage potential per square kilometre of the Cretaceous chalks in the northern part of the **Campine Basin** and in the Roer Valley Graben. Average total porosity for the Houthem and Maastricht formations measured on selected wells is  $29.3 \pm 8.5\%$ . This porosity also includes non-accessible, intragranular porosity. Based on the porosity - permeability relationship observed in the Merksplas well, samples with a porosity of less than 9.5% have a permeability of less than 1 mDarcy, and hence should be classified as poor reservoir rocks. Packages with such a low permeability were excluded from the volume assessment. The accessible pore volume of the Houthem and Maastricht formations within the Campine area is estimated to be about  $11 \times 10^6 m^3/km^2$ . The estimates span a large range due to the uncertainty on the effective porosity.

Notwithstanding the moderate to high porosities, the permeability of most of the samples taken at Molenbeersel (**Roer Valley Graben**) are low to very low. Samples with a porosity less than 17% reveal permeability values below 1 mDarcy. It is therefore assumed that a large part of the porosity will not be accessible under the anticipated reservoir conditions. The accessible pore volume is estimated at a low  $0.11 \times 10^6 m^3/km^2$ .

### 3.2.2.7 Injectivity

The injectivity for the chalks in the Campine basin was estimated for a reservoir at a depth of -1000 m with a productive interval of 50 m. A high, medium and low injectivity scenario was calculated based on the variability in porosity and permeability observed in the Merksplas well. The results are summarized in table 3-4. In the high and medium scenario, 1 well would be sufficient to store well over 1.000.000 ton/CO<sub>2</sub> per year.

### 3.2.2.8 Summary

The relatively limited surface of the target area and the lack of sufficiently large, closed structures (traps) makes the Cretaceous carbonate aquifer a less important target for CO<sub>2</sub> storage in Flanders.

The tight Gulpen chalks can contribute to the (chemical) sealing of deeper seated reservoirs. Within the Campine Basin, the high accessible porosity and moderate to high permeability results in an average storage potential of  $6.5 \times 10^6$  ton per square kilometre (for density under reservoir conditions of 610 kg/m<sup>3</sup>).

For an average chalk reservoir within the Campine Basin, injectivity is sufficiently high to allow the storage of well over 1.000.000 ton/CO<sub>2</sub> per year using a single well.

### 3.2.3 The Lower Triassic sandstones

Rocks of the Triassic contain economically important hydrocarbon reservoirs in Western Europe. For instance, the Waalwijk gas field in the Netherlands is situated in Triassic sandstones.

#### 3.2.3.1 Brief description of geological setting

Permian to Lower Jurassic strata subcrop in the Roer Valley Graben and the north-eastern Campine Basin (Delmer, 1963; Langenaeker, 2000), extending into the Netherlands and Germany (fig. 3-2). The total preserved thickness attains 550 m in the Campine Basin and about 1500 m in the Roer Valley Graben. Seismic surveys revealed that the Permian to Jurassic sequence unconformably overlies the Carboniferous coal measures and gradually wedges out toward the south below the Cretaceous unconformity (Langenaeker, 2000; Duser et al., 2001).

The only rock sequence of interest for aquifer storage in the Permian to Jurassic sequence is the Lower Triassic Buntsandstein Formation (table 3-7).

#### 3.2.3.2 Stratigraphy and lithology

A correlation scheme of the Permian to Jurassic sequence in the north-eastern part of the Campine Basin and the adjacent Roer Valley Graben is given in figure 3-3.

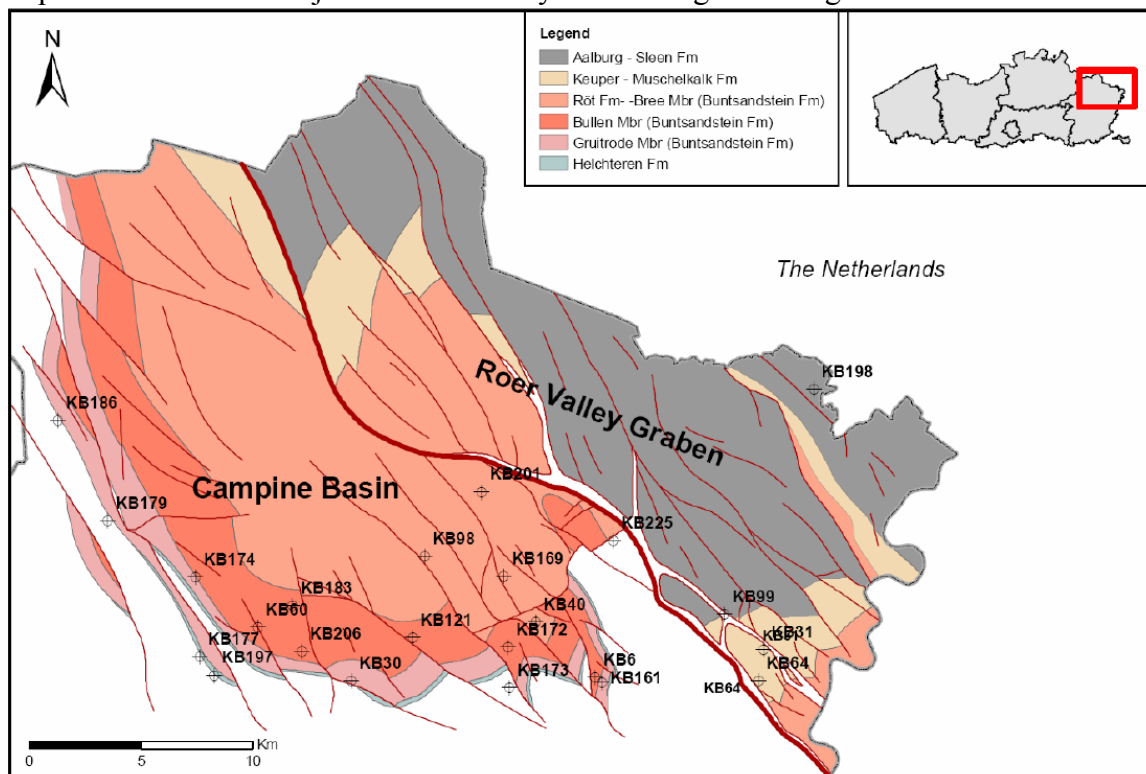


Figure 3-2: Pre-Cretaceous subcrop map of the Permian to Jurassic formations in the Campine Basin and Roer Valley Graben. The boreholes reaching the Triassic sequence are indicated (modified after Wouters & Vandenberghe, 1994).

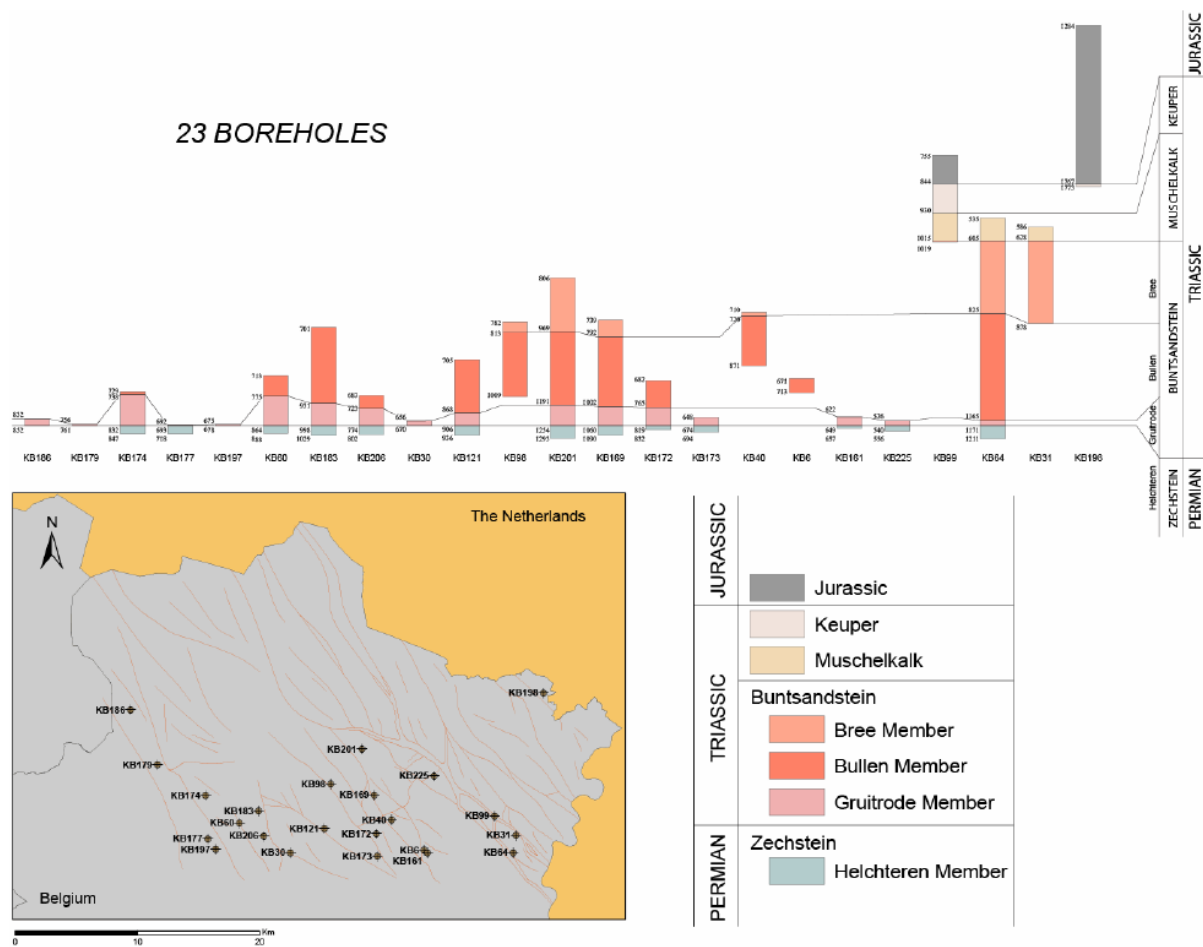


Figure 3-3: Correlation scheme for the Permian-Triassic-Jurassic in the Campine (modified after Langenaeker, 2000).

The Permian *Helchteren Formation* is made up of silty carbonates alternating with marly mudstones and siltstones (Dusar et al., 2001). The upper part of the formation consists of silty mudstones, sandstone beds, and massive claystones. Locally, a pebble layer is present at the base. The thickness amounts up to 39 m.

A sequence of reddish, sandy siliclastic rocks overlies the Helchteren Formation. They are grouped within the Buntsandstein Formation, which is of Early Triassic age (Langenaeker, 2000; Dusar et al., 2001). These sediments were deposited in a floodplain with a gradual change from fining-upwards channel fills to coarse floodsheets with intercalated clayclayas. The formation is of Early Triassic age. In the Campine Basin, the Buntsandstein Formation is divided into three members. From bottom to top, these are the Gruitrode, Bullen and Bree Members.

The *Gruitrode Member* consists of an alternation of red thick-bedded siltstones and sandstones, with a clear increase in grain size toward the top. The grain size of the sandstones varies from very fine to very coarse (conglomerates). The thickness of the member varies between 38 and 94 m.

The *Bullen Member* consists of a monotonous sequence of homogeneous medium- to coarse-grained sandstones and conglomerates. In places, the sandstone are strongly calcareous. The member has a thickness between 210 and 228 m.

The lower part of the *Bree Member* is dominated by shales. It is made up of a centimetre to meter-scale alternation of shales and very fine to medium-grained sandstones. The middle part of the member consists of a medium- to coarse-grained sandstone, locally calcareous.

The upper part of the Bree Member contains more claystones. The top of the Bree Member is only found in 2 boreholes, KB64 and KB31 (Rotem and Elen), both situated in the western part of the Roer Valley Graben. The thickness of the Bree Member is circa 250 m.

The *Röt Formation* is only present in the Roer Valley Graben (Dusar et al., 2001). It is of Middle Triassic age and is made up of red, partly bleached sandstones and shales, partly with gypsum nodules and veins, with subordinate gypsum beds and grey marls. It is up to 125 m thick.

The overlying *Muschelkalk Formation* consists of an alternation of carbonates, evaporates and fine-grained detrital rocks. It is approximately 85 m thick. The *Keuper Formation* is made up of variegated mudstones alternating with clayey dolostones, with anhydrite and gypsum beds and nodules. Its thickness attains 86 m.

The *Sleen Formation* is only present in the Roer Valley graben. It is made up of locally sandy or silty claystones. It is up to 30 m thick.

The *Aalburg Formation* is of Early Jurassic age (Hettangian to Pliensbachian). It consists of locally sandy or silty mudstones and marls. The total thickness of the clay-rich Jurassic deposits amounts to circa 400 m.

The top of the Permian-Triassic is pulverized into loose sand because of pre-Cretaceous weathering. This observation is general in the Campine Coal Basin. This weathered top can be expected to have a very high permeability, however situated below the sandy Cretaceous of the eastern mining district with poor sealing characteristics.

### **3.2.3.3 Petrophysics and petrography of potential reservoirs**

#### *a) Petrography*

Buntsandstein strata mainly consist of medium-grained sublithic arenites (Bertier et al., 2006). The mineralogical composition is given in table 3-5. This reservoir is composed of red beds alternating with diagenetically bleached zones. The red colour results from the presence of Fe oxy/hydroxides in grain coatings. Bleaching occurred during circulation of acid fluids in more permeable horizons, reducing the Fe oxides (Muechez et al., 1992).

Haematite coatings in red beds and illite coatings in bleached zones block pore throats and reduce permeability. Carbonate cements and authigenic quartz occlude porosity. Dissolution of feldspars and micas slightly increased porosity. However, part of the secondary porosity was filled with alteration products such as kaolinite (Bertier et al., 2006).

#### *b) Porosity and permeability data*

In general, the Bree and Bullen members are considered as aquifers, whereas the Gruitrode Member is considered as a possible aquifer (table 3-6). The reservoir properties of the *Gruitrode Member* vary strongly. In borehole KB172 (Gruitrode - Ophovenderheide) porosity and permeability of 11 samples were measured. The minimal and maximal values for porosity and permeability are respectively 5.6 en 19.1%, and 0.6 en 367 mDarcy. Permeability values above 250 mDarcy point to very favourable reservoir properties and are mainly found in the coarser levels. It concerns a sequence of mainly low permeable sandstones with permeable levels.

Because of the lack of clay and shale layers in the *Bullen Member*, the porosity and permeability are relatively homogenous. In borehole KB201 (Bree), porosity values between 4 and 21% were measured. The permeability varies between 2 and 74 mDarcy. The lowest values are caused by the presence of carbonate cement between the sand grains (Muechez et al., 1992).

Table 3-5: Average mineralogical composition of sandstones of the Buntsandstein Formation, based on detailed petrographical analysis on 32 samples (Bertier, 2004).

<i>Mineral phase</i>	<i>Percentage</i>	<i>Mineral phase</i>	<i>Percentage</i>
<i>Quartz (monocrystalline)</i>	30.9	Chlorite	0.0
<i>Quartz (polycrystalline)</i>	15.9	Clay minerals	1.6
<i>Quartz (microcrystalline)</i>	0.4	Fe oxi/hydroxides	5.8
<i>Quartz (authigenic)</i>	4.8	Ankerite	12.9
<i>Lithic fragments</i>	8.2	Siderite	0.2
<i>Feldspar</i>	5.3	Carbonates	2.8
<i>Mica</i>	0.5	Coal fragments	0.0
<i>Kaolinite</i>	0.4	Opaque minerals	0.1
<i>Illite</i>	2.7	Porosity	7.4

Table 3-6: Compilation of porosity and permeability measurements of the Buntsandstein Formation. Data are from laboratory analyses on samples from several boreholes (KB121, KB172, KB201). Different techniques have been combined.

<i>Member</i>	<i>Porosity (%)</i>				<i>Permeability (mDarcy)</i>			
	<i>Max</i>	<i>Min</i>	<i>Average</i>	<i>n</i>	<i>Max</i>	<i>Min</i>	<i>Average</i>	<i>n</i>
<i>Bree</i>	20.1	3.3	12.8	11	296.4	d.l.	43.5	9
<i>Bullen</i>	26.0	3.7	13.9	29	96.2	1.7	26.5	15
<i>Gruitrode</i>	19.1	0.0	10.3	35	367.0	d.l.	38.3	27

d.l.: below detection limit

Porosity and permeability data from the *Bree Member* are scarce and are all from the base of the member. Porosity fluctuates around 20% and permeability values up to 296 mDarcy were measured. The middle part of the member has an important intergranular porosity and a relatively high permeability.

### c) Contribution of different lithologies

For calculations of reservoir properties and storage capacity, the proportions of different lithologies within the reservoir formation were taken into account. For the Gruitrode and Bullen members, these proportions can be estimated based on core descriptions (table 3-8). For the Gruitrode Member, descriptions are taken from the KB172 borehole (Gruitrode-Ophovenderheide; Dusar et al., 1987). For the Bullen Member, borehole KB121 (Meeuwen-Bullen) was used. These boreholes contain the reference sections for both members. No detailed core descriptions are available for the Bree Member.

The available porosity and permeability data reveal a clear correlation (fig. 3-4). The correlation with the lithologies described in the well and core descriptions is less clear. In general, the finest lithologies, i.e., mudstones and siltstones, have the lowest porosities and permeabilities. Within the sandstone classes and for the conglomerates, the porosity and permeability values vary widely. The finest sandstone classes, i.e. fine and medium sandstones, reveal the largest variability. They contain samples that porosities that are similar to those observed in the mud- and siltstones, as well as the most porous and permeable samples. The conglomerate samples plot on the low side of most sandstones samples.

The large variability observed in the samples indicate that the porosity and permeability of the sandstones is mainly controlled by diagenesis. The sedimentology clearly is of secondary importance. This has important consequences to the delineation of potential the reservoir units. It is clear that the entire sandstone sequence can serve as reservoir units that will be separated from each other by the mud- and siltstones layers. In addition to these

sedimentological aquitards, diagenetic barriers may be present within the sandstone sequence as well.

### 3.2.3.4 Structure and sealing

The subcrop area of the Buntsandstein Formation can be subdivided in 2 areas (fig.3-2):

- An eastern area where it is covered by the Muschelkalk Formation, the Keuper Formation and Jurassic shales (Aalberg and Sleen formations);
- A western area where the Buntsandstein is covered by the Röt Formation or directly underlies the unconformity at the base of the Cretaceous.

In the eastern area the Muschelkalk, Keuper and eventually Aalburg and Sleen Formations guarantee a good sealing of any potential Buntsandstein reservoir. This area largely coincides with the Roer Valley Graben. Only some smaller areas are omitted where the Jurassic and Muschelkalk to Keuper sequence is absent.

In the western area, which is located outside the Roer Valley Graben, the Buntsandstein Formation is covered by Cretaceous sediments: sands of the Aachen Formation and sandy marls of the Vaals Formation. As a consequence the sealing can be considered to be insufficient.

Table 3-7: Stratigraphic subdivision of the Permian to Jurassic sequence in the Campine Basin and Roer Valley Graben (after Dusar et al., 2001).

<b>Chronostratigraphy</b>		<b>Formation/Member</b>	<b>Lithology</b>
<i>Jurassic</i>	Early	Aalberg Fm	Shales
	Late (from 228.0 ± 2.0 to 199.6 ± 0.6 Ma)	Sleen Fm Keuper Fm	Sandy or silty claystones Shales and clayey marls
<i>Triassic</i>	Middle (from 245 ± 1.5 to 228.0 ± 2.0 Ma)	Muschelkalk Fm	Shales, with limestone, dolomite and evaporates (anhydrite, gypsum)
		Röt Fm	Sandstones and shales, gypsum beds, marls
	Early (from 251.0 ± 0.4 to 245.0 ± 1.5 Ma)	Bree Member Upper Buntsandstein Fm	Lower part mainly shales, above medium to coarse-grained sandstones
		Bullen Member Middle Buntsandstein Fm	Medium to very coarse-grained sandstones and conglomerates
Gruitrode Member Lower Buntsandstein Fm		Alternation of silt- and sandstones (very fine to very coarse)	
<i>Permian</i>		Helchteren Fm	Conglomerate, followed by nodular or marly-sandy limestones and shales

Table 3-8: Percent fraction of different lithologies within the Gruitrode and Bullen members, based on core descriptions from wells KB172 and KB121 respectively.

	<b>Gruitrode Member</b>	<b>Bullen Member</b>
<i>Conglomerate</i>	8	6
<i>Coarse sandstone</i>	14	18
<i>Medium sandstone</i>	45	73
<i>Fine sandstone</i>	16	1
<i>Siltstone</i>	6	1
<i>Mudstone</i>	11	0

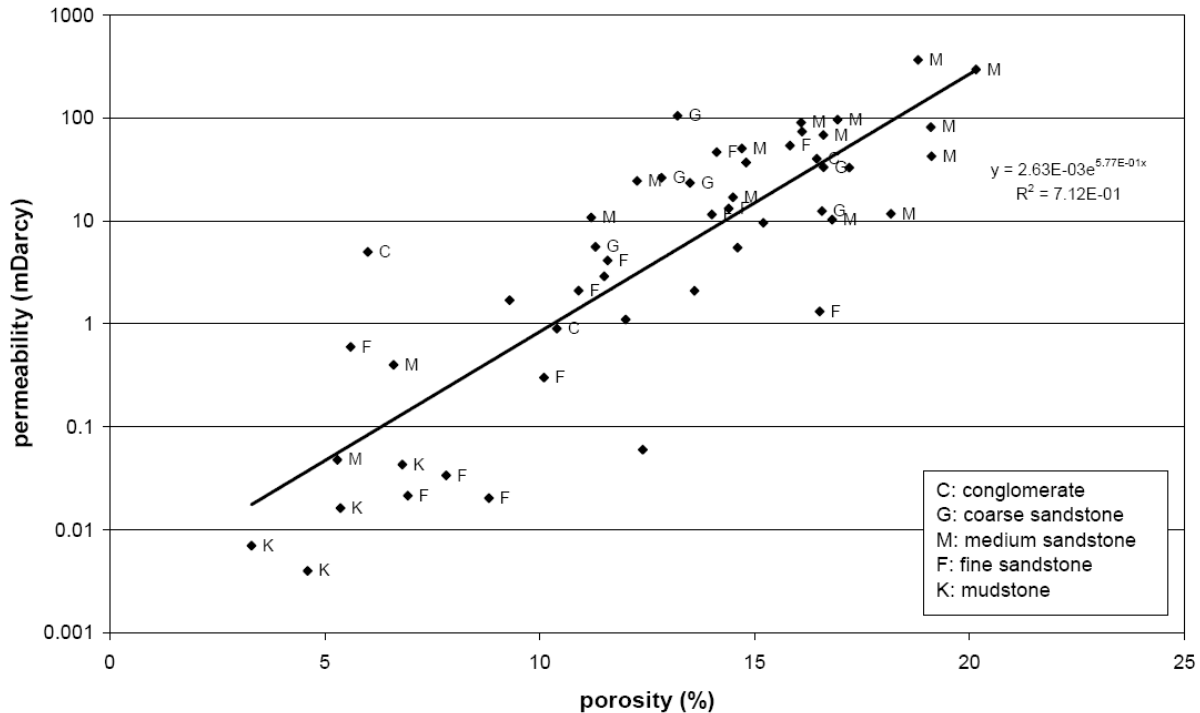


Figure 3-4: Porosity versus permeability plot for samples from the Buntsandstein Formation taken from wells KB172 and KB201. The labels refer to the broad lithologies recognized in the Buntsandstein sequence of the Campine Basin and Roer Valley Graben.

### 3.2.3.5 Outline of target area

In the southern part of the subcrop area, west of the Roer Valley Graben, the top of the Buntsandstein Formation is present at a depth of 600 to 800 m, i.e. mostly above the cut-off depth of 800 m. Towards the north, the formation is present at a greater depth (fig. 3-5). However, no good sealing formation (e.g. Jurassic shales) is present. The Buntsandstein Formation is covered by Cretaceous sediments, which do not constitute an adequate seal in that area. In most of the Roer Valley Graben, the depth is sufficient. Here, Triassic strata are buried beneath a thick pile of Jurassic (up to 800 m) and Cretaceous sediments. Middle and Upper Triassic deposits are present as well. The top of the formation is present at a depth of up to 1500 m and deepens towards the northeast. Hence, the main part of the Roer Valley Graben can be taken into consideration as a potential target area for CO<sub>2</sub>-storage reservoirs. Only some smaller areas are omitted, where Jurassic and upper Triassic sediments are absent.

### 3.2.3.6 Estimated reservoir volume

#### a) Average accessible pore volume

Based on the measured porosity and permeability values, the useful volume of the Buntsandstein sequences observed in wells KB121, KB169 and KB172 has been estimated. For this purpose, all mud- and siltstone intervals were omitted. This gives in a potential reservoir thickness of 200 m. For the sandstones, the porosity - permeability relationship shown in figure 3-4 was used. The irreducible water content was calculated using the formula (Battacharya et al., 2002):

$$S_{wi} = -0.15 \times \log_{10}(k_i) + 0.45 \quad (16)$$

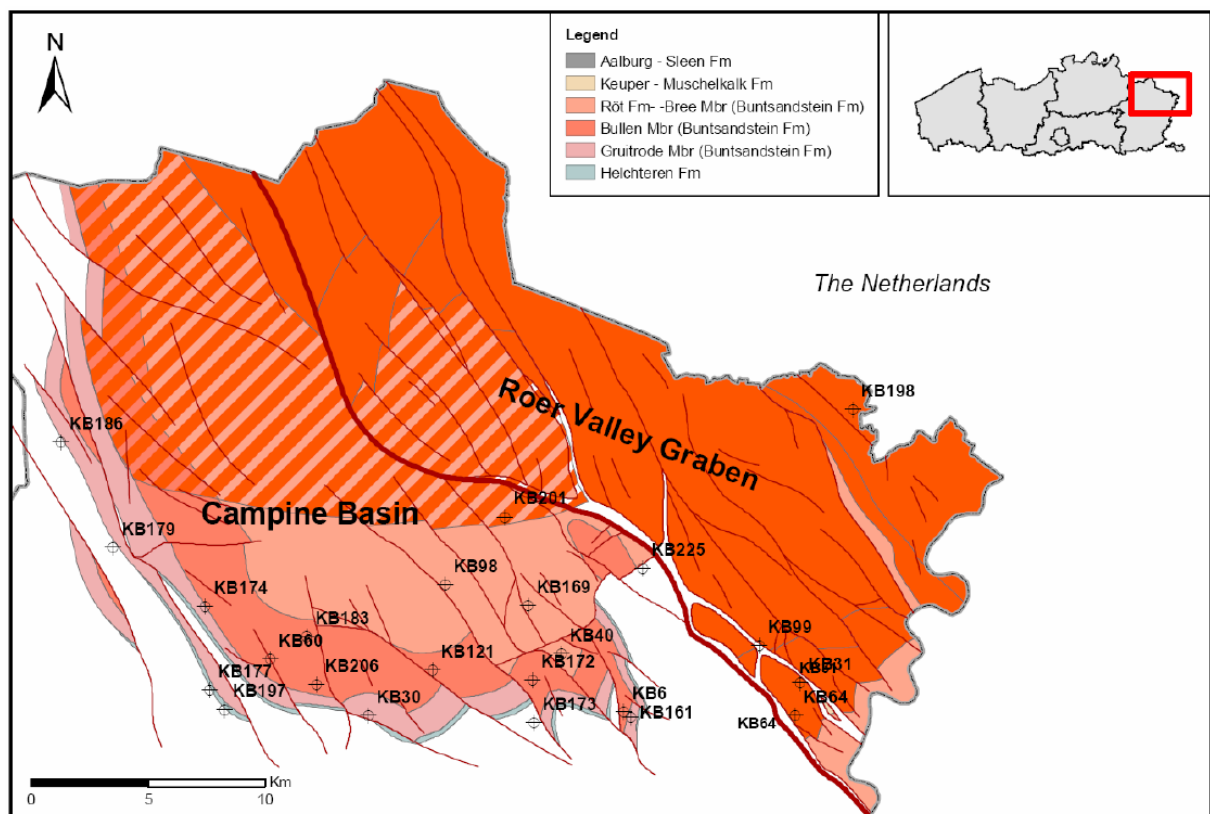


Figure 3-5: The target area of the Lower Triassic Buntsandstein Formation in the Campine Basin and Roer Valley Graben. Fully coloured area: present at minimum depth with sealing – high confidence or proven by borehole; hatched area: presence at sufficient depth, but no adequate seal.

The estimated useful volume of an average Buntsandstein reservoir is estimated to be in the order of  $16 \times 10^6 \text{ m}^3/\text{km}^2$ . The 10% and 90% percentiles are  $12$  and  $24 \times 10^6 \text{ m}^3/\text{km}^2$ , respectively (table 3-9).

*b) Case study of a structural trap: Verloren Kamp*

In addition to the accessible pore volume per square kilometre of the Buntsandstein Formation, estimated above, an estimation can be made for a structure avoiding the lateral migration of the stored gas, i.e. a trap. Such a structure covers a much more restricted area.

Table 3-9: Average useful reservoir volume of the Buntsandstein per square kilometre.

Area	Surface (km <sup>2</sup> )	Reservoir thickness (m)	Porosity (%)	Permeability measured (mDarcy)	Permeability used in model (mDarcy)	Accessible porosity* (10 <sup>6</sup> m <sup>3</sup> /km <sup>2</sup> )
Campine Basin & Roer Valley Graben	275	200	$13.4 \pm 3.9$	$37 \pm 70$	$2.63 \cdot 10^{-3} \cdot e^{0.577 \cdot \text{poro}}$	16:12–24

\* mean value and 10% and 90% percentiles

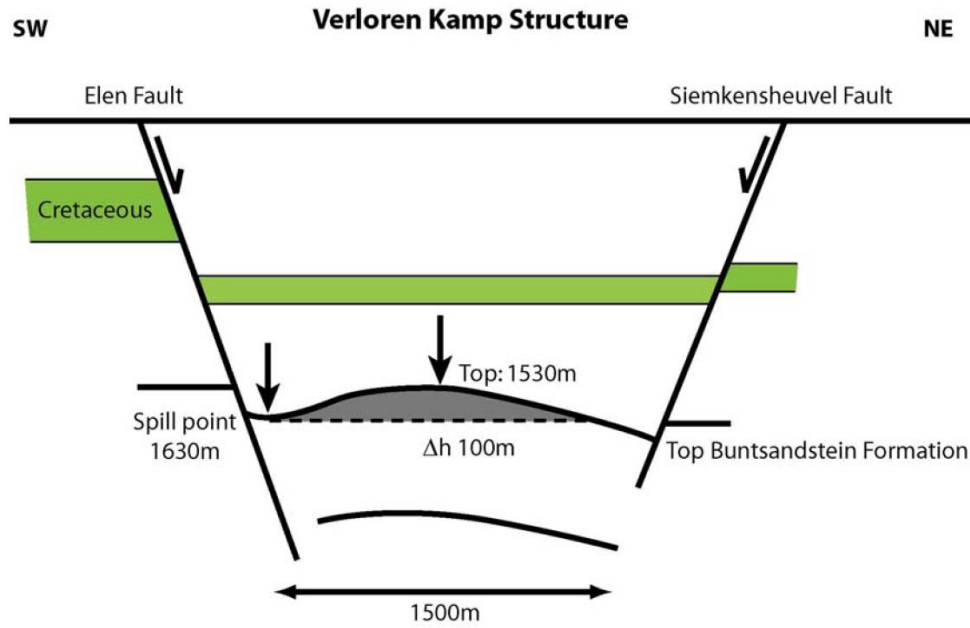


Figure 3-6: Conceptual model of the Verloren Kamp structure (not to scale).

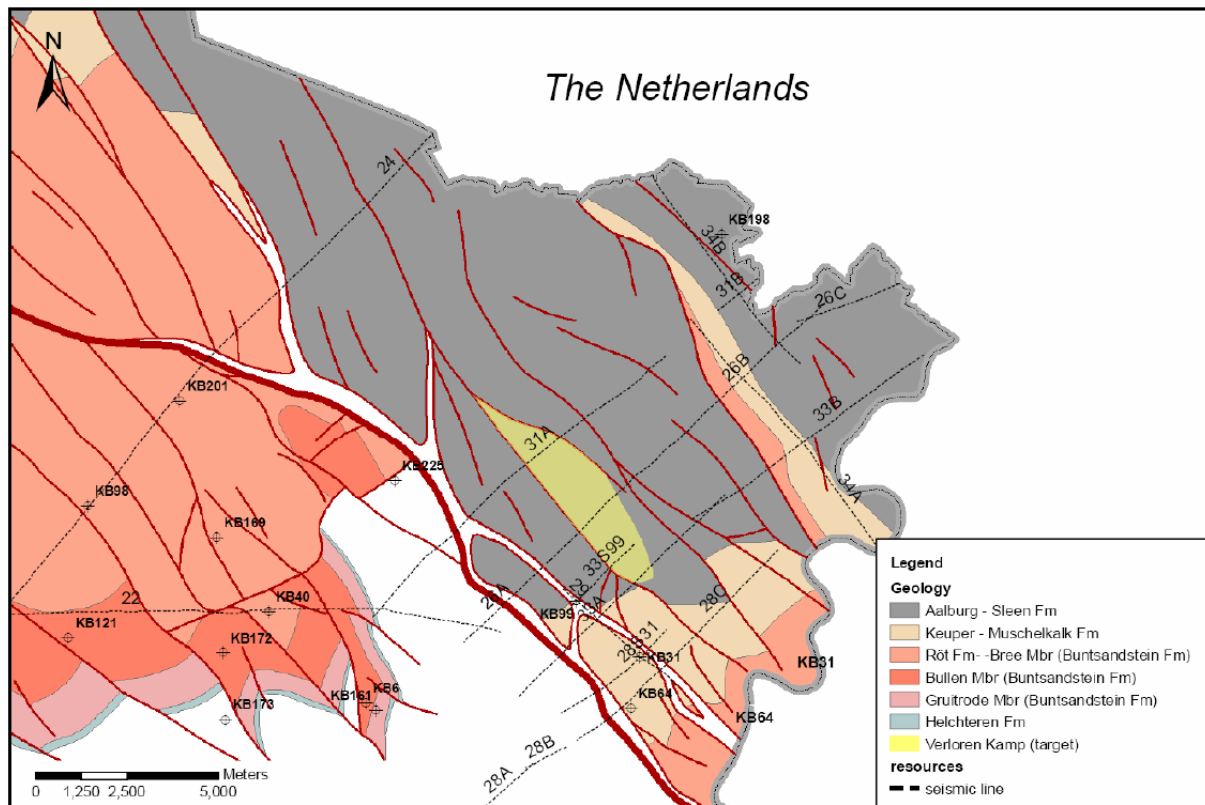


Figure 3-7: Location map of the Verloren Kamp structure in the Roer Valley Graben. Yellow area: trapped volume. Dashed lines indicate seismic lines of the 1953-1956 campaign. See figure 3-2 for legend on geology.

Based on reprocessed seismic lines 26 and 31 of the 1953-1956 campaign, the presence of a dome structure can be deduced in the Triassic sequence between the Elen and Siemkensheuvel faults (fig. 3-7). The dome is covered by upper Triassic and Jurassic sediments. The structure is approximately 7 km long, and 1.5 km wide. The surface area is approximately 7 km<sup>2</sup>. The Elen Fault constitutes the western edge of the structure. The top of the structure is situated at a depth of  $\pm$  1530 m. The spill point is located near seismic line 33B, and lies at a depth of approximately 1630 m (fig. 3-6). Hence, the estimated height of the structure is 100 m.

These dimensions can be used to estimate the volume of the structure, which amounts to  $233 \times 10^6$  m<sup>3</sup>. The accessible porosity and the density of CO<sub>2</sub> should be taken into account. The density of CO<sub>2</sub> at this depth and temperature (1550 m, 62°C) is about 600 kg/m<sup>3</sup> (Span & Wagner, 1996; Lemmon et al., 2005). Hence, a total of 15 to 40 Mton CO<sub>2</sub> could be stored in the Verloren Kamp structure.

#### *c) Mineral trapping*

Within the sandstones of the Buntsandstein Formation, potentially reactive phases for mineral trapping of CO<sub>2</sub> are feldspar, clays (mainly illite and some smectite), carbonates (zoned dolomite/ankerite), micas and iron-oxides/hydroxides.

The mineral trapping potential of the sandstones is promising, due to the presence of Fe oxo/hydroxides and Fe, Mg rich clays and micas. Feldspars are dominantly K(Na)-rich.

#### **3.2.3.7 Injectivity**

The injectivity for the Buntsandstein Formation was estimated for a reservoir at a depth of -1500 m with a productive interval of 50 m. A high, medium and low injectivity scenario was calculated based on the variability in porosity observed in the wells that penetrated the Buntsandstein in the Campine Basin and in the Roer Valley Graben. The results are summarized in table 3-10.

#### **3.2.3.8 Summary**

The Lower Triassic Buntsandstein Formation appears to be promising for storage of CO<sub>2</sub>. It occurs at sufficient depth within the Roer Valley Graben. In this area it is covered by Upper Triassic to Jurassic sediments forming an adequate seal.

Trapping structures, e.g., Verloren Kamp, may be present.

The high accessible porosity and moderate to high permeabilities observed in certain intervals result in an average storage potential of  $10 \times 10^6$  ton per square kilometre (for density under reservoir conditions of 620 kg/m<sup>3</sup>).

The injectivity of the Buntsandstein Formation is relatively low.

### **3.2.4 The Upper Carboniferous sandstones**

The good reservoir properties of the Neeroeteren sandstones are known for decades. The sandstones have a high porosity and permeability. Therefore, they are interesting to consider as a potential reservoir formation.

#### **3.2.4.1 Brief description of geological setting**

Westphalian<sup>13</sup> strata are present in the subsurface of a large part of the Campine Basin (fig. 3-8). The Westphalian sequence contains coal layers. Coal deposits of Westphalian age in Belgium, France, the Netherlands, and Germany formed part of the extensive Northwest European paralic coal basin.

<sup>13</sup> The names Westphalian and Namurian are still used by Belgian geologists. However, new names have been introduced in the international stratigraphic chart, as indicated in table 3-11.

Table 3-10: Injectivity of the Buntsandstein in the Campine Basin and Roer Valley Graben for three porosity and permeability conditions based on the analytical model described in section 3.2.2.5

Scenario	$\Phi$ (%)	$k$ (mDarcy)	PI ( $m^3(n)/s.bar.m$ )	Ip ( $bar^2.h/m^3$ )
High	17.5	64	0.020	0.094
Medium	15	15	0.0049	0.379
Low	11	1.5	0.0012	1.54

In the western part of the Campine Basin (Antwerp), only lower Westphalian deposits are present, with limited coal reserves. In the eastern part of the Campine Basin (Limburg), there is a fully preserved coal-rich Westphalian sequence. Mining occurred in the Limburg Campine area only. The most complete section is present towards the Roer Valley Graben, where Westphalian D deposits have been preserved.

Westphalian strata are buried beneath a cover of Mesozoic and Cenozoic sediments. The thickness of the cover varies from 500 in the south to more than 1000 m in the northeast of the Campine basin. The thickness of the Westphalian sequence amounts up to more than 2000 m. Towards the east, in the Roer Valley Graben, the thickness is unknown, as these strata are deeply buried to a depth of more than 2500 m.

The Westphalian sediments were deposited during a period of gradual regression, evolving from a marine-influenced to a continental environment. A transition from marine pro-delta, lower and upper delta plain, to lower and upper alluvial plain can be recognized (Langenaeker & Dusar, 1992; Dreesen et al., 1995). This transition culminated in the deposition of thick fluvial sandstone bodies in a braided river system during late Westphalian times (Westphalian

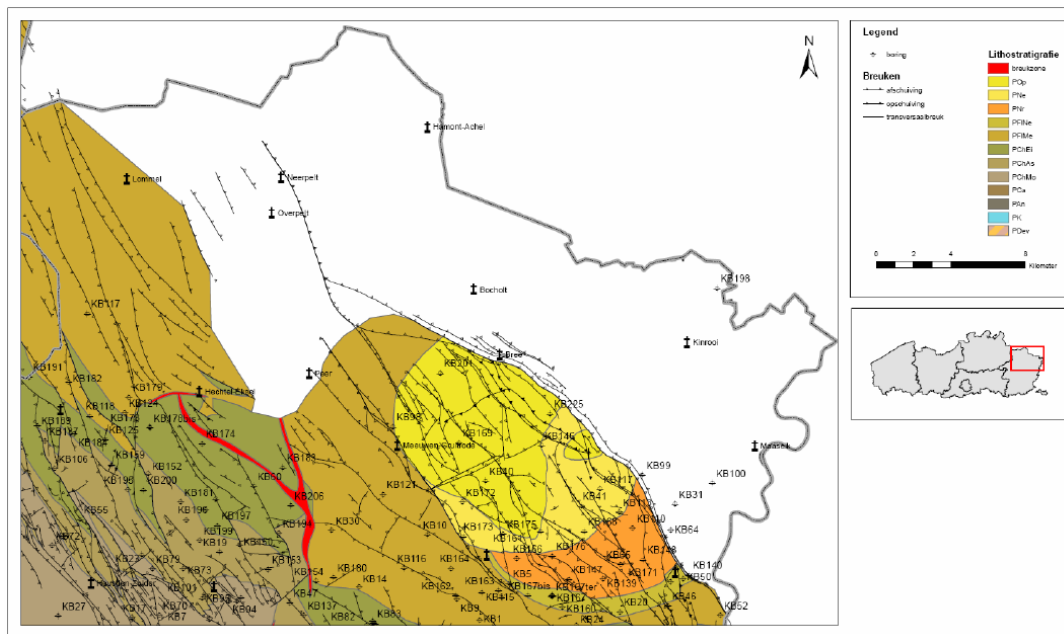


Figure 3-8: Pre-Permian subcrop map of the eastern Campine Basin (Limburg), showing the occurrence of Westphalian strata (Van Tongeren, 2004, modified after Langenaeker, 2000). Boreholes mentioned in the text are indicated.

D, Neeroeteren Formation<sup>14</sup>) (Laenen et al., 2004; Paproth et al., 1983; Langenaeker, 2000). Within the Westphalian sequence, the Neeroeteren Formation is the prime target for aquifer storage.

### 3.2.4.2 Stratigraphy and lithology

The Westphalian sequence (table 3-11) is subdivided into four units (A, B, C, & D). Boundaries between A, B, and C are determined by the presence of marine horizons. A formal subdivision in formations is presented by Delmer et al., (2001). It is worth mentioning that these subdivisions and the descriptions of strata are based not only on observations from the Campine Basin, but also from the Hainaut and Liège areas.

The lower Westphalian deposits are mudstone-dominated. Siltstones and sandstones become more abundant higher up.

The sandstone bodies of Westphalian A, B and C are lenticular river deposits and are surrounded by impermeable shales and coal layers. The thickness of the sandstone bodies varies from a few tens of centimetres up to several tens of metres. They have a width of several hundreds of metres and can be several km long. The morphology and the spatial distribution (and also specific reservoir characteristics) from these sandstone reservoirs are function of the palaeofluvial system.

Table 3-11: Stratigraphic subdivision of the Westphalian strata in Belgium (after Delmer et al., 2001).

<i>Chronostratigraphy</i>	<i>Formation</i>	<i>Member</i>	<i>Description</i>	
<i>Moscovian (from 311.7 ± 1.1 to 306.5 ± 1.0 Ma)</i>	<i>Westphalian D</i>	Neeroeteren	Massive coarse-grained to conglomeratic sandstones	
	<i>Westphalian C</i>	Flénu	Neerglabbeek	Rhythmic succession of coal-mudstone-sandstone sequences
			Wasmes	
			Meeuwen	Coal seams are frequent, and up to 5 m thick
	<i>Westphalian B</i>	Charleroi	Eikenberg	Rhythmic succession of coal-mudstone-sandstone sequences
			As	
<i>Bashkirian (from 318.1 ± 1.3 to 311.7 ± 1.1 Ma)</i>	<i>Westphalian A</i>	Mons	Coal seams are frequent and up to 3 m thick	
		Châtelet	Floriffoux	Non-marine, partly silty shales, sandstones
			Ransart	

<sup>14</sup> The Westphalian C-D boundary is located approximately 50 m below the base of the Neeroeteren Formation.

Table 3-12: Average composition of sandstone of the Neeroeteren Formation, based on point counting on 21 samples (Bertier, 2004).

<i>Mineral phase</i>	<i>Percentage</i>	<i>Mineral phase</i>	<i>Percentage</i>
<i>Quartz (monocrystalline)</i>	38.0	Chlorite	0.0
<i>Quartz (polycrystalline)</i>	19.2	Clay minerals	6.5
<i>Quartz (microcrystalline)</i>	0.4	Fe oxi/hydroxides	0.3
<i>Quartz (authigenic)</i>	4.9	Ankerite	1.5
<i>Lithic fragments</i>	9.2	Siderite	1.2
<i>Feldspar</i>	7.5	Carbonates	0.9
<i>Mica</i>	1.0	Coal fragments	0.2
<i>Kaolinite</i>	2.3	Opaque minerals	0.1
<i>Illite</i>	0.6	Porosity	6.3

The Neeroeteren Formation consists of coarse-grained to conglomeratic, white sandstones. The formation shows a series of fining-upwards sequences. These start with coarse-grained sandstone to gravel, giving way to fine-grained sandstone. Mudstones and/or coal seams are sometimes interbedded with the sandstones.

The thickness of the Châtelet Formation is estimated at 500 m. The Charleroi and Flénu formations are 1100 m and 950 m thick respectively. The maximal thickness of the Neeroeteren Formation observed in wells is approximately 275 m. Based on seismic evidence, a maximum thickness of up to 500 m is reached along the Feldbiss Fault (Dusar, 1989).

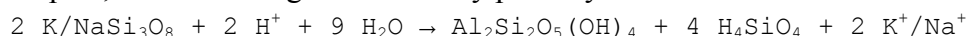
Van Tongeren & van Amerom (2003) and van Tongeren (2004) propose a different lithostratigraphy, based on palaeobotanical and seismic evidence. Van Tongeren (2004) introduces the Opitter Formation and the Neerheide Formation. They are present above and below the Neeroeteren Formation respectively. Their stratigraphy is indicated on the map. However, the meaning of the Neeroeteren Formation remains the same: the sandstone-dominated formation of Westphalian D age, with KB146 (Neerglabbeek) as the reference borehole.

### 3.2.4.3 Petrophysics and petrography of potential reservoirs

#### a) Petrography

Classification of Westphalian sandstones ranges from lithic greywacke for Westphalian A and B (Lorenzi et al., 1992), sublitharenite (Swennen et al., 1996) to subarkose (Caers et al., 1996) for Westphalian C and D.

The Westphalian sandstones contain important amounts of feldspars and lithic fragments (table 3-11). Feldspars are predominantly K-rich. They are most often weathered and converted to kaolinite or illite. Kaolinite fills most pores generated by the dissolution of feldspars, hence limiting the secondary porosity.



The Neeroeteren Formation consists of quite homogeneous, medium to coarse-grained subarkosic to sublithic arenites (Bertier et al., 2006). The porosity and permeability of these sandstones are reduced by the presence of authigenic quartz, clays (authigenic kaolinite and illite), and small quantities of authigenic carbonates (dolomite/ankerite and siderite). Porosity is enhanced by dissolution of feldspars and by preservation of primary porosity due to the presence of grain-coating clays. Feldspar is predominantly altered to illite. However, as the influence of meteoric processes shortly after deposition was restricted (Bertier et al., under review), the amount of feldspar alteration was limited. More feldspar was preserved, and less clay minerals formed (table 3-12). This had a positive effect on the porosity and permeability of the sandstone.

Table 3-13: Porosity and permeability data of the Neroeteren Formation from several boreholes. A distinction is made according to grain size, based on core descriptions.

Lithology	Porosity (%)				Permeability (mDarcy)			
	Max	Min	Average	n	Max	Min	Average	n
Fine sandstone	26.0	6.5	13.1	41	10	0.1	2	35
Medium sandstone	19.8	5.0	15.1	50	315	d.l.	86	41
Coarse sandstone	30.0	3.5	16.8	61	1172	d.l.	172	44
Conglomerate	19.2	11.5	16.2	13	2473	143	336	10

d.l. below detection limit of 0.05 mDarcy

Table 3-14: Percentage (%) of different lithologies within the Neroeteren Formation, based on core descriptions from wells KB146, KB161 and KB172.

	KB146	KB161	KB172
Conglomerate	6	3	2
Coarse sandstone	20	31	17
Medium sandstone	19	30	41
Fine sandstone	29	27	33
Siltstone	17	2	6
Mudstone	8	4	1
Coal	2	3	0

#### b) Porosity and permeability data

The Neroeteren Formation shows significant variations in porosity and permeability (table 3-13). A compilation of data was made, distinguishing according to grain size. Data are from samples taken from boreholes KB113, KB117, KB146, KB161/161B, KB168, KB172, and KB173.

The porosity and permeability are clearly correlated (fig. 3-9). The relationship between both petrophysical properties and lithology is less clear. In general, the highest porosities and permeabilities are observed in the coarse grained sandstones and conglomerates, whereas the fine grained lithologies show an overall lower porosity and permeability.

Nevertheless, in all lithology classes the porosity and permeability values vary widely. The large variability observed in the samples indicate that the porosity and permeability of the sandstones is mainly controlled by diagenesis. The sedimentology clearly is of secondary importance. The strong variations reveal that one should be cautious when extrapolating data from a limited number of samples. Differences result from varying sedimentary and diagenetic conditions. This is important with respect to the delineation of potential the reservoir units. It is clear that the entire sandstone sequence can serve as reservoir units, that can be separated from each other by both sedimentological and diagenetic flow barriers.

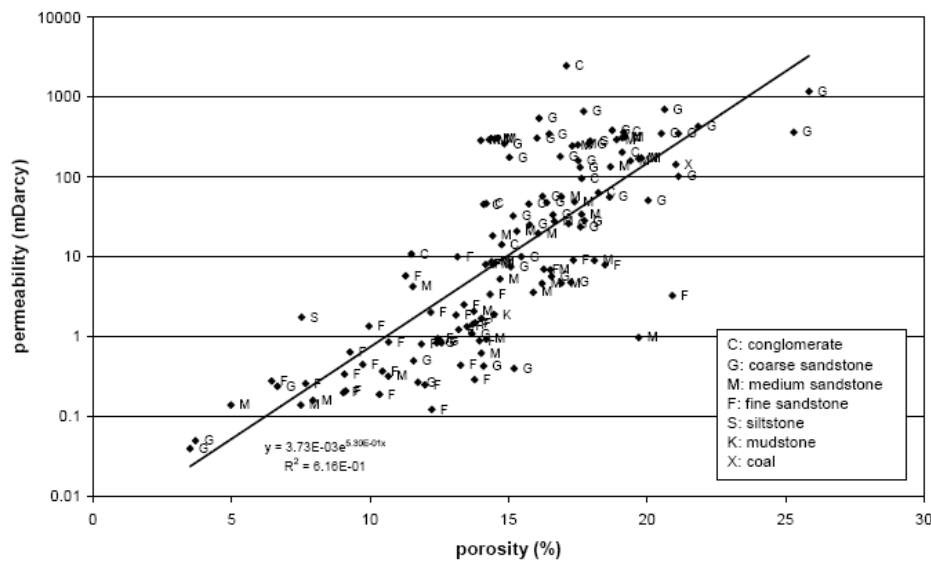


Figure 3-9: Porosity versus permeability plot for samples from the Neroeteren Formation. The labels refer to the lithology of the samples.

### c) Contribution of different lithologies

The thickest section of the Neroeteren Formation was encountered in the KB146 borehole (Neerglabbeek; Duser & Houllberghs, 1981): 275 m<sup>15</sup>. Based on the core descriptions, the proportions of different lithologies were calculated (table 3-14). Almost 29% of the Neroeteren Formation consists of fine-grained sandstone. 20% is made up of medium-grained sandstone, 20% of coarse-grained sandstone, 6% of conglomerate. Siltstone makes up 17% of the formation, mudstone almost 8%, and coal layers nearly 2%.

The proportions of each lithology are not exactly the same in every borehole. Boreholes KB161 and KB172 have a higher percentage of sandstone (around 90%), compared to less than 70% for KB146. On the other hand, KB161 and KB172 contain less siltstone, mudstone, and coal. Another difference is the percentage of conglomerate, which is higher in borehole KB146.

The proportions were used to calculate a weighted average of the porosity, resulting in an average value of 14.1% for KB146. Despite the differences between the boreholes, the calculated weighted average of the porosity only differs slightly (< 1%).

#### 3.2.4.4 Structure and sealing

An angular unconformity constitutes the top of the Neroeteren Formation. It is partly overlain by Permian and Lower to Middle Triassic sediments<sup>16</sup>. The Permian Helchteren Formation consists of calcareous shales and argillaceous limestones. The base of the Triassic sequence starts with an alternation of silt- and sandstones of the Gruitrode Member (Buntsandstein Formation).

Where there is no Permian-Triassic cover, Cretaceous sediments are resting immediately on top of the Neroeteren Formation. They consist of sands and chalks. Hence, these strata do not constitute an adequate seal.

<sup>15</sup> 275 m is the stratigraphical thickness, i.e. corrected for the dip of the strata. The drilled thickness is 283 m.

<sup>16</sup> According to Van Tongeren (2004), the Neroeteren Formation is partly covered by the Opitter Formation, also of late Carboniferous age. It is made up of more pelitic sediments.



Therefore, it appears more interesting to consider the Neroeteren Formation in the Roer Valley Graben. There, the formation should be present at greater depth. However, the few boreholes drilled in that area were not deep enough, and did not reach the Neroeteren Formation. Hence, the presence of the Neroeteren Formation and its reservoir properties in this area remain to be proven.

For the present assessment is assumed that the reservoir characteristics in the graben area are the same as in the explored part of the Campine Basin. All mud- and siltstone intervals were omitted. This roughly results in a potential reservoir thickness of 200 to 250 m. For the sandstones, an empiric porosity - permeability relationship was used. The irreducible water content was calculated using the formula:

$$S_{wi} = -0.15 \times \log_{10}(k_i) + 0.45 \quad (\text{Battacharya et al., 2002}) \quad (17)$$

Under these assumptions, the useful reservoir volume within the Neroeteren sequence will be in the range of 15 to 24 x 10<sup>6</sup> m<sup>3</sup>/km<sup>2</sup> (table 3-15). This estimate is made assuming a cumulative pay zone thickness of 200 m, and porosity values in the range of 8 to 15%.

Table 3-15: Average useful reservoir volume of the Neroeteren Formation per square kilometre.

Area	Surface (km <sup>2</sup> )	Reservoir thickness (m)	Porosity (%)	Permeability measured (mDarcy)	Permeability used in model (mDarcy)	Accessible porosity* (10 <sup>6</sup> m <sup>3</sup> /km <sup>2</sup> )
Campine & graben area	325	200	15.0 ± 3.9	115 ± 272	3.73 10 <sup>-3</sup> exp <sup>0.530.poro</sup>	19: 15 - 24

\* mean value and 10% and 90% percentiles

#### b) Mineral trapping

Potentially reactive phases in the sandstones of the Neroeteren Formation with respect to mineral trapping are feldspar, clays (mainly illite) and carbonates (zoned ankerite/dolomite; and siderite). The mineral trapping potential is rather low, as most reactive silicates contain only monovalent cations (K and Na) (Bertier et al., 2006).

#### 3.2.4.7 Injectivity

The injectivity for the Neroeteren Formation was estimated for a reservoir at a depth of -1500 m with a productive interval of 50 m. A high, medium and low injectivity scenario was calculated. The scenarios were defined on the variability in porosity observed in the core samples. Only samples ranging from fine sandstone to conglomerate were taken into account. The results are summarized in table 3-16.

#### 3.2.4.8 Summary

Sandstones of the Neroeteren Formation provide sufficient porosity and permeability for storage of CO<sub>2</sub>. However, the reservoir is not always sealed, and it is not always present at sufficient depth.

The requirements on depth and sealing may be met in the Roer Valley Graben, but the presence of the Neroeteren Formation and its reservoir properties in that area remain to be proven.

The high accessible porosity and high permeabilities observed in certain intervals result in an average storage potential of 11.8 x 10<sup>6</sup> ton per square kilometre (for a density of CO<sub>2</sub> under reservoir conditions of 620 kg/m<sup>3</sup>).

The injectivity of the Neroeteren Formation is relatively low.

### 3.2.5 The Lower Carboniferous carbonates

The karstified limestones in the top of the Viséan are potentially excellent storage aquifers. This is demonstrated by the Heibaart structure (near Loenhout), where natural gas is stored in a karstified dome structure.

#### 3.2.5.1 Brief description of geological setting

Lower Carboniferous (locally known as Dinantian) strata were drilled in several boreholes in the western part of the Campine Basin: Halen, Loksbergen, Rillaar, Booischoot, Kessel, Turnhout, Merksplas-Beerse, Poederlee, and Heibaart (Wouters & Vandenberghe, 1994). There are also various wells near Heibaart, executed by Distrigas. The top of the Lower Carboniferous strata is situated at a depth of 1000 to more than 2000 m. Towards the southern edge of the basin, the depth decreases to about 300 m (Loksbergen, Rillaar). The Dinantian formations are buried beneath a cover of Upper Carboniferous, Cretaceous and Cenozoic strata.

Table 3-16: Injectivity of the Neroeteren Formation for three porosity and permeability conditions based on the analytical model described in section 3.2.3.5.

Scenario	$\Phi$ (%)	$k$ (mDarcy)	$PI$ ( $m^3(n)/s.bar.m$ )	$I_p$ ( $bar^2.h/m^3$ )
High	20	150	0.046	0.040
Medium	15	11	0.0035	0.529
Low	11	1.3	$6.3 \times 10^{-4}$	3.00

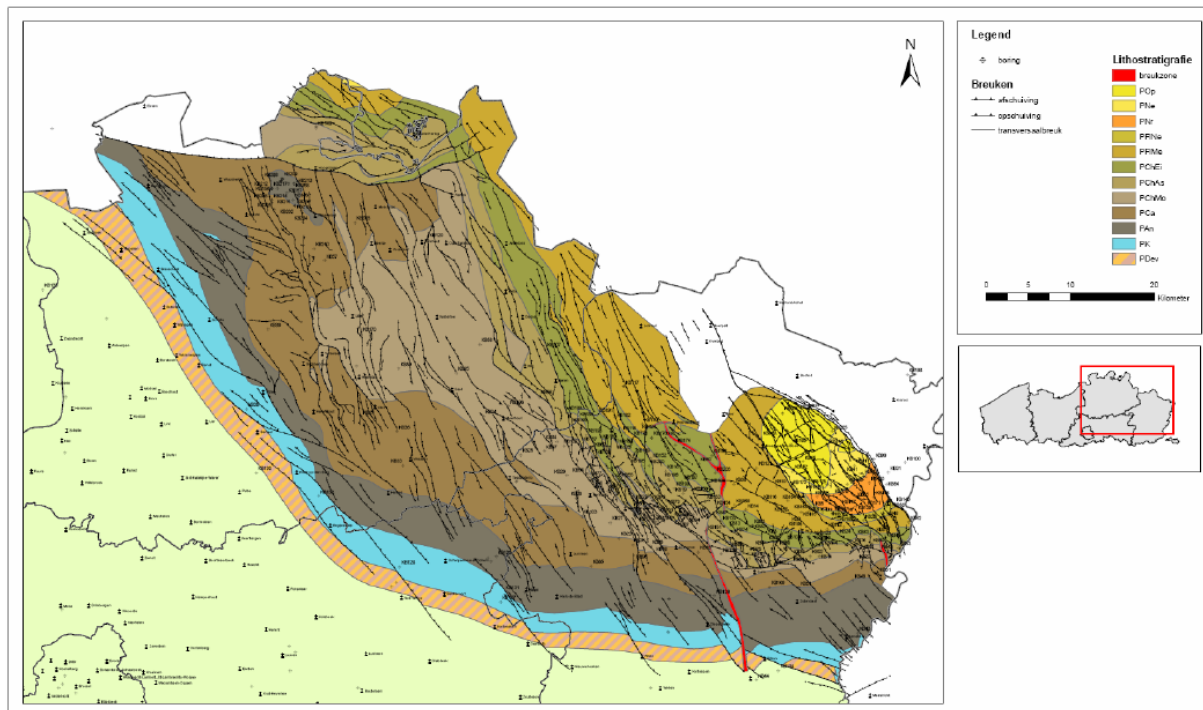


Figure 3-11: Pre-Permian subcrop map of the Campine Basin (Van Tongeren, 2004, modified after Langenaeker, 2000), showing the occurrence of Carboniferous strata, including the Carboniferous Limestone Group.

The dominant lithologies of the Lower Carboniferous sequence are limestone and dolostone. Locally, calcareous clay- and sandstone are present. Together they make up the Carboniferous

Limestone Group. The Carboniferous Limestone Group overlies siliciclastic deposits of Devonian age, and is covered by siliciclastic deposits of Late Carboniferous age (Namurian and Westphalian), i.e., the Coal Measure Group. Towards the margins of the basin (south and west) Upper Carboniferous deposits have been eroded. Here the Carboniferous Limestone Group is overlain by Cretaceous marls and chalks (fig. 3-11).

The thickness of the Carboniferous Limestone Group varies between 350 and 750 m in the western part of the basin, and 800 to more than 1200 m in the eastern part. Both parts of the basin are separated by the Donderslag fault zone. In most boreholes, the base of the Lower Carboniferous sequence is not reached, with exception of the Heibaart and Booischot wells. In these 2 wells, drilling continued into Devonian strata.

### **3.2.5.2 Stratigraphy and lithology**

The various boreholes show strong differences in the thickness of the strata and in facies (Wouters & Vandenberghe, 1994). Whereas a thick pile of sediments of a certain age can be present in one location, the corresponding deposits may be missing altogether in another location (hiatus). These differences result from block faulting, active during the deposition of the limestones. Hence, there is a differentiation between shallow and deep sedimentation areas, and open versus restricted depositional environments. Reef-like structures are present in some locations.

The main part of the Limestone Group in the boreholes is of Visean age. (Wouters & Vandenberghe, 1994; Langenaeker, 2000). In Booischot and Halen, the lower part of the carbonate sequence consists of dolostones. These are considered to be of Tournaisian age. No Tournaisian strata were drilled in Heibaart. There, the Visean limestones directly overlie Famennian sandstones. The overlying Souvré Formation is of late Visean to Serpukhovian age. In the Campine basin, the top of the Carboniferous Limestone Group is widely karstified. The Carboniferous Limestone Group in the Campine Basin is divided into five formations (from top to bottom; table 3-17): Loenhout, Velp, Kessel, Steentje-Turnhout, and Vesder (Laenen, 2003).

#### *a) Loenhout Formation*

The Loenhout Formation is made up of pale grey limestones: fossiliferous lime mudstones, bio- and lithoclastic wackestones and grainstones, and boundstones. Locally, thin layers of dark-grey argillaceous limestone or carbonaceous claystone are present. Some fossiliferous mudstones and boundstones are interpreted as reefal limestones. Laterally, massive, fossil-poor limestones were deposited in a restricted environment. In Loenhout, the formation is 185 m thick.

#### *b) Velp Formation*

The Velp Formation consists of compact bioclastic limestones, with locally argillaceous layers. The lower 5 m of the formation is made up of dolostones. The formation is divided into an upper and a lower part, separated by an argillaceous zone below a brecciated interval. The thickness varies considerably, with a maximal thickness of 131 m in Booischot.

Table 3-17: Stratigraphic subdivision of the Dinantian strata in the Campine Basin (after Laenen, 2003). The Carboniferous Limestone Groups comprises five formations (Vesder, Steentje-Turnhout, Kessel, Velp & Loenhout).

<b>Chronostratigraphy</b>	<b>Formation</b>	<b>Description</b>	
<i>Mississippian*</i>	Serpukhovian	Souvré	Dark (silicified) mudstones, limestones and dolostones
	Visean (from $345.3 \pm 2.1$ to $326.4 \pm 1.6$ Ma)	Loenhout	Pale grey limestones, including bioclastic limestones Limestone breccia
		Velp	Bioclastic limestones, some dolostones at the base
		Kessel	Limestones, nodular limestones, red sandstones and claystones
		Steentje-Turnhout	Massive limestones and some dolostones
	Tournaisian (from $359.2 \pm 2.5$ to $345.3 \pm 2.1$ Ma)	Vesder	Dolostones, intercalations of limestones and claystones

\* Formally, the name Mississippian is used instead of Early Carboniferous or Dinantian. The Early Carboniferous and Dinantian include the Tournaisian and Visean, whereas the Mississippian includes the Serpukhovian as well.

Table 3-18: Porosity and permeability data from the Carboniferous Limestone Group from the Poederlee well.

<b>Porosity (%)</b>				<b>Permeability (mDarcy)</b>			
Max	Min	Average	n	Max	Min	Average	n
3.6	0.4	1.3	23	1.5	d.l.	0.5	23

d.l.: below 0.01 mDarcy

#### c) Kessel Formation

The Kessel Formation is characterised by an alternation of massive grey to red-brown limestones with argillaceous nodular limestone beds, red calcareous sandstones, and red mottled and black claystones. Locally, thin dolostone beds are present. The thickness is approximately 80 m.

#### d) Steentje-Turnhout Formation

The Steentje-Turnhout Formation consists of massive grey to light grey limestones and dolostones, locally karstified, with some breccia levels. The thickness varies considerably: it attains 399 m in Turnhout, but the formation is absent or very thin at Heibaart.

#### e) Vesder Formation

The Vesder Formation is made up of grey to beige dolostones with dark organic-rich intervals and silicified beds. Locally, there are thin limestone beds and claystone layers. The thickness of the formation amounts up to more than 200 m in the Halen borehole. It is absent in Heibaart.

### 3.2.5.3 Petrophysics and petrography of potential reservoirs

#### a) Porosity and permeability data

Porosity measurements on Visean limestones from the Poederlee well are in the range of 0.5 to 2% (table 3-18). On average, the porosity is below 1.5%. The low porosity results in a low

permeability, often below the detection limit of 0.1 mDarcy. The permeability amounts to a few mDarcy at the most. The low porosity values are in agreement with the geophysical logs. However, the logs reveal a second population with values around 4.5%, and in some intervals even exceeding 20%. These high values are due to the presence of open fractures and voids. The low values represent the porosity of the limestone matrix.

The results from the core samples are not in agreement with formation tests, which indicate average reservoir permeability values in the order of a hundred mDarcy at a distance from the well. Pump tests were also performed in the Merksplas-Beerse well (KB165). These resulted in permeability values of 1000 to 3000 mDarcy (Vandenberghe et al., 2000).

The difference between the core samples and the field tests can be explained by a dual porosity model. Fractures play an important role in the flow properties on a reservoir scale, whereas the massive limestone does not determine the large-scale characteristics of the reservoir. Hence, the analyzed core samples are not representative for the overall reservoir.

#### **3.2.5.4 Structure and sealing**

The Carboniferous Limestone Group is overlain by Namurian & Westphalian strata (mudstones, intercalated with sandstones and coal layers). The Loenhout Formation is covered by mudstones and silicified limestones of the Souvré Formation (Laenen, 2003). This boundary may be an angular unconformity, e.g. in well KB120 in Turnhout. Where the Souvré Formation is absent, the Loenhout Formation is covered by clay- and siltstones of the Chokier Formation or of the Andenne Formation (Namurian). Towards the southern and western margin of the Campine Basin, Namurian strata are absent. There, the limestone sequence is covered by Cretaceous marls and chalks.

#### **3.2.5.5 Outline of target area**

Carbonate deposits of Early Carboniferous age are present in a large part of the Campine Basin. Karst cavities and voids provide a significant porosity and permeability. Therefore, these strata can be taken into consideration for storage of CO<sub>2</sub>.

Only part of the subcrop area is considered. To the north, the Hoogstraten Fault is taken as the limit. North of this fault, the Carboniferous Limestone Group is present at greater depth. To the northeast, the carbonate deposits are present at increasing depth. Therefore, an arbitrary limit is chosen, running more or less along the boundary between the Mons and As members of the Charleroi Formation (Westphalian A-B boundary). This limit also coincides roughly with a depth of 2500 m of the top of the Limestone Group.

Within the delineated area (fig. 3-12), a further differentiation is made (high versus low importance). In the central part of the target area, Late Carboniferous strata (i.e. Namurian and Westphalian) are present above the Limestone Group, and it is at suitable depth. This is the area of highest potential.

Towards the east, the area of high importance is limited. Further east, no borehole data are available, and the presence of karst phenomena is not proven. Moreover, boreholes in The Netherlands reveal the presence of sediments deposited in a deeper environment. Therefore, this region is indicated as an area of low importance.

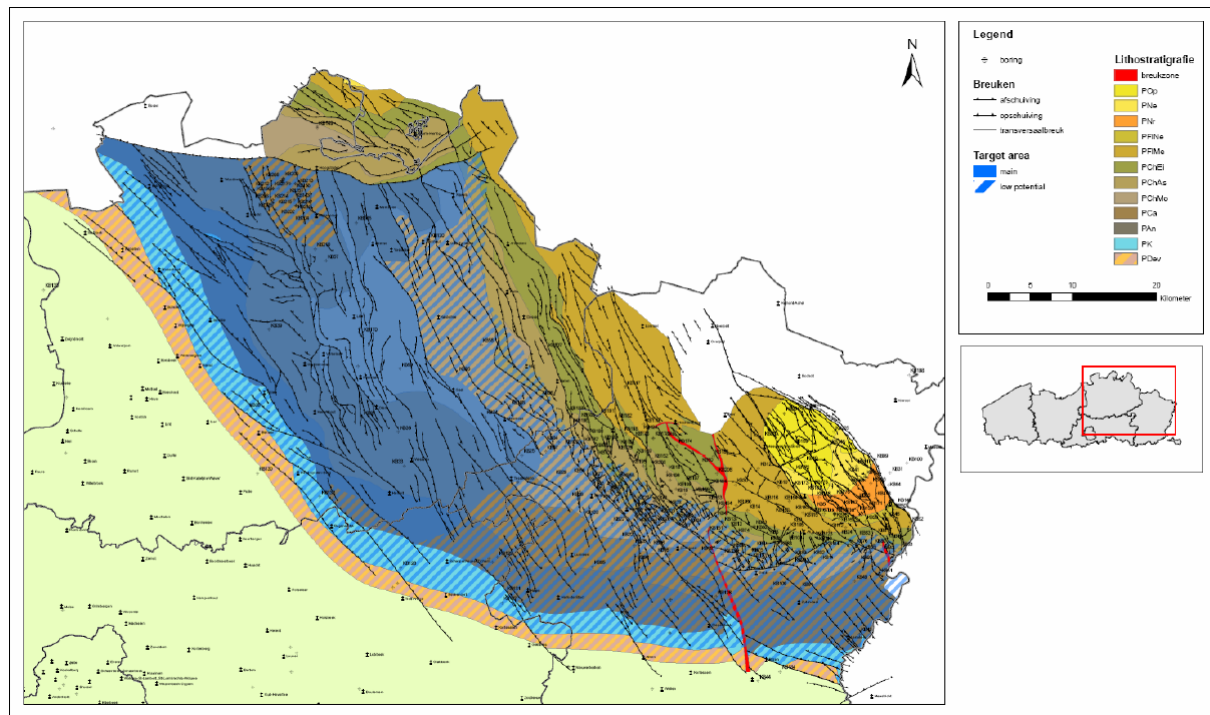


Figure 3-12: Pre-Permian subcrop map of the Campine Basin showing the target area for the Carboniferous Limestone Group. The full-coloured area indicates where the limestones are at sufficient depth, and where karst phenomena occur. The hatched area denotes the region where the limestones are probably not deep enough, or where no karst phenomena are documented. To the northeast, the limit is chosen at roughly 2500 m depth. See text for explanation.

Along the western and southern limit of the subcrop area, the carbonate deposits are overlain directly by sediments of Cretaceous age. Moreover, the top of the Limestone Group is at less than 800 m depth. Therefore, this zone is of less interest. To the northeast, where the top of the Carboniferous Limestone Group deepens, another band of lower interest is indicated, because of the greater depth. The area around Loenhout-Heibaart is omitted as well, because of the presence of an underground storage site for natural gas. Hence, there is no potential in this area.

### 3.2.5.6 Estimated reservoir volume

Limestones in the upper part of the Carboniferous Limestone Group are affected by karst. These karstified horizons constitute a potential reservoir. The thickness of these intervals is approximately 50 m. Data from wells in Poederlee and Merksplas indicate that the reservoir in the Carboniferous Limestone Group has an average working porosity of 2.4% and a permeability in the range of 100 to 1000 mDarcy (table 3-19). This results in a useful reservoir volume of  $1.18 \times 10^6 \text{ m}^3/\text{km}^2$ .

Several dome structures are recognised on seismic surveys in the Antwerp part of the Campine basin (e.g. Heibaart, Poederlee, Rijkvorsel; fig. 3-13). The dome structure near Poederlee can be recognised on seismic lines 8102 and 8106 of the Oostmalle campaign. A well was drilled by Distrigas and the Belgian Geological Survey in 1983-1984 (KB170), to a (true vertical) depth of 1643 m. The top of the limestone sequence is present at a depth of almost 1500 m, beneath more than 700 m of younger Carboniferous strata.

The spill point of the structure is located 200 m deeper. The Poederlee structure has a basal surface of about 2.5 km<sup>2</sup>. The limestones have a permeability in the range of 100 to 350

mDarcy and an estimated accessible porosity of  $2.0 \times 10^6 \text{ m}^3$ . Taking into account the density of  $\text{CO}_2$  ( $610 \text{ kg/m}^3$ ; Span & Wagner, 1996; Lemmon et al., 2005), this results in a capacity in the range of 1.2 Mton  $\text{CO}_2$ .

### 3.2.5.7 Injectivity

The injectivity for the Carboniferous Limestone Group was estimated for a reservoir at a depth of -1500 m with a productive interval of 50 m. A high, medium and low injectivity scenario was calculated. The scenarios are based on the petrophysical properties of the limestones observed at Poederlee and Merksplas. The results are summarized in table 3-20.

### 3.2.5.8 Summary

Karstified horizons within the Carboniferous Limestone Group provide sufficient porosity and permeability for the storage of  $\text{CO}_2$ .

The gas can be trapped in dome structures, covered by a seal of Namurian mudstones.

The requirements on depth and sealing are met in a large part of the western Campine Basin (Antwerp). The reservoir properties of the Carboniferous Limestone Group in the eastern part of the basin (Limburg) has to be proven.

The reservoirs developed in the limestone sequence combine a low useful porosity with high permeabilities. The average storage potential is estimated to be in the range  $1 \times 10^6 \text{ ton/km}^2$  (for a density of  $\text{CO}_2$  at reservoir conditions of  $610 \text{ kg/m}^3$ ).

The injectivity of the karstified limestone reservoirs is high.

Table 3-19: Reservoir properties of the Carboniferous Limestone Group.

	<i>Working porosity (%)</i>	<i>Permeability (mDarcy)</i>	<i>Accessible porosity (<math>10^6 \text{ m}^3/\text{km}^2</math>)*</i>	<i>Capacity (Mton <math>\text{CO}_2</math>)*</i>
<i>Carboniferous Limestone Group</i>	2.4 (1.2-3.4)	100-1000	1.2 (0.6-1.7)	0.7 (0.4-1.0)
<i>Poederlee dome</i>	3 (1.5-4)	100-350	2.0 (1.05-3.0)	1.2 (0.64-1.8)

\* 10% and 90% percentiles are given

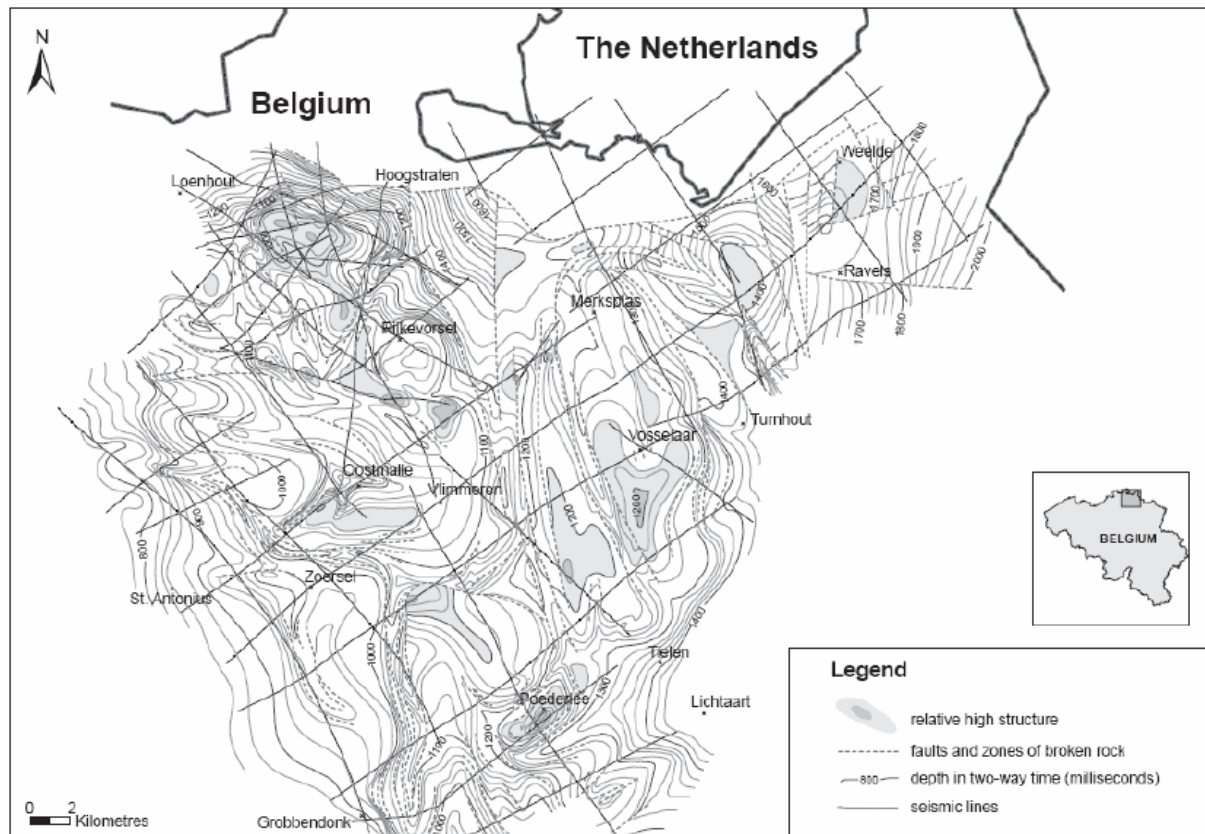


Figure 3-13: Isochrone map showing the presence of dome structures recognized on seismic surveys in the Antwerp Campine Basin (modified after Dreesen et al., 1987).

Table 3-20: Injectivity of the Carboniferous Limestone Group for three porosity and permeability conditions based on the analytical model described in section 3.2.4.5.

Scenario	$\Phi$ (%)	$k$ (mDarcy)	$PI$ ( $m^3(n)/s.bar.m$ )	$I_p$ ( $bar^2.h/m^3$ )
High	4	1000	0.30	$6.2 \times 10^{-3}$
Medium	3	100	0.031	0.060
Low	1	5	$1.56 \times 10^{-3}$	1.19

### 3.2.6 Conclusions

Based on the available well descriptions and petrophysical analyses, four potential target intervals for geological CO<sub>2</sub> storage were identified. These are:

- the chalks of the earliest Tertiary to Upper Cretaceous (Houthem and Maastricht Formations);
- the Buntsandstein Formation;
- the Neeroeteren Formation;
- karstified and fractured intervals within the Carboniferous Limestone Group.

The relatively limited surface of the target area and the lack of sufficiently large, closed structures (traps) makes the **Cretaceous** carbonate aquifer a less important target for CO<sub>2</sub> storage in Flanders (table 3-21). The reservoir units are restricted to the uppermost part of the

sequence (Houthem and Maastricht formations). The underlying, tight Gulpen chalks can contribute to the (chemical) sealing of deeper seated reservoirs. Within the Campine Basin, average accessible pore space is of the order of  $11 \times 10^6 \text{ m}^3/\text{km}^2$ . The storage potential however is limited due to the relatively shallow depth of the potential reservoirs. Contrarily, the chalks have a high injectivity.

In the northern part of the Roer Valley Graben, the Cretaceous reservoir occurs at a greater depth. Data from the Molenbeersel well however indicate that porosity and permeability in this area are much lower than in the adjacent Campine basin. Furthermore, the thickness of the Upper Cretaceous sequence is reduced to approximately 50 m in the graben area. Both observations result in a much lower storage potential. When lithologies with a permeability of less than 1 mDarcy are excluded, the average accessible pore space is estimated at a low  $0.5 \times 10^6 \text{ m}^3/\text{km}^2$ .

Table 3-21: Summary of the CO<sub>2</sub> storage characteristics of the four stratigraphic intervals that qualify for aquifer storage of CO<sub>2</sub> in Flanders.

<i>Sink</i>	<i>Geological age</i>	<i>Rock type</i>	<i>Porosity</i>	<i>Permeability</i>	<i>Reservoir type</i>	<i>Potential</i>
<i>Houthem and Maastricht formations</i>	Late Cretaceous to Paleocene	Calcarenite	High	Moderate	Small structures	Low
<i>Buntsandstein Formation</i>	Early Triassic	Sandstone	Moderate to high	Moderate	Sandstone bodies with sealing, fault-bounded in RVG	High
<i>Neeroeteren Formation</i>	Late Carboniferous	Sandstone	Moderate to high	Moderate to high	Large sandstone bodies where sealed and deeper than 800 m	Moderate
<i>Carboniferous Limestone Group</i>	Early Carboniferous	Limestone	Low to moderate	High	Relatively small karst reservoirs	High

RVG: Roer Valley Graben

The Lower Triassic **Buntsandstein Formation** appears to be promising for storage of CO<sub>2</sub> (table 3-21). It occurs at sufficient depth within the Roer Valley Graben, contains thick, porous and permeable sandstone bodies that can form good reservoirs, and it is covered by Upper Triassic to Jurassic sediments forming an adequate seal. Trapping structures may be present. The accessible pore space is estimated to be of the order of  $16 \times 10^6 \text{ m}^3/\text{km}^2$ .

The storage potential of individual reservoirs (e.g. the Verloren Kamp structure) is estimated to be in the range of 15 to 40 Mton of CO<sub>2</sub>. The injectivity of these sandstones is relatively low.

Sandstones of the **Neeroeteren Formation** provide sufficient porosity and permeability for storage of CO<sub>2</sub>. However, the reservoir is not always sealed and it is not always present at sufficient depth (table 3-21). The requirements on depth and sealing may be met in the Roer Valley Graben, but the presence of the Neeroeteren Formation and its reservoir properties in that area remain to be proven. If the reservoir characteristics in the graben area are the same

as in the explored part of the Campine basin, the accessible pore space will be in the range of 15 to 24 x 10<sup>6</sup> m<sup>3</sup>/km<sup>2</sup>, assuming a cumulative pay zone thickness of 200 m and porosity values in the range of 8 to 15%. As for the Buntsandstein, the injectivity of the Neeroeteren sandstones is relatively low

Karstified horizons within the **Carboniferous Limestone Group** (table 3-21) provide sufficient porosity and permeability for the storage of CO<sub>2</sub>. The CO<sub>2</sub> can be trapped in dome structures, covered by a seal of Namurian mudstones. The storage potential of the limestone sequence however is limited due to the low accessible pore volume (expected to be in the range of 2 to 3% of the total rock volume) and the limited thickness of the pay zone (50 m on average, but locally up to 200 m). Taking into account a net pay zone of 50 m, the accessible porosity amounts to 1.2 x 10<sup>6</sup> m<sup>3</sup>/km<sup>2</sup>. The estimated injectivity of the limestone reservoirs is high. The storage potential of individual traps is estimated to be small. For example, the amount of CO<sub>2</sub> that can be trapped within the Poederlee dome is estimated at 0.86 to 2.30 Mton.

### 3.3 Walloon Region

This section presents the sink inventory for the Walloon Region. Potential sink options in the Walloon Region were in a first stage selected on the basis of general geological requirements for CO<sub>2</sub> geological storage. Based on this screening, two types of favourable geological settings were found suitable for CO<sub>2</sub> sequestration in the Walloon Region, namely the coal deposits extending from the Hainaut to Namur and some minor potential sites near Huy and Liège and the Dinantian geothermal aquifer in Southern Belgium. Other potential aquifer sinks in the Dinant Synclinorium, such as Middle Devonian carbonates and Lower and Upper Devonian sandstones, have not been investigated in detail for the project because of 1) general geological requirements (mainly depth and presence of suitable cap rock), 2) distance of possible sinks from emission sources, which is generally >10 km and 3) exploration results for natural gas storage in these aquifers.

#### 3.3.1 Storage in (unmined) coal deposits

##### 3.3.1.1 Methodology

###### *a) Defining target areas*

Potential CO<sub>2</sub> reservoirs in coal seams were selected based on available geological and mining maps and the general geological requirements for geological storage of CO<sub>2</sub>. The Westphalian (A & B) coal beds extend from the Belgian-French border over Mons, Charleroi, Huy to Liège (fig. 3-14). In the selection for Westphalian reservoirs, those deposits were selected that lie in the 700 to 1300 m depth range (fig. 3-15). This depth range relates to the preferential supercritical state of CO<sub>2</sub> for geological storage, the optimal injectivity and adsorption capacity of the coal. Subsequently, the selection continues by removal of the mined areas from the selection (fig. 3-16), argued by obvious safety reasons. Finally, the resulting areas are screened for other geological requirements such as the occurrence of seals.

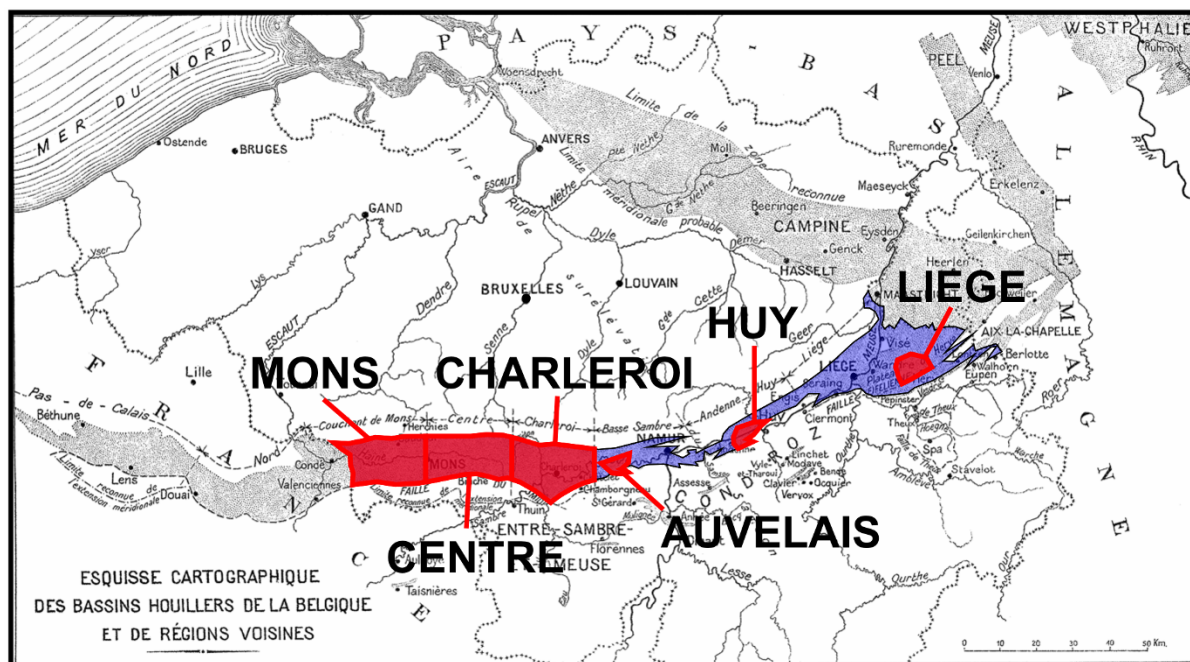


Figure 3-14: Location of the major coal deposits in the Walloon Region (in blue) and the selected area for evaluation (in red).

#### b) Data collection

Data quantity and quality are very different for each targeted sink in the Walloon Region. Data on coal seams and coalmines are abundant, but they are strongly dispersed in different institutions/associations. Moreover, with the exception of a few compilation reports, they are usually only available in raw format.

The major part of the data were collected at GSB and FPMs, while some minor additional data were provided by ULg, UNERBEL, SCBL, and SAICOM. The data mainly consist of old maps and sections, old borehole descriptions and only a few more recent reports or thesis, etc. Mined areas in the coal deposits are rendered in great detail by systematic maps and sections. It would have required an enormous amount of work to process the data (mostly digitalization) for the extrapolation in the unmined adjacent areas. It was decided not to deal with this in the framework of this project, since the unmined areas immediately surrounding mined ones have a low potential as CO<sub>2</sub> reservoirs. In the most interesting areas in terms of potential capacity, namely the virgin coal deposits lying south of the Midi fault, geological data are scarcer and they consist mainly of old (early XIXth) borehole descriptions. Although these are very difficult to use due to extreme complexity of the geological structure, lack of azimuth data and shallow depth of investigation, a compilation of borehole data was carried out using MS Excel sheets that allow analysis of the coal, sandstone and shale properties such as thickness or rank (which can be retrieved for individual seams, the whole borehole or within a given depth range).

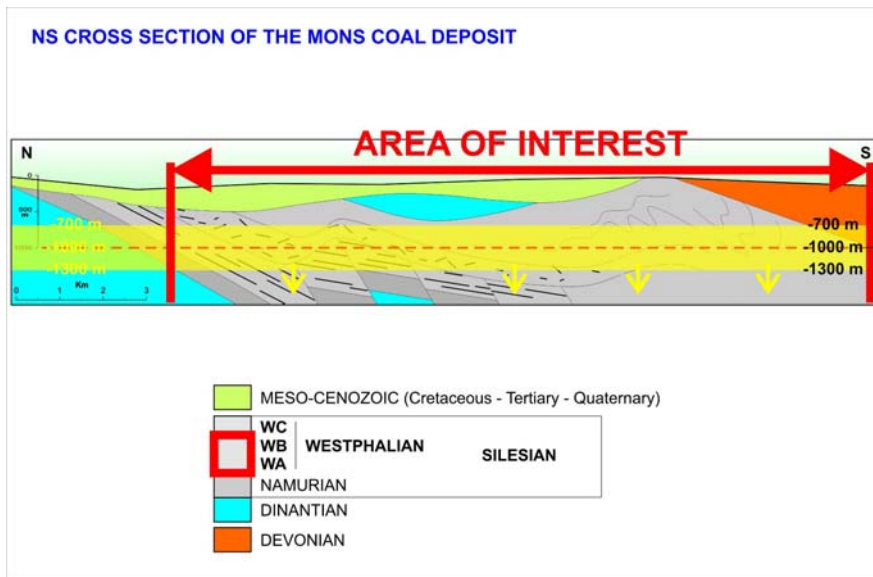


Figure 3-15: The determination of the interesting part of the coal deposits (in grey) is based on the 700 to 1300 m depth interval.

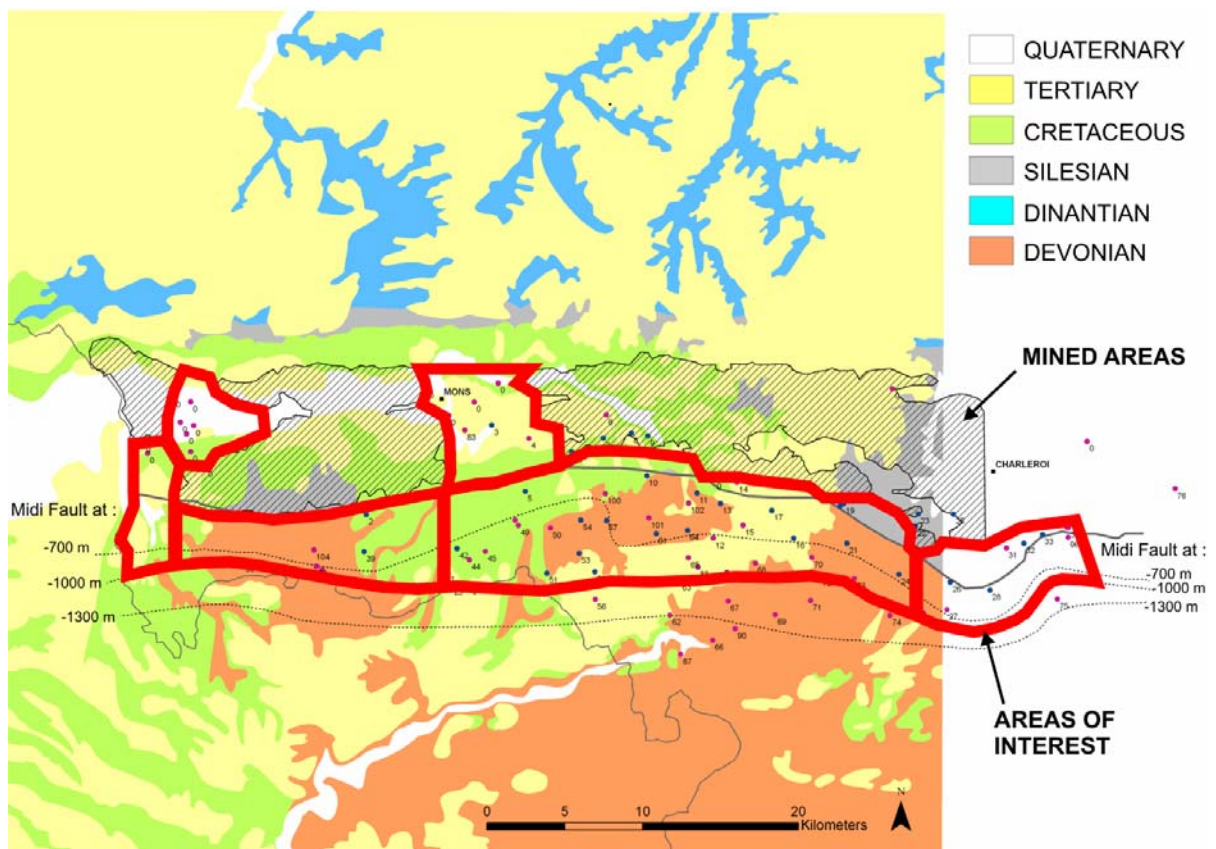


Figure 3-16: Resulting target area for CO<sub>2</sub> storage evaluation in coal deposits in the Walloon Region (Hainaut-Centre region).

*c) Evaluation of the Westphalian A & B lithology*

Six boreholes (Brasserie, Jardiné, Thulin INIEX1, Ragoda, HP14 and Thulin) were analysed for their content of coal, shale and sandstone. Coal represents only 1 to 4% of the volume of the Westphalian A & B coal deposit layers, which is rather low compared to other coal basins. In average, the coal content was 2.3%, shale 78.4% and sandstone 19.3% (table 3-22) of the studied sections (between about 480 and 1090 m long). The coal occurs in thin seams of 1 m in average.

*d) Evaluation of capacity*

The capacity evaluation was performed by the classical method using available volume, specific capacity and correction factors. However, the low coal content (2,5%) and seam thickness (<1m in average) as well as extreme folding and faulting in most of the target areas are highly unfavourable to classical single seam injection techniques. Hence, a novel approach was used here that takes into account the possible contribution of all Westphalian lithologies (siliciclastics), namely shales and sandstones along with the coal, in the perspective of multi-seam injection projects.

Storage processes vary according to the considered lithology (fig. 3-17). Physical storage, i.e. as free CO<sub>2</sub> in rock porosity, is likely to be significant in porous rock such as sandstones. Although Westphalian sandstones have never been considered as good reservoirs because of their overall low porosity (0 to 10%, lower than 5% in most cases), clearly they have a higher capacity than coal (porosity of about 0,5%) and shales (porosity less than 0,1%). As shown in figure 3-17, the assessment of the sandstone contribution to the total CO<sub>2</sub> storage capacity was limited to storage in porosity, although reactions with Fe- and Mg-bearing minerals to form stable carbonates, dissolution in formation water and adsorption on coal/clay particles are other processes that can substantially increase the storage capacity. The estimation was thus based only on realistic porosity values derived from the few analyses of reservoir properties that are available for Westphalian A sandstones. Sandstone abundance, which is approximately 10-30% volumetric of the total deposit, was retrieved from borehole descriptions (see table 3-22). The sandstone accessibility was set two times higher than that for coal.

Fine-grained sandstones as well as siltstones or shaly sandstones, sometimes called psamites or other local names, were included in the same lithology group along with true shales. It is therefore probable that the shale contribution will be larger than expected for true shales. The shale accessibility was set four times lower than that for coal. This latter value is not supported by measurements nor by published data but set arbitrarily higher than the porosity ratio (0,5% for the coal and 0,01% for the shales or 10 times lower).

*Table 3-22: Overview of lithology (coal, shale and sandstone) distribution in the studied boreholes.*

<b>Drilling</b>	<b>coal (m)</b>	<b>shale (m)</b>	<b>sandstone (m)</b>	<b>total (m)</b>	<b>coal (%)</b>	<b>shale (%)</b>	<b>sandstone (%)</b>
<i>Brasserie</i>	31.4	663.2	104.4	799.0	3.9	83.0	13.1
<i>Jardiné</i>	20.7	653.6	207.2	881.5	2.3	74.1	23.5
<i>Thulin INIEX1</i>	13.5	491.4	176.9	681.8	2.0	72.1	25.9
<i>Ragoda</i>	16.0	789.9	186.7	992.6	1.6	79.6	18.8
<i>HP14</i>	16.3	358.3	103.9	478.5	3.4	74.9	21.7
<i>Thulin</i>	6.2	943.7	137.0	1086.9	0.6	86.8	12.6
<b>AVERAGE</b>	17.4	650.0	152.7	820.1	2.3	78.4	19.3

LITHOLOGY	CO <sub>2</sub> STORAGE PROCESS		
	PHYSICAL	PHYSICO-CHEMICAL	CHEMICAL
	(Volumic)	(Adsorption)	(Mineral trapping)
COAL	Low porosity	adsorption on coal	-
SANDSTONE	medium porosity	adsorption on coal & clay particles	reaction with feldspar & clays
"SHALES"	Low porosity	adsorption on clays	reaction with clays

Figure 3-17: Storage processes that are likely to occur for each lithology in coal deposits. Some of them were neglected for this evaluation due to the lack of reliable data, but they may all contribute to significantly increase the global capacity.

Coal accessibility to injected gas, which is a crucial parameter, was inspired from German colliery experience and preliminary results from the RECOPOL Project.

Another factor that is also poorly constrained but probably crucial is the contribution of fracture porosity. Considering the vast amount of sandstone and shales in coal deposits (more than 95% vol.), there is an urgent need for collecting reliable data on intrinsic and *in situ* petrophysics for these dominant lithologies.

Physico-chemical storage, i.e. by adsorption, is the process receiving the most attention in storage projects in coal seams. Coal is able to adsorb a considerable amount of gases, especially CO<sub>2</sub>. The coal contribution by adsorption storage to the total CO<sub>2</sub> storage capacity was assessed using the classic method to obtain the coal adsorption capacity. Thereby, the method of Hildenbrand et al. (2006) was used in combination with sorption isotherms recorded at FPMs (fig. 3-18). This starts with the gas in place (GIP) evaluation from the rank (which is the only petrophysical data widely available on South Belgian coals). GIP vs. coal rank data were found in Hildenbrand et al. (2006) and CO<sub>2</sub>/CH<sub>4</sub> ratio was set to two as it is widely used for evaluation purposes. The depth range used for calculations was 700-1300 m, to ensure supercritical state for the CO<sub>2</sub>, with local possibility of deepening the reservoir bottom. However, reservoir conditions were assimilated to those prevailing at a depth of 1000 m and for a normal geothermal gradient (i.e. 30°C/km), for example, for the calculation of the density of supercritical CO<sub>2</sub>. This method was successfully checked by comparison with direct adsorption capacity measurement on a coal sample collected in a shallow stonedrift. The decrease of adsorption capacity due to humidity was taken into account using experimental data recorded at the FPMs Thermodynamics Department on the same sample as well as on a Westphalian coal sample from Silesia, Poland (sample from the injection seam used in the RECOPOL Project). Results were implemented as a factor with values ranging from 0,6 (water vapour saturation) to 1 (dry coal). Also the influence of CH<sub>4</sub> desorption (sweep efficiency) was provided by FPMs lab data.

Clay minerals may also behave in a similar way in reservoir conditions. However, the process is poorly understood since it is, for example, likely that measured adsorption capacities also include chemical reactions (Busch A., pers. communication). The shale contribution by adsorption storage was also evaluated by general assessment regarding petrophysics and by the newly discovered CO<sub>2</sub> adsorption (and/or mineral trapping) capacity of shales (RWTH-Aachen). More investigation is needed to constrain the adsorption processes and capacity of Westphalian shales from Belgium. However, we used for the evaluation a mean value of the adsorption capacity recorded in Westphalian shales from Germany. Humidity influence on shale “adsorption” was taken into account in the same way as for the coal.

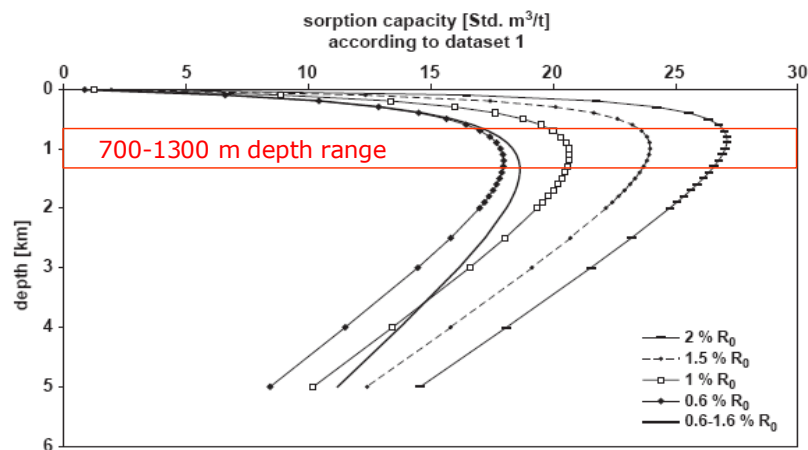
Hildenbrand *et al.* (2006)

Figure 3-18:  $\text{CH}_4$  sorption capacity of Westphalian coal from northern Belgium as a function of depth and rank. The rank is indicated in the  $R_0$  (vitrinite reflectance) range. The equivalent  $\text{CO}_2$  sorption capacity is assumed to be twice that value based on the widely reported molecular adsorption ratio for these gases.

Chemical storage, i.e. mineral trapping, is the best rated process for long-term storage. Ca, Na, Mg and  $\text{Fe}^{2+}$  silicate minerals such as chlorite and feldspar react with  $\text{CO}_2$  to form stable carbonate precipitates. Mineral trapping in coal deposits may play a significant role as chlorite and feldspar occur in Belgian Westphalian rocks. However, this process is not taken into account in this evaluation due to the lack of quantitative data.

The total capacity evaluation scheme, combining the adsorption storage capacity in coal and shale and the physical (porosity) storage in coal, shale as well as sandstone layers of the Westphalian A & B is presented in figure 3-19. It clearly shows the calculation procedure that was explained above. The volume percentages of coal, shale and sandstone are the average values based on the borehole data, as shown in table 3-22. The cumulated thickness for the different lithologies are based on the volume percentages for the interval of 700 to 1300 m depth. Based on this thickness value, the physical  $\text{CO}_2$  storage potential can easily be determined using an average value for porosity and accessibility in the respective lithologies. In contrast to the calculation of reserves for physical storage, the reserves for adsorption storage are expressed in weight per area (instead of volume per area) using the density of coal and shale. The accessible reserves in the coal layers take account of the coal accessibility, humidity and sweep efficiency, since the further calculation is only based on the amount of methane that is present in the coal layers and replacing this by the double of  $\text{CO}_2$  mole amount. In contrast, for the shale layers the value for accessible reserves given takes account of only the shale accessibility, while the shale humidity is considered in the  $\text{CO}_2$  adsorption capacity.

### 3.3.1.2 Capacity evaluation results

In figure 3-19, the calculation is presented for average values of parameters and factors in coal, shale and sandstone layers. The calculation for this base case results in an average total  $\text{CO}_2$  sequestration potential of 1.56  $\text{Mt}/\text{km}^2$ . The distribution of the storage capacity between the different lithologies and storage type is presented on figure 3-20. Based on this set of realistic parameters, the evaluation results show that coal contributes up to only 15% to the global storage capacity, which is much smaller than the sandstone (<40%) and shale (<50%)

contribution (fig. 3-20). This stresses the importance of taking account of the siliciclastics in addition to the coal.

This distribution as presented in figure 3-20 can, however, seriously change when the parameters are varied within their range given in figure 3-19. The influence of the coal accessibility, coal humidity, shale porosity, shale humidity, sandstone porosity and sandstone accessibility is examined and the total CO<sub>2</sub> potential capacity and the distribution results between different lithologies are given below.

Variations in the coal gas-in-place, coal accessibility and coal humidity within their given range result in only minor differences with respect to the total CO<sub>2</sub> storage capacity as well as the contribution of the different lithologies and storage type (fig. 3 21, 3-22 and 3-23). This minor influence is related to the low average volume percentage (2.3%) of the coal content compared to the shale and sandstone proportion in the Westphalian layers and their storage capacities.

	ADSORPTION		POROSITY		TOTAL	
COAL	Volume percentage coal (%)	2.31				
	Cumulated thickness (m)	13.85				
	Reserves (Mt/km <sup>2</sup> )	18.69				
	Accessible reserves (Mt/km <sup>2</sup> )	2.39				
	CH <sub>4</sub> adsorption capacity at 1000m (Nm <sup>3</sup> /t)	15.00	25.00			
	Corresponding moles of CH <sub>4</sub>	669.26	1115.44	Reserves (Mm <sup>3</sup> /km <sup>2</sup> )	13.85	
	Corresponding moles of CO <sub>2</sub>	1338.53	2230.88	Pore volume (Mm <sup>3</sup> /km <sup>2</sup> )	0.07	
	CO <sub>2</sub> adsorption capacity at 1000m (Kg/t)	58.90	98.16	Accessible pore volume (Mm <sup>3</sup> /km <sup>2</sup> )	0.01	
	CO <sub>2</sub> sequestration potential (kt/100m/km <sup>2</sup> )	23.49	39.15	CO <sub>2</sub> sequestration potential (kt/100m/km <sup>2</sup> )	1.50	
	CO <sub>2</sub> sequestration potential (Mt/km <sup>2</sup> )	0.14	0.23	CO <sub>2</sub> sequestration potential (Mt/km <sup>2</sup> )	0.01	0.15 0.24
SHALE	Volume percentage shale (%)	78.42				
	Cumulated thickness (m)	470.51				
	Reserves (Mt/km <sup>2</sup> )	1176.27				
	Accessible reserves (Mt/km <sup>2</sup> )	58.81		Reserves (Mm <sup>3</sup> /km <sup>2</sup> )	470.51	
	CO <sub>2</sub> adsorption capacity (mol/t)	236.00		Pore volume (Mm <sup>3</sup> /km <sup>2</sup> )	4.71	
	CO <sub>2</sub> adsorption capacity (Kg/t)	10.38		Accessible pore volume (Mm <sup>3</sup> /km <sup>2</sup> )	0.24	
	CO <sub>2</sub> sequestration capacity (kt/100m/km <sup>2</sup> )	101.79		CO <sub>2</sub> sequestration potential (kt/100m/km <sup>2</sup> )	25.49	
	CO <sub>2</sub> sequestration capacity (Mt/km <sup>2</sup> )	0.61		CO <sub>2</sub> sequestration potential (Mt/km <sup>2</sup> )	0.15	0.76
SANDSTONE			Volume percentage sandstone (%)	19.27		
			Cumulated thickness (m)	115.65		
			Reserves (Mm <sup>3</sup> /km <sup>2</sup> )	115.65		
			Pore volume (Mm <sup>3</sup> /km <sup>2</sup> )	2.31		
			Accessible pore volume (Mm <sup>3</sup> /km <sup>2</sup> )	0.93		
			CO <sub>2</sub> sequestration potential (kt/100m/km <sup>2</sup> )	100.23		
TOTAL	CO <sub>2</sub> sequestration potential (Mt/km <sup>2</sup> )	0.75 0.85		0.76	1.51 1.61	

PARAMETERS AND FACTORS		RANGES	
coal density	1.35		
coal porosity (%)	0.5	0.1	1
coal accessibility	0.2	0.1	0.3
coal humidity	0.8	0.6	1
sweep efficiency (CH <sub>4</sub> by CO <sub>2</sub> )	0.8		
shale density	2.5		
shale porosity (%)	0.01	0.001	0.5
shale accessibility	0.05	0.001	0.1
shale humidity	0.8	0.6	1
sandstone efficient porosity (%)	2	0.1	5
sandstone accessibility	0.4	0.1	0.6
sandstone water saturation	1		
planned depth (m)	700 1300		
supercritical CO <sub>2</sub> density	0.65		

Figure 3-19: Total capacity evaluation scheme for unmined coal deposits. The total CO<sub>2</sub> sequestration values are expressed in million tons per square kilometre and two results are here presented based on the minimum and maximum methane adsorption capacity in the coal layers.

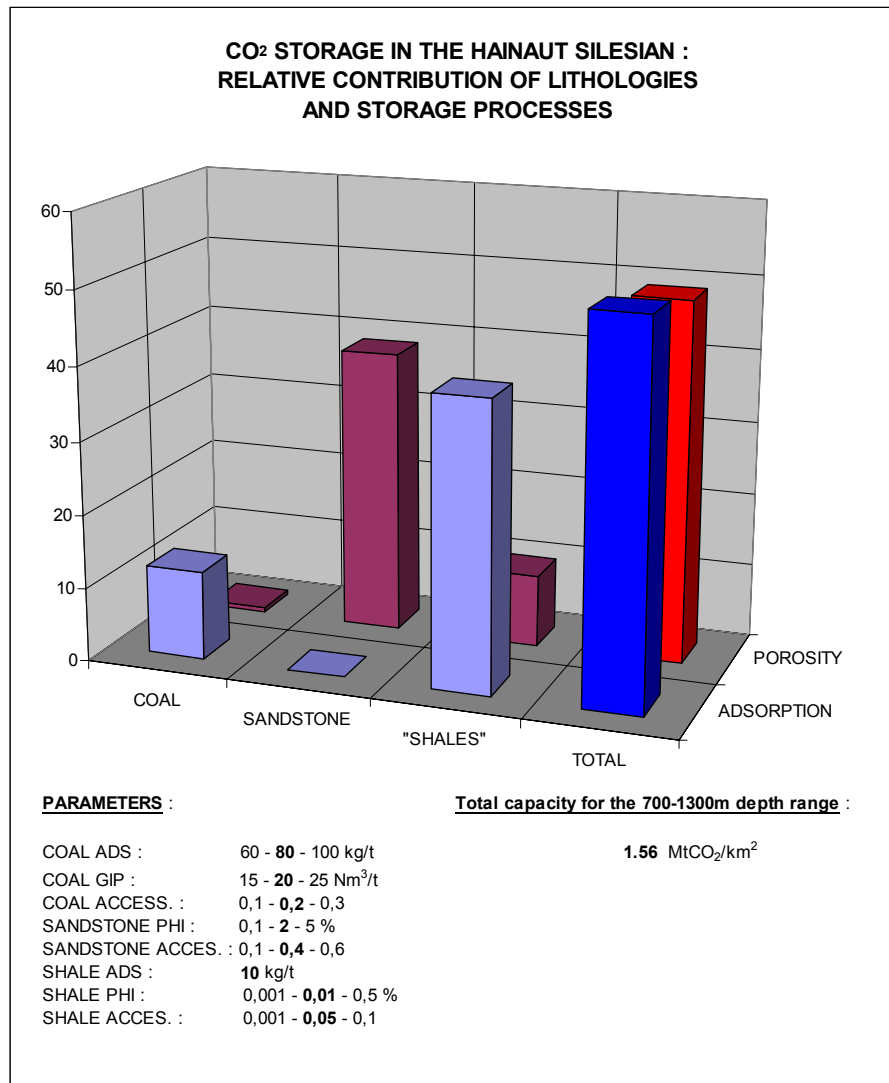


Figure 3-20: Relative contribution of the different lithologies to the global CO<sub>2</sub> storage capacity in Westphalian deposits of southern Belgium. The parameters ranges are given for coal adsorption (ads), coal gas-in-place (GIP), coal accessibility (access), sandstone porosity (phi), sandstone accessibility (aces), shale adsorption (ads), shale porosity (phi) and shale accessibility (aces). The values in bold are those used in the capacity calculation presented on this figure.

The effect of varying sandstone and especially shale characteristics has thus a more important effect on the total capacity and on the distribution between lithologies and storage types. The highest total capacity is obtained using the maximum value for shale porosity, which results then in 9.05 Mt CO<sub>2</sub>/km<sup>2</sup> (fig. 3-24), whereas the lowest capacity is obtained by using the minimum value of shale accessibility (fig. 3-25). Varying the shale accessibility, the sandstone porosity or the sandstone accessibility, the distribution in such a way affected that the dominant storage capacity changes from shale adsorption storage to sandstone physical (porosity) storage (fig. 3-25, 3-26 and 3-27). The variation of these three parameters within their given range leads to a total capacity value between 0.81 and 2.46 Mt CO<sub>2</sub>/km<sup>2</sup>.

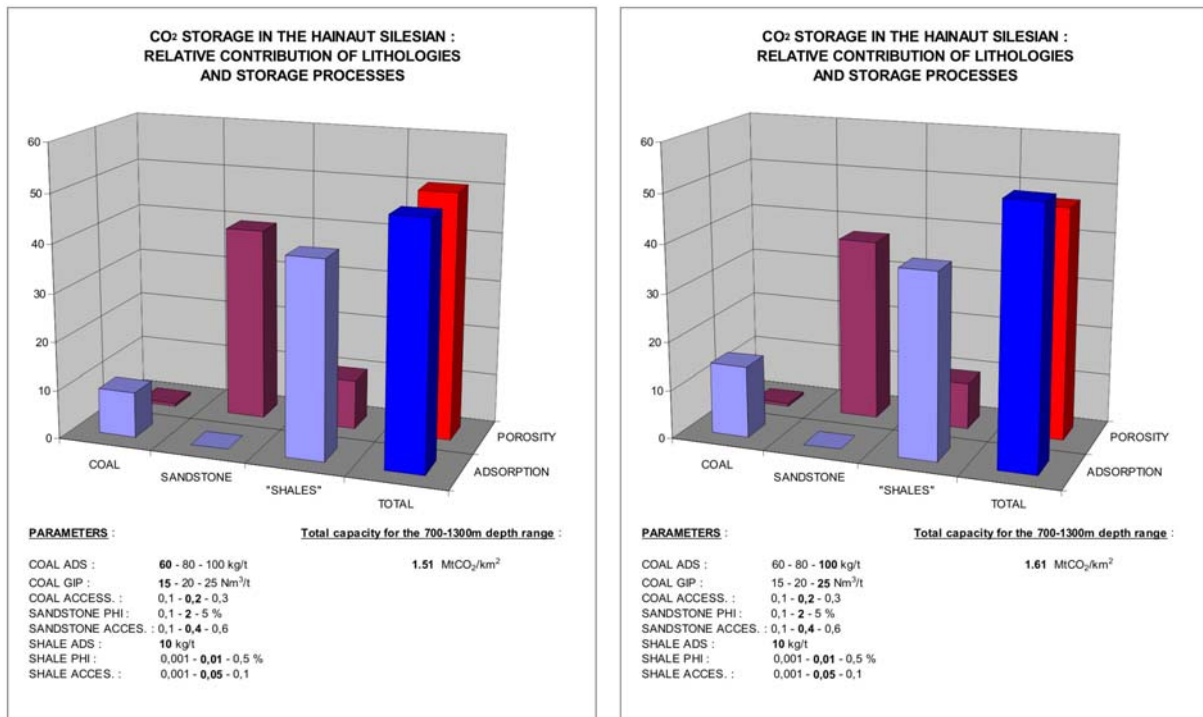


Figure 3-21: Influence of variation in coal gas-in-place (GIP) on the relative contribution of coal, shale and sandstone and storage type using the minimum and maximum value of the coal GIP range. Total CO<sub>2</sub> storage capacity lies between 1.51 and 1.61 Mt/km<sup>2</sup>.

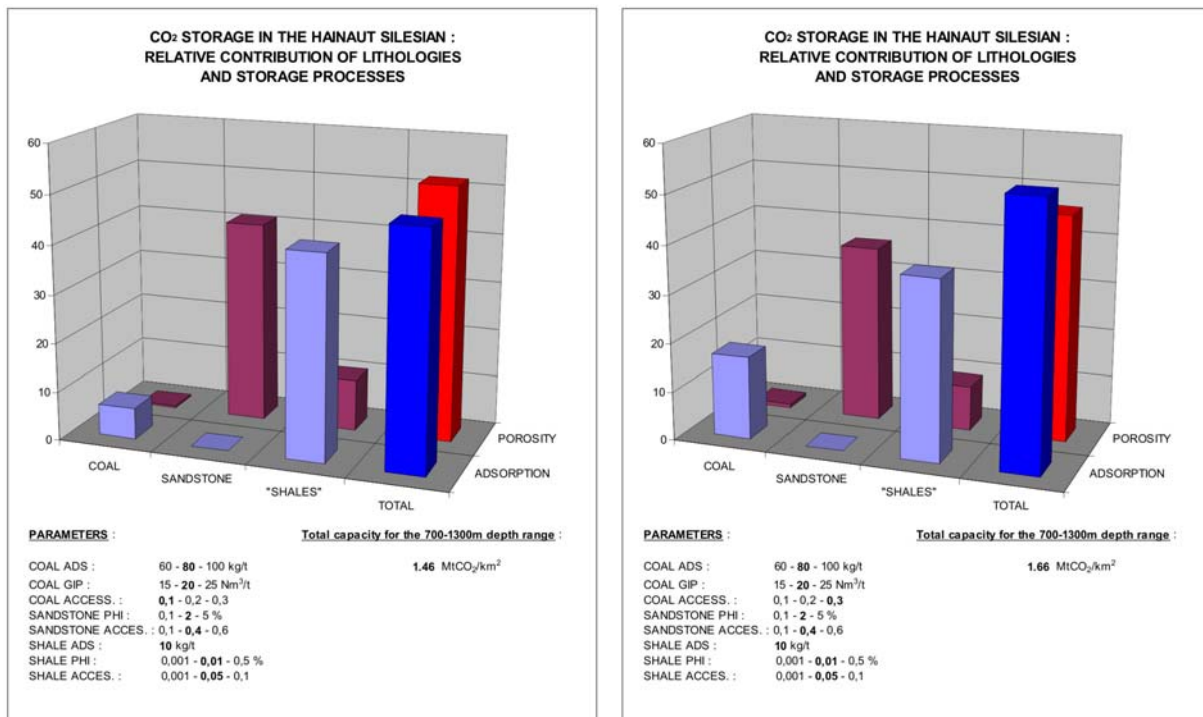


Figure 3-22: Influence of variation in coal accessibility on the relative contribution of coal, shale and sandstone and storage type using the minimum and maximum value of the coal accessibility range. Total CO<sub>2</sub> storage capacity lies between 1.46 and 1.66 Mt/km<sup>2</sup>.

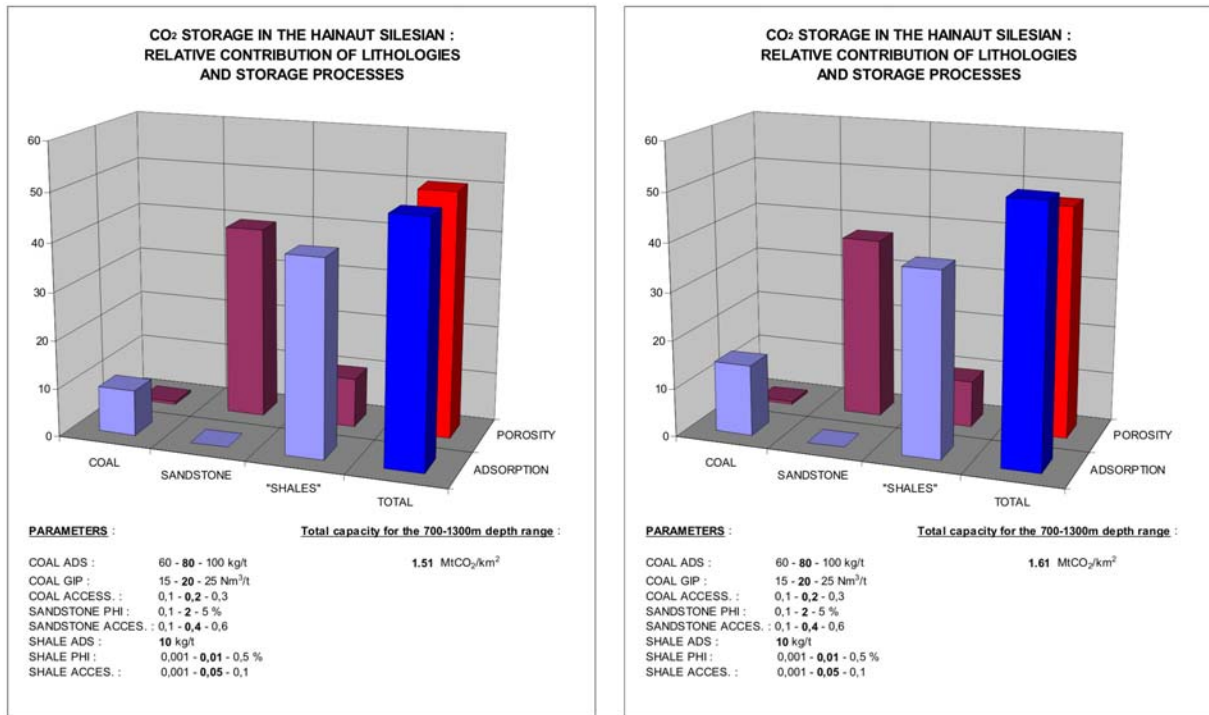


Figure 3-23: Influence of variation in coal humidity on the relative contribution of coal, shale and sandstone and storage type using the minimum and maximum value of the coal humidity range. Total CO<sub>2</sub> storage capacity lies between 1.51 and 1.61 Mt/km<sup>2</sup>.

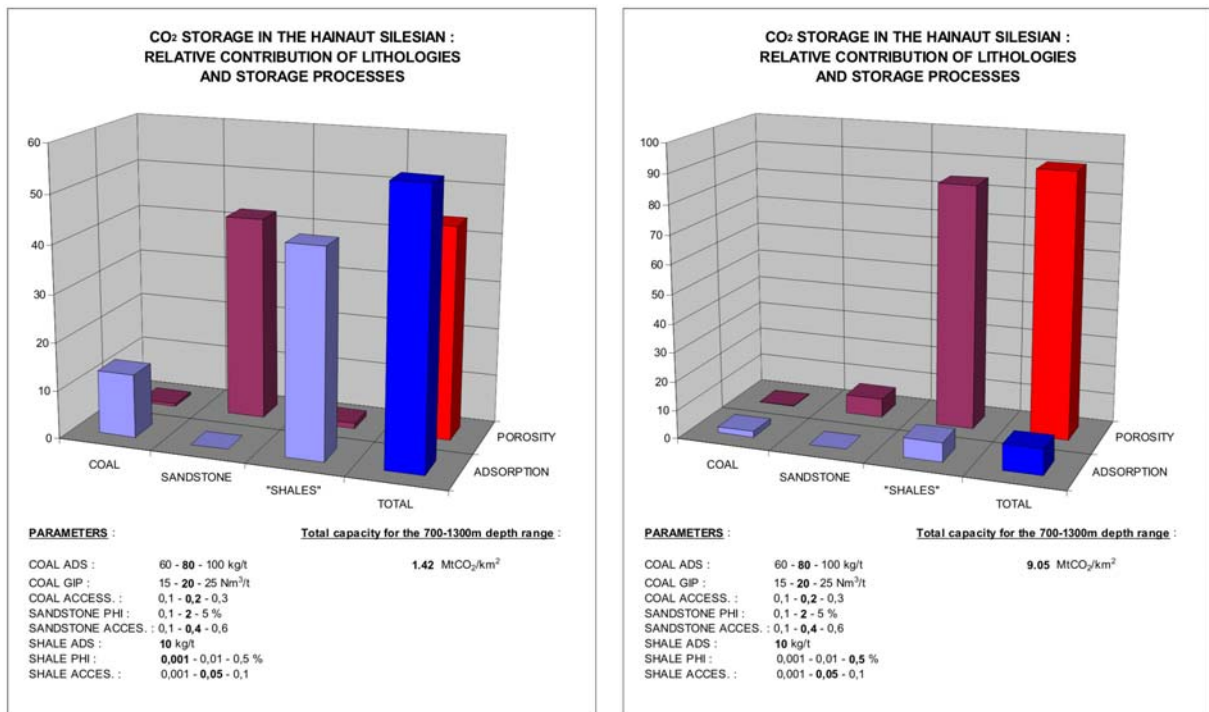


Figure 3-24: Influence of variation in shale porosity on the relative contribution of coal, shale and sandstone and storage type using the minimum and maximum value of the shale porosity range. Total CO<sub>2</sub> storage capacity lies between 1.42 and 9.05 Mt/km<sup>2</sup>.

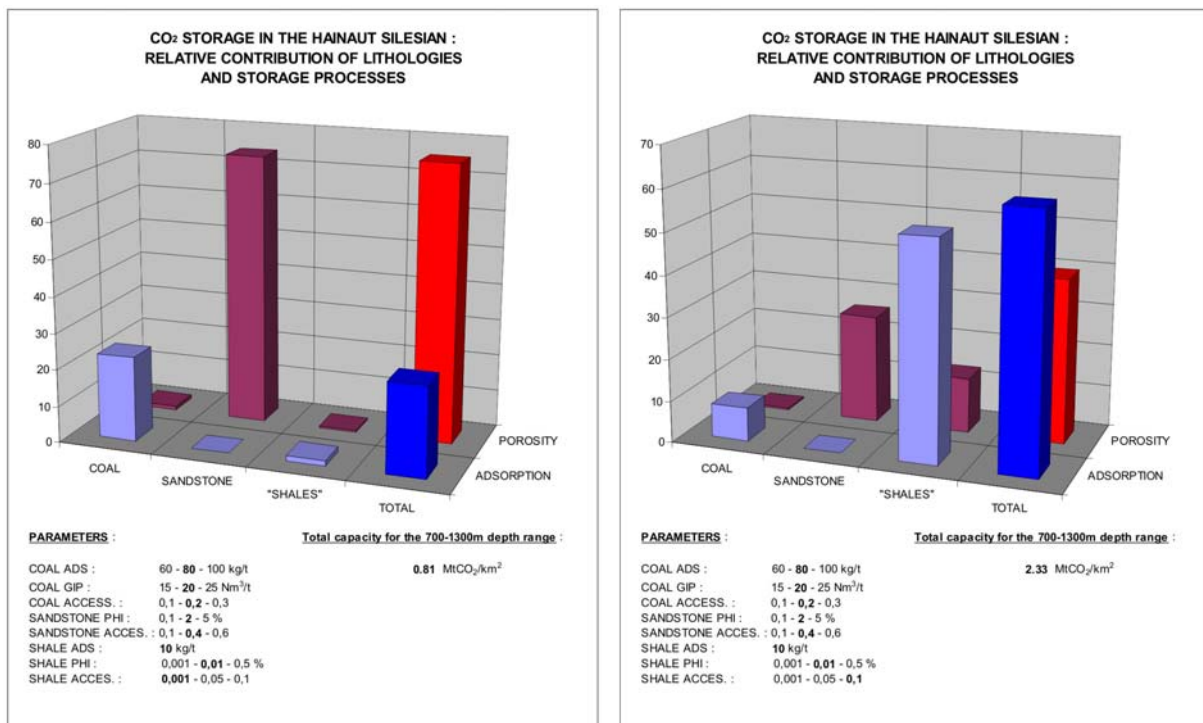


Figure 3-25: Influence of variation in shale accessibility on the relative contribution of coal, shale and sandstone and storage type using the minimum and maximum value of the shale accessibility range. Total CO<sub>2</sub> storage capacity lies between 0.81 and 2.33 Mt/km<sup>2</sup>.

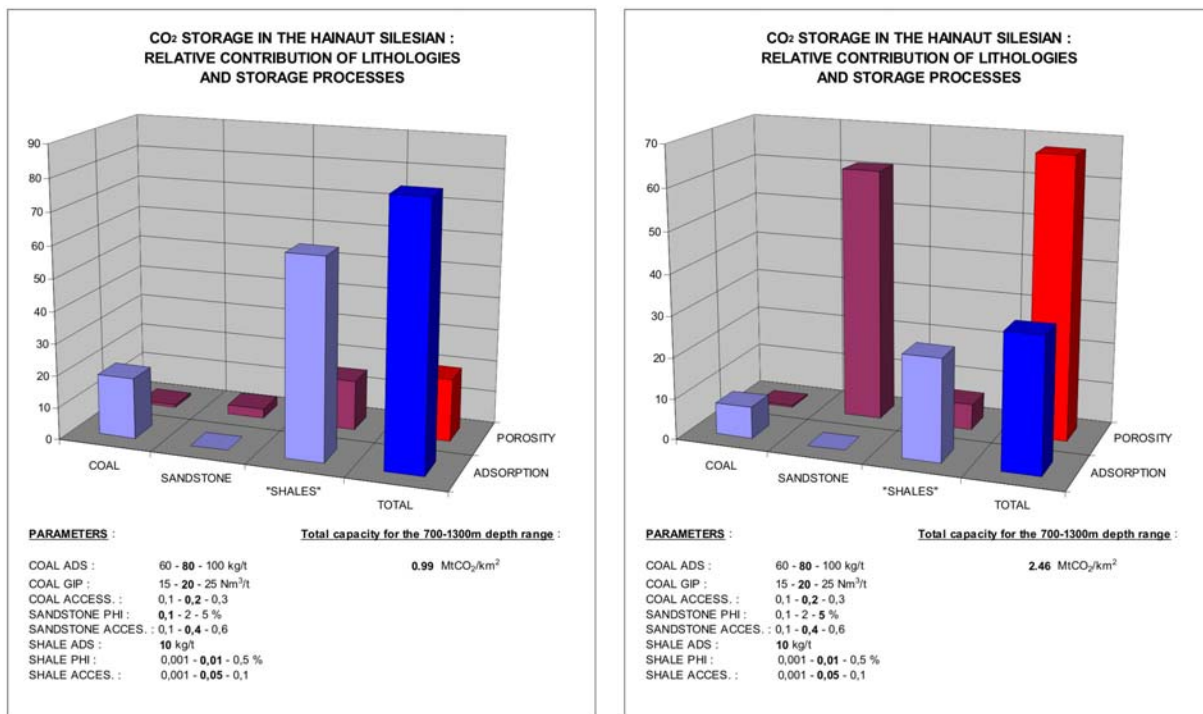


Figure 3-26: Influence of variation in sandstone porosity on the relative contribution of coal, shale and sandstone and storage types using the minimum and maximum value of the sandstone porosity range. Total CO<sub>2</sub> storage capacity lies between 0.99 and 2.46 Mt/km<sup>2</sup>.

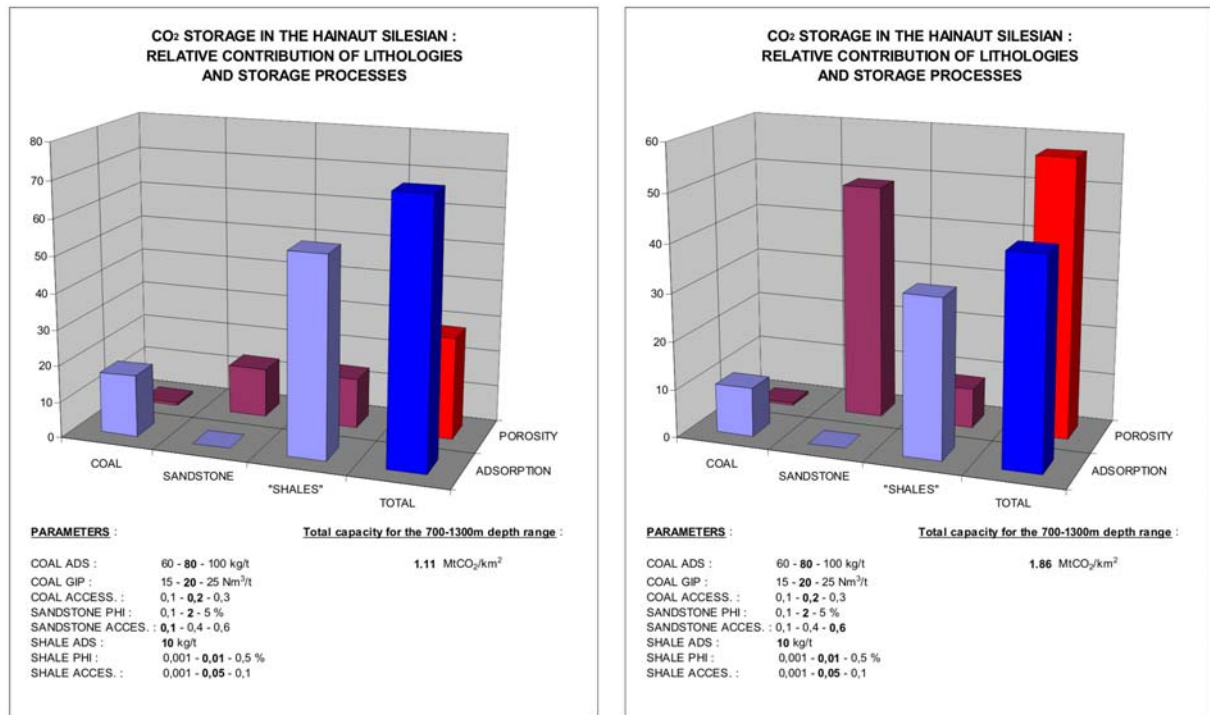


Figure 3-27: Influence of variation in sandstone accessibility on the relative contribution of coal, shale and sandstone and storage types using the minimum and maximum value of the sandstone accessibility range. Total CO<sub>2</sub> storage capacity lies between 1.11 to 1.86 Mt/km<sup>2</sup>.

Taking account of the storage capacity in shale and sandstone, has not only the effect of enhancing the overall reservoir capacity, but siliciclastics may also offer other advantages. For example, sandstone frequently occurs as thick (up to 30 m) flat lenses facilitating single seam injection. In addition, cyclothemic deposition in paralic basins predicts that sandstone is supposed to occur overlying the coal or even cutting it (wash out). As sandstone bodies should be significantly more permeable than coal, they could be used as high injectivity conduits spreading CO<sub>2</sub> over a large coal surface (fig. 3-28). This opens new perspectives in the search for bypassing or at least reducing the effects of low sorption kinetic and permeability drop due to coal swelling during injection. Sorption kinetics and swelling are major limiting factors in ECBM projects (Enhanced Coal Bed Methane recovery) using CO<sub>2</sub> as it was demonstrated by the first European ECBM pilot project RECOPOOL.

### 3.3.1.3 Selected Westphalian areas and their capacity estimation

Seven areas of Westphalian (unmined) coal deposits have been selected in the Walloon region as sink options for geological storage of CO<sub>2</sub>. These include:

- Zone Ia (Boussu-Thulin)
- Zone Ib (Frontière)
- Zone II (Sud Faille Midi – Mons)
- Zone III (St-Symphorien)
- Zone IV (Sud Faille Midi – Centre)
- Zone V (Charleroi)
- Zone VI (Auvélais-Namur + Andenne-Huy + Liège-Herve)

In order to calculate the sequestration potential of these zones, the area of each zone was determined and the complete thickness interval of 700 to 1300 m was considered. Only for Zone VI, the value is divided by two as the depth of the Westphalian A & B layers in this

zone rarely extends deeper than 1000 m. The sequestration potential in these zones varies from 35 to 330 Mt CO<sub>2</sub> and results in a total capacity of about 700 Mt CO<sub>2</sub> that could be stored in Westphalian unmined coal layers (taking into account the capacity of shale and sandstone) in the Walloon Region (table 3-23). We would like to remark here that there is a relatively high uncertainty on this value because of the uncertainty on some base parameters, as explained and shown in the methodology section.

### 3.3.1.4 Conclusion

Combining selected areas and capacity assessment per unit surface in the 700-1300m depth range yields an average total estimate of the storage potential in unmined coal deposits of about 700 Mt CO<sub>2</sub>.

The relative contribution of each of the three different lithologies to the total storage capacity is quite different, using petrophysical values chosen in accordance with common sense and care. Only about 15% of the storage capacity is attained by the contribution of coal layers. This is partially related to the low volume percentage of the coal layers in the Westphalian A & B sequence. Incorporating the storage capacity in the siliciclastic layers of the Westphalian is therefore important, not only because of the higher storage potential, but also because it opens new perspectives in the design of improved solutions for safe CO<sub>2</sub> storage in “poor” and complex coal deposits. As a major example, sandstone layers which are thicker than coal seams and are expected to have greater permeability may serve as conduits allowing (1) high rate injection and (2) greater CO<sub>2</sub> access to adjacent coal seams (provided, as it is theoretically expected, that sandstone layers are overlying or even cutting the coal seams and that the CO<sub>2</sub> will be able to sweep the formation water if it occurs).

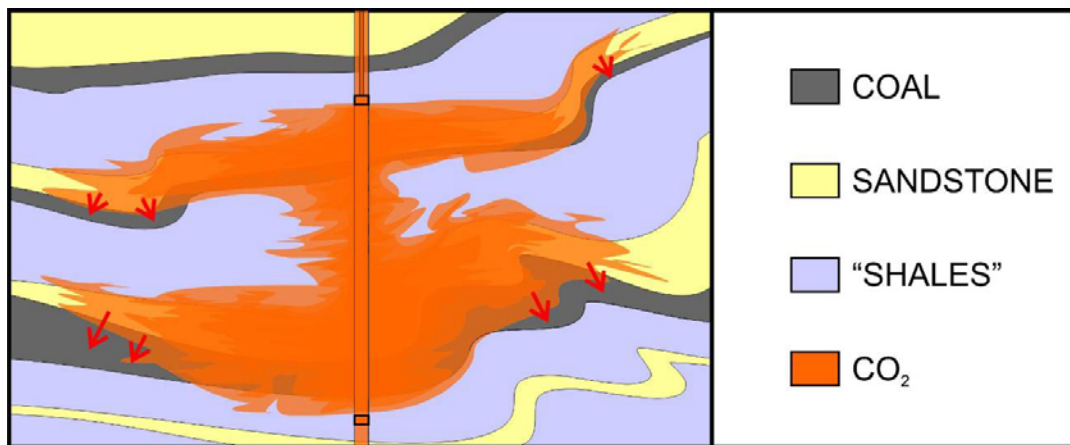


Figure 3-28: Multi-seam injection scheme using sandstone to enhance access to the coal.

Table 3-23: Results of sequestration (Mt) potential in the Hainaut Westphalian A & B layers.

	Area (km <sup>2</sup> )	Sequestration potential (Mt)				
		Porosity	Adsorption	Total		
Zone Ia (Boussu-Thulin)	27	21	20	23	41	43
Zone Ib (Frontière)	22	17	17	19	33	35
Zone II (Sud Faille Midi - Mons)	73	56	55	62	111	117
Zone III (St-Symphorien)	40	31	30	34	61	64
Zone IV (Sud Faille Midi - Centre)	205	156	154	173	311	330
Zone V (Charleroi)	50	38	38	42	76	80
Zones VI (Auvelais-Namur - Andenne-Huy - Liège-Herve)	27.5	21	21	23	42	44
TOTAL :	444.5	339	334	376	673	715

Therefore, sandstone and coal are expected to store CO<sub>2</sub> within the short- and mid-term respectively whereas storage in shales by adsorption and/or mineral trapping would require much more time due to low accessibility and reaction kinetics. Shales can also be considered as active cap rock ensuring physico-chemical and chemical CO<sub>2</sub> fixation in addition to physical sealing (but in turn, it can slow or even prevent sweeping at the formation water in the sandstone). The potential storage capacity for shales is comparable to that of the sandstone but changing the porosity from 0,01% (as in the base case) to 0,1% makes the shale contribution larger than twice the contribution of coal and sandstone together (and this multiplies the total capacity by almost 2). This value should not be considered as outrageously high for the shales we considered as the actual lithologies behind this term in Westphalian deposits comprises siltstones and fine-grained sandstones along with true shales. To support this, a hydrogeological report mentioned 0,8% as porosity value for Westphalian “shales” in the Liège area. Accessibility factor for the shales, arbitrarily set to 5%, is also a very sensitive parameter.

Further work to obtain a more accurate evaluation of the storage potential thus strongly needs detailed and reliable petrophysical and more general reservoir data, not only for the coal, but also for all other lithologies associated with it. In particular, porosity and accessibility need to be constrained and physico-chemical storage processes, mainly adsorption on clays and mineral trapping, to be investigated in more detail. Additional porosity of tectonic origin (fractures, fold hinges, etc.) is also a crucial parameter to be taken into account as it may contribute to increase storage capacity and accessibility (but in turn may decrease sealing capacity). Besides the above mentioned lack of petrophysical data of Silesian rocks, there is a great uncertainty on the nature and the structure of the coal deposits under the Midi Fault, where most of the storage potential is expected. Petrophysical data of Silesian rocks may be first investigated from core material (to be collected) or appropriate outcrops. In contrast, exploring the coal deposit under the Midi Fault is suffering from the lack of borehole and seismic data. When these data exist, their number and/or quality is too low for accurate geological interpretation.

Regarding the geological uncertainty and the distance to emission sources, two zones appear to be good candidates for CO<sub>2</sub> pilot-projects with 40 to 50 Mt storage capacity each. In addition, in these zones, the new approach could be of particular interest as coal deposits are highly fractured and faulted within a 100 to 600m thick interval called “nappe faillée du Hainaut”. This interval, which is specific to the Hainaut coal basin, is capped by a major thrust fault (Masse Fault) and produced major gas flows in the past mining activities or when it was bored. A better knowledge of geometric and petrophysic properties of the “nappe faillée” would allow to refine considerably the capacity evaluation. There is a fair possibility of an increase of the storage capacity mainly due to the higher accessibility in this interval and, in addition, ECBM production would be facilitated.

### 3.3.2 Storage in coal mines

#### **3.3.2.1 Methodology**

##### *a) Defining target areas*

Five coal mine areas were selected for this study, namely the mines of Hensies-Pommeroeul Sartis, Hensies-Pommeroeul Louis-Lambert, Blaton-Bernissart, Anderlues and Péronnes. These mines have a variable depth range; mines at intermediate depth (600 to 1000 m) were selected for supercritical storage of CO<sub>2</sub> as well as mines at shallower depth (200 to 800 m) for CO<sub>2</sub> storage in a less dense phase. The mining areas are of interest because of the large void space, but have the disadvantage of special seal requirements.

Selection criteria are mainly based on existing reports, especially for natural gas storage, historical data and likelihood of interconnection with other adjacent mines.

*b) Data collection and Westphalian A & B lithology*

Data collection and evaluation of the Westphalian A & B lithology are explained in the methodology section for storage in (unmined) coal deposits

*c) Evaluation of capacity*

The capacity evaluation is mainly performed in the same way as for the unmined coal deposits. The evaluation procedure follows the same scheme for the coal relicts and sandstone and shale layers (see above in the methodology section of unmined coal deposits), whereas there is an additional capacity potential taking account of the large void spaces of the mines. This results in a scheme with adsorption and porosity storage capacity in relict coal and shale layers and porosity storage capacity in sandstone layers, similar to the capacity evaluation scheme for unmined coal deposits in figure 3-19. In addition, for the coal mines, the CO<sub>2</sub> sequestration potential in the residual voids is taken into account. This potential is the sum of the residual volume of the extracted rock and coal and the additional residual volume due to the subsidence (fig. 3-29). The storage in residual voids is based on the GESTCO methodology (Piessens & Duser, 2003).

RESIDUAL VOIDS			
Residual volume (Mm <sup>3</sup> /km <sup>2</sup> )		Additional residual volume due to the subsidence	
Extracted coal (Mt/km <sup>2</sup> )	3.00	Additional residual volume (Mm <sup>3</sup> )	1.09
Extracted rock (Mt/km <sup>2</sup> )	0.50	Additional residual volume (Mm <sup>3</sup> /km <sup>2</sup> )	0.36
Coal volume (Mm <sup>3</sup> /km <sup>2</sup> )	2.22		
Rock volume (Mm <sup>3</sup> /km <sup>2</sup> )	0.20		
Total volume (Mm <sup>3</sup> /km <sup>2</sup> )	2.42		
Residual volume (Mm <sup>3</sup> /km <sup>2</sup> )	0.50		
<b>CO<sub>2</sub> sequestration potential (Mt/km<sup>2</sup>)</b>	<b>0.28</b>	<b>CO<sub>2</sub> sequestration potential (Mt/Km<sup>2</sup>)</b>	<b>0.20</b>

**PARAMETERS AND FACTORS**

% extracted rock compared to extracted coal	0.17
rock density	2.5
% collapse or rise	0.99
residual volume fraction	0.2
terrain uprising due to hydrostatic pressure (m)	0.15
average reservoir pressure : 120% of the hydrostatic pressure	1.2

Area of the mine (Km <sup>2</sup> )	3.00
Corresponding radius	0.98
Influence angle	20.00
Depth (km)	1.00
Subsidence area radius (Km)	1.39
Subsidence surface area (Km <sup>2</sup> )	6.03

Figure 3-29: Additional scheme for capacity evaluation of the residual void space in coal mines.

**3.3.2.2 Selected mines and their capacity estimation**

Five mine areas were selected. For the Hensies-Pommeroeul Sartis and Blaton-Bernissart mines, a depth range of 200 to 800 m was considered. The storage capacity for the Hensies-

Pommeroeul Louis-Lambert and Anderlues mines was calculated for a depth range of 600 to 1000 m. The capacity value for the Péronnes mine is based on the data from Piessens & Dusar (2003) in the GESTCO project.

For the Hensies-Pommeroeul Sartis and Blaton-Bernissart mines, the capacity is estimated based on an average value for the CO<sub>2</sub> density of 131.3 kg/m<sup>3</sup>, whereas this value is taken 550 kg/m<sup>3</sup> for the Hensies-Pommeroeul Louis-Lambert and Anderlues mines.

The sequestration potential in these mines varies from 3 to 14 Mt CO<sub>2</sub> per selected mine area and results in a total of about 40 Mt that could be stored in the five mines for the selected depth interval.

### **3.3.2.3 Conclusion**

A few coal mines have been selected for storage assessment using 1) the GESTCO methodology for storage in residual voids (Piessens & Dusar, 2003) and 2) the above mentioned approach for storage in the adjacent rock (table 3-24). Selected mines were assumed to be non flooded at the moment. Residual voids volume of the mine was estimated using past coal production (according to Piessens & Dusar, 2003), and the adjacent rock volume (which would contribute to the storage) by the product of mine depth by concession area. A more thorough estimation for the latter volume would require geometrical modelling of the mine network and gob zones as well as making delicate assumptions on CO<sub>2</sub> migration paths, which is not the scope of the project.

The selected coal mines are estimated to have a storage capacity of a few tens of Mt CO<sub>2</sub>.

## **3.3.3 Storage in aquifers**

### **3.3.3.1 Methodology**

#### *a) Defining target areas*

A number of arguments point out that investigations for aquifer storage in the Walloon Region should first focus on the geothermal field of Hainaut. It is indeed a large aquifer located at great depth and capped by thick Westphalian coal deposits. In addition, the aquifer is producing large quantities of geothermal water by pure artesian flow (150 m<sup>3</sup>/h for 20 years in the Saint-Ghislain well alone) and it is located near important emission sources. However, the question of conflict of interest with geothermal energy production is currently addressed. It is worth noting that both utilizations are not completely incompatible, but require a high degree of geological, hydrogeological and geothermal knowledge of the aquifer, which is not the case at the moment. Also, this option is very far from a mature technology but significant scientific progress is expected in the coming years, as it is a concern for many other low-T geothermal aquifers.

Table 3-24: Results of sequestration (Mt) potential in the Hainaut Westphalian A &amp; B mine areas.

	Surface deep part (km <sup>2</sup> )	Sequestration potential (Mt)					
		Volume	Adsorption		Residual voids	Total	
Hensies- Pommeroeul Sartis	3	0.9	0.9	1.2	1.4	3.3	3.5
Hensies- Pommeroeul Louis- Lambert	3	2.6	0.9	1.2	1.4	4.9	5.2
Blaton- Bernissart	8	2.5	3.6	5.0	0.7	6.7	8.2
Anderlues	8	6.8	2.4	3.1	4.4	13.6	14.3
Péronnes	8					8.9	9.3
<b>TOTAL</b>						37	40

### b) Data collection

Aquifer data are very scarce since the most promising aquifer for CO<sub>2</sub> storage, the Hainaut geothermal aquifer, is one of the least known deep aquifers. The Dinantian aquifer structure and boundaries were extrapolated from available seismic lines and published geological sections.

The Dinantian aquifer studied is delineated:

- at the west side: by a NS line approximately coinciding with the Belgian border
- at the east side: by a NS line through Mons
- at the south side: by a EW line at the southernmost point of the Belgian border
- at the north side: by a EW line through Douvrin and Ghlin, where the Dinantian layer occurs in the subsurface at a depth below 800 m.

Two compartments were distinguished and used for capacity calculations. The first compartment is idealized as a south dipping formation which is connected at ~2000 m depth with a second, tabular compartment.

Outcrop and borehole data were used for evaluating the thickness and the petrophysical parameters. Only two boreholes can substantially be used for this purpose: the Saint-Ghislain (5406 m) and the Jeumont (4939 m) boreholes.

### c) Evaluation of capacity

The thickness of the Dinantian ranges from ca. 500 to 2500 m and an average of 1500 m was retained for the calculation. Porosity was set ranging from 4 to 6% according to the neutron-porosity log recorded at Saint-Ghislain. The aquifer was then considered as homogeneous and isotropic, which is of course not the case as, among others, evaporite and highly transmissive (karstified?) layers occur in the upper part of the formation (one of the latter is used for geothermal water production). Capacity evaluation was then performed assuming that the injected CO<sub>2</sub> is able to sweep the formation water. This assumption is somewhat supported by the 20 year experience of geothermal production and the current knowledge of the aquifer but actually needs further investigations (modelling etc.). Dissolution and mineral trapping processes were not investigated so far. Also, correction terms including for example rock compressibility were omitted because they are likely to be negligible relative to geometrical and petrophysical uncertainties. Accessibility was set to 6% according to the evaluation of the Dogger geothermal aquifer of the Paris Basin, which is one of the closest analogues for CO<sub>2</sub> storage projects in deep limestone aquifers (unpublished BRGM report).

### **3.3.3.2 Results and conclusions for storage in the Dinantian aquifer**

Results from the evaluation of the Dinantian aquifer give a total of 800 to 1300 Mt CO<sub>2</sub> that could be stored. Omitting the contribution of the dipping compartment, which is more likely to allow the CO<sub>2</sub> to migrate to the surface, the storage capacity is lowered to 300-500Mt in the deep, tabular compartment (with only 180-270Mt under areas that are still on the Belgian territory). Although accessibility factor determination and modelling of lateral migration of CO<sub>2</sub> is needed for going significantly further in the evaluation of the Hainaut Dinantian aquifer, the overall comparison with other storage projects in tabular (and dipping) carbonate aquifers is very encouraging.

## **3.4 International storage assessments**

### **3.4.1 Introduction**

In this report we describe the results of the assessment of potential and costs of CO<sub>2</sub> transport and storage in foreign areas. This report contributes to the process of developing a tool that provides for an economic evaluation of carbon capture and storage (CCS). This so-called Policy Support System (PSS) is primarily developed for the Belgian national context.

Storage reservoirs abroad Belgium could form an alternative destiny to store CO<sub>2</sub> captured in Belgium. CO<sub>2</sub> from Belgium can be stored abroad when sufficient infrastructure is available and fields are accessible. This may differ from country to country, as the development of the implementation of CCS will not necessarily develop in parallel in all countries.

In this report we discuss the approach and calculation methodology to determine storage capacity and costs for storage of CO<sub>2</sub> outside Belgium. In this approach we consider only the adjacent countries/regions with Belgium, i.e. The Netherlands, Germany, France and the North Sea area.

In section 3.4.2 we pose assumptions and starting conditions underlying the calculations. In section 3.4.3 we illuminate the calculation methodology and provide the results. In the Annex we provide examples (graphical representations) of the lay-out of the transport infrastructure.

### **3.4.2 Assumptions to calculate CO<sub>2</sub> storage potential and costs outside Belgium**

To be able to systematically calculate the cost for various supply scenarios of CO<sub>2</sub> we made the following assumptions:

- CO<sub>2</sub> is delivered at one of the four fixed interconnection point at the border, from which it is further transported to storage locations
- For practical and logical reasons, the number of foreign areas have been limited to four, i.e.:
  - o The Netherlands (NL)
  - o Germany (GE)
  - o France (Fr)
  - o North Sea area (NS: consisting of Norwegian and UK storage locations)
- The presence of CO<sub>2</sub> pipeline backbone (large trunk line) structure in each of those four areas. These backbones connect satellite pipelines from to the sinks in the areas itself, and is open to CO<sub>2</sub> from Belgium
- In case of the Netherlands, Germany, and France, the backbone dimensions are depending on country's own supply of CO<sub>2</sub> to the backbone and the CO<sub>2</sub> supply from Belgium. We distinguish four scenarios with respect to supply from the various countries. The amount of CO<sub>2</sub> transported through the pipeline is equal to 0%, 10%, 20%, 30% of countries emission in 2005. In case of the North Sea, the pipeline will be able to transport the combined supply of the Netherlands, UK, Denmark, Germany Norway and France for the same percentages.

- Costs are ‘flat rate’ costs, i.e. that the costs for every tonne of CO<sub>2</sub> transported and stored are the same, regardless at which point the CO<sub>2</sub> is put in the transport system or is taken out to stored in that area. The costs are determined by the backbone costs (starting from the border with Belgium) and satellite pipelines from the backbone to individual storage locations.
- Transport costs are calculated using the same methodology and cost values as elsewhere in this PSS-study. Storage costs are taken from the IEA, 2005 study. These costs have been verified with the costs estimates developed in this PSS study. Both cost estimates were found to be comparable.
- Costs figures will be generated for the following the assumption that the supply from Belgium varies from 5 to 60 Mt per year (in steps of 5 Mt)

### 3.4.3 Methodology

The following methodology was used to calculate storage potential and transport costs.

In the first step, considering all possible source-storage structure combinations, the source-storage structure combination with the lowest specific costs is determined (i.e. the sum of the transport costs and storage costs, expressed in euro per tonne of carbon dioxide stored). The source is represented by one of the four interconnection points of Belgium with the surrounding areas. The storage locations are the storage reservoirs as indicated in studies performed for the EU (GESTCO, 2003, updated in IEA, 2005).

The costs are determined by calculating for all possible combinations the distance between the source and storage structure. The total costs are the sum of the transport costs and the storage costs. Transport costs are a function of the length of the transport system and the (average) flow size.

This calculation procedure is repeated until one of the following three criteria are met:

- there is no storage structure capacity left;
- all CO<sub>2</sub> supply from the sources have been matched with capacity of storage structures;
- one of the cut-off criteria for costs are met; this criteria can be set in the beginning of the calculation procedure (e.g. a cut-off criteria is maximum specific costs).

As the CO<sub>2</sub> is transported from Belgium to a cluster of storage locations outside the country in one direction it is cost-effective to construct a backbone pipeline. The trajectory and size of the backbone is (manually) outlined at the hand of information obtained by the position of the storage structures and sources (figs. 3-30, 3-31, 3-32 and 3-33).

The inclusion of a backbone serves computational as an additional storage structure. It is assumed that sources that deliver carbon dioxide to the backbone pay a uniform fee to cover the costs for the backbone and the costs for constructing the satellite pipelines connecting the backbone with the storage structures. The total costs for transport outside Belgium comprise therefore the transport costs for the backbone and from the backbone to the storage locations.

When a storage location is available near the interconnection point, the system may choose – for costing reasons) for only a satellite pipeline and neglecting the backbone. The fee costs for the backbone have been derived through an iterative calculation process. In the first loop, the fee of the backbone is put very low. The result of the first loop is that a relatively large amount of carbon dioxide is delivered to the backbone. Subsequently, the required storage structures are selected with sufficient capacity to be connected the backbone (selection based on lowest costs). The fee of the backbone is determined by dividing the total costs of the backbone and satellite backbone-storage structure connections by the amount of carbon dioxide transported through the backbone.

Table 3-25: Basic cost data for storage costs outside Belgium.

<b>Activity costs</b>	<b>unit</b>	<b>onshore</b>	<b>Offshore</b>
<i>Drilling costs</i>	€/m	1250	1750
<i>Deviated drilling costs</i>	€/m	2500	3500
<i>Completion costs (including platform costs)</i>	M€	0.4	25
<i>Monitoring (gas)</i>	M€	0.2	0.2
<i>Monitoring (aquifer)</i>	M€	1.8	1.8
<i>Monitoring (oil)</i>	M€	4.2	4.2
<i>Site exploration</i>	M€	1.6	1.8
<i>O&amp;M (incl Monitoring)</i>		7%	8%
<i>Max rate well</i>	Mt/y	1.25	1.25
<i>max well per location/platform</i>		6	6
<i>interest rate</i>		10%	10%
<i>Lifetime</i>	y	20	20

The capacity of the backbone is calculated by taking a certain percentage of the total amount yearly delivered to the backbone. The calculation process is repeated with the newly calculated backbone fee. As the fee is now reflecting a higher and more realistic value, a number of sources will prefer to store their captured carbon dioxide in a nearby reservoir when this will be a cheaper option than delivering it to the backbone. This will again result in a new backbone fee. This calculation process is repeated until the fee remains stable.

Table 3-25 shows the basic cost data which is used to calculate the storage costs. The transport costs are based on the same costs assumptions which have been used elsewhere in this project. The costs have been adjusted based on expert information for the various regions. Compared to Belgium, transport costs of the Netherlands and the North Sea – because of their difficult terrain conditions - are considered to be somewhat higher, i.e. about 40%. The specific transport for France and Germany are considered to be equal to Belgium.

### 3.4.4 Results

Table 3-26 shows the calculated costs per tonne of CO<sub>2</sub> stored for the four regions considered. The costs are shown for various scenarios as explained above (first column gives required storage capacity for Belgium in steps of 5 Mt/y. Costs are generated for four scenarios varying in own countries' supply (equivalent to 0%, 10%, 20% and 30% of total CO<sub>2</sub> emissions in 2005).

Table 3-26: Costs for transporting CO<sub>2</sub> from Belgium to abroad for various scenarios.

<b>Netherlands</b>				
	0%	10%	20%	30%
Total supply (kt/y) ->	60000	80000	100000	120000
Supply from Belgium (kt/y)	€/t	€/t	€/t	€/t
5000	6.36	6.36	6.36	4.98
10000	4.98	4.98	4.42	4.10
15000	4.42	4.10	3.89	3.73
20000	4.10	3.89	3.73	3.52
25000	3.89	3.73	3.52	4.38
30000	3.73	3.52	4.38	4.40
35000	3.62	4.42	4.38	4.29
40000	3.52	4.38	4.34	4.20
45000	4.42	4.40	4.24	4.13
50000	4.38	4.34	4.20	4.20
55000	4.38	4.29	4.13	4.39
60000	4.40	4.20	4.20	4.39

<b>Germany</b>				
	0%	10%	20%	30%
Total supply (kt/y) ->	60000	150000	240000	330000
Supply from Belgium (kt/y)	€/t	€/t	€/t	€/t
5000	3.65	3.07	2.71	4.94
10000	3.07	4.94	4.35	4.16
15000	2.84	4.50	4.09	4.09
20000	2.71	4.23	4.09	3.91
25000	4.94	4.09	3.91	3.92
30000	4.70	4.09	3.92	4.05
35000	4.50	4.09	3.92	4.03
40000	4.35	3.91	4.05	4.10
45000	4.29	3.91	4.03	4.22
50000	4.23	3.92	4.03	4.33
55000	4.16	3.92	4.10	4.51
60000	4.09	4.05	4.22	4.61

<b>France</b>				
	0%	10%	20%	30%
Total supply (kt/y) ->	60000	100000	140000	180000
Supply from Belgium (kt/y)	€/t	€/t	€/t	€/t
5000	2.82	2.82	4.21	3.79
10000	4.21	3.79	5.34	4.76
15000	3.79	5.10	4.57	4.36
20000	5.34	4.76	4.36	4.12
25000	5.10	4.47	4.19	4.12
30000	4.76	4.25	4.12	4.07
35000	4.57	4.19	4.11	4.08
40000	4.47	4.12	4.07	4.05
45000	4.36	4.12	4.08	4.01
50000	4.25	4.11	4.03	4.00
55000	4.19	4.07	4.05	4.12
60000	4.12	4.08	4.04	4.12

<b>North Sea</b>				
	0%	10%	20%	30%
Total supply (kt/y) ->	60000	280000	500000	720000
Supply from Belgium (kt/y)	€/t	€/t	€/t	€/t
5000	8.56	6.31	8.28	7.76
10000	7.19	8.15	7.76	7.17
15000	6.63	7.76	7.17	7.00
20000	6.31	7.76	7.17	7.18
25000	7.90	7.76	7.00	7.38
30000	8.71	7.17	7.18	7.42
35000	8.47	7.17	7.18	7.59
40000	8.28	7.00	7.38	7.63
45000	8.15	7.00	7.42	7.66
50000	8.00	7.00	7.42	7.85
55000	7.86	7.18	7.59	7.98
60000	7.76	7.18	7.63	7.98

### 3.4.5 Conclusion

Storage of CO<sub>2</sub> abroad Belgium costs about 4 to 6 € per tonne of CO<sub>2</sub>. The costs comprises the transport costs outside Belgium and storage costs. Storage in the North Sea is considerably more expensive than the in the neighbouring countries and costs about 8 to 11 € per tonne, despite the higher volumes assumed to be sup-plied to the transport system from surrounding countries.

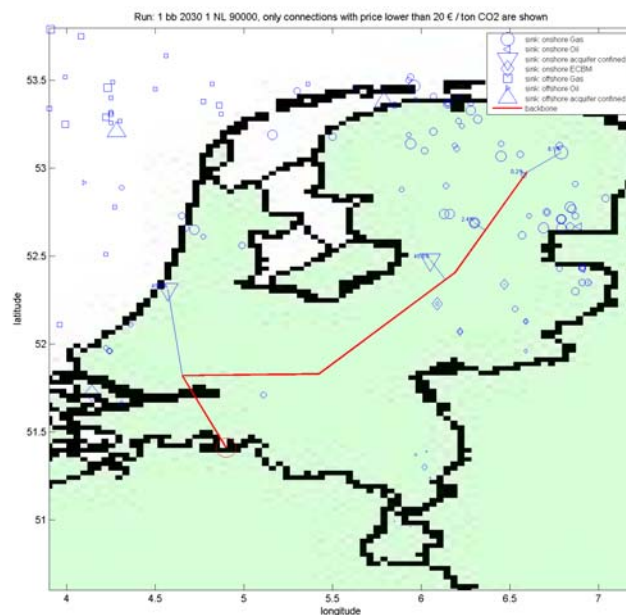


Figure 3-30: Transport and storage of 90 Mt of CO<sub>2</sub> per year to Netherlands.

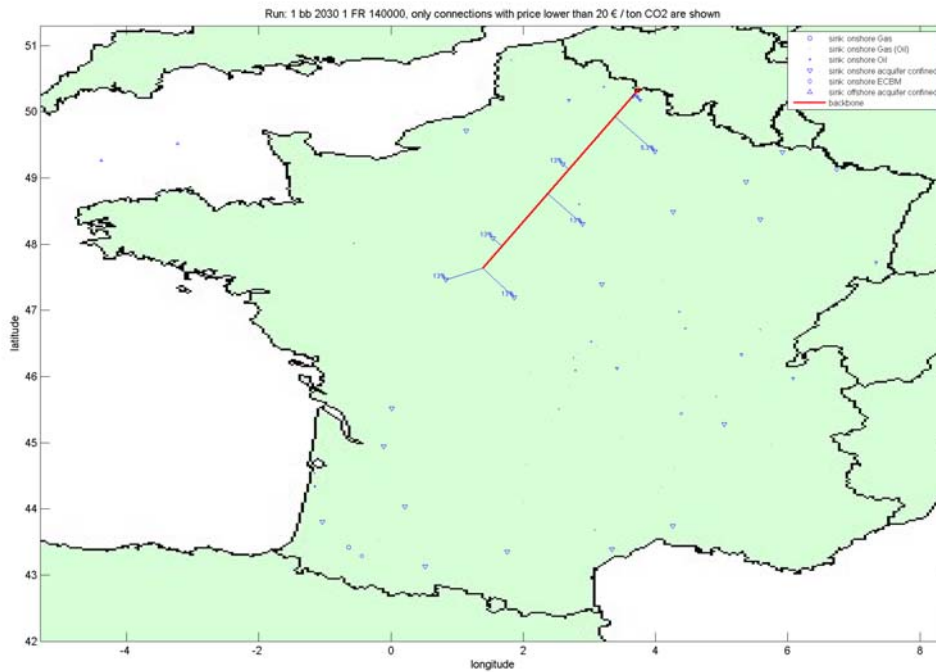


Figure 3-31: Transport and storage of 140 Mt of CO<sub>2</sub> per year to France.

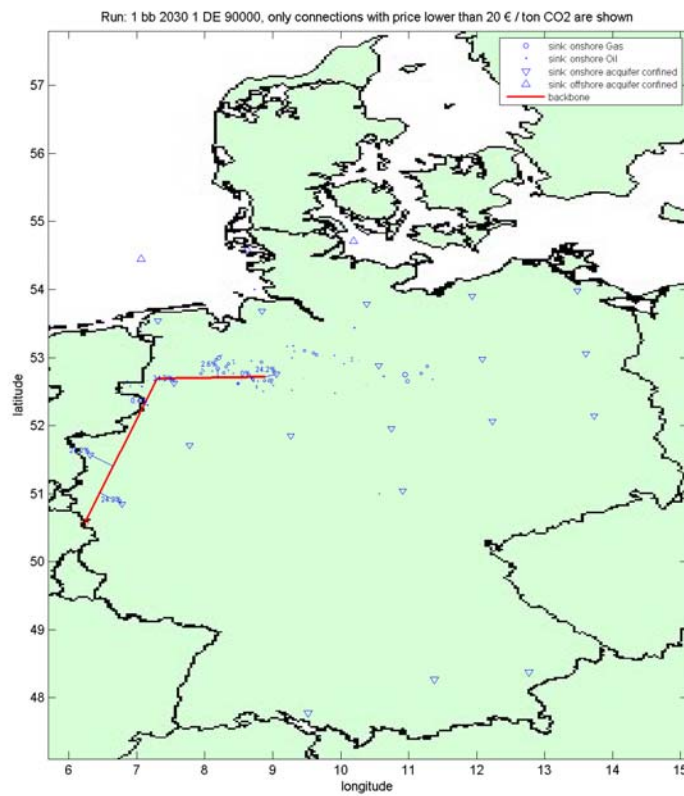


Figure 3-32: Transport and storage of 90 Mt of CO<sub>2</sub> per year to Germany.

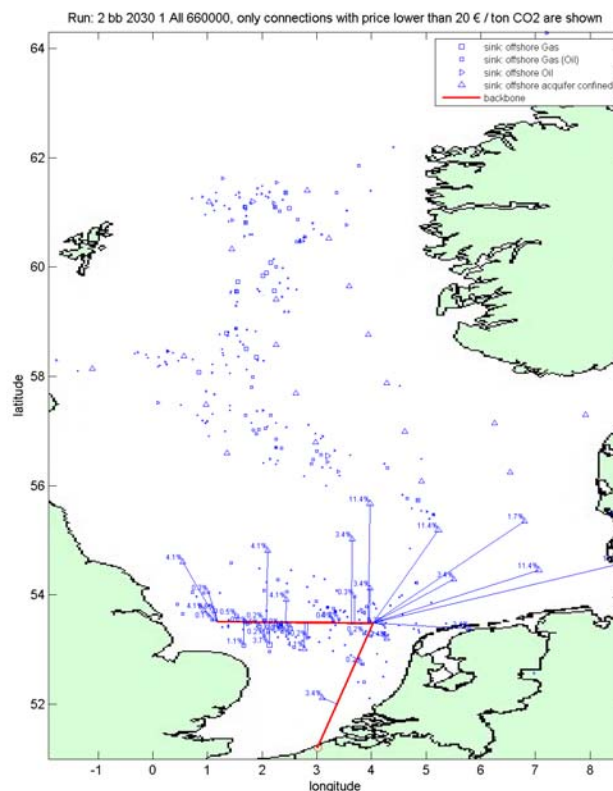


Figure 3-33: Transport and storage of 660 Mt of CO<sub>2</sub> per year to North Sea area.

### 3.5 References

- Bachu, S., 2003. Screening and ranking of sedimentary basins for sequestration of CO<sub>2</sub> in geological media. *Environmental Geology*, 44, 277-289.
- Battacharya, S., Byrnes A.P., Gerlach, P. & Olea, R., 2002. Reservoir characterization to inexpensively evaluate the exploration potential of shallow Morrow incised valley-fill field. Oil & Gas reports, Kansas Geological Survey, open-file report 2002-9.
- Bertier, P., 2004. Petrografische, geochemische en petrofysische karakterisering van potentiële reservoirgesteenten voor de opslag van broeikasgassen (CO<sub>2</sub>) in het Kempisch Bekken. Verslag doctoraatsonderzoek 2003-2004. VITO Report 2004/MAT/R/096, 29p.
- Bertier, P., Swennen, R., Laenen, B., Lagrou, D. & Dreesen, R., 2006. Experimental identification of CO<sub>2</sub>-water-rock interactions caused by sequestration of CO<sub>2</sub> in Westphalian and Buntsandstein sandstones of the Campine Basin (NE-Belgium). *Journal of Geochemical Exploration*, 89, 10-14.
- Bertier, P., Swennen, R., Lagrou, D., Laenen, B. & Kemps, R., under review. Contrasting diagenesis of the Westphalian C & D sandstones in the Campine Basin (NEBelgium). *Sedimentology*.
- Caers, J., Swennen, R. & Duser, M., 1996. Diagenetic history of Westphalian A and B fluvio-deltaic deposits: an example from the KB206 Peer borehole (Campine Basin, NEBelgium). *Zentralblatt für Geologie und Paläontologie*, 11/12, 1211-1236.
- Delmer, A., 1963. Carte des mines du Basin Houiller de la Campine (with correlation scheme by Legrand, R.). *Annales des Mines de Belgique*, 6, 739-754.
- Delmer, A., Duser, M. & Delcambre, B., 2001. Upper Carboniferous lithostratigraphic units (Belgium). In Bultynck P. & Dejonghe L. (eds), *Guide to a revised lithostratigraphic scale of Belgium*, Geologica Belgica, 4 (1-2), 95-103.
- Demyttenaere, R., 1989. The Post-Paleozoic geological history of North-Eastern Belgium. *Mededelingen van de Koninklijke Academie voor Wetenschappen, Letteren en Schone Kunsten van België, Academiae Analecta*, 51, 51-81.

- Dreesen, R., Bouckaert, J., Dusar, M., Soille, J. & Vandenberghe, N., 1987. Subsurface structural analysis of the late-Dinantian carbonate shelf at the northern flank of the Brabant Massif (Campine Basin, N-Belgium). *Toelichtende Verhandelingen voor de Geologische en Mijnkaarten van België (Memoirs of the Geological Survey of Belgium)*, 21, 37 p.
- Dreesen, R., Bossiroy, D., Dusar, M., Flores, R.M. & Verkaeren, P., 1995. Overview of the influence of syn-sedimentary tectonics and palaeo-fluvial systems on coal seam and sand body characteristics in the Westphalian C strata, Campine Basin, Belgium. In Whateley M.K.G. & Spears D.A. (eds), *European Coal Geology*, Geological Society, London, Special Publications, 82, 215-232.
- Dubelaar, C.W., Dusar, M., Dreesen, R., Felder, W.M. & Nijland, T.G., 2006. Maastricht limestone: A regionally significant building stone in Belgium and the Netherlands. Extremely weak, yet time-resistant. In Fort R., Alvarez de Buergo M., Gomez- Heras M. & Vazquez-Calvo C. (eds). *Heritage, Weathering and Conservation*, 9-14.
- Dusar, M., 1989. Non-marine lamellibranchs in the Westphalian C/D of the Campine coalfield. *Bulletin van de Belgische Vereniging voor Geologie*, 98, 483-493.
- Dusar, M. & Houllberghe, E., 1981. De steenkoolverkenningboring van Neerglabbeek (Boring 146 van het Kempens bekken). *Annalen der Mijnen van België*, 11, 913-1003.
- Dusar, M. & Lagrou, D., 2007. Cretaceous flooding of the Brabant Massif and the lithostratigraphic characteristics of its chalk cover in northern Belgium. *Geologica Belgica*. 10/1-2, 27-38.
- Dusar, M., Bless, M.J.M., Borremans, G., Burger, K., De Loose, J., Fairon-Demaret, M., Felder, P.J., Gullentops, F., Lie, S.F., Muchez, Ph., Paproth, E., Pierart, P., Rossa, H.G., Smolderen, A., Somers, Y., Steurbaut, E., Streel, M., Viaene, W., Witte, H. & Wouters, L., 1987. De steenkoolverkenningboring Gruitrode-Ophovenderheide (Boring 172 van het Kempens Bekken). *Kaartblad Opoeteren*, 63E 224. Professional Paper, 1987/3, Nr 230, 235p.
- Dusar, M., Langenaeker, V. & Wouters, L., 2001. Permian-Triassic-Jurassic lithostratigraphic units in the Campine Basin and the Roer Valley Graben (NE Limburg). In Bultynck P. & Dejonghe L. (eds), *Guide to a revised lithostratigraphic scale of Belgium*. *Geologica Belgica*, 4 (1-2), 107-112.
- Felder, P.J., 2001. Bioklasten-stratigrafie of ecozonatie voor het Krijt (Santoniaan – Campaniaan – Maastrichtiaan) van Zuid-Limburg en oostelijk België. *Memoirs of the Geological Survey of Belgium*, 47, 141 p.
- Felder, W.M. & Bosch, P.W., 2000. Krijt van Zuid-Limburg. *Geologie van Nederland*, deel 5. NITG, 90-6743-710-7, 192 p.
- Gaussens, P., 1986. *Manuel pour le transport et la distribution du gaz*. Association technique de l'industrie du gaz en France, Paris. ISBN 2-86655-031-5
- GESTCO, 2003. EU study to Geological Storage of Carbon Dioxide in Western Europe, GEUS et al., study for fifth framework programme of the European Commission, 2003
- Hitchon, B., 1996. *Aquifer disposal of carbon dioxide: hydrodynamic and mineral trapping - Proof of concept*. Geoscience Publishing Ltd., Sherwood Park, Alberta, Canada, 165p.
- IEA, 2005. *Cost curves for CO<sub>2</sub> Storage - Part 2: European sector*, IEA GHG Pro-gramme, Wildenborg, T., S. Holloway, C.A. Hendriks, E. Kreft, A. Lokhorst, M. Brook, R. Brandsma, P. Egberts, and M. Larsen, *Cost curves for CO<sub>2</sub> Storage - Part 2: European sector*, TNO-NITG, Ecofys, BGS and GEUS, 2005
- Laenen, B., 2003. *Lithostratigrafie van het pre-Tertiair in Vlaanderen. Deel II: Dinantiaan & Devoon*. Unpublished report of VITO for Flemish Department of Natural Resources and Energy (ANRE), 2003/ETE/095, 96p.
- Laenen, B., van Tongeren, P., Dreesen, R. & Dusar, M., 2004. Carbon dioxide sequestration in the Campine Basin and the adjacent Roer Valley Graben (North Belgium): an inventory. In Baines S.J. & Worden R.H. (eds), *Geological Storage of Carbon Dioxide*, Geological Society, London, Special Publications, 233, 193-210.
- Langenaeker, V., 2000. The Campine Basin. Stratigraphy, structural geology, coalification and hydrocarbon potential for the Devonian to Jurassic. *Aardkundige Mededelingen*, 10, 142p.
- Langenaeker, V. & Dusar, M., 1992. Subsurface facies analysis of the Namurian and earliest Westphalian in the western part of the Campine Basin. *Geologie en Mijnbouw*, 74, 161-172.
- Lemmon, E.W., McLinden, M.O. & Friend, D.G., 2005. Thermophysical Properties of Fluid Systems. In Linstrom P.J. & Mallard W.G. (eds), *NIST Chemistry WebBook*, NIST Standard Reference Database Number 69, National Institute of Standards and Technology, Gaithersburg MD, 20899 (<http://webbook.nist.gov>).

- Lorenzi, G., Bossiroy, D. & Dreesen, R., 1992. Les minéraux argileux au service des corrélations stratigraphiques des formations houillères du Carbonifère. EGKS final report, contract 7220-AF/206, ISSeP, Liège, 164 p.
- Muchez, Ph., Viaene, W. & Duser, M., 1992. Diagenetic control on secondary porosity in flood plain deposits: an example of the Lower Triassic of northeastern Belgium. *Sedimentary Geology*, 78, 285-298.
- NIRAS/ONDRAF, in preparation. The 96-ON acquisition and processing, the reprocessing of former seismic campaigns, internal report, unpublished.
- Paproth, E., Duser, M., Bless, M.J.M., Bouckaert, J., Delmer, A., Fairon-Demaret, M., Houilleberghs, E., Laloux, M., Piérart, P., Somers, Y., Streel, M., Thorez, J. & Tricot, J., 1983. Bio- and lithostratigraphic subdivisions of the Silesian in Belgium. A review. *Annales de la Société Géologique de Belgique*, 106, 241-283.
- Robaszynski, F., Dhondt, A.V. & Jagt, J.W.M., 2001. Cretaceous lithostratigraphic units (Belgium). In Bultynck P. & Dejonghe L. (eds), *Guide to a revised lithostratigraphic scale of Belgium*. *Geologica Belgica*, 4 (1-2), 121-134.
- Span, R. & Wagner, W., 1996. A New Equation of State for Carbon Dioxide Covering the Fluid Region from the Triple-Point Temperature to 1100 K at Pressures up to 800 MPa. *Journal of Physical and Chemical Reference Data*, 25 (6), 1509-1596.
- Swennen, R., Keppens, E., Muller, A. & Steingrobe, B., 1996. Sedimentology, diagenesis and burial history of Westphalian sandstones of Floverich 2E-1 borehole (Aachen-Erkelenz coal district: Germany). *Zentralblatt für Geologie und Paläontologie*, 11/12, 1237-1260.
- TNO-NITG, 2001. *Geologische Atlas van de Diepe Ondergrond van Nederland*. Toelichting bij kaartbladen XIII en XIV: Breda-Valkenswaard en Oss-Roermond.
- Vandenbergh, N., Duser, M., Laga, P. & Bouckaert, J., 1988. The Meer well in North Belgium. *Toelichtende Verhandelingen bij de Geologische en Mijnkaarten van België*, 25, 23p.
- Vandenbergh, N., Duser, M., Boonen, P., Lie, S.F., Voets, R. & Bouckaert, J., 2000. The Merksplas-Beerse geothermal well (17W265) and the Dinantian reservoir. *Geologica Belgica*, 3, 349-367.
- Van Tongeren, P.C.H., 2004. Nieuwe inzichten m.b.t. de geologie van het gebied Meeuwen-Rotem (noordoost Kempen) (een seismische herinterpretatie). VITO report for Flemish Department of Natural Resources and Energy (ANRE), 2004/MAT/R/138, 68p.
- Van Tongeren, P.C.H. & van Amerom, H.W.M., 2003. Datering en reconstructie van het afzettingsmilieu van de jongste Boven Carboon strata in enkele Kempense boringen, m.b.v. fossiele plantenassociaties en seismische interpretatie. VITO report for Flemish Department of Natural Resources and Energy (ANRE), 2003/ETE/R/129, 118p.
- Wouters, L. & Vandenbergh, N., 1994. *Geologie van de Kempen*. Een synthese. NIRAS/ONDRAF, 208 p.

## 4 Transport

### 4.1 Nature of CO<sub>2</sub> transport

The most profitable way to transport CO<sub>2</sub> is as a dense phase (e.g. IEA GHG, 2005). Skovholt (1993) suggested CO<sub>2</sub> transportation as liquid or as a high density gas. However, the same author noticed that during transportation of CO<sub>2</sub> as a liquid phase, topographic variations could induce pressure differences, turning liquid into gas. This would cause two-phase flow, which is complicated to handle (e.g. Kruse and Tekiela, 1996; Skovholt, 1993; Svensson et al., 2004). Therefore, most authors state that the most efficient way to transport CO<sub>2</sub> is as a supercritical phase, which occurs at a pressure higher than 7.38 MPa and a temperature of more than 31.1°C (e.g. Odenberger and Svensson, 2003; Shafeen et al., 2004; Skovholt, 1993). However, there is no need for a temperature limit. CO<sub>2</sub> can be transported as a liquid phase as long as the pressure is kept higher than 7.38 MPa and high enough to overcome a phase change due to topographic variations (e.g. Golomb, 1997). In the pipeline diameter calculations, the ambient temperature (-2 to 25°C depending on summer or winter and Nordic or warmer countries; 12°C assumed in Skovholt, 1993) of the (buried) pipeline is assumed in most cases and CO<sub>2</sub> is compressed to transport it as a supercritical or liquid phase (e.g. Bock et al., 2003; IPCC, 2005; Wong, 2005). Especially because of environmental, security and safety reasons, pipelines are often buried, which provides more stable temperatures than at the surface where pipelines can reach high temperatures by sun exposure (e.g. Zhang et al., 2006). The composition of the transported CO<sub>2</sub> has implications on the pipeline design, which influences the transport costs. The design of a pipeline should reflect the requirements of the appropriate regulations and standards, namely 1) pressure (wall thickness, over-pressure protection systems), 2) resistance to degradation (internal due to e.g. corrosion and external due to environmental conditions), 3) protection from damage (e.g. burying the line), 4) appropriate monitoring facilities and safety systems and 5) location considerations (IEA GHG, 2002). Skovholt (1993) assumed coated high quality carbon steel pipelines with cathodic protection, sectioning valves (each 30 km) and corrosion control points for the transport of CO<sub>2</sub>. Furthermore, high durometer (>90) elastomer seals are needed for CO<sub>2</sub> pipelines (Gale and Davison, 2004). In order to prevent hydrate formation and internal corrosion of the carbon and low-alloy steel pipelines, the transported CO<sub>2</sub> should be treated to a very low water content (ppm amounts; Skovholt, 1993) or a relative humidity of less than 60% (IEA GHG, 2002; IPCC, 2005). For example, the transported CO<sub>2</sub> in the Weyburn pipeline contains less than 20 ppm H<sub>2</sub>O (IPCC, 2005). According to Heddle et al. (2003), the CO<sub>2</sub> flow is dried to a -40°C dewpoint to prevent corrosion and contains N<sub>2</sub><300 ppm, O<sub>2</sub><40 ppm and Ar<10 ppm. Dry CO<sub>2</sub> has, however, poor lubricating properties requiring special design features for compressors, pumps, etc and it should be taken into account that some lubricants can harden and become ineffective in the presence of CO<sub>2</sub> (Gale and Davison, 2004). The concentration of H<sub>2</sub>S, which may be contained in CO<sub>2</sub> captured in gasification plants without proper desulphurization, are preferred to be kept very low to prevent sulphide stress corrosion cracking and also because of safety reasons where pipelines pass populated areas (IEA GHG, 2002). Furthermore, some safety measures require increased pipe wall thickness and shorter distances between sectioning valves in zones of a high population density (Skovholt, 1993). The total transport cost is the sum of the investment cost, the fixed operation and maintenance cost and the variable operation and maintenance cost of the pipeline as well as the compressor station, if needed.

## 4.2 CO<sub>2</sub> quality requirements for pipeline transport

### 4.2.1 Introduction

In addition to technical requirements that can be needed by the different parts of the CCS system, the question of requirements and standards on CO<sub>2</sub> quality have logistical importance in a perspective of large scale CO<sub>2</sub> transport network that might develop in Europe. Little attention has been paid to this topic until now.

However, there is a risk that components other than CO<sub>2</sub> in the captured stream could have a negative effect on the transport and storage parts, both from a technical and environmental and health point of view, and therefore need to be removed. There are generally no strong technical barriers to provide high purity of CO<sub>2</sub> from the flue gas of fossil fuel-fired power plants. However, stringent purity requirements are likely to induce additional costs and energy requirements resulting in a loss of power plant efficiency.

The opportunity to co-capture other main pollutants from power plant operations such as SO<sub>2</sub> and store them together with CO<sub>2</sub> could also influence greatly the cost of CO<sub>2</sub> capture and storage by excluding costly and energy-demanding flue gas cleaning equipment. A study (IEA GHG, 2003) found that capture and storage of hydrogen sulphide (H<sub>2</sub>S) along with CO<sub>2</sub> in pre-combustion capture systems can reduce overall capture costs by about 20% (although this may increase transport and storage costs). Vattenfall estimated that a cost of electricity reduction of almost 10% could be achieved if the sulphur removal is left out of the oxy-fuel process and SO<sub>2</sub> is co-captured with the CO<sub>2</sub>.

The quality of the captured CO<sub>2</sub> stream will differ depending on the fuel used, approaches used for the combustion and the capture method. The CO<sub>2</sub> quality requirements are defined by the limitations set by CO<sub>2</sub> transport, storage, safety and environmental regulations and the cost.

The CO<sub>2</sub> transport links are the interface that will put the CCS chain together. Also, the transport links will be the interface between requirements on CO<sub>2</sub> quality and physical state at the capture side delivery point and at the storage side receiving point.

Further co-operation and discussions are needed between the stakeholders of Carbon Capture and Storage, and EOR and EGR, to define a good compromise on CO<sub>2</sub> compositions for a full CCS chain, consisting of guidelines and a practice with a set of likely limit values for defined applications (ship/pipeline, onshore/offshore, aquifer/oil field/gas field), that the CO<sub>2</sub> sources (power plants) could reasonably meet. This practice would guide the legislative adaptation process.

### 4.2.2 Experience

At the storage related side, long experience and established commercial standards exist for CO<sub>2</sub> to be injected for enhanced oil recovery (EOR) in North American oil fields, where the main objective is to increase the oil recovery from old oil fields through injection of CO<sub>2</sub>. These existing specifications are mainly established as a compromise between technical requirements for transport of CO<sub>2</sub> at high pressure in pipelines and the requirements for miscibility of the CO<sub>2</sub> with the oil when injecting into the oil fields. In addition, the present knowledge and experience in this field are mainly based on CO<sub>2</sub> that has been extracted from natural sources, with a slightly different composition than in the case where CO<sub>2</sub> is captured from a power plant. In Europe, experiences from CO<sub>2</sub> storage exist (e.g. Sleipner in Norway with CO<sub>2</sub> extracted from gas production), and some coming studies will evaluate CO<sub>2</sub> quality demands based on geological prerequisites.

Today, mainly three established purity levels (compositions) exist in practice for CO<sub>2</sub> as a commodity:

The first is food grade CO<sub>2</sub> with a typical purity level of > 99.9% CO<sub>2</sub>, with a variant of technical CO<sub>2</sub> (that also occur in an odourised variant) with a CO<sub>2</sub> concentration of > 99.5%. The second is the practice for enhanced oil recovery in the USA, with a required CO<sub>2</sub> concentration of at least 95% CO<sub>2</sub>. Table 4-1 gives an example from the Canyon Reef project. The third is ongoing storage projects, using CO<sub>2</sub> quality from capture plants connected to natural gas exploration, with CO<sub>2</sub> removal. Sleipner injects a 95% pure CO<sub>2</sub>.

IPCC (2005) reports the following CO<sub>2</sub> quality specifications (for enhanced oil recovery from the Canyon Reef project):

- Carbon Dioxide: Product shall contain at least ninety-five mole percent (95%) of Carbon Dioxide as measured at the SACROC delivery meter.
- Water: Product shall contain no free water, and shall not contain more than 0.489 m<sup>-3</sup> in the vapour phase.
- Hydrogen Sulphide: Product shall not contain more than fifteen hundred (1500) parts per million, by weight, of hydrogen sulphide.
- Total Sulphur: Product shall not contain more than fourteen hundred and fifty (1450) parts per million, by weight, of total sulphur.
- Temperature: Product shall not exceed a temperature of 48.9°C.
- Nitrogen: Product shall not contain more than four mole percent (4%) of nitrogen.
- Hydrocarbons: Product shall not contain more than five mole percent (5%) of hydrocarbons and the dew point of Product (with respect to such hydrocarbons) shall not exceed -28.9°C.
- Oxygen: Product shall not contain more than ten (10) parts per million, by weight, of oxygen.
- Glycol: Product shall not contain more than 4 x 10<sup>-5</sup> L m<sup>-3</sup> of glycol and at no time shall such glycol be present in a liquid state at the pressure and temperature conditions of the pipeline.

#### 4.2.3 Components in the captured CO<sub>2</sub> stream

The types and concentrations of impurities in the captured CO<sub>2</sub> stream are presented in table 4-1 according to the type of capture process.

A study carried out by Vattenfall evaluates possible components present in the captured CO<sub>2</sub> stream and their approximate concentration levels when applying a minimum level of gas purification equipment in the power plant with CO<sub>2</sub> capture (a “worst case” scenario). This evaluation is made for a German lignite coal. Two additional cases with sulphur removal to “conventional” levels were added to the pre-combustion IGCC case and the oxy-fuel case.

Table 4-1: (From IPCC 2005) Concentrations of impurities in dried CO<sub>2</sub>, % by volume.

	SO <sub>2</sub>	NO	H <sub>2</sub> S	H <sub>2</sub>	CO	CH <sub>4</sub>	N <sub>2</sub> /Ar/O <sub>2</sub>	Total
<b>COAL FIRED PLANTS</b>								
Post-combustion capture	<0.01	<0.01	0	0	0	0	0.01	0.01
Pre-combustion capture (IGCC)	0	0	0.01-0.6	0.8-2.0	0.03-0.4	0.01	0.03-0.6	2.1-2.7
Oxy-fuel	0.5	0.01	0	0	0	0	3.7	4.2
<b>GAS FIRED PLANTS</b>								
Post-combustion capture	<0.01	<0.01	0	0	0	0	0.01	0.01
Pre-combustion capture	0	0	<0.01	1.0	0.04	2.0	1.3	4.4
Oxy-fuel	<0.01	<0.01	0	0	0	0	4.1	4.1

Table 4-2: Critical components present in the CO<sub>2</sub> based on the components and concentrations as given by the CO<sub>2</sub> capture options (in the left part of the table). NA – not available = knowledge gap; C – critical; NC – not expected to be critical.

Case	Component	Type* Unit	Capture from				CO <sub>2</sub> Com-pression train				Storage				Environment, health		Hazar-dous waste	
			Oxyfuel		Post-combustion	IGCC	CO <sub>2</sub> Com-pression train		Transport		Injection equipment		Cap rock	reservoir	Risk transport	Risk storage		
			CO <sub>2</sub> /SO <sub>2</sub>	CO <sub>2</sub> +SO <sub>2</sub>	MEA absorption	CO <sub>2</sub> /H <sub>2</sub> S	CO <sub>2</sub> +H <sub>2</sub> S	CO <sub>2</sub> /H <sub>2</sub> S	CO <sub>2</sub> +H <sub>2</sub> S	Pipeline	Ship	Ability to move oil ("EOR")	Injection equipment	Cap rock	reservoir	Risk transport		Risk storage
			Concentration															
	H <sub>2</sub> O	1 vol%	0.14	0.14	0.14	0.14	0.14	0.14										NC
	CO <sub>2</sub>	2 vol%	91	90	99.8	97.8	95.6											NC
	SO <sub>2</sub>	2 vol%	0.076	1.5	0.001	-	-											C <sup>[a]</sup>
	NO	2? 3 vol%	0.25	0.24	0.002	unknown	unknown											C <sup>[a]</sup>
	H <sub>2</sub> S	2 vol%	-	-	-	0.01	2.3											C <sup>[a]</sup>
	HCl	2, W ppmv	Trace	Trace	Trace	Trace	Trace											NC
	HF	2, W ppmv	Trace	Trace	Trace	Trace	Trace											NC
	CO	2? 3? ppmv	unknown	unknown	10	1700	1700											NC
	Ar	3 vol%	5.7	5.6	0.021	0.050	0.049											NC
	O <sub>2</sub>	3 vol%	1.6	1.6	0.003	unknown	unknown											NC
	N <sub>2</sub>	3 vol%	0.61	0.60	0.021	0.030	0.030											NC
	H <sub>2</sub>	3 vol%	-	-	-	1.7	1.7											NC
	CH <sub>4</sub>	3, 4 ppmv	-	-	-	350	350											NC
	Hydrocarbons	4 ppmv	-	-	30	unknown	unknown											NA
	HCN	4 ppmv	Trace	Trace	-	<5	<5											NC
	COS	4 ppmv	-	-	-	<5	<5											NC
	Mercaptanes	4 ppmv	-	-	-	220	220											C <sup>[a]</sup>
	NH <sub>3</sub>	5, W ppmv	Trace	Trace	unknown	30	30											NC
	Hg	6 ppmv	Trace	Trace	Trace	Trace	Trace											C <sup>[a]</sup>
	Metals	6 ppm	Trace	Trace	Trace	Trace	Trace											NC
	Particulates	7 ppm	<1	<1	<1	<1	<1											NC
	MEA	8, 4 ppm	-	-	unknown	-	-											NA
	Selexol	8, 4 ppm	-	-	-	unknown	unknown											NA

*Notations used in table 4-2:*

*[a] - corrosion; [b] - two-phase flow and/or changes of properties; [c] - hydrate formation, dependent of water content; [d] - decreased miscibility; [e] - changed redox conditions; [f] - decreased permeability; [g] - asphyxiating; [h] - greenhouse gas; [i] - acidification; [k] - toxic; [l] - nutrient (eutrophication); [m] - flammable / explosive; [n] - ozone depletion, [o] - technically acceptable to at least 1 vol%; [p] - reacts with oil; [r] - volume efficiency; [s] - strong odour*

*\*According to the physicochemical properties, the identified components could be categorized into following groups:*

*Group 1 - water; Group 2 - acidic components; Group 3 - non-condensable components; Group 4 - organic components; Group 5 - alkaline components; Group 6 - heavy metals; Group 7 - solid components; Group 8 - solvents and reagents; and Group W - water-soluble components.*

*\*\* The components affect the purity of the extracted oil product*

Subsequently, the study summarizes the present knowledge of what components could be of concern and for what reason (see table 4-2). This analysis is performed for CO<sub>2</sub> compression, pipeline transport in supercritical phase or ship transport in liquid phase, storage in a saline aquifer or CO<sub>2</sub> storage in oil fields combined with EOR operation. Aspects related to environmental and health, as well as legal aspects related to the classification of the CO<sub>2</sub> are also investigated.

Major critical components for each step of the CCS system are taken up in the next section.

#### 4.2.4 Critical components in each step of the CCS system

##### **4.2.4.1 CO<sub>2</sub> capture process**

In this section, the concentration of the components from the capture process is estimated at the boundary condition which is defined by the stage of CO<sub>2</sub> compression before possible liquefaction, removal of non-condensable components and dehydration, with a maximum water removal by condensation through intercooling during the compression (as it is the case of table 4-2).

For some CO<sub>2</sub> capture processes, pre-treatment of flue gas may be required before the capture process. This is the case for post-combustion capture and pre-combustion capture for which the solvents are attracted by acidic components. That is the reason why de-NO<sub>x</sub> and de-SO<sub>x</sub> treatments have to be upgraded (if not efficient enough) to avoid too much loss of solvent. The concentration of impurities is less dependent on fuel composition for post-combustion capture and for pre-combustion capture. The H<sub>2</sub>S level in IGCC with capture is affected by the sulphur content of the fuel in the case of co-capture. As for oxy-fuel combustion, relatively high levels of impurities are expected in the captured CO<sub>2</sub> stream. On the other hand, a more complicated composition is generally found in the captured CO<sub>2</sub> stream from IGCC, in which there are many organic impurities such as various hydrocarbons and mercaptans.

There are still some knowledge gaps related to CO<sub>2</sub> quality (properties of CO<sub>2</sub> in a multi-component system, properties of non-condensable components, corrosion behaviour...). These are greater for oxy-fuel combustion and IGCC than for post-combustion capture.

##### **4.2.4.2 CO<sub>2</sub> compression**

Main concerns related to the CO<sub>2</sub> compression train are operation in two-phase flow, change in gas properties that might affect the efficiency of the compression process and conditions for phase transitions, hydrate formation and costs (corrosion). It is important to have an efficient dust and water droplet removal system before the compressors to avoid problems related to depositions on compressor blades, erosion, and corrosion.

#### **4.2.4.3 CO<sub>2</sub> transport in pipeline and ship**

Important for the transport conditions are the physical properties of CO<sub>2</sub>. We can identify two technically different cases, pipeline transportation system and marine transportation systems. Major identified factors of concern, with possible impact or to be avoided, for CO<sub>2</sub> transportation where other components may occur in the CO<sub>2</sub> stream, are summarized as follows:

- Water content.
- Hydrate formation. CO<sub>2</sub>, H<sub>2</sub>S and CH<sub>4</sub> can form hydrates in presence of free water.
- Corrosion. Existing CO<sub>2</sub> pipelines are made of carbon steel. CO<sub>2</sub> as well as other acidic components (e.g. SO<sub>2</sub>, H<sub>2</sub>S) form corrosive acids together with liquid water.
- Two-phase flow. If CO<sub>2</sub> is mixed with components with different physical properties, e.g. Ar, O<sub>2</sub>, H<sub>2</sub>, H<sub>2</sub>S.
- Toxic components, in case of leakage.

Generally, the water content is the most important factor to keep controlled and at a low level, for a CO<sub>2</sub> transport system. If the supercritical/dense phase fluid CO<sub>2</sub> stream in pipeline transport is dry enough, the CO<sub>2</sub> itself as well as several other components cannot create corrosive acids. Pipeline transport is expected to be somewhat more tolerant to some degree of unwanted components, than the ship transport (tank transport) will be. The major identified difference in the ship case is the risk at low temperatures for hydrate formation between water content and CO<sub>2</sub>, H<sub>2</sub>S or methane.

Pipeline design requirements dictate that, to avoid corrosion in the carbon-manganese steels generally used for pipelines, the CO<sub>2</sub> mixture should not exceed a relative humidity of 60%. This requirement takes into account the likely presence of N<sub>2</sub>, NO<sub>x</sub> and SO<sub>x</sub> contaminants (Oryshchyn et al. 2006). If the CO<sub>2</sub> cannot be dried, it may be necessary to build the pipeline of a corrosion-resistant alloy ('stainless steel'). This is an established technology though more expensive.

#### **4.2.4.4 CO<sub>2</sub> storage in saline aquifers and depleted oil fields**

Storing CO<sub>2</sub> together with other compounds has been investigated considering the possible impact on the storage reservoir, the cap rock, the injection facilities, and the use of CO<sub>2</sub> for Enhanced Oil Recovery (EOR). The possibility of a leakage and geochemical reactions interfering with the injection of the captured gas stream are the main risks associated with geological storage. The leakage may be the result of a defect cap rock or poorly sealed well. Geochemical reactions between the gas stream components and the minerals and water present in the aquifer can cause problems during the operational phase, such as reduced permeability, increased pore pressures, corrosion and hydrate formation (in the injection facilities). The amount of chemical reactions that will occur in the aquifer will to a large extent depend on the specific composition of the storage rocks and conditions in the water such as redox potential, pH, buffering capacity...

Components in the gas stream that have been identified as critical for the storage process are H<sub>2</sub>O, SO<sub>2</sub>, NO, CO<sub>2</sub>, H<sub>2</sub>S, O<sub>2</sub>, CH<sub>4</sub>, HCN, Ar, N<sub>2</sub>, H<sub>2</sub> and particulates. CO<sub>2</sub>, SO<sub>2</sub>, NO and H<sub>2</sub>S are acid-forming compounds that may form corrosive acids in the presence of water. H<sub>2</sub>O, H<sub>2</sub>S and CH<sub>4</sub> are hydrate-forming compounds. Oxygen present in the gas stream may lead to changed redox conditions in the reservoir, which can cause precipitation reactions and reduce the permeability. Oxygen present can further, in the case of EOR, react exothermally with oil and cause overheating at the injection point. Particulates are critical to the reservoir since they can block pores near the injection well and reduce the permeability. When using the gas stream for EOR, it will also be important to look at the total concentration of components immiscible with oil (CH<sub>4</sub>, Ar, N<sub>2</sub> and H<sub>2</sub>). Toxic compounds, such as H<sub>2</sub>S, COS, CO, SO<sub>2</sub> and NO<sub>x</sub> are of concern for the EOR case as they are reproduced together with the oil at the

pumping well when there is a break through of the CO<sub>2</sub> front. Sulphur components will also increase the sulphur content of the oil, which is a concern in cases when the raw oil has very low sulphur content.

#### **4.2.4.5 Effects on environment and health**

Components in the injected stream that need to be considered from an environmental point of view are CO<sub>2</sub>, SO<sub>2</sub>, H<sub>2</sub>S, NO, and CO, since the concentrations of these compounds in some or all of the investigated cases, exceed occupational limit values and environmental quality standards. The limits and standards apply to a release to air and the components identified would add to the safety precautions already needed for transport and storage of pure CO<sub>2</sub>. The injected gas might also contain a low concentration of mercury. The environmental benefits and risks of co-storing Hg and CO<sub>2</sub> could be argued.

#### **4.2.4.6 Legal aspects**

The legal implications associated with CO<sub>2</sub> purity levels are mainly related to safety requirements for workers, the public and the environment and the classification of CO<sub>2</sub> as waste and potentially hazardous waste. An assessment has been made if the CO<sub>2</sub> would be classified as hazardous waste according to today's EU regulation based on the estimated concentration levels in the CO<sub>2</sub> stream as given in table 4-2. The regulation and classification of hazardous waste can be found in the directive on hazardous waste, (91/689/EEG). The conclusion of this analysis is that CO<sub>2</sub> with the non-CO<sub>2</sub> component levels in table 4-2 will not be regarded as hazardous waste according to the hazardous waste directive. However, as stated earlier, other restrictions could be placed upon the handling of the CO<sub>2</sub> stream from other perspectives, such as workers, the public and the environment.

#### **4.2.4.7 Conclusion**

Further investigations of the CO<sub>2</sub> specification, especially from the transport, storage and environmental points of view, is needed in order to understand the impacts and limitations of various impurities on different procedures of CO<sub>2</sub> capture and storage. However, even with this uncertainty, CO<sub>2</sub> quality demands for hypothetical CO<sub>2</sub> capture-transport-storage scenarios have been discussed and developed in the European ENCAP project and now form the basis for the guidelines for CO<sub>2</sub> quality requirements used in this project.

### **4.2.5 Gas conditioning**

The composition of the CO<sub>2</sub> will not change during the transport for neither of the transport methods provided that the chains are designed without leakage. Hence, the specifications have to be met by the CO<sub>2</sub> capture and conditioning process. Basically, it is possible to treat CO<sub>2</sub> to near 100% purity in the capture and conditioning processes. However, in most cases it is preferable to have less rigid specifications to reduce both energy and capital costs.

#### **4.2.5.1 Conditioning process**

In pipeline transport the gas must be conditioned to pipeline and reservoir specifications and compressed to a pressure high enough to overcome the frictional and static pressure drops and deliver the CO<sub>2</sub> at a high enough pressure to avoid flashing of gas (fig. 4-1). Two processes are presented, (P1) - Compression, condensation against seawater at 60 bar, pumping to 150 bar and (P2) - Direct compression to 150 bar.

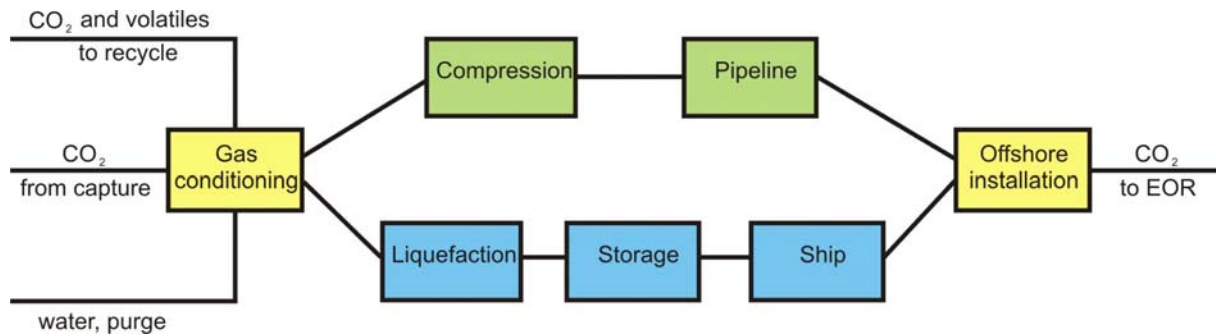


Figure 4-1: (From NTNU) The CO<sub>2</sub> transport chain.

In ship transport the gas must be conditioned to ship and reservoir specifications and liquefied at approximately 6-7 bar at -52°C. The liquid CO<sub>2</sub> is sent to an intermediate storage before it is pumped to a semi-refrigerated ship, which transports the CO<sub>2</sub> to site. The CO<sub>2</sub> feed is first compressed in stages to a pressure higher than the transport pressure and is thereafter cooled by ambient air or water after each compressor stage. At the highest pressure heat is rejected from the CO<sub>2</sub> and the CO<sub>2</sub> is expanded to transport pressure. A process (S1) with condensation against seawater at 60 bar (below the critical point) is expounded.

The compression and liquefaction processes have many similarities, both as it concerns process equipment and minimum energy requirement. The processes are distinguished by different gas conditioning possibilities and requirements. P2 is the conventional direct compression process for pipeline transport, the process is not able to remove non-condensable components (volatiles). In P1 the gas is condensed at 60 bar and pumped to pipeline transport pressure, hence volatiles can be removed by flashing or distillation. Process S1 follows the same path as P1, however, after condensation, the volatiles must be removed and the liquid is expanded to transport pressure. In some cases the CO<sub>2</sub> volatiles from P1 and S1 can be recycled back into the capture process.

#### 4.2.5.2 Removal of water and other liquids in the vapour-liquid separator drums

Vapour-liquid separator drums are needed to ensure no liquid entrainment to the compressors. Separation by gravity is the simplest and most cost and energy effective way to remove the bulk of components with higher density than gaseous CO<sub>2</sub>. Components with high solubility in water or components with higher boiling points than CO<sub>2</sub> will be removed together with the water in the separator drums. The solubility of water in CO<sub>2</sub> gas decreases with higher pressure and lower temperatures. Therefore, most of the water is removed in the vapour-liquid separator drums after compression and cooling. The last free water should be removed at a pressure between 20 and 40 bar and at a temperature close to the hydrate formation curve. With proper design the vapour-liquid separator drums can, in theory, remove water down to approximately 400 - 500 ppm. After the separator drums the CO<sub>2</sub> gas is dried to 50 ppm by regenerative adsorption columns, which can be regenerated with heated CO<sub>2</sub>. Contaminants like H<sub>2</sub>S can also be removed at this point. The purge gas from the adsorption column should be cooled and recycled into one of the first vapour-liquid separator drums to avoid purging of CO<sub>2</sub>.

It has been assumed here, based on previous industrial experience, that the CO<sub>2</sub> can contain maximum 50 ppm water. This water content may, however, be too low as free water and thereby corrosion hydrate and ice problems will probably not occur before the water content is more than ten times higher than this specification. This does, of course, depend on the maximum pressure and minimum temperature in the CO<sub>2</sub> pipeline. A more realistic specification could be achieved using only separator drums. Thus it may be possible to

remove the adsorption driers from the process both for pipeline and ship transport. Liquid CO<sub>2</sub> can contain more water than gaseous CO<sub>2</sub> at all pressures. Note that if an adsorption drier is installed the CO<sub>2</sub> will be dried to ppm level anyway, hence there will be little to gain by changing the specification from e.g. 50 to 200 ppm water.

Since most of the water is removed in the separator drums, the amount of water will hardly have any effect on the process efficiency or capital cost and O&M cost. However, as some CO<sub>2</sub> will dissolve in water there will be a loss of CO<sub>2</sub> to the ambient, unless the process is designed with the purpose to avoid this. The solubility of CO<sub>2</sub> in water will decrease with higher temperature and increase with higher pressure. The water from intermediate pressure separator drums should be sent to a final drum at ambient pressure. If waste heat is available the water can be heated prior to the final drum. The solubility of CO<sub>2</sub> in water at 1 bar and 20°C is approximately 0.1 mol%.

#### **4.2.5.3 Removal of volatile gases**

Volatiles, like nitrogen and oxygen will usually not account for any safety or operational problems for the pipeline transport process or the reservoir. However, as transport is both energy and cost intensive it makes little sense to process and transport the volatiles. One mole% of nitrogen will increase energy requirement and capital and O&M costs in the transport chain with approximately 1% as it will need (roughly) the same compression work and occupy an equal percentage of the pipeline. Hence, the purity in pipeline transport is determined by technical and economical evaluations as there also is an energy and capital penalty for removing unwanted components. In ship transport near the triple point, however, most volatiles must be removed to avoid dry ice (= solid CO<sub>2</sub>) formation during liquefaction or transport, giving less room for economical evaluations here in the optimization of the CO<sub>2</sub> processing.

The volatiles should be removed in a column instead of a flash separator to reduce the amount of CO<sub>2</sub> in the volatile purge stream. The quality of the purge stream depends on feed gas composition and the column condenser and re-boiler duty. A high condenser duty will reduce the content of CO<sub>2</sub> in the purge stream. A high re-boiler duty will reduce the content of volatiles in the CO<sub>2</sub> product. If deemed necessary a two column system can be used to enhance the purity of the CO<sub>2</sub> product and reduce the CO<sub>2</sub> in the purge stream. As a rule of thumb, in a one column system, the loss of CO<sub>2</sub> to the purge stream in moles will be equal to the amount of volatiles in moles.

An example of volatiles removal is given for the oxy-fuel process in section 2.4.2.2.

Most of the components with low boiling points, as N<sub>2</sub>, O<sub>2</sub>, NO, CO, H<sub>2</sub>, CH<sub>4</sub>, and Ar will be found in the volatile purge stream. The purge stream flow will be much smaller than the total flue gas flow and could typically be recycled back to the power process with CO<sub>2</sub> capture. This method also offers a potential to avoid other NO<sub>x</sub> cleaning measures (low-NO<sub>x</sub> gas turbines, SCR), since NO recycled to a point upstream of the combustion chamber may be further oxidized into NO<sub>2</sub> and removed in separator drums as mentioned above. Also, the heating value of components such as CO, CH<sub>4</sub> and H<sub>2</sub> can be made use of if they are recycled to a point prior to the combustion chamber. H<sub>2</sub> and Ar are valuable products that may be recovered as saleable products.

#### **4.2.5.4 Chemical or physical treatment or advanced separation processes**

Components with boiling points and densities similar to CO<sub>2</sub> will be accumulated in the CO<sub>2</sub> if not removed by the means of more advanced separation techniques. If it is possible to inject the component in the reservoir together with the CO<sub>2</sub>, the presence of these components is merely a design, safety and operational challenge. If not, the unwanted components must be removed at a potentially high cost

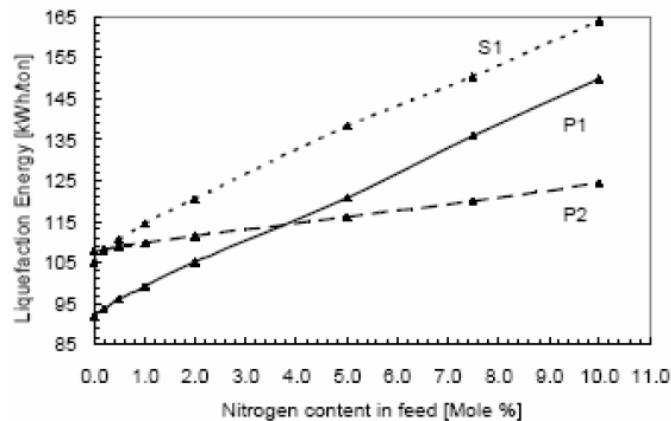


Figure 4-2: (From NTNU) Variation of energy requirement for P1, P2, S1 as a function of inert gas content.

Components that cannot easily be separated from CO<sub>2</sub> by flashing or simple distillation are for example H<sub>2</sub>S and SO<sub>2</sub>. H<sub>2</sub>S might be a safety hazard. SO<sub>2</sub> poses a particular problem, since it is not clear yet if it might be regarded as industrial waste and therefore cannot be injected in reservoirs or aquifers due to legal restrictions.

Unwanted components that cannot be removed in the Vapour-liquid separator drums or in the inert column must be removed by e.g. absorption or adsorption towers, advanced distillation, membranes or burnt in catalytic processes. Advanced separation techniques are also necessary to obtain high purity CO<sub>2</sub>, an example being removal of water from 500 ppm to 50 ppm in an adsorption column. Unwanted components that cannot be a part of the CO<sub>2</sub> product or be removed in the separator drums or inert column should be avoided in the capture process or be removed as early as possible in the capture, conditioning or transport process to avoid unnecessary handling.

#### 4.2.5.5 Energy requirement in the conditioning process

The most important factors for the energy requirement in the conditioning processes are inlet pressure, amount of volatiles in the feed, ambient temperature and the compressor efficiency. The effect of volatiles in the feed is shown by adding nitrogen to the feed and presented in figure 4-2. As expected the process with direct compression (P2) increases linearly with approximately 2 kWh/mole nitrogen. In the two processes with condensation of CO<sub>2</sub> and removal of the volatiles in an inert column, (P1) and (S1), there is a linear increase in energy requirement of 6 kWh/mole nitrogen. The reason for the increased energy requirement in the processes is twofold. First the condensation pressure will increase with larger amount of volatiles, second the column condenser and re-boiler duty will increase.

Very little CO<sub>2</sub>, less than 0.4% of the total feed for any of the processes, is lost with water purge. This CO<sub>2</sub> can, however, not be recovered. Furthermore, if the CO<sub>2</sub> solved in water is not in equilibrium due to too short settling time in the water/gas separators additional CO<sub>2</sub> will be lost in the processes with water recycles.

Figure 4-3 shows the energy requirement for the three processes as a function of inlet pressure. Process P1, has approximately 10% higher energy efficiency than P2 and S1. At atmospheric pressure the energy requirement is approximately 95 and 105 kWh/ton CO<sub>2</sub> respectively. Hence, P1 is the preferred solution for process plants with access to seawater with a relatively low temperature. However, P2 will have lower investment costs and is favourable for higher seawater temperatures.

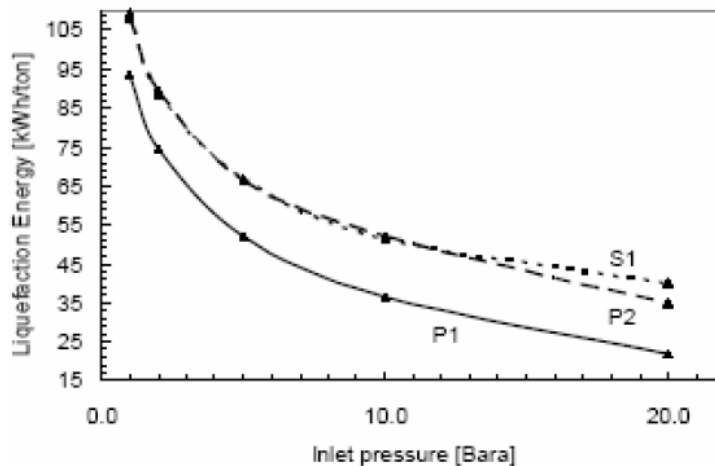


Figure 4-3: (From NTNU) Variation of energy requirement for P1, P2, S1 as a function of inlet pressure.

The CO<sub>2</sub> content in the product stream will be close to 100% for the two processes with condensation and an inert removal column (P1 and S1). The quality for the direct compression process (P2) will depend on the inlet feed composition as all the volatiles will be present in the product stream. In the process P2 it is neither required nor possible to remove any of the volatiles as the process operates in the superheated gas phase. In the processes P1 and S1 the removal of volatile components is done in a separation column after condensation close to the dew point line. At condensation pressures of 60 bar, moderate fractions of volatiles, up to 5 mole%, will be in the liquid phase. By implementing a re-boiler in the column lower compositions, down to 0.25 mole% of volatiles, can be achieved. A condenser at sub ambient temperatures is required in order to reduce the content of CO<sub>2</sub> in the volatile purge. The condenser duty and the optimal temperature is dependant on the amount of volatiles and if the purge gas can be recycled.

Power processes with CO<sub>2</sub> capture should be optimized together with the transport processes in order to reduce the total costs, increase the efficiency and minimize the CO<sub>2</sub> emissions.

### 4.3 Cost estimation

The total transport cost is the sum of the investment cost, the fixed operation and maintenance cost and the variable operation and maintenance cost of the pipeline as well as the compressor station, if needed.

#### 4.3.1 Pipeline investment cost factors

The pipeline investment cost comprises four components, following the cost division applied in the Oil & Gas Journal Pipeline Economics reports, material, labour, ROW & damages and miscellaneous cost. The material cost includes pipeline, coating and cathodic protection; the miscellaneous cost consists of supervision, surveying, engineering, contingencies, telecommunications equipment, freight, taxes, allowances for funds used during construction, administration and overheads and regulatory filing fees. For each of the cost types, a formula is proposed that is dependent on the pipeline diameter and the pipeline length.

##### 4.3.1.1 Material cost

The formula of the material cost is based on the cost of the volume of steel that is needed for the pipeline with optimal diameter. For the calculation of the volume, the pipeline thickness is taken into account, which is dependent on the pipeline diameter and the transport CO<sub>2</sub>

pressure. The value of the steel cost per kg is necessary input in the formula. Furthermore, the formula incorporates a factor expressing the regional economic dependence and product cost. The formula includes also a component that takes account of a lower cost for long pipelines, which was empirically derived from cost reports found in the Oil & Gas Journal. Finally, the equation can be written as:

$$\text{Material cost} = L \times St \times FP \times \left( \frac{\pi \times 7850}{4} \right) \times \left( OD^2 - (OD - Th)^2 \right) - 10 \times OD \times \ln(L) \times L \quad (18)$$

with pipeline thickness:

$$Th = \left( \frac{2}{1 - FT} \right) \times \left( \frac{P \times OD}{2 \times (S + 0.4 \times P)} + FC \right) \quad (19)$$

and

L: pipeline length (in m)

OD: outer diameter of pipeline (in m)

FP: factor for steel product (included in regional economics factor)

P: (transport) pressure of CO<sub>2</sub> in pipeline (Pa): 9500000

S: allowable stress in pipeline, related to pipeline degree (Pa):  
246000000

St: steel cost (euro/kg): 0.472

FT: under-thickness tolerance factor: 0.125

FC: factor allowing for threading, mechanical strength and corrosion:  
0.00127

#### 4.3.1.2 Labour cost

An empiric equation for the labour cost was derived from pipeline investment costs reported in the Oil & Gas Journal of the last years.

$$\text{Labour cost} = (650 \times OD - 35 \times OD \times \ln(L)) \times L \times TF2 \quad (20)$$

with

TF2: terrain factor for labour cost

#### 4.3.1.3 ROW & Damages cost

The ROW & Damages cost is based on a working area 15 m wide for a 4-inch pipeline and 25 m wide for a 12-inch pipeline (based on personal communication with Tractebel), whereby 3 euro per m<sup>2</sup> costs (personal communication with Nationale Maatschappij der Pijpleidingen) can be considered. This leads to the following formula.

$$\text{ROW \& Damages cost} = (150 \times OD + 30) \times L \times TF3 \quad (21)$$

with

TF3: terrain factor for ROW & Damages cost (22)

#### 4.3.1.4 Miscellaneous cost

The Miscellaneous cost formula is empirically deduced from data from the Oil & Gas Journal.

$$\text{Miscellaneous cost} = (400 \times OD - 15 \times OD \times \ln(L)) \times L \times TF4 \quad (23)$$

with

TF4: terrain factor for miscellaneous cost

### 4.3.2 Determination of diameter and length of pipeline

The mentioned cost component formulas are all expressed in function of pipeline diameter and length. The pipeline length or trajectory will be determined by a least-cost router application, developed for the current project and discussed in chapter 8.4.

Concerning the diameter, a new equation has been developed that makes a detailed calculation based on a diversity of variable factors. This equation was defined after an extensive review of existing diameter calculation formulas, currently used or proposed in the framework of CO<sub>2</sub> transport.

#### 4.3.2.1 Diameter calculation using hydraulic equations for turbulent flow

##### a) Origin of the formula

The equation:

$$D^5 = \frac{32 f_F Q_m^2}{\rho \pi^2 \left( \frac{\Delta p}{L} \right)} \quad (24)$$

with

D = diameter (m)

f<sub>F</sub> = Fanning friction factor

Q<sub>m</sub> = mass flow rate (kg/s)

ρ = density (kg/m<sup>3</sup>)

Δp = pressure drop (Pa)

L = length (m)

is used in Bock et al. (2003), Hamelinck et al. (2001), Heddle et al. (2003) and IEA GHG (2002). The equations stated in the original publications may look different, but after converting the stated units into the standard units as used above, they can all be transformed into the formula shown here. In the equation published in IEA GHG (2002), an erroneous km – m switch for unit pipeline length was corrected.

The basic formula is derived from hydraulic equations for turbulent flow in circular-shaped pipelines. It is based on the law of Bernoulli that can be presented as:

$$z_1 + \frac{p_1}{\rho g} + \frac{v_1^2}{2g} = z_2 + \frac{p_2}{\rho g} + \frac{v_2^2}{2g} + \frac{\Delta F}{1} \quad (25)$$

With

z = place height (m)

p = pressure (Pa)

v = velocity (m/s)

F = total of frictional and local losses

In the mentioned publications, no difference in topographic height is assumed (z<sub>1</sub> = z<sub>2</sub>) and analyzing the hydrostatic line (v<sub>1</sub> = v<sub>2</sub> = 0; fig. 4-4), the following is then valid:

$$\frac{p_1}{\rho g} = \frac{p_2}{\rho g} + \frac{\Delta F}{1} \quad (26)$$



Figure 4-4: Sketch of the stream line in a straight pipeline connecting two reservoirs. The hydrostatic line is considered between two points at equal place height ( $z_1 = z_2$ ) and with equal minimal velocity ( $v_1 = v_2 = 0$ ).

Only frictional losses, and no local losses (due to bends or differences in diameter), are taken into account. The Fanning friction factor is used and is assumed independent of the flow rate. As a result and based on the definition of the friction factor, the frictional losses can be written as:

$$\frac{\Delta F}{1} = \frac{f_F}{2g} \frac{v^2}{R} L \quad (27)$$

With

$v$  = velocity (m/s), which is defined by volumetric flow rate on surface

$f_F$  = Fanning friction factor

$R$  = hydraulic radius (m), which is defined as the ratio of the cross sectional area of flow on the wetted perimeter; hence, for a circular-shaped pipeline:  $R=D/4$

Equations 26 and 27 can be used to express diameter as a function of flow rate for a given friction factor, pressure loss and length of the pipeline trajectory, as presented in Equation 24. The Fanning friction factor can be found by using an appropriate roughness factor and the White-Colebrook law (visualized as the Moody chart), which can be defined as:

$$\frac{1}{\sqrt{f}} = -2 \log \left( \frac{e}{14.8R} + \frac{2.51}{Re \sqrt{f}} \right) \quad (28)$$

with

$f$  = Darcy-Weisbach friction factor =  $4 \cdot f_F$

$e$  = roughness height (m)

$Re$  = Reynolds number

for full flow (closed conduit). This equation can be used to iteratively solve for the Darcy-Weisbach friction factor, which was the method used in Bock et al. (2003), Hamelinck et al. (2001) and Heddle et al. (2003). Note that the Darcy-Weisbach friction factor is four times larger than the Fanning friction factor.

Since an iterative determination of the friction factor by the White-Colebrook equation can be quite time-consuming, the Swamee-Jain equation (for a full-flowing circular pipe) was used here to determine the friction factor for the reconstruction of the diameter vs flow rate curves:

$$f = \frac{1.325}{\left[ \ln \left( \frac{e}{3.7D} + \frac{5.74}{Re^{0.9}} \right) \right]^2} \quad (29)$$

with

$e$  = roughness height (m)

$D$  = pipe diameter (m)

$Re$  = Reynolds number

Here, still the Reynolds number needs to be defined:

$$Re = \frac{\rho v l}{\mu} \quad (30)$$

With

$\rho$  = fluid density (kg/m<sup>3</sup>)

$v$  = mean fluid velocity (m/s), which can be substituted by the ratio of flow rate on surface

$l$  = characteristic length, which is equal to the diameter if the cross-section is circular

$\mu$  = (absolute) dynamic fluid viscosity (Pa.s)

The Reynolds number in equation 29 can be substituted by the formula given in equation 30. Subsequently, the resulting equation for the friction factor can be used in equation 26, which can then be combined with equation 25 to be transformed in an equation that is written in function of the diameter. Still, the resulting equation can only be solved iteratively for the diameter. As also explained in Bock et al. (2003), a value for the diameter should first be guessed, after which the correct value can be approximated by iterative calculations.

#### b) Parameter values

For the diameter calculation, there are differences in the absolute values assigned to parameters. An overview of the assigned values for the parameters is given in table 4-3. First, Hamelinck et al. (2001) assume CO<sub>2</sub> transport conditions at a temperature of 10°C and a pressure of 7.5 MPa. These authors relate these conditions to a CO<sub>2</sub> density of 899 kg/m<sup>3</sup> and a CO<sub>2</sub> viscosity of 8.22 10<sup>-5</sup> Pa.s. Furthermore, they use a roughness height of 0.0457 10<sup>-3</sup> m for commercial steel as cited by Perry et al. (1987). The calculated pipeline diameter in function of mass flow rate is presented in figure 4-5 (symbol curves). On this figure, the line curves also present the refereed equations, but based on a temperature of 15°C and pressure of 10 MPa with corresponding CO<sub>2</sub> density of 890.1 kg/m<sup>3</sup> and CO<sub>2</sub> viscosity of 8.9151 10<sup>-5</sup> Pa.s (Span and Wagner, 1996) in order to compare different equations using the same parameter values.

Table 4-3: Overview of parameter values used in the calculation of the pipeline diameter in Bock et al. (2003), Hamelinck et al. (2001), Heddle et al. (2003), IEA GHG (2005), Zhang et al. (2006) and in our own proposed equation. The height difference, amount of bends and bend degree depend on the pipeline route and are only taken as an example here to show their influence on the pipeline diameter.

<b>Parameters</b>	<b>Hamelinck et al. (2001)</b>	<b>Heddle et al. (2003) and Bock et al. (2003)</b>	<b>IEA GHG (2005)</b>	<b>Zhang et al. (2006)</b>	<b>Proposed standard values in this study</b>
Temperature (°C)	10	25		40 (inlet)	15
Pressure (MPa)	7.5	10.3 to 15.2		15.0 (inlet)	10
CO <sub>2</sub> density (kg/m <sup>3</sup> )	899	884	800		890.1
CO <sub>2</sub> viscosity (Pa.s)	0.0000822	0.0000606			0.000089151
Roughness height (m)	0.0000457	0.0000457			
Velocity (m/s)			2		
Pressure loss (MPa)					5
Pipeline length (m)					200000
Manning n-factor					0.009
Height difference: z <sub>1</sub> -z <sub>2</sub> (m)					200
Amount of bends					2000
Bend degree					45

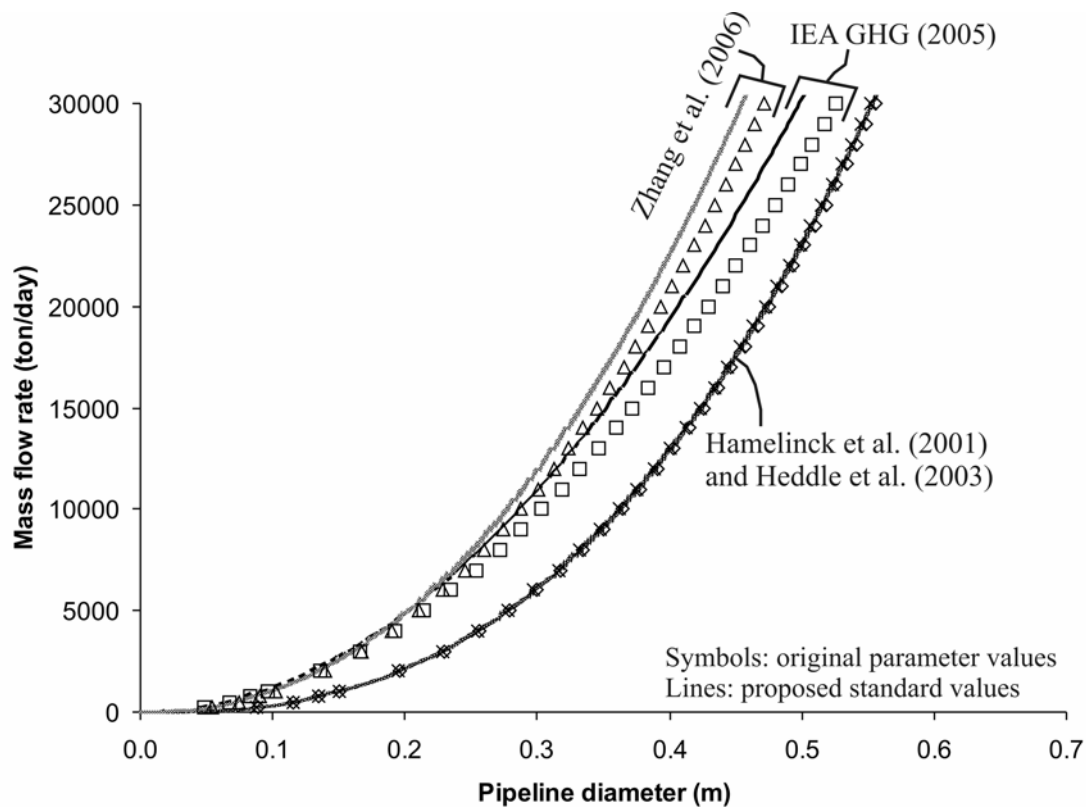


Figure 4-5: Pipeline diameter in function of mass flow rate calculated using the equation from Hamelinck et al. (2001), Heddle et al. (2003), IEA GHG (2005) and Zhang et al. (2006). The symbol curves are based on the parameter values in the respective papers, whereas the lines represent the calculations based on the parameter values used in our proposed equation, as discussed in the text, namely temperature and pressure conditions of 15°C and 10 MPa, respectively, and related CO<sub>2</sub> density and viscosity.

Second, Heddle et al. (2003) and Bock et al. (2003) use the same set of parameters. They assume an inlet pressure of 15.2 MPa, an outlet pressure of 10.3 MPa and a temperature of 25°C. A value of 884 kg/m<sup>3</sup> was calculated for the CO<sub>2</sub> density based on a temperature range of 5 to 27°C and a pressure range of 8 to 14 MPa. CO<sub>2</sub> viscosity was calculated to be 6.06 10<sup>-5</sup> Pa.s based on Kreith and Bohn (2000). Heddle et al. (2003) and Bock et al. (2003) take a roughness height of 0.15 10<sup>-3</sup> feet (equal to 0.0457 10<sup>-3</sup> m) based on Perry and Green (1997) for carbon steel. Results for the diameter calculation using these assumptions are presented on figure 4-5. The small differences in the values used for CO<sub>2</sub> viscosity and density do not result in significantly different outcomes compared to Hamelinck et al. (2001).

Third, in IEA GHG (2002), a friction factor of 0.015 for turbulent flow is assumed, but no other parameter values are provided. Hence, this reference is not included in table 4-3, but results of the diameter calculation assuming a CO<sub>2</sub> density of 890.1 kg/m<sup>3</sup> are presented in figure 4-6.

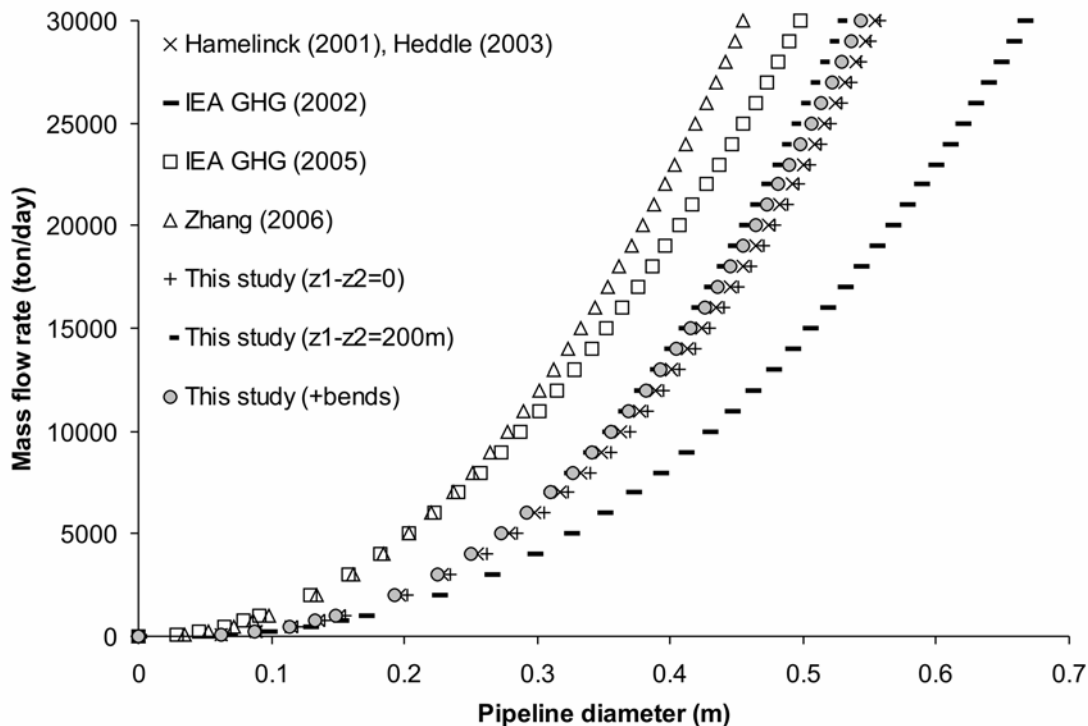


Figure 4-6: Pipeline diameter in function of mass flow rate calculated with the equations presented in Hamelinck et al. (2001), Heddle et al. (2003), IEA GHG (2002, 2005), Zhang et al. (2006) and this study, using the proposed standard values as discussed in the text. These include the temperature and pressure conditions of 15°C and 10 MPa, respectively, and related CO<sub>2</sub> density and viscosity.

### c) Evaluation and discussion

The formula for the calculation of the diameter used by Bock et al. (2003), Hamelinck et al. (2001), Heddle et al. (2003) and IEA GHG (2002) is based on hydraulic laws for turbulent flow. The proposed equation takes fluid characteristics, such as density and viscosity, and also pipeline characteristics, such as the roughness height, into account. Moreover, the diameter depends on the flow rate and the pressure drop per unit length. Nevertheless, some characteristics of the pipeline trajectory are not considered, such as topographic height differences and the occurrence of bends or valves in the pipelines and the calculation of the diameter is done in an iterative process.

With regard to the cited values for the parameters, some inconsistencies were encountered. First, for the temperature and pressure conditions assumed in Hamelinck et al. (2001), 10°C and 7.5 MPa, a CO<sub>2</sub> viscosity of  $9.12 \cdot 10^{-5}$  Pa.s is calculated with the formula of Span and Wagner (1996) instead of the reported  $8.22 \cdot 10^{-5}$  Pa.s in their study. Second, the density and viscosity used by Heddle et al. (2003) and Bock et al. (2003) are not coherent characteristic values for the temperature-pressure window they cite. A CO<sub>2</sub> viscosity of  $6.06 \cdot 10^{-5}$  Pa.s can, within their stated temperature (5-27°C) and pressure (8-14 MPa) range, only occur at marginal temperature-pressure combinations with a temperature higher than 25.5°C and a pressure lower than 8.7 MPa. The density related to this viscosity value in the given temperature and pressure range is  $772 \text{ kg/m}^3$ , which is considerably lower than the value used in these reports.

#### 4.3.2.2 Diameter calculation using hydraulic equation with velocity as parameter

##### a) Origin of the formula

In IEA GHG (2005), the pipeline diameter is calculated by:

$$D = \sqrt{\frac{4Q_m}{v\pi\rho}} \quad (31)$$

with

D = diameter (m)  
 $Q_m$  = mass flow rate (kg/s)  
 $\rho$  = density (kg/m<sup>3</sup>)  
 v = velocity (m/s)

where a given value of 2.0 m/s for velocity is assumed. This equation is derived from the relation between velocity and flow rate:

$$v = \frac{Q}{A} = \frac{4Q_m}{\rho\pi D^2} \quad (32)$$

with

Q = volumetric flow rate (m<sup>3</sup>/s), which is equal to  $Q_m/\rho$   
 A = surface (m<sup>2</sup>), which is  $\pi r^2$  or  $\pi(D/2)^2$  for a circular-shaped pipeline

##### b) Parameter values

A CO<sub>2</sub> density of 800 kg/m<sup>3</sup> and a velocity of 2.0 m/s is assumed. Pipeline diameter in function of mass flow rate is presented in figure 4-5.

##### c) Evaluation and discussion

In this approach, the only parameters defining a value for the diameter are flow rate, velocity and density. Consequently, an average velocity needs to be assumed. When designing the pipeline transport system, velocity is not a primary parameter as it depends on pressure losses in the turbulent CO<sub>2</sub> flow (due to height differences in the pipeline trajectory and frictional losses related to the pipeline material). Moreover, comparing the assumed value of velocity, namely 2 m/s, with the calculated velocity values from the flow rates and pipeline diameter data using the equations in the other references, it can be concluded that a value of 2 m/s is quite high (figure 4-7), certainly for flow rates lower than 75000 ton per day.

No specific conditions of temperature and pressure are provided in IEA GHG (2005). Considering the assumed value of 800 kg/m<sup>3</sup> for CO<sub>2</sub> density used in that report, a temperature-pressure condition of, for example, 25°C and 9.0 MPa can be deduced based on the equation of Span and Wagner (1996).

#### 4.3.2.3 Diameter calculation following optimal design

##### a) Origin of the formula

Zhang et al. (2006) use

$$D_{opt} = 0.363 \left( \frac{Q_m}{\rho} \right)^{0.45} \rho^{0.13} \mu^{0.025} \quad (10)$$

With

$D_{opt}$  = optimum inner diameter (m)  
 $Q_m$  = mass flow rate (kg/s)  
 $\rho$  = density (kg/m<sup>3</sup>)  
 $\mu$  = viscosity (Pa.s)

This equation was derived from Peters et al. (2003), who presented an equation for the calculation of the economic pipe diameter. Since the pressure drop decreases with increasing pipe diameter, also the required power to pump or compress is lower with a larger pipe diameter. Hence, the cheapest scenario is not necessarily the one with the smallest diameter, but the economic diameter is calculated on the base of the minimum total cost of the installation of the pipeline system (pipe, pumps, valves, etc) and the annual cost of electric power.

*b) Parameter values*

Zhang et al. (2006) assume inlet conditions of 15.0 MPa and 40°C. Other assumptions used for the calculation of the annual cost of electric power and installation of the pipeline system include a cost of electrical energy of US \$ 0.05/kWh, 8760 hours of pipeline operation per year, 50% motor/pumps efficiency, 35% frictional loss due to fittings and bends, 1.4 for the ratio of total cost for fittings and installation to pipe purchase, US \$ 2.43 capital cost per meter for 1-inch diameter steel pipe and 20% of capital cost for annual fixed charges including maintenance. Results of the pipeline diameter calculation in function of mass flow rate is presented in fig. 4-5.

*c) Evaluation and discussion*

The only parameters in the formula presented in Zhang et al. (2006), are flow rate and fluid characteristics, namely CO<sub>2</sub> density and viscosity. In the derivation of this equation, an approximation is made for the determination of the friction factor for turbulent flow in new steel pipes, which decreases the accuracy of the result.

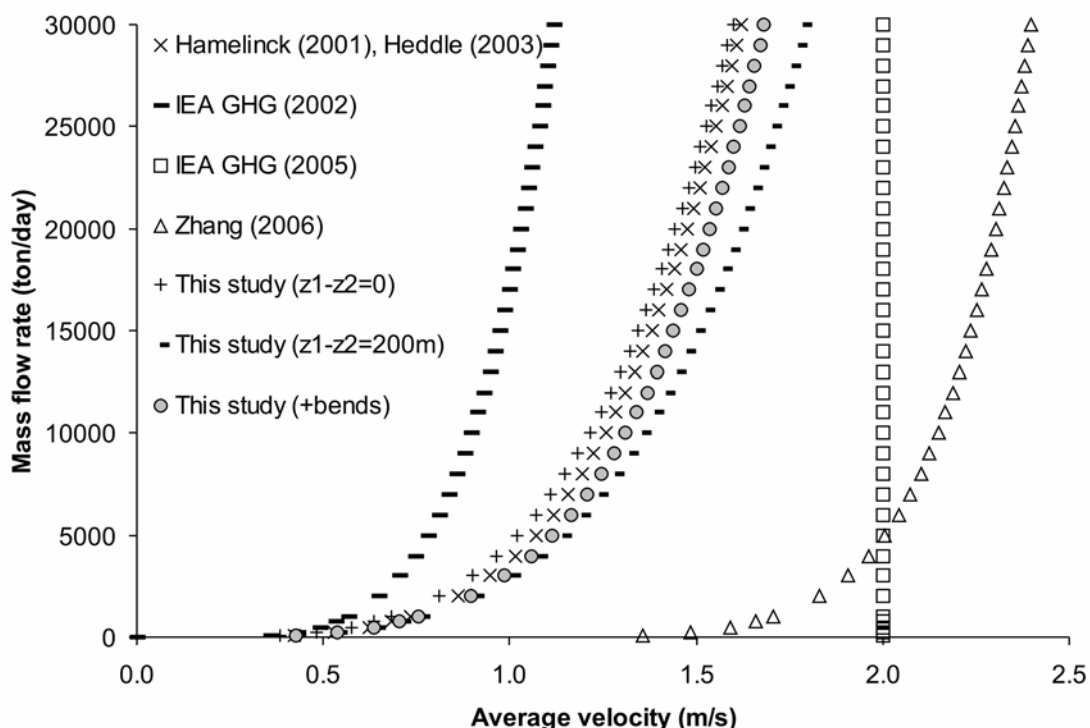


Figure 4-7: Average velocity in function of mass flow rate related to the calculated pipeline diameter using the equations presented in Hamelinck et al. (2001), Heddle et al. (2003), IEA GHG (2002, 2005), Zhang et al. (2006) and this study with the proposed standard values as discussed in the text. These include the temperature and pressure conditions of 15°C and 10 MPa, respectively, and related CO<sub>2</sub> density and viscosity.

Moreover, other values are intrinsically included in the presented formula, namely those related to the annual cost of electric power and the installation of the pipeline system. As a result, this formula lacks flexibility and may only be applicable for very specific situations.

The pressure, which should be controlled to avoid a mixture of gas and liquid phases in the CO<sub>2</sub> flow, is not taken into account in the formula itself. As an alternative, graphs are shown in Zhang et al. (2006) that show the maximum safe pipeline length for specific CO<sub>2</sub> inlet temperatures related to ‘choking’ or very high pressure drops and also the CO<sub>2</sub> density variation over pipeline length is presented indicating the transition to two-phase flow. Based on these observations, the maximum safe distances between booster stations are derived in Zhang et al. (2006). Comparing the diameter results using this formula with the diameters calculated with the equations of Bock et al. (2003), Hamelinck et al. (2001), Heddle et al. (2003) and IEA GHG (2002) using the proposed standard values, it is clear that the diameters calculated by Zhang et al. (2006) have a smaller value (fig. 4-6). This probably indicates that the equilibrium between pump costs (pressure gradient) and pipeline construction costs (pipeline diameter) occurs at a higher pressure gradient than the gradient assumed in the former references.

#### 4.3.2.4 Diameter calculation of this study

##### a) Origin of the formula

The formula we propose to work with is also based on the conventional hydraulic laws for turbulent flow in pipelines and therefore based on the law of Bernoulli for a stream line:

$$z_1 + \frac{p_1}{\rho g} + \frac{v_1^2}{2g} = z_2 + \frac{p_2}{\rho g} + \frac{v_2^2}{2g} + \frac{\Delta F}{1} \quad (33)$$

with

- z = place height (m)
- p = pressure (Pa)
- ρ = density (kg/m<sup>3</sup>)
- v = velocity (m/s)
- F = total of frictional and local losses

By assuming equal velocities (v<sub>1</sub> = v<sub>2</sub>) or a reservoir at the beginning and the end of the pipeline (v<sub>1</sub> = v<sub>2</sub> = 0; fig. 4-8), the hydrostatic line can be presented as:

$$z_1 + \frac{p_1}{\rho g} = z_2 + \frac{p_2}{\rho g} + \frac{\Delta F}{1} \quad (34)$$

This equation can be rewritten with incorporation of the formula of Manning, which is an empirical law for frictional and local losses as a function of flow rate, length, diameter. Substitution of ΔF results in:

$$(z_1 - z_2) + \frac{(p_1 - p_2)}{\rho g} = \frac{4^{10/3} n^2 Q^2 L}{\pi^2 D^{16/3}} + \frac{8Q^2 \sum \zeta_i}{g \pi^2 D^4} \quad (35)$$

with

- n = Manning factor, characteristic for roughness of pipeline material
- Q = volumetric flow rate (m<sup>3</sup>/s)
- L = length of pipeline (m)
- D = diameter of pipeline (m)
- ζ = loss factor dependent on bend characteristics and roughness of pipe material

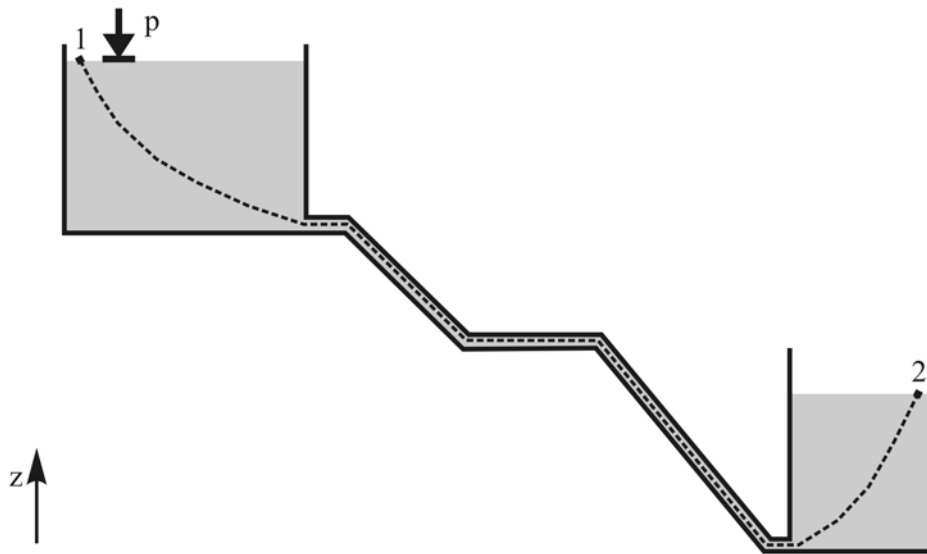


Figure 4-8: Sketch of the stream line in a pipeline with bends connecting two reservoirs at different topographic height. The hydrostatic line is considered between two points with equal minimal velocity ( $v_1 = v_2 = 0$ ).

In this equation, the first two members represent difference in topographic height and difference in pressure heads, while the third component is frictional loss and the fourth stands for local losses due to bends in the pipeline.

In a first step, not considering local losses, the diameter can be calculated by:

$$D = \left( \frac{4^{10/3} n^2 Q_m^2 L}{\pi^2 \rho^2 \left( z_1 - z_2 + \frac{P_1 - P_2}{\rho g} \right)} \right)^{3/16} \quad (36)$$

with

$Q_m$  = mass flow rate (kg/s)

The equation becomes a fourth order polynomial when taking local losses into account:

$$-\frac{4^{10/3} n^2 L Q^2}{\pi^2 \left( z_1 - z_2 + \frac{P_1 - P_2}{\rho g} \right) E^4} - \frac{8 Q^2 \sum_i \zeta_i}{g \pi^2 \left( z_1 - z_2 + \frac{P_1 - P_2}{\rho g} \right) E^3} + 1 = 0 \quad (37)$$

with

$$E = D^{4/3}$$

for which four solutions can be calculated. Two of the solutions have negative values, while the other two lie close to each other. In order to extract the correct value of the latter, the two values are compared with the calculated pipeline diameters assuming no local losses. The pipeline diameter of the two values that is higher than the result without taking local losses into account, is the correct solution:

$$D = E^{3/4} = \left( \frac{1}{2} \sqrt{t_1 + t_2} + \frac{1}{2} \sqrt{-t_1 - t_2 - \frac{2b}{\sqrt{t_1 + t_2}}} \right)^{3/4} \quad (38)$$

with

$$t_1 = \frac{4\sqrt[3]{\frac{2}{3}a}}{\sqrt[3]{9b^2 + \sqrt{3}\sqrt{27b^4 - 256a^3}}}$$

$$t_2 = \frac{\sqrt[3]{9b^2 + \sqrt{3}\sqrt{27b^4 - 256a^3}}}{3^{2/3}\sqrt[3]{2}}$$

$$a = -\frac{4^{10/3}n^2LQ^2}{\pi^2\left(z_1 - z_2 + \frac{P_1 - P_2}{\rho g}\right)}$$

$$b = -\frac{8Q^2\sum_i \zeta_i}{g\pi^2\left(z_1 - z_2 + \frac{P_1 - P_2}{\rho g}\right)}$$

#### b) Parameter values

A temperature of 15°C and a pressure of 10 MPa is assumed and based on this, the density and viscosity of CO<sub>2</sub> is calculated with Span and Wagner (1996) and used in the equations. A pressure loss of 5 MPa on a distance of 200 km is taken and a Manning n-factor of 0.009. Current literature presents Manning roughness coefficients of 0.010 to 0.014 for welded steel pipes (e.g. Corzine et al., 2007) and of 0.011 for new unlined commercial steel (equivalent to a Darcy-Weisbach roughness height of 0.045 mm; Haestad Methods, 2002). However, comparing flow rate versus diameter graphs for Manning and Darcy-Weisbach equations, it appears that a Manning factor of 0.009 better corresponds to a Darcy-Weisbach roughness height of 0.045 mm. As a matter of fact, this was confirmed by measurements performed by Simicevic and Sterling (2003) on a particular pipe.

Three cases are presented in figure 4-6. First, a situation is considered where no height difference exists between beginning and end point and it is assumed that there are no bends in the pipeline. Second, a height difference of  $z_1 - z_2 = 200$  m is assumed, but no bends in the pipeline are considered. Third, a height difference of 200 m is considered and 2000 bends of 45° in a relatively rough pipeline are assumed. An overview of velocity change in function of mass flow rate based on the different equations is presented in figure 4-7.

The diameter calculated in the first situation (without topographic differences) is very similar to the results of Hamelinck (2001) and Heddle (2003), but smaller than the results from IEA GHG (2002) and larger than the diameters calculated with the other reviewed formulas. Looking at the second case, figure 4-6 shows that the topographic difference (with the end point being topographically 200 m lower than the start point of the pipeline) results in a decrease of the diameter compared to the first case considering the same flow rate. The effect of adding bends to the considered pipeline system results in a small increase of the pipeline diameter. This effect is minimal, though. A situation of 2000 bends of 45° (with also the topographic difference of 200 m as in the second case) shows that the influence on the calculated diameter is much smaller than the effect of topography (fig.4-6).

#### 4.3.2.5 Evaluation and discussion on the diameter calculation of this study

The formula proposed in this study (eq. 38) is an elaboration of the hydraulic laws for turbulent flow in circular-shaped pipelines that were used in some earlier studies on the transport of CO<sub>2</sub>. Now it includes the effect of pipeline bends, which seems to be minimal, and that of topographic height differences between start and end point of the pipeline, which can be of major influence.

As an additional improvement, the Manning equation was introduced as an alternative to the Darcy-Weisbach formula. The Manning equation is widely accepted for describing turbulent open-channel flow and pipe flow (e.g. Brater and King, 1976; Carey and Woo, 2000; Dingman and Sharma, 1997) and has as major advantage that it avoids the use of iterative calculations. This not only makes the final diameter formula easier to use and implement, but it is also of especial importance for simulators that evaluate multiple sink and source connections, or for economic optimization of individual projects. In these repetitive calculation schemes, calculation time becomes important.

1. In contrast to the application of this formula for the presentation of the diameter results, the pressure gradient will not be incorporated as a fixed value when implementing this formula in a least-cost pipeline route planner. Based on a few basic cases, the pressure gradient can be adapted taking into account the pipeline length and the compression cost. In this way, the best economic solution is guaranteed and in a more flexible way than with an integrated optimal design formula as in Zhang et al. (2006).

The use of the Manning equation is limited by the availability of Manning factors (describing the roughness) for different pipeline materials. Having a good idea of the Manning factor is important, since for a flow rate of 15000 ton/day, the diameter increases by 0.01 m for an increase of 0.001 in the Manning factor. Hence, we also present here the Darcy-Weisbach formula, which is considered as the most accurate based on its application to an extensive range of Reynolds numbers (Liou, 1998; Bombardelli and García, 2003), with incorporation of the topographic elevation difference in contrast to the equations used in Bock et al. (2003), Hamelinck et al. (2001), Heddle et al. (2003) and IEA GHG (2002). The diameter can then be calculated by:

$$D = \left( \frac{8fQ_m^2 L}{\rho\pi^2 [\rho g(z_1 - z_2) + (p_1 - p_2)]} \right)^{1/5} \quad (39)$$

where the Darcy-Weisbach friction factor can be substituted by the White-Colebrook law as explained earlier.

#### **4.3.2.6 Application and comparison with existing CO<sub>2</sub> pipelines**

The diameter values calculated using this study's formula 38 (Manning solution) and 39 (Darcy-Weisbach solution) can be regarded as the minimum inner diameter values for a pipeline. From a practical point of view, the used pipeline will be chosen from the economic available pipeline types, of which the size is often expressed as NPS (nominal pipe size). For NPS of 1/8 to 12, the number is related to the inner diameter of the pipeline, expressed in inches, whereas for NPS of 14 and larger, this number equals the outer pipeline diameter. Hence, the first available NPS that is larger than the calculated value (converted to inches) should be chosen for NPS of 12 or smaller. For pipelines with NPS of 14 or larger, the first available NPS is taken that is larger than the calculated diameter value (converted to inches) added with two times the wall thickness. The wall thickness of, for example, a 12 and 16 inch pipeline of the SACROC pipeline is 0.34 and 0.37 inch (about 0.9 cm) wide, respectively (IPCC, 2005). The wall thickness increases with pipeline diameter.

The data of several pipelines transporting CO<sub>2</sub> were used to test and compare calculated pipeline diameters with those of CO<sub>2</sub> pipelines in operation. Some data are publicly available for pipelines owned by the Kinder Morgan Company (Kinder Morgan website). Their website lists pipeline length, location, capacity and pipeline diameter. Local losses due to pipeline bends are of minor influence and were neglected in the calculation. In contrast, the topographic height of the pipeline start and end point was taken into account in our formula. For the Weyburn pipeline, the correct inlet and outlet pressure was also considered, as this

information was available in contrast to the other pipelines. Table 4-4 shows an overview of six CO<sub>2</sub> pipelines in North America, whereby the actual pipeline diameters are compared to the diameters calculated using this study's formula 36 (Manning solution, without incorporation of bends) and 39 (Darcy-Weisbach solution). It is clear that the calculated results for the Weyburn pipeline with pressure data approximate the real pipeline diameter very well. For the other pipeline examples (without pressure information), most of our calculation results are smaller than the actual diameters, suggesting that they are designed for lower pressure gradients than the 25 Pa/m assumed in our study or for (future) higher flow rates.

The diameter was also calculated using the other reviewed formulas (table 4-5). It is clear that there is a large deviation between the IEA GHG (2005), Zhang et al. (2006) results and the actual diameter of the Weyburn pipeline, as pressure is not a parameter in these formulas. The diameter results calculated following Bock et al. (2003), Hamelinck et al. (2001), Heddle et al. (2003) and IEA GHG (2005) for the other pipelines are generally higher than the results from our formula. An important cause for this difference consists in the elevation difference between starting and end point of the pipeline trajectory. Not taking into account the topography can lead to significant over- or underestimation in pipeline diameter design.

*Table 4-4: Overview of data from a few U.S. CO<sub>2</sub> pipelines and comparison between actual and calculated pipeline diameter using pipeline length, capacity and difference in topographic height from the specific pipelines and assuming a pressure loss of 5 MPa per 200 km (or 25 Pa per meter), CO<sub>2</sub> density of 890.1 kg/m<sup>3</sup> and Manning n-factor of 0.009. The positive numbers for elevation difference indicate a decrease of topographic height from start to end point of the pipeline trajectory.*

<b>Pipeline</b>	<b>Location</b>	<b>Capacity (Mt/yr)</b>	<b>Length (km)</b>	<b>Elevation difference (m)</b>	<b>Actual diameter (m)</b>	<b>Calculated diameter (m)</b>
<i>Cortez</i>	Cortez to Denver City	19.3	808	800	0.76	0.59
<i>Transpetco</i>	Bravo Dome to Guymon	3.4	193	1094	0.32	0.30
<i>Sheep Mountain part 1</i>	Sheep Mountain to Rosebud	6.4	296	893	0.51	0.38
<i>Sheep Mountain part 2</i>	Rosebud to Seminole	9.3	360	464	0.61	0.47
<i>Bravo</i>	Bravo Dome to Denver City	7.4	351	955	0.51	0.40
<i>Weyburn</i>	Beulah to Weyburn	1.8	330	46	0.36 <sup>a</sup>	0.35

<sup>a</sup> The Weyburn pipeline consists of 2 parts with different diameter, namely 14 inch (0.36 m) and 12 inch (0.30 m).

Table 4-5: Calculated diameter values (expressed in meter) for a few example CO<sub>2</sub> pipelines using the different formulas reviewed in this paper, the proposed formula based on the Manning equation and the Darcy-Weisbach equation with the elevation difference taken into account. Also the actual diameter (outer diameter) is given for comparison. For the reviewed equations, the original parameter values are used; hence, no calculations are presented for IEA GHG (2002) as no parameter values are presented there.

<i>Pipeline</i>	<i>Hamelinck et al. (2001), Heddle et al. (2003), Bock et al. (2003)</i>	<i>IEA GHG (2005)</i>	<i>Zhang et al. (2006)</i>	<i>This study: Manning formula</i>	<i>This study: Darcy-Weisbach formula</i>	<i>Actual diameter</i>
<i>Cortez</i>	0.69	0.70	0.61	0.59	0.58	0.76
<i>Transpetco</i>	0.35	0.29	0.28	0.30	0.29	0.32
<i>Sheep Mountain part 1</i>	0.45	0.40	0.37	0.38	0.37	0.51
<i>Sheep Mountain part 2</i>	0.52	0.48	0.44	0.47	0.46	0.61
<i>Bravo</i>	0.47	0.43	0.40	0.40	0.39	0.51
<i>Weyburn</i>	0.36	0.21	0.21	0.35	0.35	0.36 <sup>a</sup>

<sup>a</sup> The Weyburn pipeline consists of 2 parts with different diameter, namely 14 inch (0.36 m) and 12 inch (0.30 m).

#### 4.3.2.7 Conclusion

In the cost estimations for CO<sub>2</sub> transport in pipelines, the pipeline diameter plays an important role. Hence, a good formula for the calculation of the diameter is necessary in the design of the pipeline network. Many technical factors play a role in the determination of the proper diameter size, namely flow rate, pressure drop per unit length, CO<sub>2</sub> density, CO<sub>2</sub> viscosity, pipeline material roughness, topographic differences and amount and type of bends. None of the refereed publications take all of these factors into account. The equations presented in Bock et al. (2003), Hamelinck et al. (2001), Heddle et al. (2003) and IEA GHG (2002) use most of these factors as variable parameters, but do not consider topographic differences nor amount and types of bends in the pipeline trajectory. IEA GHG (2005) assumes a mean velocity. However, velocity can vary quite strongly for different flow rates. The economic optimum pipeline diameter used in Zhang et al. (2006) is based on the minimum total cost considering the pumping cost and the pipeline material cost, both related to the pipeline diameter. However, in this approach, some technical parameters, such as pressure drop, are replaced by economic constraints, such as pumping costs. This makes the application of this equation less direct and the formula itself must be kept up-to-date with current and regional economic parameters.

Our proposed Manning solution takes all parameters into account, leading to the most accurate pipeline diameter results, which can then be implemented in an economic least-cost route planner by considering e.g. a variable pressure gradient depending on the length of the pipeline trajectory. The Darcy-Weisbach variant is proposed in case no accurate Manning coefficients are available. The comparison of the Manning and Darcy-Weisbach formulas has demonstrated the importance of the pipeline material roughness-related factors, which are not consistent in current literature. Furthermore, the comparison between the proposed formulas in this paper and the equations presented in papers/reports dealing with CO<sub>2</sub> transport has proved the need for the incorporation of the elevation difference in the calculations.

### 4.3.3 Compressor cost

A compressor unit can be needed at three types of locations:

at the capture site, to upgrade pressure to transport conditions;

on the transport trajectory, especially for trajectories that are longer than 200 km, but in fact it just depends on the pressure loss and inlet pressure (pressure needs to be kept higher than about 7.5 MPa);

at the storage site, pressure needs to be upgraded to reservoir pressure.

In order to calculate the compressor cost, the compressor size should be determined. This can be done using the following equation:

$$P = (E_{p2} - E_{p1}) \cdot q \quad (40)$$

with

$P$  = power needed (MJ/h)

$E_p$  = potential energy (kJ/kg)

$q$  = flow rate (ton/h)

The installed unit should then also consider the efficiency of the compressor.

The potential energy can be deduced from the thermophysical properties of CO<sub>2</sub> (Span and Wagner, 1996). Thereby, the outlet temperature should be calculated:

$$T_2 = T_1 \cdot (r_p)^{\frac{k-1}{k}} \quad (41)$$

with

$T$  = temperature (K)

$r_p = p_2/p_1$

$k = c_p/c_v$

In order to upgrade CO<sub>2</sub> pressure from, for example, 8 to 13 MPa at a temperature of 10°C, the power needed is 46600 MJ/h for a flow rate of 200 ton/h. Considering a compressor efficiency of 0.8, the installed compressor would have 21700 HP.

With respect to the actual compressor cost, a yearly cost of about 5.3 million euro can be assumed, based on Wong (2005). This yearly cost consists of a capital charge cost of 2.9 million euro (based on a discount rate of 12% and discount time of 25 years), labour and maintenance cost of 0.15 million euro and energy cost of 2.3 million euro.

## 4.4 References

- Baumert, K.A., Herzog, T., Pershing, J., 2005. Navigating the Numbers: Greenhouse Gas Data and International Climate Policy. World Resources Institute.
- Blok, K., Williams, R.H., Katofsky, R.E., Hendriks, C.A., 1997. Hydrogen production from natural gas, sequestration of recovered CO<sub>2</sub> in depleted gas wells and enhanced natural gas recovery. *Energy* 22, 161-168.
- BNCC, 2006. Belgium's Fourth National Communication on Climate Change. Under the United Nations Framework Convention on Climate Change. Belgian National Climate Commission, Federal Public Service Health, Food Chain Safety and Environment.
- Bock, B., Rhudy, R., Herzog, H., Klett, M., Davison, J., De La Torre Ugarte, D.G. et al., 2003. Economic evaluation of CO<sub>2</sub> storage and sink enhancement options. TVA Public Power Institute, DE-FC26-00NT40937.
- Bombardelli, F.A., García, M.H., 2003. Hydraulic design of large-diameter pipes. *Journal of Hydraulic Engineering* 129, 839-846.
- Brater, E.F., King, W.H., 1976. Handbook of hydraulics for the solution of hydraulic engineering problems. 6<sup>th</sup> ed., MacGraw-Hill, New York.
- Carey, S.K., Woo, M.K., 2000. The role of soil pipes as a slope runoff mechanism, Subarctic Yukon, Canada. *Journal of Hydrology* 233, 206-222.
- Corzine, J.S., Levin, S.B., Connolly, W.M., 2007. Residential Site Improvement standards. Subchapter 7 Stormwater Management. Website: <http://www.state.nj.us/dca/codes/nj-rsis>

- Dingman, S.L., Sharma, K.P., 1997. Statistical development and validation of discharge equations for natural channels. *Journal of Hydrology* 199, 13-35.
- Feron, P.H.M., Hendriks, C.A., 2005. CO<sub>2</sub> capture process principles and costs. *Oil & Gas Science and Technology – Rev. IFP* 60, 451-459.
- Freund, P., Davison, J., 2002. General overview of costs. IPCC Workshop on carbon dioxide capture and storage.
- Friedman, S.J., Dooley, J.J., Held, H., Edenhofer, O., 2006. The low cost of geological assessment for underground CO<sub>2</sub> storage: Policy and economic implications. *Energy Convers. Mgmt* 47, 1894-1901.
- Gale, J., Davison, J., 2004. Transmission of CO<sub>2</sub> – safety and economic considerations. *Energy* 29, 1319-1328.
- Golomb, D., 1997. Transport systems for ocean disposal of CO<sub>2</sub> and their environmental effects. *Energy Convers. Mgmt* 38, S279-286.
- Haestad Methods, 2002. *Computer applications in Hydraulic Engineering*. 5<sup>th</sup> ed., Waterbury CT.
- Hamelinck, CN., Faaij, A.P.C., Ruijg, G.J., Jansen, D., Pagnier, H., van Bergen, F. et al., 2001. Potential for CO<sub>2</sub> sequestration and enhanced coalbed methane production in the Netherlands. NOVEM Programma, Utrecht.
- Heddle, G., Herzog, H., Klett, M., 2003. The economics of CO<sub>2</sub> storage. Laboratory for energy and the environment, No. LFEE 2003-003 RP, Cambridge, Massachusetts.
- Hendriks, C.A., Farla, J.C.M., Blok, K., 1992. Verwijdering en opslag van CO<sub>2</sub> bij elektriciteitsopwekking (Recovery and storage CO<sub>2</sub> with power plants). Department of Science, Technology and Society, Utrecht University.
- IEA GHG, 2002. Pipeline transmission of CO<sub>2</sub> and energy. Report Number PH 4/6, International Energy Agency Greenhouse Gas R&D Programme.
- IEA GHG, 2005. Building the cost curves for CO<sub>2</sub> storage: European sector. Report Number 2005/2. International Energy Agency Greenhouse Gas R&D Programme.
- IEA, 2004. Carbon dioxide capture and storage issues – accounting and baselines under the United Nations Framework Convention on Climate Change (UNFCCC). International Energy Agency Information paper.
- IPCC, 2005. IPCC Special Report on Carbon dioxide capture and storage. Prepared by working group III of the Intergovernmental Panel on Climate Change (Metz B, Davidson O, de Coninck HC, Loos M, Meyer LA). Cambridge University Press, Cambridge, United Kingdom and New York, USA.
- Kinder Morgan CO<sub>2</sub> pipeline website: <http://www.kindermorgan.com/business/co2/>
- Kreith, F., Bohn, M., 2000. Principles of heat transfer. 6th ed., Thomson Learning.
- Kruse, H., Tekiela, M., 1996. Calculating the consequences of a CO<sub>2</sub>-pipeline rupture. *Energy Convers. Mgmt* 37, 1013-1018.
- Liou, C.P., 1998. Limitations and proper use of the Hazen-Williams equation. *Journal of Hydraulic Engineering* 124, 951-954.
- Odenberger, M., Svensson, R., 2003. Transportation systems for CO<sub>2</sub> – Application to carbon sequestration. Technical Report No. T2003-273, Department of Energy Conversion, Chalmers University of technology, Göteborg, Sweden.
- Oryshchyn D., Ochs T., Gerdemann S., Summers C., Patrick B., 2006. Developments in integrated pollutant removal for low-emission oxy-fuel combustion.
- Perry, R.H., Green, D.W., 1997. Perry's chemical engineers' handbook. 7th ed..
- Perry, R.H., Green, D.W., Maloney, J.O., 1987. Perry's chemical engineers' handbook. 6th ed., McGraw-Hill Book Co, Singapore.
- Peters, M.S., Timmerhaus, K.D., West, R.E., 2003. Plant design and economics for chemical engineers. 5th ed., McGraw-Hill Inc, New York.
- Piessens, K., Duser, M., 2004. Feasibility of CO<sub>2</sub> sequestration in abandoned coal mines in Belgium. *Geologica Belgica* 7, 165-180.
- Shafeen, A., Croiset, E., Douglas, P.L., Chatzis, I., 2004. CO<sub>2</sub> sequestration in Ontario, Canada, Part II: cost estimation. *Energy Convers. Mgmt* 45, 3207-3217.
- Simicevic, J., Sterling, R.L., 2003. Test data on the Rib Loc Machine Spiral Wound Lining System and Materials. TTC Evaluation Report, Report No. TTC-2003.02. Trenchless Technology Center, Louisiana Tech. University.
- Skovholt, O., 1993. CO<sub>2</sub> transportation system. *Energy Convers. Mgmt* 34, 1095-1103.

- Span, R., Wagner, W., 1996. A new equation of state for carbon dioxide covering the fluid region from the triple-point temperature to 1100 K at pressures up to 800 MPa. *J Phys Chem Ref Data* 25, 1509-1596
- Svensson, R., Odenberger, M., Johnsson, F., Strömberg, L., 2004. Transportation systems for CO<sub>2</sub> - application to carbon capture and storage. *Energy Convers. Mgmt* 45, 2343-2353.
- Wong, S., 2005. Module 4: CO<sub>2</sub> compression and transportation to storage reservoir, in: Harwood, J. (Ed.), *Building capacity for CO<sub>2</sub> capture and storage project in the APEC regions: a training manual for policy makers and practitioners*. APEC Reference #205-RE-01.3.
- Zhang, Z.X., Wang, G.X., Massarotto, P., Rudolph, V., 2006. Optimization of pipeline transport for CO<sub>2</sub> sequestration. *Energy Convers. Mgmt* 47,702-715.

## 5 Health, safety and environmental risks of underground CO<sub>2</sub>-sequestration

### 5.1 Introduction

The idea of storing CO<sub>2</sub> in geologic formations immediately raises questions about storage permanence, the environmental risks involved and necessary monitoring. Certain potential storage sites may not leak at all, while others may do so at an unforeseen rate. At the moment, insufficient information is available to quantify leakage from CO<sub>2</sub> storage sites. It is possible, however, to quantify upper limits for leakage and to draw conclusions from these theoretical limits and the experimental information available so far.

A strict requirement for a zero leakage rate would impose excessively stringent conditions on storage selection procedures and result in a waste of a valuable resource, i.e., potential CO<sub>2</sub> storage sites. Certain leakage rates can be accepted and permitted. It has to be emphasized, however, that selection procedures should effectively eliminate sites with a risk of sudden releases of bulk CO<sub>2</sub> due to geological imperfections and tectonic moves.

There are two types of risk associated with leakages of CO<sub>2</sub>: local, site specific, affecting health, safety and environment, and global, resulting from a return of stored CO<sub>2</sub> to the atmosphere. The majority of constraints imposed on storage permanence and also quality of monitoring will probably result from the first type.

At a *global scale*, CO<sub>2</sub>-storage could be a major contributor to reducing atmospheric levels of CO<sub>2</sub>. The major risk is that leakage of CO<sub>2</sub> injected into geological formations will limit the effectiveness of the initiative in reducing the global atmospheric CO<sub>2</sub> concentration. This global risk can be alternatively viewed as uncertainty in the effectiveness of CO<sub>2</sub> containment and of CO<sub>2</sub> storage as a climate change solution. The global risk of leakage is dependent only on the average quantity of CO<sub>2</sub> released from the storage site over time. Moreover, because of the energy penalty, the additional energy required to capture and store CO<sub>2</sub>, more fuel will be needed per unit of delivered energy if CO<sub>2</sub> is captured. Everything else being equal, therefore, there will be a corresponding increase in the various environmental impacts and risks associated with fuel production.

Taking the global risk under consideration, the minimum storage permanence time depends on future emissions. The total quantity of fossil fuels in place (about 5.67 PtC remaining) puts an upper bound on required storage time. Oil reserves are probably most limited, followed by gas and coal. Coal reserves are very large and could last for hundreds of years. If CO<sub>2</sub> concentrations should not rise above 450 ppm this would imply a retention time of 7,000 years (Zweigel and Lindeberg, 2003). On the other side of the scale, non-fossil power generation may become dominant in the second half of the 21st century. If fossil fuels are eliminated by 2100, then CO<sub>2</sub> storage for 100 years would be sufficient, according to this author. However, if large quantities of CO<sub>2</sub> are stored during this century, such a short retention time (or such a high leakage rate) will be hardly compatible with stabilizing CO<sub>2</sub> concentrations at any level, as stabilization of CO<sub>2</sub> concentrations will require near-elimination of net CO<sub>2</sub> emissions. Any storage time shorter than 100 years is thus questionable in all scenarios. In geological terms, these are extremely short periods. Oil and gas have been buried for millions of years, indicating that such favorable storage conditions are not uncommon. A retention time between 100 and 2,000 years means the maximum acceptable leakage rate can be somewhere between 0.01% and 1% per year. However the more optimistic scenario is due to an assumption of heterogeneity among reservoirs. Other studies have found that leakage rates of up to 0.1% per year allow for an effective storage policy.

At the *local scale* potentially hazardous impacts may result essentially from three different mechanisms: leakage from the storage location, alteration of ground and drinking water chemistry and displacement of potentially hazardous fluids formerly occupying the pore space being used to store the CO<sub>2</sub> (see fig. 5-1).

- Leakage of CO<sub>2</sub> from the storage location through the subsurface into the atmosphere could occur through isolated, catastrophic events, such as an earthquake, or through sustained, slow venting of CO<sub>2</sub> due to improper storage site selection and preparation. Either of these forms of leakage would result in elevated CO<sub>2</sub> concentrations at the surface or in the shallow subsurface that could negatively impact human health and safety, as well as that of plants and animals living in the area.
- Alteration of groundwater chemistry resulting from CO<sub>2</sub> dissolving in it. Such a chemical change in groundwater that is used for drinking water could impact human health. Alterations in groundwater not used for human consumption may have impacts on the ecosystem it is in contact with.
- Displacement of fluids previously occupying the underground space where the CO<sub>2</sub> is injected. By injecting CO<sub>2</sub> gas underground, salty brine water could be forced out into drinking water reserves? The increased pressure of this type of displacement could cause fractures or other physical changes in the subsurface rocks.

The local risks of leakage are dependent on the location and timing of the leak. Continued and dispersed leakage will have very different impacts than episodic and isolated leakage events. For example, while slow but sustained leakage could gradually alter long-term soil ecosystems, a sudden distinct leakage event could cause instantaneous disruption. Both human health and safety impacts must be considered in evaluating the potentials risks associated with CO<sub>2</sub>-leaking from an underground storage site. In addition to the possibility of catastrophic leaks such as well blowouts or pipeline ruptures, where large amounts of CO<sub>2</sub> are suddenly released, slow and less-obvious leaks also need to be considered.

## 5.2 Natural analogues

Although there is currently only minimal experience with engineered CO<sub>2</sub>-storage and no examples of leakage exists from existing projects to draw from, several *naturally occurring CO<sub>2</sub> underground storage sites (natural analogues)* that have released CO<sub>2</sub>, provide valuable insights into the types of hazards that could be anticipated at engineered sites. The primary natural analogs that have been studied are on several locations in Italy, the flanks of Mammoth Mountain, California, and at Lake Nyos in Cameroon.

These case studies provide indeed a useful basis for understanding both the ecosystem and human health hazards, associated with CO<sub>2</sub> leakage. However, it must be stressed that natural analogs are very different from the deep stable subsurface sedimentary storage basins that are preferred locations for engineered CO<sub>2</sub> storage. Natural analogs that are located in highly fractured and volcanic zones are generally not suited to understand the likelihood of leakage from a CO<sub>2</sub> storage site.

Additionally, extra information relevant to both the potential hazards and the likelihood of occurrence can be gained from industrial experience in underground injection: this industrial experience includes the underground injection of CO<sub>2</sub> to enhance oil recovery (EOR), store natural gas (UGS), and dispose of hazardous and non-hazardous waste.

Natural CO<sub>2</sub>-occurrences are common across Europe and their distribution is principally controlled by the Cenozoic rift system and associated Tertiary volcanisms. These occurrences can be classified into:

- CO<sub>2</sub>-rich waters both at depth and in springs. These are often exploited for mineral waters and occur in a variety of geological settings, with the sources of CO<sub>2</sub> including mantle degassing, volcanic activity and thermal metamorphism of limestones.

- Dry CO<sub>2</sub> gas vents (“moffettes”): these are associated with Cenozoic rifts such as the Eger and the Tyrrhenian rift systems. They are associated with hydrothermal fields and Quaternary to recent volcanic activity such as the Eifel volcanic complex within the Rhenish Massif, the Larderello geothermal field in Italy and currently active volcanism.
- CO<sub>2</sub> gas accumulations: these occur in Cenozoic extensional basins such as within the sub-basins of the back-arc Pannonian Basin and the Florina-Ptolemais-Aminteo graben system. Additionally, Mesozoic and Palaeozoic basins subject to Cenozoic tectonism such as the Triassic to Jurassic Southeast Basin of France (e.g. Montmiral) and sub-basins within the Southern Permian Basin in Saxo-Thuringia (Germany) can also host CO<sub>2</sub>-accumulations.
- The natural CO<sub>2</sub>-accumulations in the Pannonian basin and the small gas pools in the Southeast basin of France may be considered as the closest analogues to a storage site in Western Europe (Pearce, 2006), since CO<sub>2</sub> has been trapped here for geological timescales. Many other known CO<sub>2</sub>-accumulations are associated with volcanic regions and as such are not directly analogous to a storage site. However, they do provide opportunities to study near-surface leakage processes and the potential impacts on ecosystems on a scale not easily replicated experimentally.

### 5.3 Experimental work and modelling

Understanding the long-term effects of CO<sub>2</sub> on a reservoir is important for several reasons. In certain circumstances CO<sub>2</sub> may dissolve in the reservoir pore water and react with minerals within the reservoir, ultimately leading to long-term trapping through precipitation of carbonate minerals. Our ability to model the geochemical and geo-mechanical processes that occur in the reservoir, that could ultimately influence its long-term storage performance, can be tested by modeling natural analogues of geological storage.

The mixing of CO<sub>2</sub> and water in the pore system of the reservoir rock will create dissolved CO<sub>2</sub>, carbonic acid and bicarbonate ions. The acidification of the pore waters reduces the amount of CO<sub>2</sub> that can be dissolved. As a consequence, rocks that buffer the pore water pH to higher values facilitate the storage of CO<sub>2</sub> as a dissolved phase. *The CO<sub>2</sub>-rich water may react with minerals in the reservoir rock or cap rock matrix or with the primary pore fluid. It may also react with borehole cements and steels.* Such reactions may cause either mineral dissolution and potential breakdown of the rock or cement matrix or mineral precipitation and plugging the pore system (decreasing permeability).

A carbonate-rich formation effectively traps stored CO<sub>2</sub> as an immobile solid phase. If the mineralogical composition of the rock matrix is dominated by quartz, geochemical reactions will be dominated by simple dissolution in the brine and CO<sub>2</sub>-water-rock reactions can be neglected. However, for more complex mineralogies, sophisticated simulations, based on laboratory experimental data that use reservoir and cap rock samples and native pore fluids, will be necessary to fully assess the potential effects of such reactions in more complex systems.

As an example, an experimental setup was built at the VITO (Bertier et al, 2006) in order to evaluate the effect of CO<sub>2</sub>-water-rock interactions on sandstone aquifers in NE-Belgium: 18 experiments were performed in which sandstones were exposed to supercritical CO<sub>2</sub>. The CO<sub>2</sub>-water-rock interactions were deduced from the evolution of aqueous concentrations of 25 species and a thorough characterization of the sandstones before and after treatment. The results showed that dissolution of ankerite/dolomite and Al-silicates could indeed enhance porosity/permeability. The observed precipitation of end-member carbonates could also increase storage capacity if it exceeds carbonate dissolution. Precipitation of carbonates and of K-rich clays however can hamper the injection of CO<sub>2</sub> in the reservoir.

The shallow subsurface may be the last barrier before CO<sub>2</sub> escapes to the atmosphere. A detailed *understanding of gas migration* in this environment is therefore important to assess risks to human health and the environment.

Detailed soil gas and gas flux surveys, conducted in and around gas vents in several locations in central Italy during the EC-funded NASCENT-project, demonstrated how gas leaks occur over very small areas, on the order of a couple of meters, but that elevated CO<sub>2</sub> concentrations occur as a large halo around the actual vent, due to lateral migration in the unsaturated zone (Lombardi et al., 2006). Both soil and gas flux values indicated that a clayey cover of a non-leaking site (e.g. Sesta) prevents gas migration towards the surface. Results from gas injection tests also showed the importance of understanding the chemical and physical characteristics of the gases being monitored, as aqueous solubility, gas density and both water- and gas-phase diffusivities play an critical role in the travel times and mass attenuation features of migrating gases.

The experiences gained through this work on natural analogues in Italy has already been shown to be practical, economical and highly useful during their application to real-life CO<sub>2</sub> geological sequestration sites such as those in Algeria (In Salah EGR-project) and Canada (Weyburn EOR-project).

#### **5.4 Human health and environmental hazards**

The potential human health and safety hazards from land-based CO<sub>2</sub>-storage include (Stephens & Keith, 2005) (see also fig.5-1)

##### *a) Elevated CO<sub>2</sub> concentrations in confined areas*

The most serious human health and safety hazard associated with leaking CO<sub>2</sub> from an underground storage site is injury or death caused by elevated CO<sub>2</sub> concentrations in confined areas. Although CO<sub>2</sub> gas generally disperses quickly in the open atmosphere, CO<sub>2</sub> is denser than air so it will accumulate in confined environments including basements, tents, under snow-packs and in depressions or pits in the ground. Humans will suffer from unconsciousness and even death at CO<sub>2</sub>-concentrations above 10%. CO<sub>2</sub> causes also significant respiratory and physiological effects in humans at concentrations over 2% (see further).

Lake Nyos is the most famous example of how catastrophic events can be caused by slow leaks when the CO<sub>2</sub> is temporarily confined in the near-surface environment and then suddenly is released. Lake Nyos waters had been gradually saturated with CO<sub>2</sub> from volcanic vents over a period of time. They suddenly released a huge amount of CO<sub>2</sub> during the night, blanketing a nearby town and killing 1700 people. While the specific mechanism of the Lake Nyos event can only occur in tropical lakes, it is conceivable that leaking CO<sub>2</sub> could infiltrate caverns at shallow depths and then suddenly being vented to the atmosphere. Several deaths, including a skier at Mammoth Mountain (California) and a few individuals at a CO<sub>2</sub> degassing field in Italy, have been attributed to natural releases of CO<sub>2</sub>.

##### *b) Contamination of drinking waters*

The direct effects of dissolved CO<sub>2</sub> in drinking water are probably minor because drinking water is often carbonated with CO<sub>2</sub> without any adverse health effect. Dissolving CO<sub>2</sub> in water, however, will increase the acidity of the water causing indirect effects including increased mobilization of toxic metals, sulfates or chlorides, and changes in the odor, color or taste of the water. Groundwater used for drinking water could also be contaminated by saline brine waters that are displaced by CO<sub>2</sub> injection: this process could potentially render the water too salty to drink. The infiltration of saline water into groundwater or the shallow subsurface also could pollute surface water and restrict or eliminate the use of some land for agricultural use.

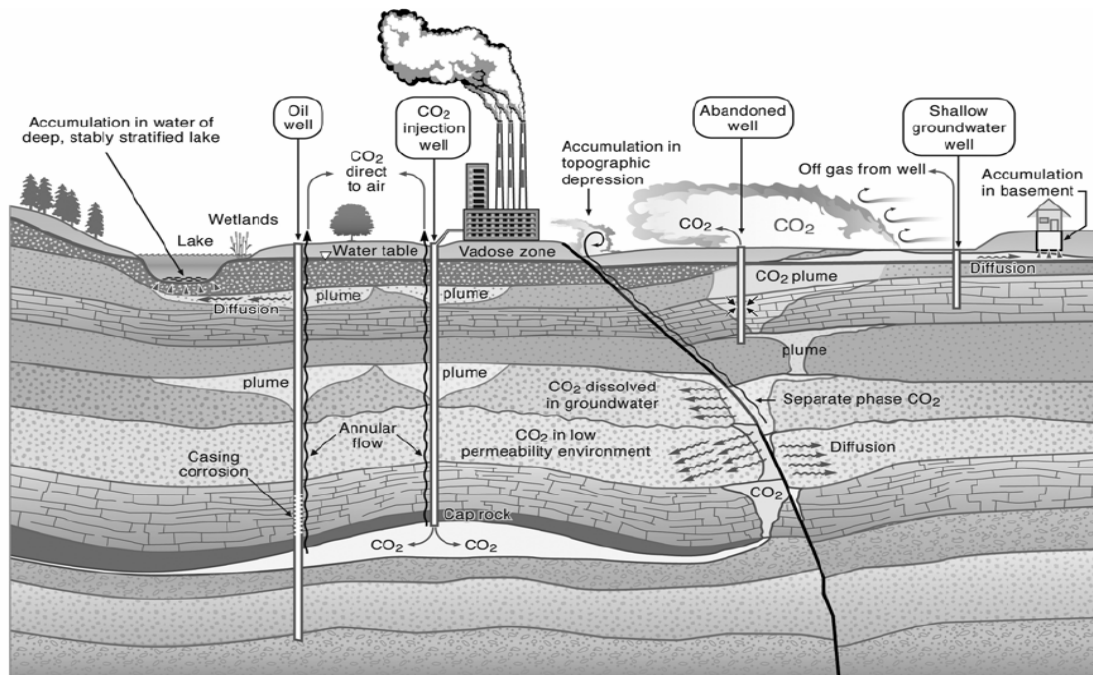


Figure 5-1: Schematic diagram showing possible pathways by which CO<sub>2</sub> might leak to the surface (Sally Benson, in Stephens & Keith, 2005)

Mammoth Mountain, California, illustrates a natural example of how steady CO<sub>2</sub> venting can impact the natural ecosystem, including the groundwater table. A fluctuating but constant flux of CO<sub>2</sub> has been flowing from the underground into the atmosphere for about 15 years. In addition to killing trees in several distinct areas and forcing the closing of a camp site to protect human health, the CO<sub>2</sub> venting has altered the soil and water chemistry in the whole region.

#### c) Local heave and seismicity

Induced seismic activity usually occurs along previously faulted rocks and may be investigated by analyzing the stress conditions at depth. Seismic events are very unlikely to occur due to injection in porous rocks unless very high injection pressures cause hydraulic fracturing. Supercritical CO<sub>2</sub> liquid is less dense than water and may cause density-driven stress conditions at depth or interact with formation water and rocks, causing a reduction in permeability and pressure buildup leading to seismic activity (Sminchak & Gupta, 2003).

Underground injection of CO<sub>2</sub> into porous rocks under pressure can induce fracturing and movement of faults, causing potentially damaging earthquakes and eventually resulting in the creation of additional pathways for CO<sub>2</sub> leakage. Several examples of induced seismicity resulting from the industrial practice of underground injection exist, including the 1967 Denver earthquake and the 1986 and 1987 Ohio earthquakes that are believed to have been induced from deep well injection of waste fluids. Experience with underground gas storage (UGS) has indicated that the risks of seismicity is minimal, which is expected to be true for CO<sub>2</sub>-sequestration as well.

## Potential leakage routes and remediation techniques for CO<sub>2</sub> injected into saline formations

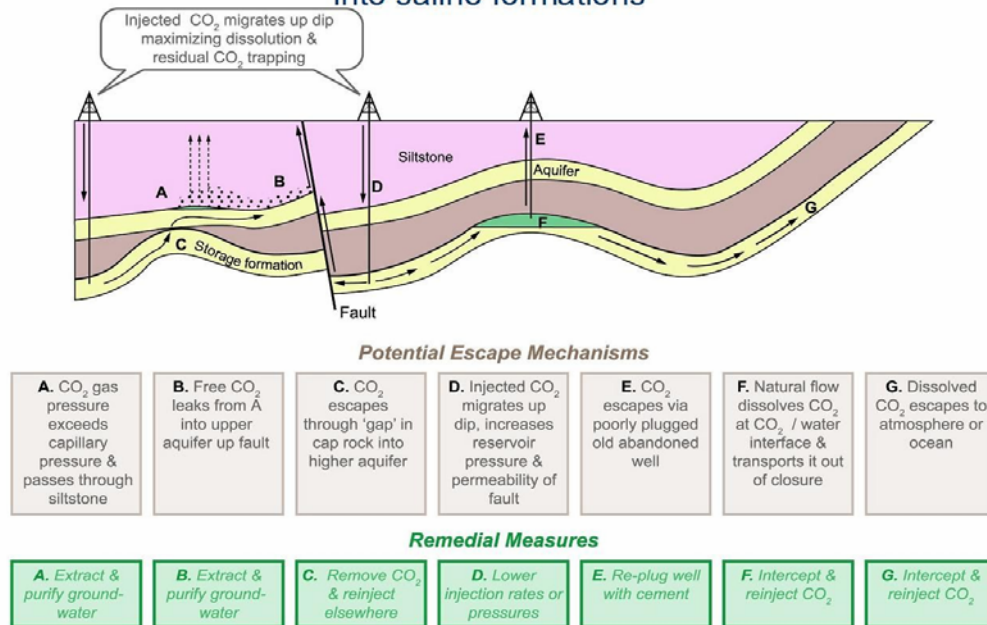


Figure 5-2: Potential leakage routes and remediation techniques for CO<sub>2</sub> injected into saline formations. The remediation Technique would depend on the potential leakage routes identified in a reservoir (CO<sub>2</sub>CRC, in IPCC-report, 2005)

The mechanisms of ground movement are understood, but prediction is difficult. Brine displacement when injecting CO<sub>2</sub> in an aquifer depends very much on local/regional conditions. Although there are still uncertainties with regard to the latter risks, the main research topic in risks associated with underground CO<sub>2</sub>-sequestration is *leakage*.

### 5.5 Main mechanisms of CO<sub>2</sub> leakage

The generally accepted scenario for injected CO<sub>2</sub> is that it is likely to rise within the storage formation roughly vertically from the injection well's perforation depth to the contact between the storage reservoir and the overlying seal or cap rock. It will then migrate updip below the top seal towards the formation's subcrop or outcrop. Key parameters influencing the migration velocity are the presence of local traps and their volume, the density difference between CO<sub>2</sub> and brine (largely a function of pressure and temperature), reservoir rock permeability, vertical and horizontal reservoir heterogeneity and the relative permeability of the reservoir to CO<sub>2</sub>. Some CO<sub>2</sub> will be dissolved into formation water in the reservoir unit, but this process is slow, operating over a time scale of 1000's of years.

When CO<sub>2</sub> is injected in geological reservoirs it might potentially migrate out of the reservoirs through the subsurface and finally to the biosphere/atmosphere (fig. 5-2). The potential for leakage will depend on well and cap rock (seal) integrity and the trapping mechanism. The latter is often a combination of physical and geochemical mechanisms: physical trapping includes stratigraphic trapping, structural trapping and hydrodynamic (residual) trapping.

CO<sub>2</sub> injected in deep saline aquifers is trapped and stored by several mechanisms (fig. 5-3): 1) in its free phase as a plume at the top of the aquifer and in stratigraphic and structural traps (similar to oil and gas accumulations); 2) as bubbles that are trapped in the pore space after passing of a plume; 3) dissolved in aquifer water; and 4) as a precipitated carbonate mineral

as a result of geochemical reactions between the CO<sub>2</sub> and aquifer water and rocks. Numerical studies have shown that, during the period of injection, up to 29% of the CO<sub>2</sub> would dissolve in the brine (Bachu, 2000).

As well as being trapped as a buoyant supercritical CO<sub>2</sub> “bubble” (physical trapping), reaction with formation water can trap CO<sub>2</sub> as a dissolved phase (solubility trapping). Furthermore, reaction of this dissolved CO<sub>2</sub> with minerals in the host formation can result in pH buffering, enhancing solubility trapping due to the formation of dissolved bicarbonate ions and complexes (ion trapping). Reaction of dissolved CO<sub>2</sub> with certain non-carbonate Ca-Fe-Mg-rich minerals can even trap the CO<sub>2</sub> as solid carbonate precipitate (mineral trapping), essentially immobilizing the CO<sub>2</sub> for geological time periods (Bacchu et al, 1994).

As CO<sub>2</sub> has a lower density than the brine, the remainder would float on top of the brine and accumulate below the cap rock. During later periods, part of this CO<sub>2</sub> may dissolve in the brine or react with the aquifer rock matrix. Dissolution would continue after injection has ceased so that, over a period of a thousand years or more, the entire plume of CO<sub>2</sub> would probably dissolve. Geochemical reaction to permanently sequester CO<sub>2</sub> would take several thousand years to have a significant effect. Where there is no stratigraphical or structural trap, the CO<sub>2</sub> would flow and spread over a large area below the aquifer cap rock. Modeling studies suggest a spread of tens or hundreds of square kilometers, depending on aquifer properties such as thickness, porosity and permeability. This also depends, however, on the topography of the cap rock and the volume injected.

Generally, modeling studies have shown that, depending on aquifer characteristics and injection rate, a plume of CO<sub>2</sub> may spread between five and twelve kilometers from the injection well over a period of 1,000 years. Other studies suggest the plume would dissolve entirely. Such a large area would complicate the monitoring and verification of leakage, but the area needed would vary by case. The lower the initial CO<sub>2</sub> saturation of the brine, the smaller the area needed, as more CO<sub>2</sub> would dissolve in the brine (IEA & OECD, 2004)

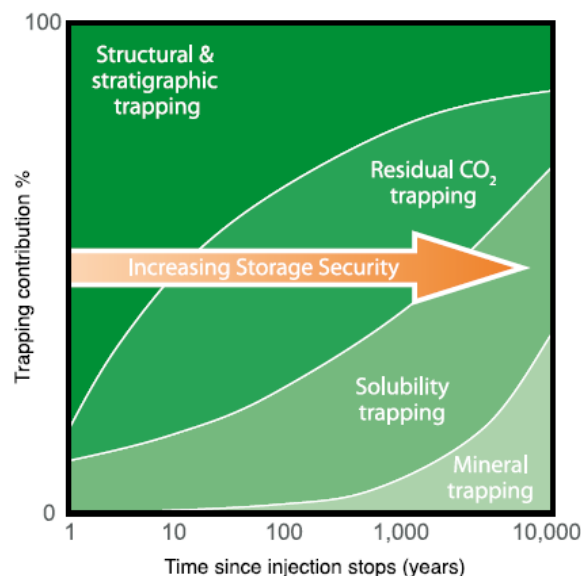


Figure 5-3: Storage security depends on a combination of physical and geochemical trapping. Over time the physical process of residual CO<sub>2</sub> trapping and geochemical processes of solubility trapping and mineral trapping increase, increasing the overall security of the storage site (IPCC, 2005)

With regard to global risks, based on observations and analysis of current CO<sub>2</sub> storage sites, natural systems, engineering system and models, the fraction retained in appropriately selected and managed reservoirs is very likely to exceed 99% over 100 years and is likely to exceed 99% over 1000 years.

CO<sub>2</sub> can migrate by several mechanisms from the reservoir through the subsurface and finally to the atmosphere/biosphere. These mechanisms are discussed for depleted oil and gas fields and saline aquifers only (based on the overview of Damen et al, 2006). Risks of CO<sub>2</sub> leakage from unminable coal seams will not be discussed in this overview. Leakage from abandoned oil and gas reservoirs or from deep saline aquifers basically occurs via the same pathways, although some differences exist (see further)

### 5.5.1 Depleted oil and gas fields

Hydrocarbon reservoirs are generally considered to be safe sinks for CO<sub>2</sub> sequestration, since they have held oil & gas for millions of years, without large spontaneous releases. However, there is a risk that CO<sub>2</sub> escapes from the reservoir *through or along wells* or by means of a *cap rock failure*. Moreover, CO<sub>2</sub> might also *escape via spill points* or dissolve in fluid flow in the reservoir rock beneath the CO<sub>2</sub>-accumulation to surrounding formations.

CO<sub>2</sub>-leakage *through or along wells* after the injection phase can be caused by (fig. 5-4):

- casing or cementation defects due to improper design or construction,
- corrosion of the casing and deterioration of cement plugs by CO<sub>2</sub> and/or brine

Abandoned wells can be an important migration pathway since depleted oil/gas reservoirs are generally “punctured” by a large number of non-operative exploration and production wells, some of them in bad condition. Especially unidentified and poorly (improperly plugged) abandoned wells are potential point sources.

Diffusion of CO<sub>2</sub> through the cement or steel casing caused by corrosion is a slow process (fig. 5-5), in the order of 20 cm in 100 years. However it is uncertain how the well bore integrity and especially the cement is affected by CO<sub>2</sub> and brine considering a sequestration timescale of hundreds to ten thousands of years.

As a first step to *assess well bore integrity*, a laboratory study of well bore materials from Sleipner was undertaken, using techniques based upon those used in previous CO<sub>2</sub>-storage projects and during the SACS-project (Chadwick et al, 2007). The experiments used realistic borehole materials (samples of casing steel and cement provided by Statoil) and synthetic formation waters based upon measured compositions of nearby fluid samples. The experimental conditions were representative of the in situ conditions within the lowest part of the Sleipner cap rock (30°C, 8MP). Experiments were pressurized with either N<sub>2</sub> or CO<sub>2</sub>.

- Borehole liner experiments involved small billets of steel and ran for 2 months. All experiments showed some evidence of relatively minor surface oxidation. However, experiments pressurized with CO<sub>2</sub> produced significant dissolution of steel in the immediate contact with the water phase: deep etching along inter-granular boundaries of the steel. Siderite was also observed as a later stage carbonation reaction product.
- Borehole cement experiments used small discs of cement and ran for 2 months. They produced significant carbonation reactions on and within the cement samples. These involved the breakdown of portlandite and CSH-phases, being replaced by silica gel and calcium carbonates: calcite precipitated on the surface of the cement whereas vaterite and calcite precipitated within the cement matrix. Significantly enhanced porosity was found in the outermost parts of the cement, suggesting overall leaching. An unexpected observation was the formation of aluminum oxide chloride hydrate: it would appear that this phase was the main sink for Al in the experiments. It appears to have formed in preference of dawsonite.

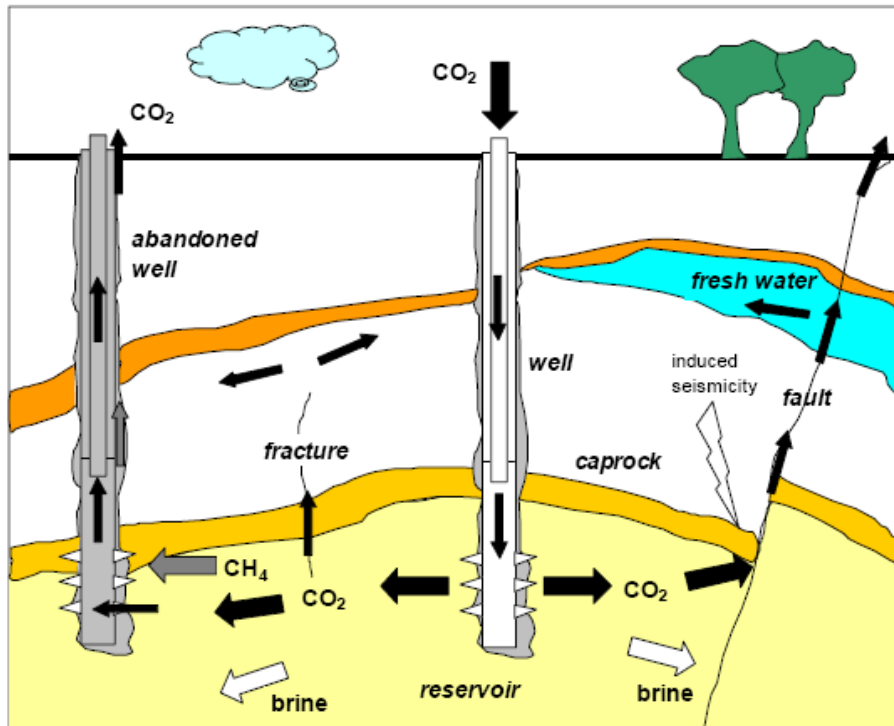


Figure 5-4: Risks of underground CO<sub>2</sub>-sequestration. Black and grey arrows represent CO<sub>2</sub> and CH<sub>4</sub> flows (along abandoned wells, fractures and faults). White arrows represent brine displacement as a consequence of CO<sub>2</sub>-injection (Damen et al., 2006)

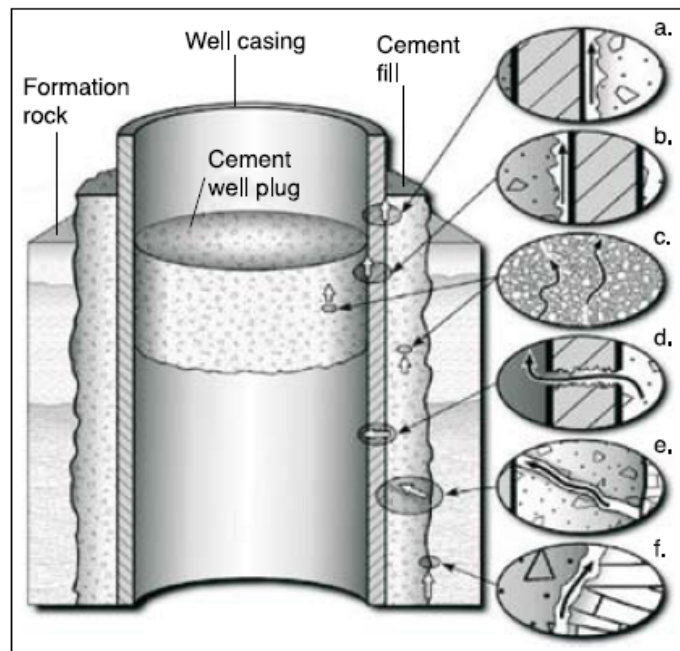


Figure 5-5: Possible leakage pathways in an abandoned well: (a) and (b) between casing and cement wall and plug, respectively; (c) through cement plugs; (d) through casing; (e) through cement wall; and (f) between the cement wall and rock (IPCC, 2005)

A *cap rock failure* is a generic term for various mechanisms:

- *Capillary leakage* occurs when the pressure difference of fluid phase and the water phase in the pores adjacent to the cap rock is higher than the capillary entry pressure of the cap rock. Since the capillary entry pressure of a cap rock has generally been sufficient to retain hydrocarbons and the capillary entry pressure can be measured by means of core testing, capillary leakage of CO<sub>2</sub> is not considered to be a problem.
- *Diffusion of CO<sub>2</sub>* (caused by a difference in CO<sub>2</sub> concentration) through the cap rock is expected to be a very slow process, but can be the controlling mechanism for leakage on the long-term.
- CO<sub>2</sub> might leak through man-made fractures, known as *hydraulic fracturing*, created by *over-pressuring the reservoir*. In order to avoid fracturing, the maximum injection pressure should always be kept below the level at which the cap rock may shear (fracture pressure). The risk of leakage is low as long as the storage pressure does not exceed the initial reservoir pressure. However, there is a certain level of overpressure, at which CO<sub>2</sub> can safely be contained. This safety factor depends on the stress state of the cap rock, which depends in turn on depth, pore pressure, rock properties and sedimentary and tectonic history.
- High-permeability zones might be formed due to chemical reaction of CO<sub>2</sub> with the cap rock, causing the cap rock to dissolve.
- CO<sub>2</sub> might leak through open or non-sealing faults and fractures, which extend into the cap rock. The risk for leakage can be strongly reduced by performing a detailed analysis of the geological-structural setting of the reservoir prior to injection.
- Seismic disturbances might cause cap rock failure.

Of all the above mechanisms, leakage along or through wells, faults and fractures are generally considered as the most important leakage pathways.

### 5.5.2 Deep saline aquifers

Leakage from deep saline aquifers occurs via the same mechanisms as those for depleted oil and gas fields. A major difference with hydrocarbon reservoirs is that aquifers generally do not have cap rocks or seals that have stood the test of time. Furthermore, since deep saline aquifers are not of economical interest such as hydrocarbon reservoirs, the number of wells in aquifers, and consequently the potential for CO<sub>2</sub>-leakage through/along wells is relatively low. However, exploration and production wells have been drilled through some deep saline aquifers and this might have created potential leakage pathways.

Another difference is the fact that CO<sub>2</sub> storage in an aquifer will induce a temporary pressure increase in the reservoir because the space to store CO<sub>2</sub> only becomes available as a result of compression of fluids and rocks in the reservoir, or the displacement of formation water into adjacent formations or to the surface (Holloway, 1996)

Deep saline aquifers have not been investigated as thoroughly as hydrocarbon reservoirs. The Sleipner project is the first commercial CO<sub>2</sub> injection in a deep saline aquifer (the Utsira Formation) where an extensive research program is running to study and monitor CO<sub>2</sub> behavior in the aquifer. Reactive transport models simulations indicate that after 120 years, mineral precipitation caused by CO<sub>2</sub> will have decreased the porosity and permeability of the cap rock base from 5% to 2,3% and from 3 to 0.3 mDarcy respectively (Johnson & Nitao, 2003). These results suggest that the sealing properties of the cap rock are enhanced by CO<sub>2</sub> sequestration (at least for the Sleipner cap).

Leakage from a typical deep saline aquifer has been modeled to estimate leakage rates from the wellhead and cap rock failure, which is used as input for risk assessment. Results indicate that *leakage through a failed cap rock poses the highest risk to all environmental media* (Saripalli et al., 2003).

The calculated flux from a continuous fracture aperture of 2000  $\mu$  corresponds to a leakage rate of 0.1% of the total volume stored per year. Leakage rates through permeable zones in the cap rock are estimated at 0.05% of the total volume stored per year. Spatial frequency of cap rock failures within the area of review was estimated at 0.01 for both a fractured cap rock and high-permeability zone, assuming that 1% of the cap rock area spread over an area of review of 50 km radius is fractured and another 1% is highly permeable.

The caprock(s) form(s) a barrier that will prevent CO<sub>2</sub> from migrating out of the reservoir rock. Therefore, understanding the *sealing capacity of the low permeability rocks for CO<sub>2</sub>* specifically will be necessary for site characterization and estimating storage capacity. Capillary breakthrough measurements with CO<sub>2</sub> have been performed on initially water-saturated cap rock samples from natural CO<sub>2</sub> sites (Hildenbrand et al, 2004). For a given cap rock permeability, the pressure at which CO<sub>2</sub> enters the cap rock is lower for CO<sub>2</sub> than for nitrogen or methane. Considering the strong variability of permeability and capillary breakthrough values in natural cap rocks, this effect is not expected to result in a substantially increased risk of capillary leakage when storing CO<sub>2</sub> in depleted methane- or nitrogen-dominated natural gas reservoirs. Although diffusive loss of CO<sub>2</sub> through cap rocks is considered negligible, the rate of potential geochemical corrosion of the cap rock is determined by diffusion.

Laboratory experiments have provided some basic information on the diffusion coefficients of CO<sub>2</sub> in seal rocks and have shown evidence of chemical interactions of the CO<sub>2</sub> with the minerals (Hildenbrand et al, 2004). Volumetric sorption experiments conducted by Busch et al (2007) demonstrated that shaly sequences in cap rocks, in addition to their sealing properties, could also represent a significant sink for CO<sub>2</sub> stored in the subsurface by fixing and immobilizing it, hence reducing the risks of leakage to the surface. Storage capacities were found to vary significantly but can be as high as 0.14 mmol CO<sub>2</sub>/g sample. This is significantly higher than the solubility of CO<sub>2</sub> in the pre waters. The CO<sub>2</sub> storage potential is not only related to the organic carbon content: the experiments showed that the sorptive CO<sub>2</sub> storage potential of clay minerals (such as montmorillonite and kaolinite) is significantly high.

A better knowledge on *CO<sub>2</sub> reactivity with reservoir rocks and cap rocks* has been gained through studies of several CO<sub>2</sub> storage sites: Sleipner and Weyburn (“industrial sites) and Montmiral (a natural site) (Czernichowski-Lauriol et al, 2006).

Modeling of long timescale upward diffusion of Dissolved CO<sub>2</sub> through the thick clay cap rock at Sleipner (North Sea) shows that diffusion is rather very slow and that it is retarded further by geochemical reactions. The overall net result is that only the bottom meters of the cap rock adjacent to the reservoir is exposed to chemical reactions. As a consequence the overall of the cap rock seal is likely to be good. That said however, migration of CO<sub>2</sub> may still be possible through pre-existing or newly formed fractures, or via the well bore.

Laboratory experiments, modeling and field monitoring at Weyburne (Canada) show that the carbonate reservoir undergoes mainly dissolution reactions and no increase of porosity, especially close to the injection zone. However, mineral trapping could play a significant role in the long term. A full 3D dynamic modeling study still needs to be undertaken, where flow, transport and chemical processes are coupled in order to quantify the temporal and spatial changes in CO<sub>2</sub> solubility and mineral trapping, and consequent porosity changes.

Although CO<sub>2</sub> has accumulated over millions of years in the Montmiral sandstone reservoir (France), observed chemical reactivity is low. Detailed mineralogical and fluid characterization combined with numerical modeling show that the dissolution of feldspars is the main reaction and that the porosity has increased by less than 3%. Mineral trapping is very limited and is restricted to minor precipitation of dolomite. Dawsonite was neither observed nor modeled at Montmiral, although often referred to in the literature as an important trapping

mineral. The absence of dawsonite is also confirmed by the experiments conducted on various reservoir sandstone samples at VITO (Bertier et al, 2006).

CO<sub>2</sub> reactivity is highly site-specific and time dependent. Investigations need to be based on a very precise characterization of minerals and fluids from the host formation.

## 5.6 Risk assessment methodology

### 5.6.1 Risk assessment

Risk assessment aims to identify and quantify potential risks caused by the underground injection and storage of large quantities of CO<sub>2</sub>. Risk denotes here a combination or the product of the probability of an event happening and the consequences of the event. Risk assessment should be an integral part of risk-management, including site selection, site characterization, storage system design, monitoring and remediation.

Risks arising from the operation of surface facilities such as pipelines, compressors and wellheads, are routine practice in the oil and gas industry. Assessment of such risks can be made with considerable confidence because estimates of failure probabilities and the consequences of failure can be based directly on experience.

In contrast, analysis of the risks posed by geological storage of CO<sub>2</sub> is a rather new field and no well-established methodology for assessing such risks exists.

Risks assessment methods dealing with the long-term risks related to the subsurface transport and storage of hazardous and nuclear waste may provide a useful basis for assessing the risks of CO<sub>2</sub> storage. However, their applicability is limited because the focus has been on assessing the low-volume disposal of hazardous materials, whereas the geological storage of CO<sub>2</sub> is high-volume disposal of a material that involves comparatively mild hazards.

Several substantial efforts are under way to assess the risks posed by particular storage sites. These risk assessment activities cover a wide range of reservoirs, use diverse methods and consider a very wide class of risks. A representative selection of these risk assessment efforts is summarized in table 5-1, taken from the IPCC special report on CO<sub>2</sub> capture and storage (2005).

*Table 5-1: A representative selection of these risk assessment efforts.*

Project title	Description and status
Weyburn/ECOMatters	New model, CQUESTRA, developed to enable probabilistic risk assessment. A simple box model is used with explicit representation of transport between boxes caused by failure of wells.
Weyburn/Monitor Scientific	Scenario-based modelling that uses an industry standard reservoir simulation tool (Eclipse3000) based on a realistic model of known reservoir conditions. Initial treatment of wells involves assigning a uniform permeability.
NGCAS/ECL technology	Probabilistic risk assessment using fault tree and FEP (features, events and processes) database. Initial study focused on the Forties oil and gas field located offshore in the North Sea. Concluded that flow through caprock transport by advection in formation waters not important, work on assessing leakage due to well failures ongoing.
SAMARCADS (safety aspects of CO <sub>2</sub> storage)	Methods and tools for HSE risk assessment applied to two storage systems an onshore gas storage facility and an offshore formation.
RITE	Scenario-based analysis of leakage risks in a large offshore formation. Will assess scenarios involving rapid release through faults activated by seismic events.
Battelle	Probabilistic risk assessment of an onshore formation storage site that is intended to represent the Mountaineer site.
GEODISC	Completed a quantitative risk assessment for four sites in Australia: the Petrel Sub-basin; the Dongra depleted oil and gas field; the offshore Gippsland Basin; and, offshore Barrow Island. Also produced a risk assessment report that addressed the socio-political needs of stakeholders.
UK-DTI	Probabilistic risk assessment of failures in surface facilities that uses models and operational data. Assessment of risk of release from geological storage that uses an expert-based Delphi process.

### 5.6.2 FEP—methodology and scenarios

The development of a comprehensive catalogue of the risks and mechanisms that underlie them, provides an ideal foundation for systematic risk assessment. Many of the ongoing risks assessment efforts are now cooperating to identify, classify and screen all factors that may influence the safety storage facilities, by using the features, events and processes (FEP) methodology. In this context features includes a list of parameters, such as storage reservoir permeability, caprock thickness and number of injection wells. Events includes processes such as seismic events, well blow-outs and penetration of the storage site by new wells. Processes refers to the physical and chemical processes, such as the multiphase flow, chemical reactions and geo-mechanical stress changes that influence storage capacity and security.

Most risk assessment systems involve the use of scenarios that describe possible future states of the storage facility and vents that result in leakage of CO<sub>2</sub> or other risks. Each scenario may be considered as an assemblage of selected FEPs. Scenarios are the starting points for selecting and developing mathematical-physical models. Such performance assessment models may include representations of all relevant components including the stored CO<sub>2</sub>, the reservoir, the seal, the overburden, the soil and the atmosphere. Many of the fluid-transport models used for risk assessment are derived from well-established models used in the oil and gas or groundwater management industries.

Generally, the parameter values (e.g. permeability of a caprock) and the structure of the performance assessment models (e.g. the processes included or excluded) will both be uncertain. Risk analysis may or may not treat this uncertainty explicitly. When risks are assessed deterministically, fixed parameter values are chosen to represent the often unknown probability distributions. Often these parameter values are selected “conservatively”, that is they are selected so that risks are overestimated. Wherever possible it is recommended to treat uncertainty explicitly. In probabilistic risk assessments, explicit probability distributions are used for some or most parameters: Monte Carlo simulations are then used to produce probability distributions fore various risks.

A good example of the EFP methodology is the *CO<sub>2</sub> online FEP database*, developed by Quintessence. The latter bas can be used as a base for setting up a screening system and a guide in the risk assessment (<http://www.quintessence-online.com>)

This database contains details of Features, Events and Processes associated with the geological sequestration of carbon dioxide. The database is generic, in that it is not specific to any particular sequestration concept or location, but has the capability to cross-reference to project-specific databases for specific sites. The FEPs included in the database have been chosen for their relevance to the long-term safety and performance of the sequestration system after injection of carbon dioxide has ceased, and the injection boreholes have been sealed but some FEPs associated with the injection phase are included where these can affect long-term performance and the initial status of the sequestration system.

*For each FEP in the database a description is provided, together with a discussion of its relevance to long-term safety and performance of the system. Further information is provided in the form of relevant publications and websites. The database provides a central source of information on the geological sequestration of carbon dioxide, and can be used as part of systematic assessments of safety and performance.*

The database has a hierarchical structure with FEPs being grouped into categories and classes with an associated numbering system. Thus FEP 1.2.3 is the 3rd FEP in the second class of category 1. If required, FEPs can be further broken down into a fourth tier of sub-FEPs. There are eight categories of FEPs, as follows:

0. The *Assessment Basis* category of FEPs determines the 'boundary conditions' for any assessment, specifying what needs to be assessed and why. The Assessment Basis helps to

determine which FEPs need to be considered in the analysis and which can be 'screened out' as outside the scope of the assessment.

1. The *External Factors* category of FEPs describes natural or human factors that are outside the system domain. These FEPs are most important in determining scenarios for the future evolution of the system.
2. The *CO<sub>2</sub> Storage* category of FEPs specifies details of the pre- and post-closure sequestration concept under consideration.
3. The *CO<sub>2</sub> Properties, Interactions and Transport* category of FEPs is concerned with those Features, Events and Processes that are relevant to the fate of the sequestered fluid. Carbon dioxide's properties can vary greatly between conditions at depth and near-surface, and a wide range of physical and chemical reactions can be important.

In the latter category, important geological parameters affecting safety and performance of CO<sub>2</sub> storage are listed under “CO<sub>2</sub>-interactions”, including:

*a) Effects of pressurization of reservoir on cap rock*

A storage reservoir will experience enhanced pressure due to injection of CO<sub>2</sub>. This may exceed original ‘natural’ pressurization due to hydrocarbon emplacement, or clay mineral transformations during diagenesis.

‘Over-pressuring’ of the reservoir may involve leakage of CO<sub>2</sub> through the cap rock due to fracturing or enhanced interactions with CO<sub>2</sub>.

*b) Displacement of saline formation fluids*

Injection of CO<sub>2</sub> into a geologic formation may result in displacement of saline formation fluids into potable water supplies. Limitations on the pressure in a formation (for seal integrity) will mean that existing fluids are displaced/replaced. Displaced fluids are highly likely to be saline. Because the pressure wave created by injection travels much further than the physical CO<sub>2</sub> front, displacement of saline formation fluids can occur at locations outside the CO<sub>2</sub> storage area. Inter-connection of aquifer systems may enable saline fluids to enter potable water formations. Displaced saline formation fluids may contaminate near-surface aquifers with subsequent impacts, such as contamination of potable water supplies.

*c) Mechanical processes and conditions*

Features and processes related to the mechanical processes and conditions resulting from the injection of CO<sub>2</sub> that affect the rock, boreholes and other engineered features, and the overall mechanical evolution with time. This includes the effects of hydraulic, mechanical and thermal loads imposed on the rock by the injected CO<sub>2</sub>. Injection of CO<sub>2</sub> into a reservoir can cause (directly or indirectly) changes of the geomechanical properties of the reservoir rock. Direct changes can be due to change of reservoir pressure and temperature (PVT system). Indirect changes (of rock properties) might result from geochemical and mineralogical changes after storage of CO<sub>2</sub>. Mechanical changes of the reservoir resulting from CO<sub>2</sub> injection (such as generation of fractures, reactivation of fractures/faults, changes of bulk elastic properties and effective reservoir) could lead to subsidence/uplift (at surface), induced seismicity, changes in migration pathways, even burst/leakage of the seal. Examples of other relevant processes are: borehole lining collapse; rock volume changes, leading to cracking

*d) Induced seismicity*

Injection of CO<sub>2</sub> may cause and trigger seismic events and earthquake hazards through processes such as reducing friction at existing faults. This may occur both in seismically active areas and in areas characterized by a low background seismicity (reactivation of ancient fault planes, changes in the orientation, fluid-pockets occurrence). This FEP includes microseismicity. Seismicity can introduce sudden physical changes to the sequestration system and may expose any local population to earthquake hazards.

*e) Subsidence or uplift*

Injecting the CO<sub>2</sub> may cause acidification of formation water, leading to mineral dissolution and subsidence. This is of particular relevance to shallow storage sites.

Injection of large quantities of CO<sub>2</sub> into a confined aquifer may increase pore pressure and 'lift' the overlying rocks upwards. Deformation may affect geological processes and may result in impacts of concern at the surface.

*f) Thermal effects on the injection point*

Temperature of the injected fluid could result in geological modification of the region around the point of injection due to thermal gradients. These thermal effects could influence the mobility of the injected CO<sub>2</sub> and impurities

*g) Water chemistry*

Water phase geochemistry of sequestered CO<sub>2</sub>. This includes the solubility trapping of CO<sub>2</sub> in water (H<sub>2</sub>O) to form carbonic acid (H<sub>2</sub>CO<sub>3</sub>). Subsequent ionic trapping of carbonic acid with hydroxide ions (OH<sup>-</sup>) forms bicarbonate ions (HCO<sub>3</sub><sup>-</sup>), which can react in turn with further hydroxide ions to form carbonate (CO<sub>3</sub><sup>2-</sup>).

Modification of the water phase geochemistry can disturb the equilibria between the water and solid phase of the reservoir and result in further geochemical (for example, solid phase geochemistry) and physical changes with resulting implications for the long-term performance of the sequestration system.

*h) Heavy metal release*

Heavy metal ions may be dissolved in formation fluids or sorbed on rock/mineral surfaces. Complexation may occur between CO<sub>2</sub> and heavy metals dissolved in formation fluids. The influence of dissolved CO<sub>2</sub> on pore water chemistry can also reduce the pH and change the equilibrium between sorption/desorption of metals, thereby resulting in significant release of these metals. This process has the potential to release heavy metals, which may then migrate to the near-surface environment with resulting impacts of interest. These heavy metals will also change pore water chemistry, which could impact on carbonate complexation.

*i) Mineral phase*

Geochemistry of the mineral phase relevant to sequestered CO<sub>2</sub>, including ion exchange and mineral dissolution. Geochemical reactions between sequestered CO<sub>2</sub> and the mineral phase of the storage system will affect the evolution of the system and the sorption (and therefore mobility) of the CO<sub>2</sub>

*j) Mineral dissolution and precipitation*

The dissolution of minerals due to the addition of CO<sub>2</sub> (an 'acid gas') to the geochemistry and precipitation. For example, the dissolution of albite and precipitation of calcite modeled for the Sleipner site by Gaus et al. (2003). CO<sub>2</sub> reaction with the host rock will modify: the porosity and permeability of the reservoir; fluid flow (direction or velocity); mechanical properties (e.g. strength); and CO<sub>2</sub> storage capacity.

*k) Ion exchange*

The process of exchanging one ion in the liquid phase for another ion on a charged, solid substrate. Injected CO<sub>2</sub> may perturb ion exchange equilibria between relevant minerals (such as sheet silicates) and the pore fluid. Some cations may be released to the pore fluid and others fixed as a consequence.

Disturbance of the rock-pore fluid equilibria may affect the capacity of the rock to store CO<sub>2</sub>

*l) Desiccation of clay*

CO<sub>2</sub> is likely to be dried to prevent corrosion during transport. Injection of dry CO<sub>2</sub> will cause it to take up water from the pores of the host formation and overlying rocks. It has the

potential to 'suck' water out of an overlying clay. If clay dehydrates, it will shrink and crack. This might aid CO<sub>2</sub> migration upwards

## **5.7 Environmental and human toxicology**

### **5.7.1 Effects on the environment**

Carbon dioxide is an integral part of living systems and as such it is considered non-toxic under normal conditions. However, as for any other molecule, the applied dose determines whether effects are seen or not. Two scenarios relevant for this study can be envisaged: 1. sudden release of large quantities of CO<sub>2</sub>, and 2. slow seepage of CO<sub>2</sub> from storage places with gradual increases of local concentrations of CO<sub>2</sub> in ground water (drinking water), surface waters, top soil and in ambient air in ill ventilated areas (e.g. buildings) as a result. Since CO<sub>2</sub> has a higher density than air, it will tend to form a blanket on the earth's surface. Leakage of relatively small quantities of CO<sub>2</sub> may pose a lethal threat when CO<sub>2</sub> is able to accumulate in confined spaces such as valleys or cellars. On the other hand, CO<sub>2</sub> is not explosive or inflammable.

Sudden releases of large quantities of CO<sub>2</sub> are not to be expected in our study area. However, slow migration or seepage of CO<sub>2</sub> from underground storage places (geological reservoirs) along fault planes, as a result of cap rock failure and through or along abandoned wells, is quite possible (see above).

There are many places in the world where CO<sub>2</sub> naturally emanates from the subsurface (Holloway, 1996) and many of these do not appear to pose a danger to man.

Natural seeps are widely distributed in tectonically active regions of the world and regions influenced by volcanism (Morner & Etiope, 2002). CO<sub>2</sub> is emitted from vents, surface degassing and diffuse emissions from CO<sub>2</sub>-rich ground waters. Fluxes from vents in central Italy, for example, range from less than 100 to more than 430 t CO<sub>2</sub> per day, which have shown to be lethal to animal and plants. However, because those seeps occur in highly fractured volcanic zones, unlike the interiors of stable sedimentary basins which are the likely locations for CO<sub>2</sub> storage, they do not represent a useful basis for estimating the spatial and temporal distribution of CO<sub>2</sub> fluxes leaking from a deep storage site (IPCC, 2005).

Another example of "harmless" naturally emanating CO<sub>2</sub> are the so-called "mofetten" or geothermal CO<sub>2</sub>-exhalations in the passive volcanic area of the Eifel (NW-Germany). These exhalations represent a potential danger in confined places only (e.g. depressions in the immediate surroundings).

Natural and engineered analogues show that it is possible, though improbable, that slow releases from CO<sub>2</sub> reservoirs will pose a threat to humans. However, the Lake Nyos disaster (Le Guern et al, 1989) demonstrates that the results of leakage from a man-made underground CO<sub>2</sub> storage should be considered. During the lake Nyos disaster in 1986, a huge mass of concentrated CO<sub>2</sub> was emitted from Lake Nyos, a volcanic crater lake in Cameroon and killed more than 1700 people in a thinly populated area, and all animal life along its course as far as 14 km from the crater. Most probably the disaster was caused by a sudden and violent release of CO<sub>2</sub> caused by the overturn of the 220 m deep lake, the lower layer of which became oversaturated with CO<sub>2</sub> of volcanic origin, caused by a slow leak of CO<sub>2</sub> into the lake waters from below (Holloway, 2005). However, this kind of catastrophic event is rather exceptional and restricted to active volcanic areas only.

### **5.7.2 Ground- and drinking water**

The local risk resulting from leaking CO<sub>2</sub> is very site specific. When migrating upwards from the reservoir, CO<sub>2</sub> may affect the quality of soil, ground and surface water as well as their ecosystems. In general, the environmental effects are less well understood as the health effects

on man. Fresh, potable groundwater could be contaminated by CO<sub>2</sub> leakage with a possible significant deterioration of its quality. Dissolved CO<sub>2</sub> forms carbonic acid, altering the pH of the solution and potentially causing indirect effects, including mobilization of toxic metals, sulphate and chloride, and possibly giving the water an odd odour, colour or taste, excluding the use of groundwater for drinking or irrigation (IPCC-report, 2005). An increase in CO<sub>2</sub> concentration might cause a decrease in pH to a level of 4 to 5, which might increase calcium dissolution, increase in the hardness of water and change in the concentration of metals and trace elements (Damen et al., 2006). In poorly buffered aquifers the decrease in pH may cause the release of trace metals to levels that exceed groundwater clean-up standards and/or drinking water standards (Jaffé and Wang, 2003). The same authors used a chemical transport model (Wang and Jaffé, 2004) to investigate the effect of releasing CO<sub>2</sub> from a point source at 100m depth into a shallow water formation that contained a high concentration of mineralized lead (galena). They found that in weakly buffered formations, the escaping CO<sub>2</sub> could mobilize sufficient dissolved lead to pose a health hazard over a radius of a few hundred meters from the CO<sub>2</sub> source.

Because the effects of CO<sub>2</sub> in groundwater are very site-specific (i.e. dependent on local soil characteristics), no generic ecotoxicological guidelines on groundwater are reported. When it is assumed that mobilisation of trace metals is the major risk to be considered, soil clean-up values or drinking water limits for heavy metals could be forwarded to determine maximum CO<sub>2</sub> levels in groundwater. Groundwater clean-up standards as well as drinking water standards for heavy metals that apply for the Flanders Region of Belgium are given in table 5-2. It should be noticed that these values are based on human health.

Next to mobilisation of trace metals, groundwater and surface water can also be contaminated due to brine displacement as a result of the injection of CO<sub>2</sub> in saline aquifers. Brines displaced from deep geological formations by injected CO<sub>2</sub> can potentially migrate or leak through fractures or defective wells to shallower aquifers and contaminate drinking water formations by increasing their salinity. In the worst case, infiltration of saline water into groundwater or into the shallow subsurface could impact wildlife habitat, restrict or eliminate agricultural use of land and pollute surface waters (IPCC-report, 2005). Contamination of groundwater by brines displaced from injection well is rather rare. It is therefore expected that contamination arising from large-scale CO<sub>2</sub> storage activities would also be rare.

Table 5-2: Clean-up standards (OVAM, 1996) and drinkwater standards (Flemish Decree dd. 13/12/2002) for heavy metals in the Flanders Region in Belgium)<sup>17</sup>

<b>Metal</b>	<b>Clean-up value groundwater (µg/l)</b>	<b>drinkwater standard (µg/l)</b>
Arsenic	20	10
Cadmium	5	5
Chromium <sup>1)</sup>	50	50
Copper	100	2
Mercury	1	1
Lead	20	25
Nickel	40	20
Zinc	100	-

1) clean-up standard for Cr(III)

<sup>17</sup> Both drinking- and groundwater clean-up standards are based on assumption of human consumption and human health effects

### 5.7.3 Surface water

Surface water could also be contaminated by leakage, which could affect aquatic ecosystems by decreasing the pH, thus increasing mobility and bioavailability of metals and trace metals, especially in stagnant or stably stratified waters (Benson et al., 2002). Carbon dioxide in water systems is reported to be harmful to some species of aquatic life (not further specified) in concentrations of less than 20 mg/l (IPCC, 2005).

### 5.7.4 Soil

Elevation of CO<sub>2</sub> concentrations in the soil due to leakage is likely to lower the pH, and adversely impact the chemistry of nutrients, redox sensitive elements and trace elements, as well as plant growth (Saripalli et al., 2003). Although plants are usually more resistant against CO<sub>2</sub> than animals, persistent leaks could suppress respiration in the root zone. Tree kills have been observed associated with soil CO<sub>2</sub> concentrations of 20 to 30% (volcanic outgassing of CO<sub>2</sub> (Damen et al., 2006)).

Elevated CO<sub>2</sub> concentrations above ground may also increase the primary production of plants. These effects will however generally be overwhelmed by the detrimental effects of elevated CO<sub>2</sub> in soils, because CO<sub>2</sub> fluxes large enough to significantly increase concentrations in free air will typically be associated with much higher CO<sub>2</sub> concentrations in soils (IPCC, 2005). Whereas normal soil gas usually contains about 0.2-4% CO<sub>2</sub>, concentrations above 5% may be dangerous for vegetation and as concentrations approach 20%, CO<sub>2</sub> becomes phytotoxic (IPCC, 2005). Soil CO<sub>2</sub> levels above 10-20% are reported to inhibit root development and decrease water and nutrient uptake (Mammoth Mountain Site in California were due to a series of small earthquakes the area of dead and dying trees amounted 40 ha; cited in IPCC (2005)).

The effects of CO<sub>2</sub> on subsurface organisms in soils are not well known (Damen et al, 2006). Still, slow leaks of CO<sub>2</sub> are known to have detrimental effects on burrowing fauna and flora. This is because surface air is far better mixed than air in soils, which means that hazardous concentrations may result from CO<sub>2</sub> fluxes far smaller than those required to produce harm to above-ground organisms (Chadwick et al., 2007). However, no data have been found to quantify this effect.

Also, the effect of CO<sub>2</sub> on subsurface microbial populations is poorly understood. A low pH, and high CO<sub>2</sub> environment may favour some species and harm others. In strongly reducing environments, the injection of CO<sub>2</sub> may stimulate microbial communities that could reduce CO<sub>2</sub> to CH<sub>4</sub>; or Fe(III) reducing communities in some siliciclastic reservoirs (Onstatt, 2004 cited in IPCC, 2005).

Up to date, there is no evidence of any terrestrial impact from current CO<sub>2</sub> storage projects. Likewise, there is no evidence from EOR projects that indicate impacts to vegetation such as those described above.

### 5.7.5 Ecotoxicity studies

#### 5.7.5.1 Invertebrates

Childs et al. (1983; cited in HSDB) investigated exposure of different life stages of *Lasioderma serricornis* (cigarette or tobacco beetle) reared on tobacco to CO<sub>2</sub>. Overall, an atmosphere of 65% CO<sub>2</sub> was more toxic to the eggs, larvae, pupae, and adults than an atmosphere of 35 or 92% CO<sub>2</sub>. The pupal stage tolerated CO<sub>2</sub> the best, some pupae surviving exposure of 7 days. Other insect stages, in increasing order of CO<sub>2</sub> susceptibility, were larva, adults, and eggs. More than 3 days of exposure of the eggs was required for a mortality rate of 99.9% (Childs et al., 1983).

### 5.7.5.2 Fish

Neurological responses to carbon dioxide (CO<sub>2</sub>) dissolved in distilled water in (carp) *Cyprinus carpio*, were studied by Kawamura et al. (1989; cited in HSDB). Results showed that CO<sub>2</sub> stimulation of carp pit organs produced a large phasic response followed by a long period (60-90 sec) of depression in impulse discharges. These responses were CO<sub>2</sub> specific and differed from those of various acids (fumaric, tartaric, succinic, acetic, etc) tested. The magnitude of the CO<sub>2</sub> response was slightly pH dependent.

Also some ecotoxicity values are reported by Environment Canada (1984). Lethality in rainbow trout occurred at concentrations of 240, 60-240 mg/l and 35 mg/l after exposure times of 1, 12 and 96 hr, respectively.

### 5.7.5.3 Macrophytes

Seedlings of 5 tropical trees, *Cecropia obtusifolia*, *Nyriocarpa longipes*, *Piper auritum*, *Senna multijuga* and *Trichospermum mexicanum*, were grown both as individuals, and in competition with each other at ambient levels (350 µl/l) and 2 levels of elevated CO<sub>2</sub> (525 and 700 µl/l) for a period of 111 days (Reekie et al., 1989; cited in HSDB). Elevated CO<sub>2</sub> did not affect photosynthesis or overall growth of the individually grown plants but did affect canopy architecture. Stomatal conductance decreased slightly as CO<sub>2</sub> increased from 350 to 525 µl/l but this had no significant effect upon whole plant water use or leaf water potential. Soil moisture content for the individuals increased marginally as CO<sub>2</sub> increased, but this did not occur in the competitive arrays. There was a marked effect of CO<sub>2</sub> upon species composition of the competitive arrays; *Senna* decreased in importance as CO<sub>2</sub> increased while *Cecropia*, *Trichospermum* and *piper* increased in importance.

### 5.7.5.4 Ecotoxicity Values (Environment Canada, 1984)

- Trout 240 mg/l/1 hour, toxic effect: lethal
- Rainbow trout 35 mg/l/96 hr, toxic effect: lethal
- Rainbow trout 60-240 mg/l/12 hr, toxic effect: lethal
- Harmful to some species of aquatic life in concentrations less than 20 mg/l (not further specified).

*BIG- data base*

LC<sub>50</sub><sup>(18)</sup> fish (*Salvelinus* sp.): 45 mg/l, toxic effect: lethal

## 5.7.6 Effects on humans

### 5.7.6.1 Toxicokinetics and metabolism

Approximately 200 ml per minute of carbon dioxide are produced by the body's metabolism at rest, and up to ten times that much during heavy exercise. The gas diffuses readily from the cells into the bloodstream, where it is carried partly as bicarbonate ion, partly in chemical combination with haemoglobin and plasma proteins, and partly in solution in mixed venous blood. It is transported to the lung, where it is normally exhaled at the same rate at which it is produced (Gilman et al., 1990 cited in HSDB).

In the blood, CO<sub>2</sub> is essential for the internal respiration. The internal respiration is the process by which oxygen is transported to body tissues and CO<sub>2</sub> is carried away from them. Carbon dioxide is essential to keep the pH of blood within narrow homeostatic levels, which is essential for survival. This so called carbonate buffer system is made up of bicarbonate ions

<sup>18</sup> Lethal Concentration for 50% of test animals.

and dissolved carbon dioxide, with carbonic acid, and is responsible to keep H<sup>+</sup> ions in the blood within narrow boundaries (Lenntech, 2004).

Carbon dioxide is excreted by the lungs and, in the form of bicarbonate ion, by the kidney, intestine and the skin (Osol and Pratt, 1973 cited in HSDB).

#### **5.7.6.2 Effects on laboratory animals**

##### *a) Acute toxicity*

Experiments with animals suggest that continuous exposure and high concentrations of CO<sub>2</sub> may alter normal physiological processes. The gas is a weak CNS (central nervous system) depressant at 30000 ppm (3%) causing elevated blood pressure and pulse, and decreasing hearing acuity. At 50000 ppm (5%) a thirty minute exposure produces signs of intoxication and at 70000 and 100000 ppm (7 and 10%) produces unconsciousness in a few minutes (from HSDB data base).

Inhalation of air containing 68% carbon dioxide for 5 min caused death from asphyxia in pigs (Humphreys, 1988 cited in HSDB).

To investigate the effects of very high concentrations of CO<sub>2</sub> upon the course of respiration and circulation, dogs were allowed to breath high concentrations of CO<sub>2</sub> while intrathoracic pressure, blood pressure in the femoral artery, electrocardiogram and electroencephalogram readings were registered (Ikeda et al. 1989, cited in HSDB). The respiratory movements either increased just after inhalation of high concentrations of CO<sub>2</sub> and then ceased in 1 min, or decreased and continued for a while according to the concentrations of CO<sub>2</sub>. The blood pressure showed an initial depression, then returned to the original level, then fell again rapidly or maintained an appreciable level for a while until circulatory breakdown. In the dogs allowed to breathe the gas mixture of 80% CO<sub>2</sub> with 20% O<sub>2</sub>, the respiratory movement ceased in 1 min, and the terminal respirations were seen with the circulatory breakdown after apnoea of several minutes. These findings showed that the cause of death in breathing high concentrations of CO<sub>2</sub> is not hypoxia, but CO<sub>2</sub> poisoning.

Morphological changes in the rat lung after carbon dioxide exposure were examined by Morita (1988; cited in HSDB). Male Wistar-rats were placed in an observation box and exposed to 20 percent oxygen, 30 to 50 percent CO<sub>2</sub>, then 100 percent CO<sub>2</sub> until asphyxiation occurred. After death, the lungs were removed, and fixed for light and electron microscopic examination. CO<sub>2</sub> inhalation, which caused death to the rats after 10 to 30 minutes, resulted in dark red, shrunken lungs. It was concluded that the morphological changes are probably due to a lack of oxygen rather than the presence of CO<sub>2</sub>.

##### *b) Repeated dose toxicity*

No information was retrieved on repeated dose toxicity in animals.

##### *c) Reproduction toxicity, embryotoxicity en teratogenity*

Rats exposed during a single gestational day to 6% carbon dioxide, 20% oxygen and 74% nitrogen showed 23% cardiac malformations in offspring as compared to 6.8% in controls (Shepard, 1986; cited in HSDB). Highest incidence occurred on the 10th day. Cardiac lesions were characterized as due to overgrowth.

Administration of 10-13% carbon dioxide to rabbits between the 7th and 12th day of gestation caused 16 foetuses of 67 to have defects of the vertebral column. Only 1 abnormal animal was found among 30 controls.

##### *d) Genotoxicity*

No information retrieved.

##### *e) Carcinogenicity*

One limited animal study could not be evaluated (CCOHS, 1997).

*f) Immunotoxicity*

No information retrieved.

*g) Irritation*

No information retrieved.

*h) Chronic toxicity*

Exposure to levels of 27 000 mg/m<sup>3</sup> (15 000 ppm) or more for several days has induced reversible changes in the lung membrane of guinea pigs (Health Canada, 2007).

### **5.7.6.3 Effects on humans**

The circulatory effects of carbon dioxide are the result of its direct local effects and its centrally mediated effects on the autonomic nervous system. The direct effect results from pH changes causing vasodilatation (Gilman et al., 1990 cited in HSDB). Carbon dioxide causes widespread activation of the sympathetic nervous system<sup>19</sup> and increases the plasma concentrations of several vasoactive peptides. The results of sympathetic nervous system activation are, in general, opposite to the local effects of carbon dioxide (Gilman et al., 1990 cited in HSDB). There are at least two sites where carbon dioxide acts to stimulate respiration: interference with the respiratory integration areas in the brainstem and bronchodilatation (elevated CO<sub>2</sub> levels) or vasoconstriction of airway smooth muscle (decreased levels) (Gilman et al., 1990 cited in HSDB) .

*a) Acute toxicity*

Carbon dioxide is naturally present in the atmosphere at levels of approximately 0.035%. Short term exposure to CO<sub>2</sub> levels below 2% (20,000 ppm) has not been reported to cause harmful effects (CCOHS, 1997). Higher concentrations can effect respiratory function and cause excitation followed by depression of the central nervous system. High concentrations of CO<sub>2</sub> can displace oxygen in the air, resulting in lower oxygen concentrations for breathing. Therefore effects of oxygen deficiency may be combined with effects of CO<sub>2</sub> toxicity (CCOHS, 1997). The international Labour Office (1971) considers the greatest danger of CO<sub>2</sub> as an asphyxiant. Asphyxiants are substances that replace oxygen in the inhaled air. The concentration of oxygen in the air should not drop below 18% (normal oxygen concentration equals 21%). When the oxygen concentration in the inhaled air drops under 8%, very often unconsciousness results (W&G, 2007).

In the HSDB (NIH, 2007) four stages following exposure to asphyxiants are described, depending on the arterial oxygen saturation.

1. **INDIFFERENT STAGE** (%O<sub>2</sub> Saturation: 90%): only decreased night vision has been reported.
2. **COMPENSATORY STAGE** (%O<sub>2</sub> Saturation: 82 to 90%): Compensatory increase of respiratory rate and pulse. Night vision is further decreased and performance ability and alertness is somewhat reduced. Symptoms may begin in those with significant pre-existing cardiac, pulmonary, or hematologic diseases
3. **DISTURBANCE STAGE** (%O<sub>2</sub> Saturation: 64 to 82%): General compensatory mechanisms become inadequate. Symptoms such as air hunger, fatigue, tunnel vision, dizziness, headache, belligerence and euphoria may occur. Visual acuity is reduced and numbness and tingling of extremities may happen. This stage is further characterized by hyperventilation, poor judgement, memory loss, cyanosis and a decreased ability for escape from toxic environment

---

<sup>19</sup> The sympathetic nervous system is responsible for up- or down-regulating many homeostatic mechanisms in living organisms.

4. **CRITICAL STAGE** (%O<sub>2</sub> Saturation: 60 to 70% or less): Deterioration in judgement and coordination may occur in 3 to 5 minutes or less. Total incapacitation and unconsciousness follow rapidly.

The NIH (2007) states that signs of asphyxia will be noted when atmospheric oxygen is displaced such that the oxygen concentration in air is 15 to 16% or less.

Argonne National Laboratory (ANL, 2007) documents Oxygen Deficiency Hazards (ODH). Table 5-3 contains a list of some of these effects and the sea level oxygen concentrations at which they occur. At higher altitudes the same effects generally occur at greater volume concentrations since the partial pressure of oxygen is less. If exposure to reduced oxygen is terminated early enough, effects are generally reversible. If not, permanent central nervous system damage or lethality result. Major effects hindering escape from the vicinity of an oxygen deficiency are disorientation and unconsciousness. In general, the intensities of the effects increase rapidly with falling oxygen concentration and longer exposure duration: reduced abilities, then unconsciousness, then death. It can be concluded that any exposure to an atmosphere containing less than 17% oxygen presents a risk.

Two percent carbon dioxide in inhaled air increased pulmonary ventilation with 50%, 5% CO<sub>2</sub> will increase pulmonary ventilation with 100 %, and 7.2% of CO<sub>2</sub> with 200%. Dizziness, headache, confusion and an inability to breathe (dyspnea) occur at 5% carbon dioxide; 8 to 10% causes severe headache, sweating, dimness of vision and tremor, and consciousness is lost after 5 to 10 minutes (Thienes and Haley, 1972; cited in HSDB).

In a normal person inhalation of 1.6% carbon dioxide in air approximately doubles the respiratory minute volume (volume air inhaled/minute) and 5% almost triples it. A concentration of 10% produces unbearable dyspnea after a few minutes, continued exposure results in vomiting, disorientation and hypertension (Osol and Pratt, 1973 cited in HSDB).

*Table 5-3: Relationship between concentration off-gas or asphyxiant in the ambient air, percentage O<sub>2</sub> and health effects after short-term exposure (ANL, 2007).*

<b>% ambient air</b>	<b>% off-gas</b>	<b>% O<sub>2</sub> in mixture</b>	<b>Mass off-gas (g/m<sup>3</sup>) air</b>	<b>symptoms</b>
75	25	17.8	306	-
70	30	17.1	367	Decreased night vision, increased pulse
65	35	16.5	429	
60	40	15.8	490	Dizziness, Reaction time doubled
55	45	15.2	551	Impaired attention, judgment & coordination
30	70	11.9	857	12%: unconsciousness

*Measured at a pressure of 1.2245 kg/m<sup>3</sup>, and a temperature of 15°C*

Volunteers exposed to 3.3 or 5.4 % CO<sub>2</sub> for 15 minutes experienced increased depth of breathing. At 7.5%, a feeling of dyspnea, increased pulse rate, headache, dizziness, sweating, restlessness, disorientation, and visual distortion developed. Twenty-minute exposures to 6.5 or 7.5 % decreased mental performance (CCOHS, 1997).

Adding 1% CO<sub>2</sub> to air increased the human pulmonary ventilation rate by 37% and 7% on the ground and under a pressure simulating a 5000 m altitude, respectively. Blood flow to the brain increased at 2 but not 1% CO<sub>2</sub>. CO<sub>2</sub> at 0.5 or 1% stimulated hyperventilation to a degree

which prevented a decrease in the psychomotor performance at a simulated 5800 m, but not a 5000 m altitude (Vieillefond et al., 1981 cited in HSDB).

Irritability and discomfort were reported with exposures to 6.5% for approximately 70 minutes. Exposure to 6% CO<sub>2</sub> for several minutes, or 30% for 20-30 seconds, has affected the heart, as evidenced by altered electrocardiograms (CCOHS, 1997).

Concentrations greater than 10% have caused difficulty in breathing, impaired hearing, nausea, vomiting, a strangling sensation, sweating, stupor within several minutes and loss of consciousness within 15 minutes (CCOHS, 1997). Exposure to 30% has resulted in unconsciousness and convulsions, and several deaths have been attributed to exposure to concentrations above 20% (CCOHS, 1997).

IPCC (2005) states that most people with normal cardiovascular, pulmonary-respiratory, and neurological functions can tolerate exposure up to 0.5 to 1.5% CO<sub>2</sub> for one to several hours without harm although noticeable physiological changes occur (increased ventilation rates) (IPCC, 2005; fig. 5-6). Acute exposure to CO<sub>2</sub> concentrations less than or equal to 3% may significantly affect the health of the general population (IPCC (2005). Hearing loss and visual disturbances occur above 3% CO<sub>2</sub>.

A summary of the results discussed above is given in table 5-4.

*Table 5-4: Levels of CO<sub>2</sub> and associated health effects for short term exposure (concentrations in ppm and %)*

<i>Level (ppm)</i>	<i>Level (%)</i>	<i>Health effect</i>	<i>Reference</i>
20.000	< 2.0 3.3 – 5.4 7.5 6.5 - 7.5	- No effect - Increased depth of breathing (15 min) - Feeling of dyspnea <sup>2</sup> , increased pulse rate, headache, dizziness, sweating, restlessness, disorientation, and visual distortion developed (15 min) - Decreased mental performance (20 min)	CCOHS, 1997
16.000 50.000 100.000	1.6 5 10	-Doubling of respiratory minute volume <sup>1</sup> -Tripling of respiratory minute volume; - Dyspnea <sup>2</sup> after a few minutes, vomiting, disorientation and hypertension after continued exposure	Osol and Pratt, 1973
10.000	1	Increased pulmonary ventilation rate with 37%	Vieillefond et al., 1981
20.000 50.000 72.000 80.000-100.000	2 5 7.2 8-10	- Increased pulmonary ventilation with 50%, - Increased pulmonary ventilation with 100%,; dizziness, headache, confusion and dyspnea <sup>2</sup> - Increased pulmonary ventilation with 200%, - Severe headache, sweating, dimness of vision and tremor, and consciousness is lost after 5 to 10 minutes	Thienes and Haley, 1972
30.000	3	- Hearing loss and visual disturbances	
65.000 - 75.000 65.000	6.5 or 7.5 6.5	- Decreased mental performance, feeling of dyspnea, increased pulse rate, headache, dizziness, sweating, restlessness, disorientation, visual distortion - Irritability and discomfort (approx. 70 min) -Effect on heart (altered electrocardiograms)	CCOHS, 1997
65.000-300.000	6.5 (min.) – 30 ( sec.)		
5000-15000 30.000	0.5-1.5 >3	- No effect for healthy people - Hearing loss and visual disturbances	ICPP, 2005

*1) volume air inhaled/minute; 2) inability to breathe*

*b) Repeated dose toxicity*

Several studies have monitored workers repeatedly exposed to elevated levels of CO<sub>2</sub> gas. Exposure to 1-1.5% for 42 – 44 days caused a reversible acid-base imbalance in the blood and an increased volume of air inhaled/minute. In another study, harmful effects were not observed in 19 brewery cellar workers repeatedly exposed to average concentrations of 1.1% CO<sub>2</sub>, with levels occasionally up to 8% for a few moments. Submarine occupants exposed to 3% CO<sub>2</sub>, 16 hours/day for several weeks experienced flushing of the skin, an impaired response of the circulatory system to exercise, a fall in blood pressure, decreased oxygen consumption, and impaired attentiveness. Adaptation to some of the effects of long-term exposure to CO<sub>2</sub> has been reported. (source: CCHOS, 1997).

*c) Reproductive toxicity, embryotoxicity en teratogenicity*

There is no human information available on reproductive toxicity. No conclusions could be drawn from limited animal information (CCOHS, 1997). There is no information on embryotoxicity in humans. There is limited information available in animal studies that exposure to very high levels of CO<sub>2</sub> gas during pregnancy may cause developmental effects (CCOHS, 1997).

*d) Genotoxicity*

No information retrieved.

*e) Carcinogenicity*

There is no human information available. One limited animal study could not be evaluated (CCOHS, 1997).

Carbon dioxide is not classifiable as to its carcinogenicity to humans (IARC, 2004).

*f) Immunotoxicity*

No information retrieved.

*g) Irritation*

CO<sub>2</sub> gas is not irritating the skin (CCOHS, 1997). Only contact with liquefied CO<sub>2</sub> can cause frostbite. Exposure to very high concentrations of the gas may cause stinging sensation in the eyes (CCOHS, 1997).

*h) Chronic toxicity*

Long-term exposure to levels between 0.5 and 1%, as may occur in submarines, is likely to involve increased calcium deposition in body tissues, including the kidney (International Labour Office, 1983).

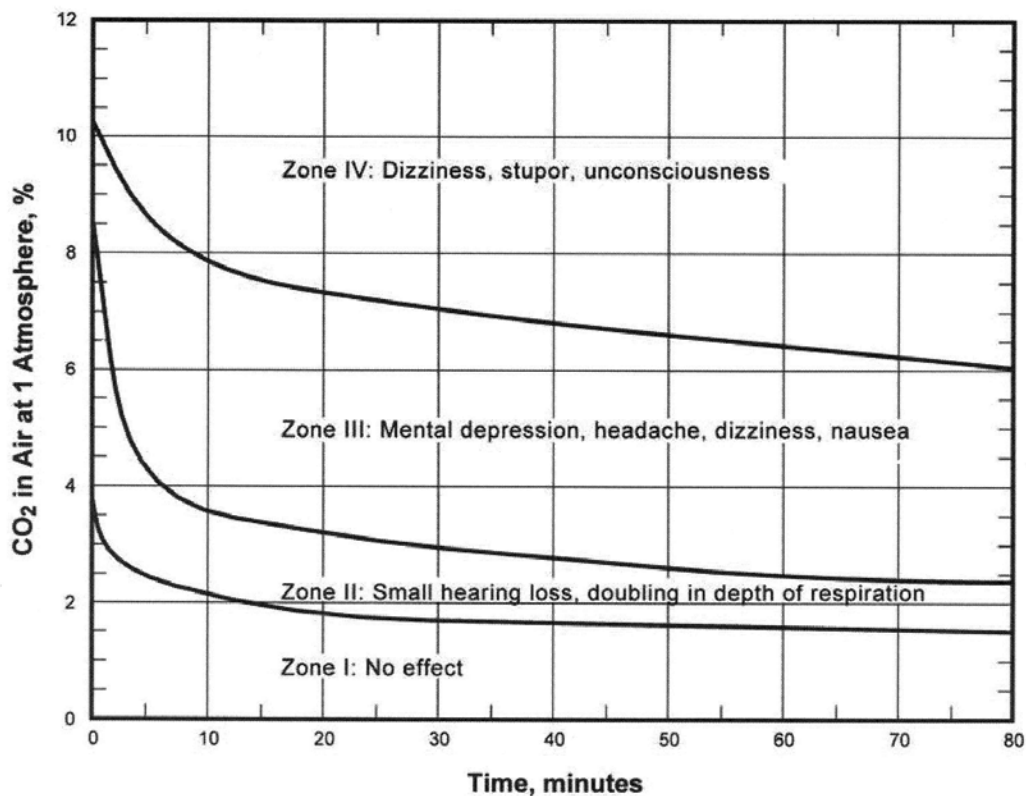


Figure 5-6: Effects of CO<sub>2</sub> exposure on humans (Fleming et al., 1992) (retrieved from IPCC, 2005).

As mentioned before, IPCC (2005) states that most healthy people can tolerate exposure up to 0.5 to 1.5% CO<sub>2</sub> for one to several hours without harm although noticeable physiological changes occur (increased ventilation rates) (IPCC, 2005; fig. 5-6). Higher concentrations or exposures of longer duration are hazardous – either by reducing the concentration of oxygen in the air to below the 16% level required to sustain human life, or by entering the body, especially the bloodstream, and/or altering the amount of air taken in during breathing – such physiological effects can occur faster than the effects of displacement of oxygen depending on the concentration of CO<sub>2</sub> (IPCC, 2005). IPCC, 2005 concludes that healthy young adults exposed to more than 3% CO<sub>2</sub> during exercise experience adverse symptoms, including laboured breathing, headache, impaired vision, and mental confusion. CO<sub>2</sub> acts as an asphyxiant in the range 7-10% and can be fatal at this concentration; at concentrations above 20%, death can occur in 20 to 30 minutes (Fleming et al., 1992).

Table 5-5: Levels of CO<sub>2</sub> and associated health effects for long term exposure (concentrations in ppm; %)

Level (ppm)	Level (%)	health effect	reference
1.000 – 2.000	0.1 – 0.2	-Complaints of drowsiness	WDHFS, 2005
2.000 – 5.000	0.2 – 0.5	- Headaches, - Sleepiness	WDHFS, 2005
> 5.000	> 0.5	-Serious oxygen deprivation resulting in permanent brain damage, coma and even death.	WDHFS, 2005
5.000-15.000	0.5 -1.5	- Supported by most healthy people for several hours	IPCC, 2005
30.000	3%	- During exercise experience adverse symptoms, including laboured breathing, headache, impaired vision, and mental confusion.	
70.000-100.000 200.000	7-10 > 20	- Asphyxiation - Death	
500-3.200	0.05-0.32	- Subjective symptoms (fatigue, headaches, increased perception of warmth and unpleasant odours) - Increased blood acidity (Lowest effect level)	Health Canada, 2007
7.000	0.7	-Headache and dizziness, visual distortions; cardiovascular effects	
50.000	5		
Between 5.000 and 10.000	between 0.5 and 1	- Increased calcium deposition in body tissues	International Labour Office, 1983
10.000-15.000	1 – 1.5	– Irreversible acid-base imbalance - Increased volume of air inhaled/minute	CCHOS, 1997
30.000	3	- Flushing of the skin, impaired response of the circulatory system to exercise, a fall in blood pressure, decreased oxygen consumption, impaired attentiveness	CCHOS, 1997

When asphyxiation is considered the primary effect of concern oxygen concentration in the air should not drop below 16-18% (normal oxygen concentrations are 21%). In their chemical fact sheets on carbon dioxide the Wisconsin Department of Health and Family Services (WDHFS, 2005)<sup>20</sup> summarizes the potential effects of increasing concentrations of CO<sub>2</sub> in the ambient air as follows:

- 250 - 350 ppm (0.025 – 0.035%) – background (normal) outdoor air level
- 350- 1000 ppm (0.035 – 0.1%) - typical level found in occupied spaces with good air exchange.
- 1000 – 2000 ppm (0.1 – 0.2%) - level associated with complaints of drowsiness and poor air.
- 2000 – 5000 ppm (0.2 – 0.5%) – level associated with headaches, sleepiness, and stagnant, stale, stuffy air. Poor concentration, loss of attention, increased heart rate and slight nausea may also be present.

<sup>20</sup> It is not explicitly mentioned in the report that a chronic exposure scenario applies.

- >5000 ppm (> 0.5%) – Exposure may lead to serious oxygen deprivation resulting in permanent brain damage, coma and even death.

According to Health Canada (2007) an increase in the ambient level of carbon dioxide brings about a rise in the acidity of the blood and an increase in the rate and depth of breathing. Over prolonged periods, of the order of days, regulation of blood carbon dioxide levels occurs by kidney action and the metabolism of bone calcium. The latter process leads to some demineralization of the bone. In humans, exposures to carbon dioxide levels of over 90 000 mg/m<sup>3</sup> (50 000 ppm) have produced effects on the central nervous system, such as headache and dizziness and visual distortions; there is some evidence of cardiovascular effects at similar concentrations. Subjective symptoms such as fatigue, headaches and an increased perception of warmth and unpleasant odours have been associated with carbon dioxide levels of 900 to 5800 mg/m<sup>3</sup> (500 to 3200 ppm). In some of these studies the symptoms may have been caused by other substances, with the carbon dioxide acting as a surrogate measure of air quality.

The lowest concentration at which adverse health effects have been observed in humans is 12 600 mg/m<sup>3</sup> (7000 ppm), at which level increased blood acidity has been observed after several weeks of continuous exposure (Health Canada, 2007).

A summary of the results discussed above is given in table 5-5.

*i) Carcinogenic effects*

Not relevant

*j) Toxicological limit values*

Limit values general public:

According to Health Canada (2007), the acceptable long-term exposure range (ALTER) for carbon dioxide in residential indoor air is  $\leq 6300 \text{ mg/m}^3$  ( $\leq 3500 \text{ ppm}$  or  $\leq 0.35 \%$ )<sup>21</sup>. No acceptable short-term exposure range (ASTER) for CO<sub>2</sub> is defined. In its motivation Health Canada states that a maximum exposure level of 6300 mg/m<sup>3</sup> should provide a sufficient margin to protect against undesirable changes in the acid-base balance and subsequent adaptive changes such as the release of calcium from the bones. This level should also provide an adequate safety margin for sensitive groups. At such a level, the effect of carbon dioxide as a ventilatory stimulant is likely to be small and so would not greatly increase the dose received of other pollutants present in the air. Changes in the acid-base balance and release of calcium from bones occur in response to chronic carbon dioxide exposure rather than to brief excursions in concentration. Thus, a short-term exposure range is not required for this substance.

No ADI for carbon dioxide is specified by JECFA (WHO). US-EPA has no national ambient air quality standard on CO<sub>2</sub>. Also no data were retrieved from ATSDR and RAIS databank.

In Belgium also an indoor chronic air quality guideline of  $\leq 900 \text{ mg/m}^3$  has been adopted Flemish Decree on Indoor Pollution as of 11 June 2004). This value is half the CO<sub>2</sub> concentration (i.e., 1800 mg/m<sup>3</sup>) which is experienced as unpleasant by 20% of the interviewees. TÜV Süddeutschland considers indoor concentrations > 1000 ppm CO<sub>2</sub> as potentially indicative of an increased risk (TÜV, 2000).

NIOSH (1991) uses peak carbon dioxide (CO<sub>2</sub>) concentrations over 1000 ppm as an indicator of underventilation.

---

<sup>21</sup> Derived by dividing the lowest effect level of 7000 ppm by 2.

*k) Occupational health standards:*

Apart from health standard for the general public, also occupational limit values have been derived by several authorities. An overview of these limit values is given in table 5-6.

Table 5-6: Compilation of occupational limit values in different countries (source: BIG data base)

Country	Limit value
USA	5.000 ppm / 0.5% (TLV-TWA) <sup>(1)</sup>
	30.000 ppm / 3 % (TLV-STEL) <sup>(2)</sup>
	40.000 ppm / 4 % (IDLH) <sup>(3)</sup>
Germany	5.000 ppm / 0.5 % (MAK) <sup>(4)</sup> (9.100 mg/m <sup>3</sup> )
	10.000 ppm/1 <sup>7</sup> /4x (short term value) <sup>(5)</sup> (18.200 mg/m <sup>3</sup> /1 <sup>7</sup> /4x)
The Netherlands	9.000 ppm / 0.9 % (MAC-TGG) <sup>(6)</sup>
European Commission	5.000 ppm / 0.5 % (TLV-EC) <sup>(7)</sup> (9.000 mg/ m <sup>3</sup> )
Belgium	5.000 ppm / 0.5 % (limit value) <sup>(8)</sup> (9.131 mg/m <sup>3</sup> )
UK	15.000 ppm / 1.5 % (WEL-STEL) <sup>(9)</sup> (27.400 mg/m <sup>3</sup> )

(1) Threshold limit value – time weighted average (Average concentration above which it cannot be guaranteed that a normal, healthy subject will not suffer health effects when exposed to it 8 hours/day during the entire career (occupational exposure). Source: ACGIH (American Conference of Governmental Industrial Hygienists) 2006.

(2) Threshold limit value – short time exposure limit (value that cannot be exceeded for more than 4 times during a working day for a period of 15 minutes or more with an interval of at least 60 min.)

(3) Immediately Dangerous to Life and Health concentration (revised value from NIOSH as of 3/1/1995).

(4) Maximal accepted concentration

(5) Maximal accepted concentration – short term exposure: Maximum concentration that cannot be exceeded for a period longer than indicated (value/time period/number of times).

(6) Maximal accepted concentration – Time weighted average: time weighted maximal accepted value that cannot be exceeded during an exposure period of 8 hour/day and 40 hours/week. Source: National MAC-list 2006.

(7) Indicative limit values according to EC-directive 2006/15/EG and 2000/39/EG.

(8) time weighted maximal accepted value that cannot be exceeded during an exposure period of 8 hour/day and 40 hours/week. Based TLV-EC. source: K.B. van 12 maart 2002

(9) Workplace exposure limit - Short-Term Exposure Limit (15 min. exposure) source: EH40/2005, Workplace Exposure Limits 2005, OEL (UK).

### 5.7.7 Evaluation of environmental and health effects

Increased levels of CO<sub>2</sub> may affect both biota in soil and aquatic environments and man. In general, the effects of increased levels of CO<sub>2</sub> on ecosystems are much less documented than the effects on man. The limit values for all relevant environmental targets (including man) that are proposed after careful scrutiny of the literature survey given above, are listed in table 5-7. A motivation for this choice is given below.

With regard to the effects on ecosystems, both direct (displacement of oxygen required for aerobic metabolism) and indirect effects (decrease in the ambient pH with an increase in mobility and bioavailability of trace metals as a consequence) should be considered. Although it is generally assumed that metal toxicity to soil biota (including terrestrial plants) is due to

free ion concentrations in the soil solution, no generic ecotoxicological limit values exist based on soluble metal concentrations in soil because they are highly site specific, i.e. they depend on local soil characteristics. As such, the ground- and drinking water limit values presented in table 5-7 are based on assumptions on human drinking water consumption and human health effects. No limit values have been retrieved from public literature on the effects of subsurface soil organisms. Soil CO<sub>2</sub> concentrations above 10% were reported to inhibit root development of terrestrial plants (IPCC, 2005). For aquatic organisms, a value of 35 mg/l derived by Health Canada (1984) is proposed.

In case of long-term exposure of humans to CO<sub>2</sub>, the aim is to protect the whole population, including sensitive groups, at the no-effect level. A limit value for long-term exposure is therefore proposed at the lowest of the no-effect levels reported for chronic exposure, i.e. 0.35% (3.500 ppm) (Health Canada, 2007)

In case of accidents, in which a sudden release of high levels of CO<sub>2</sub> takes place, the data reported by IPCC (2005) which provide a time-dose-response relationship, can be used to protect the general population (fig. 5-6). Indeed, for acute exposure an acceptable level should be defined corresponding to the protective measures that are in place at the site, e.g. depending on the availability of a monitoring system for CO<sub>2</sub>, the reporting time of the system and intervention time. If no protective measures are in place the public should be protected at the no-effect level. In case of acute exposure, CO<sub>2</sub> concentrations should not exceed 1% (based on IPCC, 2005).

Table 5-7: Selected limit values for CO<sub>2</sub> in drinking water, for soil- and aquatic biota, and for human health effects.

Target	Limit value	End point	Remarks
<b>Ground- and drinking water</b>	Clean-up values for heavy metals in groundwater <sup>1)</sup>	Human health (metal specific)	Corresponding CO <sub>2</sub> levels are site specific (i.e. depending on buffering capacity of soils)
<b>Subsurface soil organisms</b>	-	-	
<b>Terrestrial plants</b>	10 % in soil	Root development	
<b>Aquatic biota</b>	35 mg/l	Lethality after 96 h.	
<b>Acute human health effects</b>	(1%)		Depends on the protective measures in place
<b>Chronic human health effects</b>	0.35 %	Increased blood acidity Increased calcium deposition	Based on a LOEc of 0.7%

1) Published in the Flemish decree on soil pollution (VLAREBO, OVAM, (1996)

## 5.8 Case study and risk modelling

### 5.8.1 Background - Leakage mechanisms

Migration of gas through seal lithologies with low permeabilities (nDarcy range; 1 nDarcy  $\sim 10^{-21} \text{m}^2$ ) can occur by pressure-driven volume flow and by molecular diffusion (molecular

transport). In initially water-saturated rocks the former process involves both single-phase flow, capillary pressure phenomena (“gas breakthrough”) and two-phase flow.

In general the conductivity of a rock is characterised by its permeability. In a **single-phase system**, where water moves through a water saturated rock, one speaks of the absolute permeability ( $k_{abs}$ ,  $m^2$ ) of a rock. The volume flux  $Q$  [ $m^3/m^2/s$ ] through a rock is defined by Darcy’s law:

$$Q = k_{abs}/\eta * \Delta x/\Delta p$$

where

$\eta$  [ $Pa \cdot s$ ] is the dynamic viscosity of the permeating fluid

$\Delta P/\Delta x$  [ $Pa/m$ ] is the pore pressure gradient.

In the presence of two or more immiscible fluid phases in a porous rock (e.g. gas and water), **two-phase or multiphase flow** will occur. The conductivity of rock is then given by the effective permeability ( $k_{eff}$ ) of the rock to the gas or water-phase. The term relative permeability often found in literature is defined as follows:

$$k_{rel}(gas) = k_{eff}(gas)/k_{abs} \quad \text{or} \quad k_{rel}(water) = k_{eff}(water)/k_{abs}$$

However, before the gas-phase can enter/penetrate a water saturated seal the minimum capillary (entry) pressure ( $P_c$ ) must be overcome. Per definition the capillary pressure is the pressure difference between the water and the gas-phase. For static conditions the gas pressure can be calculated as a function of gas column height:

$$h = (\rho_{water} - \rho_{gas})/g/P_c$$

with

$\rho$  the density of water and gas ( $CO_2$  with  $\rho \sim 650$   $kg/m^3$  at 15 MPa and 55°C, Nist database)

$g$  the acceleration due to gravity.

After gas breakthrough the gas mass flow is calculated according to Darcy’s law for compressible media. A continuous gas flux ( $Q$ ) will evolve from higher to lower pressures:

$$Q = \Delta V_2/\Delta t = k_{eff}/\eta * A * (P_2^2 - P_1^2)/(2*\Delta x*\Delta P_2)$$

Where

$V_2$  [ $m^3$ ] is the volume of the low pressure side (e.g. top of seal)

$P_2$  [ $Pa$ ] the corresponding pressure

$P_1$  [ $Pa$ ] the high pressure e.g. at the base of the seal

$k_{eff}$  [ $m^2$ ] is the effective permeability to the gas phase

$A$  [ $m^2$ ] is the cross section area

$\eta$  [ $Pa s$ ] is the viscosity of the gas

$\Delta x$  [ $m$ ] is the migration path length.

A general observation is that the effective permeability to the gas-phase tends to be about 1 order of magnitude lower than the absolute permeability (Hildenbrand et al. 2002).

The **diffusive mass flow** is calculated as follows:

$$Q = -D_{eff} * (\Delta C * \phi) / \Delta x$$

with  $C$  the solubility of the gas phase in water,  $\phi$  the porosity and  $\Delta x$  [ $m$ ] the distance between the points of concentration difference. The diffusional leakage is independent of capillary pressure phenomena and occurs as soon as  $CO_2$  dissolves in the reservoir water.

Recently  $CO_2$  diffusion measurements were performed at the RWTH-Aachen (Germany). The experiments performed on several fine-grained rocks and limestones investigated during the Nascent project (EU funded project) resulted in effective diffusion coefficients ( $D_{eff}$ ) varying between  $10^{-9}$  to  $10^{-11}$   $m^2/s$ . During an other study repetitive  $CO_2$  diffusion tests on a water

saturated Muderong shale sample yielded effective diffusion coefficients of  $3.1\text{E-}21$  and  $4.8\text{E-}21$   $\text{m}^2/\text{s}$  (Busch et al., 2007).

### 5.8.2 The Poederlee structure

According to the lithostratigraphy of well 30W371 (Laenen et al, 2005) the major sealing lithology at the Poederlee structure is made out of an approx. 500 m thick claystone sequence of Namurian age, followed by a 250 m tight Westphalien sandstone body. Additionally further sealing bodies are present, like the 90 m thick Boom clay formation. All these lithologies are characterised by high capillary entry pressures and by low water permeabilities (table 5-8). The Namurian permeabilities were shown to be below the detection limit of the performed measurements ( $<0.01$  mDarcy =  $<10^{-17}$   $\text{m}^2$ ) and were estimated to be in the order of  $10^{-20}$  to  $10^{-21}$   $\text{m}^2$ , which are typical values for compacted claystones.

Table 5-8: Petrophysical properties of lithologies occurring in well 30w371; measurements performed for sequences below a depth of 989 m.b.s. Boom clay properties taken from Hildenbrand et al. (2004).

	Base of sequence; depth m.b.s. (meters below surface)	lithology	density ( $\text{g}/\text{cm}^3$ )	He porosity (fraction)	permeability ( $\text{m}^2$ )	capillary entry pressure (Pa)	gas saturation pressure
<b>Miocene</b>	92	sand	2.6	0.2	1E-12	3.00E+05	
<b>Boom</b>	179	clay		0.25	1E-20		
<b>Maldegem</b>	234	sand/clay		0.15	1E-15		
<b>Brussel</b>	280	sandstone					
<b>Kortrijk</b>	384	clay					
<b>Hannut</b>	505	sand/clay/marl					
<b>Heers</b>	531	Ca-arenit					
<b>Maastricht</b>	586	chalk/marl					
<b>Gulpen</b>	717	chalk/marl					
<b>Vaals</b>	743	sandstone					
<b>Westph.</b>	989	sandstone	2.7-2.8	0.03-0.04	4E-17	1.55E+07	
<b>Namurian</b>	1486	claystone	2.7-3	0.01-0.02	1E-20 – 1E-21	2.40E+07	
<b>Belgian limestone group (reservoir)</b>	1690	limestone, very heterogenous	Matrix: 2.7	Matrix: 0.015	Matrix: < 1E-15 Fracture related: 1e-12	Matrix: 4.50E+06	Matrix: 9.00E+06
<b>Belgian limestone group (reservoir)</b>	1890	limestone, start of brecciation	Matrix: 2.7	Matrix: 0.01-0.03	Matrix: 2e-17 - 1.5e-15	Matrix: 1.90E+05	Matrix: 4.50E+06

#### 5.8.2.1 Theoretical leakage rates & risk for leakage

At the Poederlee structure the maximum gas column that can be established has a height of 204 m (top to spill point), which corresponds to a maximum static gas overpressure of

0.7 MPa. According to Darcy's law for compressible medium the theoretical leakage rates through the seal can be modelled taking into account the following simplifications:

- vertical gas flow through the seal (no sidwards movement of gas),
- a porosity of 0.15 %,
- that 10 % of the rock porosity is used for gas transport, and
- a gas overpressure of 0.7 MPa

For a permeability of  $1\text{E-}20$  to  $1\text{E-}21$   $\text{m}^2$ , the calculated maximum leakage rates vary between  $6\text{E-}2$  to  $6\text{E-}3$   $\text{kg/m}^2/\text{year}$  ( $9\text{E-}5$   $\text{m}^3/\text{m}^2/\text{year}$ ), respectively. This mass/volume flow may be converted to a flow velocity within a rock column of a cross sectional area of  $1$   $\text{m}^2$ :

$$\text{volume flux } Q [\text{m}^3/\text{m}^2/\text{year}] = v [\text{m}/\text{year}]$$

and

$$v(\text{eff}) = v / \phi(\text{eff}) [\text{m}/\text{year}]$$

with

$\phi(\text{eff})$  the effective porosity used for gas transport

According to this approach the gas would need about 8,000 to 80,000 years ( $k = 1\text{E-}20$  to  $1\text{E-}21$   $\text{m}^2$ ) to move through the seal ( $\sim 500$  m thickness).

This calculation can be done for the entire sequence up to the surface (fig. 5-7). The viscosity and density of  $\text{CO}_2$  were taken for temperatures and pressures following a geothermal gradient of  $32$   $^\circ\text{C}/\text{km}$  and a hydrostatic pressure of approx.  $10$   $\text{MPa}/\text{km}$ . **Following the petrophysical properties listed in table 5-8, and a seal permeability of  $1\text{E-}20$   $\text{m}^2$ , the gas would take about 14,000 years to migrate up to the surface (fig. 5-8). For a seal permeability of  $1\text{E-}21$   $\text{m}^2$  a time of about 85,000 years is required.**

However, one has to take into account that the leakage rates calculated according to the permeability listed in the table above are maximum and steady state values! As long as the seal has not reached its maximum gas saturation after breakthrough, the effective permeability will not be at a maximum (Hildenbrand et. al., 2004). Values for a saturation (or capillary pressure) dependent effective permeability, however, are not available for the Namurian rocks.

Additionally, one has to take into account capillary phenomena. Reported gas entry pressures for the Westphalien and Namurien lithologies are as high as  $15$  and  $24$   $\text{MPa}$ , respectively (Laenen et al, 2005). These pressures would correspond to a theoretical static  $\text{CO}_2$  column of  $4000$  to  $7000$  m. According to Laenen et al. (2005) the total maximum reservoir height (top of reservoir to spill point) is  $204$  m. Assuming the reservoir to be filled down to the spill point a maximum overpressure of  $0.7$   $\text{MPa}$  could be established, which is much below the mentioned entry pressures. **Therefore, on can state that no gas volume flow through the intact Poederlee structure will be established.**

Fracturing of the seal by overpressure generation during injection is unlikely until roughly  $80\%$  of the lithological pressure has been overcome, thus for pressures above  $30$   $\text{MPa}$  ( $P_{\text{litho}} \sim 38$   $\text{MPa}$  at  $1500$  m depth). Numerical modelling (see next chapter) shows that for an injection rate of  $0.05$   $\text{kg/s}$  ( $4320$   $\text{kg CO}_2/\text{day}$ ) the maximum pressure at the top of the seal is  $23$   $\text{MPa}$ , thus below fracture pressure.

**In conclusion, only the diffusional  $\text{CO}_2$  transport must be taken into account for the Poederlee structure, with maximum steady-state diffusive leakage rates through the seal as low as  $6\text{E-}6$   $\text{kg/m}^2/\text{year}$  (table 5-8). If  $\text{CO}_2$  would escape at these velocities from the reservoir some  $1\text{E}8$  years would be necessary for leakage up to the surface.**

Table 5-9: Potential maximum leakage rates ( $Q$ ) through the Namurian caprock, assuming an overpressure of 0.7 MPa and permeabilities of  $1E-20$  and  $1E-21$  m<sup>2</sup>.  $P_{gas}$  is the overpressure generated by the gas column,  $P_2$  and  $P_1$  are the pressures at the top and the bottom of the seal,  $\Delta x$  is the thickness of the seal,  $P_{hydro}$  is the hydrostatic pressure,  $P_{litho}$  is the lithological pressure,  $\eta$  is the gas viscosity (NIST database),  $Q(k_{eff})$  and  $Q(D_{eff})$  are the leakage rates due to viscous volume flow and diffusion. For diffusion a dissolved CO<sub>2</sub> mass fraction of 0.06 (Pruess, 2005), a reservoir porosity of 0.015 and an effective diffusion coefficient of  $1E-10$  m<sup>2</sup>/s has been taken.

$\kappa_{eff}$ (m <sup>2</sup> )	$P_{gas}$	top of seal ( $P_2$ )	$P_2$ ( $P_r$ )	bottom seal ( $P_1$ )	$P_1$ ( $P_{hydro} + P_{gas}$ )	$\Delta x$	$P_{hydro}$	$P_{litho}$	$\eta$ *	$Q$ (kg/m <sup>2</sup> /year)	$Q(D_{eff})$ (kg/m <sup>2</sup> /year)
<b>1E-20</b>	0.69	989	9.7	1486	15.3	497	14.6	37.9	5E-5	6E-2	6E-6
<b>1E-21</b>										6E-3	

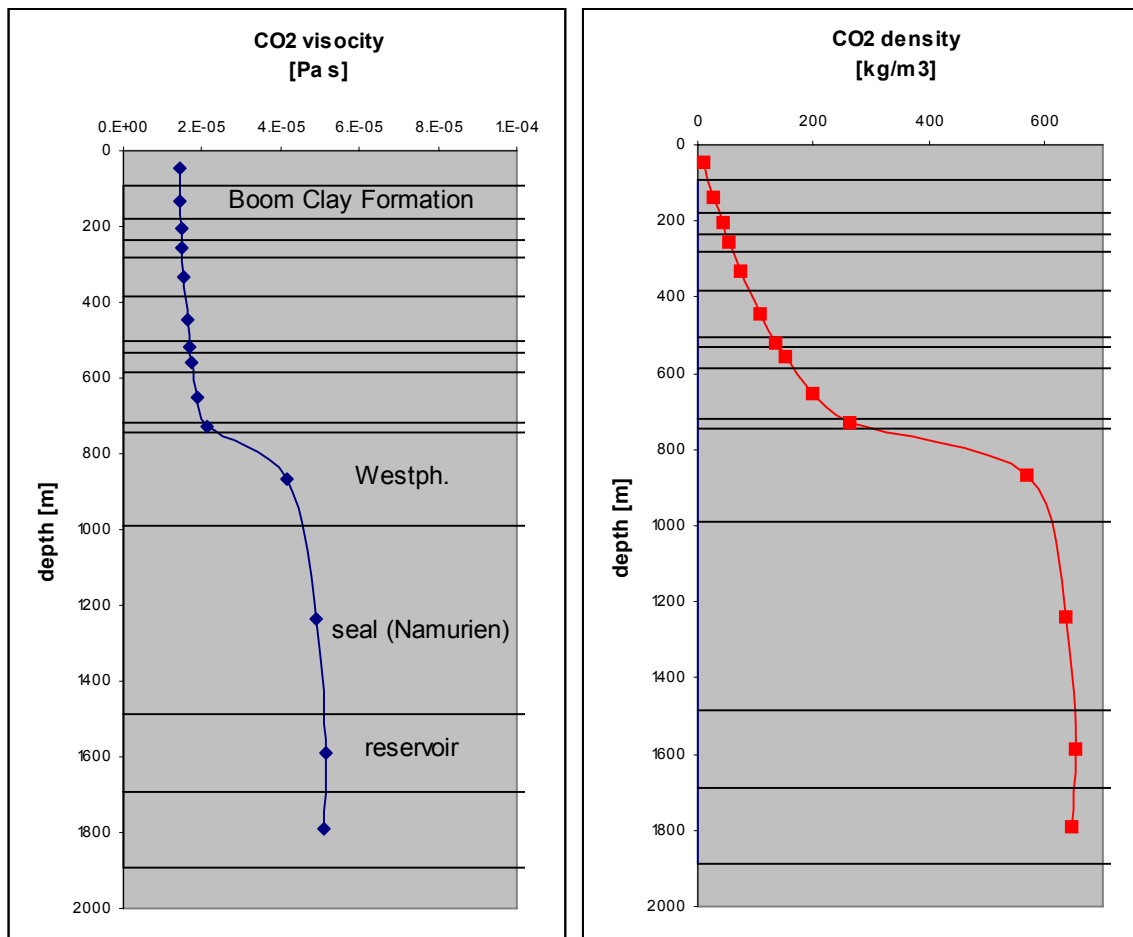


Figure 5-7: CO<sub>2</sub> viscosity and density as a function of depth (NIST database).

### 5.8.2.2 Dynamic pressure (injection) history

Numerical modelling was performed in order to make an estimation about the pressure history during and after CO<sub>2</sub> injection. For this purpose a very simplified isothermal (55 °C) model with only three different lithologies was designed. In this model the pressure development only depends on the fluid flow characteristics of the surrounding lithologies: the seal and the

less conductive rocks below the reservoir (fig. 5-11). The lithologies below and above this structure were set to a unique lithology with high porosity and permeability to allow a non-limited flow regime at larger distances. The sides/boundaries of the model were set to fixed pressure conditions. The total number of cells is 6860. The injection rate is 0.05 kg/s, which is approximately 4320 kg CO<sub>2</sub>/day or 1.6 kg/year. Diffusion was set to 1E-10 m<sup>2</sup>/s of CO<sub>2</sub> in water.

It is shown that the pressure builds up until CO<sub>2</sub> is able to penetrate the underlying less permeable layers (overcoming the capillary pressures) and migrates sideways (at time 8.6E7 s ~ 34 month). Thereafter pressure successively drops, which is additionally supported by the dissolution of CO<sub>2</sub> and the downward movement of the heavier CO<sub>2</sub> enriched water. The maximum pressure at the top of the seal reached in this scenario is 23 MPa, which is 7 MPa above the hydrostatic pressure (fig. 5-9).

As predicted above, no CO<sub>2</sub> is able to migrate through the seal, nor by a distinct volume flow nor by diffusion. Figure 5-12 shows the gas saturation development within the reservoir during injection. Figure 5-10 shows the distribution of the dissolved CO<sub>2</sub>, which starts to move downwards because of density differences. Figure 5-13 the pressure plot reveals that after a time of 200 years the pressure is nearly equilibrated to hydrostatic conditions.

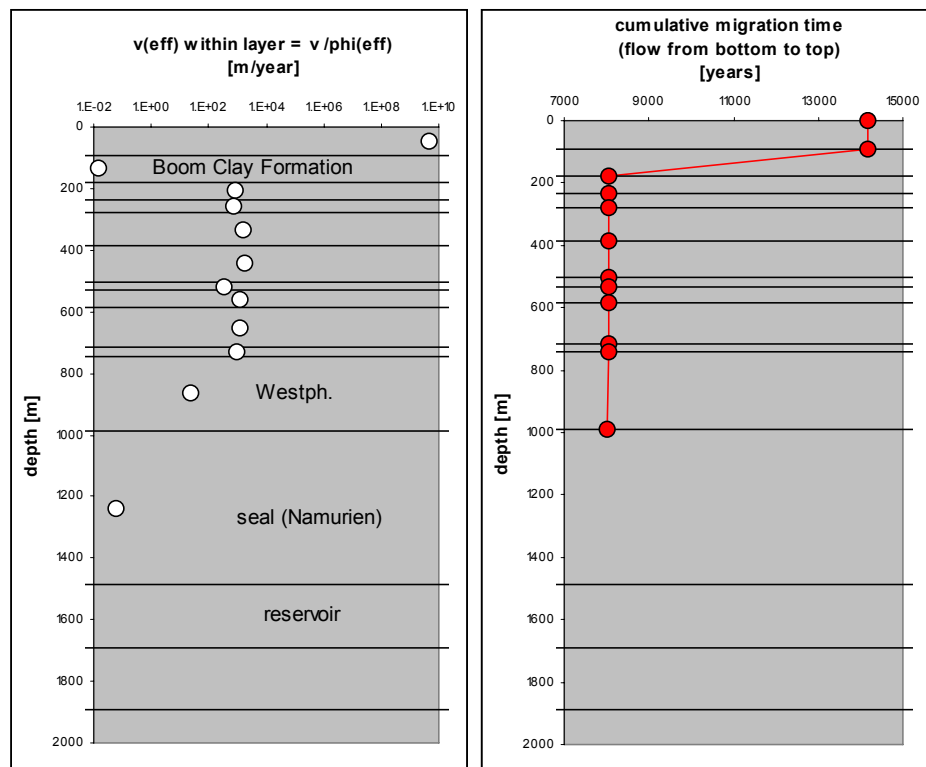


Figure 5-8: (left) Volume flow velocity [m<sup>3</sup>/m<sup>2</sup>/year] within each layer, assuming that only 10% of the porosity serves for gas transport and (right) cumulative time necessary for leakage up to the top. The top of the seal is located at about 1000 m depth. The calculation is based on the petrophysical properties listed in table 5-8.

Pressure profile for isothermal 2D model of Poederlee (55°C)

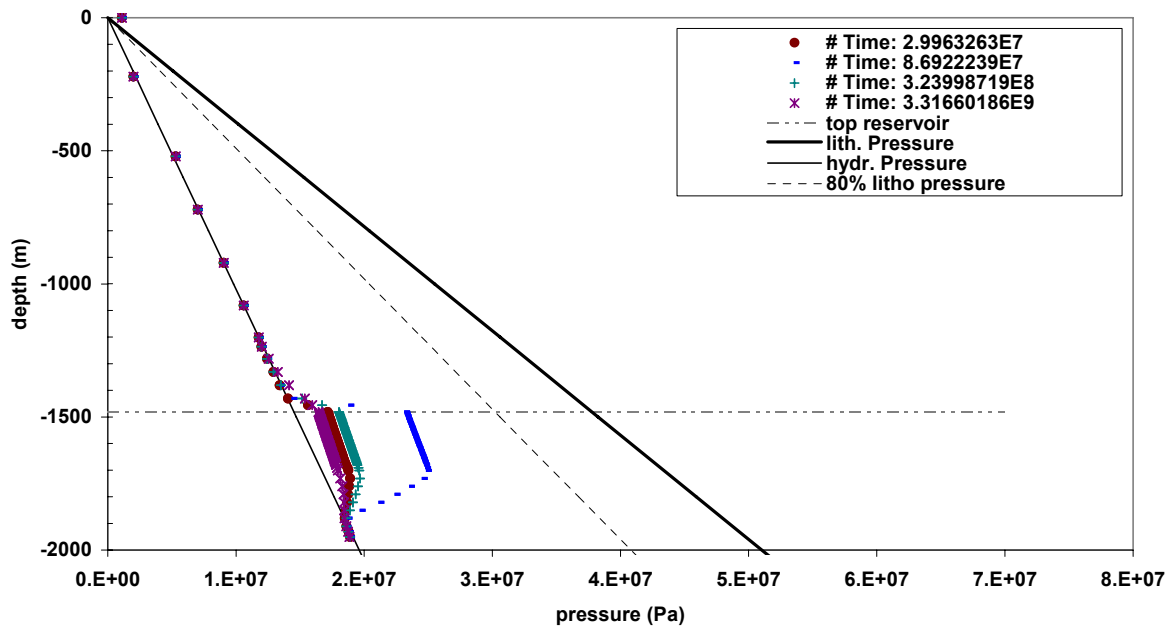


Figure 5-9: Pressure as a function of depth for different times of injection.

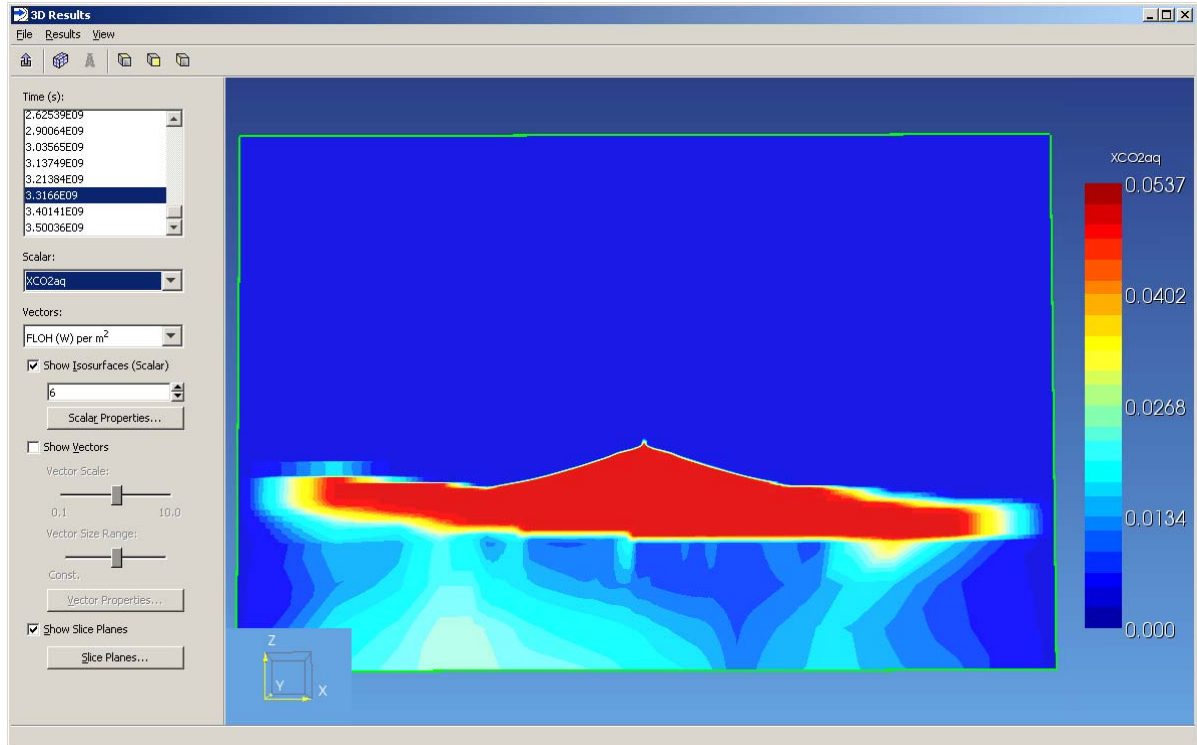


Figure 5-10: Mass fraction of dissolved CO<sub>2</sub> after 100 years.

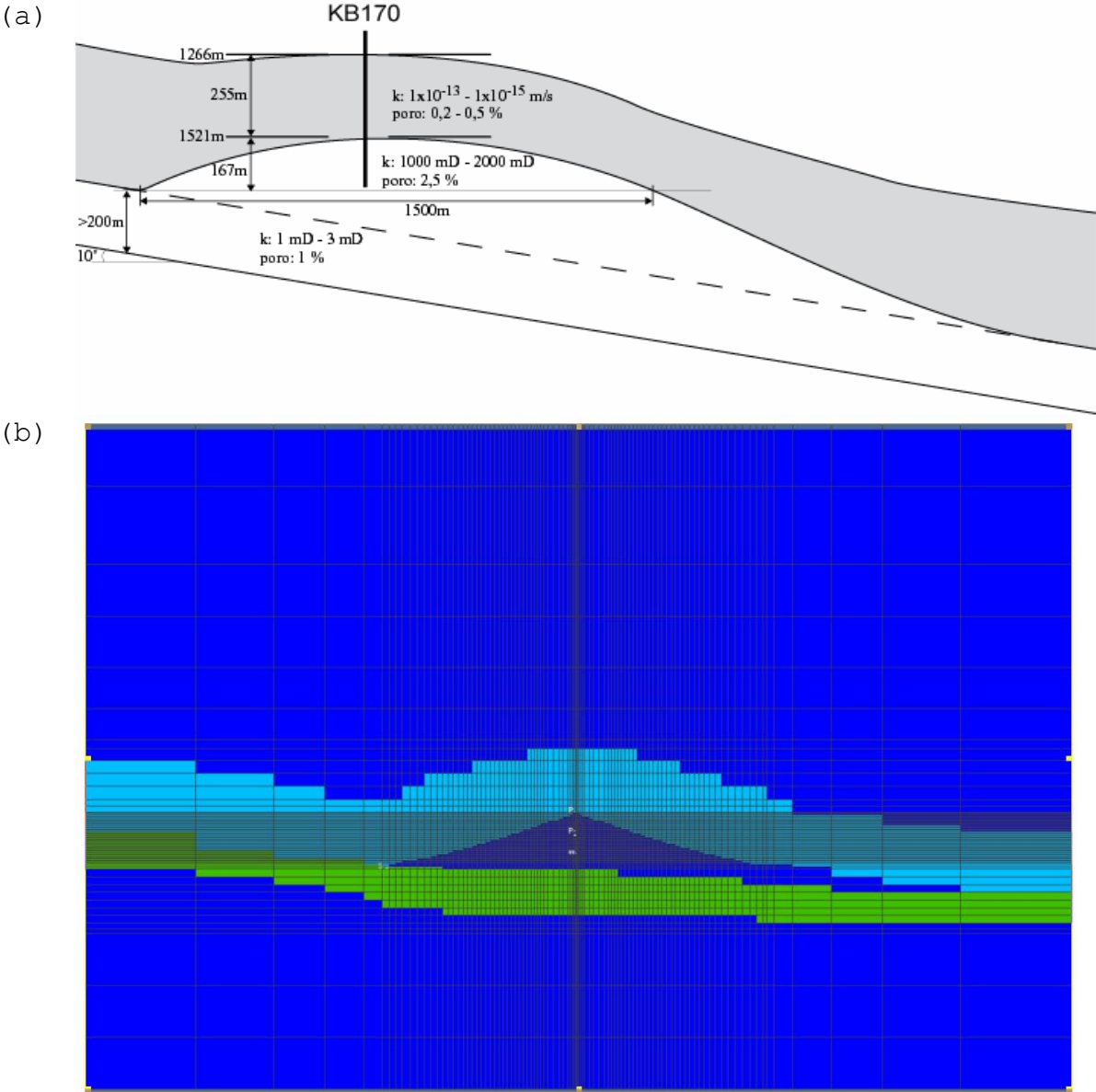


Figure 5-11: (a) Simplified Poederlee structure, (b) mesh of the 2D model.

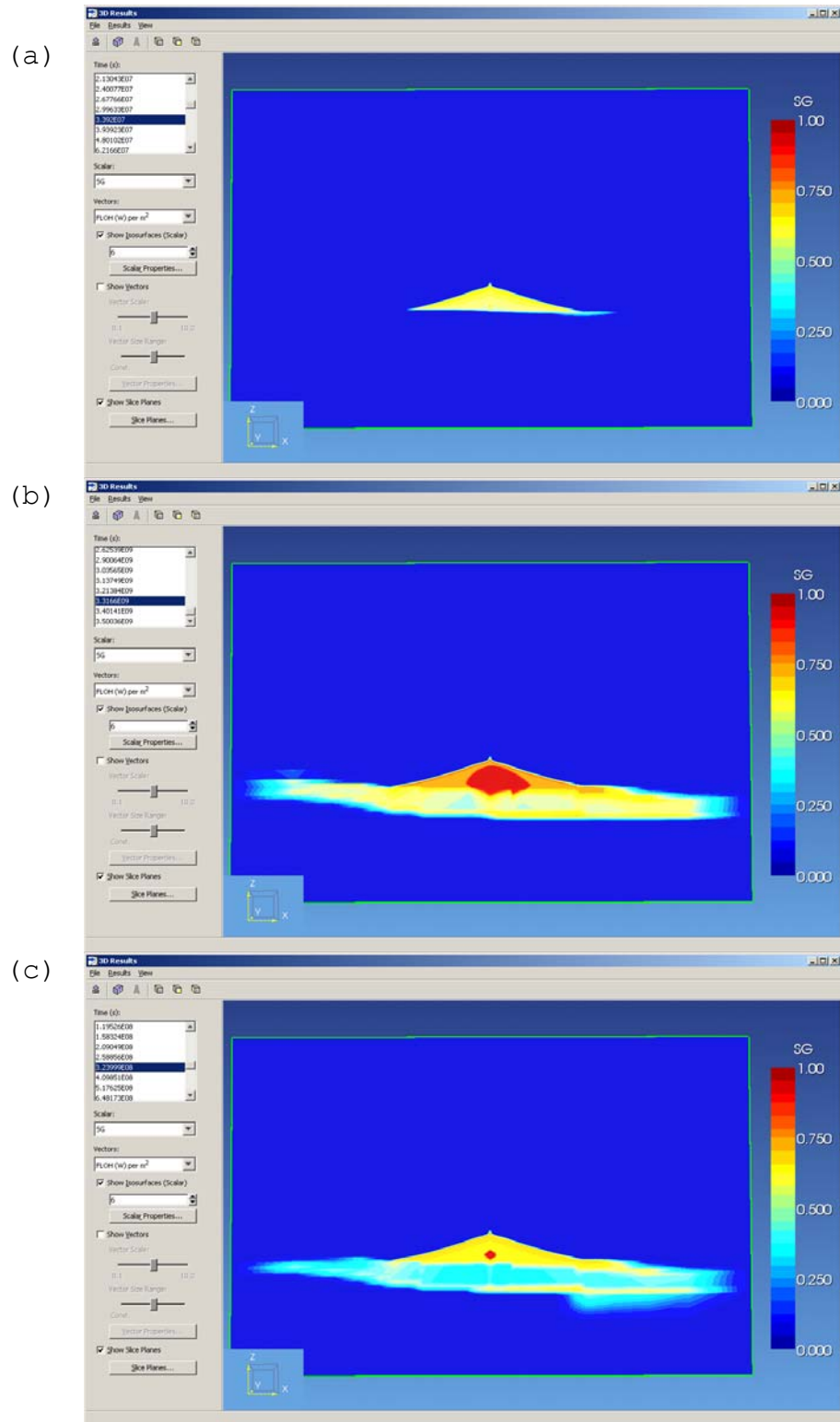


Figure 5-12: Gas saturation after (a) 1 year, (B) 10 years, and (C) 100 years of injection. After 10 years approx.  $17 \cdot 10^6$  kg of  $\text{CO}_2$  were injected.

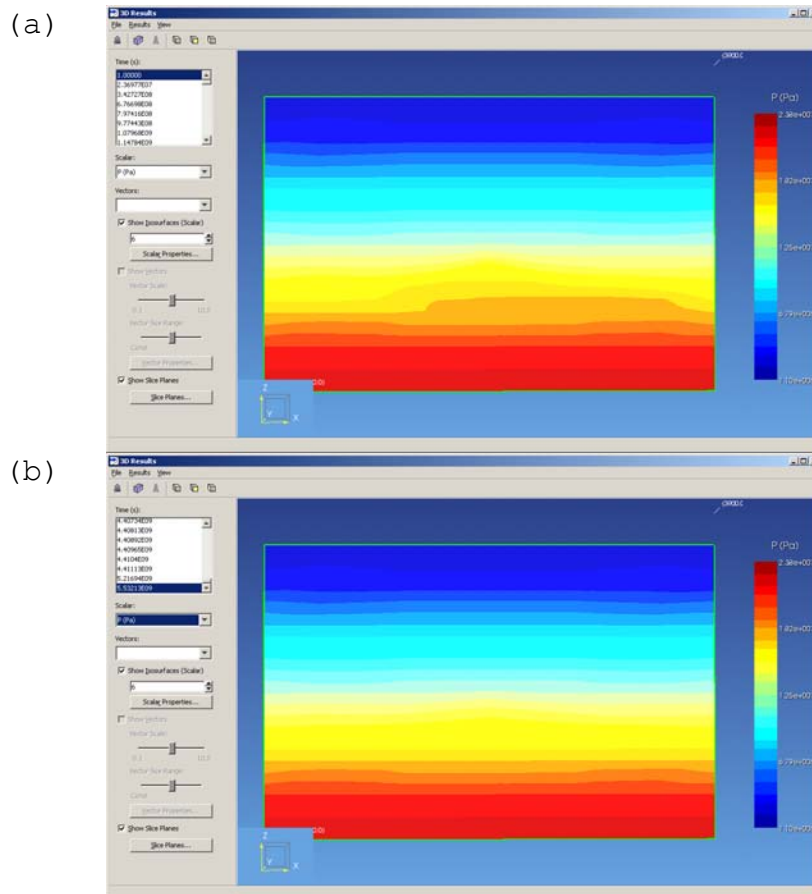


Figure 5-13: Pressure after ca. 100 years Pressure after ca. 200 years.

### 5.8.3 The Verloren Kamp structure

The following leakage (risk) estimations are done for a structure described by Laenen et al. (2006). In this report the presence of a dome structure was deduced in the Triassic sequence between the Elen and Siemkensheuvel faults (fig. 5-14). The dome is covered by upper Triassic and Jurassic sediments. The structure is approximately 7 km long, and 1.5 km wide. The surface area is approximately 7 km<sup>2</sup>. The Elen Fault constitutes the western edge of the structure. The top of the structure is situated at a depth of  $\pm 1530$  m. The spill point lies at a depth of approximately 1630 m (fig. 5-14). Hence, the estimated height of the structure is 100 m, corresponding to a static gas column pressure of 0.34 MPa. The volume of the structure is  $233 \times 10^6$  m<sup>3</sup>.

Based on well data KB99 and on Laenen et al. (2006) the overburden and its petrophysical properties were estimated in order to set up a leakage model like in the previous chapter (table 5-10). Again, a geothermal gradient of 32 °C/km and a hydrostatic pressure of approx. 10 MPa/km was used in order to derive the viscosity and density data for CO<sub>2</sub> (fig. 5-15). Following the concept described above it is shown, that for the case of a CO<sub>2</sub> leakage out of the reservoir, and assuming permeability values for the seal of 1E-19 to 1E-20 m<sup>2</sup>, a time of approx. 16,000 years would be necessary for leakage up to the surface (fig. 5-16). However, one has to take in mind that the permeabilities used are only estimations; measurements are not available.

With respect to the risk for leakage by means of capillary entry pressure, no measured capillary data are available for the Triassic/Jurassic sediments. According to Hildenbrand et. al. (2004) a correlation exist between the effective permeability and the capillary entry pressure:

$$\log (P_d / [\text{MPa}]) = -0.38 \cdot \log (k_{eff} / [\text{m}^2]) - 7.84 \quad R^2 = 0.70$$

According to this formula a risk for leakage would be given if the permeability of the rocks is in the order of  $1\text{E-}19 \text{ m}^2$ , corresponding to capillary entry pressures of 0.24 MPa. Thus leakage would occur when the gas column has reached a height of 70 m. For the case that the effective permeability is smaller ( $1\text{E-}20 \text{ m}^2$ ), the capillary entry pressure increases as such, that the sealing efficiency would be appropriate for a save  $\text{CO}_2$  storage.

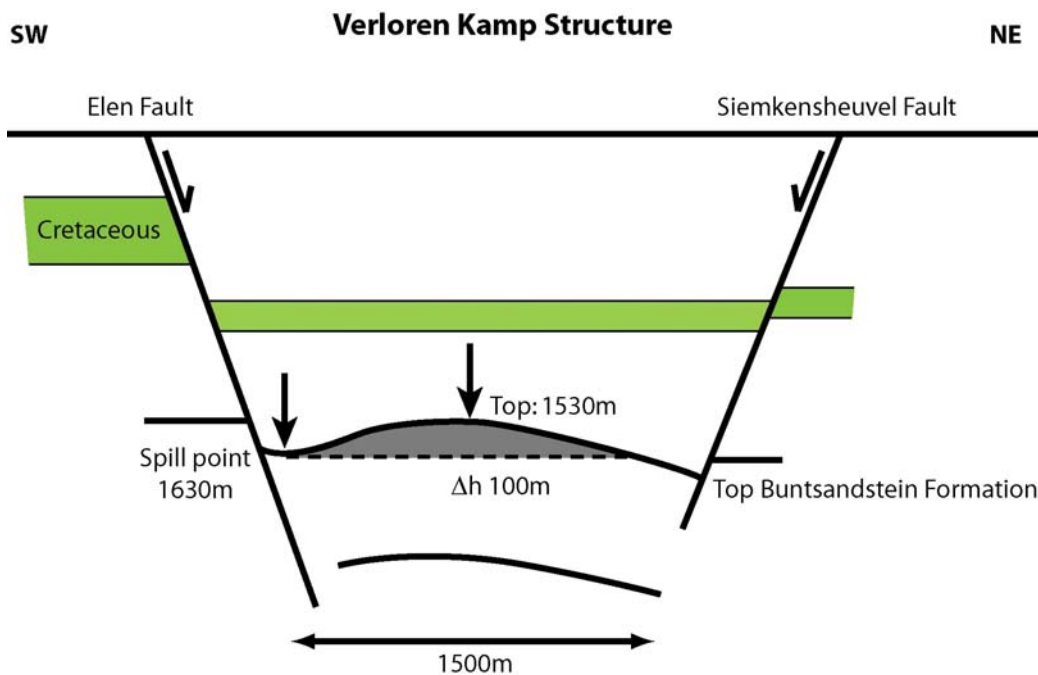


Figure 5-14: Conceptual model of the Verloren Kamp structure (not to scale; after Laenen et al, 2006).

Table 5-10: Estimated petrophysical properties of lithologies occurring at well KB99 and Laenen et al. (2006).

	Base of sequence; depth m.b.s. (meters below surface)	lithology	Rock density (g/cm <sup>3</sup> )	He porosity (fraction)	permeability (m <sup>2</sup> )	Calculated capillary entry pressure (Pa)
<b>Quarternary/Tertiary</b>	1120	Sand, grind, clay	2.6	0.2	1e-12	0.00
<b>Cretaceous</b>	1170	Marl, limestone, shale		0.25	1E-15	0.01
<b>Jurassic</b>	1250	shales		0.1	1e-20	0.58
<b>Upper Triassic (Keuper/Sleen)</b>	1440	Shales, silt, marls		0.05	1e-19	0.24
<b>Middle Triassic (Roet/Muschelkalk)</b>	1530	Shales with limestone, tight sandstones				
<b>Lower Triassic Buntsandstein Formation</b>	1630	sandstone		0.13	3.7E-14	0.00

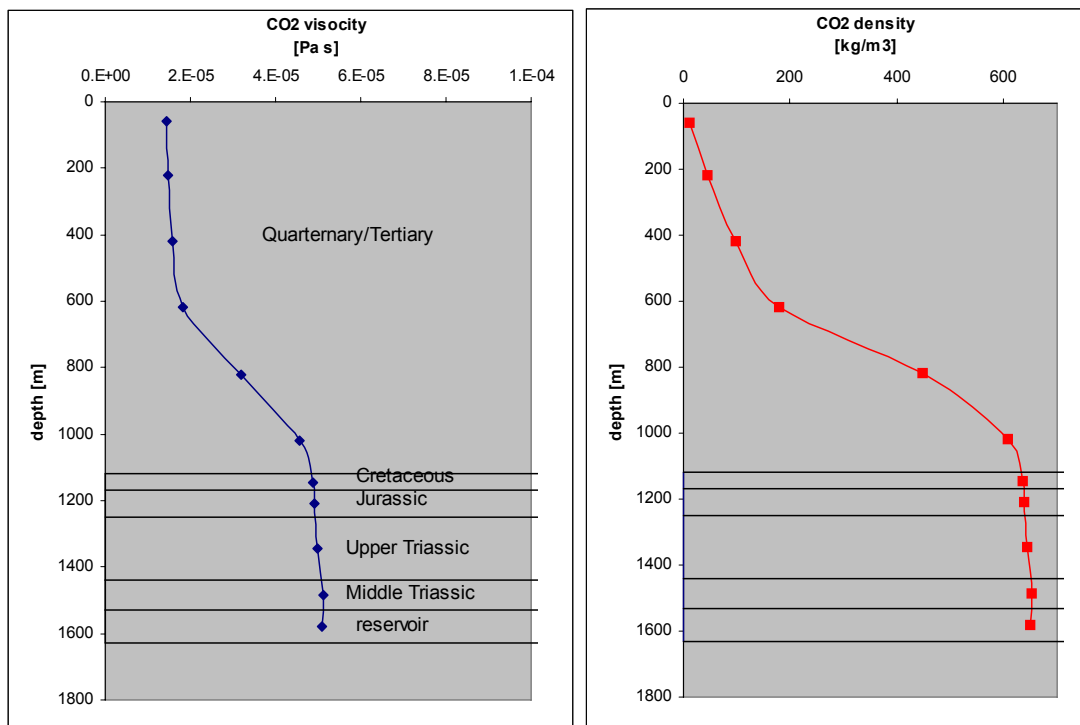


Figure 5-15: CO<sub>2</sub> viscosity and density as a function of depth (NIST database).

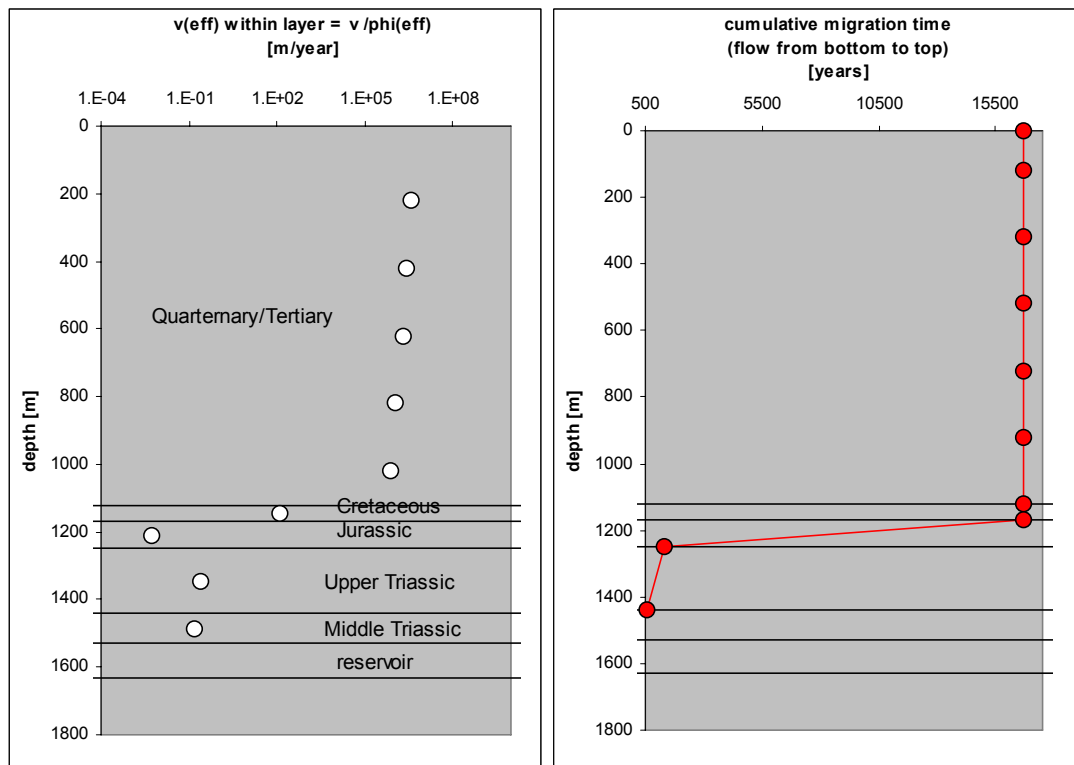


Figure 5-16: (left) Volume flow velocity [ $m^3/m^2/year$ ] within each layer, assuming that only 10% of the porosity serves for gas transport and (right) cumulative time necessary for leakage up to the top. The top of the seal is located at about 1000 m depth. The calculation is based on the petrophysical properties listed in table 5-10.

## 5.9 References

- ANL (2007) Argonne National Laboratory. Appendix 3: Oxygen Deficiency Hazards (OHD). Online source <http://www.phy.anl.gov/div/esh/Cryogenic/Appendix%203/Appendix%203.htm>.
- Bachu, S., 2000: Sequestration of CO<sub>2</sub> in geological media: criteria and approach for site selection in response to climate change. *Energy Conversion and Management*, 41, 9, pp. 953-970.
- Bachu, S., Gunter, W.D. & Perkins, E.H., 1994: Aquifer disposal of CO<sub>2</sub>: hydrodynamic and mineral trapping. *Energy conversion and management*, 35, pp. 269-279.
- Benson S., L. Myer (2002) Monitoring to ensure safe and effective geologic sequestration of carbon dioxide. In: IPCC workshop on carbon dioxide capture and storage, Regina.
- Bertier, P., Swennen, R., Laenen, B., Lagrou, D. & Dreesen, R., 2006: Experimental identifications of CO<sub>2</sub>-water-rock interactions caused by sequestration of CO<sub>2</sub> in Westphalian and Buntsandstein sandstones of the Campine Basin (NE Belgium). *Journal of Geochemical Exploration*, 89, 2006, pp. 10-14.
- BIG (2007) Brandweerinformatiecentrum Gevaarlijke Stoffen (Fireman Department Information Centre – Hazardous Substances). Online source <http://www.big.be>.
- Busch, A., Alles, S., Krooss, B. & Dewhirst, D., 2007: Potential of cap rocks as CO<sub>2</sub> storage reservoirs. *Geophysical Research Abstracts*, vol. 9, 06734. European Geosciences Union General Assembly, Vienna, Austria, 15-20 April 2007.
- CCOHS (1997) Canadian Centre for Occupational Health & Safety. Online source <http://www.ccohs.ca/oshanswers>.
- Chadwick, A., Arts, R., Bernstone, C., May, F., Thibeau, S. & Zweigel, P. (eds), in Gelein De Koeijer (ed.), 2007: Best practice for the storage of CO<sub>2</sub> in saline aquifers. Observations and guidelines from the SACS and CO2STORE projects. Statoil, 273 p.

- Chernichowski-Lauriol, I., Rochelle, C., Gaus, I., Azaroual, M., Pearce, J. & Durst, P., 2006: Geochemical interactions between CO<sub>2</sub>, pore-waters and reservoir rocks. Lessons learned from laboratory experiments, field studies and computer simulations. In: Lombardi, S. et al (eds): Advances in the geological storage of carbon dioxide, pp. 157-174. NATO Science Series, IV; Earth and Environmental Sciences, vol. 65, Springer
- Damen K. A. Faaij, W. Turkenburg (2006) Health, safety and environmental risks of underground CO<sub>2</sub> sequestration. *Climate Change* 74 (1-3):289-318.
- Health Canada (2007) Canadian exposure guidelines for residential air quality. Online source: [http://www.hc-sc.gc.ca/ewh-semt/pubs/air/exposure-exposition/appendix-a-annexe\\_e.html](http://www.hc-sc.gc.ca/ewh-semt/pubs/air/exposure-exposition/appendix-a-annexe_e.html)
- Hildenbrand, A., Schlomer, S., Krooss, B.M., Littke, R., 2004: Gas breakthrough experiments on pelitic rocks: comparative study with N<sub>2</sub>, CO<sub>2</sub> and CH<sub>4</sub>. *Geofluids*, 4 (1), pp. 61-80.
- Holloway S. Safety of the underground disposal of carbon dioxide. Proceedings of the third international conference on carbon dioxide removal, Boston, MA; 8–11 September, 1996.
- Holloway, S, 1997: safety of underground disposal of carbon dioxide. *Energy Conservation and management*, 38, pp. 241-245.
- IEA & OECD, 2004: Prospects for CO<sub>2</sub> capture and storage. CCS characteristics: technologies, potential, permanence and cost, pp.90-92 – 94-97
- IPCC, 2005: IPCC Special Report on Carbon Dioxide Capture and Storage. Prepared by Working Group III of the Intergovernmental Panel on Climate Change [Metz, B., O. Davidson, H. C. de Coninck, M. Loos, and L. A. Meyer (eds.)]. Cambridge University Press, Cambridge, United Kingdom and New York, NY, USA, 442 pp.
- Jaffe P.R., S. Wang (2003) Potential effect of CO<sub>2</sub> releases from deep reservoirs on the quality of fresh-water aquifers. In: Gale J. and Kaya Y. (eds.) Sixth International Conference on Greenhouse Gas Control Technologies, Kyoto, Japan, vol. II. Amsterdam: Pergamon p1657-1660.
- Johnson, J.W. & Nitao, J.J., 2003: Reactive transport modeling of geologic CO<sub>2</sub> sequestration at Sleipner. In: Gale, J. & Kaya, Y. (eds). Sixth International Conference on Greenhouse Gas Control Technologies, Kyoto, Japan, Vol. I? Pergamon, pp. 327-323.
- Laenen, B., Broothaers, M., Lagrou, D., 2006. Inventory of the CO<sub>2</sub> storage potential within deep saline aquifers. Study commissioned by the Belgian Federal Science Policy Office, WP 2.3, Vito report 2006/MAT/R/188.
- Laenen, B., van Tongeren, P., Dreesen, R. , De Koninck, R., Hildenbrand, A., 2005. Re-evaluation of the gas storage potential of the poederlee structure. Internal report (2005/MAT/T/214).
- Le Guern F, Sigvaldason GE, editors. The Lake Nyos event and natural CO<sub>2</sub> degassing. *J Volcanol Geotherm Res*, 39, 1989. p. 95–276.
- Lemmon EW, McLinden MO, Friend DG (2001) Thermophysical properties of fluid systems. In: NIST Chemistry WebBook, NIST Standard Reference Database Number 69, (ed. PJ Linstrom, WG Mallard), National Institute of Standards and Technology, Gaithersburg MD, 20899 (<http://webbook.nist.gov/chemistry>).
- Lombardi, S., Annunziatellis, S.E. & Ciotoli, G., 2006 : Near-surface gas geochemistry techniques to assess and monitor CO<sub>2</sub> geological sequestration sites. The use of natural analogue sites in Italy as field laboratories. In: Lombardi, S. et al (eds.), Advances in the geological storage of carbon dioxide, pp. 141-156. NATO Science Series, IV; Earth and Environmental Sciences, vol. 65, Springer
- Metz, B., Davidson, O., De Coninck, H., Loos, L. & Meyer, L. (eds), 2005: Carbon dioxide capture and storage. IPCC Special Report. Prepared by Working Group III of the Intergovernmental Panel on Climate Change. Cambridge University Press, Cambridge, UK, 442 p.
- NIH (2007) National Institute of Health. Hazardous Substances Data Base – HSDB. Online source <http://toxnet.nlm.nih.gov>.
- NIOSH (1991) National Institute for Occupational Safety and Health. Building Air Quality. A guide for building owners and facility managers. Oline available at <http://www.cdc.gov/niosh/pdfs/iaq.pdf>
- OVAM (1996). Basisinformatie voor risico-evaluaties. D/1996/5024/19. OVAM, Mechelen, België.
- Pearce, J.M., 2006: What can we learn from natural analogues? An overview of how analogues can benefit the geological storage of CO<sub>2</sub>, in: S. Lombardi et al (eds.): Advances in the geological storage of carbon dioxide. NATO Science series, IV. Earth and Environmental Sciences – Vol. 65, pp. 129-139, Springer.
- Plumier, A., Doneux, C., Camelbeeck, Th., Van Rompaey, G., Jongmans, D., Wathélet, M., Teerlynck, H. & Nguyen, F., 2005: Seismic risk assessment and mitigation for Belgium in the frame of EUROCODE 8., 69 p, BELSPO, Politique Scientifique Fédérale.

- Pruess, K., 2005. ECO2N: A Tough2 Fluid Property Module for Mixtures of Water, NaCl, CO<sub>2</sub>. LBNL-57952, 66pp.
- Reid RC, Prausnitz JM, Poling BE (1988) The properties of gases and liquids, McGraw-Hill, New York, 741 pp.
- Saripalli, K.P., Mahasenan, N.M. & COOK, E.M., 2003: Risk and hazard assessment for projects involving the geological sequestration of CO<sub>2</sub>. In: Gale, J. & Kaya, Y. (eds). Sixth International Conference on Greenhouse Gas Control Technologies, Kyoto, Japan, Vol. I. Pergamon, pp. 511-516.
- Sminchak, J. & Gupta, N., 2002: Issues related to seismic activity induced by the injection of CO<sub>2</sub> in deep saline aquifers. Journal of Energy & Environmental Research, US DOE, NETL, vol.2 n° 1, pp. 32-46.
- Stephens, J. & Keith, D., 2005: Health, safety and environmental risks of CO<sub>2</sub>-storage, in: Delphi Group & Alberta Research Council: Building capacity for CO<sub>2</sub> capture and storage in the APEC region. A training manual for policy makers and practitioners. APEC Energy Working Group. Project EWG 03/2004T, March 2005. Module 8.
- TÜV Süddeutschland (2000) Luftqualität und Schadstoffe in Innenräumen. Physikalische, chemische und biologische Risikofaktoren, Messverfahren und Analytik, Untersuchungsstrategie, Bewertungsmaßstäbe und Sanierungsverfahren. <http://www.tuev-sued.de>
- W&G (2007) Wonen en gezondheid: 1 luchtkwaliteit. Online publication: ([http://www.gezondheid.be/index.cfm?fuseaction=art&art\\_id=2305](http://www.gezondheid.be/index.cfm?fuseaction=art&art_id=2305))
- Wang, S. & Jaffé, P.R., 2004. Dissolution of trace metals in potable aquifers due to CO<sub>2</sub> releases from deep formations. Effect of dissolution kinetics. Energy Conversion and Management, vol. 45, 18-19, p. 2833-2848.
- WDHFS (2005) Wisconsin Department of Health and Family Services. Chemical Fact Sheets – Carbon Dioxide (CO<sub>2</sub>). Online source: <http://www.dhfs.state.wi.us/eh/ChemFS/fs/CarbonDioxide.htm>.
- Zweigel, P., Lindberg, E.G.B. 2003: Leakage rate - the main quality criterion for underground CO<sub>2</sub> storage. Third Nordic Mini symposium on Carbon Dioxide Capture and Storage, 2-3 October 2003, Trondheim, Norway.



## 6 MARKAL Model

The potential development of CO<sub>2</sub> Capture and Storage in Belgium has been evaluated with the Markal model in collaboration with VITO (Flemish Institute for Technological Research). VITO uses Markal since 1992.

Markal (acronym for MARKET ALlocation) is a dynamic<sup>22</sup>, process oriented<sup>23</sup> optimization model of an energy system developed by the Energy Technology Systems Analysis Programme (ETSAP) of the International Energy Agency (IEA). In Belgium, maintaining the database of Markal and this international collaboration in ETSAP is funded by Federal Science Policy. Mostly, Markal is used with the linear programming (LP) variant. Markal describes both the energy supply and demand side of the energy system. As a result, this modelling framework has contributed to national and local energy planning, and to the development of carbon mitigation strategies. Implementation in more than 40 countries indicates wide acceptability.

### 6.1 Markal methodology

The Markal model is a software that enables a user to represent a complex energy system - national, regional, local, or sectorial- as a linear system. We generally call 'model' the combination of this software with a database specific to the energy system being modelled.

#### 6.1.1 Presentation of Markal

The database specifies the energy demands -industrial, commercial, residential, and transportation- that will need to be satisfied over a specified time horizon which is divided into a number of time-periods. It describes the available sources of supply of energy, either domestic resources or imports of oil, coal, natural gas, nuclear fuel, and renewable energy sources. It provides a menu of technologies for extracting, transporting, converting, and using energy, both existing technologies and those expected to be available within the time horizon of the model. The essential characteristics of the technologies are specified: for example, their investment cost, operating and maintenance costs, service life, fuel use, efficiency, availability, emissions, existing installed capacity, and maximum expected market penetration. A distinction is made between existing technologies and new technologies that could be added. The investment costs of existing technologies are treated as sunk costs and thus not taken into account in the total cost of the energy system.

In addition to time-periods, Markal recognizes three seasons (Winter, Summer, Intermediate), and two diurnal divisions (Day, Night). These time divisions result in six time-slices. Time-slices are implemented only for technologies producing electricity (seasonal and diurnal) or low-temperature heat (seasonal), both of which may not be easily stored and thus require a finer time disaggregation than other energy carriers. In addition, a peak requirement is imposed for these two energy carriers, which forces enough additional capacity to be installed to meet the peak demand.

The model chooses the best combination of these technologies (existing equipment and investments in new technologies) to satisfy the projected energy demands. A linear program is a set of linear equations (or, more precisely, inequations that specify "greater than" or "less than" relationships) with variables and coefficients. All these equations are constraints. A

---

<sup>22</sup> Investment decisions can not be separated from what is happening in other time-slices (seasons and night / day / peak) or in other periods (future years).

<sup>23</sup> Also called Bottom-Up model, this has a rich representation of the variety of technologies (existing and / or future) available to meet energy needs, and, they often have the capability to track a wide variety of traded commodities. On the other hand, Top-Down models encompass macroeconomic variables beyond the energy sector proper, such as wages, consumption, and interest rates.

typical variable is the amount of installed capacity (which will be determined by the model) of a specified coal-fired power plant producing electricity. A typical coefficient (defined by the user) is the investment cost per installed kilowatt of such a plant. A typical constraint states that the installed capacity of such a power plant must be less than or equal to the maximum projected capacity in a future year, also defined by the user. There are also non specific constraints (i.e. not defined by the user). For example, supply must be superior or equal to demand.

A function of the variables, called the objective function, is minimized or maximized subject to the specified constraints. In a typical Markal model, the total cost of the energy system over the entire time horizon is minimized subject to limited resource supply and other constraints. This total cost is the sum of the discounted present value of the stream of annual costs incurred in each year of the horizon. This means that a spending realised in a distant future will have a smaller weight in the evaluation than an immediate spending.

$$NPV = \sum_{t=1}^{t = NPER} (1 + d)^{NYRS(1-t)} \cdot AnnCost(t) \cdot \left( 1 + (1 + d)^{-1} + (1 + d)^{-2} + \dots + (1 + d)^{1 - NYRS} \right) \quad (42)$$

where:

NPV = net present value of the total cost (the Markal objective function)

ANNCOST(t) = annual cost for period t, discussed below

d = general discount rate, equal to 5%<sup>24</sup> as advised by VITO

NPER = number of periods in the planning horizon

NYRS = number of years in each period t

The total annual cost ANNCOST(t) is the sum over all technologies, all demand segments, all pollutants, and all input fuels, of the various costs incurred, namely: annualized investments<sup>25</sup>, annual operating costs (including fixed and variable technology costs, fuel delivery costs, costs of extracting and importing energy carriers), minus revenue from exported energy carriers, plus taxes on emissions.

The solution of the linear program describes a set of energy technologies (capacities and operating levels) and energy flows that constitute an energy system that is feasible and optimal. Feasibility means that all the numbers add up correctly and that all the constraints are satisfied. Optimality means that of the hundreds or thousands of feasible solutions, this is the one that has the lowest cost. The model chooses the least costly combination of technologies that satisfies the specified demand. Beginning with the least costly technology, some candidate technology will be used up to its maximum market penetration potential. At the margin, one or several technologies will probably be used at less than their maximum.

<sup>24</sup> The choice of discount rate depends on the approach (prescriptive versus descriptive) used. A prescriptive approach typically uses lower discount rates, especially for long-term issues like climate change. Lower discount rates (4% to 8%) may also be used to appraise public sector projects. A descriptive approach uses relatively high rates (10% to 30%).

<sup>25</sup> The annualized unit investment cost is obtained via the following formula:

$$ANNUALIZED\_INVCOST = INVCOST / \sum_{j=1}^{LIFE} (1+h)^{-j}$$

where:

INVCOST is the unit investment cost of a technology

LIFE is the physical life of the technology

h is the discount rate used for that technology. If the technology specific discount rate is not defined, the general discount rate d is used instead.

The Markal linear programming solution gives also an interesting characteristic called the shadow price. For each constraint the shadow price tells us how much the objective function will change if we change the right-hand side of the corresponding constraint of one unit. It is often called the “marginal value” or “dual value” for that constraint. Note that, if the constraint is loose the shadow price is zero (as if the constraint is loose a small change in the right-hand side cannot alter the optimal solution). For example, for a constraint on technology capacity, the shadow price indicates the value of an additional unit of this technology by the difference it would make in the total system cost. Indeed, an additional unit of different technologies may bump out of the solution different marginal technologies so changing the total system cost. The shadow price makes it possible to compare on the same scale the value of an additional unit of capacity of different technologies. This sensitivity information gives us a measure of how robust the solution is i.e. how sensitive it is to changes in input data. This only holds for very small changes (that is why marginal) thus no extrapolation is possible; that is the reason why we do scenarios.

### 6.1.2 Presentation of the electricity model

The energy predictions for the electricity sector in Belgium have been developed by VITO with a detailed Markal model (to the level of individual power plants). The problem is how to generate the specified electricity demand at the lowest cost. It is possible to include several additional constraints. For example, a limitation on pollutants emission can be imposed or a penalty can be applied if specific conditions are not respected. A percentage of electricity generation by renewables can be forced and so on.

The time horizon of the model extends from 2004 to 2030 with 2 years time-periods. According to the current evolution, it seems that power plants fitted with CO<sub>2</sub> capture will only be available from 2025. So the major changes will take place between 2025 and 2050. However, VITO possesses only scenarios up to 2030. Nevertheless, it is sufficient to observe if these technologies are chosen by the model as soon as they appear on the market.

Given the specific situation of Belgian electricity sector, the choice has been made to model the sector for all the country. Indeed, Belgium owns a distribution grid that allows large transportation across regional borders. At regional level, supply and demand are not strictly linked. A rising demand in Flanders can be filled by a rising production in Wallonia and vice versa. Furthermore, Brussels consumes an appreciable amount of energy, but its production is marginal. Electricity stream goes beyond regional borders according to the grid load, the composition of the equipment park, the energy prices and others factors. Although electricity is also traded at international level, there exists in the committee of experts a general agreement that Belgium can be considered an entity on the electricity market.

Combined heat and power plants produce just as well electricity as heat. The efficiency of combined production can be higher than the separated production of the same quantity of electricity and heat with conventional installations. That is why an increase in combined heat and power plants results in an energy saving although this is not obvious in the reported figures (there is an increase in fuel consumption when CHP is used instead of conventional electricity generation).

Concerning CO<sub>2</sub> emissions, heat production and CO<sub>2</sub> related will vary according to the fraction of combined heat and power plants chosen by the model. To work on a same basis over the different scenarios, a device has been implemented. The heat demand, if not satisfied by cogeneration, will be produced with conventional methods (boiler). An important remark is that **‘total CO<sub>2</sub> emissions’ represent thus CO<sub>2</sub> emitted by the electricity sector plus CO<sub>2</sub> emitted to provide a certain amount of heat.**

### 6.1.3 Limits of the model

Each model is a simplification of the reality. In practice, it is generally difficult to take all conditions into account. Some conditions that in the reality can play a significant role are not taken into account in this model. For example, the model has no geographical localisation and can consequently not take into account the limitations of the grid. It is also the case for costs and losses of electricity transport and distribution. It will also be a problem to take account of the CO<sub>2</sub> transport cost. Power plants' flexibility to restart or stop in the model is higher than in the reality.

We use here the simplest version of Markal. Other versions are available for example to address changes in demand levels that respond to changes in energy prices or to deal with uncertainties (Stochastic Programming) or with endogenous technology learning. Some can be used in combination with each other. These versions have been created in order to get closer to the reality.

## 6.2 Reference scenario

The reference scenario (REF) constitutes the energy system skeleton. It comprises all the technologies and energy carriers that represent the energy system. The reference scenario represents a baseline that lets the energy system evolve based on existing legislation and measures and boundary conditions. This means that no post-Kyoto limits are set and that the decommissioning of the nuclear plants will take place. Some parameters have a large effect on the result and the uncertainty on those parameters is high. The difference between gas and coal prices in the future is an example. These uncertainties can be taken into account into different scenarios. The reference scenario is made up of the most probable values. It serves as a baseline for other scenarios.

Hereafter, the policies and measures as well as the assumptions on the evolution of a number of variables of the reference scenario are described. All of these influence the CO<sub>2</sub> emissions evolution.

### 6.2.1 Policies and measures

#### 6.2.1.1 Commitment under the Kyoto Protocol

The following measures introduced in the scenario are related to the Belgium's commitment under the Kyoto Protocol.

The promotion of renewable energies is taken into account by the introduction in the scenario of green certificates (modelled by a negative operation and maintenance cost of 90% of the penalty level). A certificate system for cogeneration in Flanders is introduced in a similar manner. For some technologies, an upper limit on investment has been fixed to take into account the maximum market penetration potential (the certificate system being very interesting).

Table 6-1: Assumption on CO<sub>2</sub> trading price evolution.

[€/ton CO <sub>2</sub> ]	2004	2006	2008	2010	2012	2014	2016
CO <sub>2</sub> trading price	0	23	40	42	45	47	49
	2018	2020	2022	2024	2026	2028	2030
	52	54	56.4	58.8	64	72	80

Since 1 January 2005 the European Emission Trading Scheme (2005-2012) is operational. The European Union Allowances (EUAs) price<sup>26</sup> is, as in any market, set by supply and demand. The supply is here determined by the allowances and carbon credits available to the market. Demand is set by the amount of emissions through the year in relation to the overall allocation. If member states allocate less allowances or if they emit more CO<sub>2</sub>, the carbon price will increase. An assumption (of VITO) on the trading price of emission permits is incorporated in this scenario. Selling emission permits (and thus emit less CO<sub>2</sub> than allowed) is for the sector an opportunity and not selling them is seen as a loss. In the model, this has thus been translated by a fictitious CO<sub>2</sub> tax. The reasoning followed to estimate the CO<sub>2</sub> trading price is that the raising gap between natural gas price and coal price has to be compensated for a high CO<sub>2</sub> tax so that the gas remains competitive compared with coal. Assumption on CO<sub>2</sub> trading price evolution is shown in table 6-1.

### **6.2.1.2 NOx and SO<sub>2</sub> reduction**

On 12 December 2003, the Flemish government examined the emissions reduction program of sulphur dioxide (SO<sub>2</sub>), nitrogen oxides (NOx), volatile organic compounds (VOCs) and ammonia (NH<sub>3</sub>). In the framework of the European National Emissions Ceilings (NEC) directive, significant reduction of NOx and SO<sub>2</sub> discharge in the atmosphere will have to be achieved in the electricity sector.

The Flemish electricity sector commits itself in an environmental policy agreement to strongly reduce its NOx and SO<sub>2</sub> emissions. The settled emissions ceilings are available in table 6-2. These figures do not take into account auto-producers and heat production of combined heat and power plants (CHP). Wallonia also intends to decide an environmental policy agreement with the electricity sector. The effects of such a decision can not be estimated for the moment.

New power plants are created in Markal for Wallonia and for Flanders. A constraint on investments distribution is defined (60% in Flanders and 40% in Wallonia). Otherwise, Markal would choose only Wallonia's power plants because they are not constrained.

This regulation will not have an effect on the electricity consumption but well on the way the electricity is produced and consequently also on the primary energy use. The bound values on emissions bulk are explicitly imposed in the model. If the above-mentioned measures are not sufficient to respect these limits, then the model can decide to apply additional measures. For example, the model can choose not to use the coal power plants not fitted with deNOx and deSOx and to replace them by modern combined cycle power plants with better environmental performance (NOx, SO<sub>2</sub> and also CO<sub>2</sub>). That is the way the NEC directive can influence the primary energy use.

## **6.2.2 Energy prices evolution**

Prices of oil, natural gas and coal are determined by the supply and demand on the world market. History taught us how difficult it is to make predictions on energy prices but the energy scenarios are necessarily based on assumptions on the evolution of energy prices. The fuel prices used in Markal are derived from the assumptions on the international fuel prices evolution in the new baseline scenario with PRIMES<sup>27</sup> (table 6-3).

---

<sup>26</sup> Carbon 2007 A new climate for carbon trading (Point Carbon) presents an overview of the state of the carbon market in 2006, an outlook for 2007 and expectations for the future.

<sup>27</sup> It is assumptions which have been put at disposal by the Federal Planning Bureau and which have been manipulated by PRIMES for the new baseline scenario in development for the European Commission (DGTREN)

Table 6-2: Emissions ceilings for NO<sub>x</sub> and SO<sub>2</sub> for the Flemish electricity sector.

[kton]	2008	2010	From 2014
NO <sub>x</sub>	14	12.5	11
SO <sub>2</sub>	7.5	7.5	7.5

Table 6-3: Assumptions on fuel prices.

[€2005/GJ]	2004	2006	2008	2010	2012	2014	2016
Natural gas	4.53	5.26	5.45	5.64	5.64	5.64	5.73
Coal 1.5%S	2.35	2.35	2.35	2.35	2.35	2.35	2.38
Coal 1%S	2.66	2.63	2.57	2.50	2.57	2.63	2.69
Coal 0.45%S	2.66	2.63	2.57	2.50	2.57	2.63	2.69
Fuel 1%S	4.20	5.79	5.38	4.96	4.96	4.96	5.03
Fuel 0.5%S	5.17	6.76	6.34	5.93	5.93	5.93	6.00
[€2005/GJ]	2018	2020	2022	2024	2026	2028	2030
Natural gas	5.92	6.10	6.48	6.86	7.08	7.14	7.20
Coal 1.5%S	2.44	2.50	2.57	2.63	2.67	2.69	2.72
Coal 1%S	2.76	2.82	2.82	2.82	2.83	2.85	2.87
Coal 0.45%S	2.76	2.82	2.82	2.82	2.83	2.85	2.87
Fuel 1%S	5.17	5.31	5.68	6.05	6.28	6.37	6.46
Fuel 0.5%S	6.14	6.28	6.64	7.01	7.24	7.34	7.43

### 6.2.3 CO<sub>2</sub> emission factors

Most emission factors are derived from the IPCC values. They are fuel-specific. Values for several fuels are shown in table 6-4.

### 6.2.4 Electricity importation evolution

Table 6-5 presents the assumptions on the electricity importation in Belgium. The importation increases until 2012, then decreases until 2020 to again increase until 2030.

### 6.2.5 Electricity demand evolution

The evolution of the electricity demand from 2004 to 2030 is presented in table 6-7. After 2020, the figures are given for the combination of Wallonia and Brussels. Values for these two regions until 2020 are these reported in the framework of the CAFE<sup>28</sup> program and are related to a 'with measures' scenario. The electricity consumption in Flanders has been obtained from the activities of the various sectors in a recent VITO study.

Table 6-4: CO<sub>2</sub> emission factor.

[kton/PJ]	Real CO <sub>2</sub> emission factor
Coal	92.71
Heavy oil	76.59
Natural gas	55.82
Coke oven gas	47.43
Blast furnace gas	258.00
Waste	104.89

<sup>28</sup> Clean Air For Europe: the European reduction program for emissions of acidifying substances and ozone precursors

Table 6-5: Assumption on the electricity importation in Belgium.

<i>[TJ]</i>	<b>2004</b>	<b>2006</b>	<b>2008</b>	<b>2010</b>	<b>2012</b>	<b>2014</b>	<b>2016</b>
<i>Electricity import</i>	25432	24891	25618	26665	30447	27525	24936
<i>% variation per year</i>		-1.06	1.46	2.04	7.09	-4.80	-4.70
<i>[TJ]</i>	2018	2020	2022	2024	2026	2028	2030
<i>Electricity import</i>	22679	20423	21103	21783	22417	23006	23595
<i>% variation per year</i>	-4.53	-4.97	1.66	1.61	1.46	1.31	1.28

For Flanders, the previsions are an increase in electricity demand by 14% between 2004 and 2020. It is 21% for Wallonia and 44% for Brussels. The two latter and particularly Brussels seem quite high compared to Flanders but we do not know the assumptions used to estimate them.

### 6.2.6 Heat demand evolution

A certain amount of heat has to be produced either by cogeneration or by conventional methods (boiler). It is shown in Table 6-6.

### 6.2.7 Efficiency of generating facilities

Table 6-8 gathers the net efficiencies of the main types of power plants in the model. Assumptions on the equipment mix, existing plants (e.g. planned closure) and future plants (e.g. maximum market penetration), are not explained here but can be seen in the results (chapter 7).

## 6.3 CCS scenarios

The modifications introduced in the model consist in the addition of new technologies and energy carriers that represent the system CCS.

### 6.3.1 Performance and costs of CO<sub>2</sub> capture technologies

These have been evaluated in chapter 2. The data have been converted into the unit system of the database (Energy: TJ, Capacity: MW, Emission: kton for CO<sub>2</sub>, ton for NO<sub>x</sub> and SO<sub>2</sub>, Cost: thousands of (2005) €).

Six technologies for CO<sub>2</sub> capture have been defined; each of the three capture technologies (post-combustion, pre-combustion and oxy-fuel combustion) for coal-and for gas-fired plants. We have also created new power plants without capture in the model: one Pulverised Coal-fired power plant (PC), one Natural Gas Combined Cycle power plant (NGCC) and one Integrated Gasification Combined Cycle power plant (IGCC).

All these technologies (with and without capture) have been created in duplicate, one for Wallonia and one for Flanders, because of the Flemish electricity sector commitment to reduce its NO<sub>x</sub> and SO<sub>2</sub> emissions. These emissions have thus to be specified for the 'Flemish' power plants.

Table 6-6: Heat demand evolution.

<i>[TJ]</i>	<b>2004</b>	<b>2006</b>	<b>2008</b>	<b>2010</b>	<b>2012</b>	<b>2014</b>	<b>2016</b>
<i>Heat demand</i>	88931	94554	100177	106735	107054	107857	109745
	2018	2020	2022	2024	2026	2028	2030
	110599	111453	112455	113458	111679	114073	115025

Table 6-7: Electricity demand evolution in Belgium.

[TJ]	2004	2006	2008	2010	2012	2014	2016
<i>Flanders</i>	191241	196368	198449	203194	206661	209857	212649
<i>% increase per year</i>		1.34	0.53	1.20	0.85	0.77	0.67
<i>Wallonia</i>	88343	89970	91305	92660	95296	98075	100961
<i>% increase per year</i>		0.92	0.74	0.74	1.42	1.46	1.47
<i>Brussels</i>	20830	21793	22800	23854	24957	26142	27368
<i>% increase per year</i>		2.31	2.31	2.31	2.31	2.37	2.34
<i>Wallonia + Brussels</i>	109173	111763	114105	116514	120252	124216	128329
<i>Belgium</i>	300414	308131	312554	319708	326913	334073	340978
<i>% increase per year</i>		1.28	0.72	1.14	1.13	1.10	1.03
[TJ]	2018	2020	2022	2024	2026	2028	2030
<i>Flanders</i>	215041	217432	219621	221810	224001	226195	228389
<i>% increase per year</i>	0.56	0.56	0.50	0.50	0.49	0.49	0.48
<i>Wallonia</i>	103956	106950					
<i>% increase per year</i>	1.48	1.44					
<i>Brussels</i>	28635	29901					
<i>% increase per year</i>	2.31	2.21					
<i>Wallonia + Brussels</i>	132590	136851	141578	146305	151198	156260	161321
<i>Belgium</i>	347631	354283	361198	368114	375199	382455	389710
<i>% increase per year</i>	0.98	0.96	0.98	0.96	0.96	0.97	0.95

One power plant was already entered in Markal by VITO with a possibility to retrofit it with post-combustion capture. That is a new classical power plant that will produce electricity from the siderurgical gases produced by the steel producer Sidmar in Gent. The plant of a capacity of 350 MW should be operational by 2010. The investment cost of the power plant without capture is perhaps a bit too low (607 €/kW which is more like a NGCC), and because the fuel is for free, the power plant will always be chosen. Siderurgical gases (a blend of blast furnace gas, converter gas and possibly coke oven gas) contain a large quantity of carbon monoxide and thus have a great CO<sub>2</sub> emission factor (238 kton/PJ). Given the 45% efficiency, it results in a CO<sub>2</sub> emission of 1900 g/kWh, around 2.5 times higher than a coal plant. Big mass flow rate and CO<sub>2</sub> concentration are favourable for the cost of the installation per ton of CO<sub>2</sub> captured. The cost of the retrofit is based on the difference between a fluidized coal plant with and without capture (values coming from PRIMES) corrected by the following factor:

$$\left(\frac{238}{93}\right)^{0.7}$$

where

Blast furnace gas emission factor = 238 kton/PJ

Coal emission factor = 93 kton/PJ

Proportionality factor = 0.7

That is to say an investment cost of 2148 €/kW for the post-combustion capture unit. This is quite high but the quantity of CO<sub>2</sub> captured per kWh is also very high.

Table 6-8: Efficiencies of different power plants.

<i>[%]</i>	<i>Electrical efficiency</i>	<i>Thermal efficiency</i>
<i>Coal power plant 280 MW</i>	37%	
<i>Old coal power plant</i>	36%	
<i>Gas turbine repowering</i>	40%	
<i>Classical gas power plant</i>	35%	
<i>Blast furnace gas power plant</i>	36%	
<i>Combined cycle power plant 1995</i>	50%	
<i>Combined cycle power plant 2000</i>	54%	
<i>Combined cycle power plant 2015</i>	61%	
<i>CHP gas turbine</i>	36%	42%
<i>CHP gas turbine 2010</i>	40%	47%
<i>CHP gas engine</i>	35%	59%
<i>CHP gas engine 2010</i>	35%	59%
<i>CHP diesel engine</i>	33%	44%
<i>CHP diesel engine 2010</i>	39%	51%
<i>Pumped-storage plant</i>	74%	

### 6.3.2 Costs of CO<sub>2</sub> transport and storage

We have seen that the technologies of transportation and storage are very dependent on local circumstances and therefore it is difficult to estimate the costs. Capacity of potential storage sites and maximum injection rate are also very complicated to assess. In addition, the cost of CO<sub>2</sub> transport is dependent on the distance and the model has no geographical localisation and so does not allow measuring the distance between a power plant and a storage site.

In the report ‘Markal/TIMES, a model to support greenhouse gas reduction policies’, transport and storage are regarded as one technology. Two cases are considered in the model: a ‘close’ storage (less than 20 km) with a maximum capacity of 100 Mton and a cost of 5.5 €(2005)/ton CO<sub>2</sub> and a ‘far’ storage with a maximum capacity of 1000 Mton and a cost of 13 €(2005)/ton CO<sub>2</sub>. This potential in deep aquifers and coal sinks is in Belgium. The 100 Mton can be preformed with high certainty in Belgium; 1000 Mton is uncertain (although, if not in Belgium, this could represent foreign sinks). The costs are derived from a VITO study ‘Geotechnische en financiële aspecten van ondergrondse CO<sub>2</sub>-opslag in Vlaanderen’. The same values have been taken in our work.

We are aware of the lack of detail in the transport and storage modelling, but it was not feasible at this time to cross check this data with more detailed results from the PSS simulator.

### 6.3.3 Scenarios

CCS technologies are entered in the reference scenario but can not be chosen by the model as the ‘transport and storage’ technology is set available from 2032. In the CCS scenario, the start year of the ‘transport and storage’ technology is set to 2010. Thus the model will be able to choose a post-combustion capture coal or gas plant or a coal-fired oxy-fuel boiler from 2025. The pre-combustion technologies are only available from 2030 and the NGCC oxy-fuel plant from 2050 (thus beyond the scope of this study).

The **CCS scenario** is based on the REF scenario. All assumptions are thus also valid in the CCS scenario. Variants of this CCS scenario are also included: the CCSPLUS scenario, the CCSPRO scenario and the CCSNUC scenario.

The **CCSPLUS scenario** assumes a faster development of CCS technologies than foreseen. In this scenario, the model can choose among post-combustion capture technologies and coal-fired oxy-fuel boiler from 2020 and among all the technologies (except the NGCC oxy-fuel plant) from 2025.

The two other scenarios show the influence of some policies on the CCS scenario. The **CCSPRO scenario** assumes more investment possibilities in new capacity of renewables and cogeneration and the **CCSNUC scenario** assumes no nuclear phase-out (2856 MW in Wallonia and 2937 MW in Flanders until 2030).

## 7 Presentation and discussion of the MARKAL results

This chapter discusses the combination of the different scenarios and the results provided by Markal. It is sometimes difficult to explain all the variations in the results because the model possesses a great number of variables. For example, the energy prices, exogenously defined, will influence whether coal technologies or gas technologies will be chosen (in combination with investment cost, emissions tax...). Sometimes the model will choose a technology but will only use it at partial load or the model will not invest anymore in a technology because the resources are limited. An explanation of a change in the use of a technology requires looking at all the variables which could influence it. It results that the explanations given in this chapter are sometimes partial. Moreover, since the model is dynamic and perfect foresight<sup>29</sup>, some decisions are taken in expectation of future changes. For example, if the model knows that a very interesting technology will be available from the next time-period and that meanwhile new capacity is needed, investment will be made in the cheapest technology in the short term (low investment cost) even if this technology presents high CO<sub>2</sub> emissions or high operation and maintenance costs.

We are going to use two ways for presenting the results. First, we are simply going to observe the results obtained for different scenarios. Second, we are going to construct marginal cost curves. These two ways of proceeding are not comparable and the drawn conclusions are independent.

### 7.1 Model outputs

We first briefly present the outputs of the model. The two main outputs of the model are the installed capacity and the activity of the different technologies in the database. The model encompasses power plants that are exploited by central electricity producers (Electrabel – SPE) as well as units that are exploited by auto-producers. Some power plants are not included in the database. It is the case for turbojet engines and some open cycle gas turbines but these are used as back-up group.

The installed capacity of each type of electricity power plant from 2004 to 2030 can be seen in the tables ‘CAPACITY’ for Flanders, Wallonia and Brussels. Biomass co-combustion takes place in the coal power plants (as an imposed percentage of fuel energy).

The electricity production of each type of facility or else utilization of the installed capacity is presented in the tables ‘ACTIVITY’ for Flanders, Wallonia and Brussels.

The table ‘DEMAND AND SUPPLY’ gives a summary of the total demand and supply of electricity in Belgium. The total supply is constituted of electricity produced in Belgium plus electricity imported. The consumption of electricity by the pumped-storage plants (Coo) needs to be included in the total demand. The difference between total supply and total demand represents the transmission losses on the electricity grid.

The table ‘CO<sub>2</sub>’ shows the quantity of CO<sub>2</sub> emitted and the quantity of CO<sub>2</sub> sequestered and from what plant.

The tables ‘FUEL CONSUMPTION’ give an overview of fuel use for coal, natural gas and so on.

### 7.2 Comparison of different scenarios

In this section, we define different scenarios and compare the results provided by Markal.

---

<sup>29</sup> In such a model, dynamic and perfect foresight, all investment decisions are made in each period with full knowledge of future events. ‘Perfect foresight’ means that costs are fixed and known, even for the long period.

Table 7-1: Assumption on CO<sub>2</sub> trading price evolution.

[€/ton CO <sub>2</sub> ]	2004	2006	2008	2010	2012	2014	2016
CO <sub>2</sub> trading price	0	23	40	42	45	47	49
	2018	2020	2022	2024	2026	2028	2030
	52	54	56	59	64	72	80

### 7.2.1 Major assumptions

The choice of the CCS scenarios has been made in collaboration with VITO. All these scenarios can be compared with the reference scenario (REF) defined in the previous chapter.

- CCS scenario in which CCS technologies are available from 2025 except pre-combustion capture technologies, available from 2030
- CCSPLUS scenario in which CCS technologies are available from 2020 except pre-combustion capture technologies, available from 2025
- CCSPRO scenario, similar to the CCS scenario, but with more investment possibilities in new capacity of renewables and cogeneration
- CCSNUC scenario, similar to the CCS scenario, but with no nuclear-phase out

Assumptions taken in the reference scenario are valid in the other scenarios as well. The one on the CO<sub>2</sub> trading price defined by the VITO in the framework of the European Trading Scheme is thus taken up in each scenario (see table 7-1). It is important because the choice of technologies is greatly influenced by this CO<sub>2</sub> price. There is no constraint on the CO<sub>2</sub> emissions in the model.

### 7.2.2 Total cost and CO<sub>2</sub> emissions according to the different scenarios

The CO<sub>2</sub> emissions evolution over the time horizon provided by Markal for the different scenarios is presented in figure 7-1.

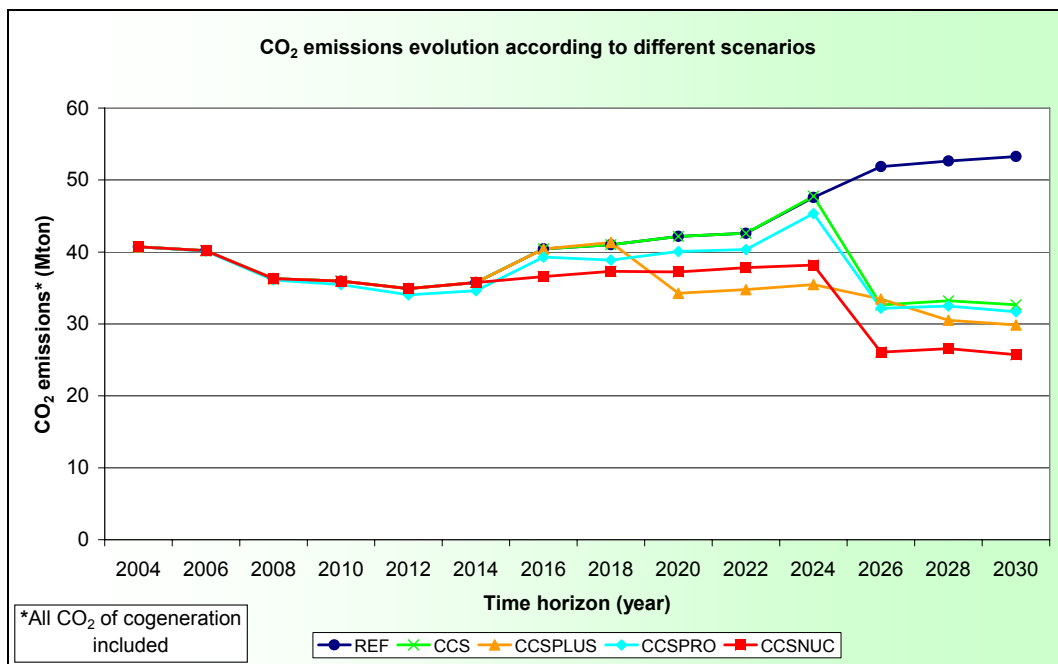

 Figure 7-1: CO<sub>2</sub> emissions evolution according to different scenarios.

Table 7-2: Total cost and CO<sub>2</sub> emissions in 2030.

	$\Delta$ Total CO <sub>2</sub> tax	$\Delta$ Objective function	CO <sub>2</sub> (2030)	$\Delta$ CO <sub>2</sub> (2030)
	(M€)	(M€)	(Mt)	(%)
<i>REF</i>	0	0	53.3	0
<i>CCS</i>	-2567	-1323	32.7	-38.7
<i>CCSPLUS</i>	-4029	-1908	29.9	-43.9
<i>CCSPRO</i>	-3304	-5734	31.7	-40.5
<i>CCSNUC</i>	-4708	-9891	25.7	-51.7

Table 7-2 shows the difference in the results of the objective function of all alternative scenarios compared to the reference scenario. The objective function result is decreased for the alternative scenarios. The difference in total CO<sub>2</sub> tax is also presented. The availability of CCS technologies allows a CO<sub>2</sub> reduction of 38.7% compared to the REF scenario in 2030. A more intensive use of renewables gives only less than 2% extra. A faster development of CCS allows reducing CO<sub>2</sub> emissions by 5.2% further. Since capture technologies are available from 2020, investments in new NGCC power plants are not required anymore. It results in about four times less new NGCC plants than in the classic CCS scenario. No nuclear phase-out brings a CO<sub>2</sub> emissions reduction of 51.7% compared to the REF scenario and with a total cost and CO<sub>2</sub> tax much lower. Indeed, this scenario allows producing an important fraction of the electricity without CO<sub>2</sub> emissions until CCS technologies become available.

### 7.2.3 Results and interpretation of technology choices

In this section, the major changes in the combination of technologies to provide the required electricity at the lowest cost are described.

The capacity of renewables and cogeneration increases over the time horizon. They are promoted with certificates and emit no or few CO<sub>2</sub> in the case of renewables and less CO<sub>2</sub> than separated production of electricity and heat in the case of cogeneration. This increase is similar in the different scenarios (excluding CCSPRO in which higher capacity is observed) and can cover a part of the power loss resulting from the nuclear phase-out and the closure of existing coal and gas-fired power plants. Co-combustion of biomass in coal plants is also promoted.

In general, we can say that, in compensation for the closure of existing plants, new NGCC plants are installed but when CCS technologies become available, the model invests very much in these technologies and decreases the capacity factor of the new NGCC plants. With the assumptions taken in the database, among capture technologies, oxy-fuel boiler power plants will be implemented first, followed by IRCC power plants if available and finally post-combustion capture NGCC power plants.

Starting from 2016, the electricity park in each time-period is compared to the electricity park in the previous period. Markal gives the optimal solution but it will become clear that another choice of technologies could be taken which would not penalize the total cost too much. Most of the time, investments made in new power plants are much more important than the changes in the use of existing plants (in produced PJ). It is also important to stress that changes in technologies can not always be explained in comparison with the previous periods.

In 2016, the nuclear power is reduced by 1376 MW (cf. fig. 7-2). To supply the electricity demand in the REF scenario, the model chooses to invest in 1293 MW of NGCC power plants (33.8 PJ) in Flanders and in Wallonia. The investment cost of this technology is low. Gas is more expensive than coal but CO<sub>2</sub> emissions from gas combustion is two times lower than those of coal combustion (and CO<sub>2</sub> price is quite high (49 €/ton, starting from 2016)). The limitation on NO<sub>x</sub> and SO<sub>2</sub> emissions is also favourable to NGCC power plants. The annual

load of existing plants increases with a preference for coal-fired plants in Wallonia and for gas-fired plants in Flanders (7 PJ extra). Although using coal plants is cheaper in Flanders, existing coal plants are already used at full load because of the promotion of co-combustion. In the CCSPRO scenario, the proportion of renewables and cogeneration is higher and thus the investment in new NGCC power plants is lower than in the REF scenario. By replacing nuclear fuel by mainly natural gas, CO<sub>2</sub> emissions thus increase in a similar way in all scenarios with nuclear phase-out. In the CCSNUC scenario, there is no investment in new capacity compared to 2014, apart from renewables and cogeneration. The demand increase is satisfied by an increase of load factors of NGCC power plants in Flanders and PC power plants in Wallonia (for the same reason as explained above).

In 2018, there is no major change in the equipment mix. A part of existing combined cycle power plants closes. In the REF scenario, the model keeps investing in new NGCC power plants. In the CCSPLUS scenario, the investment in new NGCC capacity is lower because the capture technologies will be available in the next period and will be more interesting than the NGCC plants. The model thus uses the existing plants to a larger extent to satisfy the demand (combined cycle and classical gas power plants). In the CCSPRO scenario, the capacity of offshore wind turbines increases by 584 MW. The capacity of other renewables and the cogeneration increases further (plus increase in load factors of classical gas power plants) and there is no new investment in NGCC power plants. In the CCSNUC scenario, the model chooses to invest in new NGCC power plants.

In 2020, there are fundamental changes in the generating facilities compared to 2018: closure of 451 MW of nuclear power, 460 MW of combined cycle power plant, 259 MW of coal plant and 317 MW of classical gas power plant. In the reference scenario, the model makes up this loss with further investment in NGCC power plants (1056 MW). In the CCSPLUS scenario, some capture technologies are available. The model chooses to invest in 3470 MW of new oxy-fuel boiler power plants with CO<sub>2</sub> capture and the load factors of existing power plants (coal and natural gas) are decreased significantly. In the CCSPRO scenario, an investment in 1336 MW of NGCC power plants is needed since there is no CCS available (this is more than in the REF scenario but the installed capacity remains lower; 2267 MW to 3006 MW in the REF scenario)

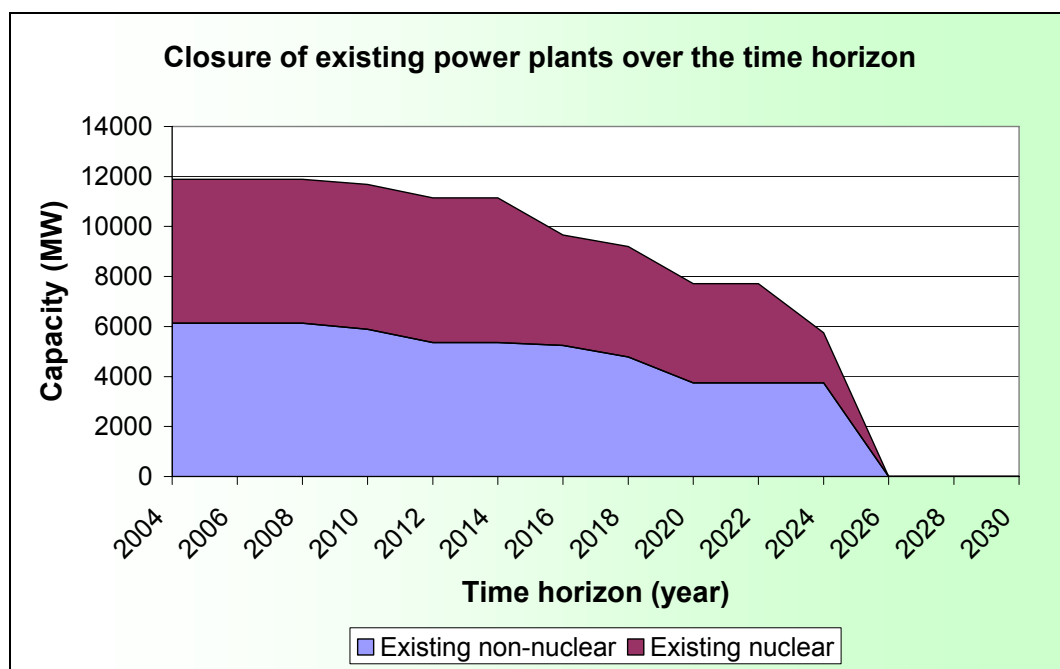


Figure 7-2: Closure of existing power plants over the time horizon.

.In the CCSNUC scenario, Markal invests in 720 MW of NGCC power plants and increases the load factors of existing plants.

In 2022, the combination of technologies remains unchanged. In the REF scenario and in the CCSNUC scenario, there are some investments in NGCC power plants. In the CCSPLUS scenario, the model does not invest in NGCC power plants but in a few oxy-fuel boiler power plants.

In 2024, a further closure of 1966 MW of nuclear power is offset by an investment in 2341 MW of new NGCC plants in the REF scenario. The load factor of coal plants is also decreased. This results in an increase in CO<sub>2</sub> emissions. In the CCS scenario, the investment in NGCC power plants is a bit lower (2162 MW) as capture technologies will be available in the next period. The load factor of coal plants is decreased but less than in the REF scenario. The load factor of existing gas plants is increased. In the CCSPLUS scenario, 2170 MW of new oxy-fuel boiler power plants are installed. Existing NGCC power plants are used at a higher load factor. In the CCSPRO scenario, the investment in new NGCC power plants amounts to 1915 MW. These are used at quasi full-load. No major change occurs in the CCSNUC scenario.

In 2026, the equipment mix is totally renewed (5747 MW loss) as can be seen on figure 7-2. To satisfy the demand, an investment of 5250 MW of new NGCC power plants is carried out in the REF scenario. In the CCS scenario, the model invests in 6098 MW of new oxy-fuel boiler power plants and 2717 MW of new NGCC power plants with post-combustion capture. SIDMAR is fitted with CO<sub>2</sub> post-combustion capture. While oxy-fuel boiler power plants are used as base-load, post-combustion capture NGCC power plants are used at partial load (44% in Flanders and full load in Wallonia<sup>30</sup>). This means that using post-combustion capture NGCC plants (lower investment cost and higher operation cost) at partial load in addition to oxy-fuel boilers is cheaper than using only oxy-fuel boiler plants at full load. The load factor of the new NGCC plants in which the model has invested since 2016 is reduced. In the CCSPLUS scenario, there is no retrofit of SIDMAR plant. Investments are made in 4877 MW of IRCC power plants instead of oxy-fuel boiler power plants. Again oxy-fuel boiler power plants are used as base-load and IRCC power plants are used at partial load (44% in Flanders and full load in Wallonia). The explanation given for post-combustion capture NGCC plants is also valid in this case. In the CCSPRO scenario, the retrofit of SIDMAR is included in the solution. Investment in new oxy-fuel boiler power plants and post-combustion capture NGCC power plants is a bit lower than in the CCS scenario, 5435 MW and 2430 MW respectively. We can make the same remark about load factors of these capture plants and existing NGCC plants as in the CCS scenario. In the CCSNUC scenario, 3940 MW of new oxy-fuel boiler power plants are installed and SIDMAR is retrofitted.

In 2028, the model keeps investing in NGCC plants in the reference scenario. In the CCS scenario, investment is made in the post-combustion capture NGCC plants (with similar load factors as in 2026). In the CCSPLUS scenario, SIDMAR is retrofitted and 210 MW IRCC plants (with similar load factors as in 2026) and 430 MW post-combustion capture NGCC plants (also used at partial load: 12% in Flanders and full load in Wallonia) are installed. In the CCSPRO, investment goes on in the post-combustion capture NGCC plants like in the CCS scenario (42% load in Flanders and full load in Wallonia). In the CCSNUC scenario, the model increases slightly the capacity of oxy-fuel boiler power plants.

---

<sup>30</sup> This difference between the capacity factor in Flanders and in Wallonia can be explained partly by the limitations on NO<sub>x</sub> and SO<sub>2</sub> imposed in Flanders. But when we execute the model without this constraint, we can see that the distribution between Flanders and Wallonia of the electricity production by these plants is arbitrary. In Markal, the grid load is not modelled so that power plants can be put in Wallonia or in Flanders without difference in the objective function.

In 2030, the model satisfies the demand by investing again in NGCC plants in the REF scenario. In the CCS scenario, new investment in 994 MW of IRCC power plants is made. These are used at a load of 42% in Flanders (the load factors of other technologies remain more or less unchanged). In the CCSPLUS scenario, the model goes on investing in the post-combustion capture and in the IRCC power plants. Load factors are similar to those in 2028. In the CCSPRO scenario, 1157 MW of new IRCC power plants are installed. Load factors also remain similar as in 2028. In the CCSNUC scenario, the model goes on investing in the oxy-fuel boiler power plants.

The Technology Investment Marginal (INVEST.M) values of new technologies were also entered in Markal. These values represent the quantity to subtract from the investment cost of the technology so that the latter is chosen in the solution. For example, in the CCS scenario in 2030, the investment cost of the post-combustion capture NGCC plant has to be reduced by 2.36 €/kW to integrate the solution. For oxy-fuel boiler power plants, the value is 12.35 €/kW. These values are very low and tell us that, given the uncertainty on performance and costs of capture technologies, it is not possible to claim that it will be this or other technology which should primarily develop. There is no difference enough between technologies' characteristics.

#### 7.2.4 CO<sub>2</sub> storage: limitation of CO<sub>2</sub> injection rates

So far, no limit on CO<sub>2</sub> injection rates in geological reservoirs has been considered. The table 7-3 shows the number of Megatons CO<sub>2</sub> stored annually according to the different scenarios. The 'close' storage is full after two or three years (capacity of 100 Mton).

The maximum injection rate for a reservoir can be determined roughly by its size and the real/economic lifetime of a source, if such rates are technically feasible. Lifetime would be anything between 25 and 50 years. So, for the 'close' storage, the maximum injection rate would be around 2-4 Mton/y and for the 'far' storage around 20-40 Mton/y. For the 'close' storage this would mean ~2 and for the 'far' one ~10 injection sites, which is realistic. At least for aquifers, injection in coal would probably be completely different (communication of Kris Piessens). We made an additional CCS scenario in which the injection rate of the 'close' storage is limited to 3 Mton/y and the one of the 'far' storage is limited to 30 Mton/y. In this case, Sidmar is retrofitted from 2022 so that CO<sub>2</sub> captured is exactly 3 Mt/y. In 2026, the model chooses oxy-fuel boiler and NGCC plants with capture and in 2030, IRCC plants add to those so that CO<sub>2</sub> captured stays below or equal to 30 Mt/y. It obviously results in higher CO<sub>2</sub> emissions in 2030, 36.4 Mt instead of 32.7 Mt, but all the same it allows a reduction of 31.7% compared to the reference scenario. The total cost and total CO<sub>2</sub> tax also increase. These limitations are very arbitrary as the way we modelled the 'transport and storage' technology. A more detailed description of this part of the CCS system may be required to get more precise information.

Table 7-3: Quantities of CO<sub>2</sub> stored annually.

[Mton/y]		2020	2022	2024	2026	2028	2030
CCS	close	0.0	0.0	0.0	44.6	5.4	0.0
	far	0.0	0.0	0.0	0.0	39.5	46.1
CCSPLUS	close	20.4	21.0	8.7	0.0	0.0	0.0
	far	0.0	0.0	25.2	41.9	46.1	47.6
CCSPRO	close	0.0	0.0	0.0	40.2	9.8	0.0
	far	0.0	0.0	0.0	0.0	31.0	42.3
CCSNUC	close	0.0	0.0	0.0	25.8	24.2	0.0
	far	0.0	0.0	0.0	0.0	2.6	31.9

### 7.3 Marginal Abatement Cost curves

In this section, we have constructed Marginal Abatement Cost (MAC) curves from the results given by Markal. We have proceeded as follows.

#### 7.3.1 Proceeding

The MAC curves are given as stepwise curves relating abatement costs (the marginal cost) and abatement potentials (CO<sub>2</sub> emitted) as shown in figure 7-4. Among the possibilities for abatement the principle is to start to reduce discharges by using the cheapest option, and then continuing with the second cheapest, etc., ending up with the most expensive option.

There are two ways to obtain these curves with Markal. The first is to impose a constraint on CO<sub>2</sub> emissions and to observe the corresponding marginal cost given in the results (i.e. the shadow price of the constraint). The second consists in imposing a CO<sub>2</sub> tax and observing the corresponding CO<sub>2</sub> emissions. These two ways result in the same curve. We chose the second option because it was easier to implement.

The fictitious CO<sub>2</sub> tax imposed in the REF scenario to represent the CO<sub>2</sub> trading price on the European Emission Trading market (assumption of VITO) has been replaced by a CO<sub>2</sub> tax increasing by step as shown in figure 7-3. It was chosen to increase the price gradually from 0 to the value in question until 2020, this being more realistic than an abrupt change from 0 to this value.

In a discussion with VITO, we defined the scenario which would be evaluated by means of MAC curves. It is the same scenario as CCSPRO defined in the first part of this chapter but with no financial support or other mechanism which would promote a technology. These technologies, classical, with CO<sub>2</sub> capture or using renewable energies, are thus compared only on their techno-economic characteristics and MAC curves can be seen as an academic exercise.

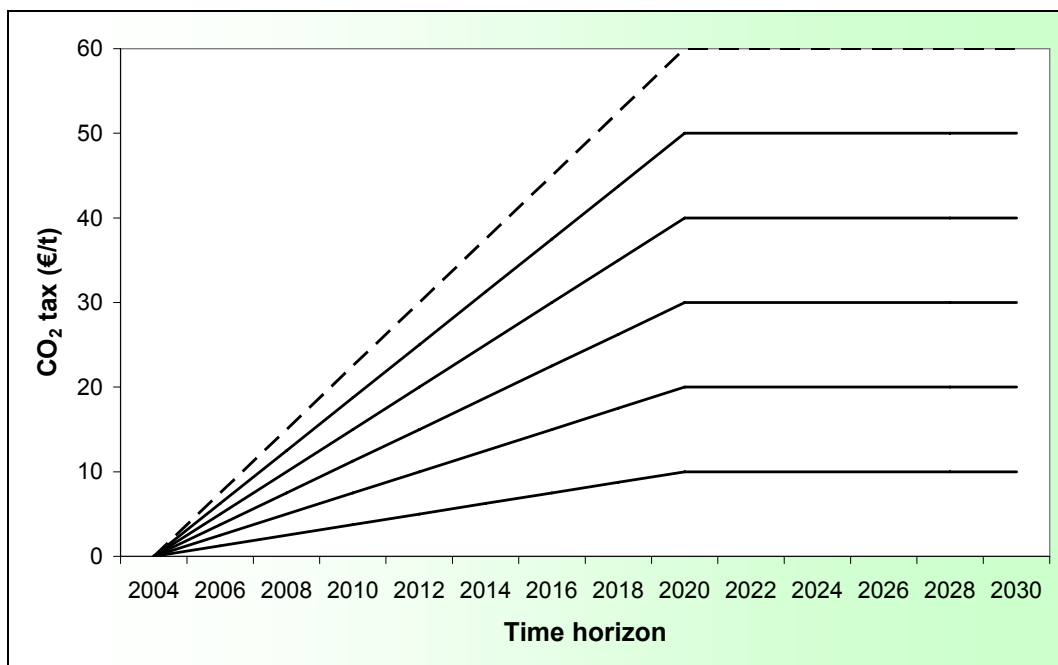


Figure 7-3: CO<sub>2</sub> tax versus time horizon for MAC curves construction.

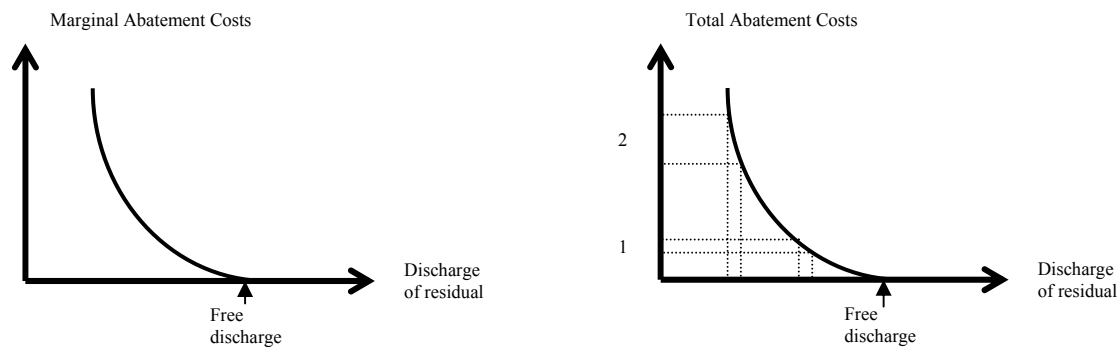


Figure 7-4: Marginal Abatement Cost (TAC) curve and Total Abatement Cost (MAC) curve.

By imposing a tax on CO<sub>2</sub> emissions, the model will modify the combination of technologies to produce the required electricity at the lowest cost. MAC curves will be plotted for two years, 2020 and 2030. In these two years, the electricity demand, the available technologies and other constraints are different so resulting in two different curves.

We can also plot the Total Abatement Cost (TAC) curve. On the basis of the above-mentioned principle, the Marginal Abatement Cost is increasing when discharge in the atmosphere is reduced, as shown by the change in total costs at 1 and at 2 on figure 7-4 (the Marginal Abatement Cost curve being the derivative of the TAC curve).

The two figures show the result obtained theoretically. A “pure” TAC curve has an increasing slope. In our exercise, when taxes go up, the model can choose to invest in an earlier year (2020 instead of 2030 for example) so that the total cost (over the period 2004-2030) is not influenced by it. We do not calculate “pure” cost curves. If desired, these curves could be elaborated when having an increasing tax only in the year for which we plot the curve, 2020 or 2030, and 0 in all other years instead of the evolution shown in figure 7-3. But in that case, the investment decisions chosen by the model are based on “short-term thinking” and the model will always prefer an installation with a life of 10 years instead of one with 20 years which maybe will be chosen in a long-term exercise.

It should be noted that each point on the curves represents a complete energy system solution, rather than the result of an individual abatement option.

The figures 7-5 to 7-7 show the results obtained with Markal for the MAC curves in the year 2020 and 2030, as well as the TAC (all periods) curve versus CO<sub>2</sub> emissions in the year 2030.

## 7.3.2 Results interpretation

### 7.3.2.1 Year 2020

The figure 7-8 shows the electricity production by type of power plant versus the CO<sub>2</sub> tax. It also shows the corresponding CO<sub>2</sub> emissions.

Nuclear power contributes to 32% of the total electricity production. The fraction of coal plants decreases from 18% when no CO<sub>2</sub> tax is imposed to constitute less than 1% from 60 €/ton. New coal plants is around 70% of this fraction for no CO<sub>2</sub> tax, decrease sharply for a CO<sub>2</sub> tax of 15 €/ton and become null from 20 €/ton. Classical gas power plants are not used anymore when the tax reaches 30 €/ton. The contribution of cogeneration increases from 12% to 19% when the tax goes up to 150 €/ton. Concerning renewables (wind turbines, photovoltaic cells, “green” CHP plants, biomass/biogas-fired plants and hydroelectric plants), their part increases from 3.7% to 10.7%. Sidmar is retrofitted when the tax is higher than

70 €/ton. NGCC power plants are used to complete the equipment mix. Their contribution varies between 29 and 40% of the total electricity production.

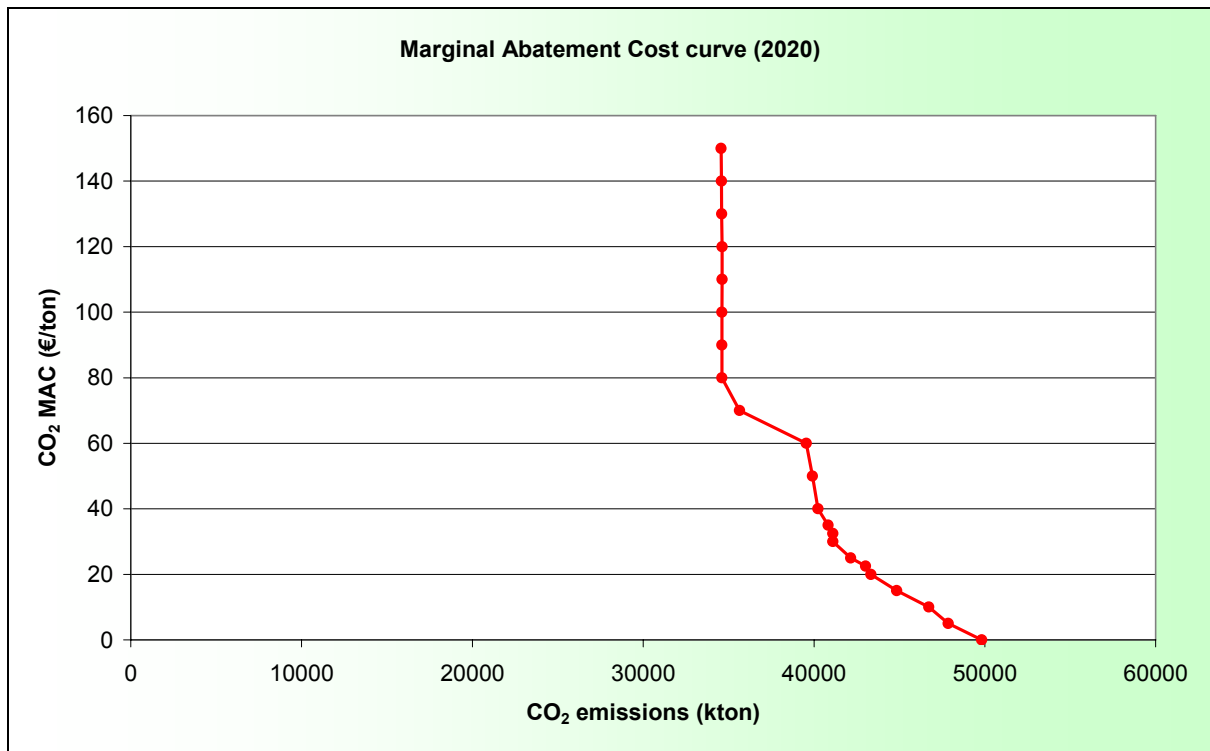


Figure 7-5: Marginal Abatement Cost curve for the year 2020.

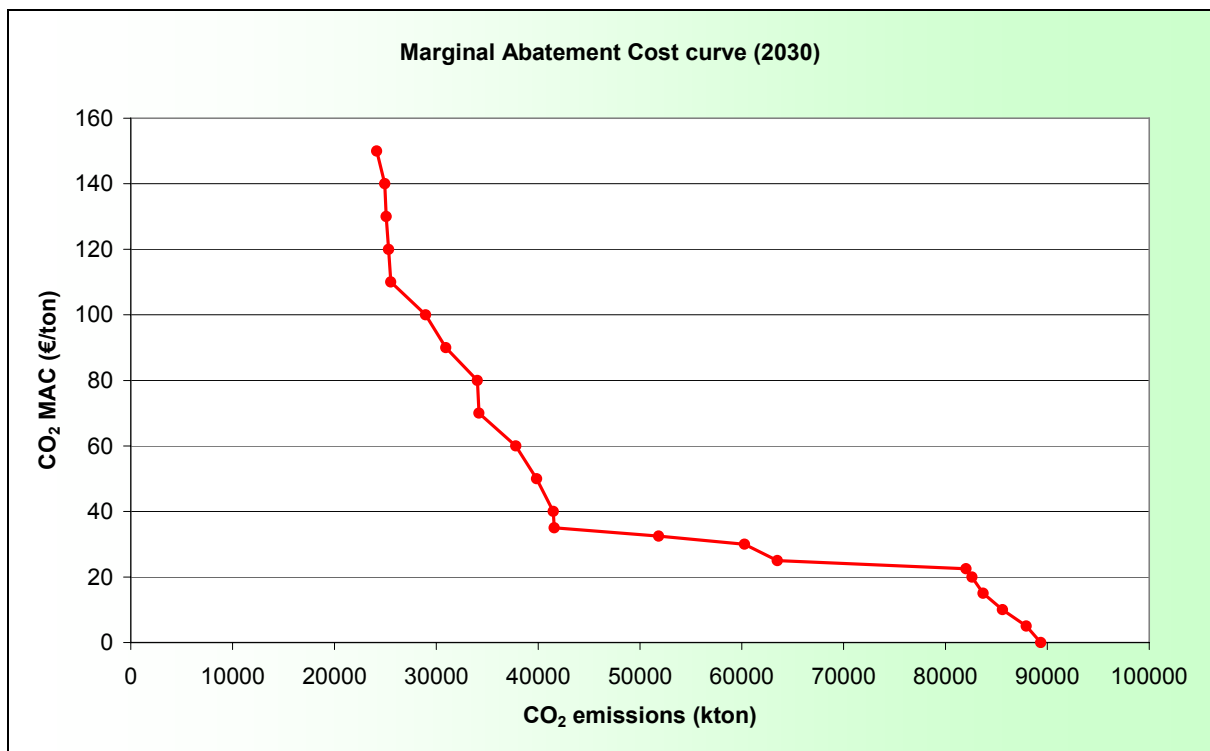


Figure 7-6: Marginal Abatement Cost curve for the year 2030.

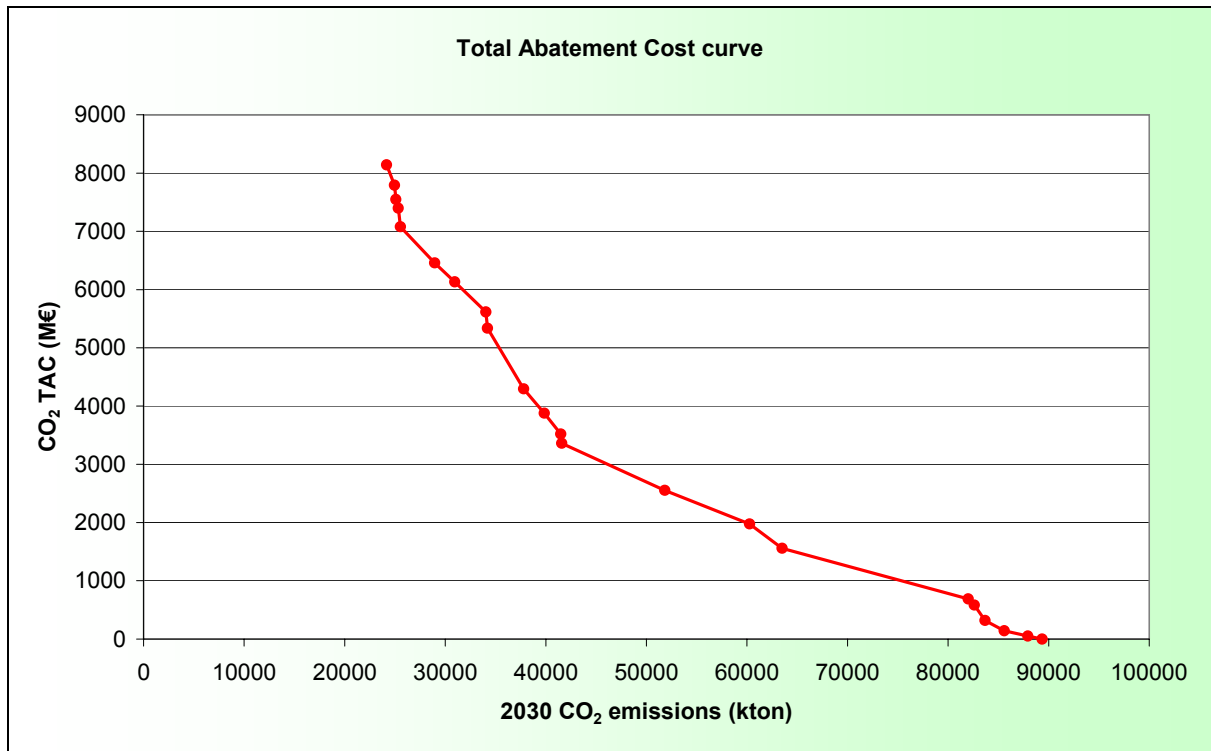


Figure 7-7: Total Abatement Cost curve versus CO<sub>2</sub> emissions in 2030. TAC for all periods.

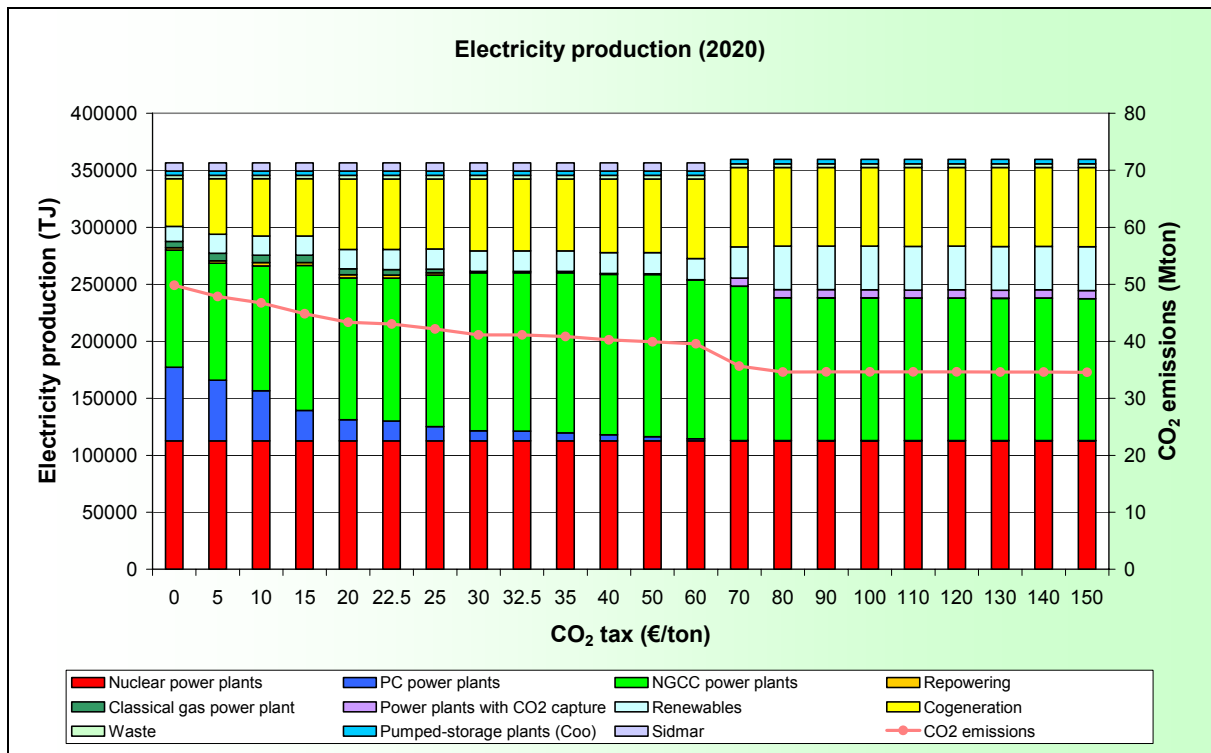


Figure 7-8: Electricity production by type of plant (2020).

We can see on figure 7-9 the contribution of offshore wind turbines when the CO<sub>2</sub> price goes up beyond 60 €/ton. These wind turbines (onshore and offshore) reach their upper bound on capacity very quickly. Hydraulic energy is already at its maximum. Photovoltaic cells are too expensive and are not chosen by the model even with a CO<sub>2</sub> tax of 150 €/ton (although there is an existing capacity which produces 3 TJ electricity). The electricity produced by “green” CHP plants is doubled with a tax of 150 €/t. The model does not allow investing very much in biomass/biogas-fired plants. Co-combustion in coal plants is not chosen by the model. Indeed, the fuel price of wood is quite high and CO<sub>2</sub> is still emitted which make the option uninteresting (no green certificates).

### 7.3.2.2 Year 2030

With regard to the year 2030 (cf. fig. 7-10), all the power plants that composed the equipment mix in 2004 are now closed. The new PC power plants constitute the major part of the electricity production (79.7%) if there is no tax on CO<sub>2</sub> emissions. This fraction decreases gradually and coal plants are no longer used when the tax reaches 35 €/ton. The proportion of NGCC plants in the electricity production rises from 5 to 33.1% when the tax reaches 35 €/ton and then decreases to 0% for 120 €/ton. Power plants with CO<sub>2</sub> capture appear at a CO<sub>2</sub> cost of 25 €/ton (20.3%) in the guise of oxy-fuel boilers. Their fraction in the electricity production grows until 83.1% for a CO<sub>2</sub> tax of 150 €/ton.

Concerning power plants with CO<sub>2</sub> capture (cf. fig. 7-11), the NGCC plant is included in the solution when the tax reaches 60 €/ton and the IRCC plant when the tax reaches 80 €/ton. The fraction of NGCC plants with capture grows at the expense of oxy-fuel boilers. NGCC plants with capture have lower CO<sub>2</sub> emissions than oxy-fuel boilers. Although natural gas price becomes high, the lower emissions tax favours NGCC plants. Retrofit of Sidmar is considered for taxes higher than 70 €/ton.

Renewable energies (wind turbines, photovoltaic cells, “green” CHP plants, biomass/biogas-fired plants and hydroelectric plants) grow from 4.2% to 9.6% when the tax increases until 150 €/ton. As in 2020, we can see on figure 7-12 the great contribution of offshore wind turbines when the CO<sub>2</sub> price goes up beyond 40 €/ton. All others remarks made for the year 2020 are equally valid for the year 2030.

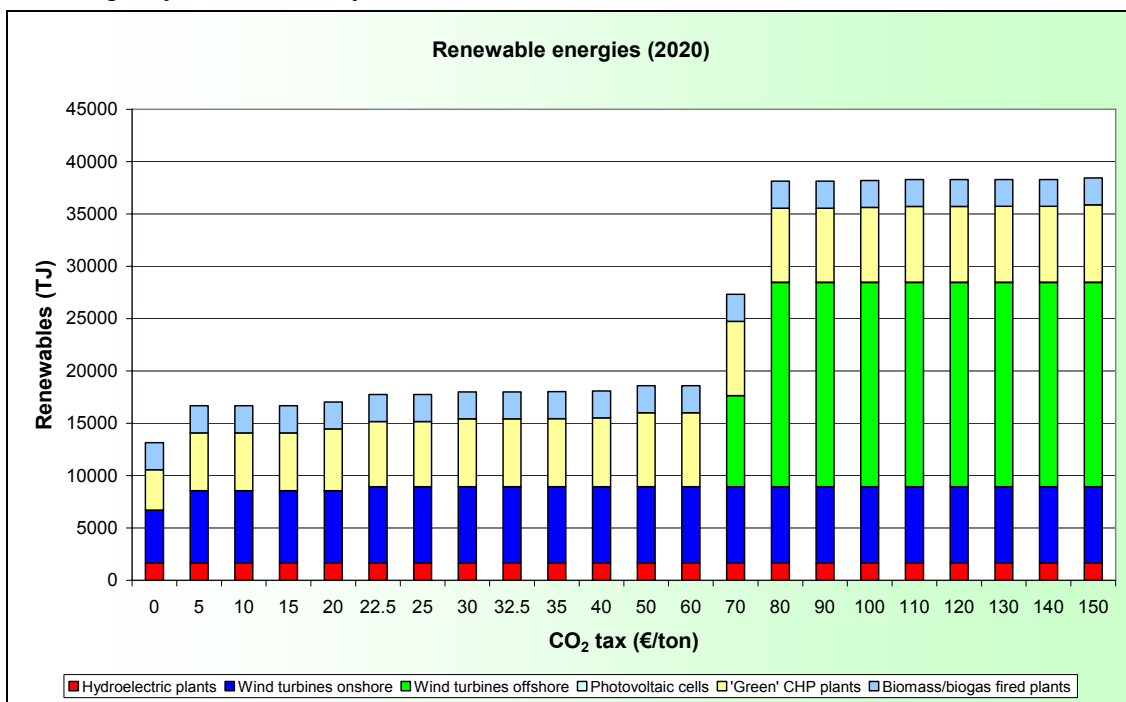


Figure 7-9: Electricity production by renewable energies (2020).

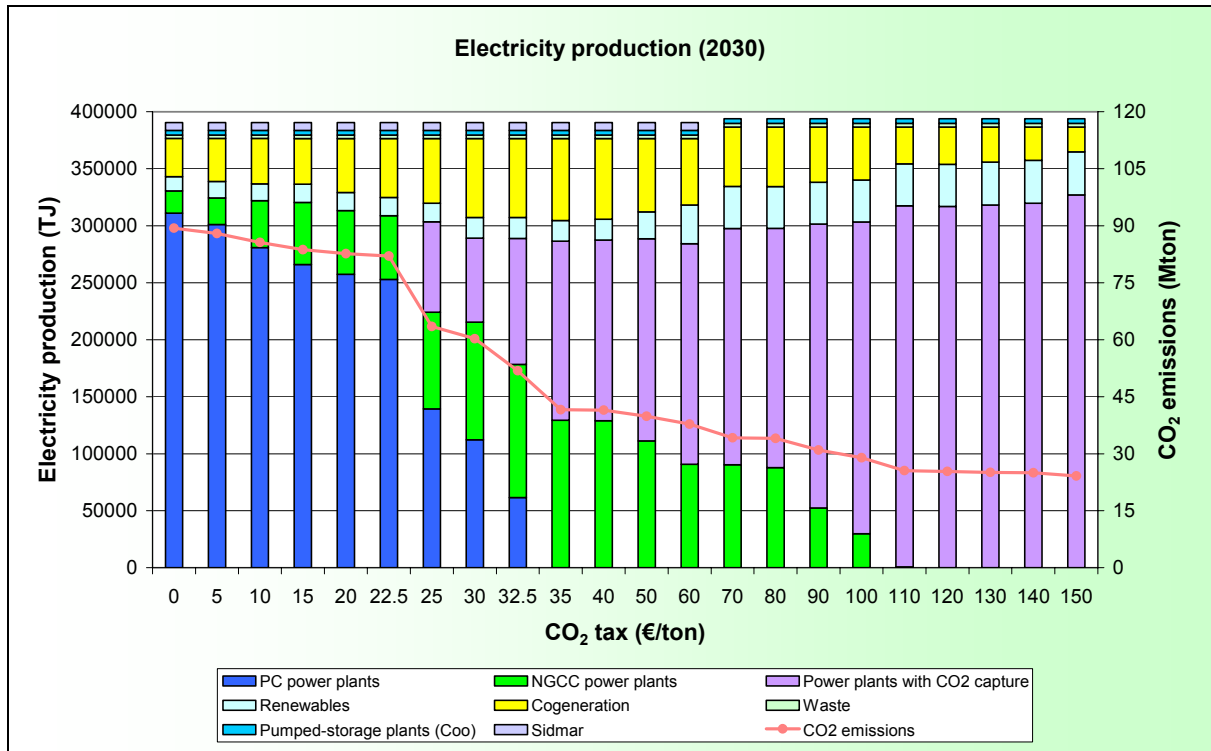


Figure 7-10: Electricity production by type of plant (2030).

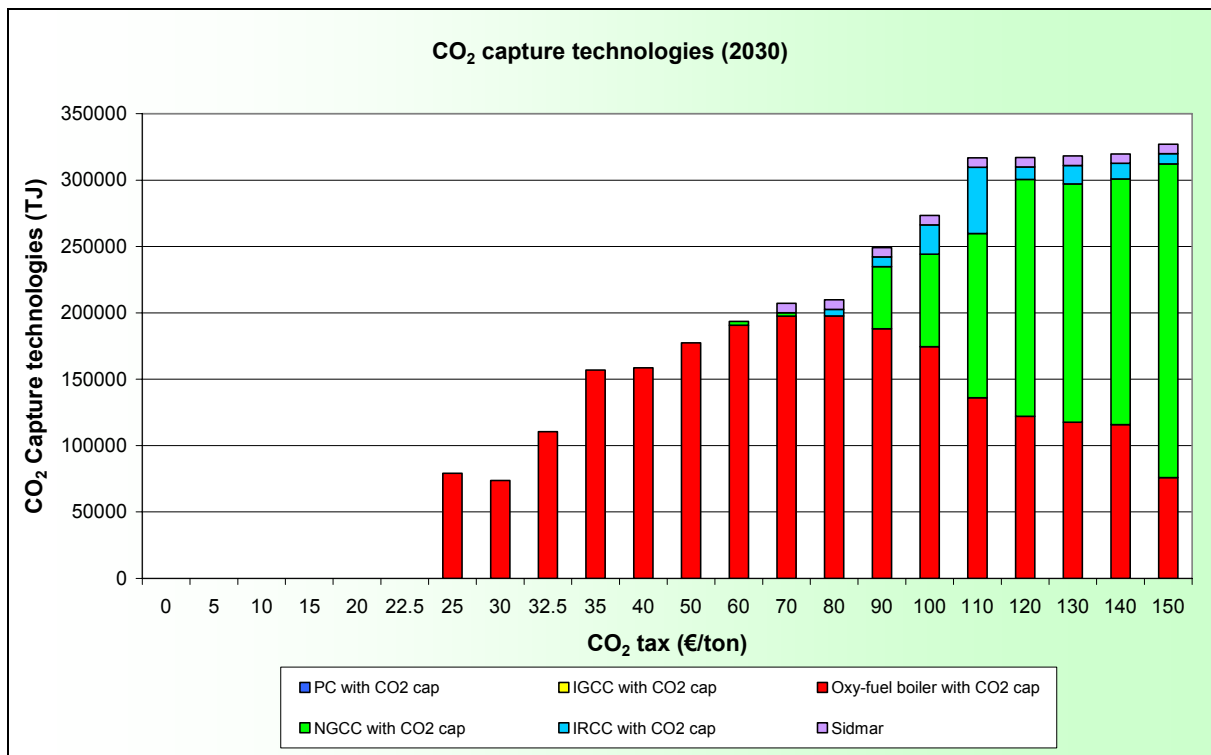


Figure 7-11: CO<sub>2</sub> capture technologies (2030).

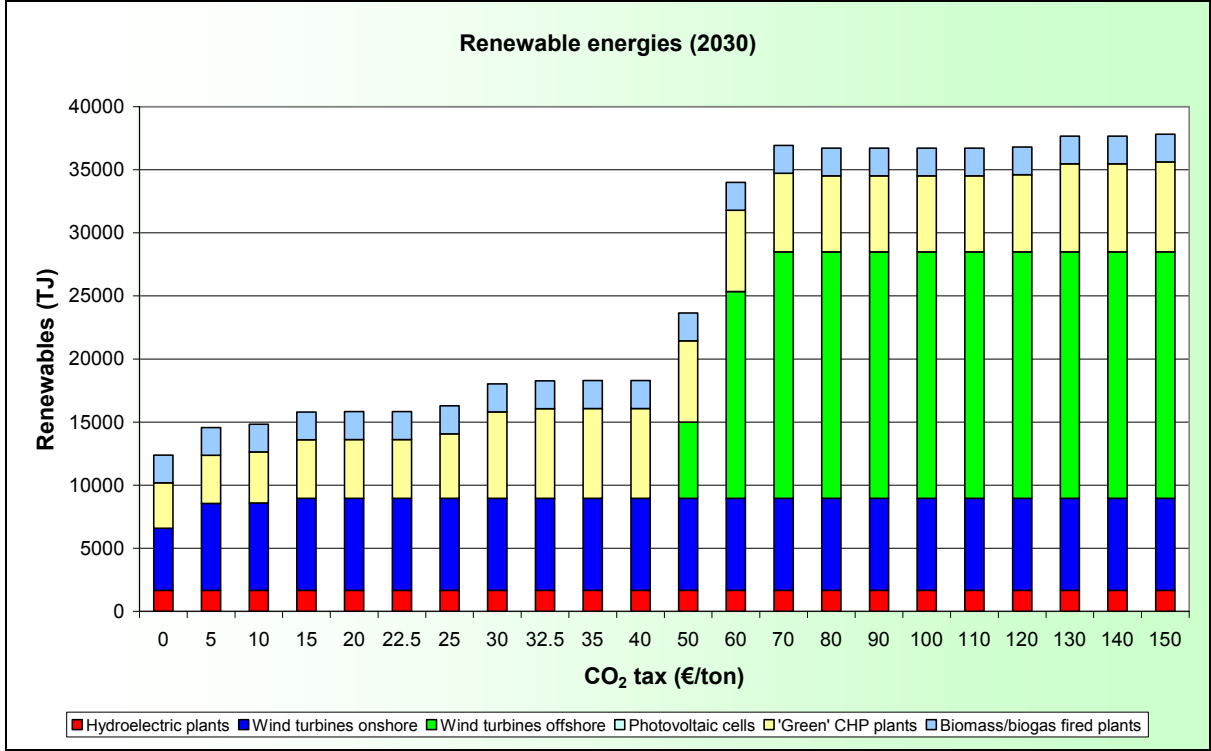


Figure 7-12: Electricity production by renewable energies (2030).



## 8 PSS simulator

Developing the PSS simulator is the central goal of the PSS-CCS project. The source, sink and transport aspects discussed in previous chapters provide the necessary data for making projections. This chapter discusses the methodology and principles on which the PSS simulator is built.

### 8.1 Principles of bottom-up simulation

PSS is a true bottom-up simulator, which means that it is individually based and spatially explicit. In more practical terms this means that the actions of individual entities (for PSS these are CCS projects and their elements) are simulated in a spatial environment (sources, sinks and transport pipelines are geographically referenced). Other simulation techniques are for example optimisation models, such as Markal-Times.

Bottom-up simulators usually retain a close link with reality. For that reason they can address, when well designed, a large variety of practical issues. For PSS this is demonstrated in chapter 9.

The main items that PSS discriminates are sources, sinks and pipelines. Each of these has a number of properties that allows to define e.g. sources for different sectors, existing sources, potentially new-built sources, retrofits, etc. The same flexibility exists for sinks and pipelines. Sinks may for example be aquifer or ECBM projects, but also one of the export possibilities.

At time intervals of one year, PSS will consider if existing projects (CCS and others) should be retrofitted, and if and which new ones have to be built. This is the actual essence of the simulation, because here PSS tries to take a realistic approach, or more precisely, tries to take decisions that would also be taken in the real world.

For PSS the basis for that decision is the cost of production, expressed in euro per unit of production (€/UoP). In the most basic case, it will have the option to build a standard facility (no-CCS), or one with carbon capture and storage. From these two options, it will choose the most economic one, which is the one with the lowest production cost. In real simulations, PSS will choose between a large number of possible projects, as it will combine all (for that year) available sources and sinks, and on top of the range of potential technologies associated with the different sources.

After activating the necessary and most economic projects, PSS will move to the next year to evaluate the possible decisions then, until it has completed its forecast for the desired time interval (2010-2050). This bottom-up approach through time is also referred to as organic approach or organic growing.

### 8.2 Environment and Architecture of PSS

An MS Access VBA (Visual Basic for Applications) environment was chosen early on in the project as the common environment for development, because this allowed to establish a close and direct link between an existing database environment and the simulator. The structure of the PSS is highly modular, which is essential as it allowed the different partners to introduce their specific expertise, translated into formulas and decision trees, into the system. It also makes the overall architecture more transparent and facilitates debugging and overall verification of the code.

It is necessary to make clear conventions on the input and output parameters, more precisely definitions, names and units. This was realised through a the system that refers to parameters at different grouping levels. This parameter reference system has proven to facilitate data handling and allows for easy introduction of additional parameters.

The input values are stored in different ways, depending on their nature. Data regarding names of input/output databases, tables, and field names are stored in public modules and

loaded during initialisation of the simulator. Input data for the simulations is grouped in different databases according to their nature and use (e.g. a database for grid data, vector data, projected economical data...) that each contains several data tables. In total PSS uses 8 satellite databases that contain over 50 tables that serve as direct input tables to PSS, and a multitude of original or conversion tables and queries. One set of 8 databases forms one specific simulation scenario.

This way of arranging data facilitates running different scenario variants, e.g. the influence of different economic outlooks can simply be modelled by replacing the 'projected economical data' database. This does not require data handling, but is done by automatically linking the specified combination of databases and tables to the central PSS-CCS database. Databases themselves contain relational data tables, e.g. for time variable data linked to objects and spatial vector data linked to non-spatial properties (an example is given in fig. 8-7).

The parameter definitions in the algorithm mimic this data structure, usually using a system of variably dimensioned indices. The definition of the parameters and parameter groups is summarised in a structured MS Excel spreadsheet<sup>31</sup> for ease of reference.

At predefined moments, MS Excel spreadsheets or other files are produced during programme execution to give an overview of the data read into the programme variables and constants, the pre-processed data (e.g. links between vector and grid data), and intermediate or final results. This is essential for verifying that variables are correctly read into the memory resident parameters and that the code is operating correctly. In total 7 different types of output files can be created.

The current code has been structured into following modules: Main, Initialiser, Linker, Reader, Stochaster, Sourcer, Sinkers, Router, Economist, and Abstracter<sup>32</sup>. These modules and the blocks of code that they contain correspond to the elements of the PSS flow-scheme that serves as the blue print for the simulator, and situates and orders the different tasks and subtasks (fig. 8-1).

The Main-module calls the procedures in the other modules in the correct order. The Reader-module first assembles the input scenario data by linking to the tables in the different input scenario tables, using the links defined in Initialiser and set by Linker. Then the data from the tables is read into the parameters, either directly or by calling on procedures in other modules when module-private data has to be read (extensive datasets, e.g. those for grid data, are kept private at module level). It also takes care of the interpolation of time series down to the time resolution used by the simulator.

Sourcer and Sinkers (pre-)process the data for CO<sub>2</sub>-sources and sinks in order to update it yearly, and to keep it in a format compatible with Economist.

Stochaster is the first module executed after starting a new Monte Carlo loop. It resets the appropriate stochastic parameters for source and sink parameters.

The Router-module determines the least-cost routes for pipelines, and is discussed in detail in § 8.4.

The Abstracter-module produces an overview of the data read into the parameters and shows intermediate and final results. Overviews are stored as spreadsheets that can be viewed during or after programme execution. Also GIS-output files are produced that can be visualised using GIS applications.

---

<sup>31</sup> Included in the PSS light version.

<sup>32</sup> In reality, PSS counts 50 different modules, but the situation is obviously simplified for this discussion.

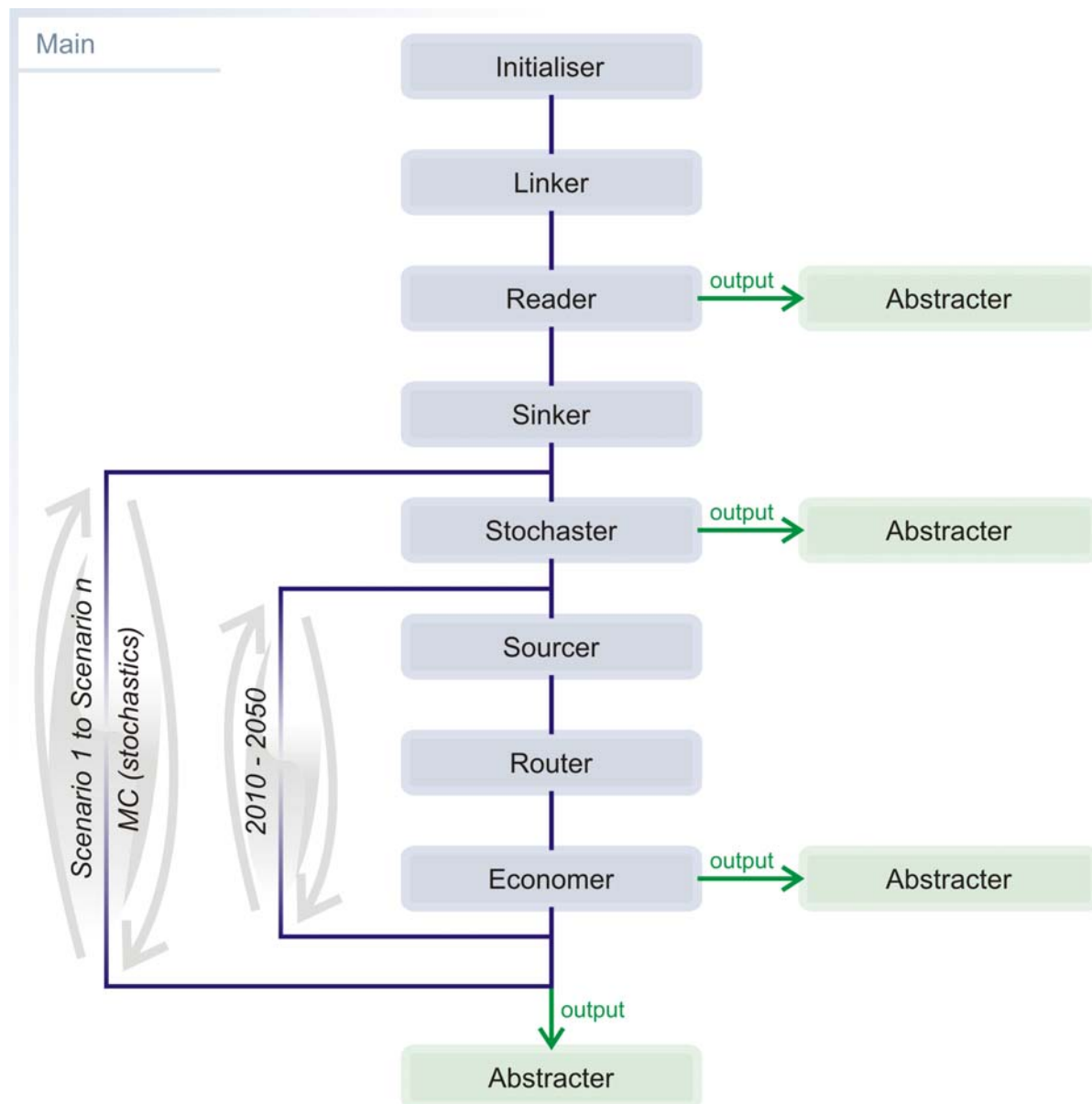


Figure 8-1: Generalised flow-scheme of the PSS simulator. The first three modules establish the link between the satellite databases and the PSS parameters, and determine for a large part the user friendliness of PSS (and therefore its capability of handling large and complex datasets). Abstracter stores at specific points the input and result values. Economer is the core of the simulator, nested within the time and stochastic (MC for Monte Carlo) loops.

### 8.3 The power of stochastic modelling

Next to determining the average cost picture for carbon capture and storage, also the uncertainty on the cost estimates should be considered as a key parameter when prediction the evolution of CCS. It is indeed undisputed that uncertainty is one of the major concerns when considering large investment decisions, such as have to be made for CCS projects. The PSS simulator is a tool that allows making detailed projections on CCS, but stands out because it specifically addresses uncertainties. It does this for current and future cost aspects of capture technologies, and also for storage site specific uncertainties on the other end of the CCS chain.

When making simple calculations, uncertainties on the result can be calculated directly from the uncertainty on the parameters. This technique becomes very complex or impossible for complex calculations or probability distributions. The simulations made by PSS are an example of such complex calculations. In order to determine the uncertainty envelope of the result, a stochastic approach can be used which is commonly referred to as Monte Carlo (a group of methods named in the 1940's after the casino located in Monte Carlo, Monaco).

The principle relies on randomly changing the input parameters of the calculation according to their uncertainty distribution. Subsequently, the result of this calculation will not be a fixed or average value, but vary corresponding to its uncertainty distribution. Repeating this calculation a sufficient number of times will then allow to determine the uncertainty distribution of the result.

PSS does not produce one result, but a series of parameters that show an evolution through time from 2010 to 2050. An uncertainty distribution is calculated for each of these parameters. It is further noteworthy that the 'average' result may sometimes be meaningless, because it may fall in between discrete results (for PSS: projected trends). An example of such a situation is shown in fig. 9-6.

It is obvious that this approach is calculation intensive, especially for calculations that are by themselves already quite lengthy. For the calculation of the demonstration results (see chapter 9), 12 computers were set up for an over-weekend calculation. In order to minimise impacts of e.g. power failure, the computers were placed on three different locations. In total an amount of 2.2 Gb of data was produced.

This immediately highlights the issue of analysing and presenting the results of stochastic multiparameter calculations. It is not only the amount of data, but also the multidimensional aspect which requires the combination of distributions, multiple parameters and geographic information in one graph. A number of graphical presentations was designed just for this purpose.

Stochastic simulation in general also relies on the access to high-quality random number data. If not, it is potentially possible that the structure of the pseudo random numbers, such as those produced by pseudo number algorithms, causes patterns or relationships in the output data.<sup>33</sup> In order to prevent this, PSS makes use of real random number data that were obtained from atmospheric noise. PSS has access to 60 Mb of binary random numbers provided by Random.org.

## **8.4 Router: determining pipeline trajectories**

### **8.4.1 Principles of raster routing**

The goal of routing theorems is to determine paths of least impedance. In practice these may be least-cost trajectories, fastest or shortest routes, etc. Routing is performed on a grid of linked nodes. For a map with road, the nodes are the crossings and the roads the links between the nodes.

A roadmap is an example of an irregular grid, which means that the distance (or other parameter that will affect impedance) between the different nodes is not constant. Paths of least impedance are most efficiently determined using the Dijkstra algorithm (Dijkstra, 1959) or comparable approaches. The calculation speed of these approaches is limited by the need to sort the routing options.

---

<sup>33</sup> The complex and branched calculations within PSS probably may make this possibility theoretical, but it was nevertheless ruled out with regard to general criticism on the pseudo random number generators standard for Microsoft Office.

This is why for regular grids or rasters, spread algorithms usually outperform the ones based on the Dijkstra approach. The efficiency is gained by assuming that straighter trajectories have lower impedance than highly irregular ones (with many curves and bends). When this condition is met, as in the case of for example pipeline trajectories, then the geographical structure of the raster itself can be used instead to rank the routing options. Corrections will naturally have to be made because the least impedance trajectory is rarely a straight line, but for most raster cases these vastly outweigh the calculation-intensive sorting needed in the Dijkstra approach.

The principle of the spread algorithm designed for the PSS-CCS project is illustrated in figure 8-2. What is shown is a small raster of 25 cells, and moves can be made from a cell to each of its eight neighbours. Costs are not indicated, but assume that the red shaded area is a zone of higher cost. The steps shown in figure 8-2 are the following:

- a. When a least-cost route has to be determined from point A to point B, the algorithm starts by evaluating the least-cost routes from each of the 8 neighbouring cells to B. The result is quite obvious 8 straight lines towards B which are remembered.
- b. In a next step, it will do the same, but now from the cells adjacent to those just evaluated. Now the choices are less evident, but a possible solution is shown.
- c. After having done this, the directions evaluated for the inner cells have to be checked, because now more options have become available which may (in this case theoretically) be cheaper.
- d. On this small grid, we have here a first estimation of the least-cost route from A to B, which is in this case a straight line. The cells farthest away from B are now also taken into account. As is indicated by the arrows, the least cost routes will avoid the expensive, red shaded area.
- e. As in step c, the inner cells need to be verified again. This time, the routes determined in d offer options for cheaper routes for two of the inner cells, including the one containing A. The checking of the next inner range needs to be performed as long as changes are made.
- f. The final result including the least cost route from A to B. Note however that not only the least-cost route from A to B has been determined, but in fact the least cost route from any cell to B. This is a property that is also exploited by Router.

This example shows only the basic principle, and Router has been optimized in several ways, some of these discussed in § 8.4.3.

#### 8.4.2 Geographic cost parameters

The cost for pipeline construction differs from location to location. In urban areas, for example, costs may be multiple those for grassland. Most pipeline routers try to accommodate for these differences by the introduction of a terrain factor (TF) that indicates the relation of the standard cost to the actual cost at a certain geographic location.

PSS Router takes a more advanced approach. In section 4.3.1 it was shown that the four major cost factors (material, labour, ROW and miscellaneous) are all to a different degree dependent of pipeline length and diameter. This means that the shares of the four cost factors are not constant, but differ for each pipeline in relation to its length and diameter.

They cost factors also depend in different ways on site characteristic aspects. The type of soil, for example, may strongly influence the labour costs, but does not have any influence on material costs.

Because the shares of the four cost factors is not constant, and they show a different dependence on different terrain factors, means that one terrain factor is insufficient to calibrate the pipeline costs with respect to the terrain characteristics.

PSS Router therefore defines four discrete terrain factors, one for material, one for labour, one for ROW and one for miscellaneous costs. Each of these cost factors is defined on the basis of soil type, topography, land use and regional information.

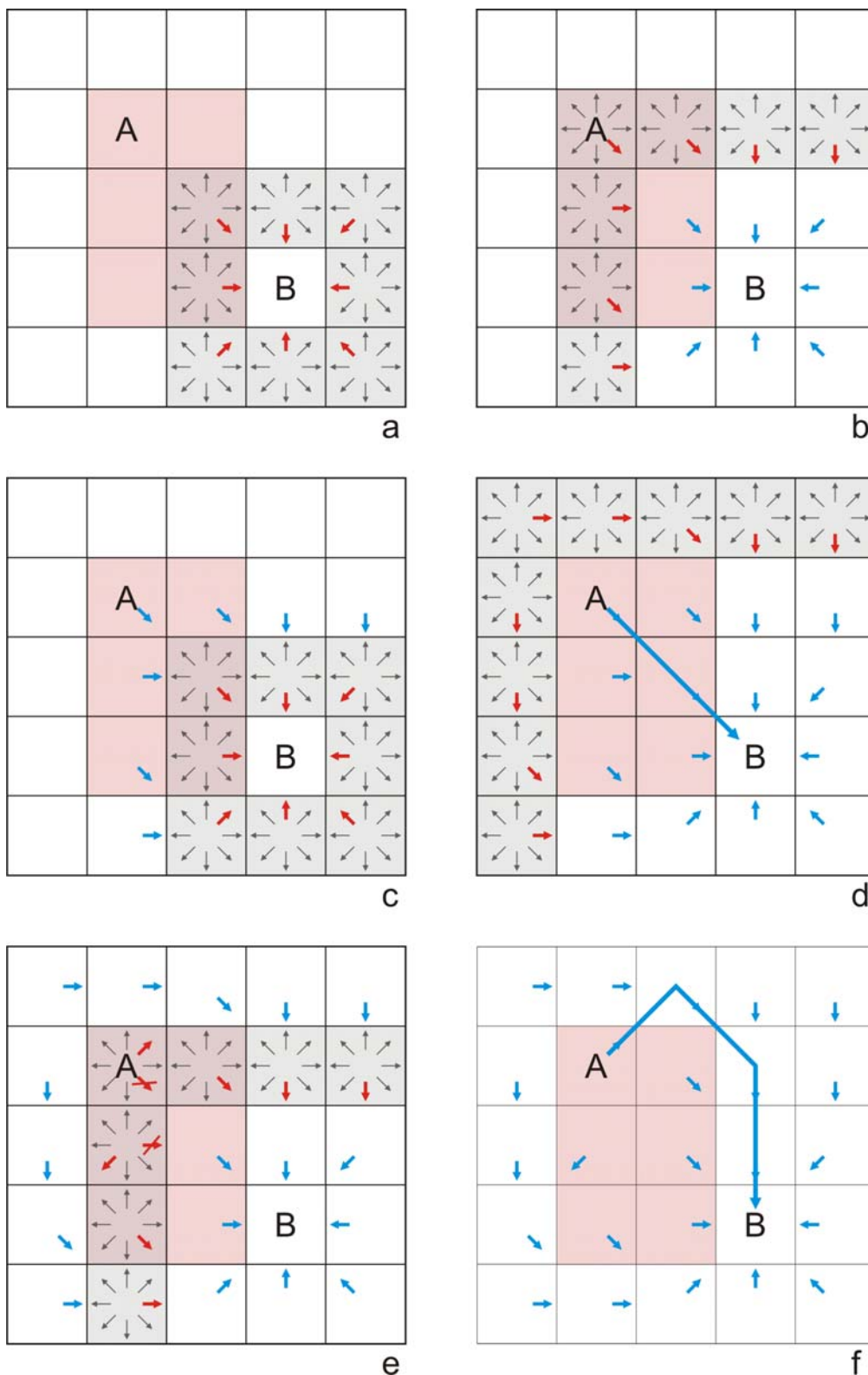


Figure 8-2: Explanation of the principles of spread algorithm, as it is used in Router. The goal is to find the least-cost trajectory from point A to point B on a 5 by 5 raster grid. Cost factors are not indicated, but the red shaded cells represent an area with higher construction costs. The steps to come to solution f are described in the main text.

This geographic and geologic information is converted into a raster format that matches the resolution of the Router grid. Thereby, each location or raster cell on the map is characterized by a certain soil type, slope, land use, region. The soil type map assigns each location to sand, sandy loam, loam, clay, peat, sandstone, shale with sandstone, shale, limestone (and lime) or zones with very steep slopes. The topography maps are divided in zones with slopes of 0 to 3°, 3 to 6° and 6 to 9°. The land use consists of areas of grassland, horticulture, arable land, arable land or forest, forest, nature reserve, urban zone and arable land or grassland. Different defined regions are Antwerp, Brussels, Flanders (except Antwerp), Walloon Region or Belgium as a whole.

Also the four cost factors are further subdivided. This is done solely for the ease of calibration. Terrain expertise forms the basis of this calibration scheme, and is indeed easier translated into these cost factors when split down into subcosts that are also discriminated in real projects. A list of these is given in figure 8-4. This list of cost factors is flexible, and can be modified at any time. The subcosts are used in two ways. Firstly, a matrix between the subcosts and the geoinformation types defines how much each of costs groups depends on terrain specific elements (fig. 8-4). Secondly, for each of the subcosts, the actual influence of terrain elements is defined as detailed terrain factors (fig. 8-5).

All of this information is then summarised into four main terrain factors, and used in PSS according to the following formula:

$$INV_{\text{pipe}} = TF_{\text{Mat}} \cdot INV_{\text{Mat}} + TF_{\text{Labor}} \cdot INV_{\text{Labor}} + TF_{\text{ROW}} \cdot INV_{\text{ROW}} + TF_{\text{Misc}} \cdot INV_{\text{Misc}} \quad (43)$$

The above procedure is capable of providing accurate estimates of the investment cost of a pipeline based on information from four raster layers. Also operational costs depend on location aspects, but in a different and less complex way. The issue can be simplified to height differences between the start and end point of the pipeline. The necessary information is read from a fifth raster layer (terrain model).

Next to raster data, also vector information is used in order to obtain the most correct estimate of pipeline investment costs. The basic difference is that raster data describe general terrain properties, characteristic for a certain area of land (e.g. woodland, urban area...). Such terrain properties are efficiently described by a set of terrain factors. Since these properties are characteristic of a certain area of land, the accuracy of the cost estimate is not very dependent of the resolution of the rasters. Router typically uses a 2.5 km mesh<sup>34</sup>.

Vector information, on the other hand, is much more efficient to describe discrete elements, such as main roads, rivers or railways. If these elements, referred to in this text as hinder elements or hinder objects, would have to be included as raster information, then the resolution would have to be decreased to the decametre level, which would have a very serious impact on calculation time of Router, and as Router is the slowest step in PSS, also on overall calculation time.

This is why Router is designed to handle vector data directly. Crossing a hinder object implies an additional cost, of which the elements are shown in figure 8-3. In order to make this information compatible with the raster calculations used by Router, following derivation is made. We would desire a solution that has the following format.

$$INV = INV_{TF} \cdot HF \quad (44)$$

with

$INV$  = total investment cost for pipeline construction, including the hinder objects

<sup>34</sup> Note that Router is capable of handling much higher resolutions. The limit is determined by the available memory of the computer system, and the required calculation speed. Successful test runs have been made at a resolution of less than 50 m. This was done in order to test if Router could be used at the scale of Europe.

$INV_{TF}$  = investment cost for pipeline construction, only considering terrain data

HF = hinder factor, accounting for the combined effects of the hinder objects encountered while moving from raster to raster cell

This definition assumes that the hinder factor also depends on the terrain factors. In other words, constructing a work in an area where the costs for pipeline construction are high, also implies that the works (e.g. tunnelling) are more expensive. In general this assumption is probably justified.

As shown in the figure 8-3, the additional costs are spend over distance  $W$ . Assume that the total distance between the two raster cells is distance  $L$ . Then the cost over that distance  $L$  can be expressed as:

$$INV = INV_{TF} \cdot (L - W) + INV_{TF} \cdot H \cdot W \quad (45)$$

with  $H$  the additional cost factor for crossing distance  $W$

This can be rewritten as:

$$INV = INV_{TF} \cdot \left( 1 + \frac{(H - 1) \cdot W}{L} \right) \quad (46)$$

For  $n$  multiple hinder objects, this expands to:

$$INV = INV_{TF} \cdot \left( 1 + \frac{\sum_{i=1}^n (H_i - 1) \cdot W_i}{L} \right) \quad (47)$$

which reduces to the desired equation 44, when the hinderfactor HF is defined as:

$$HF = 1 + \frac{\sum_{i=1}^n (H_i - 1) \cdot W_i}{L} \quad (48)$$

The introduction of the hinder factor allows to compile the hinder data prior to running a PSS simulation, and from then on use it with the same efficiency and comparable methodology as the raster data (terrain factors) are used. This approach has clear advantages, including the fact that after compilation, calculation speed is constant regardless of the number of hinder objects. Router currently uses a set of over 18000 hinder objects, consisting of over 100 000 segments, but this could potentially be much larger.

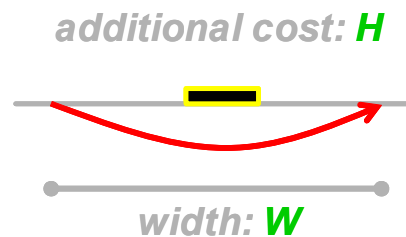


Figure 8-3: When a hinder object, such as a main road, railway or waterway, has to be crossed, then a work has to be performed that represents an additional cost. In this cartoon, the black block is a main road, and the red arrow the deviated drilling necessary for crossing that road.  $H$  is then the additional cost, in €/m, that has to be paid for a distance  $W$  (in m).

ID_	Label_CostGroup	SoilType_Ai	Topography_Ai	LandUse_Ai	RegionalEconomics_Ai	Check
<b>1 Materials</b>						
ID_	Label_CostClass	SoilType	Topography	LandUse	RegionalEconomics	
1	Line pipe				1	
2	Pipe coating					
3	Cathodic protection					
<b>2 Labor</b>						
ID_	Label_CostClass	SoilType	Topography	LandUse	RegionalEconomics	
1	Not specified	0.35	0.35	0.2	0.1	
<b>3 ROW</b>						
ID_	Label_CostClass	SoilType	Topography	LandUse	RegionalEconomics	
1	Obtaining ROW			0.5		
2	Allowing for damages			0.5		
<b>4 Miscellaneous</b>						
ID_	Label_CostClass	SoilType	Topography	LandUse	RegionalEconomics	
1	Surveying	0.16			0.04	
2	Engineering	0.1	0.07		0.03	
3	Supervision				0.1	
4	Contingencies		0.15			
5	Telecommunications equipment					
6	Freight (charges for transportation)				0.1	
7	Taxes				0.15	
8	Allowances for funds used during construction					
9	Administration and overheads				0.1	
10	Regulatory filing fees					

Figure 8-4: Example of the calibration matrix that defines the dependence of the different subfactors of the cost parameters versus the four groups of geoinformation that are taken into account. Together with the terrain factor data, these will determine the overall cost correction for pipeline construction at a certain location.

### 8.4.3 Advanced raster routing with Router

In the above sections, several background aspects of Router were discussed. As these and other properties make it stand out in front of other applications, they are briefly summarized here. In the simplified scheme in figure 8-2 routes to the eight immediate neighbours are considered. Router takes a similar approach, but evaluates 32 routing directions, not only to neighbouring steps, but in jumps up to 3 cells wide. This increases performance as well as smoothing the pipeline trajectories in a more realistic way.

Figure 8-5: Screen shot of the calibration form in which the cost dependency of, in this case Miscellaneous-Engineering costs are influenced by soil type, topography, land use and regional economics.

Router also exploits the basic principle of routing applications that simultaneously routes from one starting point to a large range of end points can be determined. In practice this means that the routes from one source, with known CO<sub>2</sub> production, are determined to all potential sinks within range.

Router estimates the pipeline investment cost by differentiating between material, labour, ROW and miscellaneous costs. An equation was derived for each of these cost factors, based on theoretic evaluation, US data of real pipelines, and general information for Belgium. These equations are used to estimate an average cost.

This average cost is then corrected for four location specific parameters, implying the use of four independent terrain factors. As such, Router makes use of multiple raster layers during cost calculation.

The operational cost of the pipeline, dominated by the compression and recompression costs, is balanced against the investment cost in order to optimise for pipeline diameter. Also height differences over the pipeline trajectory are taken into account for the calculation of the compression costs, making for this purpose use of a terrain model.

Linear elements (e.g. main roads) are identified as vector elements. A virtually unlimited number of these can be included without affecting calculation time. The specific use of vector elements in a basically spread algorithm allows to keep the size of the raster grid optimised for terrain specific data.

## **8.5 Economer: NPV based project evaluation**

The methodology is first explained for sources that are newly built. After this, the required modifications are detailed for retrofitting the new and old sources. A summary of all parameters is given in table 8-1 at the end of this section.

### **8.5.1 Methodology for 'New Sources'**

New sources are industrial facilities that are presently not existing, but may become active during the simulation time. New sources are only defined for the power sector, but the methodology is kept general in order to allow extension to other sectors. This is the reason why figures are e.g. expressed in UoP, which corresponds to GWh/y and needs to be converted to the more typically cited MW. The NPV<sup>35</sup> methodology was first detailed and implemented for these so called new sources, and later modified and extended to allow e.g. retrofit (see subsequent sections).

#### **8.5.1.1 Source capacity**

The PSS-simulator starts from the assumption that it is known how much production is needed at a certain year in the future (exogenous input).

For power production, this means that the share of fossil fuels in the energy production needs to be known. Other simulators, such as Markal/Times, can be used to determine the energy share. No distinction needs to be made between natural gas, coal, or energy technologies. The available technologies will be compared by PSS, and the ones with the highest NPV selected until demand is saturated. Import/export of electricity is necessary in order to exactly match production and demand.

For other industries, a comparable approach can be used, although it may be less clear what a realistic national capacity may be, since off-shoring is more of an issue in these sectors.

---

<sup>35</sup> NPV or Net Present Value: The current value of an asset as determined using appropriate discounting techniques. This means that costs and revenues are in an appropriate way added. A positive NPV therefore represents a profitable project.

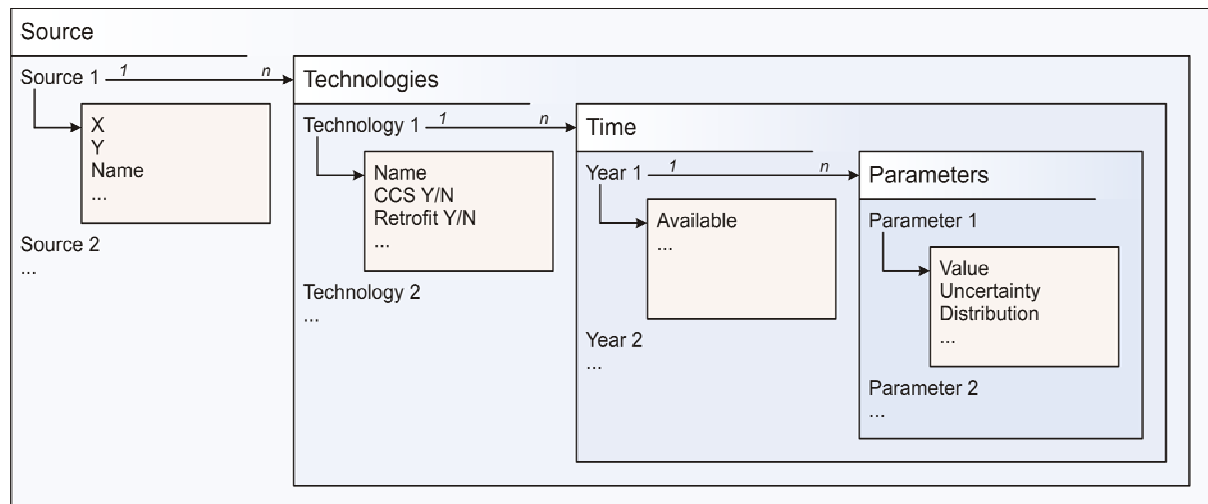


Figure 8-6: Generic presentation of how source data is organised in the PSS databases. For each source option, a number of technologies are available. For each technology option, time dependent data is defined. As parameters are stochastic, a 4<sup>th</sup> level is needed to defined these.

A conservative approach is currently followed, assuming that current production levels are maintained during the next decades. Alternatively, projections could be made where a link is defined with the rate of growth of the economy, or results from other models could be used.

#### 8.5.1.2 Source technologies

For most sources, a range of potential technologies needs to be assessed. A power plant may e.g. be developed after evaluation of different no-capture and capture technologies. It is the most economic one that will be selected, taking into account cost aspects for transport and storage.

These technological variants are characterised by different sets of operational parameters, but are located at the same site (XY are identical). The way the data is handled at database level is shown in the generic scheme in figure 8-6 and a screenshot in figure 8-7. The data is organised in four nested relations, starting at the top (level 1) with the general data of the site (name, location, sector, etc.). For each site, a range of technological options are listed by name (level 2), detailing also whether it concerns a retrofit or CCS technology. After this, a time relation is defined in order to make further parameters time dependent (level 3). Main parameters here are the year and whether the technology is available in that year. For each year, a parameter list is given (level 4), in which the value or uncertainty distribution for each parameter is defined.

#### 8.5.1.3 NPV source calculation

NPV related calculations are made for:

- Source
- Transport
- Storage
- CO<sub>2</sub> emissions (atmospheric emissions)

This is not completely possible for storage (see 8.5.1.6). Note that the cost of CO<sub>2</sub> (environmental cost) is excluded from the production cost.

ObjectID	Name	X	Y	Location	Operator	Sector	Unit of Production	Remark					
001	Coal and gas reference					Power	GWh	Based on Bertrand (2007), total investment costs & FOM were calculated with					
OptionID	Technology	RetroFitTechID	CCSTechID	ReferenceObject	ReferenceTechnology			Remark					
1	PC no capture			0				Reference for PC post combustion					
YearID	Available							Remark					
2000	0												
ParameterID	Remark	ValueDefinition	0_Estimate	1_Value	2_Min	2_Max	2_Round	3_Min	3_ProbMin	3_Max	3_ProbMax	3_Precision	4_Min
INV_s		1_Exact		489.888	436.32	610.416							
VOM_s		1_Exact		3852									
FOM_s		1_Exact		12.3984									
ProdCap_s		2_Block		4733.510	4049.7811	6644.4461	0						
AvF_s		1_Exact		0.8									
DiscRate_s		1_Exact		0.05									
DiscTime_s		1_Exact		40									
LifeTime		1_Exact		40									
FuelType_s		1_Exact		1									
FuelEm_s		1_Exact		9.27E-08									
ProdEff_s		2_Block		1.19E-10	1.083E-10	1.244E-10	12						
CaptEff_s		1_Exact		0									
FuelPrice_s	Coal 1.5%S	1_Exact		2.35E-06									
TL_INV_s		1_Exact		-0.074									
TLRefY_INV_s		1_Exact		2000									
TL_ProdEff_s		1_Exact		0.029									
TLRefY_ProdEff_s		1_Exact		2000									
CarbPressure_s		1_Exact		12									
+	2005	1											
+	2016	1											
+	2018	1											
+	2020	1											
+	2022	1											
+	2024	1											
+	2026	1											
+	2028	1											
+	2030	1											
+	2 PC post combustion		0	1									
+	3 IGCC no capture		0	0									Reference for IGCC pre combustion
+	4 IGCC pre combustion		0	1									
+	5 PC no capture		0	0									Reference for PC oxyfuel
+	6 PC oxyfuel		0	1									
+	7 NGCC no capture		0	0									Reference for NGCC post combustion
+	8 NGCC post combustion		0	1									
+	9 NGCC no capture		0	0									Reference for NGCC pre combustion

Figure 8-7: A screen shot from the source database, of which the structure is shown in figure 8-6.

For the source part calculation is based on the methodology described in chapter 2 for power plants and generalised for other sectors. It is important that all costs are converted to the same basis, which is €/UoP<sup>36</sup> (€/kWh for power plants). Project and project variants can then easily be compared on an economic basis, which is the production price.

$$\text{ProdCost}_{\text{UoP},s} = \text{INV}_{\text{UoP},s} + \text{FOM}_{\text{UoP},s} + \text{VOM}_s + \text{FuelUse}_{\text{UoP},s} \quad (49)$$

with

$$\text{INV}_{\text{UoP},s} = \frac{\text{INV}_s \cdot \text{FCF}_s}{\text{AvF}_s \cdot \text{ProdCap}_s} \quad (50)$$

$$\text{FOM}_{\text{UoP},s} = \frac{\text{FOM}_s}{\text{AcF}_s \cdot \text{ProdCap}_s} \quad (51)$$

$$\text{FuelUse}_{\text{UoP},s} = \frac{\text{FuelCost}}{\text{ProdEff}_s} \quad (52)$$

$$\text{FCF}_s = \frac{\text{DiscRate}_s}{1 - (1 + \text{DiscRate}_s)^{-\text{DiscTime}_s}} \quad (53)$$

Technological parameters, especially efficiency and investment costs, vary with time. However, these are ‘locked’ the moment the power plant appears in the simulation (the technology of the building year is used, plant is not modified later on, unless through a specifically defined retrofit).

<sup>36</sup> UoP: Unit of Production. UoP corresponds to kWh for the power sector, kTon NH<sub>3</sub> in the ammonia sector, etc.

### 8.5.1.4 NPV transport

Router calculates the transport costs in relation to the CO<sub>2</sub> emissions of the source plant (or that fraction that will be stored). This can also be expressed in €/UoP:

$$\text{TrCost}_{\text{UoP},p} = \text{TrCost}_{\text{Me},p} \cdot \text{ProdCost}_s \quad (54)$$

Router is designed to account for all compression costs, and are therefore not detailed in the former formula. Note however that Router also has a parameter to exclude compression costs at the source completely or partly from the economic evaluation, e.g. for making sensitivity analysis.

In general, however, this means that production efficiency takes into account the reduced performance of the capture installation, such as separation of CO<sub>2</sub>, but not compression, since this is part of the transport emissions.

### 8.5.1.5 NPV CO<sub>2</sub>

#### a) CCS-projects

CCS projects may compete with non-CCS projects because of the offsets obtained through the market price of CO<sub>2</sub>. Here we will assume that emitting CO<sub>2</sub> is penalized according to the CO<sub>2</sub> market price, which is an endogenous parameter. Calculation is as follows:

$$\text{CarbEmCost}_{s,p,r} = \text{CarbPrice} \cdot \frac{(\text{CarbEmNet}_s + \text{CarbEmNet}_p + \text{CarbEmNet}_r) + (1 - \text{AccF}) \cdot \text{CarbCounted}}{\text{ProdCap} \cdot \text{AvF}} \quad (55)$$

With

$$\text{CarbEmNet}_s = \text{CarbEmTot}_{\text{UoP},s} - \text{CarbCapt}_s \quad (56)$$

$$\text{CarbEmNet}_r = \frac{\text{CarbCapt}_s}{\text{StEff}_r} \cdot \text{FuelEm}_r \quad (57)^{37}$$

$$\text{CarbEmNet}_p = \frac{\text{VOM}_p}{\text{FuelCost}_p} \cdot \text{FuelEm}_p \quad (58)^{38}$$

with

$$\text{VOM}_p = \text{VOM}_{\text{SourceCompression}} + \text{VOM}_{\text{BoosterCompression}} \quad (59)$$

$$\text{CarbCounted} = \begin{matrix} \text{CarbStore} \\ \text{or} \\ \text{CarbAvoided} \end{matrix} \quad (60)$$

with

$$\text{CarbStored} = \text{CarbCapt}_s \quad (61)$$

$$\text{CarbAvoided} = \text{CarbEmNet}_{\text{ref}} - \text{CarbEmNet}_{s,p,r} \quad (62)$$

with

$$\text{CarbCapt}_s = \text{CarbEmTot}_s \cdot \text{CaptEff}_s \quad (63)$$

$$\text{CarbEmTot}_s = \frac{\text{ProdCap}_s \cdot \text{AvF}_s}{\text{ProdEff}_s} \cdot \text{FuelEm}_s \quad (64)$$

Note that part of the energy needed for transport (initial compression) can be provided by the source, e.g. when the compressor uses electricity from the source. This requires correcting the fuel consumption by reducing it with the fuel provided by the source, but this will also influence the net production of the facility (reduced power output for sale). Therefore this is

<sup>37</sup> These values can be calculated based on the compression needed for injection. For demo purposes, a 10 MW natural gas compressor was assumed for an injection of 1Mton/y. This gives following parameters:

$\text{FuelEm}_r = 55.82 \text{ kton/PJ} = 55.82 \cdot 10^{-9} \text{ ton/kJ}$

$\text{StEff}_r = 3.17 \cdot 10^{-6} \text{ ton/kJ}$  (currently  $3.85 \cdot 10^{-6}$  is used).

<sup>38</sup> This function uses the output of Router. In this output, VOM is a summary of the fuel costs for compression.

currently not included, and energy for compression and also injection is typically considered to be provided by natural gas.

The cost for emitting carbon is basically calculated by summing up the carbon emissions throughout the CCS chain, and then multiplying it by the market price (penalty) of CO<sub>2</sub>. In order to allow taking into account measures that discourage or stimulate CCS activities, a second term is used that is based on the amount of CO<sub>2</sub> stored and an ‘acceptability factor’. If this factor is, e.g. 0.75, then this means that only 75% of the stored CO<sub>2</sub> is regarded as counted (not emitted into the atmosphere). In a regime where the technology is (temporarily) stimulated, it can also be larger than 1 (e.g. 2), implying that the amount of CO<sub>2</sub> stored is counted double (this would imply a certain regime of subsidised activities, as are currently suggested). In the current scenarios, it is set to 1 (calculation only based on net emissions, acceptability term becomes zero).

#### b) No-CCS projects

For no-CCS technologies, the formulas are reduced to:

$$\text{CarbEmCost}_{s,p,r} = \text{CarbPrice} \cdot \frac{\text{CarbEmNet}_s}{\text{ProdCap} \cdot \text{AvF}} \quad (65)$$

$$\text{CarbEmNet}_s = \text{CarbEmTot}_{\text{UoP},s} \quad (66)$$

#### 8.5.1.6 NPV storage

Following the Real Options approach for estimating realistic storage probabilities and capacities (see §8.4.1), storage costs can not be calculated independently as is done for the other steps. Instead a stepwise approach is followed, detailed below.

First the no-capture technologies available at a certain site are evaluated, and from that the most economic one is selected (the local reference technology).

$$\text{ProspCost}_{\text{ref}} = \text{Min}_{\text{ec}} (\text{ProspCost}_{\text{NoCCS}}) \quad (67)^{39}$$

Then the potential capture technologies can be evaluated, using the following starting equation:

$$\text{StCost}_{\text{UoP},r} \leq \text{ProspCost}_{\text{ref}} - (\text{ProdCost}_{\text{UoP},s} + \text{TrCost}_{\text{UoP},p} + \text{CarbEmCost}_{\text{UoP},s,p,r}) \quad (68)$$

which states that the storage costs should be smaller than the difference between the expected (average) costs of the reference project and the sum of the other project costs.

This allows using the results from the real options sink evaluation (see §8.4.1), where the starting point is the maximum allowed cost for storage. This is done in a 3 step process:

1. Evaluate the Poison probability corresponding to the maximum storage cost.
2. On go: sample corresponding yearly capacity.
3. If sufficient: determine the cost corresponding to the needed storage capacity, which replaces the initial (conservative) estimate of the storage cost.

Note that capacity and costs are treated in the above scheme as independent parameters, although they are to a certain degree related.

#### 8.5.1.7 NPV prospect

In PSS prospects are potential projects, still under evaluation. The NPV, or more precisely the levelized costs of prospects can now be expressed as:

$$\text{ProjCost}_{\text{UoP}} = \text{ProdCost}_{\text{UoP},s} + \text{TrCost}_{\text{UoP},p} + \text{StorCost}_{\text{UoP},r} + \text{CarbEmCost}_{\text{UoP},s,p,r} \quad (69)$$

<sup>39</sup> The function  $\text{Min}_{\text{ec}}$  implies that project uncertainty is taken into account (e.g. in an NPV or options approach).

This allows to select the most economic technology at a certain site, and afterwards select from the range of prospects evaluated the actual (most economic) projects needed order to meet demand.

#### **8.5.1.8 Source database**

A general overview of the way source technology parameters are structured is given in §8.5.1.2. There are however additional, more technical requirements that this database and the parameters structure in PSS needs to meet. These can be summarised as follows:

1. Ability to define standard technologies.
2. Make reference to these standard technologies for actual technologies.
3. Indicate when or for what parameters an actual technology differs from a standard technology.
4. Include existing facilities.
5. Group technology variants for one site (in order to distinguish them from other potential sites).
6. Distinguish between CCS and no-CCS technologies (necessary for storage calculation).
7. Allow for time dependent parameters.

#### **8.5.2 Retrofit for 'New Sources'**

The retrofit technology for new sources was implemented directly in code, but was changed at a later time to be more parallel with the evaluation procedure of old sources.

The basic steps in the retrofit procedure for new sources are:

1. Check which retrofit technologies exist for an existing plant, given the technology activated and the current year.
2. Calculate the economics, including the effects of the retrofit technologies.
3. If retrofitting is more economic, then choose the most economic retrofit option.

Retrofit technologies are defined in the same table set as new technologies. The data definitions are at this level identical, with one exception: the  $INV_s$  is the incremental investment cost, or the cost to retrofit the plant.  $INV_s$  is therefore  $\Delta INV_s$ . All other parameters, such as O&M costs, are defined for the whole installation.

The methodology to calculate the economics of retrofitting new sources is largely parallel to that of old sources (discussed in § 8.5.3), but since more actual data are considered to be known, the calculation is more direct. In view of the many parallels and for reason of recurrence, the actual formulas are not cited here.

The main drive for a retrofit to gain an economic advantage through time, are the increased prices of CO<sub>2</sub> and the learning curves.

#### **8.5.3 Retrofit for 'Old Sources'**

The so called old sources are sources that are present in the current database (with a reference year of ~2005). Major difference with the new sources is that the data is much more limited. Evaluating a retrofit of these technologies therefore requires a modified methodology than for the new sources.

##### **8.5.3.1 Data available for 'Old Sources'**

The fact that less data is available for currently existing sources, has a simple reason. Making an economic evaluation of new sources requires knowing all relevant operational parameters. The uncertainty on the assumed values of these parameters is an essential part of an economic evaluation.

For existing or old sources the operating parameters are exactly known, but not publicly available. There is however less need to have an estimate on all of these parameters, since it can be assumed that the facility is economic.

For simple simulation purposes, without evaluating CCS-retrofits, it is sufficient to know the production capacity, CO<sub>2</sub> production and expected lifetime of existing sources. When evaluating retrofits, some additional parameters need to be known for reasons provided further on.

*a) ProdCap<sub>s</sub> and AvF<sub>s</sub>*

Production capacity is taken directly from the source database, as well as the typical AvF for this installation. The production is therefore a calculated estimate, instead of the actually reported production for a certain reference year.

*b) CarbEmTot<sub>s</sub>*

Two numbers are provided in the database: an actual reported yearly number from around 2005, and an estimate provided by the source database (section 2.1). The latter is used, because it is generally considered as a better average than the reported emission from a specific year, since the estimate is based on typical operating conditions.

*c) ProdEff<sub>s</sub>, FuelType and EmFact<sub>s</sub>*

The production efficiency indicates how much energy is consumed to produce 1 UoP. It is not provided by the database, but can be estimated from the emission factor (expressed in tonCO<sub>2</sub>/UoP) and the fuel type (with known energy and emission parameters).

*d) StartYear<sub>s</sub> and EndYear<sub>s</sub>*

The starting year is normally exactly known, the end year is the year in which the facility is expected to close down.

### **8.5.3.2 Modified methodology**

The modification compared to the one used for the retrofit of new sources is basically that the incremental costs and fuel use are used, instead of total parameters. For retrofit of new sources, this was only done for the investment cost.

This overcomes the problem that these exact numbers are not known for the existing source. In brief, in this way the net additional cost of the retrofit is calculated. When this is negative, then the additional costs are offset by the mitigation returns, and the retrofit is economic.

*a) Alternative and new parameter definitions*

Following parameters are defined as the difference between the retrofitted and original plant when preceded by a delta sign: ProdCost<sub>s</sub>, INV<sub>s</sub>, FOM<sub>s</sub>, VOM<sub>s</sub>, FuelUse<sub>s</sub>, CarbEmTot<sub>s</sub> and ProdCap<sub>s</sub>.

When these parameters occur as quotients, then replacing them by their increments does not result in the increment of the result. This happens for two parameters (ProdCap and ProdEff), for which new parameters are introduced that are defined as follows:

$$\Delta\text{ProdCapQ}_s = \frac{\text{ProdCap}_{s,\text{ref}} \cdot \text{ProdCap}_s}{\text{ProdCap}_{s,\text{ref}} - \text{ProdCap}_s} \quad (70)$$

$$\Delta\text{ProdEffQ}_s = \frac{\text{ProdEff}_{s,\text{ref}} \cdot \text{ProdEff}_s}{\text{ProdEff}_{s,\text{ref}} - \text{ProdEff}_s} \quad (71)$$

This Q-definition is the result from following generic derivation in which a is constant and b a variable:

$$\Delta r = \Delta \frac{a}{b} = \frac{a}{b} - \frac{a}{b_0} = a \cdot \frac{b_0 - b}{b_0 \cdot b} = \frac{a}{b_0 \cdot b} = \frac{a}{\Delta b Q} \quad (72)$$

Whereas this problem does not occur for the situation in which a is variable and b constant:

$$\Delta r = \Delta \frac{a}{b} = \frac{a}{b} - \frac{a_0}{b} = \frac{a - a_0}{b} = \frac{\Delta a}{b} \quad (73)$$

### b) Modified formulas

Once these parameters have been defined, the modifications to the formulas are relatively limited. This has effect on two parts in the calculation scheme.

For the NPV source calculation, the formulas are modified to:

$$\Delta \text{ProdCost}_{\text{UoP},s} = \Delta \text{INV}_{\text{UoP},s} + \Delta \text{FOM}_{\text{UoP},s} + \Delta \text{VOM}_s + \Delta \text{FuelUse}_{\text{UoP},s} \quad (74)$$

with

$$\Delta \text{INV}_{\text{UoP},s} = \frac{\Delta \text{INV}_s \cdot \text{FCF}_s}{\text{AvF}_s \cdot \Delta \text{ProdCapQ}_s} \quad (75)$$

$$\Delta \text{FOM}_{\text{UoP},s} = \frac{\text{FOM}_s}{\text{AvF}_s \cdot \Delta \text{ProdCapQ}_s} \quad (76)$$

$$\Delta \text{FuelUse}_{\text{UoP},s} = \frac{\text{FuelCost}}{\Delta \text{ProdEffQ}_s} \quad (77)$$

For the NPV<sub>CO<sub>2</sub></sub> calculation of the CCS retrofit, total carbon emission is affected:

$$\text{CarbEmTot}_s = \Delta \text{CarbEmTot}_s + \text{CarbEmNet}_{\text{ref}} \quad (78)$$

$$\Delta \text{CarbEmTot}_s = \frac{\Delta \text{ProdCap}_s \cdot \text{AvF}_s}{\Delta \text{ProdEffQ}_s} \cdot \text{FuelEm}_s \quad (79)$$

where CarbEmNet<sub>ref</sub> is the net emission of the old source.

## 8.6 PSS definition of CO<sub>2</sub> avoided

A clear distinction should be made between CO<sub>2</sub> captured and CO<sub>2</sub> avoided. The definition of CO<sub>2</sub> captured is rather straightforwardly the amount of CO<sub>2</sub> captured at the source. In most cases, CO<sub>2</sub> captured should be equal to CO<sub>2</sub> stored. The concept plays an important role in CCS projects, as generally the larger the amount is of captured CO<sub>2</sub>, the higher the costs for capture, transport and injection.

The environmental quality of the project, however, is determined by the amount of CO<sub>2</sub> that is, in spite of CCS, still released. This net amount is the sum of CO<sub>2</sub> emissions at the source, during transport, and during injection, and is closely related to the amount of energy that is required for these operations (see fig. 8-8). Note that projects are penalised on the amount of CO<sub>2</sub> emitted, not rewarded on the amounts stored.

From a general point of view, a third aspect is important, namely how much CO<sub>2</sub> is not emitted into the atmosphere because of CCS is applied. This answer is provided by the parameter CO<sub>2</sub> avoided as defined in section 2.5.3.2: 'CO<sub>2</sub> avoided is obtained by subtracting the emissions of a plant with CO<sub>2</sub> capture from the emissions of the reference plant without capture'. The reference plant here is not necessarily the same plant without capture. In PSS it is instead defined as the plant that would be build if CCS technology was not available, which is the most economic no-CCS plant (taking into account all cost aspects, so also the price on CO<sub>2</sub> emissions). As is shown in figure 8-8, CO<sub>2</sub> avoided will usually be smaller than CO<sub>2</sub> captured. Close inspection of the demo results (chapter 9) reveals that this is however not an absolute law, as in rare cases the reference plant may fire coal, and the CCS plant natural gas.

Table 8-1: Overview of the main parameters used in section 8.5. Note that units may differ, based on indexes that refer to a specific cost basis.

<b>Parameter</b>	<b>Unit</b>	<b>Description</b>	<b>s,p,r</b>
$X_s$		Index indicating that parameter relates to source activities, so excluding compression, transport, storage, CO <sub>2</sub> costs (s for source)	
$X_p$		Indicating transport (p for pipe)	
$X_r$		Indicating storage (r for reservoir)	
$X_{UoP}$		Index indicating that parameter is expressed as specific value per unit of production (UoP). For parameters this results in a €/UoP basis.	
$X_{CO_2}$		Specific parameter, expressed per ton <sub>CO<sub>2</sub></sub> . CO <sub>2</sub> may be CO <sub>2</sub> captured, avoided, transported, injected, etc. depending on the context.	
$X_{ref}$		Parameter of reference plant, which is the most economic no-CCS plant at that site.	
$AccF$	-	'Acceptability' factor	e
$AvF$	-	Capacity Factor (fraction, also availability factor)	s
$CaptEff$	-	Capture efficiency (fraction)	s
$CarbAvoided$	tonCO <sub>2</sub> /y	Carbon avoided	
$CarbCapt$	tonCO <sub>2</sub> /y	Carbon Emissions captured	s
$CarbCounted$	tonCO <sub>2</sub> /y	Amount of carbon that is regarded as not emitted (either avoided or stored)	
$CarbEmCost$	€/y	Cost of carbon produced	s,p,r
$CarbEmNet$	tonCO <sub>2</sub> /y	Net carbon emission (total minus captured)	s,p,r,ref
$CarbEmTot$	tonCO <sub>2</sub> /y	Total Carbon Emission (all carbon produced, including the captured carbon)	s
$CarbPrice$	€/tonCO <sub>2</sub>	Cost Of Emission per unit released	e
$CarbStored$	tonCO <sub>2</sub> /y	Amount of carbon that is geologically stored	
$DiscRate$	-	fraction	s
$DiscTime$	y	Economic life time of facility	s
$FCF$	1/y	Fixed charge factor	s
$FOM$	€/y	Fixed operation and maintenance	s
$FuelCost$	€/kJ	Fuel Cost	e
$FuelEm$	tonCO <sub>2</sub> /kJ	Amount of CO <sub>2</sub> produced per unit of energy for a certain type of fuel	s,p,r
$FuelUse$	€/UoP	Value of the amount of energy used.	s
$INV$	€	Total investment cost, except for retrofits: then this is the incremental cost (economy takes care of adding up the investment cost of the original plant and the retrofit investment)	s
$ProdCap$	UoP/y	Yearly potential capacity, beware to convert MW to GWh/y for power production <sup>40, 41</sup>	s
$ProdCost$	€/UoP	Cost Of Production (CO <sub>2</sub> cost not included)	s
$ProdEff$	UoP/kJ	Production energy efficiency (inverse of specific consumption)	s
$ProjCost$	€/y	Project cost	
$ProspCost$	€/y	Prospect cost	ref,NoCCS
$StCost$	€/y	Storage cost	r
$StEff$	tonCO <sub>2</sub> /kJ	Storage energy efficiency	s
$TrCost$	€/y	Cost Of Transport	p
$TrEff$	tonCO <sub>2</sub> /kJ	Transport energy efficiency	p
$VOM$	€/UoP €/y <sup>42</sup>	variable operation and maintenance	s p

<sup>40</sup> 1 MW = 8.76576 GWh/y (1 y = 365.24\*24 h)<sup>41</sup> ProdCap is not a stochastic value in PSS, since extrapolation procedures rely on normalisation on a fixed size for the plant. E.g. ranges for investment costs are given in function of a fixed size of the plant.

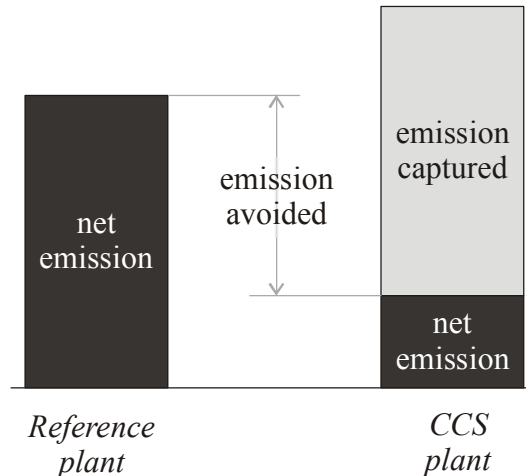


Figure 8-8: CO<sub>2</sub> avoided is defined as the difference between the net emission from a CCS plant and that of the reference plant. As such, it is usually, but not always, smaller than the amount of CO<sub>2</sub> captured.

## 8.7 Sinkers: estimating storage capacity

### 8.7.1 Introduction

In general, regional simulations regarding the potential for CCS tend to take into account only those reservoirs that are sufficiently known which implies that a usually significant number of reservoirs are not considered. Overall results will therefore be conservative. This is usually acceptable, but such an approach can only be used if a sufficient portion of the storage capacity can be regarded as nearly proven.

In other regions the degree of exploration of the deeper subsurface may be much poorer, for example, areas with little or no proven oil- and gas reserves. Resultantly, too few storage sites may qualify as sufficiently known to follow the conservative approach. Nevertheless, also in these areas significant opportunities may exist, although currently still surrounded by high uncertainties.

Arguably, an exploration campaign is what is needed to shed more light on the regional storage potential, but unfortunately the incentives to do this only for the purpose of storing CO<sub>2</sub> are currently lacking.

Belgium is in such a situation. It is also surrounded by other regions, including the North Sea, where storage opportunities for CO<sub>2</sub> are known with much more confidence. When simulations were made regarding the implementation of CCS in Belgium, an interesting aspect was the competition between exporting CO<sub>2</sub> towards neighbouring countries, versus storing it in domestic, currently largely unexplored reservoirs.

Making such an evaluation required a completely new way of assessing CO<sub>2</sub> reservoirs, which was done by combining elements from real options theory with geotechnical expert judgements. This new assessment technique forms the main topic of this publication.

### 8.7.2 Conceptual model

Making a detailed geotechnical evaluation of a certain storage reservoir is a complicated issue, involving techniques such as 3D-reservoir simulation. Without access to reliable and relatively detailed data, such an evaluation is not possible. It is also not practical when making

<sup>42</sup> This value is taken from the Router output, where specific costs are typically expressed in €/y.

an overall appraisal of a regional storage capacity. Often some quick-scan approach is used, leading to a qualitative or semi-quantitative ranking of storage sites. Such an approach also requires a significant level of knowledge. Sites with poor data are usually filtered out in a geotechnical evaluation because results are too uncertain or contested.

The basic problem that arises when uncertainties grow too large, is that absolute statements can not longer reliably be made. This problem is also known from other domains, such as economics, where appraisal techniques have been developed that successfully can handle large uncertainties. Real options as it is applied to estimate the net present value of an asset, is a technique that will show to be applicable, in a modified form, to estimating the CO<sub>2</sub>-storage capacity in poorly known areas.

### **8.7.2.1 Real Options**

An important goal of economical sciences is to correctly estimate the value of an asset before it is acquired. This is an important aspect when buying concessions or for estimating what up-front investments are justified when developing them. In the most basic approach, all revenues and expenses are estimated and compared on a discounted basis. The result is the net present value (NPV) of the asset. This NPV indicates how much money can be invested in purchasing or developing the asset.

Usually several parameters are not exactly known at the moment the asset is evaluated, and stochastic techniques, such as Monte-Carlo, are used to evaluate the impact of these uncertainties. This approach leads to a NPV distribution, rather than a single value, and gives a more realistic view of the asset and especially of the investment risks.

Yet, although all uncertainties are (at least theoretically) taken into account, this NPV approach is still unrealistic in one way. Let's, for sake of illustration, assume that Monte-Carlo is used to calculate the NPV distribution. For each run, the revenues but especially also all costs for the whole project are taken into account. This is realistic for optimistic outcomes, because then exploration and development is followed by profitable exploitation. For pessimistic assumptions, however, projects will normally be terminated when exploration shows that exploitation is not profitable.

Real options is a way to introduce such decisions in a NPV evaluation and make the result more accurate. The basic principle of real options is therefore simply including a decision scheme when calculating the value of an asset. The difference with a standard NPV technique, called the real options value, can be very significant. It has become common practice in many fields, such as the bidding for oil- and gas concessions.

### **8.7.2.2 Concept of project**

A general decision scheme was set up that describes the main steps when developing a potential CO<sub>2</sub> storage site. This schema deliberately only includes main decision points, as it is used for making a general assessment. Similar schemes for actual projects are usually more complex.

The scheme, shown in figure 8-9, shows two go/no-go points. In point 1, a potential investor decides whether or not to explore a potential site. We will show later why this is important. The decision is taken using a binomial probability, with the likeliness to explore being positively related to the price of CO<sub>2</sub>.

Between point 1 and 2, supposed investments are made in research and exploration. At point 2, it is assumed that the site is sufficiently known in order to evaluate whether development of the project will result in additional profit, or whether the project has to be abandoned. It will later be shown that the latter may be due to poor economic outlooks, or pure geotechnical reasons.

This scheme is applicable to aquifer-like reservoirs for which exploration is lacking or incomplete. It is however also valid for Enhanced CoalBed Methane (ECBM) prospects, where up-front investment may be more focussed on research and development of CO<sub>2</sub>-injection and CH<sub>4</sub>-recovery techniques.

From this scheme, it is also obvious why this approach is redundant for e.g. empty oil and gas fields or properly documented aquifers, as these storage opportunities can be assumed to be close to decision point 2.

### **8.7.2.3 Concept of storage site**

Three types of parameters can be distinguished in a real options calculation: parameters of which the values are sufficiently known to be considered as exact, those for which the uncertainties need to be evaluated, and poison probabilities deciding which branches of the binomial tree to follow.

Net present value techniques are usually applied by economists, and it is probably for this reason that in most textbook examples the stochastic parameters are purely economic parameters, such as the price of products, energy, etc. Our approach is different in this respect, as the starting assumption is that the uncertainty on the geotechnical parameters outweighs that of other relevant parameters. This is no doubt justified, considering the fact that the potential CO<sub>2</sub> reservoirs in the context of this study are very poorly known. The actual input data presented further will show that the uncertainty on key parameters may range several orders of magnitude for certain reservoirs.

Without challenging the fact that CO<sub>2</sub> injection into reservoirs is highly complex in reality, this real-world situation was strongly simplified into a conceptual context that is shown in figure 8-10. In this situation, three key issues are considered as relevant and capable of describing in a generic way aquifers and coal reservoirs.

The first basic question is whether the potential reservoir will prove to be able to actually trap the injected CO<sub>2</sub>. For aquifers this generally boils down to the question whether seal and trapping structure are adequate. One may think of this as the safety aspect, but other aspects may be found relevant as well, such as CO<sub>2</sub>-accounting or conflicts of interest. The answer is a simple yes or no, and the corresponding parameter therefore a poison probability.

Secondly, it is important to know what the total capacity of the reservoir is, or how much CO<sub>2</sub> can be stored in the reservoir if it is used completely. Given the low degree of geological data, the answer will be a continuous range of possible answers rather than a single value. The third parameter estimates how much CO<sub>2</sub> can be injected on a yearly basis in a certain reservoir. Again, this parameter needs to be defined as a stochastic parameter. The size and rate parameters obviously depend on the injection configuration, such as number and type of wells, and injection conditions.

### **8.7.3 Expert input**

Also after simplifying the storage problem by narrowing down to the essential geotechnical aspects, it is not possible to provide an objective answer to the three basic questions shown in figure 8-10. If data is available, it is usually of poor quality, of insufficient quantity, or needs to be extrapolated over larger distances.

For experts, this information is however be sufficient to form an opinion on basic reservoir properties. This opinion is of course not absolute, but enough to answer the basic reservoir questions in the manner given below, which is actually the procedure that was followed for

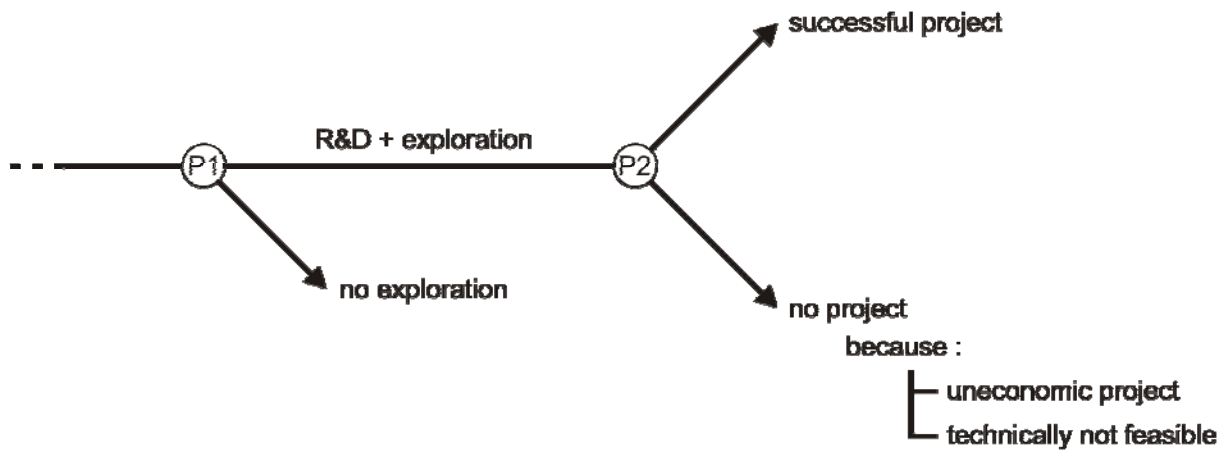


Figure 8-9: Conceptual binomial tree, illustrating the two main decision point used in the reservoir evaluation scheme.

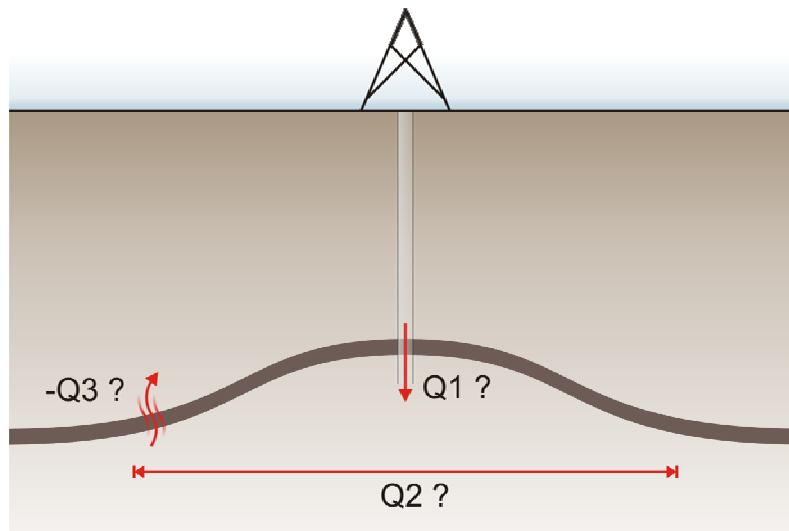


Figure 8-10: The generic reservoir with the three main parameters that need to be evaluated in order to make general cost-capacity estimates. The generic reservoir mimics an aquifer, but the principle can also be applied to coal.

making the reservoir estimates for the demonstration projections. For practical purposes, only experts from the project were at this stage asked for their opinion.

Each expert was given a list of potential reservoirs in Belgium, together with a brief description. At this moment the experts were allowed to comment on this list. As a result the definition of some of the reservoirs were clarified to make sure that the evaluations of the different experts would be comparable in terms of e.g. stratigraphic and areal delineation. Also the number of possible injection points was agreed upon.

In a next step, each of the experts individually answered the three basic questions for each reservoir on the list, unless he found himself not qualified (outside his field of expertise). The questions were organised in an excel worksheet, but can be summarised as follows:

- What is the chance that reservoir X is not suited for storing CO<sub>2</sub>? Answer: 70%.

- What is the total capacity of the reservoir? Answer: a probability distribution, drawn by the expert.
- What is the yearly injection capacity at a typical injection site? Answer: again a probability distribution.

Note that the probability distributions may span orders of magnitude, and do not necessarily approach a normal or lognormal distribution, but reflect the view of the expert. It may e.g. be justified to draw a bimodal distribution for injection capacity in a case where the reservoir rock would initially be expected to have a very good permeability, but whether it is uncertain if the reservoir has been affected by cementing.

Views of experts usually differ, but they can simply be combined by averaging the poison probabilities and the continuous probability distributions. In this way, quantitative data is obtained for the three questions that need to be answered in the real options scheme.

### 8.7.4 Real Options calculation scheme

The expert data is used in the real options calculation scheme, of which the simplified binomial tree is shown in figure 8-9. The actual calculation takes into account required rates of return, discount times, time and budgetary constraints, etc. and discriminates for each project exploration, R&D and operation phases. The cost of the project are described in terms of investment costs, variable and fixed operation costs, and the cost for emitting CO<sub>2</sub>. Monte-Carlo techniques are used to provide the stochastic outcome. The methodology deviates from standard real option forecasts, because it does not express the success of a project in the cash-flow that it returns. This parameter, expressed as net present value, is calculated in order to verify if the project is successful, but it is the amount of CO<sub>2</sub> stored that is the relevant output parameter.

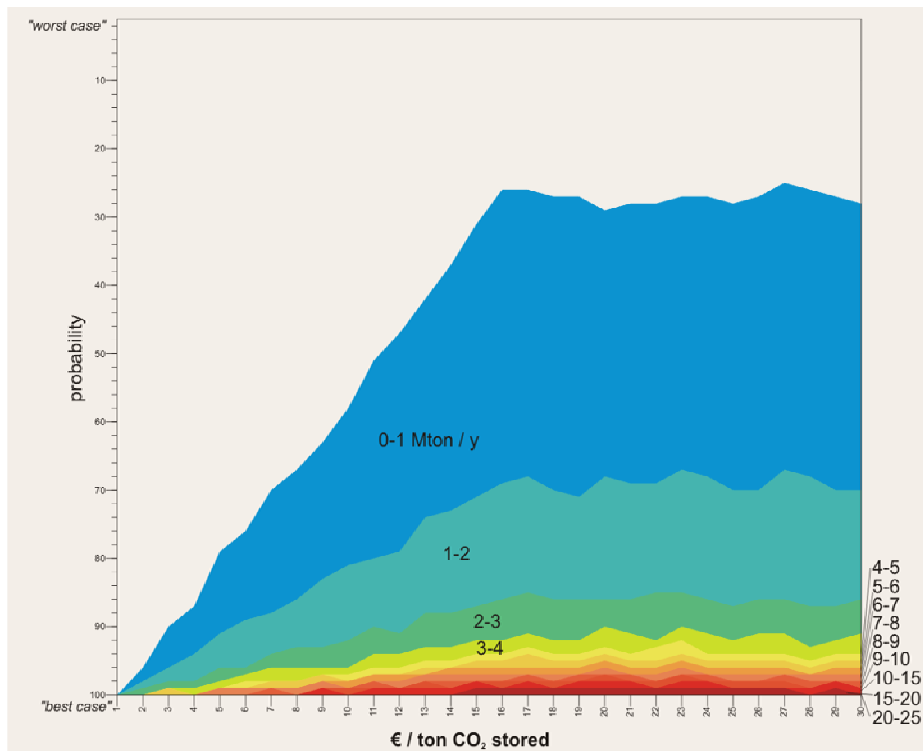


Figure 8-11: Capacity estimates, here expressed in MTon/year for a reservoir. The results are plotted in function of the affordable cost for CO<sub>2</sub> storage and future probability.

### 8.7.5 Presentation of results

The results (e.g. fig. 8-11) show a relation between the price of CO<sub>2</sub> that can be paid for storing it (so excluding capture and storage costs) which is indicated on the horizontal axis, and the amount that can be injected in a certain reservoir, which is shown as coloured areas and is expressed in Mton/y. The vertical axis indicates the probability that you are somewhere between 'worst case' and 'best case' from a storage point of view.

It is clear that there is a 25% probability that no CO<sub>2</sub> can be injected in this reservoir. This is an absolute limit. Increasing the price for CO<sub>2</sub> does not change this probability, as it is caused by the current fundamental uncertainty regarding the reservoir sealing.

On the other hand, there is a 30% probability that more than 1 Mton of CO<sub>2</sub> can be stored annually, at least when the cost for storing CO<sub>2</sub> is allowed to be higher than 15 €/ton. If storage costs can only be 5 €/ton, then this probability is only 10% for this reservoir.

The individual reservoir (fig. 8-11) is deliberately not identified, as the results are still considered as preliminary. The results of all reservoirs in Belgium can also be combined into one graph (fig. 8-12), which is probably more robust. This shows that there is a fair chance that industrial amounts of CO<sub>2</sub> can be stored in Belgian reservoirs, but that only in the most optimal cases this will be sufficient to accommodate for all potential CO<sub>2</sub> from Belgian CCS activities.

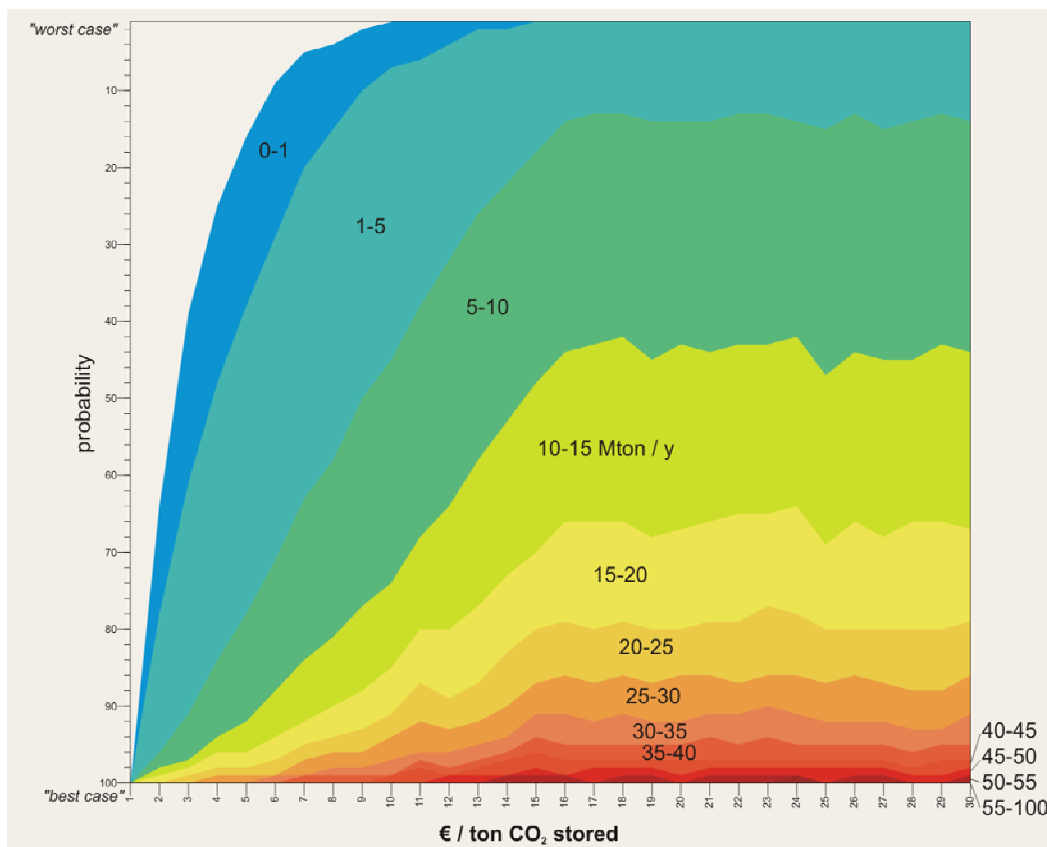


Figure 8-12: Capacity estimates for all reservoirs in Belgium. Capacities expressed in Mton/year. The results are plotted in function of the affordable cost for CO<sub>2</sub> storage and future probability.

## 9 Preliminary results from PSS

The two-year goal of the PSS-CCS project was to build the PSS simulator and its databases, not to perform and provide in-depth future forecasts. Results in this chapter are not verified. Instead they are provided for demonstrating the potential of PSS.

### 9.1 Demo scenario

The general scenario parameters are taken from the CCS scenario used in the Markal projections (see § 6.3.3). The timeframe was extended from 2030 to 2050 by keeping all values after 2030 constant, as for example for the market value of CO<sub>2</sub> (fig. 9-1). The production of electricity from fossil fuel, as predicted by Markal-Times, was used as demand curve in PSS.

Predictions on other sectors were not made by the Markal-Times model. For demonstration purposes, demand for commodities in other sectors relevant to CCS was kept constant at the 2005 level. The source inventory currently does not include source parameters for these other sectors. Realistic but rudimentary estimates for three sectors (Iron and Steel, Cement, Refineries) were included, but without uncertainty ranges. In the output graphs, this approach emphasises the current lack of reliable data.

### 9.2 Scenario variants

In order to demonstrate the flexibility of PSS, two variants of the demo-scenario were run, which were given the names ‘friendly’ and ‘hostile’.

In the friendly scenario, our neighbouring regions are considered open for the export of CO<sub>2</sub>

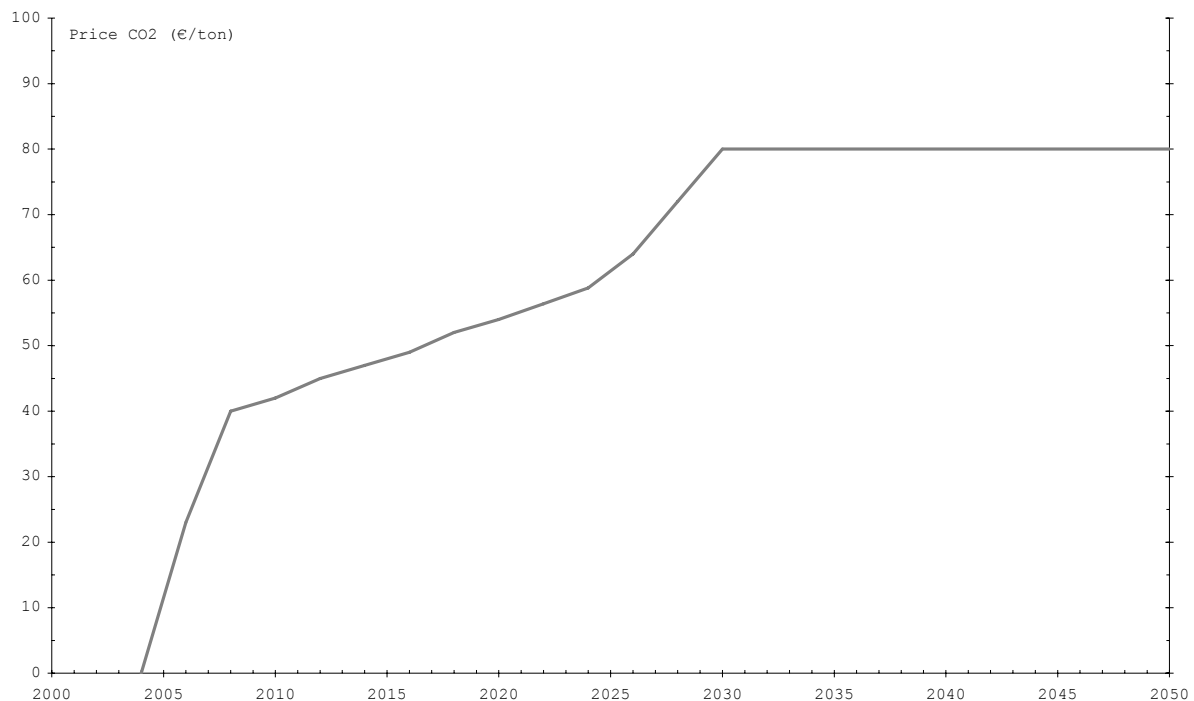


*Figure 9-1: The price of CO<sub>2</sub> is increasing through time, as such mimicking the assumptions made during Markal-Times modelling up to 2030. After 2030, the CO<sub>2</sub> price is assumed to remain constant. PSS uses the price assumptions between 2010 and 2050.*

produced in Belgium, while in the hostile one, CO<sub>2</sub> can only be stored on Belgian territory. This situation is inspired by certain discussions during the preparation of the EU directive on CCS. Around May 2008, open access to international transport and storage infrastructure for CO<sub>2</sub> was on the table, with some clearly opposed views, which are here simplified and radicalised into friendly and hostile.

### 9.3 Friendly scenario (export allowed)

The status of the PSS forecasts currently has a demonstration status only. The accurateness of the results can therefore not be guaranteed. The discussion on both scenario input and results is kept less detailed than in case of presentation of policy relevant final results.

PSS makes forecasts from 2010 and to 2050. As shown in figure 9-1, the price for CO<sub>2</sub> is expected to go up from around 40 to 80 €/ton during these four decades. The currently installed capacity in different sectors, based on fossil fuels, will decrease rapidly due to decommissioning of aged installations. This is shown for the power sector in figure 9-2. At the same time, the demand may rise, as demonstrated by the demand curve that is based on Markal-Times projections (fig. 9-3). Note that the reference scenario assumes a phasing-out of nuclear. From these outlooks follows that a new power and other plants will be built at a faster than current rate during the next decades. Under the reference scenario used for the PSS-demo simulations, CCS only becomes available from 2025 and 2030 onwards, which is usually well visible in the different projections.

This discussion on the demo scenario will focus on the global environmental aspects (CO<sub>2</sub> emission). A full analysis would also dig in the different economic and technical implications, and evaluate the results at a more detailed level. We will focus first on results from the power sector.

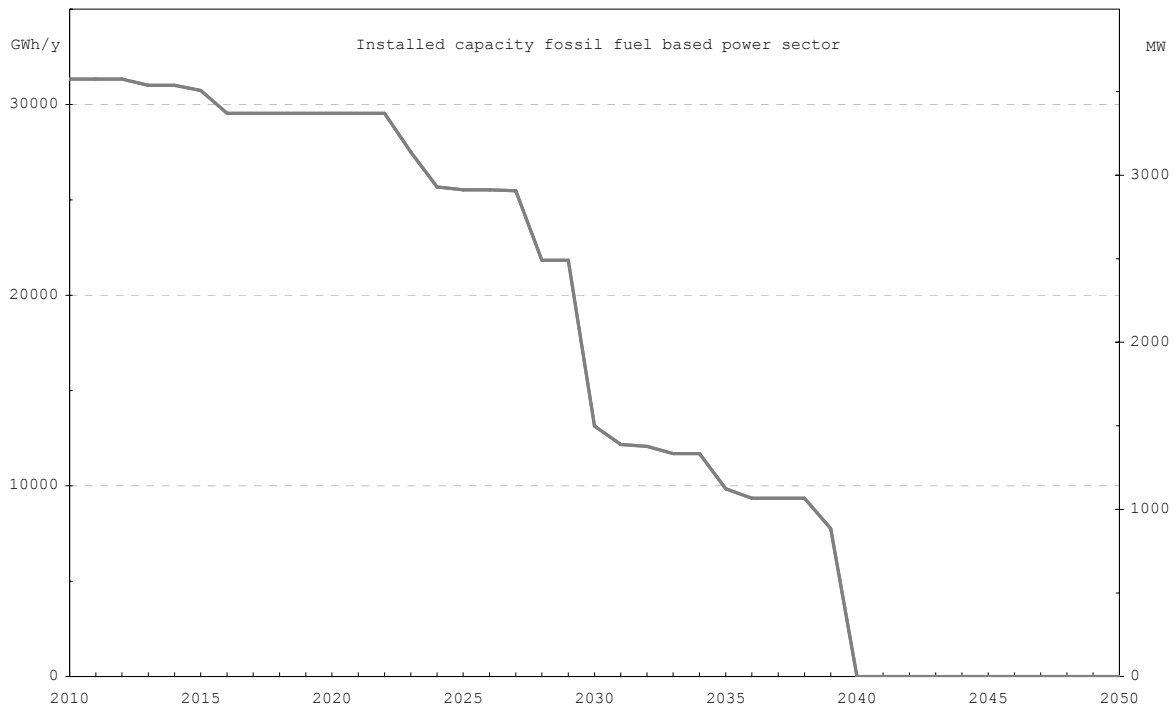


*Figure 9-2: The evolution of the currently installed capacity of the power sector in the next decades, based on the data in the PSS source database, demonstrating a quick drop after 2020 due to the age of the facilities.*

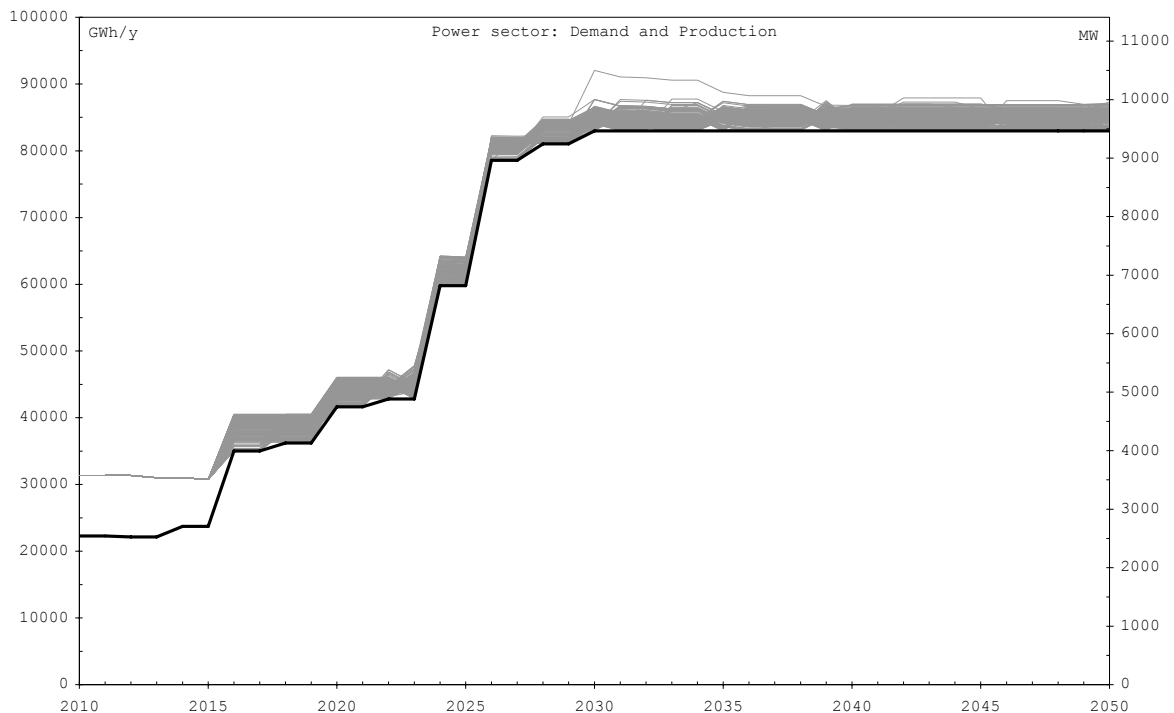


*Figure 9-3: Demand and production for the power sector (CCS relevant only). The black line represents the demand curve, based on Markal-Times projections up until 2030. Grey lines show the PSS projections. The mismatch during the first 5 years (demand lower than installed capacity) was traced down to an incorrect input parameter in PSS.*

The introduction of CCS technology shows clearly when looking at the amount of CO<sub>2</sub> captured on a yearly basis (fig. 9-4). The fast growth of CCS from 2025 onwards (first year when this technology is allowed under the demo scenario) shows that it is clearly economically viable to invest in CCS at that time. A next jump occurs in 2030, mainly due to the retrofit of (capture ready) power installations. From 2040 onwards, each year between 20 and 65 Mton of CO<sub>2</sub> is expected to be captured and stored each year, with a most likely value around 40 Mton. On a cumulative basis, this means that between 500 and 1200 Mton of CO<sub>2</sub> from Belgian sources would be captured and stored by 2050.

CO<sub>2</sub> avoided (fig. 9-5) gives a better idea of the environmental contribution of CCS. Again the steady increase towards 2040 shows the growth of CCS activities, with clear jumps at 2025 and 2030. By 2050, between 20 and 60 Mton of CO<sub>2</sub> would be less emitted into the atmosphere because of CCS activities. This amounts on average to a cumulated total of 800 Mton by 2050.

Another way of presenting this data, is by means of the total net emission of a certain sector (fig. 9-6). The CO<sub>2</sub> emission increase until 2025, because demand increases and CCS technology is assumed not to be available. At 2024, a last investment is made in non-CCS technology due to an increase in demand, which is clearly visible as a steep increase in CO<sub>2</sub> emissions. In almost all scenarios, technologies are chosen (NGCC) that can not be retrofitted until 2030, which explains why emissions stay high until 2030. In a future version, the limited foresight code of PSS will be activated, enabling PSS to make more rational choices.

After 2030, in spite of the strongly grown energy demand, the absolute emissions drop to below the 2010 level. However, they also break up along two distinct paths, with almost a factor 2 difference between the higher and lower projected emission paths. The cause is technology lock-in. In the source options, two very similar variants of NGCC are defined. The

main difference is that variant one can be retrofitted after 2030, while for variant 2 no retrofit is possible. Because both are very similar, in about 50% of the scenarios, the retrofittable variant is chosen (resulting in the low emission path), and in the other half the non-retrofittable one. This clearly demonstrates the danger and impact of construction of not capture-ready installations, even for natural gas fired facilities. It also shows the power of stochastic modelling, as this is a clear example of a situation where the average truth does not exist.

In order to make abstraction of the impact of demand, specific emission is used, which is the CO<sub>2</sub> emission normalised per unit of production. In figure 9-7 the relative specific emission is shown, where the specific emission in 2010 is taken as the 100% reference. Also before 2025, which marks the introduction of CCS technology, it is clear that the emission per kWh produced decreases, which is due to the replacement of existing sources by more efficient ones. In 2030 the effect of CCS becomes very clear, and also the technology lock-in is evident from the two emission trajectories. According to the lowest ones, the power sector as a whole could become 80 to 85% less CO<sub>2</sub> intensive due to increased efficiency and CCS. Even if part of the sector fails to retrofit, the gain may drop to less than 70% under the assumptions of the reference scenario.

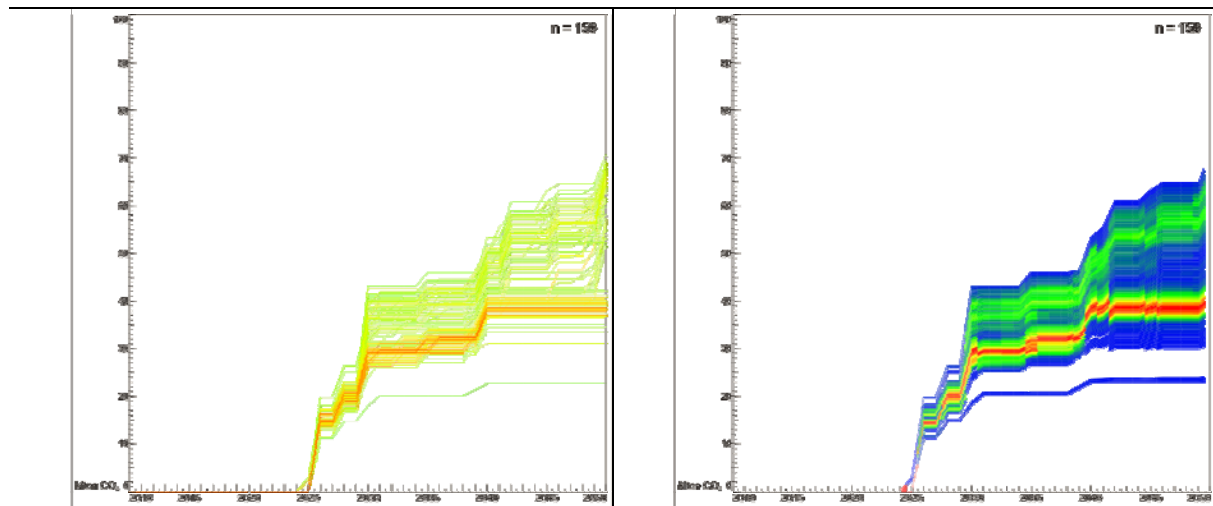


Figure 9-4: The amount of CO<sub>2</sub> (Mton/y) captured over time for the power sector. Left figure the individual graphs of the 159 stochastic runs. Right figure a density plot of the same results, with red values indicating the futures with the highest probability.

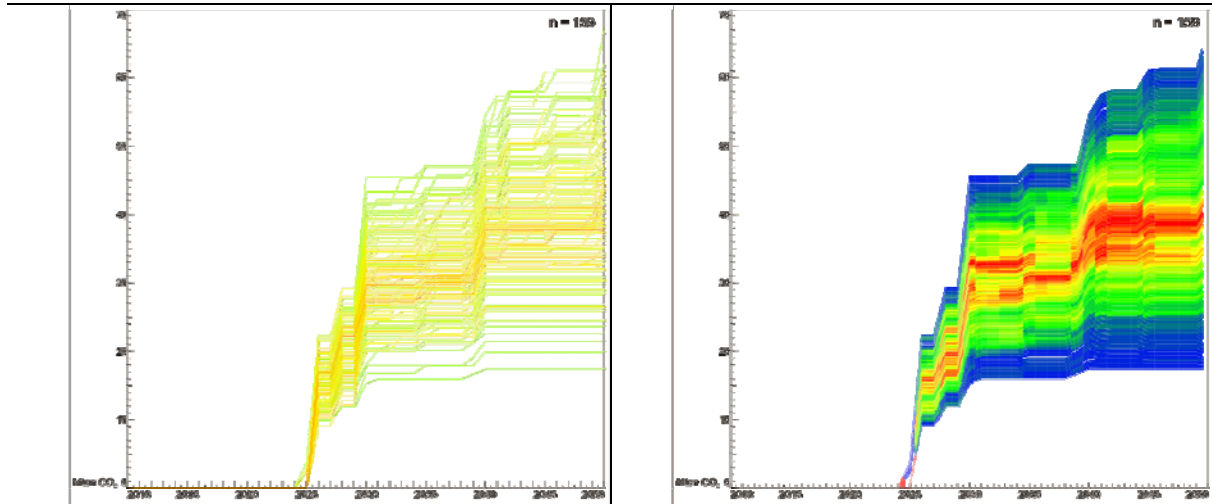


Figure 9-5: The amount of CO<sub>2</sub> (Mton/y) avoided due to CCS activities for the power sector. Left figure the individual graphs of the 159 stochastic runs. Right figure a density plot of the same results, with red values indicating the futures with the highest probability.

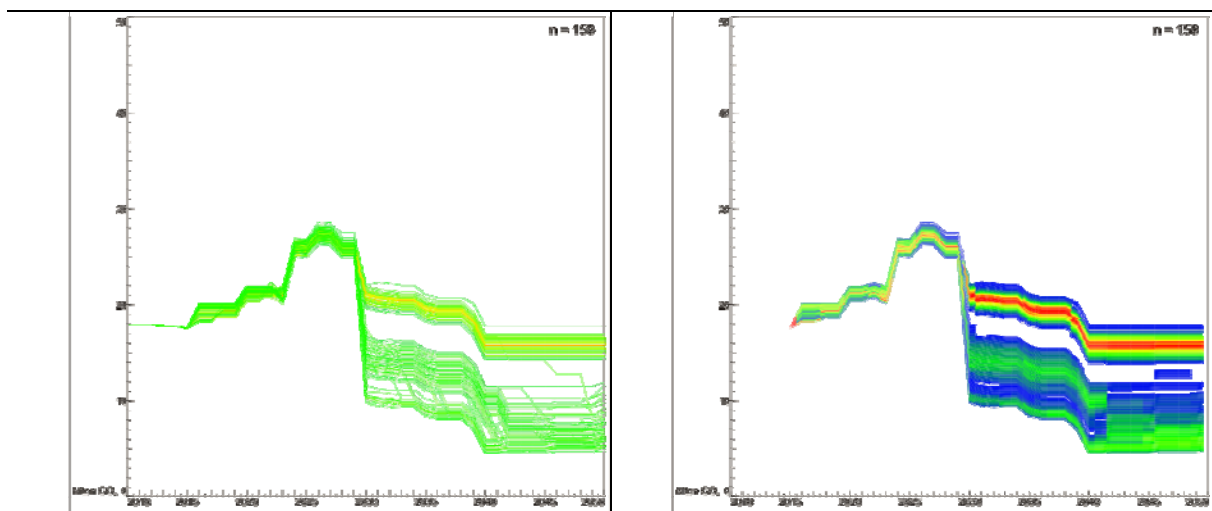


Figure 9-6: The net emissions of CO<sub>2</sub> (Mton/y) for the power sector. The discrete paths after 2030 is an example of technology lock-in, where the path of highest emission values is due to investment in non-CCS compatible technology (retrofit not feasible). Left figure the individual graphs of the 159 stochastic runs. Right figure a density plot of the same results, with red values indicating the futures with the highest probability.

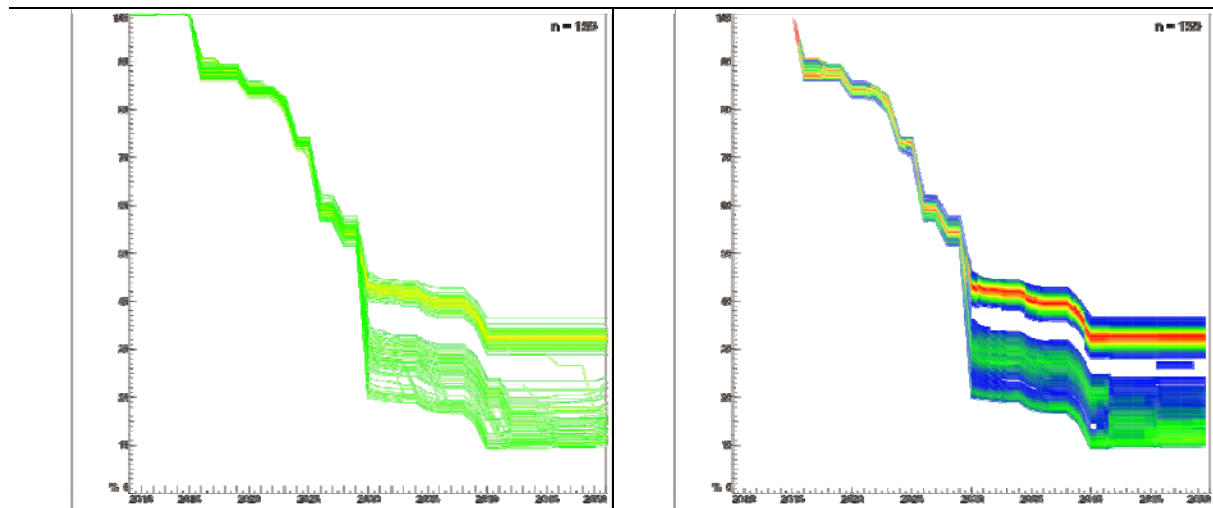


Figure 9-7: The specific net emissions of CO<sub>2</sub> for the power sector, expressed in percentage relative to the starting year 2010. The effect of technology lock-in is again clearly visible. In absolute numbers, specific emission is expressed in tonCO<sub>2</sub>/UoP. Left figure the individual graphs of the 159 stochastic runs. Right figure a density plot of the same results, with red values indicating the futures with the highest probability.

#### 9.4 Hostile scenario (no export possible)

In the friendly scenario, the total amount of CO<sub>2</sub> that need to be stored up until 2050 can exceed 1 Gton. The amount that is exported to neighbouring countries is very variable, but in most cases above 50% and often near 100% (fig. 9-8). From this graph, it is clear that Belgium is likely to export large amounts of CO<sub>2</sub>, but it is unclear whether this is due to economic reasons (cheapest option), or if this indicates a true dependency (no other option). The hostile scenario provides these answers, because it evaluates if CCS projects are feasible and economic when CO<sub>2</sub> needs to be stored in Belgium.

The impact of a ‘closed border’ situation will be evaluated by comparing the results of the friendly and hostile scenarios. Again, this approach will be done with emphasis on CO<sub>2</sub> emissions, but an in-depth analysis would e.g. also include making a cost impact comparison of the two scenarios, which is equally feasible with PSS.

The upper limit of CO<sub>2</sub> avoided under the hostile scenario is comparable to that of the friendly scenario (fig. 9-9), but the lower limit is zero. In fact, there is 3 to 4% probability that no CCS projects will develop. Also the average expectations are clearly lower, dropping from over 35 for the friendly to around 20 Mton/y in the hostile scenario.

The impact is more clear for the total emissions from the power sector (fig. 9-10). Instead of an overall reduction, as is predicted in the friendly scenario, emissions will probably have increased (60% probability) by 2050 with respect to 2010. Worst case outlooks even indicate a more than doubling of the CO<sub>2</sub> emissions from the power sector. This is also reflected in the CO<sub>2</sub> intensity (fig. 9-11), where the possibility seems to exist that the CO<sub>2</sub> intensity in 2050 is only marginally lower than in 2010, probably due to fuel choice.

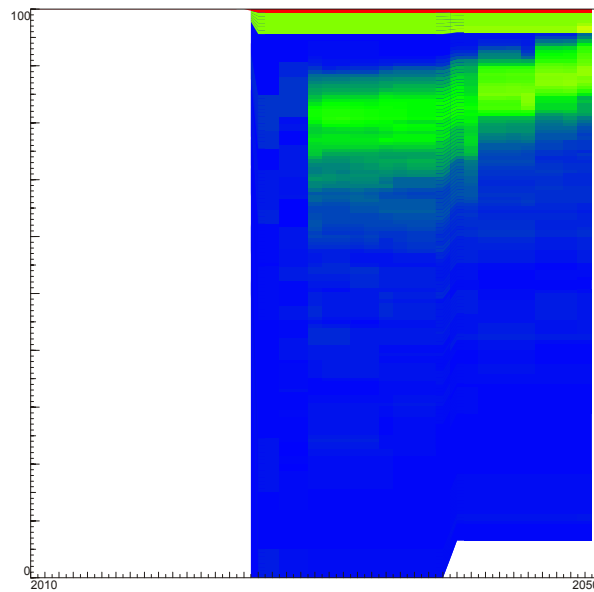


Figure 9-8: This graph shows the contribution of CO<sub>2</sub> storage in neighbouring countries versus storage in domestic reservoirs in the friendly scenario. 100% indicates that all CO<sub>2</sub> captured in Belgium is exported, which is the case in 60% of the stochastic runs. There is only a 5% probability that more than 50% of the captured CO<sub>2</sub> (on the graph: less than 50%) would be stored in Belgium.

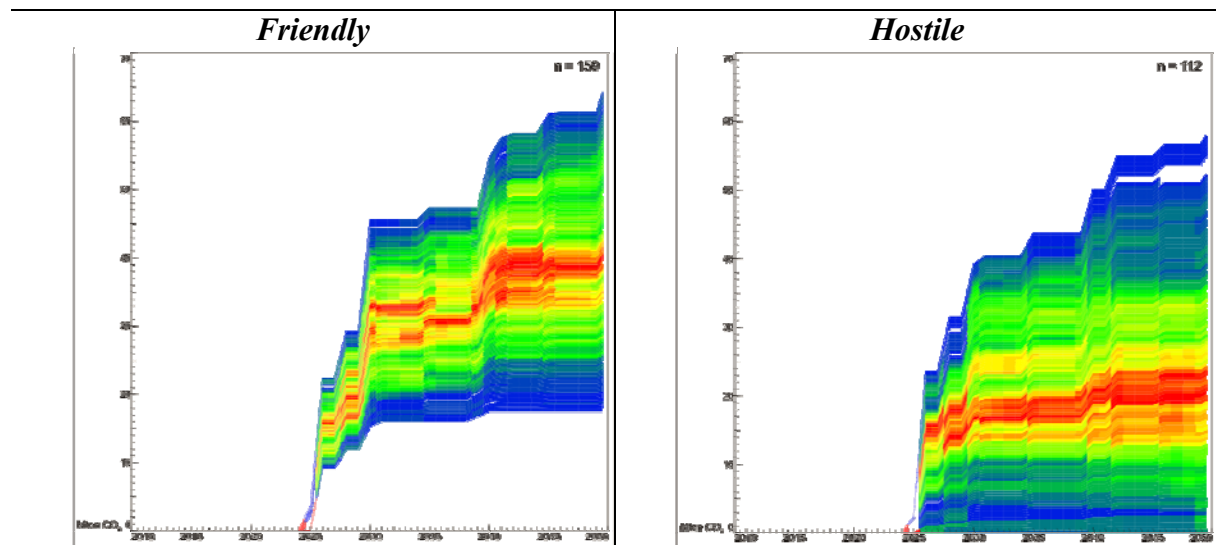


Figure 9-9: The amount of CO<sub>2</sub> (Mton/y) avoided due to CCS activities for the power sector, left for the friendly and right for the hostile scenario. Although the maximum value amount of CO<sub>2</sub>-avoided is reduced only slightly, the average and minimum values are strongly reduced in the hostile scenario. *n* indicates the number of stochastic runs. Red values show the most probable outcome.

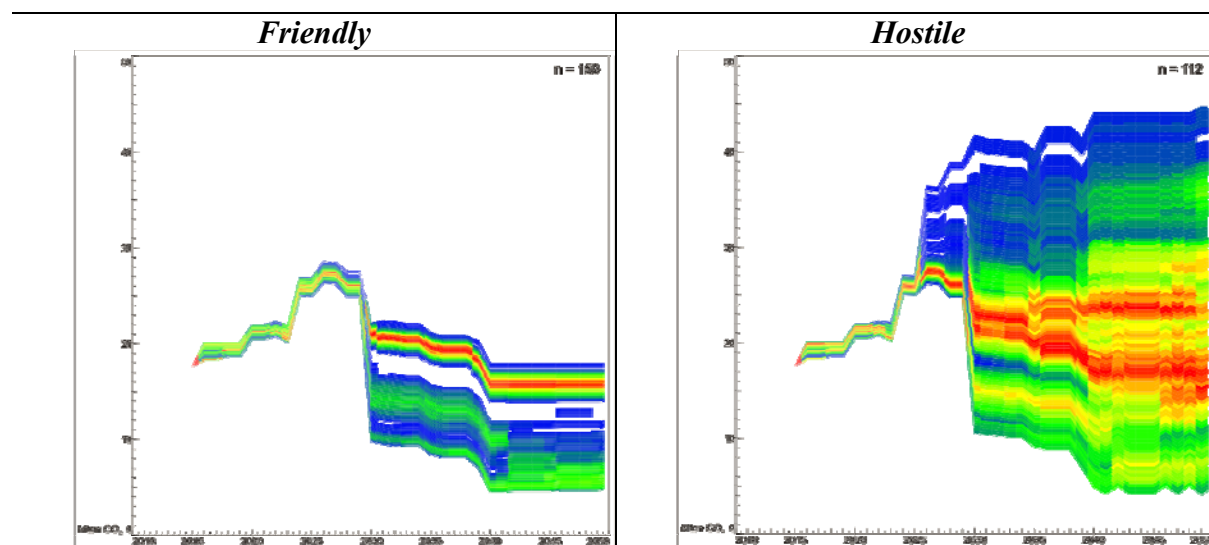


Figure 9-10: The net emissions of CO<sub>2</sub> (Mton/y) for the power sector, showing clearly the impact of the hostile scenario. In the friendly scenario, the total emissions in 2050 are always lower than in 2010, while in the hostile scenario, there is nearly 70% probability that emissions will continue to increase after 2010. *n* indicates the number of stochastic runs. Red values show the most probable outcome.

### 9.5 Discussion of the Friendly and Hostile scenarios

Both scenarios are mainly provided for demonstrating the possibilities and flexibility of the PSS simulator. The friendly scenario is based on the CCS model that was used for Markal-Times projections. PSS provides, next to a more detailed analysis of the CCS chain, also explicitly results in which the probability is clearly embedded. For the friendly scenario, the trends are usually relatively apparent. Nevertheless, two clear examples were encountered where the stochastic modelling technique was capable of trapping essential aspects that relate to future uncertainties.

In both the total and specific emissions of the power sector, there is a clear branching around 2030 into two separate future trends. Detailed inspection of the data revealed that this was caused by technology lock-in, leading to the direct conclusion that the concept of capture-readiness is crucial, not only for coal, but also for natural gas fired units.

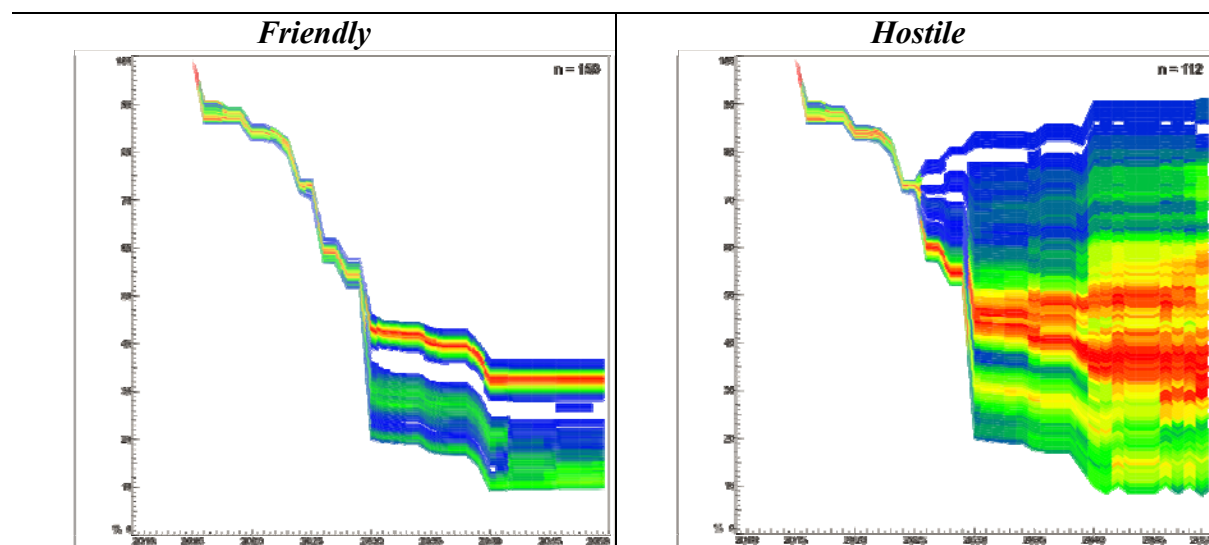


Figure 9-11: The specific net emissions of CO<sub>2</sub> for the power sector, expressed in percentage relative to the starting year 2010. In the worst-case predictions of the hostile scenario, the CO<sub>2</sub> intensity of the power sector is only marginally lower in 2050 than in 2010. The best-case projections are comparable to that of the friendly scenario. *n* indicates the number of stochastic runs. Red values show the most probable outcome.

Next to this discrete uncertainty, also more continuous ranges were identified, such as were shown for CO<sub>2</sub> captured and avoided. This uncertainty range is large, and has different causes. Essentially they are due to uncertainties in capture parameters and storage options. It is possible to identify the prime causes, and evaluate if the uncertainty can be reduced, or the overall result be improved.

Instead of actually attempting this, the opposite was done by running a second scenario variant. In this hostile scenario, the certainty of finding sufficient storage in neighbouring countries was removed. The negative impact of this is immediately clear, both in average results as in the overall increase of future uncertainty. Note that changing the scenario so drastically most likely requires the adjustment of other scenario parameters, such as the fossil fuel share. This was ignored here, which is an additional reason why one should be careful with the interpretation of these demo projections.



## 10 Conclusions

Policy Support System for Carbon Capture and Storage is truly a multi-disciplinary project. This is necessary in order to correctly assess all aspects of carbon capture and storage, which are capture, transport and geological storage of CO<sub>2</sub>. It is also an integrated study, which is shown by the way all individual elements meet in the PSS simulations.

The industrial source inventory show that two-third of the emissions from the power sector come from large sources, i.e. those that emit over 500 Mton/y. Large sources are in general more interesting for capture projects. Also in other sectors, the largest part of the emissions usually comes from the over 500 Mton/y installations. Sources which produce near-pure CO<sub>2</sub> as flue gas constitute a relatively small part of the total industrial CO<sub>2</sub> emissions.

Capture technologies in the power sector can be discriminated into three large groups: pre combustion capture, post combustion capture and oxyfuel combustion. These can be applied to both gas and coal fired installations. Although the technologies are based on different concepts and show different performance and CO<sub>2</sub> retention rate, the costs of electricity generation are quite similar. Changes in investment cost, fuel price, CO<sub>2</sub> price and other techno-economic parameters would modify the ranking. It is likely that all kinds of technologies will be developed in parallel and will find applications in different niches.

An assessment of the aquifer storage potential in Flanders identified four potential target intervals for geological CO<sub>2</sub> storage. The chinks of the earliest Tertiary to Upper Cretaceous (Houthem and Maastricht Formations) appears to be a less important target due to limited storage potential and limited distribution. The Lower Triassic Buntsandstein Formation appears promising in the Roer Valley Graben. It contains permeable sandstones and is overlain by Upper Triassic to Jurassic sediments that may act as good seals. The Neeroeteren Formation shows good reservoir properties, but does not always occur at sufficient depth or lacks proper sealing. The karstified and fractured intervals within the Carboniferous Limestone Group are good and properly sealed reservoirs, but the storage potential in the dome structures is rather small compared to the scale of CO<sub>2</sub> storage projects.

In the Walloon region, in the 700-1300m depth range an average total estimate of the storage potential in unmined coal deposits is about 700 Mt CO<sub>2</sub>, which represents a relative contribution three different lithologies (coal, shale, sandstone). Regarding the geological uncertainty and the distance to emission sources, two zones appear to be good candidates for CO<sub>2</sub> pilot-projects with 40 to 50 Mt storage capacity each. In addition, in these zones, the participation of the three lithologies could be of particular interest as coal deposits are highly fractured and faulted within a 100 to 600m thick interval. This interval, which is specific to the Hainaut coal basin, is capped by a major thrust fault (Masse Fault).

For the Dinantian aquifer, it is the deep and tabular part that appears most promising for the storage of CO<sub>2</sub>. First estimates indicate that between 180 and 270 Mton could be stored on Belgian territory.

Storage costs in neighbouring countries was estimated using the storage inventory reports for these countries, and assuming back-bone pipeline networks. For our neighbouring countries, these costs range between 4 and 6 €/ton, while in the North Sea region these costs vary between 8 and 11 €/ton CO<sub>2</sub>.

The Markal projections show a large implementation of CCS technologies as soon as they are available on the market and show CO<sub>2</sub> emission reductions in 2030 ranging from 32% to 52% in the different scenarios compared to the reference one.

Before the CCS technologies appear, the closure of existing plants (end of life of coal and gas plants and decommissioning of nuclear power plants) is offset by large investments in new Natural Gas Combined Cycle plants. The more intensive use of renewables and cogeneration and in the case nuclear plants lifetime is extended will reduce the investments in new capacity

of NGCC plants. The latter, while still in operation, is much less used once CCS technologies are implemented. If CCS technologies appear earlier than expected, then the investments in new NGCC capacities will still decrease more significantly.

Marginal Abatement Cost curves are developed where generation technologies are ranked on the basis of a CO<sub>2</sub> price and on their techno-economic characteristics. The conclusion of this exercise is that in 2030, the CCS technologies would appear as soon as the market CO<sub>2</sub> price is higher than 25 €/ton. Beyond 2030, the costs of CCS will be reduced by research and technological development and economies of scale. For information, this is the objective of the European Union project to reduce the capture cost down to 20 €/ton with a 90% retention rate.

The PSS simulator is successfully developed as an ad-hoc simulation tool for CCS technology, and details transportation issues, including pipeline routing, and sink uncertainties, which is of particular relevance to Belgium where accurate storage estimates can not be made. This uncertainty, together with that on the evolution in the capture technologies, are given specific attention by the stochastic simulation process. PSS is also highly flexible regarding different scenario assumptions. These aspects are demonstrated with a simulation of two scenario variant, based on the CCS scenario used in the Markal projections. Although intended for demonstration purposes only, some results already indicate or confirm future trends.

It is also clear from the PSS simulations that CCS can play a major role in the reduction of industrial CO<sub>2</sub> emissions, as was already indicated by the Markal projections and is indeed the general expectation of CCS.

Specifically for Belgium, it is likely that, given the current uncertainties regarding domestic storage capacity, a large part, or even all of the captured in Belgian CCS projects is exported to neighbouring regions. This dependency, emphasised by the two end-member export scenarios, is economically and environmentally a clear burden for the future in terms of uncertainty. This uncertainty can be controlled by ensuring export possibilities (cf. Rotterdam Climate Initiative) and by exploring or pre-exploring the Belgian subsurface.

The former danger is an example of potential technology lock-in due to insufficient or non-available storage possibilities. Also the effect of source technology lock-in is evident in the PSS demo simulations. Per scenario, randomly preference was given to capture-ready and non-capture ready NGCC technology. Although this is only one of the six technology groups, and natural gas has a relatively low-carbon intensity, the effects of this technology lock-in on overall emission show clearly.

These two potential pitfalls clearly illustrate the large impact that counterproductive effects may have. Carbon Capture and Storage is a technology that is likely to make a large contribution to reducing the industrial CO<sub>2</sub> emissions in the next decades, but it is advisable to plan and to some degree guide its implementation. This requires in-depth analyses which can be made using the PSS simulator, that itself relies on technological, technical and geotechnical assessments.